

STRENGTH AND FAILURE MECHANISMS OF UNIDIRECTIONAL CARBON FIBRE-REINFORCED PLASTICS UNDER AXIAL COMPRESSION

by

Dipl.-Ing. Jürgen Häberle

A thesis submitted for the degree of Doctor of Philosophy
of the University of London and for the Diploma of
Imperial College of Science, Technology and Medicine

December 1991

Department of Aeronautics
Imperial College of Science, Technology and Medicine
Prince Consort Road
London SW7 2BY

ABSTRACT

The main objective of the present study has been to develop a model predicting the compressive strength of unidirectional composites, and carbon fibre-reinforced plastics in particular, from the properties of the constituents.

A literature survey was carried out considering topics such as compression test methods for composites, failure modes and theories predicting the compressive strength of unidirectional carbon fibre-reinforced plastics. The survey revealed a variety of test methods with great variation of associated test results. It was therefore felt that an intensive study was necessary in order to establish a meaningful test method. The intention was to keep the specimen and the test procedure as simple as possible whilst reducing hardware-induced stress concentrations in the test piece.

The development of a new test method is described and limitations of a coupon test in general are discussed. The influence of several parameters of test piece preparation and design was assessed experimentally and by finite element investigations. As a result of this investigation, the mechanism of tab tip debonding was found to play an important role in compression testing, and an improved specimen with tab tip debonds is proposed.

In order to study the influence of the test method on the measured compressive strength of composites, several established compression test methods were compared and assessed. The new test fixture was used successfully for a range of materials and specimen configurations, and the test results are presented and discussed.

Two parameters were found to be most important for the compressive strength of unidirectional composites with volume fraction and fibre type given. The first one is the shear response of the composite, which is largely determined by the shear properties of the matrix. The second one is the axial alignment of the fibres within the composite. A technique which evaluates polished sections of composite samples cut at a small angle was applied on several materials. This technique enabled the degree of fibre misalignment to be quantified in terms of angular deviations of individual fibre segments. The shear response of unidirectional composites was determined by tension of ±45°-laminates.

Macroscopic instability was identified, experimentally and analytically, as a major problem in compression testing of CFRP because of the reduction of the elastic properties of CFRP under compression. By including nonlinear effects in classical buckling predictions the experimental findings could be verified.

Compressive failure of the composite was modelled as local shear instability using a simple micromechanical model incorporating the nonlinear shear stress-strain response of the composite, as well as initial fibre deflection. With the experimentally determined input data the model offered satisfactory answers for the compressive strength of the composites examined. Light and scanning electron microscopic investigations strengthened the assumptions made on the failure mechanism.

ACKNOWLEDGEMENTS

A large experimental programme would not be possible without considerable assistance from many sides, and I would like to express my gratitude to all Imperial College staff who helped to perform the various tasks during the project.

In particular, I would like to thank the Aeronautics structures workshop for their efforts in producing the hardware, essential for the work. Bill Godwin was untiringly helpful in matters of testing, and matters of the Holland Club.

Full appreciation to Darryl Williams for helping set up the image analyser; to Nick Taylor for assisting with the scanning electron microscope; and to John O'Leary for printing of too many photographs. I would also like to thank the members of the Aeronautics department for their support, particularly Ken Stevens, Ian Matthews and John Finley.

Continuous discussions with Paul Curtis, project coordinator, Andy Ingram and Michael Wisnom on the subject of compression were helpful and I hope that some of the ideas discussed will be pursued.

Special thanks go to my supervisor Frank Matthews, director of the Centre for Composite Materials, who initiated the project. His calm and professional way of dealing with any problem was very impressive and a great help.

Finally, I would like to express my deepest gratitude to Jocelyne who never failed to support me.

The support made available by the Royal Aerospace Establishment from funds of the Department for Trade and Industry is greatly appreciated.

TABLE OF CONTENTS

Abstract 2
Acknowledgements 3
Table of Contents 4
List of Symbols 7
List of Figures 9
List of Tables 18
Chapter 1 Introduction 21
Chapter 2 Literature Review 25
2.1 Compression Testing of Composites 25
2.1.1 Principles 25
2.1.2 Compression Test Methods 27
2.1.3 Comparison of Test Methods 32
2.1.4 Factors Affecting the Test Results 39
2.2 Strength Prediction 41
2.2.1 Compressive Failure Modes 41
2.2.2 Models Predicting Compressive Strength 46
2.3 Conclusions 58

EXPERIMENTAL INVESTIGATIONS
A. Compression Testing

Chapter 3 Basics of Mechanical Testing 60
3.1 Laminate Production 60
3.2 Test Piece Preparation 62
3.3 Testing Equipment and Data Acquisition 68
3.4 Fractography 69

Chapter 4 Preliminary Compression Experiments 70
4.1 Comparative Compression Testing 70
4.2 Failure Modes 73
4.3 Discussion of Test Results and Conclusions 77

Chapter 5 Development of a Modified Compression Test Method 79
5.1 Test Fixture Design 81
5.2 Specimen Design 85
5.2.1 Finite Element Investigations 87
5.2.2 Experimental Parameter Study of Test Piece Geometry 92

5.2.3 The Role of Tab Tip Debonding 98
5.2.4 Identification of Test Piece Instability 101
5.2.5 Parameter Study of Test Piece Preparation 107
5.2.6 Improved Specimen Design 110
5.3 Proposal for a Multidirectional Specimen 113

Chapter 6 Summary of Results of Compression Testing 115
6.1 Unidirectional CFRP 115
6.1.1 XAS/914C - Different Test Methods 115
6.1.2 XAS/914C - ICSTM Method with Improved Specimen 119
6.1.3 Apollo 43-750/9106C 122
6.1.4 AS4/PEEK (APC-2) 126
6.2 Unidirectional GRP 128
6.2.1 E-Glass Fibre-Reinforced Nylon (ICI 'Plytron') 128
6.2.2 E-Glass Fibre-Reinforced Epoxy 131
6.3 Non-Standard Specimens 132
6.3.1 Woven Cross-Ply CFRP 132
6.3.2 Multidirectional CFRP 133
6.3.3 Thick Woven Cross-Ply GRP 134

B. Complementary Experimental Investigations

Chapter 7 Mechanical Characterisation 135
7.1 Tensile Tests 135
7.2 Flexure Tests 139
7.3 Interlaminar Shear Strength Tests 144
7.4 In-plane Shear Stress-Strain Response 148

Chapter 8 Quantification of Fibre Misalignment 153
8.1 Description of the Technique 153
8.2 Statistical Data Analysis 157
8.3 Results for Several CFRP Systems 161

Chapter 9 Discussion of Experimental Findings 167
9.1 Proof of Proposed Test Method 167
9.2 Influence of Test Method 173
9.3 Influence of Test Piece Parameters 176
9.4 Interpretation of Flexure Test Results 179

9.5 Correlation of Compressive Strength and Other Mechanical Properties 187
9.6 Significance of Coupon Compression Testing 190

MODELLING OF COMPRESSIVE FAILURE

Chapter 10 Macroinstability of the Test Piece 193
10.1 General Aspects on Buckling of Columns 193
10.2 Modifications of Euler Equations for Composites 197
10.2.1 Shear Correction 197
10.2.2 Nonlinear Elastic Properties 198
10.3 Comparison with Experimental Results and Discussion 201

Chapter 11 Micromechanical Model to Predict Compressive Failure ... 205
11.1 Derivation of the Model 205
11.1.1 Micromechanical Strength Model 205
11.1.2 Graphical Solution 210
11.1.3 Discussion of the Model Parameters 213
11.1.4 Modelling the Stress-Strain Response 216
11.2 Input of Experimental Data 219
11.2.1 Stress-Strain Response 219
11.2.2 Strength Prediction 220
11.2.3 Influence of Superposed Shear Stresses 223
11.3 Concluding Discussion 226
11.3.1 Discussion of the Predictions 226
11.3.2 General Comments on Compression Failure 230
11.3.3 Conclusions 232

Chapter 12 Conclusions and Suggestions for Future Work 233
12.1 Conclusions of the Experimental Work 233
12.2 Conclusions of Theoretical Investigations 236
12.3 Suggestions for Future Work 238

References 241
Figures 250
Photographs 269
Tables 282
Appendix A Papers Published During the Project
A 1 ASM-3, Guildford 301
A 2 ECCM-4, Stuttgart 316

LIST OF SYMBOLS

A	cross-sectional area	m	total number of class intervals; machining allowance
a	initial column imperfection	N	number of specimens in a sample
C	coefficient of support condition; (correction) factor	n	counting variable; number of values within a class interval; shape factor
d	diameter; debond length	P	applied load; (normal) force
E	longitudinal modulus of elasticity	p	shear curve shape parameter
e	shift of neutral axis	R	resistance
f	frequency	r	measure for surface unevenness
G	shear modulus	S	strength
I	moment of inertia	s	slenderness ratio; support length; arc length
g	gauge length	t	thickness
H	horizontal resultant	U	voltage
k	matrix shear yield strength, strain gauge factor	u	axial deformation
l	(unsupported) length; fibre half wave length	v	lateral deformation
M	(bending) moment	w	(test piece) width

Greek symbols

α	fibre inclination within kink band	μ	coefficient of friction
β	kink boundary angle	ν	Poisson's ratio
δ	central (lateral) deflection	ω	fibre angle relative to intersection plane
Δ	difference	ρ	radius of curvature
ε	direct strain	σ	direct stress, standard deviation
ϕ	fibre angle relative to nominal composite zero direction	τ	shear stress
γ	shear strain	θ	laminate ply angle
λ	half wave length	ξ	auxiliary variable

Composed symbols

C_V	coefficient of variation	σ_{n-1}	standard deviation of a sample
f_0/l	initial composite fibre waviness	σ_{cu}	ultimate compressive stress
f_V	fraction of fibre volume	V_f	composite fibre volume fraction
$\tilde{f}$	relative class frequency	w_c	class interval width

Subscripts

ax	axial	*eff*	effective
c	compression	*el*	elastic
corr	corrected, correction	*Eu*	Euler
cr	critical	*f*	fibre
e	end tab	*fl*	flexure

geom	geometric	*r*	reduced
if	interface	*s*	source; surface
is	interlaminar shear	*sp*	superposed
k	*kink band*	*t*	tension, tangential
lt	laminate	*tot*	total
m	matrix	*tr*	transverse
max	maximum	*u*	ultimate
min	minimum	*vol*	volumetric
p	proportional	*y*	yield
PC	cutting plane	0	initial

Superscripts

*	value at failure	–	mean value

Abbreviations

ASTM	American Society for Testing and Materials
BAe	British Aerospace
BS	British Standard
CFRP	carbon fibre-reinforced plastic
CRAG	Composites Research Advisory Group
DIN	Deutsches Institut für Normung (German Institute for Standardisation)
FACETS	Forum for Advanced Composites Evaluation of Testing and Standards
FE	finite element
GRP	glass fibre-reinforced plastic
ICSTM	Imperial College of Science, Technology and Medicine
IITRI	Illinois Institute of Technology Research Institute
ILSS	(apparent) interlaminar shear strength
MAX	maximum
MIN	minimum
MOD	longitudinal modulus of elasticity
PEEK	poly-ether-ether-ketone
RAE	Royal Aerospace Establishment (formerly Royal Aircraft Establishment)
SACMA	Suppliers of Advanced Composite Materials Association
SAMPE	Society for the Advancement of Materials and Process Engineers (formerly: Society of Aerospace Material and Process Engineers)
SEM	scanning electron microscope
SW	sandwich
SWB	sandwich beam
UCS	ultimate compressive stress
UCSN	ultimate compressive strain
UD	unidirectional
UTS	ultimate tensile stress
UTSN	ultimate tensile strain

LIST OF FIGURES

Figures contained within the text

Chapter 1

1-1: Ratio of tensile and compressive strength of different materials.

1-2: Test results of a European round robin in compression testing of CFRP sorted into categories of materials.

1-3: Test results of a European round robin in compression testing of CFRP sorted into categories of participating laboratories.

Chapter 2

2.1.1-1: Different methods of load introduction into a compressive specimen.

2.1.1-2: Different compression test piece types.

2.1.2-1: The Celanese and IITRI compression fixtures, shown schematically.

2.1.2-2: Modified ASTM D695, RAE and Birmingham compression test methods, shown schematically.

2.2.1-1: Principal observed failure modes of composites.

2.2.1-2: Kink band geometry.

Chapter 3

3.1-1: A typical autoclave lay-up; exploded view, not to scale.

3.2-1: Machining of the composite panel and the end tab plates.

3.2-2: Test piece plate assembly.

3.2-3: Final composite plate ready for cutting into individual test pieces.

3.2-4: Illustration of the test piece surfaces to be ground flat.

3.2-5: Illustration of composite surface roughness.

3.2-6: Resistors and strain gauge arranged to a 'Quarter Wheatstone Bridge'.

3.2-7: Illustration of the technique used to apply strain gauges.

Chapter 4

4.1-1: Dimensions of test pieces tested in the Birmingham fixture; (a) waisted, (b) plain specimen.

4.1-2: Modified gripping of the test piece using the IITRI method.

4.2-1: Main compressive failure modes of unidirectional CFRP.

4.2-2: Typical invalid failures of the modified ASTM D695 test piece.

4.2-3: Typical test piece failures CRAG/IITRI.

4.2-4: Delaminations and consequent compressive failure in the Birmingham (RAE)-type test piece.

4.2-5: Compressive failure modes of the Birmingham method specimen.

Chapter 5

5.1-1: ICSTM compression test fixture; exploded view.

5.1-2: End blocks of Birmingham and ICSTM rig, respectively.

5.1-3: Illustration of the effect of through-thickness stresses on surface fibres.

5.1-4: Mounting of the compression rig in the testing machine.

5.2-1: Preliminary standard compression test piece for the ICSTM method.

5.2.1-1: Finite element mesh of an end-loaded compression test piece with 5 mm gauge length.

5.2.1-2: Deformation of an end-loaded compression test piece.

5.2.1-3: Surface stresses in an end-loaded compression specimen from finite element analysis; plane perpendicular to laminate plane.

5.2.1-4: Stresses scanned through-thickness in an end-loaded compression specimen from finite element analysis; plane perpendicular to laminate plane.

5.2.1-5: Stresses in the centre symmetry plane in an end-loaded compression specimen from finite element analysis; plane perpendicular to laminate plane.

5.2.2-1: Poisson's ratio of XAS/914C from compression tests versus unsupported length of the test piece.

5.2.2-2: Test results for the compressive strength of XAS/914C versus specimen slenderness ratio.

5.2.2-3: Typical compressive stress-strain curves suggesting macroscopic instability of the test pieces in some cases.

5.2.2-4: Variation of compressive failure mode with slenderness ratio of test piece using the ICSTM method; 16-ply laminates.

5.2.2-5: Repeated loading of a test piece with a gauge length of 50 mm.

5.2.2-6: Illustration of an occasionally observed test piece failure.

5.2.3-1: Integral test piece: (a) machining of the test piece from a thick laminate;
(b) interlaminar cracking at the 'tab' tip.

5.2.3-2: Stress-strain signals at the instant of tab tip debonding; note that the origin is suppressed.

5.2.3-3: Typical stress-strain curve for a specimen with machined gauge section showing 'tab tip debonding'.

5.2.3-4: Illustration of initial tab tip debonding by bending of the test piece.

5.2.3-5: Illustration of tab tip debonding when compressing a unidirectional glass fibre/polyester test piece with weakly bonded tabs.

5.2.4-1: Illustration of the shape of a buckled specimen.

5.2.4-2: Unsymmetrical tab debonding in the stress-strain curve of a modified ASTM D695 test piece; thickness 1 mm, gauge length 5 mm.

5.2.4-3: Stress-strain curves of a compression test using the IITRI method showing specimen buckling.

5.2.4-4: Repeated loading of a test piece with 10 mm gauge length.

5.2.5-1: Illustration of a layer misalignment of 2°.

5.2.5-2: Proposal for loading block arrangement to allow lateral movement.

5.2.6-1: Test piece preparation with debond insert.

5.2.6-2: ICSTM test piece with debond insert.

5.2.6-3: Identification of stress concentrators in an ICSTM test piece.

5.3-1: Multidirectional test piece sandwiched between reusable tabs.

Chapter 6

6.1.1-1: Illustration of loading conditions using the CRAG compression rig.

6.1.1-2: Some typical stress-strain curves using the BAe compression test rig.

6.1.1-3: Adjustable end cap for modified ASTM D695 specimens.

6.1.2-1: Polynomial curve fits to experimental compression data.

6.1.2-2: Failure mode of an improved specimen using the ICSTM method in some cases.

6.1.3-1: Test results for the compressive strength of Apollo 43-750/9106C containing fibres with different levels of fibre surface treatment; ICSTM and Birmingham test methods.

6.1.3-2: Typical stress-strain curves for Apollo 43-750/9106C containing fibres with different levels of fibre surface treatment; ICSTM test method.

6.1.3-3: Normalised modulus of elasticity versus level of fibre surface treatment for Apollo 43-750/9106C.

6.1.4-1: Comparison of compressive stress-strain curves of an APC-2 and an XAS/914C specimen.

6.2.1-1: Typical compressive stress-strain curves of ICI 'Plytron'.

6.2.1-2: Ultimate compressive stress versus the product of modulus of elasticity and the thickness of the test piece squared.

6.2.1-3: Typical mean compressive stress-strain curves of ICI 'Plytron'.

6.2.2-1: Stress-strain curves of unidirectional glass fibre/913G ($V_f \approx 60\%$) using the ICSTM method; specimen with debond insert.

6.3.2-1: Compressive stress-strain curves of laminates L1; ICSTM method.

Chapter 7

7.1-1: Test piece for determination of tensile properties.

7.1-2: Stress-strain curves from individual tension and compression tests.

7.1-3: Illustration of a misaligned single layer in a unidirectional test piece.

7.1-4: Average stress-strain data of XAS/914C in tension and compression and curve fit.

7.1-5: Normalised modulus of elasticity versus axial strain for XAS/914C.

7.2-1: Dimensions of specimen (a), jig (b) and modified roller (c) for four-point bend tests according to ASTM D790 M.

7.2-2: Typical stress-strain curves of four-point bending tests; (a) standard loading rollers; (b) plastic padded loading rollers.

7.3-1: Specimen and jig dimensions for the short beam shear tests.

7.3-2: Illustration of failure modes of short beam shear test pieces.

7.3-3: Some typical 'shear' stress-displacement curves from short beam shear tests.

7.4-1: Test piece for determination of in-plane shear properties.

7.4-2: Typical shear stress-strain curves of APC-2 obtained by tension of a ±45° test piece.

7.4-3: Typical shear stress-strain curves of XAS/914C obtained by tension of a ±45° test piece.

7.4-4: Polynomial and exponential curve fits to a typical shear curve.

7.4-5: Representative shear stress-strain curve fits for XAS/914C and APC-2.

Chapter 8

8.1-1: Cross-sections of circular fibres sectioned at different angles.

8.1-2: Definition of fibre angles in a sectioned composite sample.

8.1-3: Illustration of the sensitivity of the technique on the sample intersection angle.

8.1-4: Possibilities of manipulating objects using an image analyser.

8.1-5: Classification of relative fibre angles.

8.2-1: Untransformed corrected discrete distribution of fibre angles.

8.2-2: Absolute fibre angle distribution used for determination of a representative mean deviation from the zero direction.

8.3-1: Fibre angle distribution for XAS/914C using an image analyser.

8.3-2: Cumulative fibre angle distribution for XAS/914C.

8.3-3: Comparison of image analyser and manual measurement.

8.3-4: Fibre angle distribution for AS4/PEEK (APC-2).

8.3-5: Comparison of fibre angle distribution for AS4/PEEK and XAS/914C.

8.3-6: Transformed fibre angle distributions for Apollo 43-750/9106C containing fibres with 0%, 10%, 50% and 100% surface treatment.

8.3-7: Results of fibre angle analysis; cumulative plots.

8.3-8: Results of the fibre angle analysis; distribution of absolute angles.

Chapter 9

9.1-1: Illustration of test fixture arrangement for assessment of frictional effects.

9.1-2: Effects of friction on the apparent modulus of elasticity.

9.1-3: Influence of operator on the test results using the ICSTM method.

9.1-4: Influence of clamping pressure on apparent compressive strength using the ICSTM method.

9.1-5: Some typical compressive stress-strain curves observed using the ICSTM method.

9.2-1: Results of tests carried out in the present study for the compressive strength of XAS/914C using different test methods and specimen configurations; abbreviations as in Table 6.1.1-1.

9.2-2: Published test results for the compressive strength of XAS/914C using different test methods and specimen configurations.

9.3-1: Effect of tabbing properties on measured compressive strength.

9.3-2: Test results for the compressive strength of XAS/914C using the ICSTM method and varying test piece parameters.

9.4-1: Sketch of strain and stress distribution in the flexure specimen.

9.4-2: Geometric linear prediction assuming test conditions described in Chapter 7.2 and test results for four-point bend test.

9.4-3: Geometric linear prediction and test results for four point bend test, compressive versus tensile surface strains.

9.4-4: Deflections of the flexure specimen.

9.4-5: Forces acting on the flexure specimen.

9.4-6: Bending moment correction factor versus tensile surface strain.

9.4-7: Nonlinear prediction of the load-strain response of the flexure test piece.

9.5-1: Compressive strength (ICSTM method with standard specimen) versus short beam ILSS for several unidirectional composites.

9.5-2: Compressive strength of several unidirectional CFRP versus fibre alignment.

9.6-1: A view of compression testing practice.

Chapter 10

10.1-1: Load deflection behaviour under compression of columns with imperfections.

10.1-2: Application of the Southwell plot: (a) Compressive stress-strain curve of an aluminium alloy specimen (gauge length 50 mm, thickness 2 mm); (b) Southwell plot using the data from (a).

10.1-3: Illustration of reduced modulus in plasticity zone of metals.

10.2.2-1: Reduction of longitudinal modulus of elasticity of XAS/914C under compression.

10.2.2-2: Demonstration of the nonlinear elastic nature of the stress-strain response of XAS/914C under compression.

10.2.2-3: Comparison of buckling stress predictions.

10.3-1: Comparison of experimental results and buckling predictions using Equations 10.2.1-2 and 10.2.2-1 to -3 with initial in-plane shear modulus G = 5.0 GPa.

10.3-2: Critical stresses versus slenderness ratio using different values for the shear modulus.

10.3-3: Comparison of test results and predictions for varying values of shear modulus and two clamping factors.

10.3-4: Comparison of experimental data and common methods of buckling prediction.

Chapter 11

11.1.1-1: Idealised fibre deflection in the composite.

11.1.1-2: Forces acting on a repeating composite element under axial compression.

11.1.1-3: Different idealizations of the unloaded unidirectional composite.

11.1.2-1: Graphical determination of the ultimate compressive stress.

11.1.2-2: Direct reading of the ultimate compressive stress.

11.1.3-1: Modelled shear stress-strain curve with different shape parameters.

11.1.3-2: Influence of the shape of the shear stress-strain curve on the ultimate compressive stress.

11.1.3-3: Influence of variation of shear modulus (a) shear strength (b) and shape of the shear stress-strain curve (c) on the ultimate compressive stress versus initial fibre deflection.

11.1.4-1: Flowchart of the computer program to model the stress-strain response of a unidirectional CFRP composite.

11.2.1-1: Modelled stress-strain response of a unidirectional composite for various initial fibre deflections.

11.2.2-1: Ultimate compressive stress versus initial fibre deflection.

11.2.2-2: Critical values versus initial fibre deflection for XAS/914C.

11.2.3-1: Sketch of modes of shear superposition. (a) increased or (b) decreased shear deformation caused by load introduction.

11.2.3-2: Illustration of the method to determine the compressive strength with shear stresses superposed.

11.2.3-3: The influence of superposed shear stresses on the predicted compressive strength of XAS/914C.

11.2.3-4: The influence of superposed shear stresses on the predicted compressive strength of AS4/PEEK (APC-2).

11.3.1-1: Comparison of predicted and measured values for the compressive strength of XAS/914C and APC-2.

11.3.1-2: Graphical determination of the compressive strength in case of interfacial failure.

11.3.1-3: Assessment of the test results for Apollo 43-750/9106C using the ICSTM compression test method (standard specimen) on the basis of predictions for XAS/914C in dry and saturated conditions.

11.3.2-1: Illustration of propagation of kink bands at a free specimen edge.

Chapter 12

12.3-1: Proposal for the use of a sandwich column in the ICSTM test rig shown in Figure 5.1-4.

Figures contained in the section "FIGURES" page 250

F-1: Compression test piece dimensions.

F-2: Stress-strain curves of unidirectional XAS/914C using the ICSTM compression method with standard test piece; gauge lengths 5 and 7.5 mm.

F-3: Stress-strain curves of unidirectional XAS/914C using the ICSTM compression method with standard test piece; gauge length 10 mm.

F-4: Stress-strain curves of unidirectional XAS/914C using the ICSTM compression method with standard test piece; gauge length 15 mm.

F-5: Stress-strain curves of unidirectional XAS/914C using the ICSTM compression method with standard test piece; gauge length 20 mm.

F-6: Stress-strain curves of unidirectional XAS/914C using the ICSTM compression method with standard test piece; gauge lengths 30 and 50 mm.

F-7: Stress-strain curves of unidirectional XAS/914C using the ICSTM compression method; test piece gauge length 10 mm; initial debond by bending.

F-8: Stress-strain curves of quasi-unidirectional XAS/914C using the ICSTM compression method; quasi-unidirectional lay-up $[(\pm 1°)_8]_S$, 10 mm gauge length.

F-9: Stress-strain curves of unidirectional XAS/914C using the ICSTM compression method; test piece 10 mm gauge length; tap tip debond by inserting a 5 mm strip of PTFE tape.

F-10: Stress-strain curves of unidirectional XAS/914C using the ICSTM compression method; test piece 10 mm gauge length; tap tip debond by inserting a 5 mm strip of cellulose adhesive tape.

F-11: Some typical stress-strain curves of unidirectional Apollo/9106C with different levels of fibre surface treatment using the ICSTM and the Birmingham (BI) method.

F-12: Stress-strain curves of unidirectional APC-2 using the ICSTM compression method; test piece 10 mm machined gauge section.

F-13: Stress-strain curves of unidirectional APC-2 using the ICSTM compression method; test piece 10 mm gauge length with 5 mm debond (cellulose tape) insert.

F-14: Stress-strain curves of quasi-isotropic XAS/914C (laminate L1) using the ICSTM compression test method with sandwiched test piece.

F-15: Stress-strain curves of unidirectional XAS/914C; tension tests.

F-16: Critical compressive stress versus longitudinal modulus of elasticity for different clamping conditions for an orthotropic column with rectangular cross-section of 2 mm thickness and 10 mm unsupported length.

F-17: Critical compressive stress versus test piece slenderness ratio for different clamping conditions for an orthotropic column with rectangular cross-section.

F-18: Chart for graphical solution of compressive strength for a given angle of misalignment; shear curves of XAS/914C ('dry' and 'saturated') and APC-2 are given.

Figures contained in the section "PHOTOGRAPHS" page 269

P-1: Various compression test jigs; same scale.

P-2: British Aerospace compression jig.

P-3: Compression jigs with specimens mounted; disassembled; not same scale.

P-4: Micrographs of compressive failure modes of CFRP; (a) in-phase buckling of fibres forming a band including several wave lengths of buckled fibres; (b) and (c) kink bands.

P-5: Typical compressive failure of a CFRP test piece using the modified ASTM D695 method; (a) gauge section failure; (b) end failure.

P-6: Micrograph of the tab tip region; specimen through-thickness loaded by a clamping device.

P-7: Micrograph of compressive failure initiated at tab tip.

P-8: ICSTM compression rig; disassembled.

P-9: ICSTM compression rig mounted in universal testing machine.

P-10: Buckling of a CFRP test piece with 50 mm (a)-(e) and 10 mm (f) gauge length using the ICSTM method; (a) initial state; (b) onset of buckling; (c) buckled shape, increased deflection; (d) shape just before failure; (e) fractured test piece; (f) 10 mm test piece just before failure.

P-11: Macroscopic failure modes of compression test pieces; details in Chapter 5.

P-12: Scanning electron micrograph of the compression fracture surface of a XAS/914C test piece.

P-13: Scanning electron micrograph showing the compression fracture surface of an APC-2 test piece; note the bent but unfractured fibres (right); buckled fibres fractured at vicinity of highest curvature form a kink band (left).

P-14: Scanning electron micrograph of a kink band surface in APC-2 (AS4/PEEK) showing ends of fibres failed in flexure.

P-15: Scanning electron micrograph at higher magnification of centre fibre end in Figure P-14 (x10000) showing details of flexural fibre failure.

P-16: Scanning electron micrograph of a compression fracture surface in APC-2 (AS4/PEEK) showing bundles of buckled fibres.

P-17: Fractured ASTM D790M-84 four-point bend test pieces; (a) compressive failure above rollers using a standard jig; (b) tensile failure above rollers using rollers with plastic sleeves.

P-18: Compression failure of non-standard specimens using the ICSTM method; (a) thick woven cross-ply GRP; (b) woven cross-ply CFRP; (c) multidirectional CFRP; width of test piece 10 mm in all cases.

P-19: Scanning electron micrograph of the compression fracture surface in the 0°-ply of multidirectional XAS/914C; lay-up: $[(+45/-45/0/90)_3]_s$; 45°-plies removed.

P-20: Micrographs taken from polished samples of unidirectional CFRP intersected at an angle of approximately 5°. (a) APC-2 (AS4/PEEK); (b) Apollo 43-750/9106C 0% fibre surface treatment.

P-21: Sample of unidirectional XAS/914C polished parallel to the fibres.

LIST OF TABLES

Tables contained within the text

Chapter 1 none

Chapter 2

2.1.2-1: Static compression test methods for composites and specimen modifications described in the literature; circular symbols indicate a comparison of methods.

Chapter 3 none

Chapter 4

4.1-1: Results for the compressive strength of HYE/1682AW using different test methods.

4.1-2: Results for the compressive axial modulus of elasticity of HYE/1682AW using different test methods.

Chapter 5

5-1: Factors influencing the results of compression tests.

5.2.1-1: Influence of some parameters on longitudinal stress concentrations factors; results of a finite element study (Kukula, 1989).

5.2.2-1: Test piece dimensions of slenderness ratio parameter study.

Chapter 6

6.1.1-1: Test results for the compressive strength of XAS/914C using different test methods.

6.1.2-1: Test results for the compressive strength of XAS/914C using ICSTM test method with improved specimens.

6.1.2-2: Ultimate compressive stresses calculated from maximum strains using the extrapolated compressive stress-strain curve.

6.1.3-1: Fibre volume fraction of Apollo 43-750/9106C as measured in different laboratories.

Chapter 7

7.2-1: Flexural test results of unidirectional XAS/914C.

7.2-2: Ultimate surface stresses at specimen centre in four-point bending tests.

7.3-1: Summary of ILSS results using the CRAG short beam shear test method; test speed 1.5 mm/min; each sample included five test pieces.

7.4-1: Mechanical properties from in-plane shear tests.

7.4-2: Coefficients of representative shear stress-strain curve fits.

Chapter 8

8.3-1: Results of statistical analysis of fibre angle distributions.

Chapter 9 none

Chapter 10 none

Chapter 11

11.2.2-1: Prediction of the compressive strength of the composites examined.

Chapter 12 none

Tables contained in the section "TABLES" page 282

T-1: Test results for the compressive strength of XAS/914C; gauge length 5 mm.

T-2: Test results for the compressive strength of XAS/914C; gauge length 7.5 mm.

T-3: Test results for the compressive strength of XAS/914C; gauge length 10 mm.

T-4: Test results for the compressive strength of XAS/914C; gauge length 12.5 mm.

T-5: Test results for the compressive strength of XAS/914C; gauge length 15 mm.

T-6: Test results for the compressive strength of XAS/914C; gauge length 20 mm.

T-7: Test results for the compressive strength of XAS/914C; gauge length 30 mm.

T-8: Test results for the compressive strength of XAS/914C; gauge length 50 mm.

T-9: Test results for the compressive strength of XAS/914C; 8-ply laminate.

T-10: Test results for the compressive strength of XAS/914C; 12-ply laminate.

T-11: Compressive strength of XAS/914C; specimen machined from 32-ply laminate.

T-12: Compressive strength of XAS/914C; specimen machined from 32-ply laminate; additional machining of the tab surfaces.

T-13: Influence of initial tab tip debonding on the compressive strength of XAS/914C.

T-14: Influence of surface finish on the compressive strength of XAS/914C.

T-15: Influence of layer alignment on the compressive strength of XAS/914C.

T-16: Influence of laminate alignment on the compressive strength of XAS/914C.

T-17: Influence of initial tab tip debonding on the compressive strength of XAS/914C; debond by inserting 5 mm PTFE tape.

T-18: Influence of initial tab tip debonding on the compressive strength of XAS/914C; debond by inserting 5 mm adhesive cellulose tape.

T-19: Test results for the compressive strength of APC-2/AS4; machined specimen.

T-20: Test results for the compressive strength of APC-2/AS4; improved specimen.

T-21: Test results for the compressive strength of Apollo 43-750/9106C with different levels of fibre surface treatment; ICSTM method with standard specimen.

T-22: Test results for the compressive strength of Apollo 43-750/9106C with different levels of fibre surface treatment; Birmingham method.

T-23: Test results for the compressive strength of ICI 'Plytron' with different levels of fibre volume fraction.

T-24: Test results for the compressive strength of woven cross-ply CFRP.

T-25: Test results for the compressive strength of woven cross-ply CFRP; Aluminium end tabs; specimens manufactured at Liverpool University.

T-26: Test results for the compressive strength of quasi-isotropic XAS/914C; lay-up L1.

T-27: Test results for the tensile strength of XAS/914C.

T-28: Influence of clamping bolt torque on the measured compressive strength of XAS/914C.

T-29: Test results for the compressive strength of XAS/914C; specimens produced at Birmingham University.

T-30: Summary of parameter study compressive strength of XAS/914C using the ICSTM method.

CHAPTER 1 INTRODUCTION

Light weight design is dominated by four criteria: strength, stiffness, stability and cost of a structure of given weight. A merit function including these factors often demonstrates the superiority of reinforced plastics over metals. The balance is still on the metals side if it comes to high temperature environment and damage tolerance. However, ceramic and metal matrix composites look promising in this respect.

Apart from a few applications such as wires, light-weight structures and substructures always include compression members, elements either under pure compression or under combined flexural and compression load. One of the principles of light weight design is to split loads into pure compression and pure tension in order to avoid relatively ineffective flexural action of full cross-sections. Flexural loading of frameworks or sandwiches, for example, is transformed into (almost) pure compression and tension loading of struts or face sheets, respectively. Composites are particularly suitable for such design due to their high orthotropy. Axial stiffness of compression members can, for a given material, only be controlled by the cross-sectional area, i.e. it is proportional to the weight. The bending stiffness of axially compressed struts or panels, which is of particular importance since buckling in service has to be avoided, can be designed by geometry, e.g. by using tubes rather than rods, or sandwiches rather than plain plates. Restrictions are given only by requirements such as aerodynamics or minimum wall thickness in order to avoid local buckling. Stresses in a member of given geometry, however, can only be lowered, thus increasing the strength, by increasing the cross-section under load. Therefore, both high specific strength and stiffness in tension as well as in compression are desirable for an ideal light-weight construction material.

Composites are particularly valued for their high tensile strength. The comparatively low compressive strength of some composites, e.g. plastics reinforced with organic fibres, e.g. aramid fibres, drastically limits their potential for application. The intrinsic low compressive strength of fibrous materials has long been recognised for wood, the first composite used to a large extent in aeronautical structures.

Brittle materials usually exhibit higher compressive than tensile strength due to different failure mechanisms. Tensile failure is controlled by flaws in the material on a micro-level. Stress concentrations around the discontinuity lead to the development of a crack and once a critical length is reached the material fails catastrophically. That is why brittle materials show a strong size effect: the smaller the typical dimension the smaller the likelihood of a flaw of critical size. The best example is glass where a fibre of a few microns diameter is several orders of magnitude stronger than the bulk material.

Compression failure of brittle materials is determined by the shear strength and failure occurs in planes of maximum shear.

Ductile metals take a mean position. In both tension and compression, failure is dictated by similar mechanisms, i.e. gliding of crystalline planes, hence compressive and tensile strengths are similar. Figure 1-1 shows the ratio of compressive and tensile strengths of some typical materials.

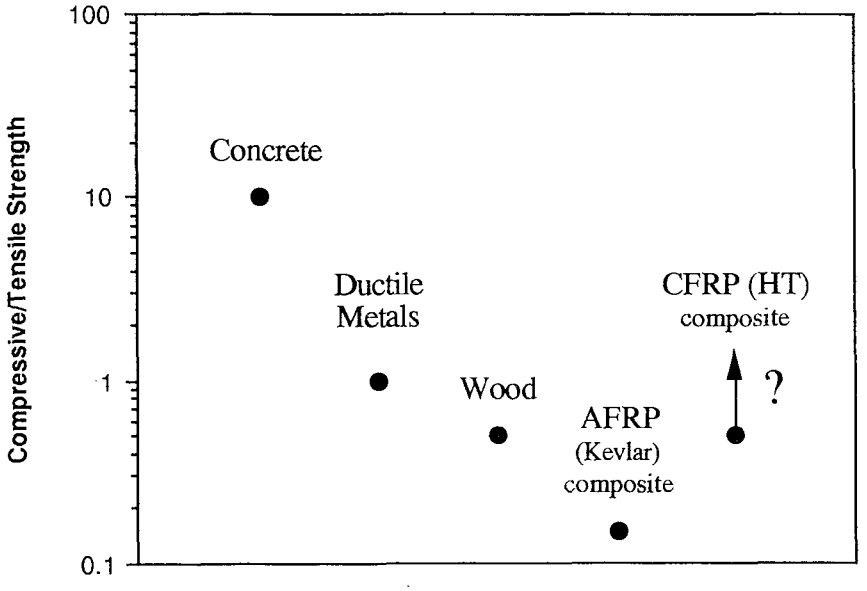


Figure 1-1: *Ratio of tensile and compressive strength of different materials.*

Ideally, fibrous composites would fail by fibre compressive failure using the whole potential of the reinforcing material. Fibre loop tests show, for instance, that high-modulus, highly anisotropic, carbon fibres and organic fibres are relatively weak in compression compared to intermediate modulus carbon fibres or glass fibres. The ratio of tensile and compressive strength is low for the highly anisotropic fibres, and the compressive strength of glass fibres is probably higher than the tensile strength. However, experimental evidence shows that the failure of composites containing fibres of high compressive strength is by buckling of the fibres rather than by fibre compression failure.

The first models developed in the 1960's to predict microbuckling failure of composites treating fibres as plates on an elastic foundation overpredicted the critical stress by a large margin. To-date nonlinear models have been developed which fit the experimental data, assuming certain reasonable boundary conditions and input data, but a

universal model to predict compressive failure from the properties of the constituents is still not available. In other words, there is still uncertainty about the mechanism triggering compressive failure. The situation is complicated by the problems in determining from experiment the compressive strength of a given composite system. The following study illustrates the difficulties encountered when defining the compressive strength of composites.

A European 'round robin' on compression testing of CFRP was conducted recently.* Seven laboratories participated in testing seven different unidirectional materials using their own testing procedures. Each laboratory manufactured one particular batch of material so that the influence of composite production was eliminated. Figure 1-2 shows the results sorted into categories of materials. Using this chart as a data base, literally any compressive strength within the measured range could be assigned to any of the materials examined. The range of results encloses a factor of two for almost all systems.

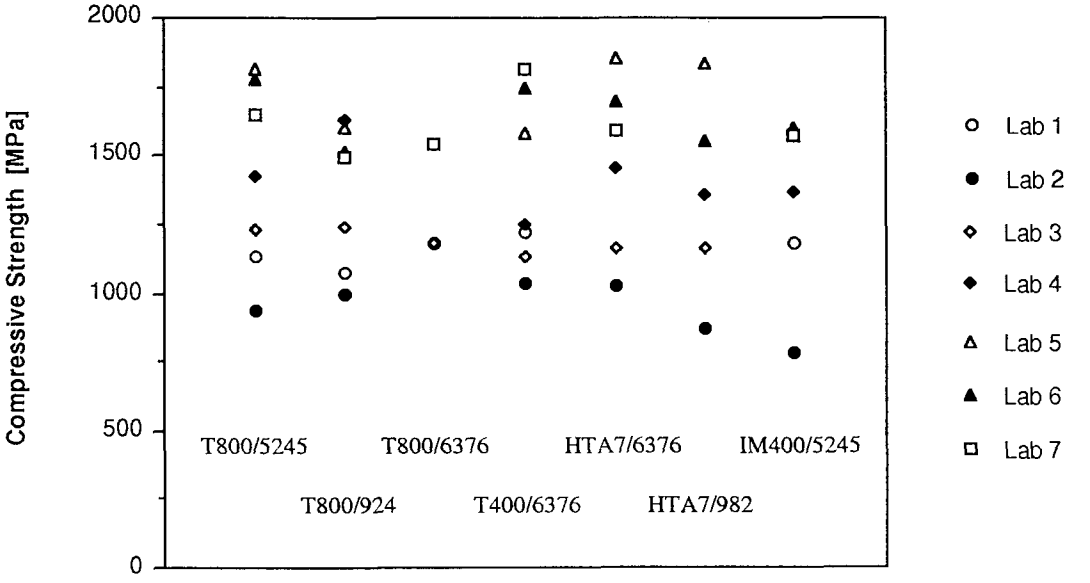


Figure 1-2: Test results of a European round robin in compression testing of CFRP sorted into categories of materials.

The following Figure 1-3 shows the results sorted into categories of the participating laboratories. A definite trend is now apparent: the test results are highly dependent on the laboratory which carried out the test. Some laboratories seemed to have generated generally higher results than others throughout the range of materials tested. And, *nota bene*, all laboratories were experienced in compression testing of composites and used standard test methods. Test results are obviously to a large extent dependent on the

* PRIVATE COMMUNICATION WITH DR P. CURTIS (RAE)

individual testing practice, which can be suspected to include parameters such as test method, testing experience and methods of specimen preparation.

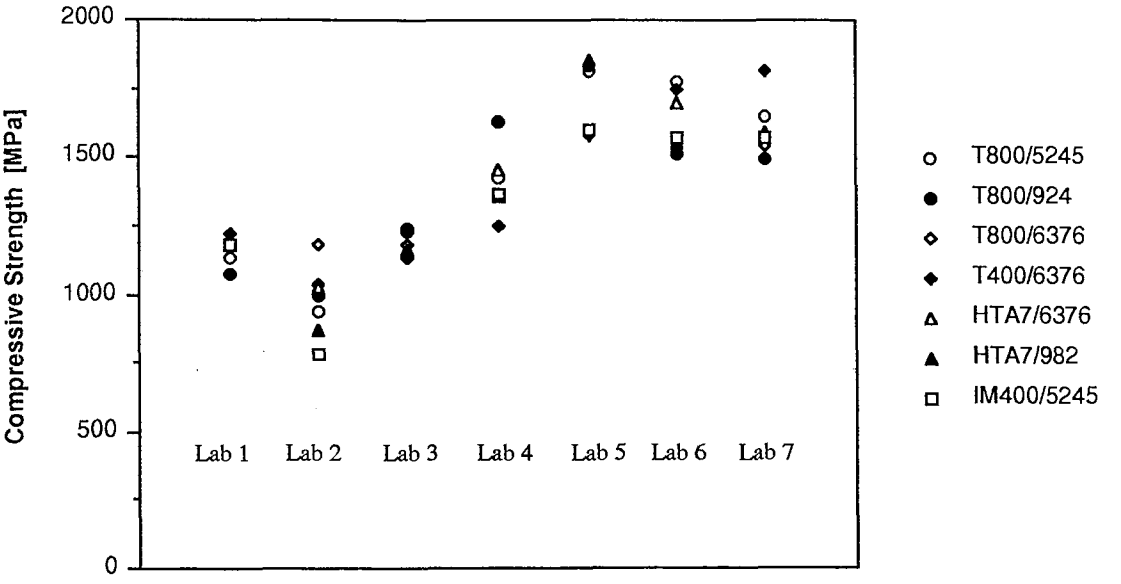


Figure 1-3: Test results of a European round robin in compression testing of CFRP sorted into categories of participating laboratories.

The comparison not only shows how desirable a standardisation of test procedures would be - currently, projects like FACETS endeavour to achieve this on a European scale - but also how difficult it is to assess factors affecting the compressive strength of a composite.

In the present investigation the approach is taken of clarifying the question of measuring the compressive strength rather than developing complex analytical models of compressive failure, the verification of which is questionable at present. Nevertheless, it will be attempted to qualify a simple model which allows the prediction of compressive properties from easy to determine other mechanical properties.

A major consideration in this context is, of course, the transfer of results gained using laboratory specimens under laboratory conditions to real structures. It is common knowledge that data generated this way are not necessarily useful design data. However, it is the intention of this project, by isolating the factors affecting the compressive strength of simple coupon specimens under simple stress conditions, to identify the basic compressive failure mechanisms. Knowledge of these will allow a more complex analysis including multidirectional stress fields, environmental and fatigue effects leading to realistic design allowables for a composite.

CHAPTER 2 LITERATURE REVIEW

During the past few years extensive research on compressive performance of composites, particularly CFRP, has taken place in laboratories all over the world. Hardly any other issue of composite testing has been subject to so much controversy as compression testing. Although recently there seems to be more consensus on modelling compressive failure, contradictory test results are still commonly observed. The review of the published literature concentrates on topics such as compression test methods, compressive failure modes of composites and theories predicting compressive strength of CFRP. Since much parallel research has been going on since the current project started, some coincident findings are unavoidable.

2.1 Compression Testing of Composites

Before comparing test methods some fundamental aspects of compression testing will be reviewed and the most widespread test methods will be described.

2.1.1 Principles

Generating a uniform one-dimensional stress state is the main objective of a compression test fixture. The need to prevent overall buckling of the compressed specimen complicates the situation. Usually, coupon specimens, cut from panels with a typical thickness of 1 to 2 mm, are used for testing rather than rods. Therefore, the gauge length of these relatively thin specimens has to be short, or they must be supported by an anti-buckling device. Short specimens with a typical gauge length from 5 to 12.5 mm are preferred for testing unidirectional material. Long gauge length, side-supported, specimens are used for testing multidirectional laminates, so that angle ply fibres are not constrained by the grips.

Stress concentrations due to load introduction increase with the degree of orthotropy of the material tested. Thus, stress concentrations present the most serious problems for unidirectional lay-ups and may cause premature failure of the specimen. This problem will be discussed later.

There are three basic methods of introducing a compressive load into the specimen: direct loading of the specimen end; loading the specimen by shear; and mixed direct and shear loading.

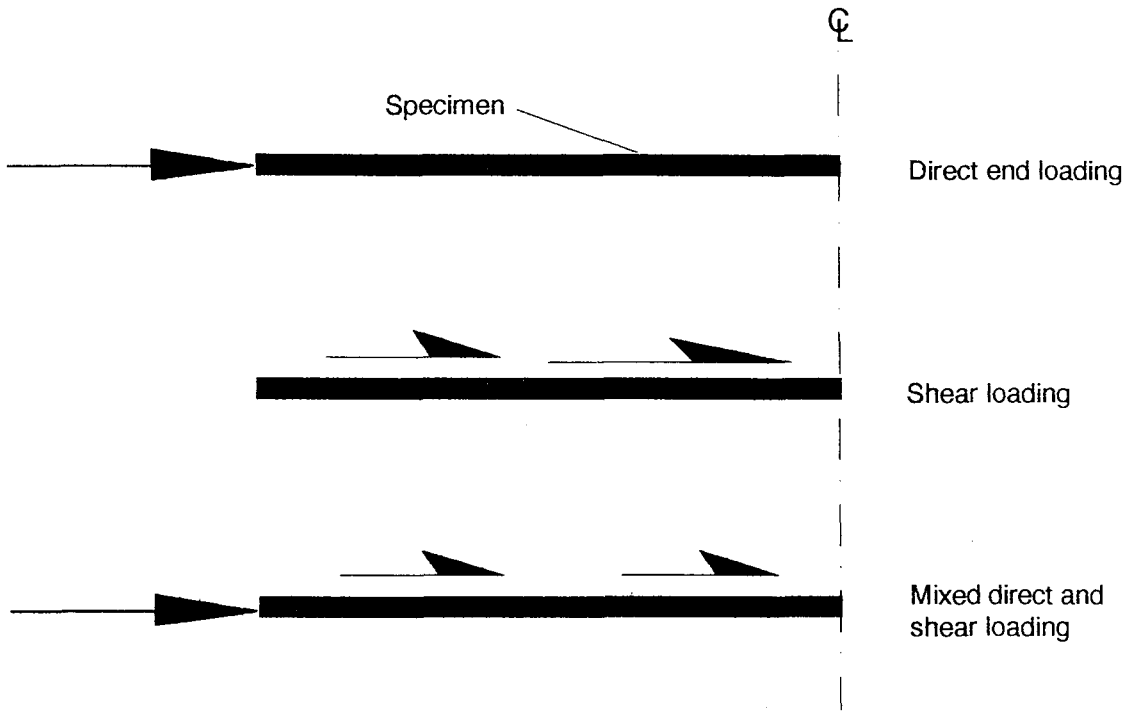


Figure 2.1.1-1: Different methods of load introduction into a compressive specimen.

Another possible way to classify compression test methods is by the type of specimen used. Generally, three types can be distinguished:

1. The short coupon specimen which is usually tabbed and used for unidirectional laminates as mentioned above. Load introduction is either by shear ('indirect') or by loading of the end ('direct') which results in a mixed shear/end-loading of the laminate.

2. The long test piece. This test piece is either tabbed or untabbed and used preferably for multidirectional laminates. Under compression a lateral support has to prevent buckling of the specimen (e.g. CRAG).

3. The sandwich specimen. Different core materials have been used for this type of specimen. The sandwich is either tested as a beam, i.e. in four-point bending (ASTM), or in a direct compression test (e.g. Crasto and Kim, 1990).

Figure 2.1.1-2 shows the three fundamental specimen types schematically.

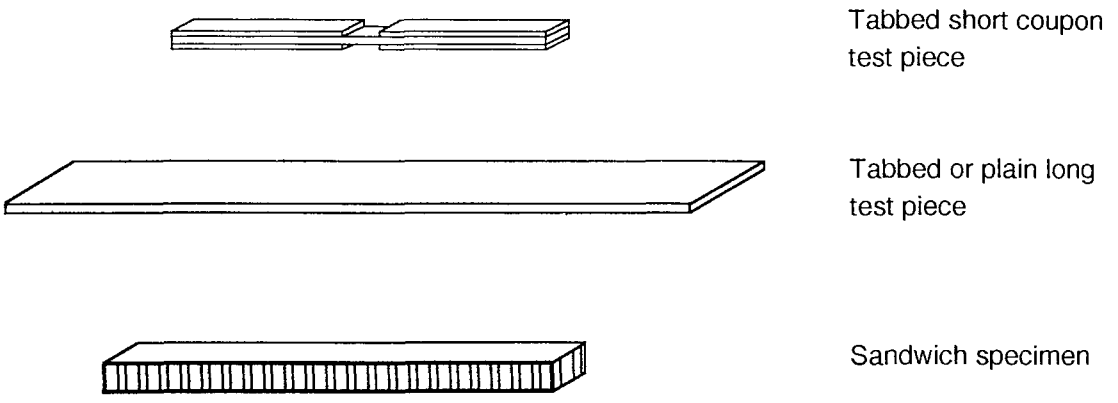


Figure 2.1.1-2: Different compression test piece types.

Clearly, there exists a variety of less widespread special purpose compression test pieces. Examples of these are the tubular specimen proposed by Swanson et al. (1988) or the ring specimen used by Kim and Tsai (1988).

2.1.2 Compression Test Methods

A vast variety of test methods and modifications of test pieces has been proposed during the past two decades as illustrated by Table 2.1.2-1. In this section the principal test methods will be described.

Direct loading of the specimen end as specified for instance in ASTM D695 'Test Methods for Rigid Plastics'. A dog-bone shaped specimen is machined from the material sheet; it is not suitable for high strength composites. Because of the low transverse strength and the low interlaminar strength of these materials the specimens fail by end crushing, sometimes referred to as 'brooming', and/or longitudinal splitting.

Shear loading of the specimen end, which is usually tabbed in the same manner as for a tension specimen, is the most common method. Shape, material and precision of the end tabs are likely to influence the failure mode and strength result. One of the first fixtures using this principle is the Celanese fixture, developed at the Celanese Research Center and later adapted as ASTM D3410 standard. The specimen is held in conical wedge grips which are accommodated in tapered sleeves. An outer cylinder maintains alignment of the parts. When the load is applied to the sleeves, it will be transmitted to the specimen by shear through friction between the specimen and the grips. This fixture needs careful adjustment to the specimen's thickness, otherwise non-uniform load distribution on the cones will lead to distortion of the sleeves and friction with the outer cylinder. The problems encountered with this method will be discussed in detail in Chapter 6.

Type of specimen	Method/specimen/ fixture	**Reference** (see legend below)																						
		1	2	3	4	5	6	7	8	9	10	11	12	13	14	15	16	17	18	19	20	21	22	23	24
Side supported specimen	ASTM D695						O			O															
	BS 2782																								
	Cambridge fixture															•									
	CRAG (multidirectional)													•											
	Northrop ETL method				O																				
	Face supported fixture		O																				O		
	Lockheed fixture	O																							
	Wyoming end-loaded fixture																	O							
Short coupon specimen	Modified ASTM D695			O						O	O		O						O					O	
	RAE method			O					O																
	Various end-loaded coupon fixtures		O									O								•					
	Birmingham method								O																
	Celanese method			O	O		O	O		O		O							O				O		
	Modified Celanese specimen			O																					
	Wyoming modified Celanese																	O							
	DIN 29971 (modified Celanese)										O														
	CRAG (unidirectional)													•											
	Modified CRAG specimen (tabs)															O									
	Modified CRAG specimen (waisted)															O									
	IITRI method		O			O	O	O										O	O		O		O	O	O
	Hercules mod. IITRI												O												
Sand-wich	(Honeycomb) SWB						O						O												
	Reusable SWB					O																			
	Mini-SWB																					•			
	IITRI Mini-sandwich																				O				O
Others	Ring specimen														•										
	Tubular specimen																•								

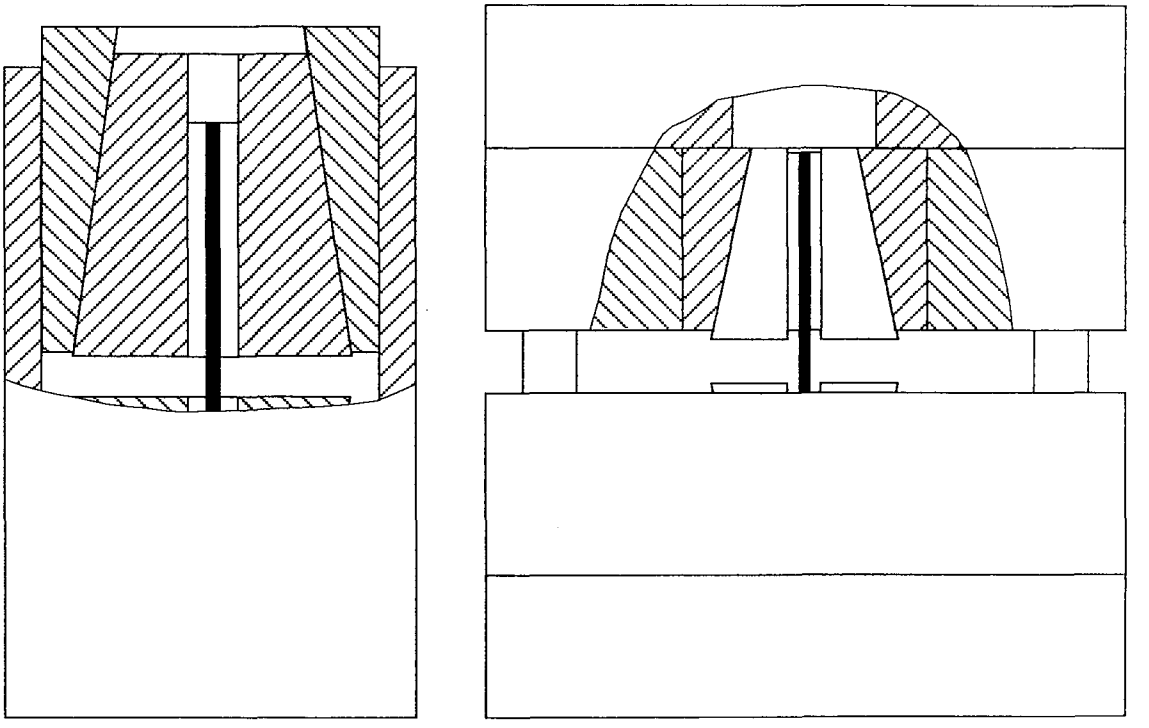
1 Ryder/Black, 1977
2 Clark/Lissagor, 1981
3 Woolstencroft et. al., 1981
4 Grimes, 1981
5 Gruber et al., 1982
6 Adsit, 1983
7 Lamothe/Nunes, 1983
8 Barker/Balasundaram, 1987
9 Gedney et al., 1987
10 Henrat, 1987
11 Lee, 1987
12 Westberg/Abdallah, 1987
13 Curtis, 1988
14 Kim/Tsai, 1988
15 Soutis/Fleck, 1988
16 Swanson et. al., 1988
17 Berg/Adams, 1989
18 Leeser/Leach, 1989
19 Poon, 1989
20 Crasto/Kim, 1990
21 Mrse/Pigott, 1990
22 Pinnell et. al., 1990
23 Adams/Lewis, 1991
24 Whitney/Guihard, 1991

Table 2.1.2-1: *Static compression test methods for composites and specimen modifications described in the literature; circular symbols indicate a comparison of methods.*

The German standard DIN 59273 and CRAG (Curtis, 1988) specify slightly modified versions of the Celanese fixture and specimens. Many internal company test standards were found to be based on the Celanese principle with various specimen types.

A fundamental modification of the Celanese fixture was developed by the Illinois Institute of Technology Research Institute (IITRI) (Hofer and Rao, 1977). Here, tapered wedge grips, which fit into matching pockets in massive steel blocks, are used rather than conical ones, so that specimens of different thicknesses can be easily accommodated. The steel blocks are aligned by pillar guides and linear ball bearings. The weight of the fixture - the one used in the present investigation weighs about 250 N - reduces the ease of use significantly.

Both the IITRI and the CRAG fixtures are shown schematically in Figure 2.1.2-1 and Figures P-1 and P-3 show the rigs in comparison to other rigs and disassembled, respectively.



CRAG (Celanese) IITRI

Figure 2.1.2-1: The CRAG and IITRI compression fixtures, shown schematically.

The Wyoming University modified Celanese fixture (Westberg and Abdallah, 1987) uses wedge grips similar to the IITRI fixture thus evading the problem of having to adjust the grips to the specimen thickness.

The fixture used by British Aerospace is a further variation of wedge action type fixtures.It combines features of the Celanese as well as of the IITRI fixture and can be regarded as a synthesis of these fixtures. The IITRI type wedge grips are accommodated in Celanese type circular tapered sleeves. The outer cylinder which aligns the sleeves is an open frame rather than a closed shell allowing access to the specimen. Quick release retaining pins additionally ease handling of the rig. The BAe jig is shown in Figure P-2 with a specimen mounted.

Note that in all of the above fixtures the gripped portion of the specimen is loaded transversely (through-thickness) in order to generate the shear load.

A typical representative fixture for mixed shear and end-loading is the configuration proposed by Purslow and Collings (1972) and modified by Port at the Royal Aircraft Establishment (RAE) (Port, 1982). The specimen, which is waisted to force failure in the centre of the gauge length, is bonded into slots in aluminium end blocks. The amount of shear loading depends on the properties of the adhesive as well as on the thickness of the bond layer. Great care is needed in specimen preparation.

A modified ASTM D695 specimen as specified, for instance, in the SACMA recommendations (1989), is loaded in a similar way. The end-tabbed and overall-supported specimen with a gauge length of 5 mm is purely end-loaded. A certain amount of the load is introduced to the specimen by shear through the end tabs, depending on the stiffness of the tabs and bond layer. An additional device for overall alignment of the test piece is recommended. Although the specimen needs careful preparation, parallelism of the specimen ends is particularly important, the test jig is of remarkable simplicity thus cheap and and very easy to handle. Due to the transverse constraint of Poisson's deformation the specimen may experience some transverse loading which in turn leads to friction between the support faces and the specimen.

A variation of the RAE method is the method developed at Birmingham University by Barker and Balasundaram (1987). Here, an RAE-type specimen with a waisted gauge section is clamped within steel cubes at the end rather than being bonded into aluminium blocks. Thus, the specimen end is loaded directly and a portion of the load is transmitted by shear. By adjusting of the torque on the clamping bolts the amount of shear can be varied. Mounting of the specimen is very simple. Frictional effects are minimised by using a die set, as discussed in Chapter 9, but the clamping causes through-thickness loading of the test piece.

Figure 2.1.2-2 shows schematically the three representative methods for mixed shear/end-loading.

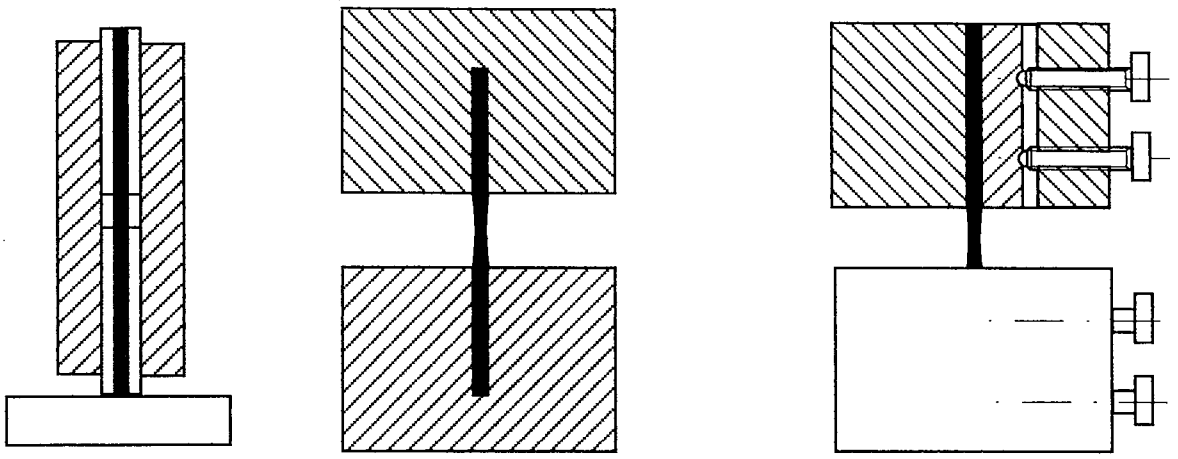


Figure 2.1.2-2: Modified ASTM D695, RAE and Birmingham compression test methods, shown schematically.

Waisting the specimen, which in fact is an optimised form of tabbing, has to be carried out carefully in order to maintain a symmetric specimen, otherwise one would be likely to introduce bending and cause premature failure. Port (1982) showed that interfacial splitting due to excessive shear stresses can be avoided when the specimen is waisted following the taper contour equation, which gives the minimum gauge length as:

$$g_{min} = t \ln\left(\frac{t}{t_{min}}\right)\frac{S_c}{S_{is}} \qquad (2.1.2\text{-}1)$$

where t is the nominal (unwaisted) specimen thickness, t_{min} the minimum (waisted) specimen thickness, S_c the compressive strength and S_{is} the interlaminar shear strength of the material.

Stress concentrations at the ends of the end tabs of unwaisted specimens initiate failure at local stress levels which can be significantly higher than the measured overall stress level. Therefore, strength results obtained with unwaisted specimens are to be regarded as a lower bound for the compressive strength. It is, on the other hand, unclear how damage caused to the surface fibres when the specimen's waist is machined influences compressive failure initiation.

Long gauge length specimens, i.e. multidirectional laminates, are either end-tabbed and shear-loaded or, as for instance recommended in CRAG (Curtis, 1988), end-loaded with end fittings to prevent brooming.

Sandwich specimens are usually designed rather as sandwich beams than sandwich columns, and are loaded in four-point bending. The composite top (compressed) cover sheet is the specimen to be tested. A metal honeycomb core, variations to be discussed later, and a bottom cover sheet with greater stiffness and strength ensure that the specimen fails on the compression side. In this way very thin specimens can be tested.

The high costs of this type of specimen led to the development of a reusable sandwich beam by Gruber et al. (1982). Here, the core in the test section is made of plexiglas and a CFRP sheet used as tension face. On the compression side the specimen, rather than being bonded, is clamped between two aluminium end caps. The drawback as with most sandwich specimens is that stresses cannot be measured directly.

2.1.3 Comparison of Test Methods

In this section comparative studies on test methods, fixtures and specimen modifications described in the literature are reviewed. Since most standards leave a wide choice of test piece parameters, a parametric study of the test piece is implicitly included in these investigations. In Table 2.1.2-1 the test methods described in the literature are listed and it is indicated which publications compare various methods.

Ryder and Black (1977) presented a test method for a large gauge length specimen. The specimen was tabbed only on one end and the gauge section of approximately 130 mm length was supported by an anti-buckling device similar to the one specified in ASTM D695. The tabbed end was gripped in the testing machine and the other end, untabbed and machined square, was butted flat on bearing plate. Alternatively, they suggested, both ends could be tabbed and gripped. The test method was found to work satisfactorily for two multidirectional laminates of T300/934 with 25% and 67% 0°-layer content, respectively. Failure in all cases occurred in the gauge section.

Only a few references can be found comparing test methods using long supported and short unsupported test pieces, as in the work done by Clark and Lisagor (1981). They investigated the influence of test method, specimen width and thickness and lay-up on the compressive strength of T300/5208. The test fixtures used were the IITRI, modified to allow testing of wider specimens, and a face-supported fixture. An end-loaded coupon fixture was used to obtain comparative data for quasi-isotropic specimens.

The IITRI method was found to provide the most consistent results for unidirectional and quasi-isotropic lay-ups, where failure is governed by the 0° plies. However, the results for the quasi-isotropic lay-up were comparable for all three methods. The face-supported fixture yielded the most consistent results for $[\pm 45°]_s$

laminates. Not surprisingly, strong influence of specimen width was found for $[\pm 45°]_s$ when tested in the IITRI rig due to constraint of the layers. The difference in the ultimate stress was greatest for unidirectional specimens, the IITRI method giving about 25% higher results than the face-supported fixture. Test results were little influenced by specimen width but by specimen thickness for all methods. The 8-ply test pieces showed signs of overall instability in all cases. The modulus of elasticity values were found to be only insignificantly different for the three fixtures examined.

Grimes (1981) described the influence of environmental conditions on the static compression and compression-compression fatigue properties of AS/3506-1. The test methods employed for static compression were the Celanese method for unidirectional laminates and the Northrop ETL method, which uses an untabbed rectangular specimen two inches wide and three inches long, for multidirectional and $[90°]_n$ laminates.

Lamothe and Nunes (1983) investigated the influence of fixture design on the compressive properties of glass, Kevlar and carbon/epoxy systems, as well as on FP alumina/aluminium and FP alumina/magnesium composites. Both methods employed, the IITRI and the Celanese, gave similar results for the tangent modulus. The IITRI method, however, was found to yield higher strength results and less scatter in data for the epoxy composites. The authors found both methods unsuitable for testing of metal matrix composites because of premature adhesive shear failure.

The properties of the core of a sandwich beam can influence the failure mode of the beam as stated by Shuart (1981). If the core takes a certain amount of the bending load, which is the case with the plexiglass core of the reusable sandwich beam, the neutral axis of the beam must be known before the load on the specimen can be determined. This is not simple when the elastic behaviour of the cover sheets is not linear, the neutral axis position being dependent on the strain state. It should also be noted that transverse stresses are built up when the curved specimen is compressively loaded. These stresses are presumed to inhibit certain compressive failure modes, particularly for multidirectional lay-ups. That tendency could be observed in compression/tension fatigue tests of a reusable sandwich specimen (Argyris et al., 1988).

Adsit (1983) stated, regarding results of a testing round robin including a (honeycomb) sandwich beam, that Celanese and IITRI methods give comparable results. The IITRI method, however, appeared to be easier to use and more flexible to varying specimen thickness.

Reducing the gauge length of the Celanese specimen down to a length of 6 mm leads to increasing compressive strength results as shown by Lee (1987). Results achieved with specimens of different gauge length should therefore be handled with care.

This is confirmed by the investigations of Woolstencroft et al. (1981) on the CFRP system XAS/914C. They compared a range of test methods including the standard Celanese method; a modified version using a waisted specimen with a gauge length of only 4 mm; the RAE method; and the modified ASTM D695 method. They found that the modified Celanese specimen yielded strength results some 50% higher than the standard version. A (linear) finite element analysis, however, revealed a poor distribution of longitudinal stress and noticeable transverse stresses in the centre of the gauge length from which they concluded that the specimen was not measuring a true compressive strength. According to the finite element analysis the ASTM specimen had a reasonable stress distribution, second only to the RAE specimen which offered the most uniform distribution with negligible transverse stresses. A design value, calculated as the mean minus three times the standard deviation of the strength results of the test, was used to assess the methods. The standard Celanese, giving a low mean value and high scatter, as well as the ASTM D695, with a reasonable mean but high scatter of results, were rejected as test methods. Because of the relatively high mean of the RAE method combined with a remarkably low scatter of results, they finally recommended that method as the most suitable to characterise compressive properties of CFRP.

Port (1982), however, demonstrated that this specimen exhibited macroinstability and therefore measured a buckling strength. This could explain why the scatter of test results achieved with the RAE method was so low. Port consequently proposed a new standard specimen with reduced slenderness ratio. He also reported similar strength results for the new RAE specimen and the modified Celanese specimen when the slenderness ratio of the latter is increased to the same order as that of the RAE specimen.

The fixture proposed by Barker and Balasundaram (1987) employed the new RAE standard specimen with the attractive feature that the specimen was not bonded, but clamped. Barker reported similar results gained with both methods and stressed the merits of an untabbed unbonded specimen when testing under various environmental conditions.

Gedney et al. (1987) examined carbon/epoxy fabrics using the ASTM D695, a Union Carbide modified D695 with tabbed specimen, and the Celanese method. The authors found that Celanese and modified ASTM methods yielded comparable results, the Celanese method strength results being slightly lower but exhibiting significantly less scatter.

Henrat (1987) compared the DIN 29971 compression test method and ASTM D695 with modified specimen of 2 mm thickness. Several unidirectional intermediate-modulus carbon fibre reinforced plastics were used in the study. The author found that the

modified ASTM D695 method gave consistently about 15 to 20% lower values than the modified Celanese method. The reason for the lower values could be attributed to end crushing of the ASTM specimens. End crushing failures can most probably be avoided when a specimen thickness of 1 mm, as suggested by SACMA, is adopted. Scatter of strength results, as well as the modulus of elasticity, were found to be independent of the test method.

Westberg and Abdallah (1987) carried out an extensive experimental and analytical study examining three test methods: Hercules-modified IITRI, the modified ASTM D695, and a sandwich beam with aluminium honeycomb core and titanium backsheet loaded in four-point flexure. The material used in their investigations was Hercules AS4/3501-6.

A finite element analysis investigated the influence of the following parameters on the stresses at the tab tip of the two coupon specimens:

nominal specimen thickness;
taper angle of the end tab (10° and 90°);
tab material (0° CFRP, 0/90° GRP, aluminium);
nut torque (modified ASTM D695).

In addition to the above-mentioned parameters, the test programme included factors such as:

unsupported length (distance between tabs);
specimen width (modified IITRI);
type of tabbing adhesive.

The finite element analysis showed, as expected, that the lower the longitudinal stiffness of the tab, the lower the longitudinal stress peaks on the specimen surface. The stress concentration factor for the longitudinal stress was found to be similar for both methods when the specimen configuration was the same, whereas transverse stresses were about twice as high for the IITRI specimen. The specimen thickness was found to have a significant influence on the peak stresses, indicating a more uniform stress distribution through the thickness for smaller thicknesses. Tapered end tabs, obviously, yielded lower surface stresses than end tabs with square ends.

Not all the findings of the finite element analysis were reflected in the test results. This might have been due to the fact that nonlinear effects like specimen buckling and material behaviour were not considered adequately in the calculations. Tapering of the end tabs, for instance, might reduce stress concentrations but at the same time the free length of the specimen is increased, which might outweigh the other effect.

Interestingly, the specimens for both methods seemed to have an 'optimum' gauge length of about 5 mm for which the ultimate compressive stress was maximum. Whilst

the predicted trend regarding the specimen thickness was confirmed for the ASTM specimen, for the IITRI specimen the opposite tendency was found. The greater the specimen thickness, the higher was the measured compressive strength of the specimen with the standard gauge length. Note that the slenderness ratios for the standard configurations as quoted in the paper are 16 and 28 for the modified ASTM specimen and the IITRI specimen, respectively. Reducing the slenderness ratio of the IITRI specimen by reducing the gauge length resulted in a strong increase in compressive strength.

The tabbing adhesive was found to have a significant influence on the test results gained with the modified ASTM D695 method. The higher the strength of the adhesive, the higher was the compressive strength of the specimen. This fact suggests that end tab debonding had played an important role regarding that test method. The tightness of the nuts of the ASTM side support influenced the result as well, but here friction, which is taking part of the applied load, cannot be separated reliably.

In flexure tests of sandwich specimens the face sheet bonding adhesive did not influence the failure stress as long as the backsheet bondline did not fail. Failure stresses dropped by 10% when the face sheet thickness was increased from 4 to 10 plies.

Westberg and Abdallah concluded that, depending on specimen configuration and test method, results could range from 120 to 300 ksi (830 to 2070 MPa). They stated that the three test methods in their optimum form each produce comparable results of around 300 ksi with comparable coefficients of variation. It is worth noting that these strength data are the highest published for this material.

Tan (1990) carried out a similar finite element analysis of the IITRI and Celanese method with findings in agreement to the investigation above. Test results using the Celanese method were very low compared to results gained with a face supported fixture, which was attributed to global instability of the Celanese specimen. The author therefore rejected the Celanese method as a meaningful method for measuring the compressive strength of unidirectional CFRP.

Following a comprehensive review on compression test methods Berg and Adams (1988 and 1989) compared experimentally the IITRI, the Wyoming-modified Celanese method and a Wyoming end-loaded specimen configuration. The materials used were CFRP (AS4/3501-6) and GFRP (S2/3501-6) in unidirectional and quasi-isotropic lay-up. The IITRI method again gave the highest strength and lowest scatter of results for unidirectional composites, a fact attributed to the superior rigidity and consequently better specimen alignment of the IITRI fixture compared to the Wyoming rig. The end-loaded fixture using an unwaisted untabbed specimen surprisingly gave similar strength results to the Wyoming fixture. Strength and modulus data for the quasi-isotropic laminates

were similar for all three methods. Comparing data gained with strain gauges and extensometers, it was concluded that both methods are equivalent, but strain gauges were recommended. Extensometers, though easier to mount, are likely to be damaged at specimen failure.

In a more general publication Adams (1989) compared state-of-the-art compression test methods for composites, concluding that the IITRI method is the current standard for comparison.

The CRAG modified Celanese method was examined by Soutis and Fleck (1988). Testing T800/924C carbon fibre-reinforced epoxy, they employed two modifications of the specimen recommended by CRAG: one with tapered rather than square tab ends and plain gauge section, and one with a waisted gauge section. The waisted specimen yielded about 10% higher compression strength than the plain specimen, which was about 70 % of the material tensile strength. The authors concluded that the CRAG modified Celanese is a method relatively easy to use and that the result gained with the waisted specimen is a true measure for the compressive strength. They also tested multidirectional laminates with and without holes. Failure strains of the unnotched specimens were found to be similar to the values of the unidirectional material. Therefore, they concluded that the failure mechanism in the axial plies was little affected by the off-axis plies. A single hole of 5 mm diameter in a 50 mm wide specimen was reported to reduce the compressive strength by 40%. Not surprisingly, further strength reduction was observed for a second hole, particularly when the edge distance of the holes was less than a hole diameter.

An end-loaded tubular specimen for testing unidirectional laminates was presented by Swanson, Colvin and Haslam (1988). In addition to the axial fibres, the tube must contain fibres in the hoop-direction. Lay-ups containing 12 axial and two or three hoop plies have been tested. The failure stresses for the unidirectional AS4/3501-6 seemed to be quite low and dependent on the content of hoop fibres (1053 MPa and 1538 MPa for the two and three hoop plies, respectively, when the stresses in the hoop plies were neglected).

Recently, two promising techniques have been introduced. Both methods use sandwich type specimens, characteristically with thin composite skins.

The first one is the 'compact sandwich beam method' proposed by Mrse and Piggot (1990 and 1991). Instead of a honeycomb core of the standard sandwich specimens they used an acrylic core of 4.35 mm thickness onto which three plies of unidirectional laminates were bonded. The laminate used in their investigation was AS4 fibre-reinforced PEEK made from four different prepregs. The samples were plasma treated

before bonding in order to ensure good adhesion. Failure occurred on the compression side in most cases; only the strongest laminate in this investigation presented problems when the acrylic core failed before the laminate. The results they gained for AS4/PEEK were considerably higher (between 1.52 and 1.85 GPa) than the data gained with conventional methods (around 1.1 GPa) for all prepregs examined. Therefore, they concluded that the 'compact sandwich beam method' should be adopted as a standard method for compression testing of composites. However, the authors regarded the core material and lever arm length which they had suggested initially as the drawbacks of the method at the time of publication.

The other part of their investigation examined the effect of fibre alignment on the compressive strength of the composite. Applying the method of Yurgartis (1987), they determined the in-plane and out-of-plane fibre angle distribution of the four laminates. They found, in general, a good correlation between the standard deviation of the fibre alignment and the compressive strength. Also, a linear correlation between the square of the angular deviation and the modulus was found.

The second method is a variation of the sandwich specimen and was proposed by Crasto and Kim (1990). The honeycomb core of the standard sandwich beam is here replaced by a slab of neat resin of the same type as the matrix of the composite to be tested, in order to avoid strain incompatibility. The composite prepreg, two or four plies, is placed on both sides of the core and the whole assembly is co-cured, thus eliminating the usual adhesive layer and accompanying procedure. The authors stated that this specimen is simple and inexpensive to fabricate, that it required a smaller volume of composite than an all-composite coupon and that it could be tested either in four-point flexure or in axial compression, using a specimen of standard dimensions in each case. Since stresses in the composite skins cannot be measured directly, they were calculated using the rule of mixtures for axial compression or engineering bending theory for flexural testing, respectively.

In an experimental programme the authors produced specimens to be tested in four-point bend flexure and the IITRI fixture. The composites used were (unidirectional) thermoset AS4/3501-6, thermoplastic AS4/PEEK (APC-2) and S-Glass/1035.

The test results of the axially compressed mini-sandwiches were substantially higher than the equivalent results of standard coupon tests for all systems examined. Most epoxy sandwich specimens failed in the gauge section and from microscopic evidence the authors suggest shearing of fibres, i.e. compression failure of the fibres, rather than a buckling mode as the triggering event of failure. APC-2 sandwich specimens partly failed in the gauge section and partly under the tabbed region. The glass sandwich

specimens failed at compressive strains of almost 4% and showed signs of fibre fracture, longitudinal splitting and delamination. Some of the AS4/3501-6 coupon specimens, and particularly the S-Glass/1035, were found to have failed in global buckling.

The AS4/3501-6 and S-Glass/1035 sandwich beams tested in four-point flexure presented problems because of core cracking yielding lower results than when tested in axial compression. For APC-2 both tests yielded similar results due to the higher toughness of the PEEK core.

Whitney and Guihard (1991) compared results from direct compression of the mini-sandwich beam and the standard IITRI specimen using two multidirectional and a unidirectional lay-up of AS4/3506-1. Whilst test results for the sandwich were obtained from a reference, the tests using a conventional test piece were carried out by the authors. Generally, they found the values obtained using the sandwich specimen higher than the equivalent values for the standard specimen, this fact being most pronounced for the unidirectional lay-up. However, it is remarkable that the mean value obtained for the 24-ply standard specimen is only 1128 MPA compared to values of 1600 to over 1700 MPa reported by Odom and Adams (1990) using the same test method. This underlines once more how much coupon test results are dependent on the experience of the tester and the particular specimen configuration. The value quoted for the mini-sandwich beam is 2086 MPa. It would be interesting to know how repeatable the sandwich results are under different laboratory conditions. Interestingly, Whitney and Guihard found bending or buckling type behaviour on all strain-gauged standard specimens before catastrophic failure, despite the very low failure stresses. It is suggested that other factors (see Chapter 5) possibly contributed to the observed behaviour.

2.1.4 Factors Affecting the Test Results

As shown above, numerous studies comparing different test methods, thus implicitly studying factors affecting the test results, have been published. However, rigourous investigations into the effects of individual factors of testing practice are relatively scarce.

One of those was the investigation by Westberg and Abdallah (1987) described in the previous section. Odom and Adams (1990) investigated failure modes of AS4/3501-6 specimens using the IITRI method. In their study they varied parameters such as tabbing material, geometry of the tabs and gripping condition. They found that a specific failure mode of the specimen is dependent on the factors examined and so was the associated strength result. However, for a particular configuration strength and failure mode could

not be correlated, suggesting that the macroscopic failure mode was a secondary effect. The test results were highest for tapered steel tabs and only for tapered glass tabs were the results significantly lower. Initial debonding of the tab tips lowered results as well but only marginal influence from gripping was found.

In a publication based on the same experimental results (Adams and Odom, 1991) the authors addressed the problem of macrobuckling. Since the test results for specimens with slightly debonded tabs were only slightly lower, they rejected the argument of Chamis and Sinclair (1985) that tab tip debonding during the test increased the effective unsupported length of the specimen significantly. Since the specimens with debonds failed at the end of the tabs rather than at the end of the bond line, they concluded that clamping forces of the IITRI rig override the stress concentrations caused by load introduction. Finally, they recommended untapered glass fibre/epoxy tabs as they yield only slightly lower results and are easier to produce. They stated that existing standards are sufficiently general that less than satisfactory results can be obtained, even if all guidelines are fully conformed to regarding testing of unidirectional CFRP.

Adams and Lewis (1991) investigated the influence of specimen gauge length and loading method on the compressive strength of unidirectional composites. The materials used were AS4/3501/6 CFRP and S2/3501/6 GRP. They found that as long as global instability of the specimen could be avoided there was little influence of the gauge length on the measured compressive strength. The limit for the slenderness ratio was quoted as 25 to 30. This was in general agreement with work by Port (1982), Barker and Balasundaram (1987) and Smoot (1982). The influence of the method of load introduction, i.e. shear loading or end-loading, were considered as being small as long as the ends of the end-loaded specimen are not crushed and the tabs in either case do not debond.

Very little has been published to quantify the so-called 'operator influence' on test results. Lee (1987), for example, when examining the influence of gauge length on the measured compressive strength using the Celanese method, quoted 10% higher results in a second attempt with much reduced scatter. Although this might be within experimental error, it is believed that test results are generally more consistent - and often higher - with increasing operator experience.

Hart-Smith (1991) presented some interesting views on testing of composites in general, illustrated on a laboratory case history. Some of his findings and suggestions had been made independently in the present investigation. He stated that design of test coupons and their imperfect manufacture and testing are serious sources of scatter in measured strengths, concluding that variation in fibrous composite material strengths is

largely a consequence of inappropriate test technique and specimen design. Tabbing of the test piece is shown to be one of the most important factors in this context. In particular, he recommended the use of friction tabs rather than bonded ones and cross-plied rather than unidirectional laminates for compression strength specimens. He strongly recommended that future test specimen specifications be more flexible with only the size of the gauge section specified, instead of the entire geometry and the method of load introduction.

2.2 Strength Prediction

2.2.1 Compressive Failure Modes of Composites

Strength prediction for a given material is much simplified if the failure mode of the material is known since, often, intrinsic properties, in particular under multi-dimensional stress conditions, are not known. A predictive model from basic (one-dimensional) properties is therefore not possible for a complex material like a composite. Unfortunately, observations of the compressive failure process in unidirectional composites are very difficult because failure is usually sudden and catastrophic. Post-failure analysis of the fracture surfaces may be misleading when the sudden release of stored elastic energy of the specimen, the testing rig, and the testing machine destroys the evidence of initial failure. Also, it is often found difficult to distinguish between primary and secondary failure modes and between testing artefacts and 'natural' failure.

In the following, the investigations will mostly be concentrated on unidirectional CFRP but supporting evidence for other composites, particularly from the early publications, is considered as well. Figure 2.2.1-1 gives a brief summary of failure modes on different levels of the composite which have been reported or suggested, as discussed in the following.

Failure modes observed in CFRP specimens, in particular, include: macrobuckling of the specimen (e.g. Port, 1982); crushing of the specimen end and longitudinal splitting (e.g Weaver and Williams, 1975); interfacial failure (e.g. Port, 1982; Weaver and Williams, 1975; Parry and Wronsky, 1982); microbuckling of a fibre bundle (e.g. Prandy and Hahn, 1990; Hahn and Williams, 1986); microbuckling of fibres in a kinking mode (e.g. Evans and Adler, 1978; Lee, 1986; Hahn and Williams, 1986; Potter, 1986; Hahn and Sohi, 1986); shear failure of the specimen (e.g. Ewins and Ham, 1973; Hancox, 1975) and shear fracture of fibres at several locations in a fibre bundle embedded in epoxy (e.g. Hahn and Sohi, 1986); compressive shear failure of fibres in a

laminate (Crasto and Kim, 1990); and local fibre 'bulging' (Melanitis and Galiotis, 1990).

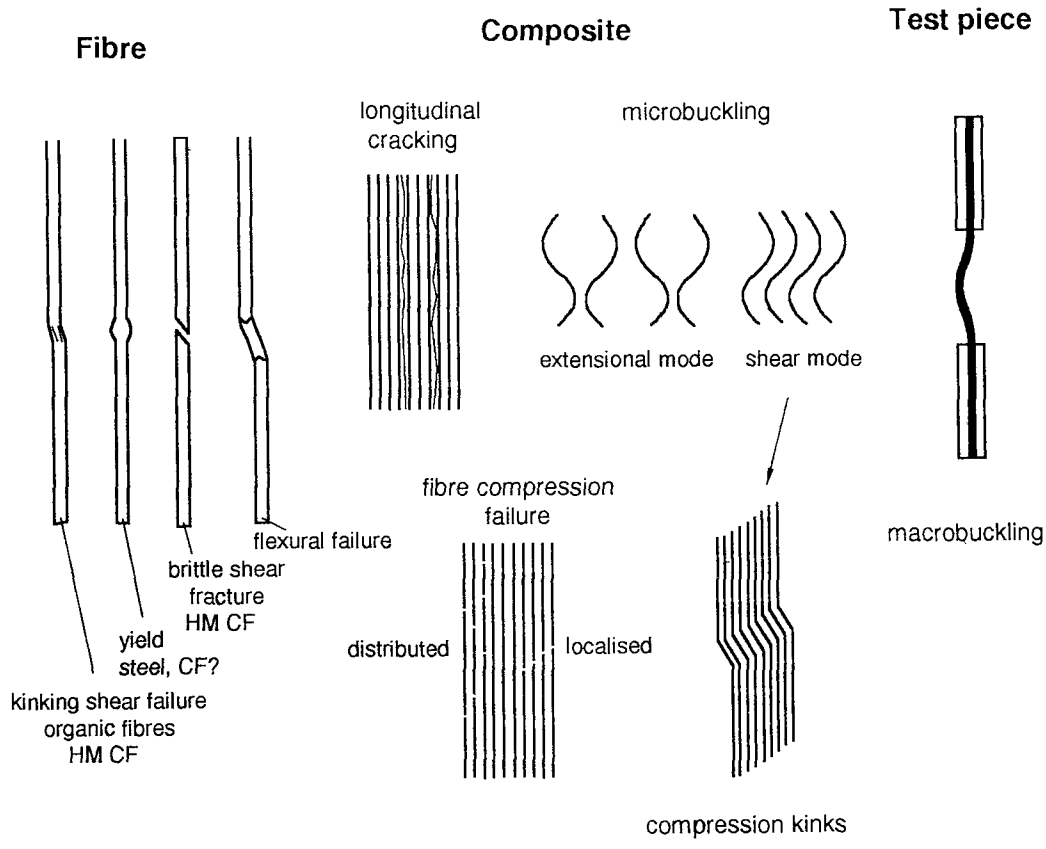


Figure 2.2.1-1: Principal observed failure modes of composites.

Shear failure of the specimen, i.e. failure in the plane of maximum shear, which is to be regarded as an upper limit for the compressive strength of any material, was observed at room temperature by Ewins and Ham (1973). Moving to higher temperatures, they discovered that the failure mode changed to a fibre microbuckling type. Port (1982) stated that such a transition is not encountered in currently used CFRP systems and that failure is always of a microbuckling type, regardless of temperature. This is due to the fact that modern matrices are less brittle and stiff than the early systems so that the fibres fail by buckling before their compressive strength is reached.

In order to elucidate compressive failure in the laminate which is, as mentioned before, difficult to observe, various studies have been carried out using single filaments or fibre bundles embedded in resin carriers.

Hawthorne and Teghtsoonian (1975) investigated compression failure of single carbon fibres of various types and modulus embedded in epoxy resin. They found a trend of decreasing compressive fibre strength with increasing modulus for pitch and rayon-based fibres. It was suggested that fibre compression failure changes from a shear to a buckling or kinking mode of microfibrils with increasing fibre anisotropy. This microkinking mode was thought to occur as fine partial microcracks initiating in individual, well-aligned but uncoupled microfibrils in the surface layer of the carbon fibre. The compression strength of PAN type II and type A fibres could not be obtained since fibre fracture was not observed before the epoxy resin failed in shear at about 3% direct strain.

In contrast, recent research on single fibres under compression using Raman spectroscopy by Melanitis and Galiotis (1990) suggested that modern high-strength intermediate-modulus fibres (Courtaulds' XAS) can fail locally in a yielding ('bulging') mode. This, however, has so far not been observed in a composite for this fibre. Crasto (1990) reported compressive failure of AS4 fibres in a laminate tested using the new mini-sandwich beam in direct compression.

Hahn and Sohi (1986) examined compression failure of fibre bundles embedded in epoxy resin rather than single filaments. The fibres used were (modern) carbon fibres T300 and T700 and high-modulus P75. Shear failure of single fibres at several locations, causing gradual failure of the composite, was observed only for high-modulus P75 fibre bundles. The other carbon fibre bundles as well as glass fibre bundles failed by microbuckling, the carbon fibre bundles failing more in a quite localised kinking type. Fibre fracture occurred immediately after buckling. Interestingly, the failure strains of the intermediate modulus bundles were higher than those of their composites.

Norita, Kitano and Noguchi (1988) investigated the compressive strength of 13 different fibres including organic, metallic, PAN and pitch-based carbon fibres by the loop method. They found in general a direct correlation between fibre shear modulus and fibre compressive strength. Testing composites fabricated from those fibres using epoxy resins, they also found that the composite compressive strength increased with increasing fibre compressive strength, i.e increasing fibre shear modulus. They emphasised that the result for the boron composite was almost the value predicted by elastic microbuckling (Rosen, 1964). For composites containing fibres with high orthotropy (such as organic fibres and pitch-based carbon fibres, where the ratio E_f/G_f is high) composite strength is dictated by fibre strength. With increasing shear strength there is a transition towards buckling domination, the upper limit of the compressive strength being the shear modulus of the composite.

Kumar and Helminiak (1990) generally confirmed the above findings in their comprehensive review on compressive strength of high performance fibres. Regarding carbon fibres they stated that compressive strength of both pitch and PAN-based fibres decreases with increasing (longitudinal) modulus of elasticity. And at a given modulus the compressive strength of a PAN-based carbon fibre is higher than that of the pitch-based one. They suggested that failure of polymeric fibres is rather by buckling of fibrils/microfibrils, whereas compression failure of high modulus carbon fibres is by brittle fracture.

Applying the fibre loop test on pitch and PAN-based carbon fibres, Tsushima (1989) concluded that failure for both fibre types was initiated on the tensile side and not affected by some pre-failure damage on the compression side. The loop strength results were about 1.5 to 2 times higher than the tensile strengths from fibres with 25 mm gauge length. The Weibull strength theory was found to be in good agreement with these findings.

Crasto and Anderson (1990) suspected that, since they found an inverse relationship between crystallite aspect ratio and compression strength of pitch-based fibres, buckling of crystallites may be involved in the compression failure mechanism. They associated relatively low fibre compressive strength with sheet or ribbon-like structure (as in pitch-based fibres), and granular or particulate morphology (as seen predominantly in PAN-based fibres) with comparatively higher compression strength.

Madhukar and Drzal (1990) examined the effect of fibre-matrix adhesion on the compressive properties of CFRP containing the high-strength intermediate-modulus carbon fibres with different surface treatment (AU-4, AS-4, AS-4C). They found that the influence of fibre surface treatment on the modulus of elasticity was only marginal, whereas the compressive strength was highly dependent. From fracture surface analysis they suggested that failure of specimens with low ILSS was due to delamination and global delamination buckling, in-phase microbuckling of fibres for intermediate ILSS and compressive failure of fibres in several planes perpendicular to the fibre axis for high values of ILSS. Compressive fibre failure was suggested from the evidence of stepped fracture surfaces. However, it should be noted that the failure stress was relatively low in that investigation (1174 MPa for the composite with the highest ILSS). Considerably higher failure stresses for AS-4 fibre-reinforced composites have been reported elsewhere so that fibre compression failure, which has to be regarded as the upper limit for the compressive strength, is rather unlikely.

Boll, Jensen and Cordner (1990) tested several single carbon filaments, including Hercules AS-4, IM6 and IM7 embedded in epoxy. In contrast to other authors they

found no evidence of microbuckling of the carbon fibres, but of a glass fibre tested for comparison. SEM studies suggested transverse shear failure of the carbon fibres. Fibre failure occurred at a fraction of the composite failures stress (about 10% for the HMS carbon fibre and the glass fibre). However, they emphasised that composite failure does not correspond to initial fibre failure but is likely to be caused by an accumulation of breaks. They supposed that compressive fibre failure is determined by a more or less uniform fibre micro-crystalline structure rather than by random effects.

Prandy and Hahn (1990) tested different pitch and PAN-based carbon fibre bundles (rather than single filaments) embedded in epoxy resin. In all pitch-based fibres failure occurred at many locations and, as stated above, the bundle did not fail catastrophically. The three types of pitch-based fibres exhibited quite different distinct failure modes, including shear failure at 45° (UHM), transverse cracks with fracture surfaces normal to the fibre axis (HS, HM) and longitudinal splitting (HM). All specimens containing PAN-based fibres failed catastrophically and failure was by fibre microbuckling followed by kinking in some cases. Failure strains increased with decreasing modulus for both types of fibres, though the absolute values of failure strains of PAN-based fibres were significantly higher. Interestingly, and in contrast to the previous author, failure strains of the PAN-based fibre bundles were significantly higher than the values generally reported for the composites (all greater than 2%).

Microbuckling of fibres or fibre bundles, i.e. local microinstability, is accepted by most authors as the principal failure mode of currently used high strength carbon fibre-reinforced plastics, although the mechanisms triggering failure are still unclear.

Woolstencroft et al. (1982) pointed out that microbuckling of fibre could be caused by loss of support due to interfacial failure caused by tension stresses. They showed that transverse tension stresses in the matrix by the mismatch of Poisson's ratio of matrix and fibre, matrix cooling shrinkage and moisture absorption can reach significant values.

Failure of a kinking type is usually observed in CFRP since brittle carbon fibres are likely to break immediately after buckling at two locations due to additional bending stresses. Since the buckled fibres disturb the equilibrium of neighbouring fibres the kink band, defined by rotated fibre segments which may experience further breakage during the failure process, will spread across the specimen.

The boundary planes of the kink bands are inclined at an angle β (see Figure 2.2.1-2) of approximately 15 to 25 degrees to the normal of the fibre 0°-direction (e.g. Budianski and Fleck, 1990) The specimen, therefore, exhibits fracture surfaces in these planes. 'Crossing' kink bands and kink bands 'reflected' at the edge of the specimen have been frequently observed. Longitudinal splitting is likely to occur as a secondary

effect when transverse tensile stresses are developed due to kinematic incompatibility in the matrix, or when a kink band intersects a void.

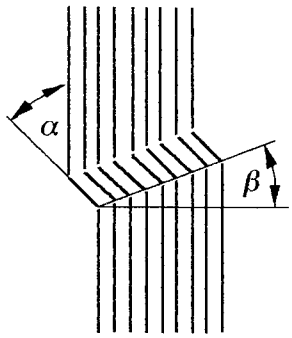


Figure 2.2.1-2: Kink band geometry.

2.2.2 Models Predicting Compressive Strength

One of the first models is commonly attributed to Rosen (1964). In a two-dimensional elastic analysis the reinforcing elements are treated as columns (of infinite width) on an elastic foundation. Two buckling modes are possible: the extensional (symmetric) mode involving matrix normal deformation and the shear (antisymmetric) mode causing mainly shear deformation (compare Figure 2.2.1-1). The shear mode was found to be the critical one for high fibre volume content of practical composites. The critical stress is the compressive strength of the composite, which is for this case:

$$\sigma_{cu} = G_m \frac{1}{1 - V_f} \qquad (2.2.2\text{-}1)$$

The compressive strength depends only on the initial shear modulus G_m of the matrix and the fibre volume fraction of the composite. However, models based on elastic buckling theory yielded results which overpredicted the compressive strength of fibre reinforced polymers by a large margin, typically by a factor of two to four.

More detailed investigations, for instance incorporating a three-dimensional continuum rather than treating matrix and fibres as two-dimensional (e.g. Sadowky, Pu and Hussain (1967) brought similar results.

Greszczuk (1973) reviewed and compared some of the early models. In a later publication (1975) he considered a three-dimensional composite containing fibres with circular cross-section and deduced for the critical stress, assuming (elastic) shear mode failure, which is the compressive strength of the laminate:

$$\sigma_{cu} = G_{lt} + K_b \qquad (2.2.2\text{-}2)$$

where K_b is a bending term including the fibre stiffness and an end constraint factor. For macroscale composites, e.g. aluminium rod reinforced resins, good agreement with experimental results was found. A size effect was observed and influence of initial fibre deflection suggested.

It had soon been realised that non-linear effects had to be taken into account to obtain realistic predictions for practical composites. Schuerch (1966) examined the compressive strength of uniaxial boron fibre-metal matrix composites. He proposed that compressive failure takes place when the matrix material is in the plastic zone due to compressive strain. The (elastic) matrix shear modulus in Equation 2.2.2-1 was therefore replaced by an effective tangent matrix shear modulus $G_{m,eff}$ which is dependent on the compressive strain.

$$\sigma_{cu} = G_{m,eff}(\varepsilon_c)\frac{1}{1 - V_f} \qquad (2.2.2\text{-}3)$$

Lager and June (1969) also proposed to modify Rosen's model by introducing an 'empirical influence coefficient' of 0.63. This led to good agreement of predictions with experimental results for boron fibre-reinforced epoxy where fibres were arranged in a nearly square array.

Herrmann et al. (1967) examined the compressive behaviour of 'initially crooked wires' surrounded by matrix. They found that only for extremely small ratios of the shear moduli of reinforcing element and matrix would buckling be possible. But it was stated that the difference of elastic modulus in tension and compression might be explained by the beam-column behaviour of initially non-straight fibres. Lanir and Fung (1972) investigated the micromechanics of fibre composite columns. They concluded that fibre buckling in the elastic range of metal matrix composites does not affect the overall mechanical behaviour, but that debonding between fibre and matrix reduced the buckling load. In the plastic range of direct strain they expected the buckling of fibres would have a significant effect since the deformation due to fibre waviness is of the order of the compressive deformation.

Hayashi (1970) modified the elastic shear buckling theory by taking into account plastic behaviour of the matrix material under axial compression. He had found that for bulk material shear instability took place when the applied compressive stress equalled the shear modulus of the material. Applied to composites he postulated that compressive failure occurred when the matrix shear modulus equalled the instantaneous axial compressive stress:

$$\sigma_m^* = G_m(\sigma_m) \tag{2.2.2-4}$$

so that the compressive strength was obtained as:

$$\sigma_{cu} = \sigma_f^* V_f + \sigma_m^* (1 - V_f) \tag{2.2.2-5}$$

where σ_f^* is the fibre stress corresponding to σ_m. This is the rule of mixture for strength and the composite compressive strength is approximately proportional to the fibre volume fraction. Since data on $G_m(\sigma_m)$ were scarce, the critical matrix (axial) stress was approximated by the matrix yield stress:

$$\sigma_m^* = \sigma_{m,y} \tag{2.2.2-6}$$

so that the compressive strength was approximately:

$$\sigma_{cu} \cong \sigma_f^* V_f + \sigma_{m,y} (1 - V_f) \tag{2.2.2-7}$$

It was noted that this equation did not give satisfactory predictions for the whole range of boron/epoxy tested by Lager and June (1969), but fairly good agreement for glass/epoxy and was therefore considered to be a large improvement on the predictions of the Rosen model. However, Equation 2.2.2-6 would significantly overpredict the compressive strength of composites containing fibres with low failure strains, due to low fibre strength (e.g. polymeric fibres) or due to high fibre stiffness (e.g. metallic fibres, carbon fibres). Piggot and Wilde (1980) pointed out that when the fibre strength is the limiting factor the rule of mixtures including the fibre compressive strength $\sigma_{cu,f}$ can be applied:

$$\sigma_{cu} = \sigma_{cu,f} V_f + \sigma_m^* (1 - V_f) \tag{2.2.2-8}$$

where σ_m^* is the matrix stress at fibre failure strain.

In a later publication (1989) Hayashi described the decrease of the effective shear modulus of epoxy under axial compression and derived the simple relation for the effective shear modulus:

$$G_{eff} = G_0 + \sigma \tag{2.2.2-9}$$

This linear relation showed good agreement with torsion/compression tests on epoxy rods for compressive stresses up to 30 MPa. For larger compressive stresses the experimentally determined reduction in shear modulus was higher than predicted by Equation 2.2.2-9. Also, for carbon fibre-reinforced epoxy cylinders in tension this equation was found to be valid, i.e. the shear stiffness of the cylinders was increased

under tension. The geometric deformation has been taken into account. The author therefore suggested that the relation is valid also for laminates.

Kulkarni, Rice and Rosen (1975) included shear deformation of the fibre, rather than treating the fibre as rigid, which reduced the compressive strength of the composite compared to the Rosen prediction to:

$$\sigma_{cu} = \frac{G_m}{(1 - V_f) + V_f \frac{G_m}{G_f}} \qquad (2.2.2\text{-}10)$$

Norita, Kitano and Noguchi (1988) accepted the validity of this equation as an upper bound which could experimentally be verified for some systems such as boron and alumina fibre-reinforced epoxies.

One of the first models incorporating implicitly plastic microbuckling of initially curved fibres is the one described by Argon (1972). He developed a model of 'shear collapse mode of failure for composites' in analogy with kink bands in metal crystals. An energy balance yielded after simplifications, such as neglecting bending terms:

$$\sigma_{cu} \approx \frac{k}{\phi_0} \qquad (2.2.2\text{-}11)$$

where k is the plastic shear strength of the matrix and ϕ_0 an initial angle of fibre misalignment. One of the shortfalls of this equation is that the effect of fibre volume fraction is not considered.

Swift (1975) discussed the effect of initial fibre curvature on the tensile elastic moduli of laminates. He found that for glass fibre composites the effect of fibre waviness is negligible both in reduction of initial modulus and strain hardening, but significant for stiffer boron fibre composites. However, it is not clear whether his input data on fibre deflections were realistic.

Davis, Jr. (1975) found experimental evidence of the shear modulus being a function of the applied compressive stress. It is not known whether a correction of geometric effects has been made. However, failure of boron epoxy in a shear instability mode was reasonably well predicted when initial fibre curvature was included and the experimentally determined $G(\sigma_c)$ was used.

Weaver and Williams (1975) tested CFRP rods with a fibre volume fraction of 36% under hydrostatic pressure and found increasing compressive strength with increasing pressure. They observed specimen failure by end crushing and longitudinal splitting from the end as well as debond failures in the specimen body at low pressures. At higher

pressures the failure mode changed to a kinking type. Parry and Wronsky (1982) (see also Wronsky and Parry, 1982) carried out compression tests with CFRP containing type-3 carbon fibres under hydrostatic pressure. They used specimens of dogbone shape with circular cross-section. Failure was by fibre kinking preceded by some longitudinal splits and interfacial failure starting from the centre of the waist at low pressure. At higher pressures longitudinal splitting was suppressed. Interfacial failure seemed to be a specimen design problem (Equation 2.1.2-1) as was longitudinal splitting from the specimen end in the case mentioned above. The ultimate compressive stress was strongly dependent on pressure. They rejected therefore any model based on shear stress controlled failure of fibres in CFRP as reported by Ewins and Ham (1973), which would be much less pressure dependent. Also, theories where the compressive strength is based on the matrix shear modulus as proposed by Rosen were ruled out, because the initial matrix shear modulus is only weakly dependent on pressure.

The shear strength of the composite, however, increases in a similar range as the compressive strength. They reported a twofold increase of the maximum interlaminar shear stress for a pressure of 300 MPa compared to ambient pressure. Therefore, they considered models based on the strength, ductility and possibly toughness of the matrix rather than the modulus as more suitable to predict the ultimate compressive stress of the laminate. A local surface condition was suggested to cause first buckling of a group of fibres which then promotes the kink band.

In 1980 Piggot and Harris rejected Rosen's model on the basis of the linear relation of fibre volume fraction and compressive strength they found for a range of fibre-reinforced polyesters of moderate volume fractions. Varying the state of cure of the matrix resin they found a strong correlation between matrix modulus and matrix yield strength as well as between composite strength and matrix yield strength. Linear variation of the compressive strength of carbon, glass and Kevlar fibre-reinforced polyesters was also reported by Martinez et al. (1981) up to a fibre volume fraction of 40%. Above this value the compressive strength did not increase significantly and even dropped at volume fractions above 60%. Surprisingly, fibre misalignment reduced the compressive strength of composites containing glass and carbon fibres only for angles exceeding 10°. The effect of deliberate fibre kinking by indenting the rod specimen was drastic and could be described by the relation

$$\sigma_{cu} = \sigma_0 + bR \qquad (2.2.2\text{-}12)$$

where R is the minimum radius of curvature of the indentation and σ_0 and b are constants. Since the composite strength of a laminate with a minimum radius of curvature of 5 mm

was equal to the strength of the plain laminate, the authors concluded that compressive failure due to fibre curvature occurred only for smaller radii of curvature. This would suggest that fibre curvature of that order was present in the composite (Piggot, 1981). Fibre/matrix adhesion was identified as being important for good compressive strength of a composite.

Wang (1978) extended the shear instability model of Argon (1972) by taking into account a nonlinear shear response of the composite. Assuming initial sinusoidal fibre deflection, the amplitude of which increased under compressive load leading to shear instability (this mechanism will be described later in detail), he developed the following relation:

$$\tau_{lt} \approx \frac{G_{lt}\,\sigma_c}{G_{lt} - \sigma_c}\,\frac{\pi f_0}{l} \qquad (2.2.2\text{-}13)$$

where f_0/l denotes the fibre amplitude over half wave length initially present in the composite. The fibre volume fraction is included implicitly by taking composite shear properties rather than matrix properties. Wang stated that f_0/l is at best a statistical quantity and difficult to measure for a given composite. He therefore proposed the following procedure to prove the validity of the strength prediction model. Firstly, the shear-stress strain behaviour of the composite is determined from stress-strain curves of a ±45° laminate under tension. With these data a value for f_0/l is selected so that the predicted result matches the experimental value in a particular test condition. This value characterising the fibre waviness is then regarded as a material property independent of test conditions. Applying the theory with shear stress-strain curves from different test conditions, i.e. temperatures, in an incremental manner, Wang found that predicted results agreed reasonably well with the experimental results.

Hahn and Williams (1986) identified compressive failure of two different carbon fibres in four different resins as shear crippling, with the development of kink bands, if the matrix was stiff, and microbuckling without regular kink band pattern but large post failure deformation of the fibre causing multiple fractures due to high bending strains if the matrix was soft. In a model similar to Wang (1978), considering forces acting on a fibre segment rather than an energy balance for a composite element, the equilibrium compressive stress was found to be (see also Tsai and Hahn, 1980):

$$\sigma_c = V_f\, G_{lt}\,\frac{\gamma_{lt}}{\gamma_{lt} + \pi\frac{f_0}{l}} \qquad (2.2.2\text{-}14)$$

which is basically the solution of Wang multiplied by the factor V_f. This factor is a

consequence of regarding a fibre rather than a fibre/matrix element and the authors supposed that it would give a more realistic estimate of the compressive strength.

Assuming elastic-perfectly plastic behaviour, the compressive strength of the composite is derived from Equation 2.2.2-14:

$$\sigma_{cu} = V_f \frac{\tau_y}{\gamma_y + \pi \frac{f_0}{l}} \tag{2.2.2-15}$$

Tsai and Hahn (1980) had deduced that approximation without the factor V_f. For weak fibres flexural failure occurs before matrix shear or interfacial failure, yielding the compressive strength:

$$\sigma_{cu} = V_f \frac{G_{lt}}{1 + \frac{\pi}{2} \frac{E_f}{S_{fl,f}} \frac{d_f}{l} \frac{\pi f_0}{l}} \tag{2.2.2-16}$$

Approximating the initial laminate shear modulus by:

$$\frac{1}{G_{lt}} = \frac{V_f}{G_f} + \frac{\eta(1 - V_f)}{G_m} \tag{2.2.2-17}$$

with

$$\eta = \frac{1}{2}\left(1 + \frac{G_m}{G_f}\right) \tag{2.2.2-18}$$

they calculated the value for the initial fibre imperfection from test results of one laminate, similar to Wang's approach. Under these assumptions, Equation 2.2.2-15 overestimated the compressive strength when the matrix tensile modulus was less than 3 GPa. But in general they found reasonable agreement with the experimental data.

Ceramic matrix materials do not exhibit yielding characteristics typical for polymers. Steif (1987) therefore extended the classical microbuckling analysis by including slippage at the fibre/matrix interface to predict compressive failure of composites with brittle, weakly bonded constituents. Imperfections were included by assuming initial fibre deflections and catastrophic failure assumed at first interfacial slip. This led to an equation similar to that found by Argon (Equation 2.2.2-11) replacing the yield strength of the matrix by the interfacial shear strength S_{if} of the composite:

$$\sigma_{cu} = \frac{E}{E_f} \frac{S_{if}}{\pi \frac{f_0}{l}} \tag{2.2.2-19}$$

where E is the composite modulus of elasticity. Published data could only be verified using this equation by chosing somewhat arbitrary input parameter for the initial fibre

deflection. However, the author concluded that the model was an improvment since its predictions were substantially below classical predictions.

Yeh and Teply (1988) considered unidirectional composites containing fibres of low shear strength. They predicted compressive failure either as local shear instability given by the maximum of the following expression (compare Equations 2.2.2-10 and 2.2.14, without the factor V_f):

$$\sigma_c = \frac{G_m}{(1 - V_f) + V_f \frac{G_m}{G_f}} \left(1 - \frac{f_o}{f}\right) \qquad (2.2.2\text{-}20)$$

where f_0 and f are typical fibre deflections in the unloaded and compressively loaded composite, respectively. Alternatively, they predicted local shear failure when the maximum of the shear stress transverse to the fibre direction given in the following equation reaches the shear strength of the composite:

$$\tau_\phi = \frac{\sigma_c}{2} \sin 2\phi + \tau \cos 2\phi \qquad (2.2.2\text{-}21)$$

where ϕ is the local fibre angle. They concluded that the fibre microbuckling model (Equation 2.2.2-19) is suitable for composites containing fibres with high shear modulus, and that local shear failure is the dominant failure mode of composites containing fibres with low shear modulus, such as Kevlar 49.

Wisnom (1990) considered the effect of a small fibre misalignment on the compressive strength of a laminate. Considering a laminate element rotated by a small angle he derived the equilibrium equivalent to Equation 2.2.2-13, expressing the laminate properties by matrix properties:

$$\sigma_c = \frac{G_m \gamma}{V_m (\gamma + \phi_0)} \qquad (2.2.2\text{-}22)$$

where V_m denotes the volume fraction of the matrix. The maximum of the right hand side gives, as in Wang's model, the compressive strength. Additionally, he suggested including the axial strain the matrix suffers, by replacing the shear strain in Equation 2.2.2-22 by the maximum shear strain γ_{max}:

$$\gamma_{max} = \sqrt{(\varepsilon_m \ (1 + \nu_m))^2 + \gamma^2} \qquad (2.2.2\text{-}23)$$

γ is the shear strain induced by fibre misalignment, ε_m the axial strain in the matrix, which is taken as the composite axial strain, and ν_m is the matrix Poisson's ratio.

Applied on XAS/914C he found that a misalignment of 0.25° is sufficient to reduce the compressive strength from 2720 MPa to 1850 MPa, or to 700 MPa for 3°, respectively.

It has to be noted that the models suggesting shear instability generally yielded reasonable agreement with experimental data only on a semi-empirical basis. The input datum for the fibre deflection was a free parameter which allowed fitting of test results. A strength prediction *a priori* was not possible because of lack of data for the initial fibre waviness. Yugartis (1987) had proposed a promising technique to quantify fibre angle distributions by analysing micrographs of polished samples. This will be described in detail later in the current investigation.

Relatively few investigations took into account experimental evidence of kink band inclination. Chaplin (1977) derived from a volumetric strain argument a relation between the kink boundary angle β and the kink fibre angle α. Expressing the volumetric strain within the kink band as:

$$\varepsilon_{vol} = \frac{\cos(\beta - \alpha)}{\cos\beta} - 1 \qquad (2.2.2\text{-}24)$$

and assuming no change in the volumetric strain, he found the relation:

$$\alpha = 2\beta \qquad (2.2.2\text{-}25)$$

Budianski (1983) generalised the elastic shear buckling solution to a kink band inclined at an angle β and deduced the critical stress for elastic buckling:

$$\sigma_{cr} = G_{lt} + E_{tr}\tan^2\beta \qquad (2.2.2\text{-}26)$$

where E_{tr} is the transverse modulus of elasticity. This, as Rosen's equation, gave the critical value for the kink boundary angle as $\beta = 0°$. Introducing perfect plasticity, the ultimate compressive stress reduced to:

$$\sigma_{cu} = \left(\frac{\gamma_y}{\phi_0 + \gamma_y}\right)\sigma_{cr,el} \qquad (2.2.2\text{-}27)$$

Regarding a kink band inclined at an angle β and using a quadratic yield condition for transverse and shear stresses:

$$\left(\frac{\tau}{\tau_y}\right)^2 + \left(\frac{\sigma_{tr}}{\sigma_{tr,y}}\right)^2 = 1 \qquad (2.2.2\text{-}28)$$

and the 'assumption-of-convenience':

$$\frac{E_{tr}}{G_{lt}} = \left(\frac{\sigma_{tr,y}}{\tau_y}\right)^2 \qquad (2.2.2\text{-}29)$$

the ultimate compressive stress was determined as:

$$\sigma_{cu} = \left(\frac{\gamma_y}{\phi_0\sqrt{\frac{\sigma_{cr}}{G_{lt}}} + \gamma_y}\right)\sigma_{cr} \qquad (2.2.2\text{-}30)$$

or with γ_y neglected:

$$\sigma_{cu} = \frac{k^*}{\phi_0} \qquad (2.2.2\text{-}31)$$

with

$$k^* \approx k\left(1 + \left(\frac{\sigma_{tr,y}}{k}\right)^2 \tan^2\beta\right)^{\frac{1}{2}} \qquad (2.2.2\text{-}32)$$

With the simplification of $\beta = 0°$, so that $k = k^*$, Argon's relation (Equation 2.2.2-11) is obtained.

An analysis of the elastic effects of localised boundary imperfections yielded the following relationships for long-wave imperfection:

$$\tan\beta = \pm\sqrt{\frac{1 - \frac{\sigma_{cu}}{G_{lt}}}{\frac{E_{tr}}{G_{lt}}}} \qquad (2.2.2\text{-}33)$$

and for short-wave imperfection:

$$\tan\beta = \pm(\sqrt{2} - 1)\sqrt{\frac{1 - \frac{\sigma_{cu}}{G_{lt}}}{\frac{E_{tr}}{G_{lt}}}} \qquad (2.2.2\text{-}34)$$

Experimentally observed kink boundary angles fell into the band defined by these two equations.

Finally, a bending analysis, assuming inextensional bending of perfectly brittle fibres and rigid-plastic behaviour of the matrix, led to the relationship for the kink band width w_k:

$$\frac{w_k}{d_f} = \frac{\pi}{4}\left(\frac{2k^*}{V_f E_f}\right)^{-\frac{1}{3}} \qquad (2.2.2\text{-}35)$$

For CFRP this expression yielded reasonable predictions (e.g. Soutis, 1991).

Hahn (1987) proposed a unified analysis of kink band formation, i.e. all three geometric parameters of the kink band are determined. A deformation tensor was used to describe the deformation within the kink band assuming a perfectly plastic matrix behaviour. He found for the kink (fibre) orientation α, i.e. the angle of fibres within the kink band:

$$\alpha = 2\frac{\tau_{ym}}{\sigma_f} \tag{2.2.2-36}$$

and the kink band width:

$$w_k = \frac{\pi d_f}{4}\sqrt{\frac{E_f}{\sigma_f}} \tag{2.2.2-37}$$

The kink boundary angle is taken as half the kink fibre orientation angle (Equation 2.2.2-25). In a semi-empirical approach experimental results for fibre stresses at failure σ_f (composite compression strength divided by fibre volume fraction) and kink boundary angle were used as input data. The analysis showed that fibres failed on the compression side at the point of maximum curvature.

The predictions for the kink band width agreed fairly well with the experimental data for Kevlar and carbon/epoxy but were too low for glass/epoxy. Predicted kink orientation angles were considerably smaller than the observed ones. It was stressed that the kink orientation angle might be increased after failure if the load is not released immediately, which is confirmed by experimental evidence.

Fleck and Budiansky (1990) emphasised, as Budiansky (1983), that compression failure of polymeric composites is a plastic rather than an elastic event. They stated that yield stress scales in a linear fashion with elastic stiffness of polymer matrices. Thus the compressive strength of the fibre composite varies linearly with elastic modulus which has led several investigators to conclude erroneously that microbuckling is an elastic event. They generalised Budiansky's analysis to include remote shear stresses. A rigid-perfectly plastic analysis approximated well the onset of yield in the elastic-perfectly plastic solid. They found that for small ratios of yield strain and initial fibre misalignment both reduced to the approximation:

$$\sigma_{cu} \approx k^*\left(1 - \frac{e}{\phi_0}\right) \tag{2.2.2-38}$$

where e has been defined as the proportionality factor between applied compressive and shear stress and k^* is defined by Equation 2.2.2-32. In the case of vanishing remote

shear stress, and the assumption for mathematical convenience from above, this reduces to:

$$\sigma_{cu} = \frac{k^*}{\phi_0 + \phi_y} \qquad (2.2.2\text{-}39)$$

They concluded that the axial compressive strength increases with decreasing fibre misalignment and increasing shear strength of the matrix, and with decreasing remote shear stress.

Their buckle propagation analysis suggested that only a small compressive stress, less than the matrix yield stress, is necessary to propagate an existing microbuckle.

Published micromechanical investigations into compression failure usually assume a homogeneous fibre-matrix pattern and uniform loading. The interaction of fibre and matrix in the microbuckling analysis was examined by Chang and Lessard (1991) for composites with non-uniform stress distributions. Their analysis, based on the minimum potential energy principle, included matrix extensional energy which they attributed to the interaction between fibre and matrix.

Interestingly, they found that local buckling strengths under non-uniform loading can be significantly higher than the uniaxial strength of the laminate under non-uniform loading. For a 'point'-load in the centre of the laminate, for instance, the local stress concentration can be almost eight times the uniaxial compressive strength before buckling occurs. They concluded that the inclusion of the matrix extensional energy is essential for predicting local fibre buckling strength in composites. A non-uniform and more concentrated load distribution can significantly affect local fibre buckling strength. Laminates under non-uniform loading conditions are typically more resistant to local fibre buckling. However, it should be noted that, as Fleck and Budiansky (1990) have pointed out, once a microbuckle due to stress concentrations is developed the stress to promote the buckled band is very small. The compressive capability of a structure can therefore be reduced to a higher degree than expected from the properties of laboratory coupons.

Empirical equations predicting the compressive strength of CFRP from other mechanical properties of the composite are presented by Sinclair and Chamis (1983). They proposed that as an upper bound the compressive strength of the composite can be calculated from the compressive strength of the fibre, which is taken as 90% of the fibre tensile strength. The compressive strength for the composite is then :

$$S_c = 0.9S_t \qquad (2.2.2\text{-}40)$$

where S_t is the tensile strength of the composite. As an estimate for the lower bound for the compressive strength, they suggested equations including the flexural strength S_{fl} or the interlaminar short beam shear strength S_{is} of the composite and the matrix tensile strength $S_{t,m}$:

$$S_c = \frac{S_{fl}}{3 - \frac{S_{fl}}{S_{t,m}}} \qquad (2.2.2\text{-}41)$$

and

$$S_c = 10S_{is} + 2.5S_{t,m} \qquad (2.2.2\text{-}42)$$

Equations 2.2.2-41 and 2.2.2-42 were found to provide a reasonable estimate for a variety of composite systems according to unpublished Lewis Research Center data (Sinclair and Chamis, 1983). Also, Lee and Springer (1988), who examined the influence of cure on mechanical properties of composites, found that Equation 2.2.2-39 applied reasonably well to the longitudinal compressive strength of the laminate examined, as did Equation 2.2.2-15 without factor V_f (Tsai and Hahn, 1980) in their investigation, when the term for initial fibre deflection was chosen to fit one case.

The failure mode of macrobuckling, an overall instability of the specimen, describes a structural rather than a material property. Therefore, macrobuckling of the specimen should be avoided during testing. Usually, the Euler buckling equations are used for an estimate of the critical stresses. A correction of these equations for highly anisotropic materials, including shear deformation in the differential equation of the deflected beam, seems to be appropriate for unidirectional composites and is included in the current ASTM D3410. Shear deflections should be taken into consideration, especially when the specimen is relatively short (Timoshenko, 1961, Chou and Kelly, 1980). A detailed investigation into the validity of classical buckling analysis will be carried out later in this study (Chapter 11). It will therefore not be reviewed in detail here.

2.3 CONCLUSIONS

Test methods

The literature survey on compression methods for composites showed that short gauge length specimens are used preferably for testing unidirectional material, and specimens with a long, supported, gauge length are used for multidirectional laminates. Load introduction is either by shear or by mixed shear/end loading.

Conflicting assessment of test methods by different authors is found in the published literature. Parameters influencing the test results are rarely identified and often not

recognised. Published test data suggest that the influence of the individual researcher and the individual rig might be greater than the influence of the test method itself. In other words, if the specification of each test method could be carefully fulfilled, the difference in test results gained with different test methods would be less significant. However, test results from specimens with different slenderness ratios are to be compared with caution.

Ease of use of the rig and the cost of rig and specimen manufacture are important criteria when choosing a test method. The IITRI fixture was found by most authors, particularly from the USA, to be easy to use and the specimen is relatively simple. An advantage of this method is that it is widely used, as well as Celanese-type methods which seemed to be the most controversial ones.

Partially end-loaded specimens require great care in machining, but they are likely to experience less stress concentrations due to load introduction. The Birmingham method is interesting, because it uses an untabbed specimen and because mounting of the specimen is very simple. Simplicity of the rig is the big advantage of the ASTM D695 method with a modified specimen.

The modulus of elasticity was found to be independent of the test method. Strain gauges are recommended for strain recording rather than extensometers.

Strength prediction

Basically, two failure modes were identified for CFRP: fibre compressive failure and fibre (micro)buckling. Highly orthotropic fibres such as high modulus carbon fibres (PAN and pitch-based) and polymeric fibres (aramid, nylon) have a low compressive strength due to their fibrilar morphology. Composites containing these fibres generally fail by fibre compression fracture.

Most authors accept microbuckling failure of a kinking type as the principal failure mode of modern high-strength CFRP. But the mechanisms of failure initiation are still unclear. Therefore, a model predicting the compressive strength of unidirectional CFRP from fundamental properties of the constituents of the composite is not yet available. Models assuming local shear instability in an elastic medium overpredict the compressive strength of fibre-reinforced polymers by a large margin. Taking into account initially non-straight fibres and plasticity of the matrix or generally non-linear behaviour the predictions become more realistic. The shortcoming of models including imperfections is that the fibre misalignment is very difficult to quantify *a priori*, thus making a verification of the model difficult. In addition, the shear stress-strain behaviour of the composite is difficult to measure and requires considerable experimental effort. However, even simplified models showed reasonable agreement with the experimental data.

CHAPTER 3 BASICS OF MECHANICAL TESTING

In this section the main subsidiary topics of compression testing will be described starting from the raw materials up to the analysis of the test data. This is to ensure repeatability of the experimental process and to document experiences gathered during the project. In particular, a simple procedure to produce test pieces of good quality is presented. Apparently, the results of compression tests, and not only compression tests but all other mechanical tests to a certain extent, can be affected by variations of all of the procedures described below. A further discussion of factors influencing test results is presented in Chapter 5.

3.1 Laminate Production

In general, laminates are produced from prepreg with a nominal thickness of 0.125 mm. The prepreg is normally stored in freezers at temperatures of about -18°C. Before laying up, the prepreg must be allowed to reach room temperature. Otherwise, condensate might be trapped between the layers. During the lay-up process care is taken in aligning each layer, which is fairly straightforward with unidirectional laminates. It is estimated that a maximum difference in angle between any two layers of less than 0.25° can be realised by careful laying up. This value of course depends on the quality of the prepreg used, as the edge of the prepreg is used as reference datum. It is also important to avoid any air entrapment between two layers of prepreg because this again might be the source of voids in the cured laminate.

The laid-up laminate is then stored in a freezer until the autoclave is available for the required curing process. A typical autoclave lay-up used in the present work is shown in Figure 3.1-1. In the case of prepregs with excessive resin content additional bleed cloth, usually one or several layers of glass cloth, are placed between the upper peel ply and the release film. A cork dam around the lay-up serves to contain excess resin emerging from the composite during curing.

Cured XAS/914C panels, typically of size 300x300 mm, are postcured in a ventilated oven according to the supplier's specifications. Particularly for thin unidirectional laminates, it was found to be necessary that the panels lie flat during the post curing process, otherwise they would distort due to residual thermal stresses.

The edges of finished panels have to be removed as soon as possible as they are very sharp and a potential risk of injury. For multidirectional laminates these edges are a reference datum and should therefore be treated carefully.

In the case of unidirectional laminates the fibre direction can be determined precisely by splitting a thin slice of material from the edge using a sharp knife to initiate the crack. This new edge is then used as datum. If for some reason the reference direction of a multidirectional laminate is lost, peeling off the single layers of a sample piece can help.

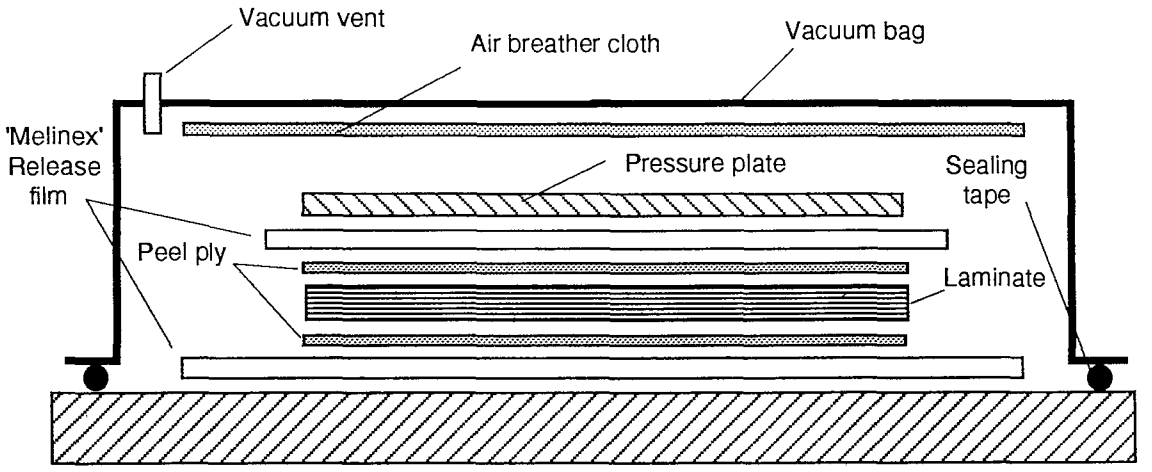


Figure 3.1-1: A typical autoclave lay-up; exploded view, not to scale.

In order to ensure a consistent quality of the material to be tested, non-destructive checks have to be carried out. In the present study a computerised ultrasonic C-scan technique is usually used to examine the cured panels. For that purpose the laminates are placed in a water tank and air bubbles carefully removed from the panel surface. After calibration of the attenuation the laminate is scanned by a probe which emits an ultrasonic sound beam. The distribution of the attenuation of the main reflected signal, which normally is the reflection from the carrier of the panel, gives an indication of the density and therefore of the quality of the panel. Delaminations and inclusions, and even cracks, can be discovered reliably when the map of attenuation is printed on the screen. The screen map or a printout can the be used to trace a fault on the original plate.

The next point to consider before the material is tested is moisture conditioning of the material. As the moisture take-up is a very slow process, thorough planning ahead is essential. In the present study mostly material in a dry condition is used for the tests. It is therefore stored in a vacuum oven at approximately 45°C. Storage in a sealed container with silica gel proved not to be feasible as the composite took up moisture.

The material is now ready for being tested and needs to be machined into test pieces as required by the appropriate standard.

3.2 Test Piece Preparation

Test Piece Fabrication

The precision of the test piece is vital for successful compression testing and a prerequisite for meaningful test results. On the other hand the preparation of test pieces is time consuming and therefore expensive, so that a reduction of the effort is highly desirable. This is true in particular for tabbed test pieces as required for many mechanical tests. A major objective of the present investigation is to keep specimen production and the testing procedure as simple as possible. The process described below has proved to be adequate to generate specimens of the required quality with reasonable effort. It is divided into the following steps for tabbed test pieces:

1. Determine the main fibre axis and cut the composite panel to the dimensions required with appropriate allowance for machining after bonding. An allowance of 1 mm on each end has proved sufficient (Figure 3.2-1). The minimum width w and the length h of the plate to be cut amount to:

$$w = nw_i+(n-1)c$$

$$h = 1+2m$$

where n is the number of test pieces, w_i is the test piece width, c is the width of the sawing slit and m is the machining allowance.

2. Cut the end tab plates to size with the same allowance as for the composite panel (see Figure 3.2-1). Woven glass fibre/epoxy which is commercially available in large sheets of different thicknesses has proved to be well suited for tabbing purposes. Using composite tabs rather than metal ones has the advantage that specimen plates manufactured as described below can be cut without problems with conventional diamond tipped saw-blades.

3. Cover the gauge section and, if required, low bond strength area (see Chapter 5) with adhesive cellulose tape. The bond surfaces have to be cleaned of remaining traces of release agent with a suitable solvent, e.g. 1,1,1-Trichlorethane, before grit blasting. This is in order to avoid contamination of the grit.

4. Grit blast the surfaces to be bonded; alumina grit of 0.003" diameter gave good results. Clean surfaces of fine grit dust, preferably with water and let dry thoroughly. Repeat cleaning with 1,1,1-Trichlorethane as the the grit may have been contaminated.

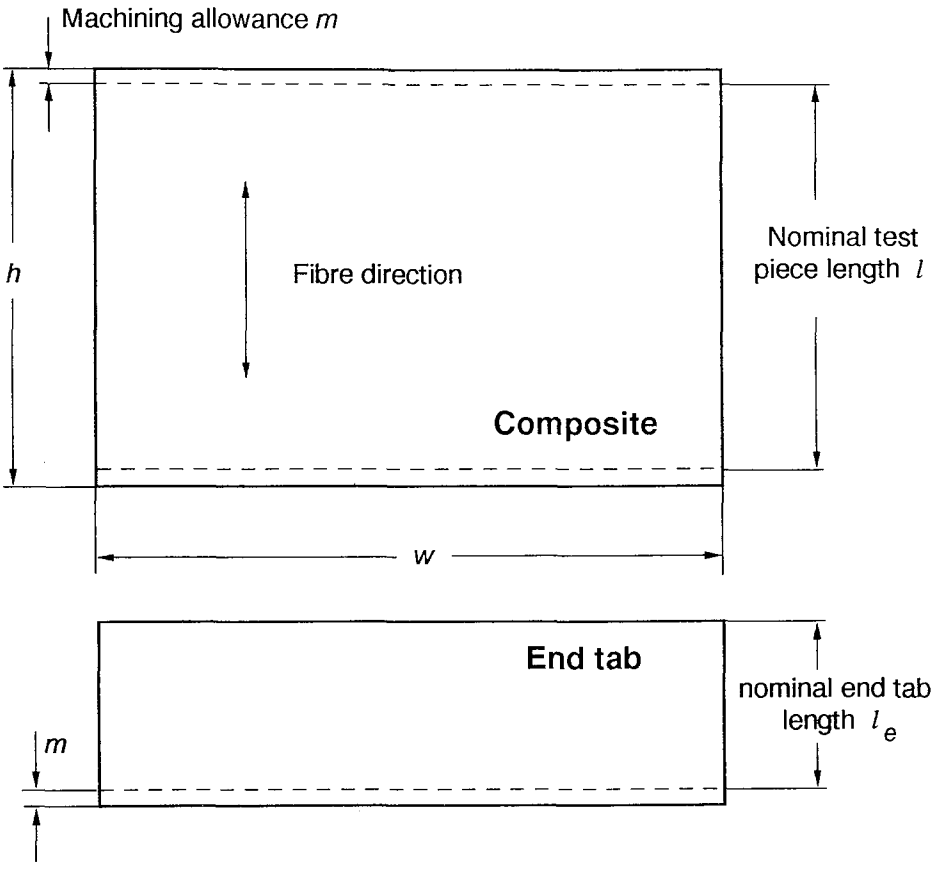


Figure 3.2-1: Machining of the composite panel and the end tab plates.

5. Apply adhesive on all surfaces to be bonded. In the present investigation room temperature setting *Araldite 2001*, a multi purpose two-pack epoxy paste, has been used for all tabbing purposes.

6. Place the end tab plates onto the composite. It is important to ensure that no air bubbles are trapped under the tab. Removing the bubbles by hand pressure immediately after positioning the tab plates gives the best results.

7. Place appropriate silicone rubber shims according to Figure 3.2-2 in order to ensure that the correct gauge length is maintained during the curing of the adhesive. Symmetric shimming is essential in order to produce a symmetric test piece. Then put the assembly onto a flat plate and adjust it as shown in the figure.

8. Put the set-up under a vacuum bag and allow the adhesive to cure. Loading with weights led to unsatisfactory results. If vacuum is applied the bond line thickness is fairly constant (around 0.1 mm) even without using spacers or filling particles in the adhesive.

9. After curing remove excess adhesive, determine the reference edge (surface 'b' in Figure 3.2-3), and trim the plate to the appropriate length *l*. This ensures that, without further effort, the ends of the individual specimens (surface 'a' in Figure 3.2-3) will later be square to the specimen axis. An accurately machined rectangular steel plate is a simple and effective guide if the saw is not equipped with a transverse carriage or if the carriage has too much play in order to give satisfactory results.

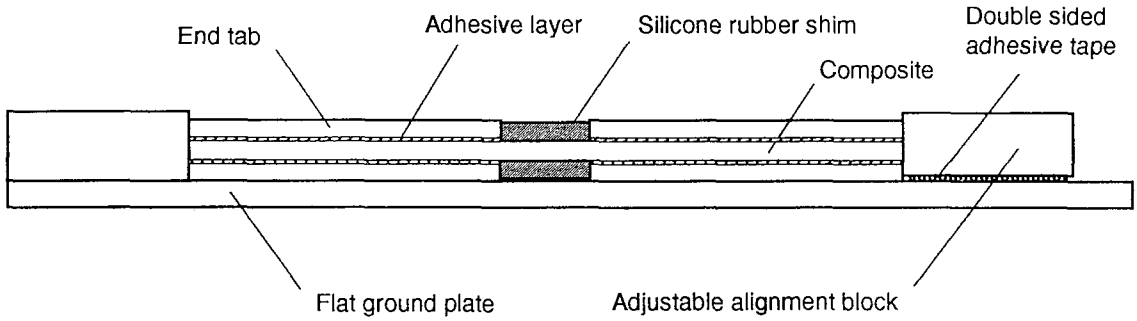


Figure 3.2-2: Test piece plate assembly.

10. Cut individual test pieces to the desired width using a saw-blade of 600 grit or, better, 800 grit, leaving an allowance for further grinding of the edges if required.

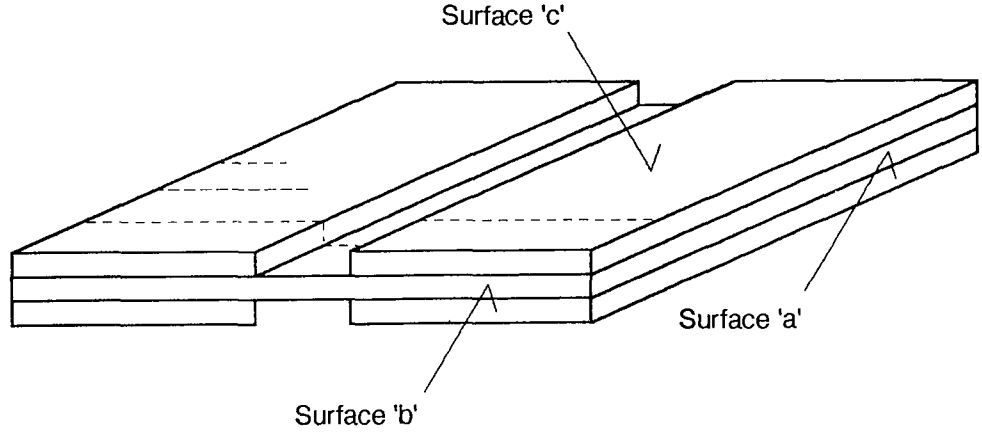


Figure 3.2-3: Final composite plate ready for cutting into individual test pieces.

11. Grind surfaces 'c' (Figure 3.2-3) manually on a flat surface with coarse emery paper, e.g. aluminium oxide paper 80 grit. The flatness of these surfaces is

important for the specimen alignment and can be improved significantly by this simple process, provided only gentle pressure is applied. The flatness can be checked easily and very effectively by stacking up the test pieces and looking at the gap between them. Typical values r (see Figure 3.2-4) for the unevenness of the tabs are up to 0.5 mm along the specimen length. Manual grinding can reduce the value to less than 0.05 mm.

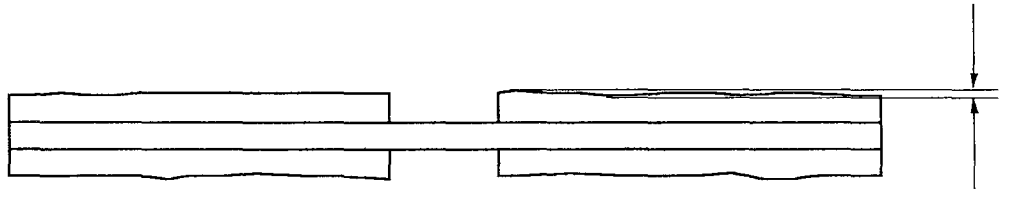


Figure 3.2-4: Illustration of the test piece surfaces to be ground flat.

The procedure for untabbed test pieces is simpler. The test piece is cut to the required dimensions from the panel. Care clearly must be taken to ensure square ends if the specimens are to be tested in compression, e.g. cross ply laminates (see Chapter 5).

A problem which can occur is furring of the edges during cutting when the surface fibres are not parallel to the cutting direction. This can be avoided by using a support, e.g. a glass/epoxy plate.

Measurement of the test piece dimensions

Some attention should be given to the measurement of the specimen dimensions as they directly affect strength and stiffness results.

All measurements in the present investigations are carried out using a micrometer with flat ends of approximately 6 mm in diameter. Width and thickness are determined to 0.01 mm.

The thickness of short compression specimens is usually measured as a mean value across the width of the specimen at the centre of the gauge section. For long specimens the mean thickness is either determined from several measurements along the length of the specimen or, in the case of strain measurement with strain gauges, from measurements across the width at the vicinity of the strain gauge.

Due to the nature of composite production the thickness of the panel can vary depending on the peel plies used. The standard peel ply used in this study leaves a pattern of approximately 0.02 to 0.04 mm roughness depth on the cured laminate. This

pattern consists purely of resin absorbed by the peel ply resulting in a mirror image of the fabric texture, and the surface fibres do not seem to be affected. Figure 3.2-5 illustrates this fact and research at RAE (Curtis and Whitehead, 1990) confirms the finding. Strictly, this resin layer should be removed before measuring the specimen thickness, especially when the test results are compared with results gained using specimens with machined gauge sections. Typical values for a standard test piece were found to be:

Average thickness as cured:	2.15 mm
Average thickness, surface resin slightly abraded:	2.09 mm

This is a difference of 2.8 % which should not be neglected. The measured surface roughness for panels with a coarse peel ply is quoted as 13.1 μm and 0.65 μm for smooth film in the RAE report. In the present investigation, as strain gauges are used for strain measurement in most cases, the surfaces are lightly abraded before strain gauge application, thus correcting the thickness measurement. If no strain gauges are used and the thickness of the composite as manufactured is measured, it is quoted separately in each case.

An attempt to normalise fibre volume fraction and to avoid inclusion of the resin rich areas on the surface is seen in the frequently practised method of using the nominal rather than the actual thickness of the laminate.

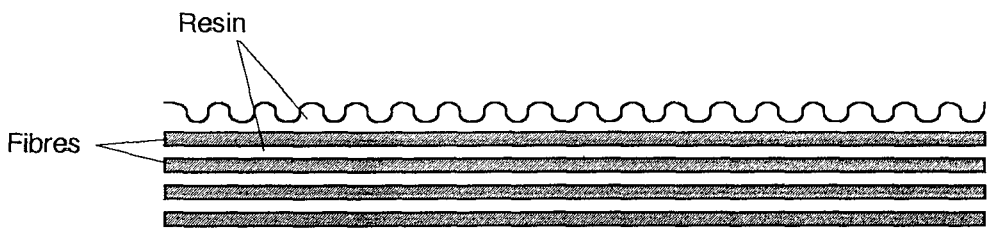


***Figure 3.2-5:** Illustration of composite surface roughness.*

Application of strain gauges

As recommended by many standards, strain gauges are preferred for strain determination in the test pieces in the present investigation. Strain gauges are usually connected to a 'Wheatstone bridge', a balanced circuit which enables one to record small changes of its resistance members. The circuit shown in Figure 3.2-6 with three fixed resistors and one variable one, i.e. a strain gauge, is called a 'quarter bridge'. A quarter bridge allows the recording of the signal of an individual strain gauge. Bending effects during the test can be assessed if the test coupon is provided with gauges on both faces. Any difference in

the signals of these then indicates bending. Typically, strain gauges designed for mild steel with a nominal resistance of 120 Ω, a gauge factor k of about 2, and a gauge length of 2 mm are used. The short gauge length is not optimum for fibrous composites, but as the gauge length of the standard compression test coupon is typically only 10 mm there is no space for longer strain gauges. For reasons of comparison most of the other test pieces, such as tension or four-point bend test coupons, are equipped with strain gauges of a similar length.

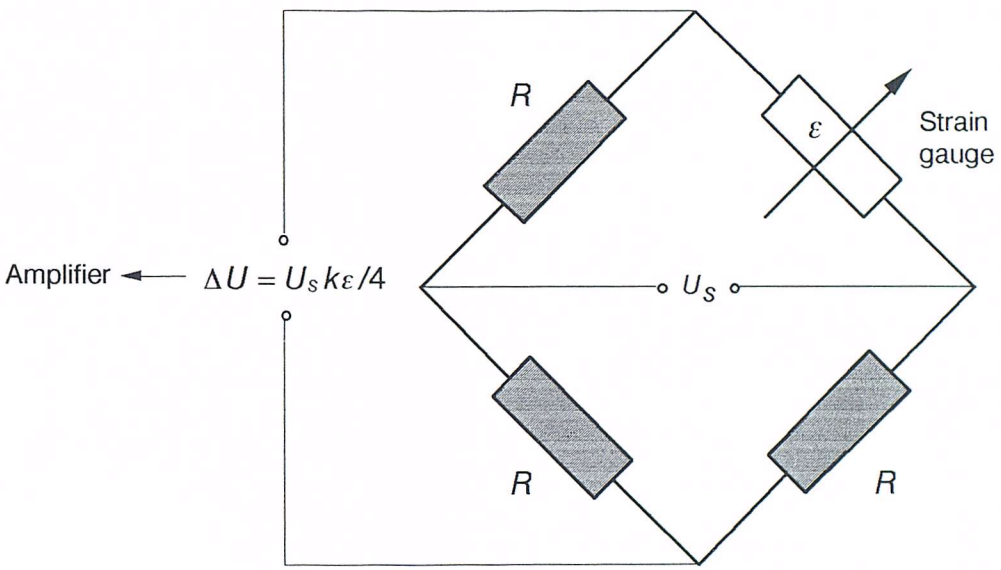


Figure 3.2-6: Resistors and strain gauge arranged as a 'Quarter Wheatstone Bridge'.

Care has to be taken when applying the strain gauges to the test coupons. The following procedure is used and yields satisfactory results in the present investigation.

Firstly, all traces of release agent have to be removed using a suitable solvent, e.g. 1,1,1-Trichlorethane. Then the area where the gauge is to be positioned is carefully abraded with fine (800 grit) emery paper. The thickness of the coupon has to be measured now and the area cleaned again. After that the strain gauge is placed on a strip of transparent adhesive cellulose tape so that the adhesive can be applied onto the carrier surface. Fast hardening Cyanoacrylate adhesive proved to be suitable for this purpose. The adhesive tape now allows adjusting of the strain gauge in the desired position before pressure with an appropriate stamp of soft rubber is applied for approximately 30 seconds which is sufficient for the Cyanoacrylate adhesive to harden. Finally, the tape can be peeled off.

Alignment by eye is quite satisfactory for the small test sections of the compressive coupons and can hardly be improved by grid lines. On wider test pieces, however, it is advisable to mark the position of the strain gauge with fine grid lines, preferably omitting the area where the gauge is actually bonded.

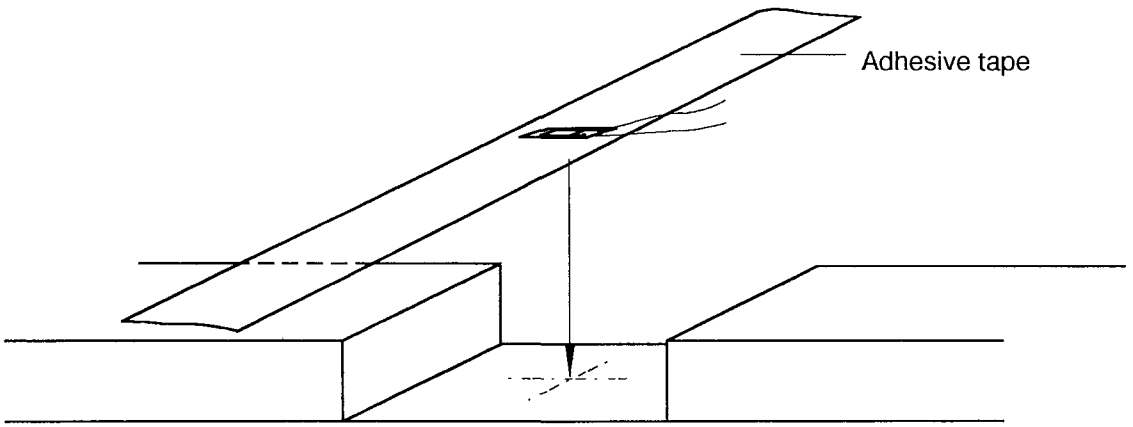


Figure 3.2-7: Illustration of the technique used to apply strain gauges.

In the present investigation strain gauges with wires already soldered on are used; no further attention to the strain gauges is then necessary. Clips used to connect the strain gauge leads to the bridge reduced the effort significantly compared to a soldered connection. Care, however, has to be taken to ensure that the clips are in good condition and the connection is properly made. Insulating the strain gauge wires with appropriate silicon rubber sleeves prevents unwanted contacts with the conductive CFRP or with the test rig.

3.3 Testing Equipment and Data Acquisition

The mechanical tests are carried out on a screw-driven ZWICK 1488 universal testing machine with a load capacity of 200 kN. For compression tests stiff steel plates of 50 mm thickness with suitable holes for the compression or bending jigs are mounted onto the crossheads. The machine can be controlled by a BBC Master computer and data from the testing machine are recorded by the computer. In-house developed software allows the recording of load and crosshead displacement as well as four additional analogue channels, e.g. strain gauge amplifier output, through an analogue input port. The data are acquired at a rate of between 2 and 3 sets of data per second and stored

internally so that they can be saved on disk files when the test is completed. The software includes some data processing utilities such as averaging, curve fitting and plotting routines. In most cases, however, the data are transferred onto a Macintosh computer where interactive data processing routines of high standard as well as compatible word processors are available.

As mentioned before, strain gauges are employed for most strain measurements. The strain gauge amplifiers were developed in-house and have a fixed gain setting of 500, i.e. with a source voltage $U_S \approx 1V$ the amplification factor is about 500. In some tensile tests the built-in extensometer on the Zwick machine is used for comparison.

The axial modulus of elasticity is usually calculated as the 0.25% secant modulus from third order curve fits of the experimentally determined stress-strain curves.

3.4 Fractography

Fractography is essential for assessing failure modes of composites. Both light and electron scanning microscopy are used to examine fracture surfaces of test pieces.

The samples for light microscopy are cast into fast hardening polyester resin. The surface of the resin block which contains the composite surface is ground first on a rotary grinder on watered silicon carbide paper of 240 grit or a similar roughness. In the next step paper of 600 to 800 grit is used. The finishing polish is achieved by a synthetic cloth-covered rotary plate with polishing fluid added. The time which is required to get a desired finish depends on the type of matrix and on the orientation of the fibres on the surface. 'Over-polishing' results in eroding the fracture surface and sediment of polishing material is built up. This falsifies, for instance, the fibre diameters when preparing 90° samples for assessing fibre volume fraction. Too little polishing, obviously, leaves part of the fibre segments covered with resin.

The polished sample is then examined under a light microscope. The microscope used has objectives with a range of magnifications and a camera is attached to it.

Scanning electron microscopy is used in some cases to analyse compressive fracture surfaces in order verify certain failure modes. For this purpose the samples have to be coated with a thin layer of gold which is done in a low vacuum Argon atmosphere. The magnification used ranges from 50 to 10000.

CHAPTER 4 PRELIMINARY COMPRESSION EXPERIMENTS

The term 'preliminary' has been chosen because the results presented are not intended to be used as base line data. The idea behind the experiments was rather to verify some of the findings in the literature, particularly the variation of ultimate compressive stress with the test method used. The findings of these preliminary investigations should help to understand the most important parameters regarding testing hardware and therefore help to choose a test method for the main experiments. It was thought that a chronological sequence of the investigations would account best for the problems encountered with compression testing. Some of the test data have been produced in a mechanical testing short course at Imperial College, others by the author himself. Since the tests during the course were supervised, the data created are regarded as comparable. In Chapter 6 further comparative testing using XAS/914C will be described.

4.1 Comparative Compression Testing

The material used in the following investigations is the experimental grade high strength intermediate modulus CFRP system, Fiberite HYE/1682AW. Specimens were manufactured as described in Chapter 3, but rather than room temperature curing epoxy paste a high temperature curing film adhesive was used for end tab bonding. The end tabbing material was 0/90° glass fibre/epoxy in all cases. The test methods used were CRAG, IITRI, modified ASTM D695 and the Birmingham method to represent load introduction by shear as well as mixed shear/end-loading (compare Figures P-2 and P-3). In addition, specimens designed for one jig were tested in other jigs in order to allow an assessment of the influence of load introduction. Details of the Birmingham fixture can be taken from Barker and Balasundaram (1987). The CRAG recommended loading fixture is a modified Celanese jig which has been described in Chapter 2. Test piece dimensions are summarised in the Figure F-1 in the sections CRAG-1, IITRI, ASTM-1. The dimensions of the test piece for the Birmingham rig are given in Figure 4.1-1.

Note that the modified ASTM D695 test piece had a nominal laminate thickness of 2 mm since only a 16-ply laminate was available. These are the same dimensions as in the investigation by Woolstencroft et al. (1981), whereas SACMA recommends the use of a 1 mm laminate and unidirectional CFRP tabs.

Most of the specimens were manufactured for a testing short course at the Centre for Composite Materials. The thickness of the 16-ply unidirectional laminates varied between 2.05 and 2.25 mm, although they were moulded to a nominal thickness of 2 mm. In

order to correct the consequent variation of fibre volume fraction a nominal laminate thickness of 2 mm was assumed. This was thought to normalise fibre volume fraction to 60%.

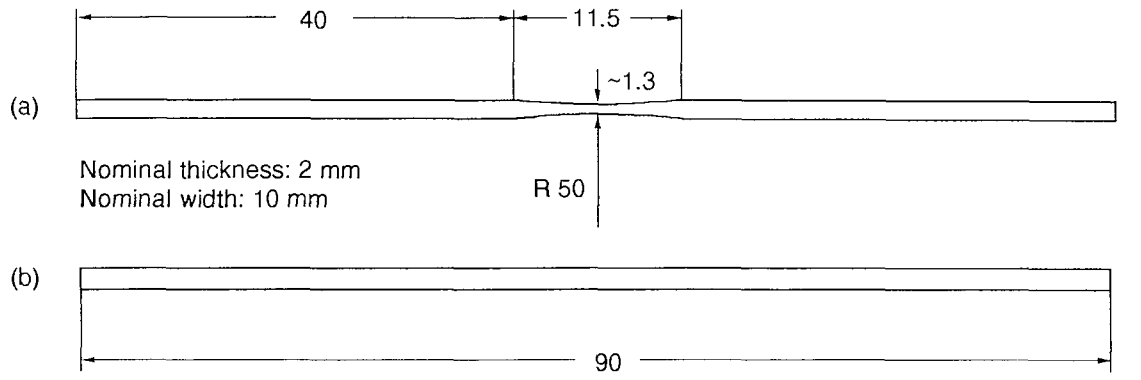


Figure 4.1-1: Dimensions of test pieces tested in the Birmingham fixture; (a) waisted, (b) plain specimen.

The results of the compression test are given in Table 4.1-1 and 4.1-2 and the test conditions are explained below.

Test Method	N	Compressive Strength [MPa]			σ_{n-1}	C_V
		Mean	Min	Max	[MPa]	[%]
CRAG	21	**1068**	752	1285	119	11.1
ASTM D695 a	24	**1460**	1102	1665	127	8.7
ASTM D695 b	15	**1457**	1236	1665	113	7.8
ASTM D695 c	8	**1431**	1313	1489	59	4.1
ASTM D695 d	8	**1517**	1411	1680	83	5.4
IITRI a	10	**1006**	825	1202	110	10.9
IITRI b	6	**1238**	1207	1291	35	2.8
ITAS	4	**1373**	1323	1428	44	3.2
CRAS	4	**1298**	1212	1357	63	4.9
BI a	7	**954**	906	1047	68	7.2
BI b	5	**1096**	1080	1159	36	3.3
BIWA	4	**1033**	966	1095	69	6.7

Table 4.1-1: Results for the compressive strength of HYE/1682AW using different test methods.

Test Method	N	Compressive Modulus [GPa]			σ_{n-1}	C_V
		Mean	Min	Max	[GPa]	[%]
CRAG	21	**133**	120	147	8.8	6.6
ASTM D695 a	22	**132**	121	145	5.9	4.6
ASTM D695 c	6	**131**	123	138	5.5	4.3
ASTM D695 d	8	**131**	127	137	3.7	2.9
IITRI a, b	13	**130**	128	132	1.1	0.9

Table 4.1-2: Results for the compressive axial modulus of elasticity of HYE/1682AW using different test methods.

The abbreviations used in the tables are:

ASTM D695

a: all specimens of testing course, specimens cut on a diamond saw.

b: specimens of testing course, end failures excluded.

c: specimens HA1-HA8; specimens same as 'a' but surfaces of end tabs (surface 'c' in Figure 3.2-3) manually ground; one operator.

d: specimens HA9-HA16, surfaces of end tabs and test piece ends machined flat and parallel on a milling machine; one operator.

IITRI

a: normal gripping of the specimen; gauge length, therefore, is 12.5 mm; one operator.

b: end tab tips emerge approximately 2.5 mm from wedge grips resulting in an unsupported length of about 18 mm; one operator (see Figure 4.1-2).

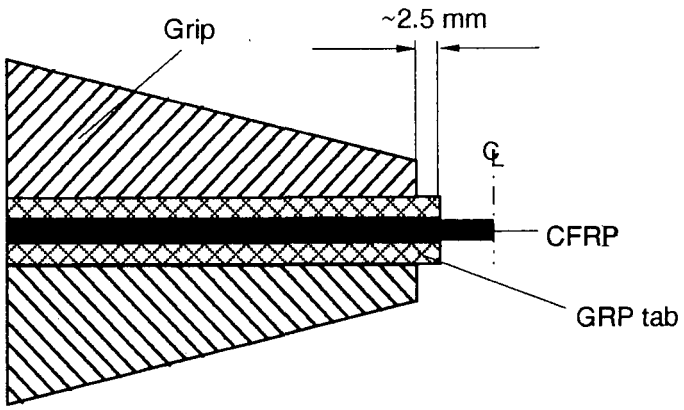


Figure 4.1-2: Modified gripping of the test piece using the IITRI method.

ITAS: IITRI specimen tested in ASTM D695 support jig; only failures within gauge section of the specimen regarded as valid; end failures excluded.

CRAS: CRAG specimen tested in ASTM D695 support jig; specimen gauge sections were slightly damaged by excessive grit blasting, which could result in lower compressive strength.

BI

a: flat unwaisted specimen (Figure 4.1-1(b)) tested in Birmingham rig; both clamping bolts tightened with a torque of 15 Nm.

b: as 'a' but bolt near specimen end: 15 Nm; bolt at gauge section: 5 Nm.

BIWA: waisted specimen (Figure 4.1-1(a)) tested in the Birmingham rig; compressive strength calculated from real cross-sectional area; therefore no normalising to 60% fibre volume fraction.

4.2 Failure Modes

Failure of unidirectional CFRP was catastrophic in all cases. This led to destruction of the fracture surfaces, the more so since in displacement controlled experiments on a screw driven machine there is no possibility to release the load acting on the specimen after fracture. Even on stiff load-controlled hydraulic systems, the chance of arresting failures is very small due to the elastic energy stored in the test pieces just before failure.

When failure occurred in the centre gauge section the test piece was partitioned into two pieces with fracture surfaces inclined at a typical angles of between 15° and 25° in either the width or thickness direction. End failures as described below offered the opportunity to examine arrested failures. There it was found that failure of the composite was due to microbuckling of the fibres forming a kink band, which is in agreement with most publications. Figure P-4 shows several cases where a complete band of buckled or kinked fibres was preserved. Since the characteristic kink band angle is similar to the fracture surface angle of test piece fragments, though usually slightly larger, there is little reason to doubt that failure in general is by microbuckling and kinking of fibres. In almost all cases kink bands started at locations of stress concentration due to load introduction, i.e. at the end of end tabs where the specimen emerges from the clamps or at the loaded specimen end.

The fracture surfaces usually exhibited some longitudinal splitting and interlaminar cracking, a fact which is attributed to post-failure damage rather than being a failure cause. At low failure stresses the surfaces were smoother with less splitting. Some observations to strengthen the assumption of the splitting being post failure damage will be presented in the following chapter. Figure 4.2-1 summarises the basic failure modes found in the CFRP composite examined.

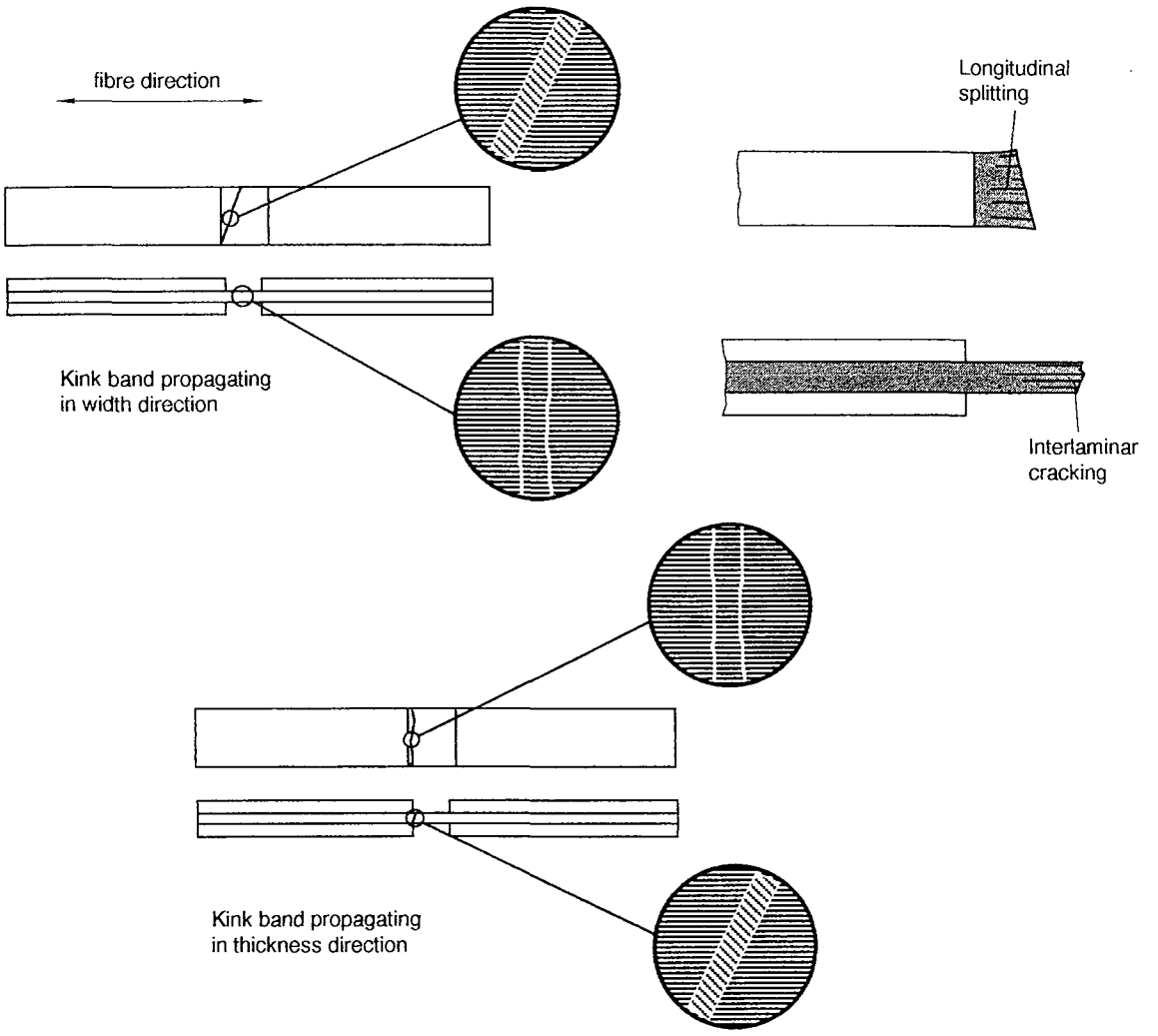


Figure 4.2-1: Main compressive failure modes of unidirectional CFRP.

Specific failure modes

Apart from the basic failure modes which are considered to be typical for CFRP, there are certain hardware-induced failure modes which have to be regarded as invalid in certain cases. In general, the most typical failure modes of the individual test methods are:

ASTM D695, modified specimen

Specimens fail by kinking of fibres across the width (compare Figure P-5(a)) as well as across the thickness of the gauge section.

Invalid

Three different invalid failure modes have been identified (Figure 4.2-2):

1. Kink bands under the end tab
2. Shear failure of the specimen end
3. Complete debonding of the end tabs, partly with delamination of CFRP surface layers (compare Figure P-5(b)).

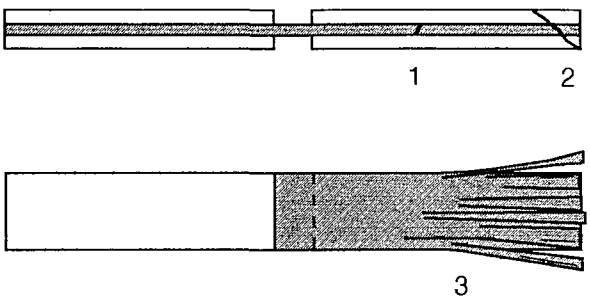


Figure 4.2-2: *Typical invalid failures of the modified ASTM D695 test piece.*

CRAG/IITRI

Kinks across the width as well as kinks across the thickness are observed, the latter ones more frequently. Kink bands often propagate underneath the tab rather than into the free gauge section. In many cases both occur simultaneously apparently initiated at the same location, or possibly one causing the other.

Invalid

Fracture initiated underneath tab.

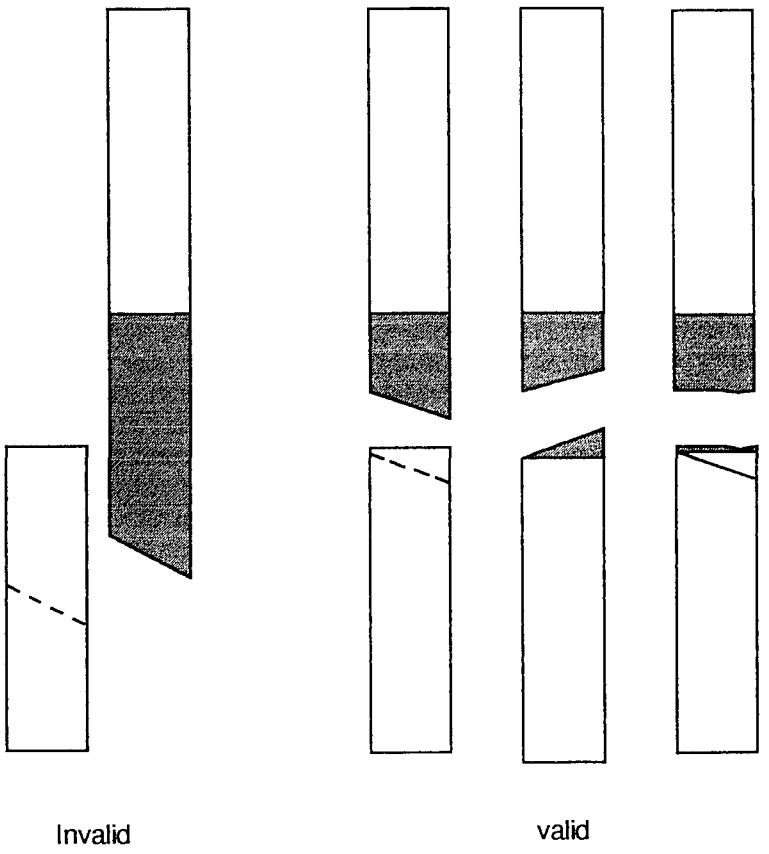


Figure 4.2-3: *Typical test piece failures CRAG/IITRI.*

Birmingham method

Flat unwaisted specimens fail in the two main modes where the specimen emerges out of the end block (see ASTM D695), if the force transmitted by shear is high enough.

The waisted specimens usually fail in the centre of the waist by fibre kinking across the width. In some cases failure was preceded by a crackling sound. This was caused by delaminations as illustrated in Figure 4.2-4, although the specimen is designed to avoid interlaminar shear failure (Equation 2.1.2-1). The test piece then fractured where it emerges from the grips.

Invalid

Both specimen types fail prematurely at the end as illustrated in Figure 4.2-5 when the clamping force is below a critical value. The angle of kinks in the restrained region is often greater than in the non-restrained region.

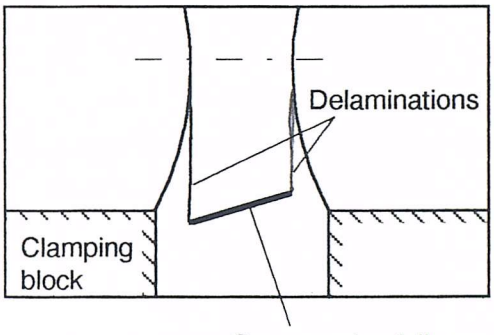


Figure 4.2-4: Delaminations and consequent compressive failure in the Birmingham (RAE-type) test piece.

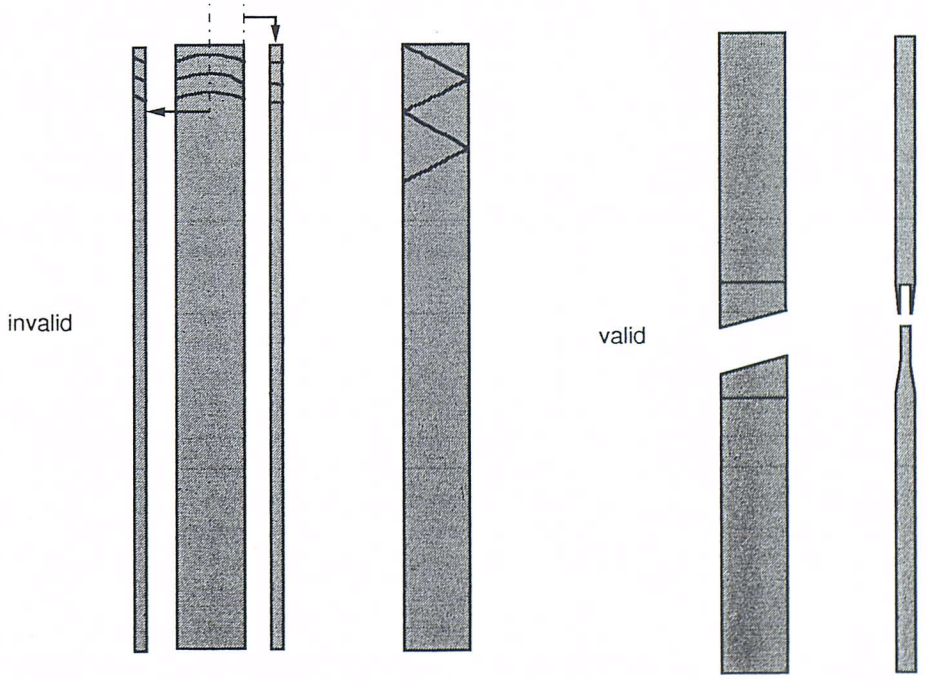


Figure 4.2-5: Compressive failure modes of the Birmingham method specimen.

4.3 Discussion of Test Results and Conclusions

The easiest method to use was the modified ASTM jig where mounting the specimen and the jig is very simple. A further advantage of the rig is that it is very small and light. The Birmingham method also proved to be user-friendly. The massive construction of the IITRI rig, which weighs about 250 N, made testing a tiring exercise. Adjusting the shims of the CRAG jaws to the specimen thickness was cumbersome, and often the test piece slipped and the test had to be restarted.

As expected, significant variation of strength results, and little variation of modulus of elasticity results, were recorded when using different compression test methods. The dominant fact is that ASTM results are considerably higher than the results of the other methods.

The relatively low values that CRAG and IITRI methods yielded are attributed to stress concentrations which seem to be more severe in the indirect compression test methods. Load introduction always causes stress concentrations, particularly at the vicinity of sudden stiffness changes, such as the ends of tabs and grip edges. The objective of a test method should be that those stress concentrations are at least smaller than any material-inherent stress concentration at voids, curved fibres, and so on. Load introduction by shear leads to higher normal and shear stresses in the surface layers than in the centre, as shown by various finite element investigations (see Chapter 5). If the shear action is by friction the accompanying transverse (through-thickness) compression causes further stress concentrations by curving the outer fibres what may act as a kink initiator. In that way transverse compressive stresses may cause premature failure even if an additional compressive stress may lower the tendency of fibre microbuckling by reducing tensional interface stresses, as pointed out by Woolstencroft (1981).

This supposition is supported by two facts. Firstly, IITRI and CRAG specimens tested in the ASTM anti-buckling guide achieved reasonably higher results than when tested in the original fixtures. Secondly, IITRI specimens with tabs sticking out from the grips yielded consistently about 20 % higher results than the ones with the tab edges flush to the grips, despite the gauge length being increased by almost 50%.

The modified ASTM D695 method yielded the highest strength results, which is thought to be due to the following factors:

1. Low transverse loading of the specimen. The transverse deformation can be considered as very small thus causing low through-thickness stresses. This can be checked by sliding the guide, which was possible even at high loads on the

specimen. The stress-strain diagram also does not show evidence of friction between specimen and jig, which would lead to apparently higher strength results.

2. Load introduction at the ends. The end tabs introduce a portion of the load by shear to the specimen, similar to the RAE method where a portion of the load is transmitted by the bond. This method of load introduction seems to generate smaller stress concentrations, provided that the tab stiffness is appropriate.
3. No jig-induced bending of the specimen.
4. The short gauge length possibly generates a non-uniform stress field suppressing certain failure modes.

The biggest problem arising with this method was the failure of the specimen end, or debonding or delamination of the end tab. Further investigations into improvement of the end tabbing material and geometry seem reasonable, considering the superior results gained with this method.

The Birmingham method led to similar results to the indirect methods (e.g. CRAG, IITRI). Unwaisted untabbed specimens gave strength values of about 1000 MPa. Reducing the clamping stress where the specimen emerges from the end block raises this value by about 10% with the specimen now failing at the end. Experiments with different specimen widths and sandwiching the test pieces between aluminium sheets of different thickness did not improve the results significantly.

Surprisingly, waisted specimens gave similar results to the unwaisted ones. Due to the better specimen design one would have expected higher strength values. The reason for that is most likely buckling of the test piece plus the fact that the slot into which the specimen is fitted was not flat, which might have caused additional stresses. Buckling could not be verified as no strain gauges were applied. The gauge lengths of the specimens, however, were found to be between 13 and 14 mm rather than the specified 11.5 mm, adding some weight to the argument. A first step to further examination of this method will be the redesign of the given fixture as described in the next chapter. Another improvement is to be expected by increasing the accuracy of machining the waist into the test piece.

The results of these preliminary tests make a combination of a Birmingham-type loading rig and a tabbed specimen look promising. It was therefore decided to look closely into this option. At a later stage this proposal will be qualified against the standard test methods.

CHAPTER 5 DEVELOPMENT OF A MODIFIED COMPRESSION TEST METHOD

Following the findings of the previous chapter an attempt has been made to devise a test procedure which combines the advantages of the test methods examined and avoids their shortcomings. A major objective was to keep the rig and the specimen as simple as possible. Carrying out the test should be simple without sacrificing repeatability and reproducibility of the test results. These two terms can be used to characterise a test method and can be distinguished in the following way:

Repeatability	**Reproducibility**
same method	same method
identical material	identical material
same lab	different lab
same equipment	different equipment
same operator	different operator
different sessions	different sessions

As the main parameters influencing compression test results the following are suggested:

Test method	1. Method of load introduction
	2. Geometry of the test piece
	3. Mechanical properties of tabbing
Laboratory/operator	4. Method of laminate and specimen production
	5. Condition of testing hardware
Operator	6. Care taken in performing the test
	7. Assessment of results

The first point, test method, is discussed in the current chapter. The method of laminate and specimen production has been addressed in Chapter 3 and the need for standardisation has been stressed. The condition of testing hardware, e.g. parallelism of loading surfaces or the calibration of the load cell, can obviously influence results and can be regarded as being part of the 'operator influence'. The 'operator influence', naturally, is not easy to define and often held responsible for a number of effects. In particular, the assessment and interpretation of failure modes and test results is important in this context and dependent on the experience of the tester. For example, partial loading of the rig will produce misleading results unless the stress-strain curves are examined critically. The aim of a test method should be to keep the possible influence of the operator as small as possible. The following Figure 5-1 tries to summarise the effects in compression testing and is thought to be a check list for potential testers.

Test Method	Test Piece Preparation
Method of load introduction - Shear - Mixed end/shear - (End) **Test piece geometry** - Width - Unsupported length - Thickness **Tabbing material** - Aluminium - Steel - GRP - CFRP	**Method of laminate production** - Prepreg lay-up procedure - Curing cycle - Curing device (Pressclave, autoclave, heated press) **Method of specimen production** - Bond surface preparation - Tabbing adhesive properties - Symmetry of tabbing - Alignment when machining - Specimen surface finish
Equipment	**Operator Influence**
Calibration - Load cell - Transducer, etc. - Strain gauges **Accuracy** - Parallelism of testing machine surfaces - Alignment of compression rig	**Measurement of test piece dimensions** - Micrometer, vernier, etc. - Removal of resin pimples **Care taken in carrying out the test** - Checking of alignment - 'Zero-load' at test start **Analysis of test data** - Assessment of failure modes - Classification of valid/non valid failures - Check of unlikely results - Method of modulus determination

Table 5-1: *Factors influencing the results of compression tests*

5.1 Test Fixture Design

The proposed new method, referred to as the ICSTM (Imperial College of Science, Technology and Medicine) method in the following, uses a specimen configuration similar to the modified ASTM D695 specimen; this is a tabbed specimen which is loaded purely on the ends. A portion of the load is therefore transmitted by shear via the end tabs, thus lowering the average stresses at the end of the test piece.

The loading fixture is similar to the one developed at Birmingham University by Barker and Balasundaram (1987) with some significant design changes, as described below. The fixture consists of two end blocks which accommodate the specimen end and prevent debonding of the tabs from the specimen end, shear failure of the end or compression failure under the tab, which are all the problems encountered with the ASTM method. The blocks rest on hardened and ground steel plates, a measure which is necessary in order to avoid indentations of the loading surfaces. One has to bear in mind that compressive stresses of up to 2 GPa can be realised in CFRP coupons. As can be seen from Figure 5.1-1, where an exploded view of the fixture is shown, the important parts are very simple. They can easily be machined flat and parallel on conventional milling machines and grinders. Great accuracy can therefore be achieved with little effort. Remachining of the surfaces, if necessary due to wear and tear, again, is straightforward and does not require specialist attention.

The high precision die set is commercially available and can be used for other test methods, where parallel loading surfaces are required, thus further reducing the costs. The lower block is not attached to the lower plate of the die set in order to keep the risk of additional constraints during testing, e.g. bending of the test piece due to misalignment of the upper and lower block, as small as possible.

One of the design changes with regard to the Birmingham fixture is that the hardened loading plate is bolted to the floating end block. This was found to improve the quality of alignment significantly as great care in setting up the test was needed in order to ensure that the specimen did not protrude from the block when the end block was open. This, in turn, would allow rocking of the block introducing bending. Another important design change is that surface A-A in Figure 5.1-2 is flat rather than provided with the slot to accommodate the specimen as in the Birmingham design.

An advantage of the fixture is that a variety of test pieces can be accommodated as shown later in the section about specimen design. It was mentioned before that Barker and Balasundaram (1987) tested untabbed, waisted, specimens referred to as the 'Birmingham method'. There the clamping bolts have the task of providing a certain

amount of frictional loading of the test piece. The proposed method relies on the shear load being mainly transferred through the end tabs in order to avoid high transverse stresses. These stresses are believed to cause additional curvature of fibres in layers near to the surface thus encouraging premature failure. This is not surprising as all transverse deformation of the test piece must be translated into surface deformation which in turn leads to short wave fibre deflection. It is suggested that, even when the tab is tapered or when the grips do not cover the whole tab, this effect causes premature failure.

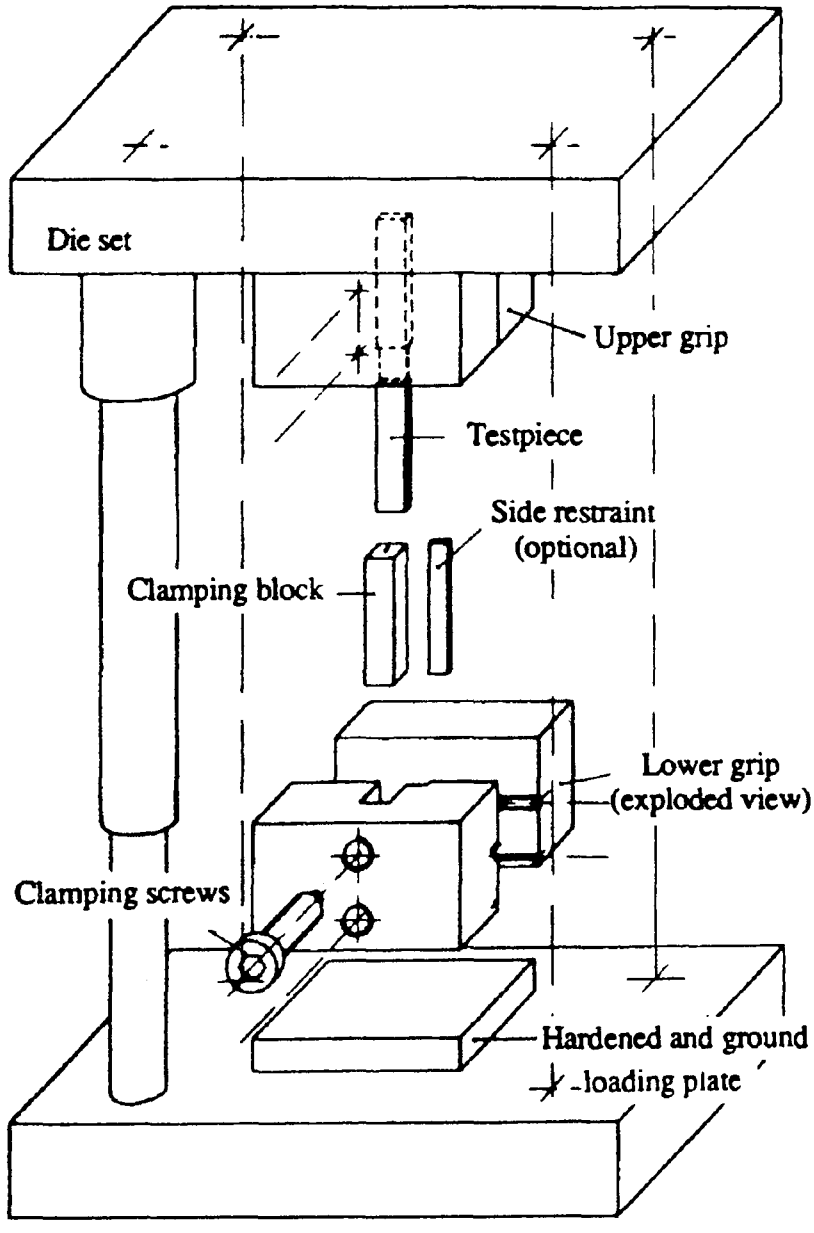


Figure 5.1-1: ICSTM compression test fixture; exploded view.

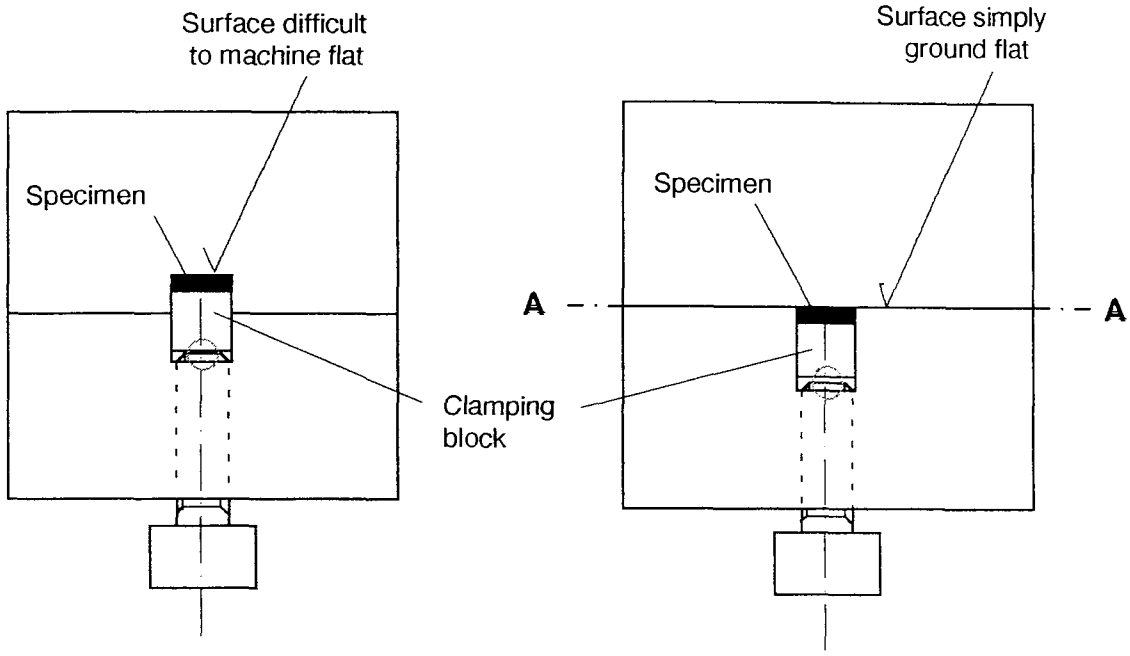


Figure 5.1-2: End blocks of Birmingham and ICSTM rig, respectively.

Figure 5.1-3 illustrates the effect of transverse stresses on surface layers. The micrograph in Figure P-6 shows a small section of a compression test piece including the tab-gauge length region compressed transversely in one of the end blocks described above. Although the stresses acting are difficult to determine - at least one can state that they are well below transverse failure stress -, the micrograph clearly shows the effect of these stresses. Fibre bundles close to the specimen surface are curved, and transverse stresses reach quite significant levels, as shown by the FE analysis (Section 5.2.1), with indirect compression test methods. Figure P-7 shows a micrograph of compressive failure in a unidirectional CFRP test piece (CRAG) initiated at the tab tip.

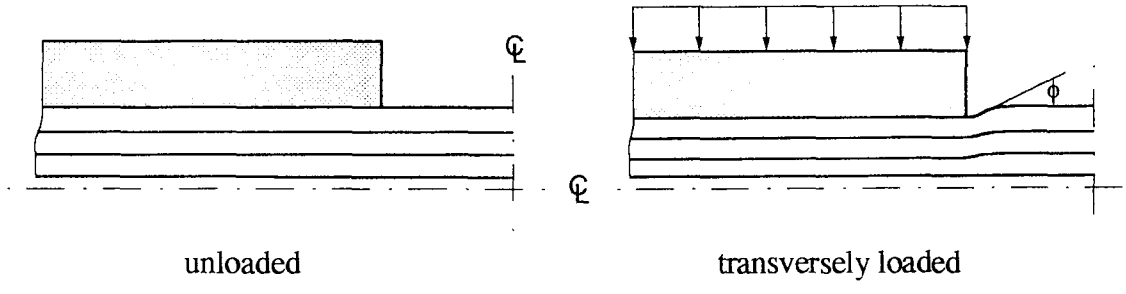


Figure 5.1-3: Illustration of the effect of through-thickness stresses on surface fibres.

From the above it is clear that the test piece ideally should not be clamped tightly but rather kept in position only with as little transverse pressure as possible. Testing experience, however, showed that a certain amount of clamping force, i.e. a certain

torque on the clamping bolts, is necessary to obtain consistent and satisfactory results as pointed out in Section 5.3.

The optional side restraint shown in Figure 5.1-1 proved to be only of limited use in practice. Originally it was designed as an aid for reliably adjusting test pieces with smaller than nominal width. It was found that this could easily be done without the support. The other intention was to create a hydrostatic pressure in the ends of untabbed waisted test pieces in order to avoid end failures. A series of tests using the device, however, showed that the additional in-plane pressure hardly influenced failure.

As illustrated in Figure 5.1-4, the mounting of the rig in the testing machine is done in an 'upside down' fashion. Two bolts attach the upper part of the rig to the upper crosshead of the testing machine. The lower parallel plate of the die set is equipped with a round ended loading pin which contacts the lower crosshead on a hardened steel plate. This steel plate is mounted so that it can rotate and act as a quick release of the rig reducing the time of changing the specimen.

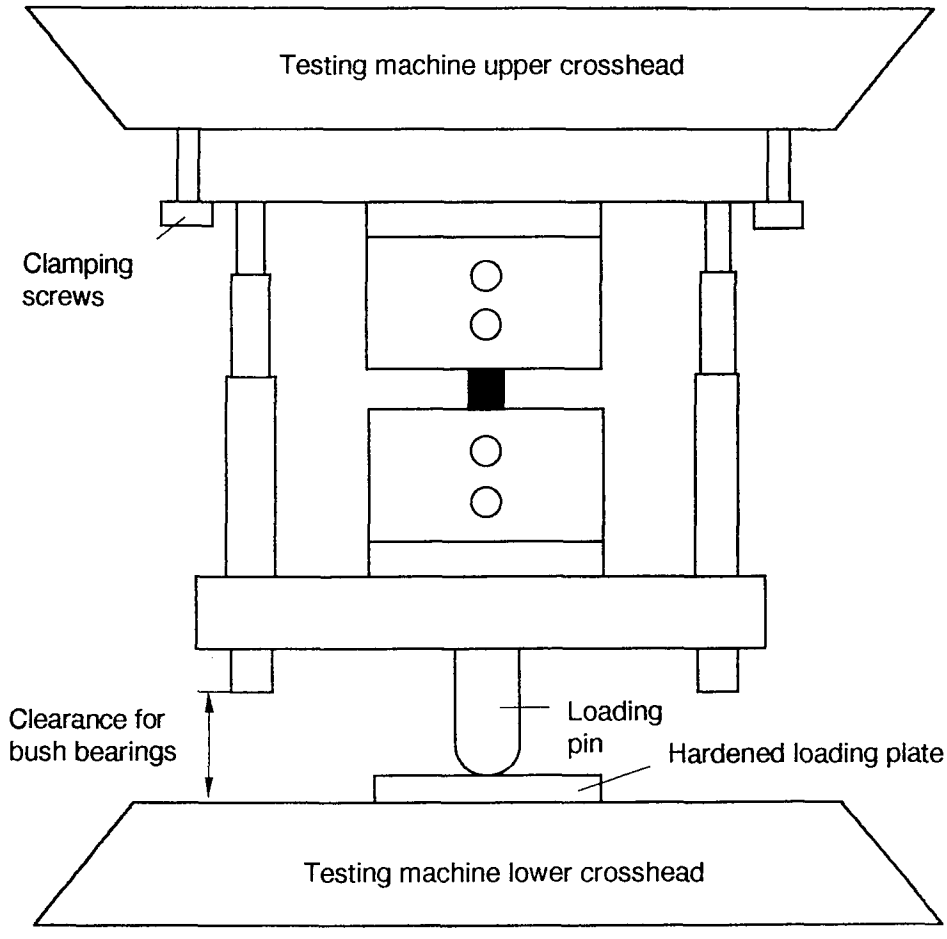


Figure 5.1-4: *Mounting of the compression rig in the testing machine.*

The arrangement guarantees that the weight of the rig is taken off the specimen during the test and that the load is introduced centrally into the test rig. In addition, mounting of the complete rig is extremely simple and requires very little time.

A further time saving issue is that removing the broken test piece is generally very simple: if fracture occurs in the gauge section the lower block is removed and after untightening the clamping bolts both the broken ends can be removed from the end blocks. The situation is complicated by end failures which can make it necessary to demount the rig and disassemble the block. However, with appropriate specimen design this should be a rare case. Figure P-8 and P-9 show the proposed fixture disassembled and mounted in the testing machine, respectively.

5.2 Specimen design

Compression test pieces should fulfil two requirements: firstly to provide a uniform one-dimensional stress field and secondly to promote a compressive failure of the material rather than macroinstability of the specimen. In other words, the test piece should be long enough for any stress concentrations to decline, and, on the other hand, it should be short enough to avoid buckling. Unfortunately, these requirements are conflicting, given the material properties and standard dimensions of unidirectional CFRP test pieces. High strength and relatively low elastic and shear moduli lead to both long decay lengths as well as low critical slenderness ratios, i.e. the maximum slenderness ratio of a strut where compressive failure occurs before buckling failure. Derived from the basic Euler equations (Chapter 10) the critical slenderness ratio for a column can be expressed as:

$$s_{cr} = \pi \sqrt{C \frac{E}{\sigma_p}} \tag{5.2-1}$$

where E denotes the bending modulus of elasticity, C the clamping condition and σ_p the proportional limit of the compressive stress or yield stress, which equals the ultimate compressive stress for composites. For mild steel ($\sigma_p = 200$ MPa, $E = 210$ GPa) and a typical aluminium alloy ($\sigma_p = 250$ MPa, $E = 70$ GPa) the critical slenderness ratios are about 200 and 100, which for a 2 mm thick test piece with clamped ends ($C = 4$) would correspond to critical unsupported lengths (Equation 10.2.2-2) of approximately 120 mm and 60 mm, respectively. For CFRP (σ_p = 1600 MPa, E = 120 GPa) the critical unsupported length is calculated as only 30 mm. In Chapter 10 it will be shown that including nonlinear material properties lowers the predicted value significantly.

As indicated in Chapter 2, attempts to find an optimum specimen configuration have been numerous, with questionable success, as the variety of published data would suggest. The main factors determining the stress distribution in a compressive test piece, and therefore the measured strength, have been identified earlier in this chapter. As far as the test piece is concerned, these are:

Test piece geometry
Properties of the tabbing material
Bond characteristics
Factors of specimen production.

Each of the factors listed are thought to influence the test result independently. A parametric study regarding these factors was therefore carried out using the proposed test rig. In addition, a finite element study considering some of the parameters was performed in order to aid the experimental programme. The test piece regarded as a preliminary standard in the experiments and the FE analysis is shown in Figure 5.2-1. Apart from the tab length, the dimensions of the CRAG compression test piece for unidirectional composites are accepted. The geometric dimensions varied in the investigations are underlined.

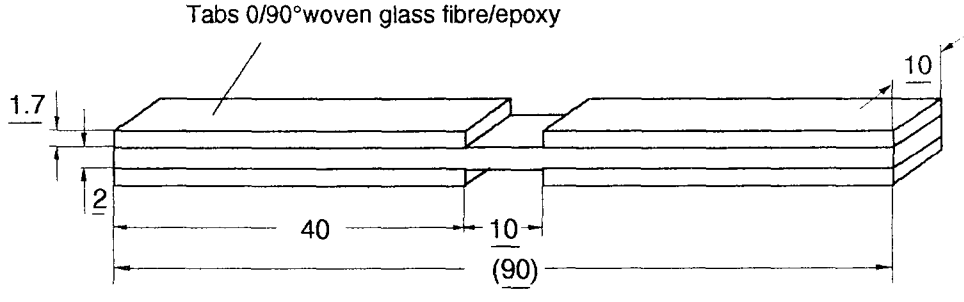


Figure 5.2-1: Preliminary standard compression test piece for the ICSTM method.

5.2.1 Finite Element Investigations

A finite element analysis was carried out in order to gain some information on the stress distribution in an end-loaded coupon specimen for various specimen configurations. The first approach was to examine a modified D695 specimen with CFRP tabs as this is supposed to be the 'worst case' regarding stress concentrations. The finite element package used was "FINEL", an in-house program developed in collaboration with BABCOCK, plc. The test pieces were idealised using isoparametric 3-dimensional 20-noded elements. The mesh used is shown in Figure 5.2.1-1 (here, the tab bond layer is not modelled). Because of symmetry only one eighth of the specimen had to be examined, using appropriate boundary conditions. The load was introduced by displacement of the end, suppressing z-displacements in the tabbed region in order to model the constraint by the end blocks.

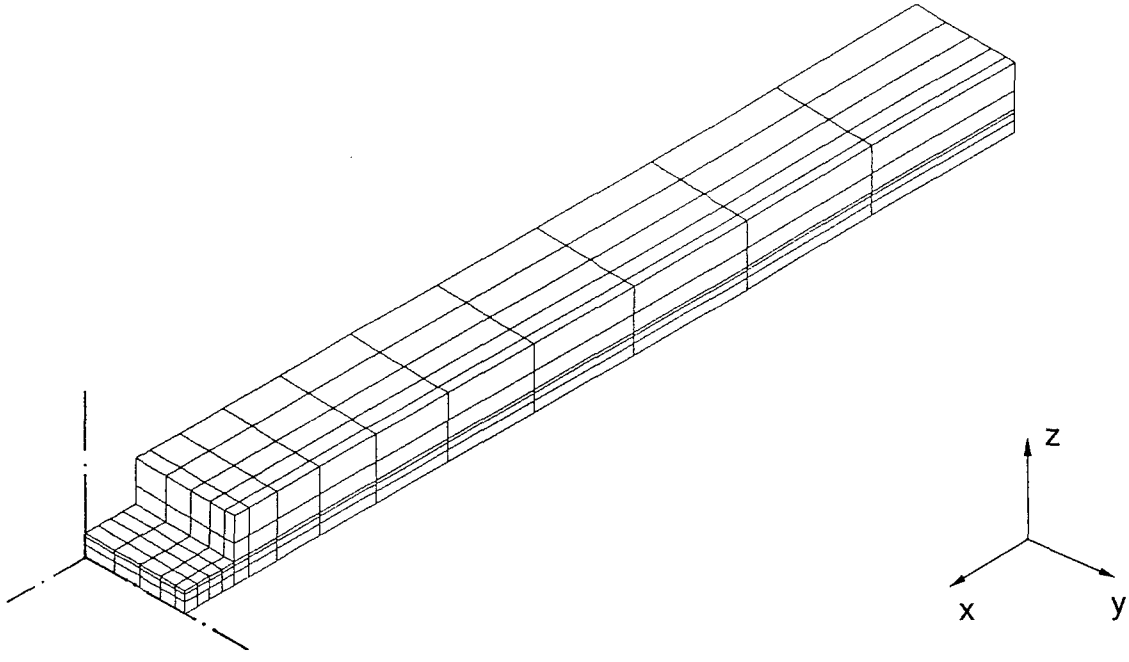


Figure 5.2.1-1: *Finite element mesh of an end-loaded compression test piece with 5 mm gauge length.*

The finite element code allowed only a linear analysis. It was found that a nonlinear analysis including plasticity of the adhesive layer was necessary in order to obtain quantitatively meaningful results. Regarding the importance of tab tip debonding (see Section 5.2.4) the information gained from this simple linear finite element analysis is of limited use. The main problem in the model of the test piece is the geometric singularity the tab end presents. Numerical results will depend on the mesh size used and on the

algorithm to average stresses. It is believed that 'quarter point' elements as used in fracture mechanic problems would be more suitable than the elements available in the package. Nevertheless, some interesting observations can be made from the simple analysis.

Figure 5.2.1-2 shows (scaled) deformations of an end-loaded compression test piece. Constraint of transverse deformation in the tabbed area is visible; also note the rotational deformation of the tab tip.

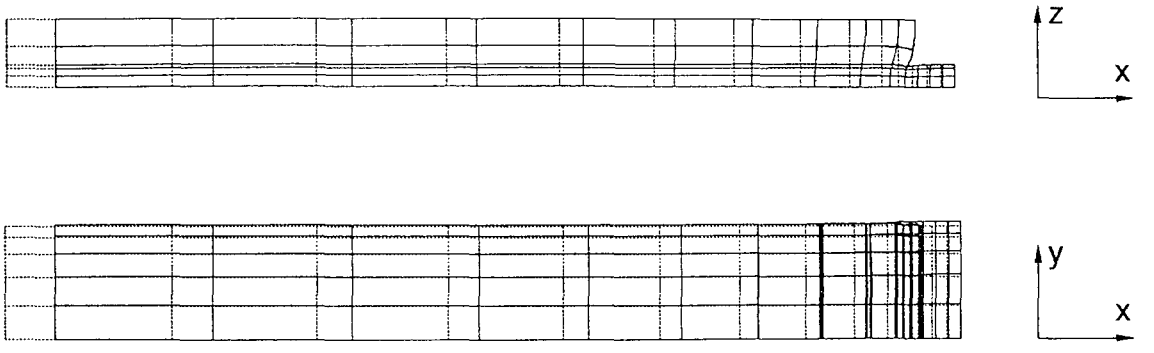


Figure 5.2.1-2: Deformation of an end-loaded compression test piece.

Figure 5.2.1-3 shows surface stresses in a plane perpendicular to the laminate plane (xz-plane). It clearly demonstrates that severe stress concentrations exist at the tab tip region for both xz-shear stresses (σ_{xz}) as well as longitudinal stresses (σ_{xx}). In a later investigation (Kukula, 1989) it was shown that these stress concentrations are of the same order of magnitude in a standard ICSTM test piece and an IITRI specimen. As mentioned above, the exact numerical results are too dependent on the modelling to be compared directly, but a qualitative comparison is still reasonable.

Several facts are remarkable about the stress plots. Firstly, most of the stress concentrations at the tab tip decline after about one and a half specimen thicknesses into the gauge section of the test piece. Secondly, stresses are constant over the first two thirds of the tab length. This would indicate that much shorter test pieces could be used. However, the load in the finite element model is introduced uniformly, whereas in practice small imperfections of the ends lead to non-uniform stresses in the tabbed region. End tabs longer than suggested as necessary from the calculations are therefore beneficial for a more uniform stress distribution in the gauge section.

Stress concentrations decline quickly in the gauge section, but there is a comparatively long region of considerable shear stresses under the tab towards the specimen end. The peak shear stress is about 25% of the average longitudinal stress in

the specimen centre plane, which shows that plasticity and fracture mechanics have to be incorporated to obtain realistic stress fields. The results indicate that interlaminar cracking at the tab tip is likely given typical values of around 0.05 for the ratio of shear-to-compressive strength of a unidirectional laminate. Note that in the example above the adhesive layer is not modelled, the specimen therefore represents a test piece where the gauge section is machined into the laminate (see Section 5.2.3). Including the adhesive layer (linear properties) changes these results only slightly (Kukula, 1989).

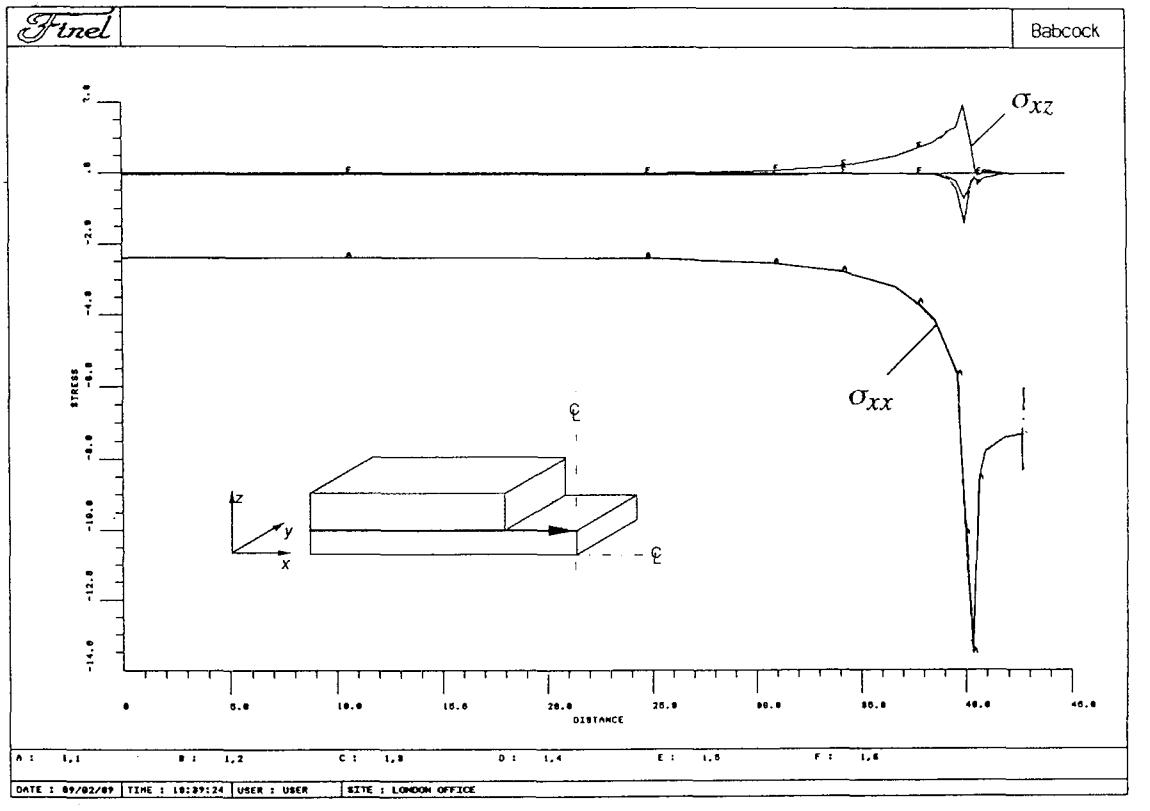


Figure 5.2.1-3: *Surface stresses in an end-loaded compression specimen from finite element analysis; plane perpendicular to laminate plane.*

Stresses scanned through-thickness in a plane perpendicular to the laminate plane are shown in Figure 5.2.1-4. It illustrates that in the thickness direction stress peaks caused by the tab tips decline quickly near the surface, but there is a gradient across the whole cross-section. This fact would support the finding that test pieces with smaller thicknesses yield higher strengths in compression since the ratio of average stress and peak stress is greater (Westberg and Abdallah, 1987, and Table 5.2.1-1, below). It would also imply that surface layers less prone to catastrophic compressive failure could buffer stress concentrations, thus increasing the measured compressive strength. This will be discussed later when analysing multidirectional laminates.

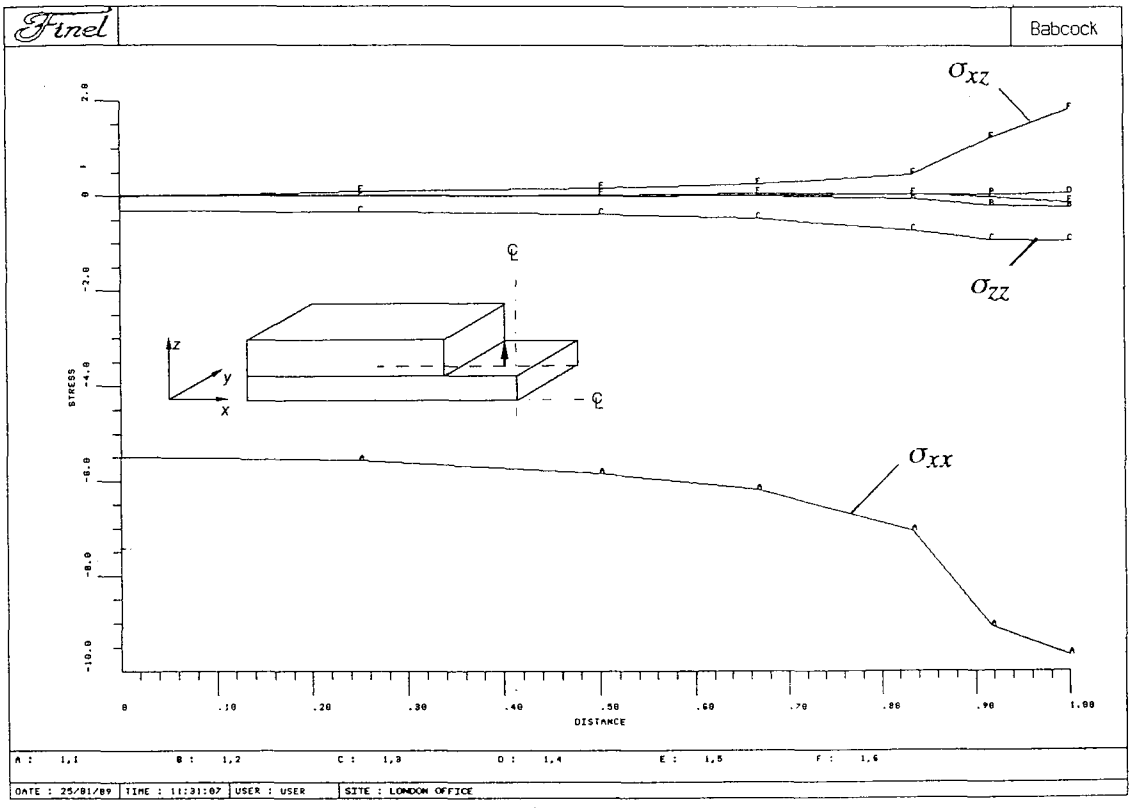


Figure 5.2.1-4: *Stresses scanned through-thickness in an end-loaded compression specimen from finite element analysis; plane perpendicular to laminate plane.*

Figure 5.2.1-5, finally, shows that stresses in the centre of the gauge section (here, 5 mm) are fairly uniform so that a uniform stress field can be expected from a test piece with 10 mm gauge length. This is confirmed by Kukula's investigation, which shows that in an ICSTM test piece with 0/90° glass fibre/epoxy tabs the variation of longitudinal stress in the centre symmetry plane perpendicular to the laminate plane is less than 2%.

In Table 5.2.1-1 some of the results of the finite element investigation are listed. As reported by Westberg and Abdallah (1987), stiffer end tabs result in higher stress concentrations, the lowest value being calculated for the GRP tabs. The stiffness of the tab is determined by the longitudinal modulus of elasticity, the thickness of the tab and the shear stiffness, which is high for metals. As pointed out earlier, no yield effects could be considered here, but yielding of the tab itself could play a role in practice, for example when using 'soft' aluminium tabs. Stress concentration factors are smaller for thinner laminates, but higher for shorter gauge lengths. So the need to compromise to avoid macroinstability might invalidate the advantage over the standard test piece.

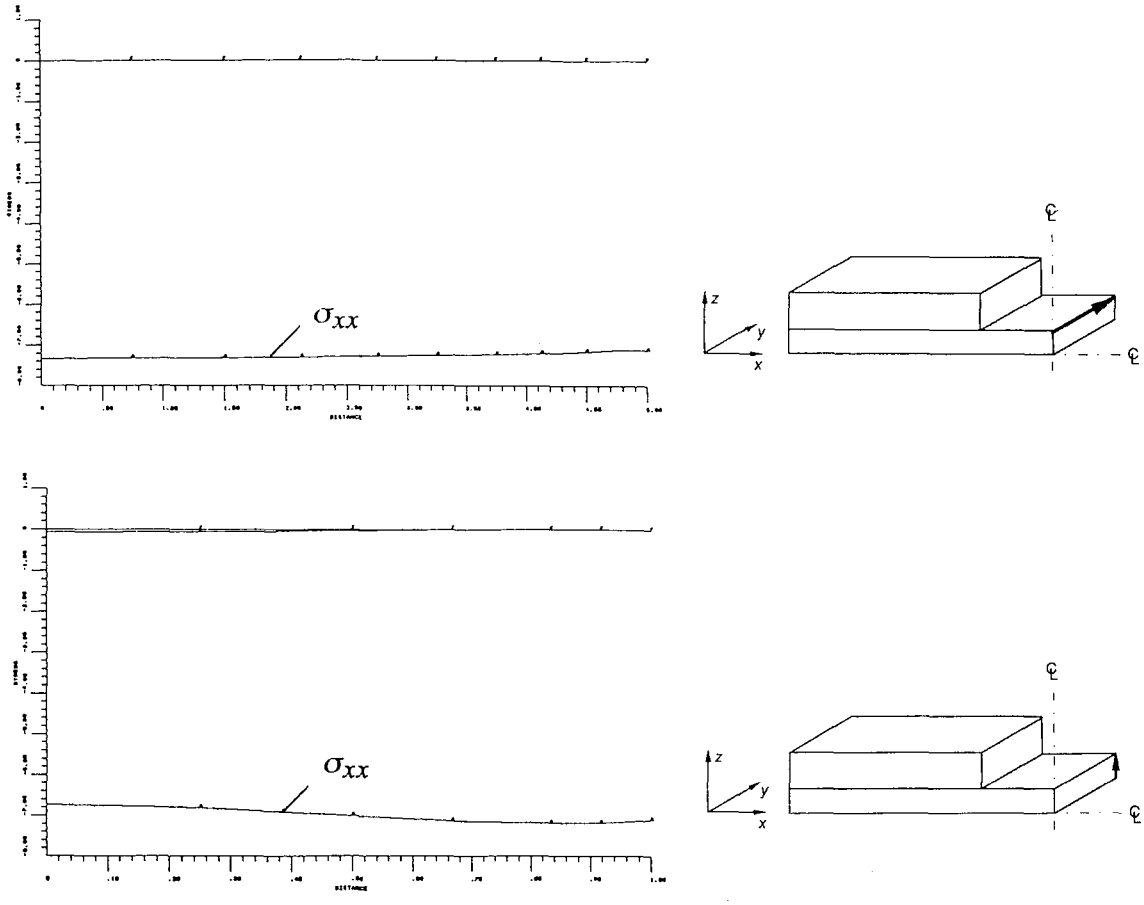


Figure 5.2.1-5: Stresses in the centre symmetry plane in an end-loaded compression specimen from finite element analysis; plane perpendicular to laminate plane.

End tab material	0/90° GRP	(standard)
	UD CFRP	+11 %
	Aluminium	+12 %
	Steel	+27 %
Laminate Thickness	2.0 mm	(standard)
	1.5 mm	- 5 %
	1.0 mm	- 13 %
Specimen gauge length	10 mm	(standard)
	7.5 mm	+ 7 %
	5.0 mm	+10 %

Table 5.2.1-1: Influence of some parameters on longitudinal stress concentrations factors; results of a finite element study (Kukula, 1989).

5.2.2 Experimental Parameter Study of Test Piece Geometry

The most important geometric parameter in compression testing is the slenderness ratio of the test piece. In the tests carried out the standard nominal specimen thickness was 2 mm, and the unsupported length ranged between 5 and 50 mm. In order to assess laminate thickness effects laminates with 12 and 8 plies, equivalent to 1.5 and 1.0 mm nominal laminate thickness were also included in the investigation. Finally, the specimen width parameter was examined by testing 5 mm wide coupons.

Gauge length [mm]	Nominal thickness [mm]	Slenderness ratio	Abbreviation
5	2	8.7	G5
7.5	2	13.0	G7
10	2	17.3	G10
12.5	2	21.7	G12
15	2	26.0	G15
20	2	34.6	G20
30	2	52.0	G30
50	2	86.6	G50
7.5	1	26.0	T8
10	1	23.1	T12

Table 5.2.2-1: *Test piece dimensions of slenderness ratio parameter study.*

In-plane Poisson's deformation was measured in some cases, using strain gauges applied axially and in the width direction. This was thought to provide information about the uniformity of the stress field and effects of end constraints. The Poisson's ratio was determined as the slope of the best fitting line between 0 and 0.5% axial strain in a transverse versus axial strain plot. Since the transverse versus axial strain curves were almost perfectly linear in this range, this method should yield the same result as the 0.25% strain ratio. The advantage of using the linear slopes is that 'noise' and other irregularities in the signals are levelled out. The results of this test series are given in Tables T-1 to T-10 and presented in Figures 5.2.2-1 and 5.2.2-2 below.

Figure 5.2.2-1 shows the effect of unsupported length on the in-plane deformation in the centre of the gauge length. It suggests that for a 2 mm thick laminate the minimum gauge length offering an unconstrained section in the centre is about 10 mm, considering that the gauge length of the strain gauge used is 2 mm. Shorter test pieces experience in-plane constraint, as implied by the lower Poisson's ratio. The plateau value, i.e. the in-plane Poisson's ratio of the unconstrained laminate, is about 0.34.

Figure 5.2.2-2, where the ultimate compressive stress versus slenderness ratio is shown, indicates a drop in UCS for slenderness ratios above 20. Regarding the 16-ply laminates, indeed, a buckling type of failure is suggested from the stress-strain diagrams

for gauge lengths of 12.5 mm and above. Remarkably, even 10 mm gauge length specimens failed in a macroinstability mode in three cases out of six (compare Figure F-3). No sign of macroinstability is observed for gauge lengths of 5 and 7.5 mm (Figure F-2). Some typical stress-strain curves are shown in Figure 5.2.2-3.

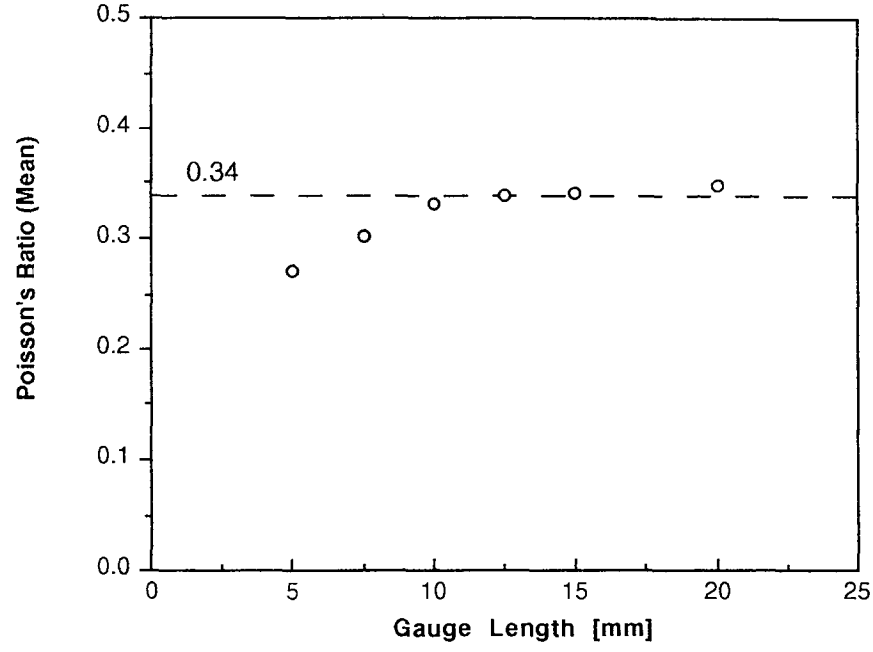


Figure 5.2.2-1: Poisson's ratio of XAS/914C from compression tests versus unsupported length of the test piece; 16 plies .

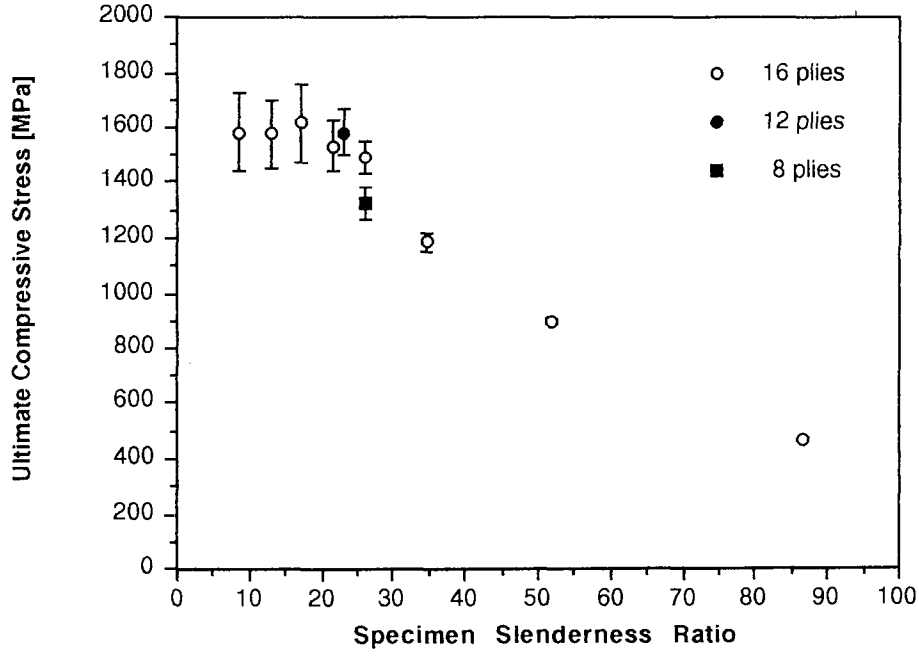


Figure 5.2.2-2 Test results for the compressive strength of XAS/914C versus specimen slenderness ratio. Error bars indicate standard deviation.

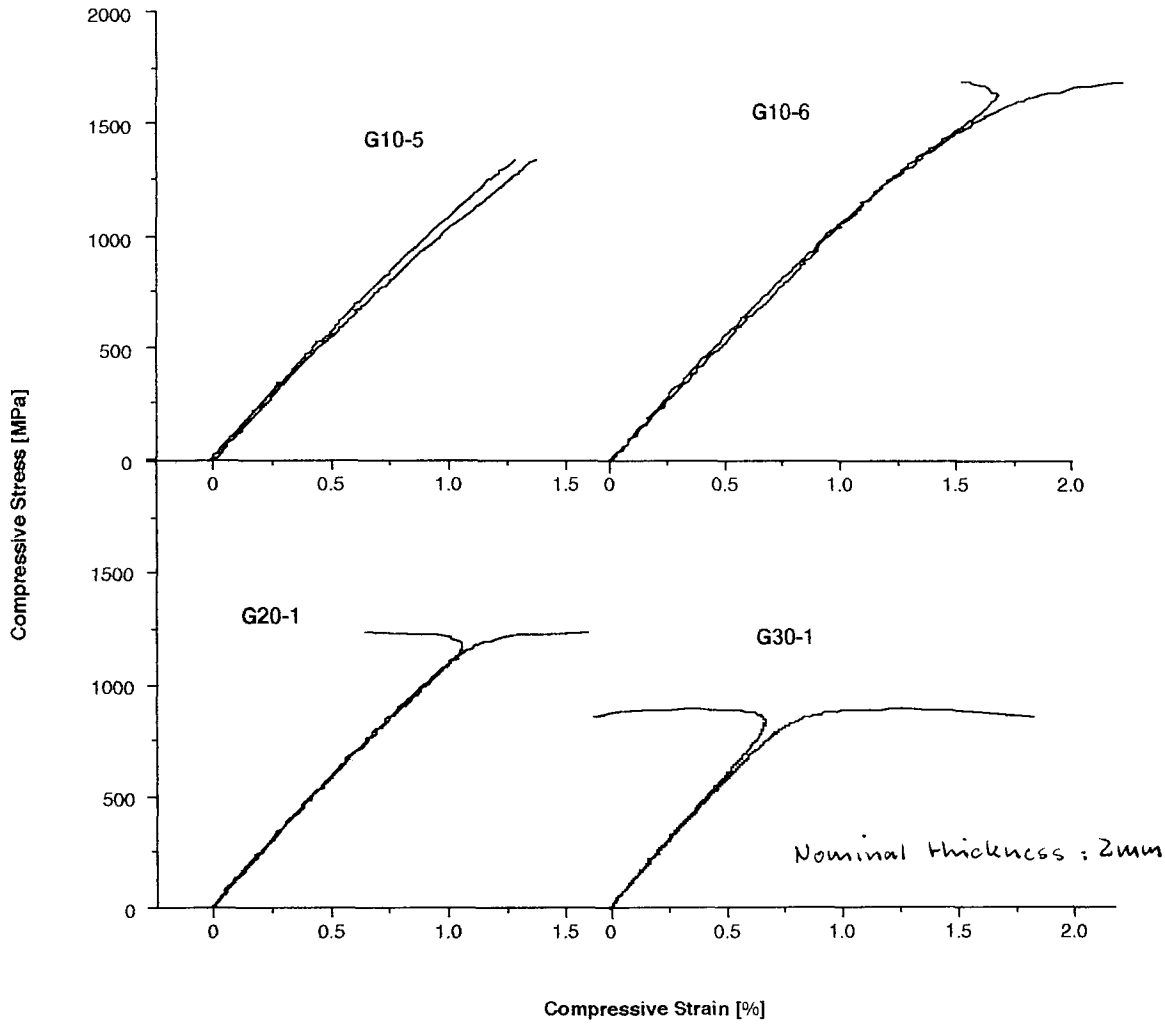


Figure 5.2.2-3: Typical compressive stress-strain curves suggesting macroscopic instability of the test pieces in some cases.

These test results already illustrate the dilemma of compression testing: there is a trade-off between the different requirements. A compression coupon test piece is always a compromise. Changing a geometric factor can have opposite effects on the conflicting properties: e.g. increasing the test piece thickness will increase the resistance to buckling but at the same time stress concentrations are likely to be higher.

Some interesting observations can be made regarding failure of the specimens. Close examination of the fractured test pieces reveals a transition from a pure interlaminar shear failure through a combined interlaminar shear and compression failure to a pure compression failure due to the amount of lateral deflection the test pieces experience. 'Pure' compression failure, as opposed to interlaminar shear failure, will be a subject of discussion in Chapter 11, and the influence of shear stresses will be investigated. In Figure 5.2.2-4 the test piece failures observed are illustrated. Photographs of some typical fractured test pieces are shown in Figure P-11.

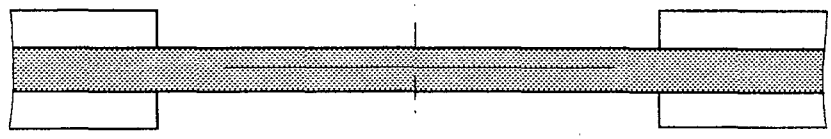
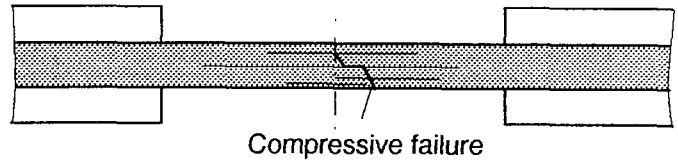
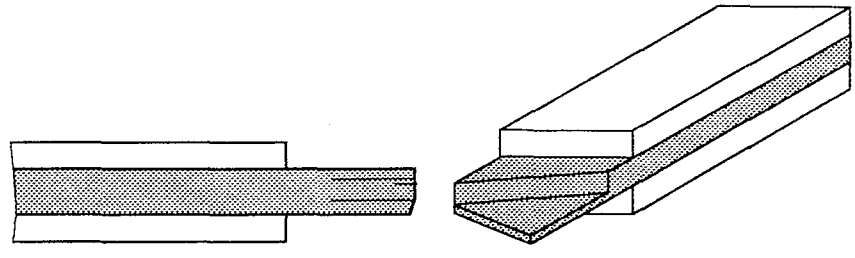
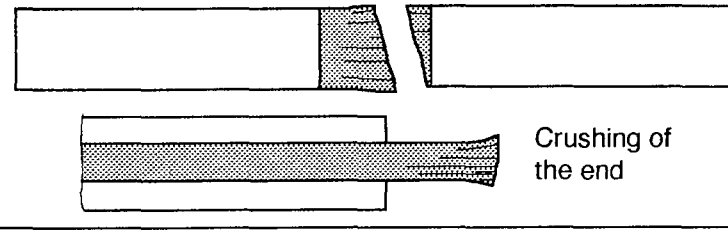
Gauge Length [mm]	Failure Mode
50	Interlaminar shear failure which leads to collapse of the test piece due to reduced bending stiffness. 
30	Extensive interlaminar splitting; compression kinks between centre and tab tips delimited by delaminations. 
20	Interlaminar cracking; 'forked' compression kinks near quarter span of gauge length in some cases. 
15	As 20 mm; three failures at end tabs with little interlaminar splitting and three failures near quarter span.
12.5	Compressive failure (kink-banding) initiated near tab tips; 'Quarter point failure' in one case.
10	Compressive failure (kink-banding) initiated at tab tips and crushing of the fracture surfaces. 
7.5	Compressive failure (kink-banding) initiated at tab tips and crushing of the fracture surfaces. Kink bands across width and thickness.
5	Compressive failure (kink-banding) initiated at tab tips and crushing of the fracture surfaces. Kink bands across width and thickness.

Figure 5.2.2-4: *Variation of compressive failure mode with slenderness ratio of test piece using the ICSTM method; 16-ply laminates.*

Obviously, it is very difficult to find the true sequence of the failure process, since, as mentioned before, most damage is done to the test piece after failure has initiated.

Only two 30 mm and 50 mm gauge length specimens have been tested, which seemed to be sufficient for determination of the buckling stress as scatter is extremely low in these cases (the scatter bars are not visible in Figure 5.2.2-2).

The 50 mm test pieces were used for repeated loading (Figure F-6). The ultimate stress was determined from the peak of the stress-strain curve when the specimen buckled. Both specimens failed by interlaminar splitting presumable when a certain centre deformation was exceeded. Test piece #1 was loaded five times and finally fractured. Fracture occurred at the tab edge as a consequence of the reduced stiffness of the test piece. The failure strain in the centre was approximately 2.2%. Figure 5.2.2-5 shows the repeated loading and the increasing divergence of the surface strains with loading cycle suggests steady growth of the delamination. Test piece #2 was loaded twice without fracturing the test piece. Figure P-11 (a) shows interlaminar failure after the second test.

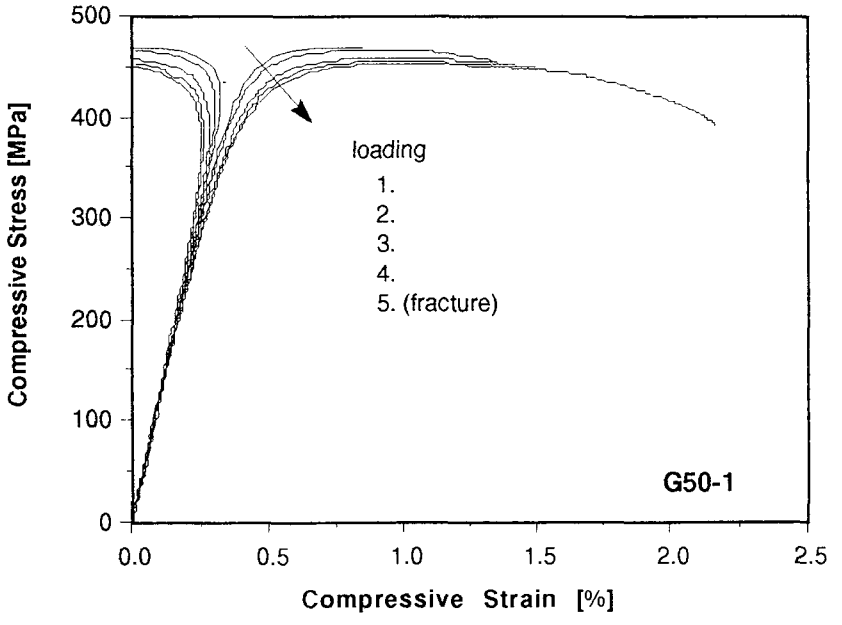


Figure 5.2.2-5: Repeated loading of a test piece with a gauge length of 50mm.

The two 30 mm test pieces showed signs of both interlaminar and compressive failure. As some of the compression kinks stretch from one delamination crack to another, it is likely that the laminate failed in shear first. The location of fracture is near the centre at approximately one third of the unsupported length from the tabs suggesting that compressive failure was promoted at the vicinity of maximum shear stress. Failure strains are clearly below 2%.

The mode of failure of 20 and 15 mm gauge length test pieces looks similar with separation of the test pieces concentrated between the centre of the gauge section and the tab tip. 12.5 and 10 mm specimens usually fail by kinking in width and thickness directions. The kink seems to initiate at the tab edge. In some rather rare cases, however, a wedge-type failure as illustrated in Figure 5.2.2-6 is observed. This failure mode shows some similarity to the one assigned to the 20 mm test piece in Figure 5.2.2-4, and the question is whether failure initiated at the tab edge or at the tip of the wedge. Since no correlation between amount of bending and associated shear stresses and failure mode could be found, it is suggested that failure started at the tab edge.



Figure 5.2.2-6: Illustration of an occasionally observed test piece failure.

Compressive strains at the location of fracture are much smaller for long gauge lengths, e.g. 30 and 20 mm, than for 10 mm specimens. The presence of shear stresses reducing the compressive capability could explain this phenomenon. Remarkably, the 10 mm test pieces which buckle, reach compressive strains of more than 2.3% in the centre, whereas the longer ones usually fail below 1.8% centre surface strains.

Influence of laminate thickness

Both thinner laminates failed mostly in a buckling mode. Therefore, an assessment of the influence of the laminate thickness on the compressive strength from the test results is not meaningful. The reason for the result for the 8-ply laminate being considerably lower than the corresponding 16-ply result is most probably the lower bending stiffness of the thinner laminate. Any load eccentricity or test piece misalignment causes lateral deflection under axial load. The induced bending moment reducing the buckling stress, is the greater the lower the bending stiffness of the test piece.

Influence of specimen width

The mean ultimate compressive stress of the 5 mm wide specimens was 1611 MPa with a coefficient of variation of 5.6 %. This result is very similar to the value for the standard 10 mm wide test piece. The width of the specimen does not seem to play an important role. Failed specimens usually exhibited more longitudinal splitting than the standard ones, which is most probably a consequence of the reduced in-plane stiffness.

5.2.3 The Role of Tab Tip Debonding

Before further discussion of results of parametric testing an important aspect of specimen design will be addressed. The aspect in question is the debonding of the tab tip at the gauge section where, as shown by the FE analysis, a severe three-dimensional stress state is present.

In order to assess the influence of tabbing material and bond properties, test pieces were produced from a laminate with a nominal thickness of 4 mm by machining a slot of 10 mm width on both sides as illustrated in Figure 5.2.3-1. The slot was machined by using a diamond tipped cutting wheel of approximately 2.5 mm width. After carefully adjusting the depth of the slot on a sacrifical plate, slots were cut by feeding the saw blade in 0.5 mm increments. This resulted in a satisfactory, if somewhat coarse, surface finish of the gauge section. Due to the geometry of the saw blade a radius of 1.25 mm was left at the edges of the slot. Individual specimens were then cut from this plate.

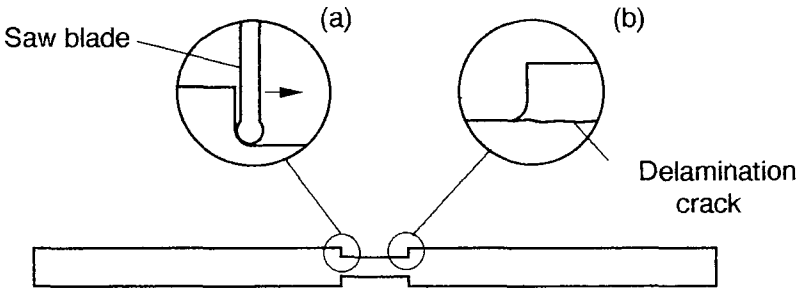


Figure 5.2.3-1: Integral test piece: (a) machining of the test piece from a thick laminate; (b) Interlaminar cracking at the 'tab' tip.

When testing these specimens cracking could be heard at about 800 MPa. Assuming an end failure, the test was interrupted, the test piece demounted and examined. Surprisingly, no damage was immediately apparent. On close inspection delamination cracks initiating at the corner of tab and gauge section, as illustrated in Figure 5.2.3-1, were discovered. These cracks show similarity to the ones mentioned earlier with the Birmingham method, but here they are initiated at lower overall stresses. Figure 5.2.3-2 shows the corresponding stress-strain recording and the likely interpretation of the curve.

Consecutively the test piece was remounted and loaded up to failure. In the following tests the samples were loaded to failure without interruption. The delamination described occurred in all cases. As illustrated in Figure 5.2.3-2, tab tip delamination initially caused asymmetric loading and therefore bending of the test piece. On further loading, however, delaminations are initiated on the other tab tips resulting in symmetric

loading. Since this happens at relatively low stress levels, the overall stability is not endangered nor are strength limits reached during the bending phase.

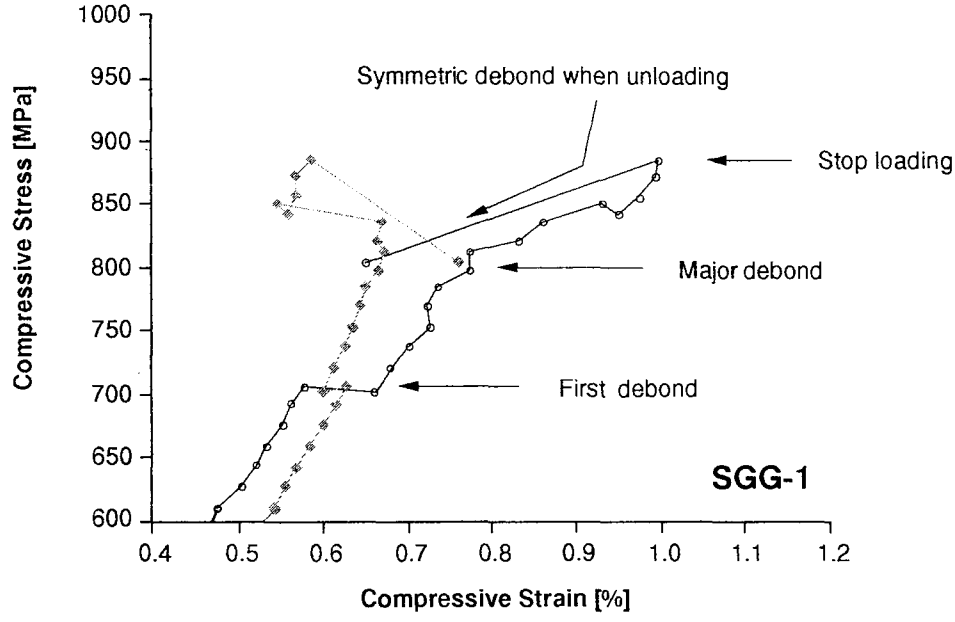


Figure 5.2.3-2: Stress-strain signals at the instant of tab tip debonding; note that the origin is suppressed.

In Figure 5.2.3-3 a complete stress-strain curve of such a specimen is given. The onset of the delamination crack causing asymmetric loading of the test piece and the following re-stabilising are clearly visible.

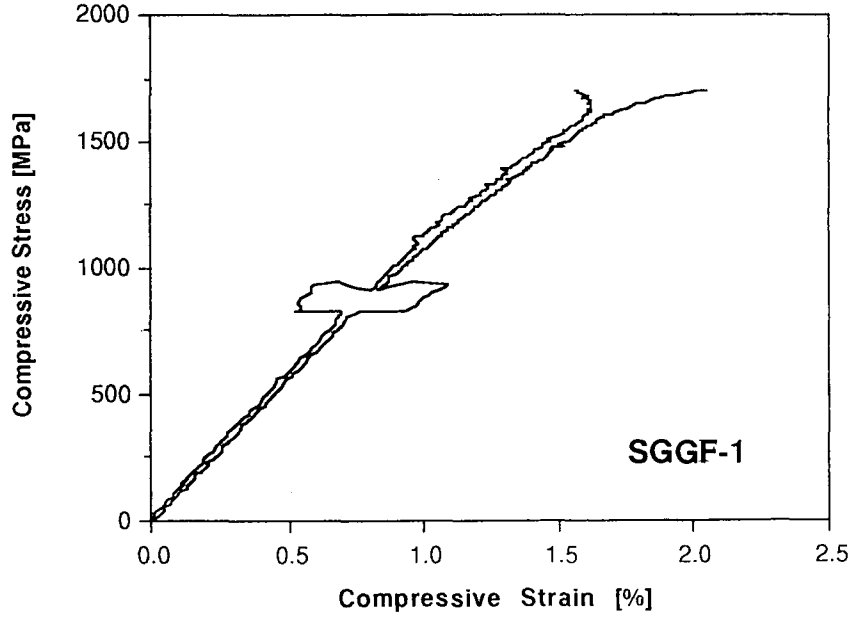


Figure 5.2.3-3: Typical stress-strain curve for a specimen with machined gauge section showing 'tab tip debonding'.

The important fact of these tests is that the strength for this specimen sample is about 6% higher than the results for the standard specimen (compare Table T-11 and T-12), despite the coarse surface finish of the gauge section. Obviously, the mechanism described above reduces stress concentrations in the area of the tab tip.

In order to prove this observation, debonds in the tab tip region were initiated by bending of the test piece as illustrated in Figure 5.2.3-4. The peel stresses introduced by bending the specimen were sufficient in most cases to 'pop off' the tab edge and to increase the debond to the desired length. This was done with five test pieces aiming for a debond length between 5 and 7 mm.

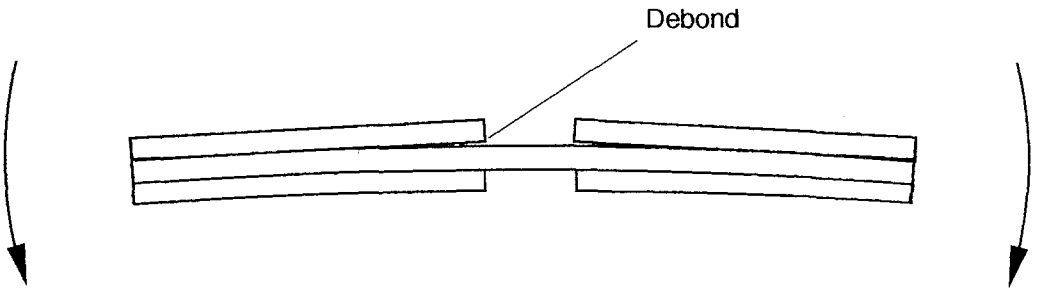


Figure 5.2.3-4: Illustration of initial tab tip debonding by bending of the test piece.

The strength results for these test pieces, shown in Table T-13, are 10% higher than those for the standard test piece, confirming the assumption made above. Another finding of these tests is that almost all specimens now fail in a macrobuckling mode. The critical stress is not affected by the debonds, but because of lower stress concentrations more test pieces reach buckling stress levels. Therefore, the mean is increased. In the next section this failure mode will be examined more closely followed by a proposal of how the evidence of stress relief by tab tip debonding can be translated into specimen design.

A final example of the self-stabilising nature of debonding tab tips is given in Figure 5.2.3-5 below. The specimen, whose stress-strain curve is shown there, presented problems when tested in a CRAG compression fixture due to a weak bond of the tabs to the composite. The load could not be transmitted by shear. Tested in the ICSTM rig compression failure in the gauge section was achieved readily. Clearly visible is the debond at very low strains and the following symmetric debond leading to axial loading with hardly any bending induced.

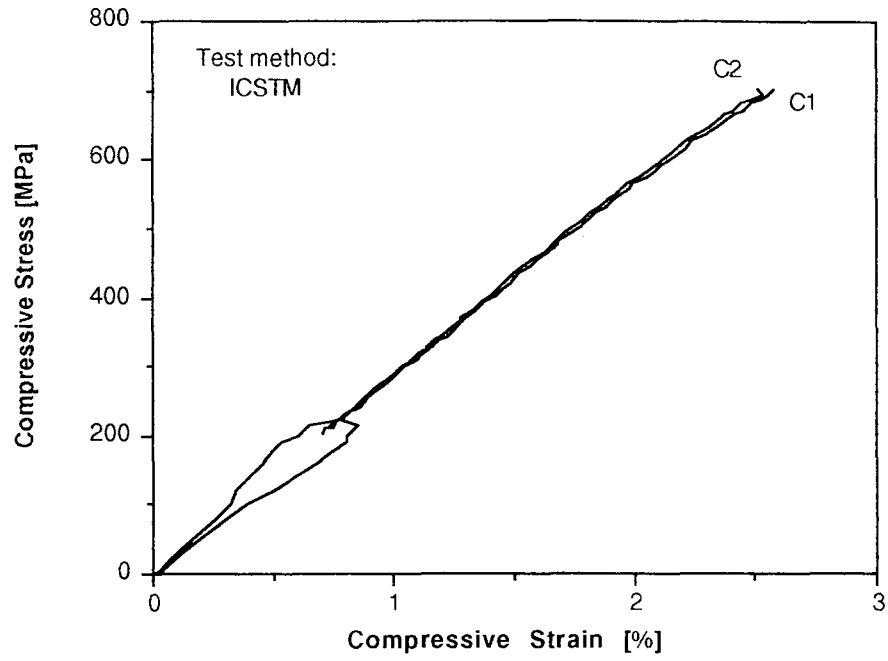


Figure 5.2.3-5: *Illustration of tab tip debonding when compressing a unidirectional glass fibre/polyester test piece with weakly bonded tabs.*

5.2.4 Identification of Test Piece Instability

So far, test piece instability, i.e. specimen buckling, was thought to take place when bifurcation of the stress-strain curve is observed as, for example, presented in Figure 5.2.2-3. However, there is a transition zone where it is not quite obvious whether the test piece bending derives from macroinstability or has other causes. One explanation which can be found for the bifurcation of the strain signals is that of asymmetric tab tip debonding preceded by plastic deformation of the tab tip adhesive layer. Investigations have been carried out to clarify this point which is thought to be of great importance for compression testing of composites.

The first observation in this context is that not all cases of bifurcation of the strain signals could be correlated to asymmetric tab debonding. Tab debonding could be checked relatively easily by visual inspection since the debonded sections were clearly identifiable as lighter areas through the glass/epoxy end tab (e.g. Figure P-11.d). Secondly, stresses at the tab tip responsible for any mode II failure are strain dependent if the load is introduced at the specimen end as in the ICSTM method. If the bifurcation of strain signal were caused by a mode II failure similar failure strains should be observed for different materials when tabs of similar stiffness are used. This is clearly not the case. Glass/nylon test pieces fail at strains of 2.5 % and more (see Chapter 6) whereas the onset of buckling of CFRP specimens is usually observed at strains of 1.5%.

These observations strengthen the assumption of a genuine buckling failure. For longer gauge lengths the onset of buckling as well as identification of the buckled shape is easily possible, as illustrated in Figure P-10. The same buckled shape can be imagined for short gauge lengths if the low shear modulus of composites is taken into account. One can probably think of buckling to be similar to in-phase buckling of the pages of a book, to give a simplified example. And, indeed, careful inspection of Figure P-10 (f) reveals such a buckling type deformation. It shows a test piece with 10 mm gauge length just before failure when bifurcation of the strain signals was observed. The thin white line underneath the strain gauge on the left side of the test piece, which is the edge of the specimen, is shaped as for the long specimens shown above. On the photograph of the unloaded test piece this line is perfectly straight.

The verification of buckling for short gauge lengths during the test, however, is difficult because lateral deflections of the test piece are very small. The following estimation may give an impression of the deformations involved in a compression test with short gauge length test pieces.

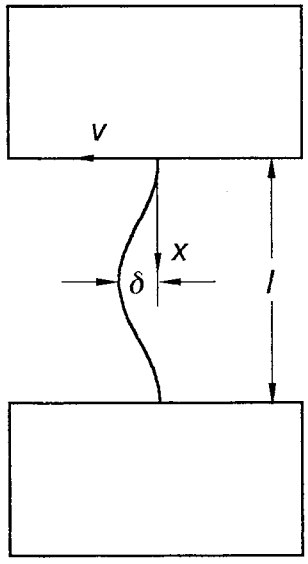


***Figure 5.2.4-1:** Illustration of the shape of a buckled specimen.*

For an estimate of the magnitude of the centre lateral deflection of the test piece before failure the deflected shape will be expressed by:

$$v = \frac{\delta}{2}\left(1 - \cos\frac{2\pi}{l}x\right) \qquad (5.2.4\text{-}1)$$

where v is the lateral deflection, δ is the maximum centre deflection and l is the unsupported length of the test piece (Figure 5.2.4-1).

The derivatives are readily obtained as:

$$v' = \frac{\pi}{l}\delta \sin\frac{2\pi}{l}x \tag{5.2.4-2}$$

$$v'' = \rho^{-1} = 2\delta\frac{\pi^2}{l^2}\cos\frac{2\pi}{l}x \tag{5.2.4-3}$$

with the radius of curvature ρ. The slope is maximum at $x = l/4$:

$$v'_{max} = v'\left(\frac{l}{4}\right) = \delta\frac{\pi}{l} \tag{5.2.4-4}$$

In order to obtain a relationship between strain and lateral deflection, linear elastic material behaviour and engineering bending theory are assumed and shear deformations are neglected as an approximation:

$$\sigma = E\varepsilon \tag{5.2.4-5}$$

and

$$\frac{EI}{\rho} = M \tag{5.2.4-6}$$

The difference of centre surface stresses can be written as:

$$\Delta\sigma = \frac{M}{I}t \tag{5.2.4-7}$$

Equations 5.2.4-5 to 5.2.4-7 together yield:

$$\Delta\varepsilon = \frac{t}{\rho} \tag{5.2.4-8}$$

And with Equation 5.2.4-3 the relation between lateral deflection and difference in surface strains $\Delta\varepsilon$ at l/2 becomes:

$$\delta = \frac{l^2}{\pi^2}\frac{\Delta\varepsilon}{2t} \tag{5.2.4-9}$$

Using Equation 5.2.4-4, the average shear stress acting on the $l/4$-cross-section can be approximated by:

$$\bar{\tau} = \frac{l}{\pi}\frac{\Delta\varepsilon}{2t}\sigma_c \tag{5.2.4-10}$$

Assuming a parabolical distribution of the shear stresses through thickness, with stresses maximum in the centre and vanishing on the surface, the maximum shear strain acting in the centre plane becomes:

$$\tau_{max} = 1.5\,\bar{\tau} \qquad (5.2.4\text{-}11)$$

With typical values (Figure 5.2.2-5): $l = 50$ mm, $\Delta\varepsilon = 0.037$ and $t = 2$ mm the central deflection is calculated as $\delta \approx 2.34$ mm. The corresponding deflected shape in Figure P-10 suggests a central deflection of around 3.5 mm. The discrepancy is most likely caused by shear deformation, increased after interlaminar shear failure, as pointed out in Section 5.2.2. For a gauge length of 10 mm the central deflection is calculated to be 0.025 mm assuming $\Delta\varepsilon = 0.01$ and $t = 2$ mm. As mentioned before, a deflection of this magnitude is difficult to detect visually during the test. Moiré interferometry would probably be a useful means to observe small deflections in situ. In the present investigation, however, it was not employed.

With the typical values for the 50 mm test piece the induced maximum (thickness) centre shear stress is calculated as approximately 90 MPa, assuming a compressive stress of 400 MPa acting on the deflected specimen. This value is close to the interlaminar shear strength measured for this material, thus predicting (central) interlaminar splitting correctly. For the 10 mm test piece a shear stress of 20 MPa for a compressive stress of 1700 MPa is obtained. Due to additional shear deformation the actual value of induced shear stress is probably higher. These shear stresses might be too small to cause direct shear failure but they might influence compressive failure as will be discussed in Chapter 11.

The assessment of the moments caused by asymmetric tab debonding is more difficult and probably best investigated by a finite element analysis. Test results, however, suggest that asymmetric tab debonding can cause the observed surface strain difference. Figure 5.2.4-2 shows a stress-strain curve of a modified ASTM D695 specimen with 1 mm gauge section thickness. The test was stopped at the moment when bifurcation of the strain signal occurred. Then the test piece was unloaded and examined and a debond of approximately 5 mm on one of the tab tips was found. Note that, in this case, the specimen does not bend in the direction which is anticipated from the bending at lower strains. Theoretically, buckling of this kind is possible for a certain combination of eccentricity of applied load and initial specimen deformation (Timoshenko and Gere, 1961). Here, the load eccentricity caused by tab debond overrides the effect of initial test piece non-symmetry. The stress-strain signal shows evidence of tab debonding as the 'unloading-path' is different from the 'loading-path'.

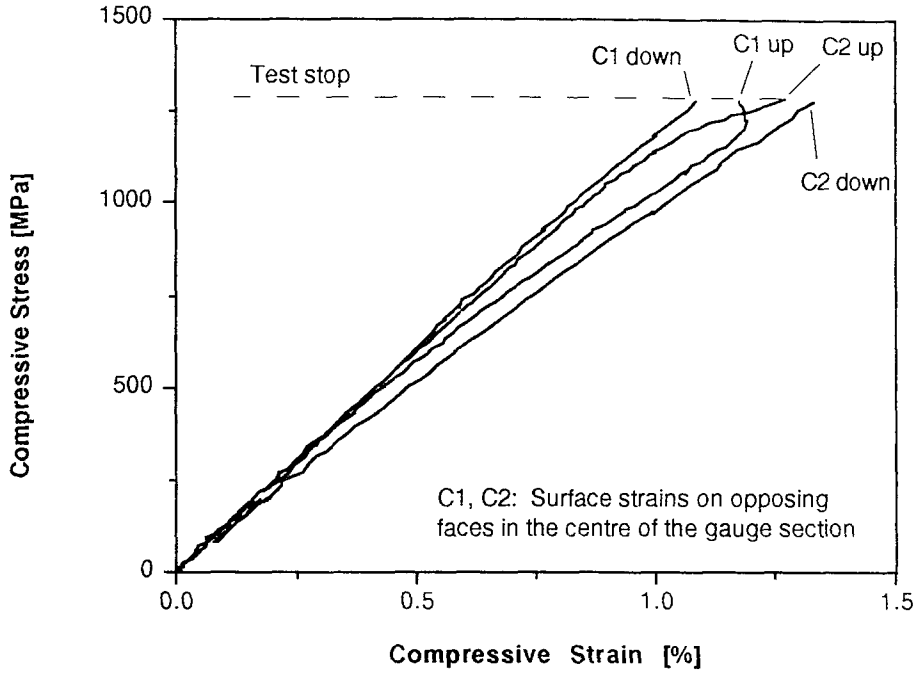


Figure 5.2.4-2: Unsymmetrical tab debonding in the stress-strain curve of a modified ASTM D695 test piece; thickness 1 mm, gauge length 5 mm.

Using the IITRI method, bifurcation of the strain signals was observed only in two cases. The specimens in these tests were clamped with tab tips sticking out from the grips as described in Chapter 4 (Figure 4.1-2), the unsupported length being around 18 mm.

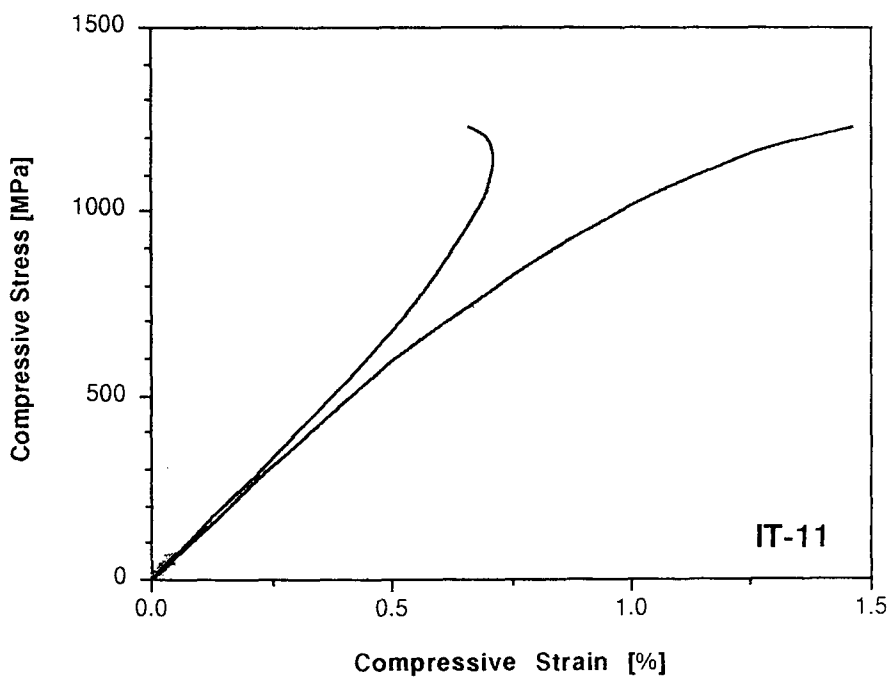


Figure 5.2.4-3: Stress-strain curves of a compression test using the IITRI method showing specimen buckling.

Two facts are remarkable about the stress-strain curves of these two tests: firstly, significant bending occurs and, secondly, bifurcation of the strain signals is apparent. One of the stress-strain curves is shown in Figure 5.2.4-3. Post-failure examination by removing the tabs layer by layer revealed tab tip debonding up to the point where the grips contacted the tabs in one case. Very little tab debonding was found in the other. The test results of around 1250 MPa are comparable to the ones gained for XAS/914C with a test piece of 20 mm gauge length. Additionally, it is suggested that the relatively large amount of bending, probably caused by inadequate specimen machining, contributes to an increased shear loading of the composite. This might in return reduce the shear modulus leading to a lower buckling load (see Chapter 10). In conclusion, the assumption of macroscopic buckling is reasonable in these cases.

Further evidence supporting the buckling assumption is the following observation. A test piece with 10 mm gauge length is loaded to the point where the strain signals diverge. Then it is unloaded and loaded again (Figure 5.2.4-4). The strains follow the same path with failure occurring before the former maximum stress is reached (an observation which has been made frequently in repeat tests). This would suggest that the divergence of the strain signal is caused by quasi-elastic macrobuckling rather than an unrecoverable mode II-type of bond failure.

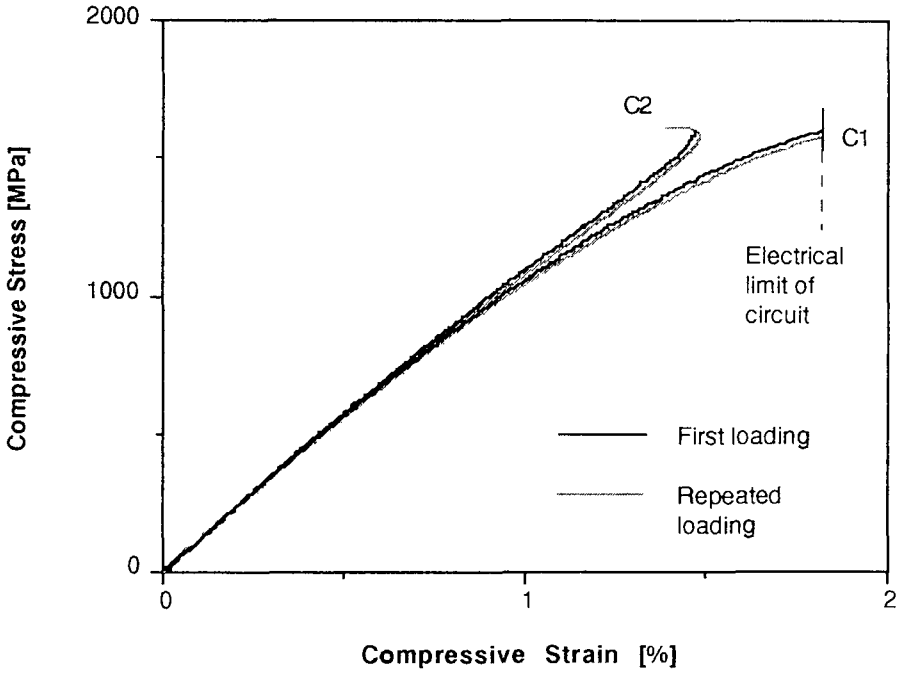


Figure 5.2.4-4: Repeated loading of a test piece with 10mm gauge length.

The fact that stresses near failure cannot be repeated, because of failure below the previously reached level, indicates that there is a certain plastic component involved. Tests of this kind are obviously very difficult to quantify because the individual failure load is not known so it is more or less coincidence if a test can be stopped near failure and repeated.

It can be concluded that tab tip debonding may cause strain bifurcation in some cases, in particular when the specimen bending stiffness is low. High test piece stiffness is therefore recommended. However, most facts suggest that bifurcation is caused by macroscopic instability of the test piece. This will be examined quantitatively in Chapter 10.

5.2.5 Parameter Study of Test Piece Preparation

In this section the influence of parameters of test piece production as described in Chapter 3, which are suspected to affect the measured compressive strength, are investigated:

1. Surface finish of the composite panel and the gauge section, respectively.
2. Small layer misalignment during laying-up.
3. Small off-axis machining of test pieces.

Surface finish

The standard peel ply used for the panels to be cured in the autoclave is porous PTFE coated glass fabric (Aerovac FF/03/PM). These peel plies leave the fabric pattern imprinted on the panel surface as pointed out in Chapter 3. An alternative panel was produced using porous release film (Tygavac RF 260/P3) which resulted in mirror surface finish (abbreviation of the specimen sample: PP3). The thickness of this panel was within the scatter of the standard panels (compare Table T-14 and, for instance, Table T-3). Compression data of a carbon fibre producer suggest that the smooth surface increases the compressive strength by approximately 30%[+]. Similarly, Curtis and Whitehead (1990) found that the flexural strength of test pieces with a smooth surface is significantly higher than that of standard ones, whereas the effect on the axial compression strength was considered to be small.

[+] Internal compression testing data using the CRAG method, Courtaulds, 1989.

Using the ICSTM method, a mean ultimate compression strength of 1688 MPa was measured (Table T-14) with a coefficient of variation of 7.1%. One of the six test pieces failed at 1921 MPa, and as it was not equipped with strain gauges it is not known if higher stiffness is the reason for the high failure stress. If this result is excluded, the mean value reduces to 1641 MPa with 2.6 % of variation.

These results are very close to those gained with the standard specimen as are the modulus values which were determined for two specimens (Table T-3 and T-14). Thus, the above mentioned considerable influence of a smooth surface on the ultimate compressive strength could not be verified. Failed test pieces showed tab debonding as observed with the standard specimens.

Also, the comparatively coarse surface finish of the test pieces machined on a saw did not influence the compressive strength detrimentally, as pointed out in Section 5.2.3. Equally, the machining of the specimen edges (surface 'b' in Figure 3.2-3) did not seem to influence the compressive strength of the test piece significantly. It could not be observed that failure was more likely to be initiated at locations where scratches from machining where present. However, since the load bearing capacity of this surface layer is reduced strength measurements are influenced via measuring the test piece dimensions. Therefore, the surfaces have been smoothed as described in Chapter 3. And, certainly, there is a critical depth where serrations act as notches causing premature failure.

Layer misalignment

Laminates with layers deliberately aligned ±1° to the main axis were produced to assess the influence of small layer (in-plane) misalignment on the compressive strength. This degree of misalignment is most certainly considerably higher than in most practical lay-ups. The 0°-direction of the cured panels was carefully determined by peeling off single plies before the specimens were produced.

Off-axis machining

Specimens were produced from standard unidirectional laminates which was cut at an angle of two degrees to the nominal fibre direction. Usually, an angle of two degrees is considered to be very small and hard to detect, but Figure 5.2.5-1 illustrates that two degrees give, in fact, the impression of severe misalignment. Again, in practice it is unlikely, that such a misalignment would be introduced into a unidirectional laminate by machining. It is possible if the fibre direction is difficult to trace, for instance in multidirectional laminates.

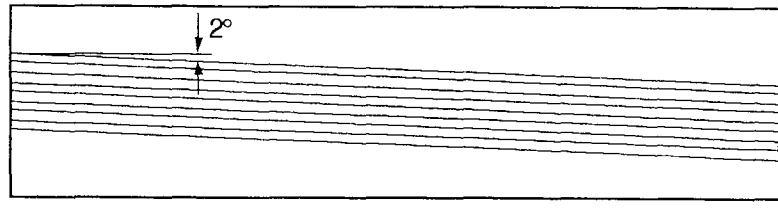


Figure 5.2.5-1: Illustration of a layer misalignment of 2°.

The results of the tests were somewhat surprising as a considerable influence of the described misalignment on the compressive strength was expected. However, the mean ultimate compressive stresses, 1710 MPa and 1648 MPa for the ±1° laminate and the off-axis test pieces, respectively, were higher than the values for the standard test pieces. The mean modulus of elasticity of the ±1° laminate was 119.1 GPa which is the usual value.

The explanation for the unexpectedly small influence of layer alignment is twofold. Firstly, in the case of the off-axis laminate the test piece is constrained by the rig from any in-plane shear deformation since the gauge length is very short. Therefore, additional shearing stresses are not built up in the composite as the resultant is absorbed by the jig. For the symmetric ±1° laminate there is no axial/shear stress coupling, but the individually misaligned layers are gripped on both ends. Again, in-plane shear deformation is suppressed by the fixture. Note the difference to short wave length misalignment: there the misalignment is anti-symmetrical with respect to the specimen axis but symmetrical with respect to the specimen end-loads. Shear deformation cannot be constrained by the jig in that case (Chapter 11).

This still does not explain why the results are even higher than the ones from the standard case. Therefore, as the second argument, tab tip debonding again seems to play a dominant role. It is believed that tab tip debonding occurred in most cases with the off-axis specimens, thus preventing low values which reduced the mean of the standard G10 specimens.

Since it proved not to be feasible to investigate misalignment effects with the standard test method, two alternatives are proposed:

1. The effect of off-axis machining can be examined by reducing in-plane constraint of the test piece. An example of achieving this is given in Figure 5.2.5-2: rollers allow lateral movement of the lower end block. The drawback of this arrangement is that there is still friction which constrains lateral movement. One test piece has been tested using this set-up yielding an ultimate compressive stress of 1542 MPa. Although a single test is no proof, it supports the assumptions made above.

2. Another method to investigate the influence of any type of layer misalignment is probably a four-point bend test as the gauge length is considerably longer and in-plane constraints are small.

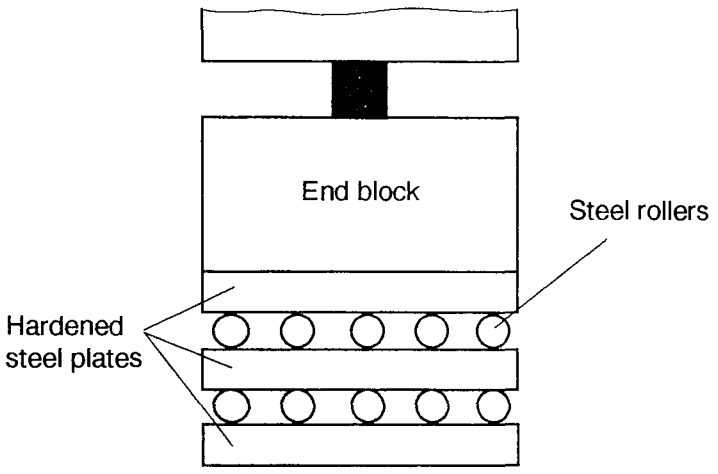


Figure 5.2.5-2: Proposal for loading block arrangement to allow lateral movement.

Conclusions

In conclusion, no influence of the surface finish on the compressive strength could be found. However, it should be noted again that the measurement of test piece dimensions might be impaired by a coarse surface. Smooth surfaces are therefore preferred and removal of saw marks is recommended, although it was not observed that they act as stress concentrators initiating compressive failure. The effect of a small layer misalignment could not be examined satisfactorily using the standard ICSTM method. A consequence of this, on the other hand, is that a small in-plane layer misalignment does not affect the results of coupon compression tests.

5.2.6 Improved Specimen Design

In Section 5.2.3 the advantages of an initial debond of tab tips were outlined. The challenge then was to produce a test piece with consistent and repeatable properties. The simplest way to realise a weak bond was to insert some kind of release tape in the tab tip region. In practice, this was done by covering part of the area under the tabbing plate with transparent cellulose tape which was used to mask the gauge section during grit blasting (see Figure 5.2.6-1).

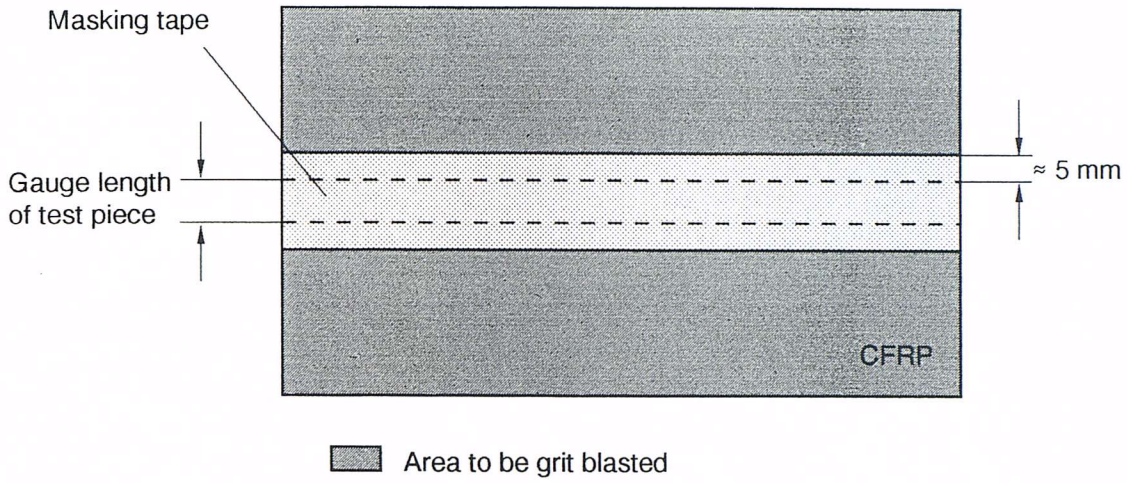


Figure 5.2.6-1: Test piece preparation with debond insert.

After bonding the tabbing plates the tape is removed from the gauge section, together with excess adhesive, and the individual test pieces are cut as described in Chapter 3. The result is a test piece as shown in Figure 5.2.6-2. It was found that inserting a PTFE tape into the adhesive layer was more difficult and less accurate than using the adhesive tape before bonding. Spraying the area with release agent was not considered since the effort required to avoid contamination of the bond areas was too high.

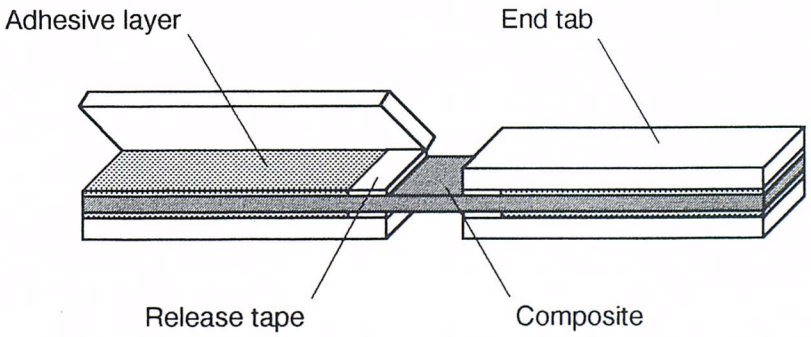
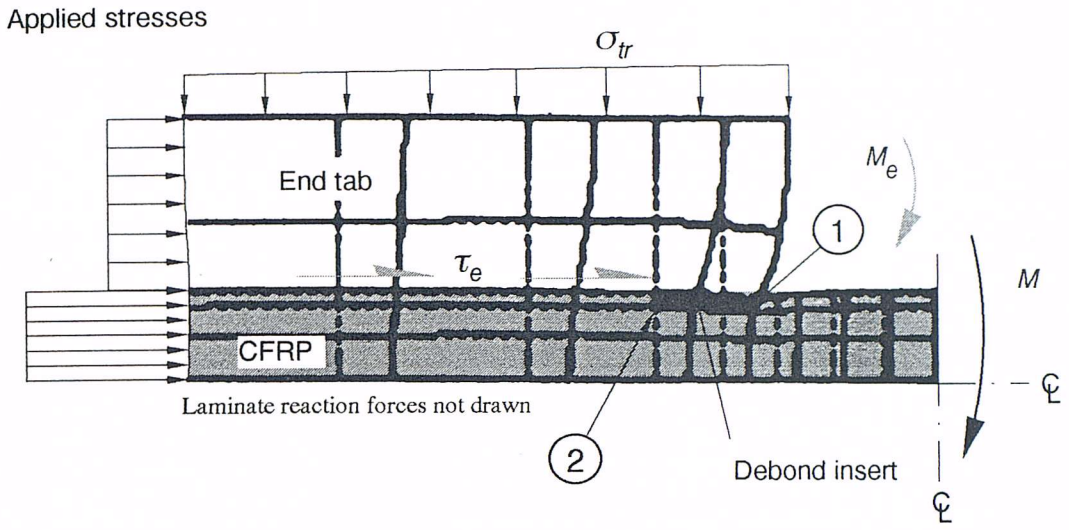


Figure 5.2.6-2: ICSTM test piece with debond insert.

The basic idea behind initial tab tip debonding is to separate the locations of stress concentrations and to lower them to some extent. As opposed to tapering the tab tips, the advantage of this method would be that lateral support is not lost in the regions of reduced load transfer, i.e the unsupported gauge length is hardly increased, which is of great importance regarding the results presented in the previous sections. To clarify this point, the main sources of stress concentrations at the gauge section borders are identified and the effect of a debond insert assessed in Figure 5.2.6-3.



Cause of stress concentration at tab tip	Stresses mainly affected	Effect of debond insert on stress concentration
Axial load carried by end tab	axial direct and shear	Moves stress concentration from (1) to (2)
Specimen bending	axial direct	reduced
Through-thickness loading	through-thickness direct	--
Constraint of through-thickness Poisson's deformation	through-thickness direct	reduced
End moment of end tab	through-thickness direct	much reduced
Constraint of Poisson's deformation in width direction	width direct	reduced

Figure 5.2.6-3: *Identification of stress concentrators in an ICSTM test piece.*

This specimen design is thought to be a further step to reducing constraints of the test piece, allowing more realistic test results for the compressive strength of the composite. The advantages expected from this 'improved' specimen design could be summarised as follows:

* Lower stress concentrations at the tab tip, thus giving a more realistic estimate for the compressive strength of the composite.
* Increased length of unrestrained area without increased unsupported length; shorter gauge length than 10 mm therefore possible.
* Reduction in scatter of results caused by erratic tab tip delaminations, thus increasing reproducibility of test results.

* Quality of the bond is not a crucial factor so that less care is needed in specimen production.
* Less influence of the tabbing material on test results.

Specimens with adhesive tape insert as well as PTFE tape insert have been produced and tested. The test results are presented in Chapter 6.

5.3 Proposal for a Multidirectional Specimen

Testing of multidirectional laminates poses different problems from those faced with unidirectional laminates. Inter-layer effects have to be considered in specimen design. Stress concentrations at the edges due to strain incompatibility of adjacent layers cause greater influence of specimen geometry than in unidirectional test pieces.

Two basic assumptions are usually made: firstly, edge stress concentrations vanish after one specimen thickness. The width of the test piece should therefore be considerably larger than the thickness. Secondly, there should be a proportion of the gauge section where angular fibres are not restrained by the clamps. According to CRAG, for example, the free length of the specimen should be chosen so that a non-axial fibre can run across the full width of the specimen and be at least half specimen width short of the end tabs, at each end. This is equivalent to the condition for the minimum gauge length:

$$g = w\left(1 + \frac{1}{\tan\theta}\right) \tag{5.3-1}$$

where w is the specimen width and θ the angle between the fibres of the angle ply and the longitudinal specimen axis.

No attempt was made in the present investigation to evaluate geometric effects in multidirectional lay-ups. But in a rather empirical attempt the behaviour of unidirectional layers within a laminate is assessed. This has been reported elsewhere: Barker and Balasundaram (1987) tested short gauge length plain specimens designed for uni-directional material, using the Birmingham method, for several stacking sequences. Clark and Lisagor (1981), as well as Whitney and Guihard (1991), used the IITRI method for testing quasi-isotropic and other multi-directional lay-ups, respectively. The effect of fibre surface treatment on the compressive strength of two multidirectional laminates has been examined by Curtis and Morton (1982) using short stable coupons in a modified Celanese jig.

The proposal here is to use an untabbed plain specimen, as shown in Figure 4.1-1 (b), but rather than clamping it directly it is sandwiched between glass fibre/epoxy tabs, which are not bonded to the composite, as illustrated in Figure 5.3-1. Only slight clamping pressure is applied at the loaded end of the sandwiched test piece in order to prevent end failures. The tabs are thought to reduce the stress concentrations in the vicinity where the test piece emerges from the grip. At the same time the in-plane constraint of angular fibres is minimised, because the tabs are not bonded and friction can be regarded as small since there is no clamping pressure on the side of the tab adjacent to the the gauge section. The equivalent gauge length is therefore increased significantly, whereas the laterally unsupported length of the test piece is still only 10 mm.

The advantages of this arrangement are obvious. Specimen preparation effort is reduced drastically, since only flat test pieces have to be machined from the composite panel. Also, tabs can be reused. Carrying out the test is very simple and dismounting of the test piece is without any problems.

In the long run it would be desirable to compare test results gained with the proposed test piece and larger standard specimens, particularly regarding the comparatively low width-to-thickness ratio proposed. Since laterally supported long test pieces often fail near the grips, the advantage of a comparatively uniform stress field in the gauge section might be overridden by the stress concentrations near the grips. Therefore, the use of a short test piece with lower stress concentrations could possibly offer more realistic design values.

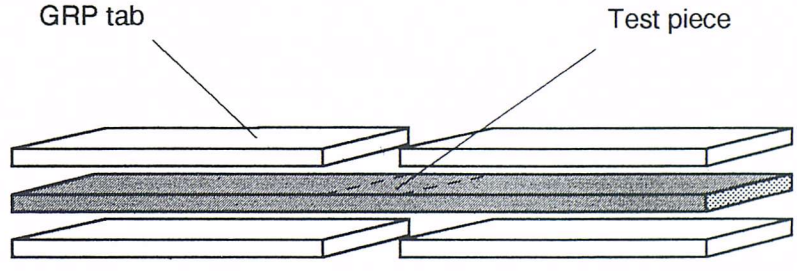


Figure 5.3-1: *Multidirectional test piece sandwiched between reusable tabs.*

In the present investigation the sandwiched test piece is used for woven cross-ply carbon fibre/epoxy and a multidirectional, quasi-isotropic, lay-up of XAS/914C (abbreviation L1):

$$[(+45/-45/0/90)_3]_S\,,$$

with a nominal thickness of 3 mm. The results of these tests are presented in Chapter 6.

CHAPTER 6 SUMMARY OF RESULTS OF COMPRESSION TESTING

In this chapter test results of compression tests other than the parametric study described in Chapter 5 are presented. Mainly the proposed new ICSTM method is used, but the results of a comparison of different test methods are also given.

6.1 Unidirectional CFRP

Three systems have been examined: two thermoset epoxy-based and one thermoplastic-based, poly-ether-ether-ketone. All three are reinforced with high strength intermediate modulus carbon fibres. The epoxy systems are XAS/914C and Apollo 43-750/9106C, the thermoplastic is ICI's AS4 carbon fibre-reinforced PEEK, APC-2.

6.1.1 XAS/914C - Different Test Methods

Six different test methods, including specimen modifications, have been compared: CRAG, IITRI, ICSTM, modified ASTM D695, Birmingham and British Aerospace method. Most of the methods have been described before. The British Aerospace method (Figure P-2) is a derivative of the Celanese method, but it uses wedge grips like the IITRI rig rather than conical ones. All test pieces were tabbed with woven 0/90° glass/epoxy tabs. The dimensions are given in Figure F-1.

The test results of the comparative compression testing using unidirectional XAS/914C are summarised in Table 6.1.1-1. The first four categories represent test results gained in a short course on mechanical testing of composites. These tests were carried out by eight different groups but always under supervision of an operator familiar with the test method and the testing equipment. For the CRAG[1] and IITRI tests an Instron universal testing machine was used rather than the apparatus described in Chapter 3 for the other tests. ASTM[2] data have been produced in a different short course under similar conditions. The remaining tests were carried out by one operator under conditions described in Chapter 3. Details of the tests with specimen modifications and the abbreviations used are as follows.

CRAG[1]: Standard CRAG specimen and fixture; several operators.

CRAG[2]: One operator; remachined grip surfaces; careful adjustment of the grip collets to the individual test piece.

CRAG[3]: As CRAG[2]; additionally tab tip debonding by bending of the test piece.

IITRI: 'Standard' IITRI specimen and fixture; several operators.

ASTM[1]: Modified ASTM D695; test piece thickness 2 mm; end cap on one end.

ASTM[2]: As ASTM[1]; test piece thickness 1 mm.

ICSTM: Standard ICSTM specimen and fixture; several operators.

BI: Birmingham method specimen tested in the ICSTM rig.

BAe[1]: BAe standard rig and specimen; one operator.

BAe[2]: Specimen fully gripped, 5 mm non grit-blasted section under the tab tip.

BAe[3]: Specimen partially gripped; 5 mm non grit-blasted section under the tab tip.

	CRAG[1]	IITRI	ASTM[1]	ICSTM	ASTM[2]	BI	CRAG[2]	CRAG[3]	BAe[1]	BAe[2]	BAe[3]
	1174	1343	1448[a]	1770	1389	1530	1337	1445	979	1109	1516
	1145	1278	1465[a]	1648	1369	1414	1536	1610	1102	1493	1361
U	1299	1232	1503[a]	1556	1395	1351	1376	1581	1235	1083	1436
C	1089	1348	1535[a]	1704	1270	1472	1494	1526	1074	1196	1491
S	1259	939	1601	1553	1304	(1319)	1348	1523	1075		1387
[MPa]	1349	1356	1434[b]	1467	1250	(1363)			1107		
	1210	1199	1601[a]	1607	1322				1366		
	1290	1278		1674	1245				1152		
Mean	**1227**	**1247**	**1512**	**1622**	**1318**	**1442**	**1418**	**1537**	**1136**	**1220**	**1438**
StDev	87.8	136.6	69.3	96.6	61.0	76.8	90.7	63.3	92.1	188.1	66.0
C_v	7.2	11.0	4.6	6.0	4.6	5.3	6.4	4.1	8.1	15.4	4.6

[a] end failure [b] tab completely debonded

Table 6.1.1-1: Test results for the compressive strength of XAS/914C using different test methods.

CRAG[1] yielded relatively low test results, comparable to those in Chapter 4. The serrations of the grip surfaces were worn so that high torque on the auxiliary grip screws was necessary in order to prevent slipping of the specimen. This could have caused severe transverse stress concentrations as pointed out in Chapter 4. This assumption is supported by the results of samples CRAG[2] and CRAG[3] which both yielded considerably higher results. It is believed that, indirectly, the most important reason for

the increase is the remachining of the grips. To explain this the geometry of the CRAG/Celanese rig has to be examined more closely. Strictly, the conical grips match the surface of the outer sleeves only in one case: when the cross-section of the grips with the specimen clamped is circular. An increase of the axial load will then not increase the transverse load on the specimen; the grips lock. A proportional increase of the transverse load, which enables the friction needed for load transfer, to the axial load is only given for an 'elliptical' cross-section as illustrated in Figure 6.1.1-1 'A'. An initial set-up 'B' shown in the figure will not create any transverse force when the specimen is loaded axially and only the friction caused by initial tightening of the mounting screws enables load transfer. During loading the cross-sectional shape changes due to two factors. Firstly, the test piece is deformed through thickness by the transverse clamping force and, secondly, the grip serrations impress themselves into the tabs. Therefore, if initially there is an appropriate elliptic shape 'A' the locking position can be reached before failure. If the frictional coefficient between the grips and the specimen is high (remachined grips) the failure load can be applied without slipping of the test piece and the failure load should be higher because of reduced transverse stresses. From that it follows that different specimen/grip combinations and small changes in specimen geometry and stiffness are likely to give different results. Ideally, using the CRAG or Celanese method, the test piece is loaded to approximately half the failure load to set the specimen and then the grip inserts are shimmed again to ensure optimum conditions.

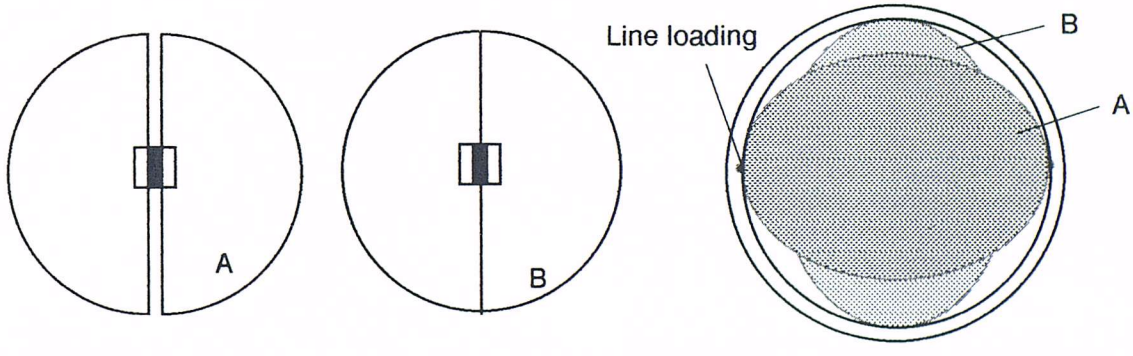


Figure 6.1.1-1: *Illustration of loading conditions using the CRAG compression rig.*

The IITRI results are similar to CRAG indicating that principal problems with the method of load introduction indeed exist. The through-thickness load on the specimen in the IITRI rig is always proportional to the applied compressive load and not dependent on the specimen geometry.

The British Aerospace rig proved to be simple to use since the fixture is very light and the open sleeve makes mounting of the test piece easy. Deep serrations in the grips

guaranteed a reliable grip of the specimen but seemed to influence the failure, generating some interesting results. The standard specimen, fully gripped, yielded the lowest mean value of the investigation. In some cases compressive failure seemed to be initiated at the serrations of the grips. It confirms what has been said about the influence of transverse stresses: the wedge grips cause transverse forces proportional to the axial load and independent of the specimen geometry. Therefore, the low results are not surprising. A weak bond of the tab tips did not influence the result significantly. When the specimen was not fully gripped (BAE^3), approximately 2 mm of the tab sticking out of the grips, the results rose by almost 20%, consistent to the observations made in Chapter 4 using the IITRI test method.

Buckling of the test piece was generally not observed when using the indirect methods. This was simply because usually the test piece fractured before a critical stress was reached for reasons suggested earlier. Figure 6.1.1-2 shows some representative stress-strain curves using the British Aerospace rig.

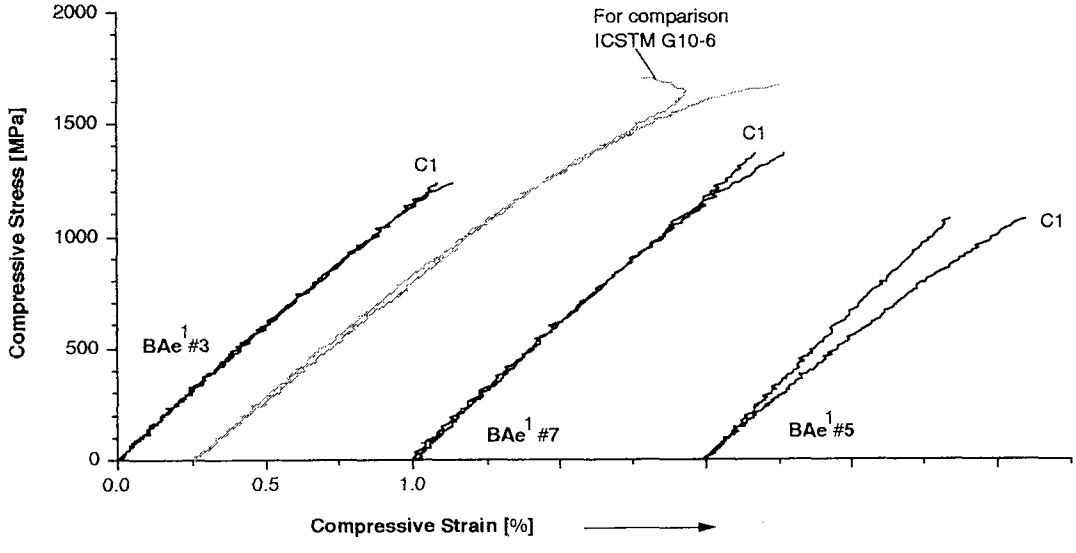


Figure 6.1.1-2: Some typical stress-strain curves using the BAe compression test rig.

The methods using end-loaded test pieces generally yielded higher test results than the indirect methods. To start with the modified ASTM D695 method using the test piece with 2 mm thickness presented the previously mentioned problems of failure at the end. For demonstration purposes a specially designed adjustable end cap (Figure 6.1.1-3) was fitted to only one specimen end. It was found that this device could prevent most of the end failures and is therefore recommended. Despite the invalid failure modes the failure stresses are comparatively high. The test piece with 1 mm gauge thickness presented no problems regarding end failures when tabs of the same thickness as for the 2 mm

specimens were used. But due to the low bending stiffness of the test piece any tab tip debonding led to strong bending causing premature failure. This is reflected in the lower mean failure stress compared to the thicker test piece.

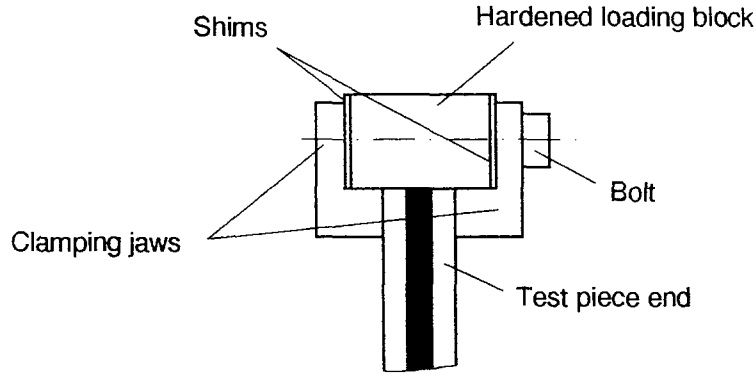


Figure 6.1.1-3: Adjustable end cap for modified ASTM D695 specimens.

The result of 1442 MPa for the Birmingham specimens tested in the ICSTM rig is consistent with the results published for the Birmingham method (Barker and Balasundaram, 1987). One of the five specimens failed at the end. As pointed out in Chapter 4, the slenderness ratio of the test piece proved be too high to cope with delaminations which occurred in the gauge section at high strains.

The ICSTM method using a standard specimen yielded the highest results with acceptable scatter in the present comparison. It has to be stressed that, at the same time, the test piece experienced the lowest constraints of all methods presented, thus evading the argument of artificially high values. Almost all stress-strain curves indicated tab tip debonding reducing stress concentrations. The different testers of the short course judged that the method was simple to use. Comparison of the results of the parametric study, where a mean compressive strength of 1617 MPa was measured, indicates good consistency of the method.

6.1.2 XAS/914C - ICSTM Method with Improved Specimen

In Section 5.2.6 the idea of the compression test piece with debond inserts has been outlined. The expectations, i.e. reduction of stress concentrations caused by load introduction and specimen constraint, seem to be fulfilled considering the results shown in Table 6.1.2-1. For comparison, the results for the test pieces where the debond was created by bending of the test piece (abbreviation DEB) are also listed. The other

abbreviations used in the table are:

DELST: 5 mm cellulose adhesive tape debond insert
DELPT: 5 mm PTFE tape debond insert,

as described in Section 5.2.6. All test pieces had a nominal thickness of 2 mm and a gauge length of 10 mm (Figure F-1).

The plain strength figures show that there is a consistent tendency and debonding of the tabs yields average results above 1700 MPa. Note that the value for the sample DELST is approximately the average tensile strength determined with a similar specimen with longer gauge length. The coefficient of variation is low in all cases, particularly for the sample DELPT with C_V being only 2%.

Specimen type	UCS		Modulus		Maximum Strain	
	Mean [MPa]	C_V [%]	Mean [GPa]	C_V [%]	Mean [%]	C_V [%]
DEB	1761	4.7	121.6	2.3	2.22	12.8
DELPT	1704	2.0	119.6	4.7	1.99	9.4
DELST	1806	4.8	123.0	2.6	2.22	13.5

Table 6.1.2-1: *Test results for the compressive strength of XAS/914C using the ICSTM test method with improved specimens.*

Table 6.1.2-1 lists the mean of the strain maxima which were recorded for the individual specimens. The stress-strain curves given in Figures F-7, F-9 and F-10 reveal the reason for the high strains in some cases: bifurcation indicating buckling of the test pieces is apparent causing additional compressive stress on the concave side of the specimen.

In Table 6.1.2-2 stresses calculated from the (extrapolated) curves using the maximum compressive strain are given. These stresses, which were sustained in the centre of the gauge section without causing any apparent damage (failure occurred near the tab tip in most cases), are of the order 1900 to 2000 MPa. This suggests that stress concentrators still promote failure and that the intrinsic compressive strength of the material is higher than the measured (mean) ultimate stress. Of course it has to be noted that the absolute value will depend on the extrapolation. Using a second order polynomial will yield even higher stresses.

	DEB		DELPT		DELST	
Specimen No	ε^*max [%]	$\sigma(\varepsilon^*max)$ [MPa]	ε^*max [%]	$\sigma(\varepsilon^*max)$ [MPa]	ε^*max [%]	$\sigma(\varepsilon^*max)$ [MPa]
1	2.57	2101	2.13	1941	1.72	1704
2	1.78	1743	1.8	1756	1.99	1869
3	2.26	1999	2.52	2088	2.25	1950
4	2.11	1931	2.21	1977	2	1874
5	2.39	2048	2.44	2064	2	1874
MEAN	2.22	**1964**	1.99	**1965**	2.22	**1854**
Buckling specimens	2.33	**2020**	2.33	**2018**	2.13	**1910**

ε^*max *maximum compressive strain at fracture*

Table 6.1.2-2: *Ultimate compressive stresses calculated from maximum strains using the extrapolated compressive stress-strain curve.*

Figure 6.1.2-1 shows different curve fits to the experimental data. It also illustrates that the declining axial stiffness of the composite suggests an ultimate compressive stress of well below 2500 MPa, an observation first made by Port (1982).

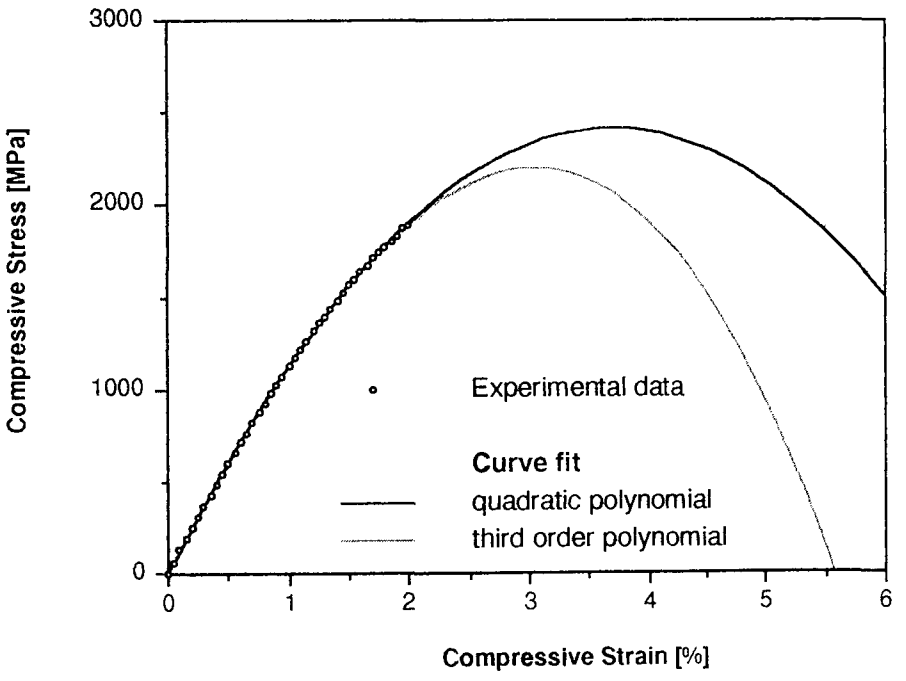


Figure 6.1.2-1: *Polynomial curve fits to experimental compression data.*

As indicated above, most of the test pieces still failed near the tab edge into the gauge section. Specimens of the sample DELST, which seemed to be the best aligned ones, occasionally failed at the end of the debond insert as demonstrated in Figure 6.1.2-2. This failure mode has to be regarded as valid as opposed to invalid end failures. The gauge section, although subjected to, so far, unrealised high (uniform) stresses, showed no signs of damage, as mentioned before. The previously made assumption that most of the damage done to the test piece is post-failure is proven by the fact that specimens which failed at high stresses at the end of the debond insert showed no splitting or other signs of interfacial failure (Figure P-11 (e)).

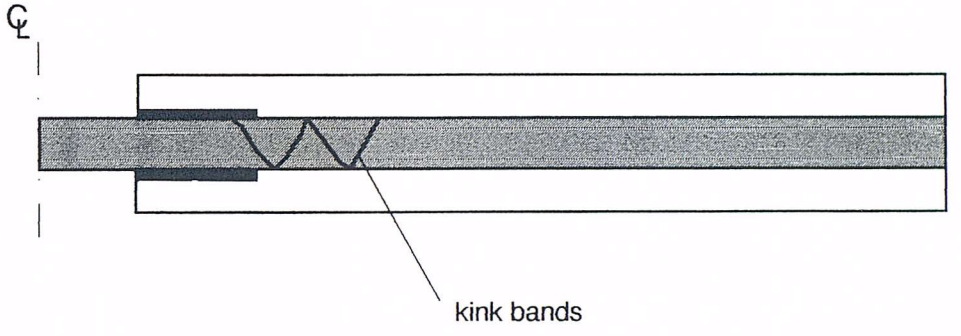


Figure 6.1.2-2: Failure mode of an improved specimen using the ICSTM method in some cases.

6.1.3 Apollo 43-750/9106C

The high-strength Courtaulds Apollo 43-750 fibre is incorporated in an experimental grade toughened epoxy resin, code 9106C. Batches of pre-impregnated tapes containing fibres with different levels of surface treatment, from non-treated fibres to fibres with 100% of the usual cycle, were produced by Courtaulds. A large experimental programme using this material was planned in order to compare the different test methods presented in Chapters 4 and 5 and to examine the influence of interfacial properties on the compressive strength of CFRP. Unfortunately, although the curing cycle for 9106C has been modified several times, the final result was not satisfactory. The cured composite panels were considerably thicker than anticipated nominal values and the compressive strength was relatively low.

Courtaulds quoted a compressive strength of around 900 MPa for the composite with fully treated fibres. Unknown factors seemed to reduce the compressive strength of the systems and were believed to override the influence of fibre surface treatment. In

particular, problems with the resin formulation were encountered at Courtaulds. When these facts became obvious most of the comparative part of the programme was discontinued. On the other hand, it was thought that the low compressive strength of the composite might reveal valuable information regarding the cause of compressive failure of CFRP.

The compression tests were therefore carried out. Standard test pieces covering the whole range of fibre surface treatment were prepared for two test methods: the Birmingham and the ICSTM methods. Four levels of fibre surface treatment were examined (in brackets are the abbreviations used in the tables): 0% (01), 10% (X), 50% (L) and 100% (C1, C2) of the standard treatment as specified by Courtaulds.

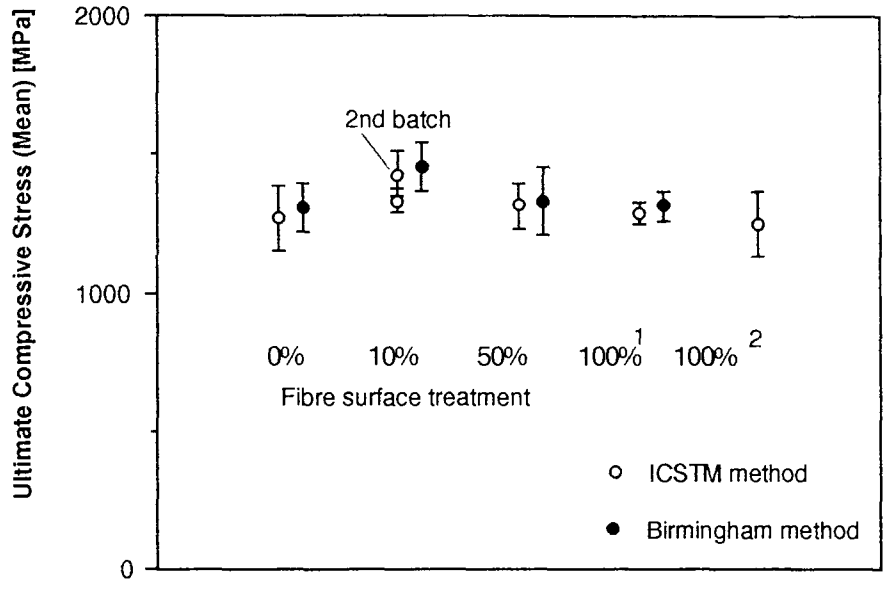
Preliminary tests showed that with a radius specified in Figure 4.1-1 most Birmingham method test pieces failed at the end. The specimens therefore had to be remachined to reduce the centre thickness. The gauge length, consequently, was slightly longer than 11.5 mm, but due to low failure stresses and high fibre stiffness no test piece buckling has been observed. Some of the ICSTM specimens also failed by kinking of fibres starting from the end. Obviously, the tab thickness, i.e. the tab stiffness, should have been adjusted to the increased specimen thickness. Unfortunately, producing another set of specimens could not be considered.

The results of all tests are listed in Tables T-21 and T-22. They are, in general, about 50 % higher than the ones quoted by Courtaulds using the CRAG method. A problem encountered with test pieces failing at the end was to decide whether a result from any invalid failure should be disregarded. It was decided to include the value if it was higher than the mean of the 'valid' failure stresses of the sample. The test results therefore represent a lower boundary of the compressive coupon strength which can be gained with the two methods, particularly regarding the ICSTM method.

Figure 6.1.3-1 shows the mean values of the compression tests. It includes a second sample of five ICSTM test pieces with 10% fibre surface treatment. This sample was accidentally left in a oven in order to post-cure the tabbing adhesive where it reached a temperature of 140°C for approximately 30 minutes. Since the curing temperature of the composite was 170°C, no significant effect from this 'post-curing' was expected. The mean result of this sample (1428 MPa, $N = 6$) was higher than the one for the first sample and comparable to the result of the Birmingham method.

In order to eliminate fibre volume fraction effects the fibre volume fractions of several samples have been determined in different laboratories, see Table 6.1.3-1. The values are consistent within ±1% fibre volume fraction between laboratories and the mean values are 57% ±1.5% FVF for the different panels.

The test results do not suggest an influence of fibre surface treatment on the compressive strength of this material. The composites containing fibres with 10% surface treatment seem to have the highest compressive strength, whereas there is little difference for the others even if the slight difference in fibre volume fraction is taken into account.



100%[1] and 100%[2] denote two different panels containing fully surface-treated fibres

Figure 6.1.3-1: *Test results for the compressive strength of Apollo 43-750/9106C containing fibres with different levels of fibre surface treatment; ICSTM and Birmingham test methods.*

	0%	10%	50%	100%
RAE 1	56.7	58.5	55.0	58.2
RAE 2	56.1	58.0	54.8	58.8
Courtaulds	54.7	57.5	57.1	59.4
Mean	**55.8**	**58.0**	**55.6**	**58.8**

Table 6.1.3-1: *Fibre volume fraction of Apollo 43-750/9106C as measured in different laboratories.*

In Figure 6.1.3-2 some typical stress-strain curves are shown. Only a few test pieces were instrumented with strain gauges and, as mentioned above, buckling did not occur. For comparison an XAS/914C stress-strain curve is also plotted.

The higher stiffness of the Apollo system is clearly visible, which is in accordance with manufacturers' data for the (tensile) fibre stiffness: 230 GPa for the XAS and 300

GPa for the Apollo fibre, respectively. There is no obvious influence of interfacial properties on the axial modulus of the composite as Figure 6.1.3-3 illustrates, where the normalised modulus is shown versus degree of fibre surface treatment. The average modulus is approximately 152 GPa, 27% higher than the average 120 GPa of XAS/914C. Taking into account a resin modulus of about 5 GPa the ratio of composite moduli is equivalent to the ratio of fibre moduli.

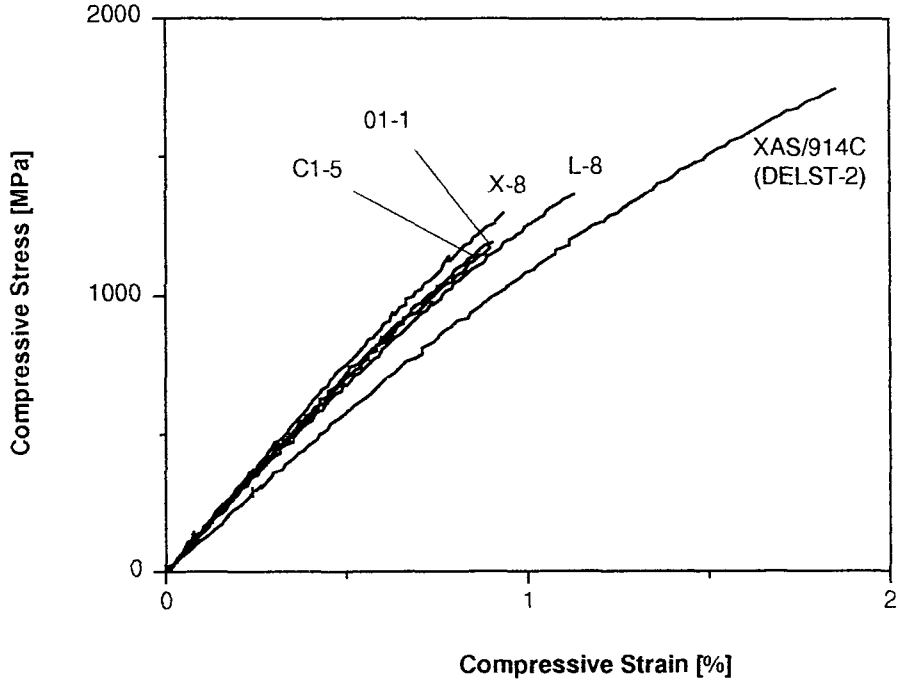


Figure 6.1.3-2: Typical stress-strain curves for Apollo 43-750/9106C containing fibres with different levels of fibre surface treatment; ICSTM test method.

Failure was similar for all materials; only the specimens containing non-treated fibres exhibited slightly more brushing, i.e. fibre/matrix debonding, of the fracture surfaces when failure occurred in the gauge section.

In conclusion, it can be said that at low failure stresses the Birmingham and ICSTM methods are comparable. This is not surprising, since the effects mentioned in Chapter 5, namely interfacial cracking and consequential bending, as well as tab tip debonding and macroscopic instability, do not occur to the same extent at the low stress and strain levels observed with this material. On the other hand, the data obtained by Courtaulds demonstrate that there is a considerable influence of the method of load introduction, even at low failure stresses. In a later chapter the fibre alignment will be shown to override the effect of interfacial properties.

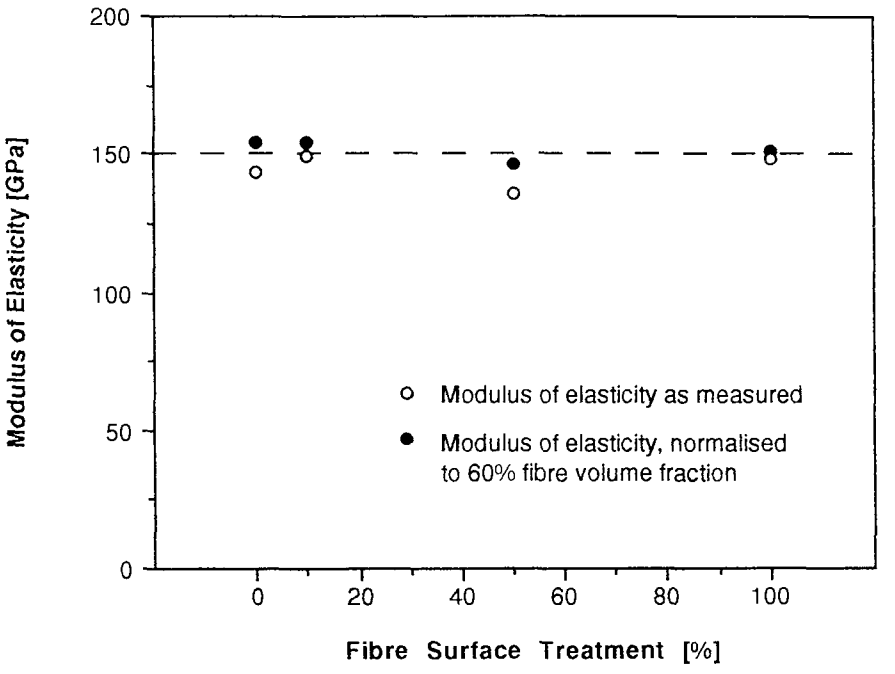


Figure 6.1.3-3: Normalised modulus of elasticity versus level of fibre surface treatment for Apollo 43-750/9106C.

6.1.4 AS4/PEEK (APC-2)

The thermoplastic poly-ether-ether-ketone reinforced with carbon fibres is known to have moderate compressive strength. ICI quotes tensile strengths of 2130 MPa for reinforcement with Hercules AS4 fibre and 2891 MPa for the Hercules Magnamite IM-7 fibre at 61% fibre volume fraction. The compressive strengths using the IITRI method are given as 1100 MPa and 1139 MPa, respectively. It was therefore of some interest to find out if there is a similar influence of the test method on the strength result as observed with carbon fibre-reinforced epoxies.

Two different panels of unidirectional APC-2 with a nominal fibre volume fraction of 61% have been manufactured at ICI for compression testing. The first panel contained 16 plies and the second 32 plies of unidirectional prepreg so that the nominal thicknesses were 2 mm and 4 mm, respectively. Specimens with a 5 mm cellulose tape tab tip debond insert, abbreviation APCS, were manufactured from the 16-ply panel and, as usual, instrumented with back-to-back strain gauges. From the 4 mm panel specimens were machined as described in Section 5.2.3, the gauge length in both cases being 10 mm.

Tables T-19 and T-20 contain the test results of the compression tests and Figures F-12 and F-13 show the corresponding stress-strain curves. The results confirm, although it is not immediately obvious, the observations and conclusions drawn in Chapter 5.

Contrary to the case of XAS/914C the ultimate compressive stress for the milled specimen is considerably lower than that for the improved specimen: 1133 MPa for the former, which is the same as the ICI-value, and 1511 MPa with an individual value as high as 1658 MPa for those with a debond insert. Scatter is comparatively low (2.2%) for the milled specimens.

The explanation for these findings is to be found in the high failure strain and high shear strength of the PEEK matrix. APC-2 has about the same axial stiffness as XAS/914C and the compressive strength is likely to be lower as the results for the specimens with debonds suggest. Consequently, tab tip delaminations which occurred in the 914-system at relatively low strains reducing stress concentrations did not happen, or not to the same extent, in APC-2. Therefore, the specimen failed compressively due to stress concentrations at the tab tips. And, indeed, tab tip delaminations were hardly found in failed specimens. For this reason, the machined specimen type cannot be recommended for APC-2. The debond insert, on the other hand, had the same effect as on the thermoset system, namely to separate stress concentrators, which is reflected in the increase of failure stress. Interestingly, one specimen of each sample (APCS-2, APCD-3 in Table T-19 and T-20) failed in the centre of the gauge section, i.e. the kink initiated at least 3 mm away from the tab tip, see Figure P-11 (f). Shear stresses (see Section 5.2.2) might have played a role since bending did occur in both cases (Figures F-12 and F-13). But since this kind of failure was never observed for the equivalent XAS/914C specimens, it is assumed that these specimens failed in 'true' compression. The low result of the centrally failed test piece without debond insert (1111 MPa, compared to 1658 MPa of the one with insert) indicates severe stress concentrators within the material. In Chapter 11 this will be discussed further.

Generally, the fracture surfaces looked similar to those of epoxy test pieces. The only noticeable difference was that much less splitting and brushing of the surfaces was present due to the toughness of PEEK. SEM micrographs of fracture surfaces are shown in Figure P-12 (XAS/914C) and P-13 to P-16 (APC-2). Figure P-13 shows evidence of in-phase fibre microbuckling in APC-2 with Figures P-14 and P-15 illustrating flexural final fibre failure. The similarity of the fracture surfaces of XAS/914C and APC-2 suggest fibre microbuckling failure for both materials.

The stress-strain curves of APC-2 show, as would be expected from the low failure stresses, no signs of a buckling type of failure, with the exception of APCS-3, where most probably compressive failure initiated macroinstability. Asymmetric delamination cannot be excluded as a cause, the more so as some tab delamination was found in this case.

The stress-strain curves exhibit a similar degree of nonlinearity to the equivalent XAS/914C curves, as can be seen from Figure 6.1.4-1, where two representative stress-strain curves are shown. As the degree of overall fibre misalignment of the two systems was found to be quite different, the nonlinearity is most probably caused by the nonlinear elastic behaviour of the carbon fibre.

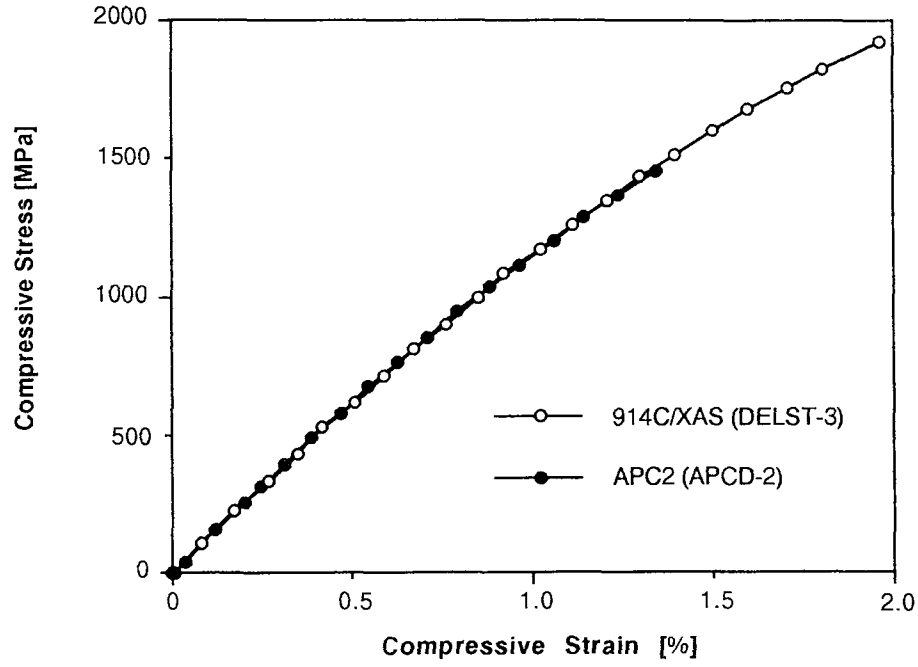


Figure 6.1.4-1: Comparison of compressive stress-strain curves of an APC-2 and an XAS/914C specimen.

6.2 Unidirectional GRP

Although not directly a subject of the present investigation, it was felt that comparative tests using glass fibre-reinforced plastics could be of use for studying the compressive behaviour of CFRP. Two systems have been examined: E-glass fibre-reinforced nylon with different levels of fibre volume fraction, and E-glass fibre-reinforced epoxy (Ciba Geigy Fibredux 913).

6.2.1 E-Glass Fibre-Reinforced Nylon (ICI 'Plytron')

Pultruded panels with nominal fibre volume fractions of 23%, 29% and 35% were available for testing. Standard specimens according to Figure 5.2-1 were produced from this material using the same tabbing material as for CFRP. The crosshead rate of motion was 2 mm/min which is approximately equivalent to 3 % strain/min. A summary of the test results is given in Table T-23.

It was mentioned before that the magnitude of stresses responsible for tab tip debonding depends on the ratio of composite stiffness and tab stiffness. For a given tab stiffness the stresses are strain dependent. Debonding of the tab tips indeed occurred in all cases, mostly in a symmetric fashion, between 1 and 2.5% strain. As the failure strain of glass fibre composites is considerably higher, tab debonding did not cause immediate failure but acted as a stress relief. Figure 6.2.1-1 shows typical stress-strain curves and an arrow points at first tab debond.

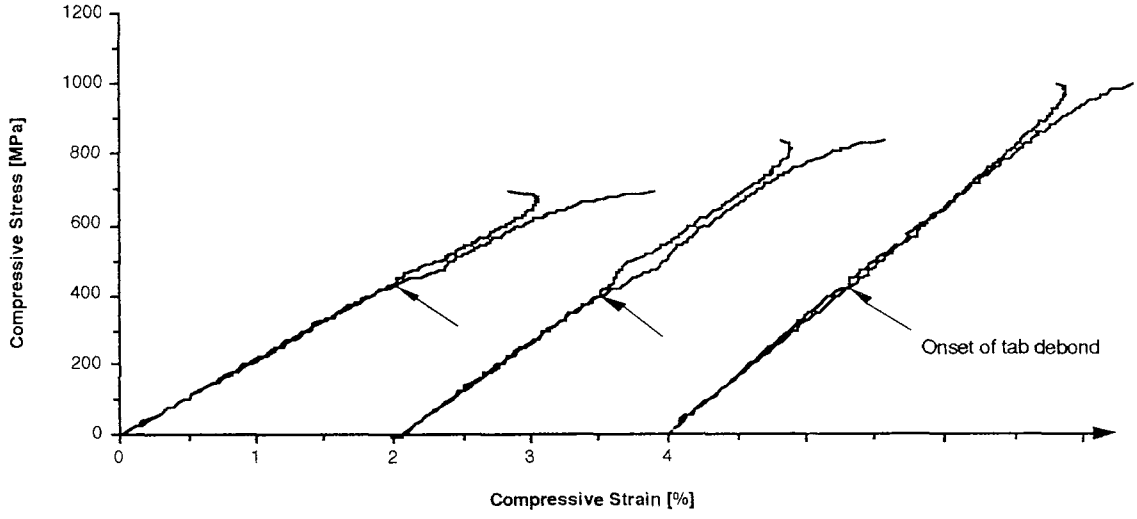


Figure 6.2.1-1: Typical compressive stress-strain curves of ICI 'Plytron'.

Most stress-strain curves exhibit well developed bifurcation, indicated by 'B' in Table T-23, suggesting macroinstability of the test piece. In Figure 6.2.1-2 the test results are presented in normalised form. The ultimate compressive stress is plotted versus the normalised bending stiffness of the test piece, which is modulus of elasticity multiplied by the square of test piece thickness. The Euler buckling load is proportional to this value. The graph clearly shows a linear relationship for the tests where bifurcation occurred, hence strengthening the assumption of macroscopic instability. This again stresses the need to design the specimen specifically for the material to be tested. The composite examined does not exhibit significant stiffness decrease as described below, but the relatively high stresses reached by reducing stress concentrations introduce the problem of macrobuckling as observed with CFRP. In Chapter 10 this will be treated analytically.

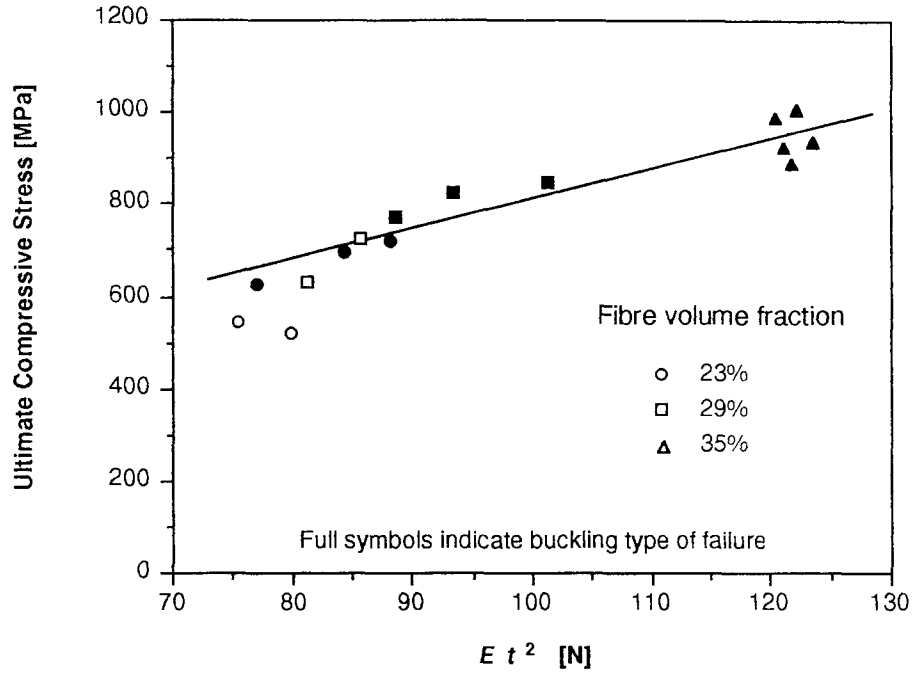


Figure 6.2.1-2: *Ultimate compressive stress for ICI 'Plytron' versus the product of modulus of elasticity and the thickness of the test piece squared.*

The following Figure 6.2.1-3 illustrates an important feature of glass fibre-reinforced composites. Here, the mean of the surface strains from Figure 6.2.1-1 are plotted versus stress. These mean stress-strain curves are almost linear reflecting the fact that the elastic behaviour of glass fibres is linear.

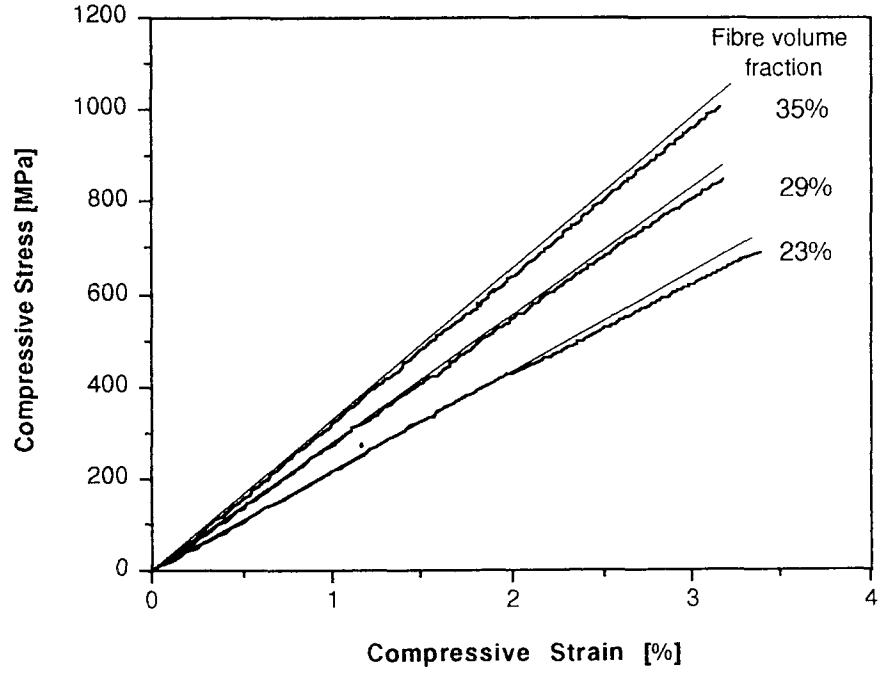


Figure 6.2.1-3: *Typical mean compressive stress-strain curves of ICI 'Plytron'.*

Two factors can be held responsible for the slight nonlinearity, i.e. reduction in stiffness. Firstly, the stiffness of the matrix decreases with axial strain, which in ~~the~~ the case of very low fibre volume fractions is not a negligible effect. Secondly, the initial imperfection of fibres which, although very small, contributes to nonlinear strain characteristics at high strains. This will be analysed in more detail in Chapter 11.

6.2.2 E-Glass Fibre-Reinforced Epoxy

Only a few compression tests using E-glass fibre/Fibredux 913G specimens were carried out in order to obtain the compressive stress-strain relationship of glass fibre-reinforced epoxy with high volume fraction (about 60%). The stress-strain curves of two ICSTM test pieces with debond insert are shown in Figure 6.2.2-1. The mean curves show only a very small degree of nonlinearity as observed with glass fibre/nylon. The mean of the compressive strength of the two tests was 1531 MPa. This value, however, should only be taken as an estimate, since the material, remaining from a former project, was several years old and the moisture content and other details were not known. It has to be mentioned that the specimen with the higher ultimate stress seemed to have failed by buckling.

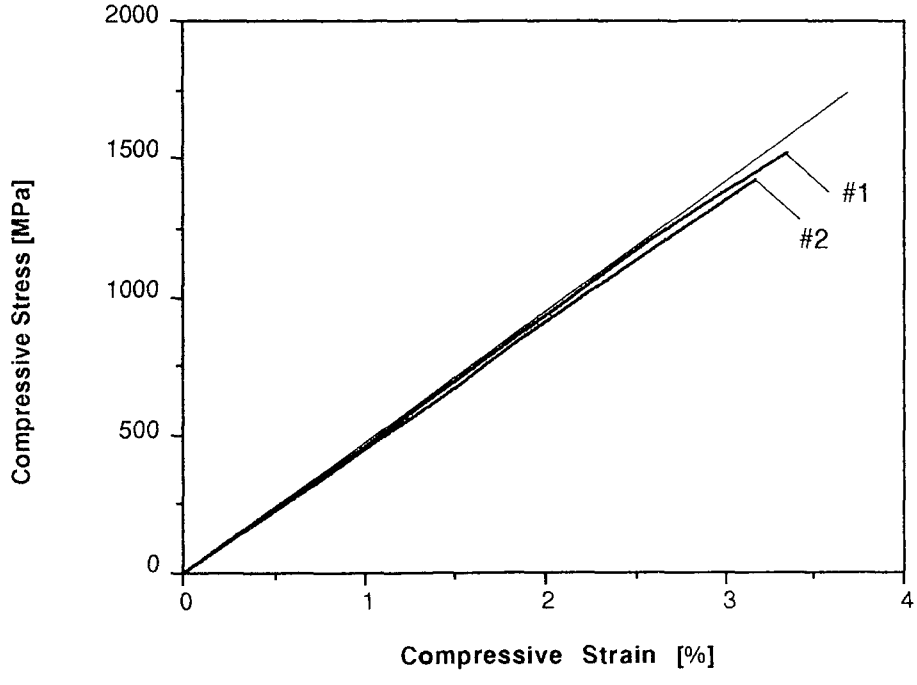


Figure 6.2.2-1: Stress-strain curves of unidirectional E-glass fibre/913G ($V_f \approx 60\%$) using the ICSTM method; specimen with debond insert.

6.3 Non-Standard Specimens

Some results of compression tests using the rig presented in Chapter 5 and the specimen design described in section 5.3 are given in this section. The intention was to prove the feasibility of the proposed test method and to gain some insight into compressive behaviour of CFRP under various experimental conditions.

6.3.1 Woven Cross-Ply CFRP

This investigation was initiated by researchers of Liverpool University. Test results they gained using the IITRI compression test method were not satisfactory as they exhibited large scatter. The material came in sheets with a mirror surface mould face and a coarse back side which made symmetric tabbing difficult.

It was felt that using the ICSTM method could lead to more consistent values. Therefore, flat test pieces sandwiched between end tabs as described in section 5.3 were prepared for testing. For comparison identical test pieces with aluminium tabs bonded on at Liverpool University were tested as well. The modulus of elasticity was determined using only one strain gauge on the flat side of the test piece.

The tests with the sandwiched test pieces did not present any problems and exhibited consistent failure modes. Failure seemed to be by buckling of individual layers as shown in Figure P-18 (b). In most cases 'pops' could be heard just before failure. These could be identified in the stress-strain diagram and are most probably caused by buckling and delamination of surface bundles.

Testing of the test pieces with aluminium end tabs was more troublesome due to the way the specimens were manufactured. In order to improve the bond to the composite, which as mentioned had surfaces of unequal roughness, serrations have been cut into the aluminium tabs. According to the standard procedure the outer surfaces of the test pieces received were ground flat and the ends were machined square to the specimen axis before testing.

These test pieces failed partially at relatively low loads under the tab near the deep serrations cut into the tabs. This introduced strong bending moments leading to an overall failure at comparatively low average stresses. Adequate bond preparations are likely to lead to similar results for the tabbed specimens as for the untabbed, as the result for specimen #5 suggests. This specimen failed centrally without a sign of failure under the tabs.

As the test piece preparation of the simple flat specimens requires much less effort than preparation and machining of tabbed specimens, the former are preferred for determination of compressive properties using the ICSTM fixture.

In comparison to the results gained using the IITRI method it is found, as before, that the ICSTM method gives higher strengths whilst specimen constraints are reduced and scatter of results is lower.

6.3.2 Multidirectional CFRP

As pointed out in the previous chapter, testing multidirectional laminates is an attempt to assess strains in unidirectional layers rather than to produce design data for the lay-up. The laminate tested was the quasi-isotropic lay-up:

$$[(+45/-45/0/90)_3]_S$$

with a nominal thickness of 3 mm.

Figure 6.3.2-1 shows the stress-strain curves of the five specimens tested. The failure strain in all cases is higher than 2.1%, which is some 30% higher than the mean failure strain of a unidirectional coupon test piece. The failure strains, however, are comparable to the maximum strains on the compressed side of the gauge section when the unidirectional test piece buckles.

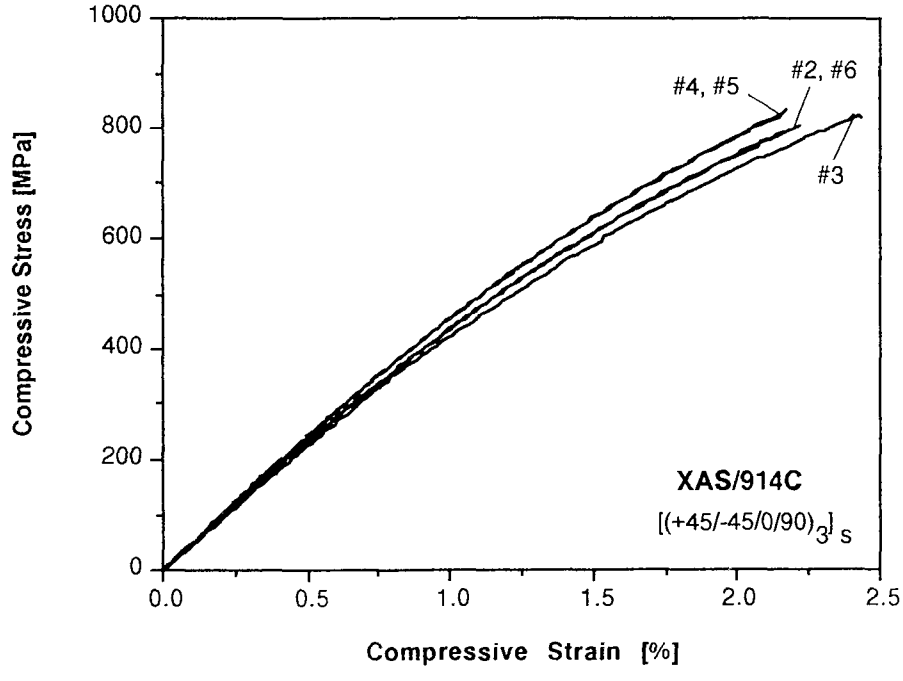


Figure 6.3.2-1: Compressive stress-strain curves of laminate L1; ICSTM method.

A typical test piece failure is shown in Figure P-18 (c). Figure P-19, where a 0°-layer within the laminate is shown, indicates that compression failure of the 0°-layer within the laminate is of similar nature to compression failure in a coupon test piece. It is therefore likely that final failure of the test piece is triggered by compressive failure of the 0°-layers, as pointed out by Soutis and Fleck (1988).

6.3.3 Thick Woven Cross-Ply GRP

The compression characteristics were required for woven cross-ply glass fibre-reinforced plastic delivered in sheets of 10 mm thickness. Preferably, the material should be tested without machining the original mould surfaces. No standard compression method was capable of accommodating a test piece of such dimensions. The decision therefore fell on a specimen with a square cross-section of 10 mm width and a unsupported gauge section of 25 mm which could be tested in the ICSTM fixture. The ends of the test piece were inserted in the end blocks of the ICSTM fixture and slightly clamped. No additional tabbing material was used.

Failure occurred in all cases in the unsupported section in a layer kinking mode shown in Figure P-18 (a). This was the anticipated mode of failure as the maximum inclination of fibres in the individual layers was as high as 10°. Stress concentrations are believed to play a minor role because the strong layer waviness overrides other effects. For the same reason end failures did not occur because through-thickness deformation and, as a consequence, layer buckling, is suppressed by the end blocks of the fixture. The measured values, therefore, should give a good estimate of the compressive strength of the material on a structural scale.

CHAPTER 7 MECHANICAL CHARACTERISATION

In this Chapter the complementary mechanical tests related to the subject of compression are described and the results are given and discussed.

7.1 Tensile Tests

Tensile tests have been carried out in order to determine the complete stress-strain response of unidirectional XAS/914C. These data are used as input for a model for the four-point bend test. The dimensions of the tensile specimen, basically a compression test piece with 100 mm gauge length, are given in Figure 7.1-1. It was not intended to produce tension design data therefore this test piece was thought to match the conditions of the compressive test piece best. Specimen preparation and testing conditions were as described for the compression test in Chapter 3.

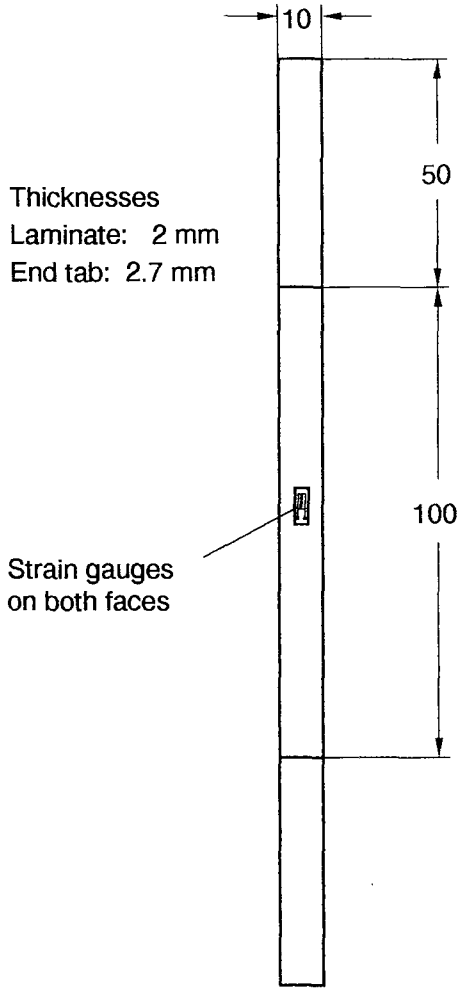


Figure 7.1-1: Test piece for determination of tensile properties.

The results for ultimate tensile stress and longitudinal modulus of elasticity are listed in Table T-27; the individual stress-strain curves are presented in Figure F-15. Figure 7.1-2 shows the stress-strain curves of the tension tests including the ones from compression tests using the improved ICSTM specimen (DELST).

The strength values, mean 1832 MPa, have to be regarded as a lower bound of the tensile strength of XAS/914C. A more appropriate specimen design as, for instance, the one with a waisted centre gauge section recommended by CRAG (Curtis, 1988), would most probably yield higher values.

Of more concern, however, are the relatively low modulus of elasticity values, the mean of the 0.25%-secant modulus being 122 GPa. Based on the curve fit given in Figure 7.1–4 the difference between the +0.25%- and -0.25%-secant modulus is 3.75%. That means that the measured tensile modulus is in agreement with the average compression modulus determined in the present investigation (see Tables T-1 to T-10). However, in literature and manufacturer sheets values between 130 GPa and 140 GPa (CIBA-GEIGY product sheet: 135 GPa; Courtaulds: XAS-fibre: 230 GPa which would give approximately 140 GPa for a composite with 60% fibre volume fraction) are quoted for the tensile modulus. The fibre volume fraction determined for several control pieces of different panels was close to the nominal value of 60%. Modulus of elasticity measurements for aluminium and steel using the same strain gauge circuit yielded 73 and 206 GPa, respectively, which are reasonable values for those materials. The calibration of the load cell was checked as well and found to be correct. Also, the tensile modulus of a CFRP test piece was the same when measured in a different laboratory. Therefore, it is assumed that the low modulus values of the tests are genuine.

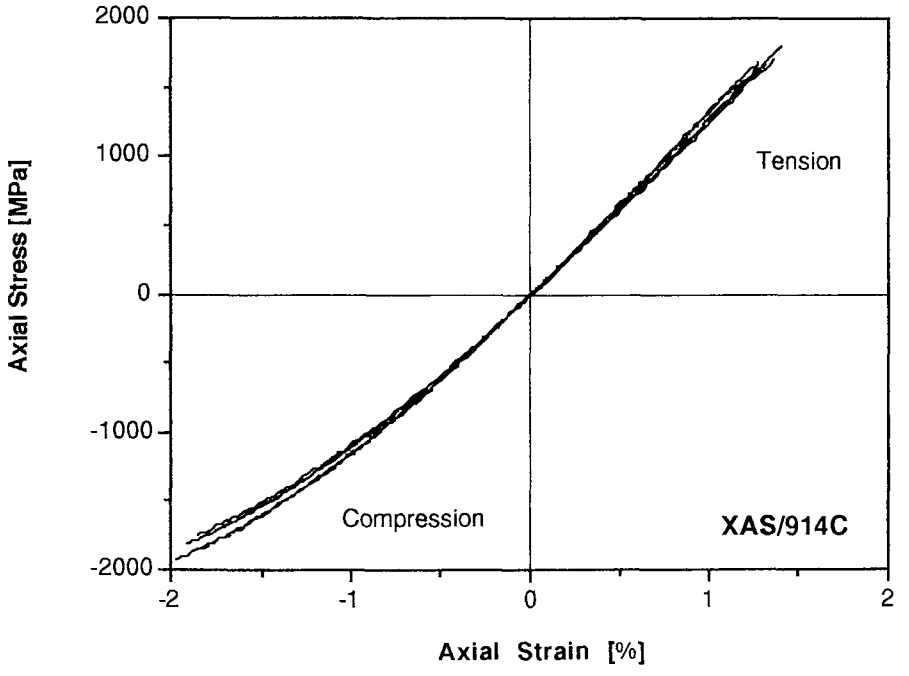


Figure 7.1-2: Stress-strain curves from individual tension and compression tests.

The tensile stress-strain curves exhibit the typical slight stiffening characteristic, well known for CFRP. It may be noted here that any layer misorientation would induce a stiffening stress-strain response if the misalignment angle is very small. Most of the

fibres are clamped on both ends so that any shear action can be neglected and under a tensile load initially inclined layers become oriented in the loading direction resulting in an increased stiffness of the test piece with increasing strain.

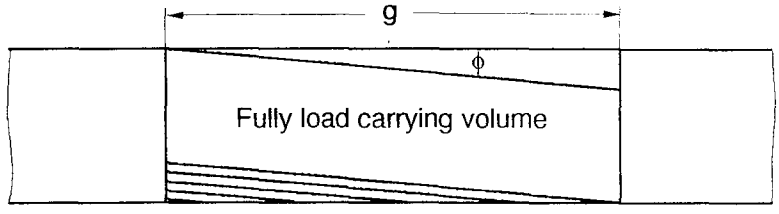


Figure 7.1-3: Illustration of a misaligned single layer in a unidirectional test piece.

At greater angles of misalignment the portion of the test piece sheared under tension gains influence causing decreasing stiffness of the test piece. An overall layer misalignment of ±1° in a test piece of 10 mm width and 100 mm gauge length results in 35% of the fibres not gripped at both ends but ending on a free surface (compare Figure 7.1-3). In compression any misalignment will be increased resulting in an increased level of nonlinearity if shear deformation is not restrained, as pointed out in Chapter 5.

Failure was in all cases accompanied by extensive longitudinal splitting. Normally, fibre failure initiated at the tab tip due to longitudinal stress concentrations. Only one of five test pieces fractured approximately 10 mm from the tab edge. Before final failure surface fibre bundles fractured causing irregular strain gauge readings (Figure F-15), giving further reason for waisting the specimen. Unfortunately, the extensometer failed to work reliably in most cases due to failure of the springs in the measuring levers which guarantee precise positioning. Often it was found that, particularly in the initial part of the stress-strain curve, slippage of the extensometer occurred making the calculation of the modulus difficult, if not impossible.

Only one comparative stress-strain curve is available (Figure F-15). The agreement with the strain gauge recordings in this case is reasonable, particularly in the initial part of the curve from which the modulus is determined. Generally, it was found that the extensometer used in this investigation needed much attention and was difficult to maintain on an operating level. Strain gauges, although requiring more preparative work and being more expensive in the long term, were found to be more reliable and are, therefore, preferred to extensometers. However, it should be stated that the extensometer in question often was not treated properly and an extensometer in good condition is likely to prove more reliable.

In order to approximate the complete stress-strain relationship of XAS/914C the individual stress-strain curves shown in Figure 7.1-2 are curve-fitted and the average polynomial in tension and compression determined. These are the data represented by 'experimental data' in Figure 7.1-4. The third order polynomial which fits these points best, representing the stress-strain curve of XAS/914C for strains ε between -1.8% and +1.4%, is:

$$\sigma = 1233\varepsilon + 90.7\varepsilon^2 - 27.0\varepsilon^3 \qquad (7.1\text{-}1)$$

or, second order:

$$\sigma = 1193\varepsilon + 108.9\varepsilon^2 \qquad (7.1\text{-}2)$$

where the stress σ is in MPa and ε in % (tensile strain positive, compressive strain negative). Obviously, this is only an approximation as the number of test pieces is small. The compression data from the sample DELST were chosen because this sample was thought to give the most representative stress-strain curves up to the highest strain level of all compression tests.

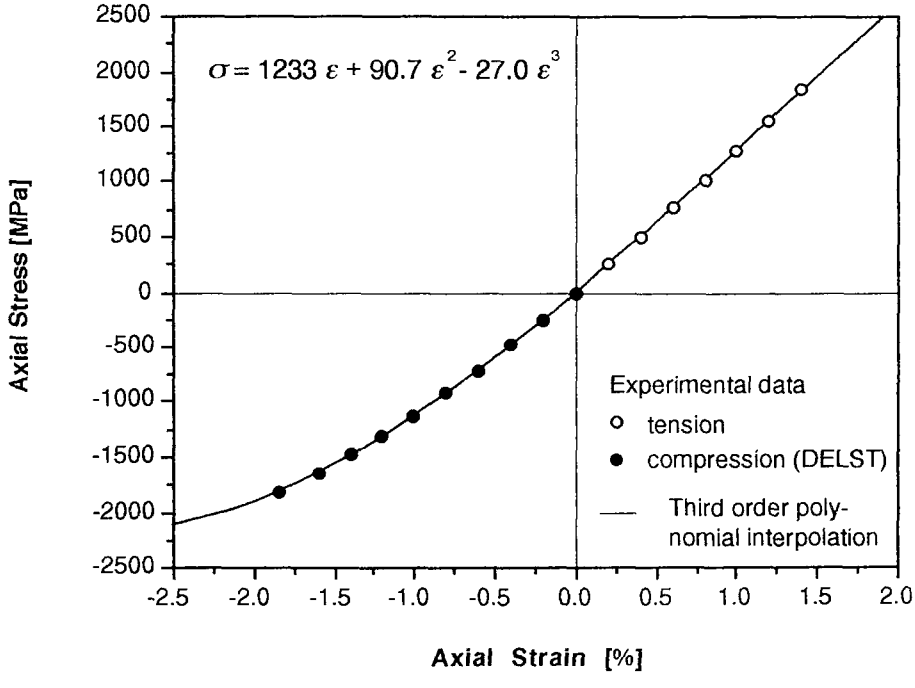


Figure 7.1-4: Average stress-strain data of XAS/914C in tension and compression and curve fit.

Tangent and secant modulus of unidirectional XAS/914C are determined as tangent and secant slope of the approximated curve fit. The values are normalised to the values at zero strain and plotted versus axial strain in Figure 7.1-5. This graph clearly illustrates

the variation of modulus with axial strain, a topic which will be a subject of discussion in Chapter 10.

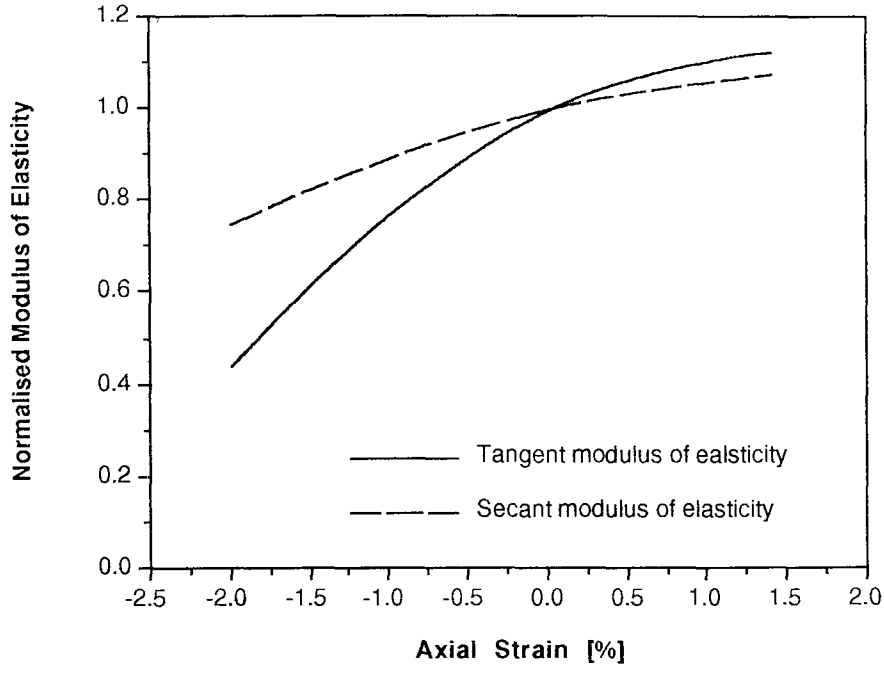


Figure 7.1-5: Normalised modulus of elasticity versus axial strain for XAS/914C.

7.2 Flexure Tests

Flexure tests are known to yield higher strengths than would be expected from results of tension and compression tests. If the material behaved linearly the flexural strength would be limited by the lower value of tensile or compressive strength of the material. Regarding CFRP this is generally not observed. The ICI data sheet for APC-2/AS4, for instance, quotes 2130, 1100 and 1880 MPa for tensile, compressive and flexural strength. Even more contradictory are data for XAS/913 quoted by Westland[+] : 2000, 1070 and 2460 MPa. The correlation of compressive strength and flexural strength, considering test results gained with the improved compression test method, seemed therefore of particular interest. Flexure test results will be described below and a nonlinear model will be used to interpret the experimental findings in Section 9.4.

Flexural properties of XAS/914C were determined using a four-point loading jig in accordance with ASTM D790M-84. The dimensions of test pieces and loading configuration are give in Figure 7.2-1.

[+] Michael Wisnom, seminar on flexural properties of CFRP at Imperial College, December 1990.

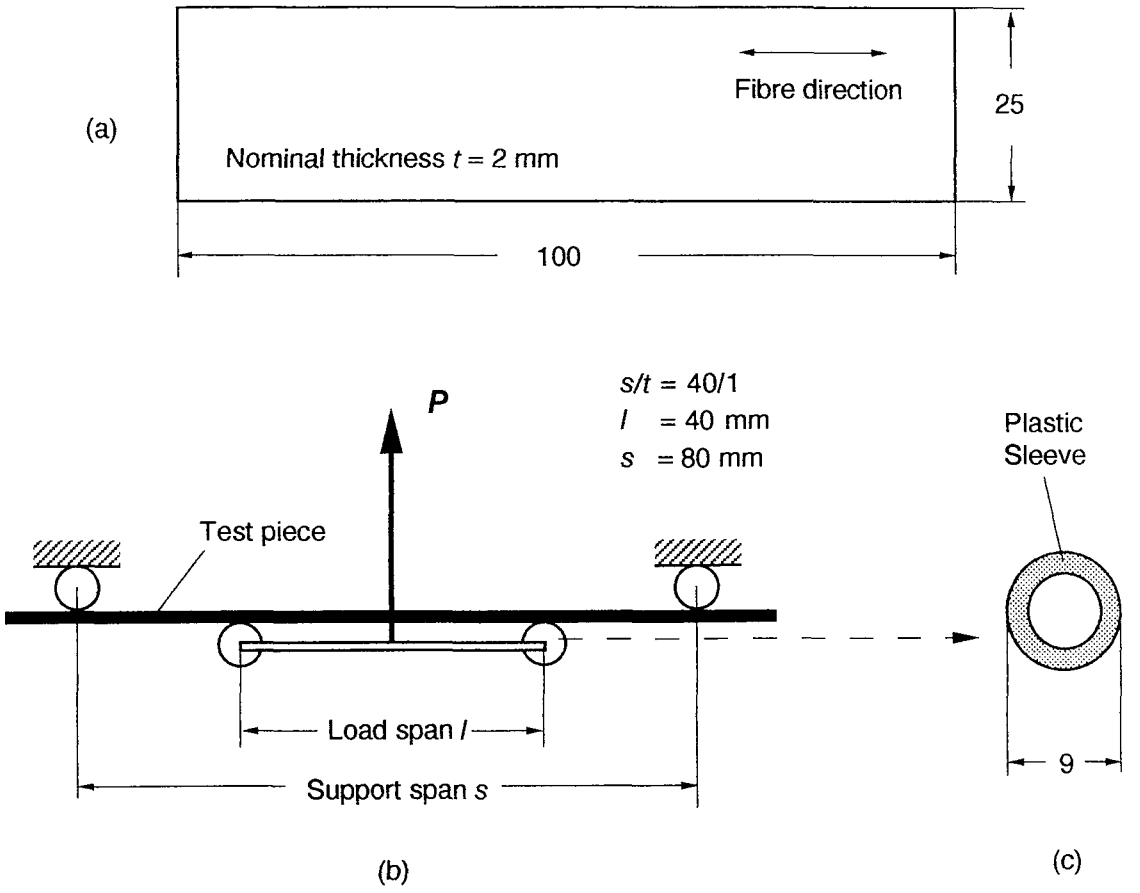


Figure 7.2-1: Dimensions of specimen (a), jig (b) and modified roller (c) for four-point bend tests according to ASTM D790 M.

Two specimens were tested using the standard rollers with a diameter of 6 mm and another two using plastic sleeves of approximately 1.5 mm thickness around the rollers. Strains are measured on the compression and tension faces of the test piece using strain gauges of the same type as in the previous tests.

According to ASTM D790M the surface stresses (equal on the compression and tension face) are calculated as:

$$\sigma_s = C\frac{3Ps}{4wt^2} \tag{7.2-1}$$

where P is the maximum load, s is the support span, w the test piece width and t the actual test piece thickness. C is a correction factor to take into account the nonlinearity of applied load and bending moment acting on the test piece due to large deformations, and is approximated by:

$$C = [1 - (10.91\frac{\delta t}{s^2})] \tag{7.2-2}$$

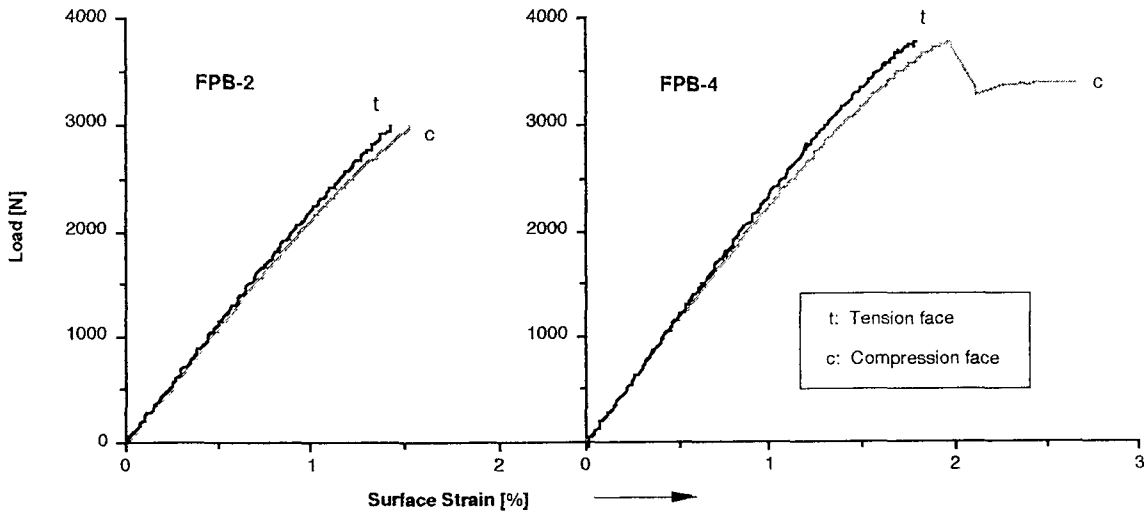
where δ is the maximum deflection of the centre of the specimen. The centre deflection, not recorded continuously in the tests, was estimated at fracture using a ruler attached to the jig.

Table 7.2-1 below summarises the results of the tests and typical stress-strain curves for both roller configurations are presented in Figure 7.2-2.

No	Loading rollers	t [mm]	w [mm]	P_u [N]	$\varepsilon_{t,u}$ [%]	$\varepsilon_{c,u}$ [%]	Mode of failure	δ (appr.) [mm]
1	standard	2.11	24.97	3048	1.33	-1.44	compr.	9
2	standard	2.04	24.72	2978	1.44	-1.54	compr.	9.5
3	plast. sl.	2.09	24.82	3696	1.69	-1.83$^+$ -1.93*	tension	12.5
4	plast. sl.	2.10	24.89	3784	1.79	-1.98$^+$ -2.65*	tension	13

$^+$ *Compressive strain at first tensile failure* * *Compressive strain at test stop*

Table 7.2-1: *Flexural test results of unidirectional XAS/914C.*



(a) (b)

Figure 7.2-2: *Typical stress-strain curves for four-point bending tests; (a) standard loading rollers; (b) plastic padded loading rollers.*

The striking result of these tests, observed earlier by Kretsis (1987) and Wisnom (1991) was that padding of the rollers changes the failure mode and increases the failure load by over 20%. With unpadded rollers failure was of a compressive nature above the loading rollers resulting in complete separation of the test piece. The plastic coated loading rollers, however, promoted tensile failure of the composite initiated, again, above the loading rollers and causing a brush-like appearance of the test piece. Remarkably, the failure process was gradual and, even when the test was continued (test piece #4) after tensile failure of the surface layers had occurred, compressive failure could not be provoked. Thus, a compressive strain of 2.65% was recorded with no sign of compression damage before the test was finally stopped. Both failure modes are shown in Figure P-17.

Table 7.2-2 summarises failure stresses calculated from ASTM D790M using Equations 7.2-1 and 7.2-2 (first and second column) and failure stresses calculated from the strains at failure - at first failure in the case of padded rollers - using the expression for the stress-strain curve given in Equation 7.1-1 (third and fourth column).

No	σ_S [MPa]	$\sigma_{S,corr}$ [MPa]	$\sigma(\varepsilon_t^+)$ [MPa]	$\sigma(\varepsilon_c^+)$ [MPa]
1	1645	1592 δ=9mm	1737	-1507
2	1737	1680 δ=9.5mm	1883	-1585
3	2043	1952 δ=12.5mm	2343	-1876
4	2068	1972 δ=13mm	2212	-1787

$^+$ strains at first failure

Table 7.2-2: *Ultimate surface stresses at specimen centre in four-point bending tests.*

In the following only the results achieved with the padded loading rollers will be discussed as the test pieces tested with standard rollers appear to have failed prematurely.

Due to the nonlinear stress-strain relationship there is a discrepancy of approximately 20% between compressive and tensile surface stress at failure, whereas the difference in strains is less than 10%. Significantly, both failure strains, the tensile as well as the compressive, are higher than the values gained in individual tension and compression tests. There are several possible reasons behind this phenomenon:

1. Longitudinal stress concentrations caused by load introduction are small in four-point bending tests.

   As the finite element analysis has shown, realistic longitudinal stress concentration factors are likely to be of the order of 1.1 to 1.2 in axial tests. Local contact stress concentrations, particularly on the compression side, are minimised by the use of plastic sleeves in the four-point bend test. They play an important role when small diameter steel rollers are used.

2. Shear stress concentrations caused by load introduction are small in four-point bending tests.

   The presence of shear stresses is believed to lower the compressive strength of a composite (see Chapter 11) .

3. Small volume of material is under maximum strain.

   Only the surface layers of the beam are subjected to maximum stresses. Wisnom (1991) observed a significant size effect in flexure tests. In particular, it was found that larger specimens failed in compression rather than in tension as the smaller ones. However, size effects are difficult to quantify experimentally. All testing hardware has to be scaled as well as the test piece. But increasing the thickness of the test piece increases the overall layer misalignment, during laying-up as well as in the curing process. Also, the fibres themselves are not scaled, so that identical stress conditions, where the load is introduced, are not obtained. This would mean that the size effect in compression is a structural rather than a material property, which explains why Weibull strength theory cannot be applied satisfactorily to compression failure of composites.

4. Three-dimensional stress state is present in the test piece.

   Compressive through-thickness stresses possibly suppress a lower strength mode of failure. It can be argued that compressive through-thickness stresses cause tensile in-plane stresses with the opposite effect on compression failure.

All these factors might contribute to the high failure strains, in particular in compression, realised in XAS/914C. The absence of severe stress concentrations (topic 1 and 2) are probably primarily responsible. This will be discussed further in connection with supporting experimental results from other tests in Section 9.6.

7.3 Interlaminar Shear Strength Tests

Short beam shear tests have been carried out on a range of materials for which compression data were available. The test according to CRAG is very simple and results usually exhibit low scatter. Figure 7.3-1 gives details of the specimen and jig used.

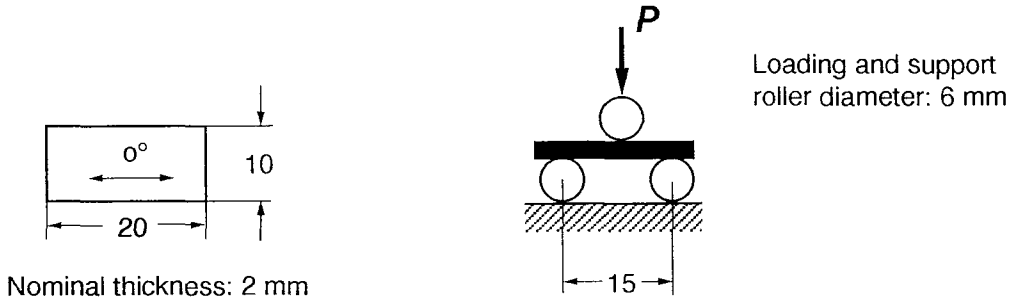


Figure 7.3-1: Specimen and jig dimensions for the short beam shear tests.

Assuming a parabolic distribution of the shear stress through the laminate thickness, with the maximum in the centre plane and vanishing shear stresses at the surface, the interlaminar shear strength (ILSS) S_{is} is determined as:

$$S_{is} = 0.75\frac{P_u}{wt} \tag{7.3-1}$$

where P_u is the ultimate load, and w and t the width and thickness of the test piece, respectively. It has to be noted that the laminate thickness of the test pieces in these tests was measured as fabricated (see Chapter 3).

The results of the short beam shear tests are summarised in Table 7.3-1 below. The abbreviations used are:

XAS/914C

ST2: XAS/914C 16-ply, standard peel ply.

ST3: XAS/914C 16-ply, standard peel ply, different panel to ST2.

PP2: XAS/914C 16-ply, peel ply: non-porous PTFE coated glass fabric with smooth surface; no compression data available.

XAS/913C

MSC89: XAS/913C, 16-ply, prepreg out-of-date and undercured to an unknown extent.

MTSC90: XAS/913C, 16-ply, prepreg out-of-date; normal cure.

Apollo 43-750/9106C

01: Apollo 43-750/9106C, 16-ply, fibres not surface treated.

X1: Apollo 43-750/9106C, 16-ply, 10% of standard fibre surface treatment.

L1: Apollo 43-750/9106C, 16-ply, 50% of standard fibre surface treatment.

C1: Apollo 43-750/9106C, 16-ply, standard fibre surface treatment.

E-Glass fibre/Nylon

23/9: Pultruded E-glass/Nylon, 9-ply, 23% fibre volume fraction.

29/8: Pultruded E-glass/Nylon, 8-ply, 29% fibre volume fraction.

35/8: Pultruded E-glass/Nylon, 8-ply, 35% fibre volume fraction.

Sample	**ILSS** (Mean) [MPa]	σ_{n-1} [MPa]	C_V [%]
XAS/914C			
ST2	**114.3**	3.1	2.7
ST3	**109.3**	2.7	2.4
PP2	**115.4**	3.5	3.1
XAS/913C prepreg had exceeded shelf life			
MSC89	**46.6**	5.2	11.2
MTSC90	**96.2**	2.4	2.5
APC-2 (AS4/PEEK)			
APC	**124.5**	0.7	0.6
Apollo/9106C			
01	**72.7** *(78.5)**	2.6	3.5 *(2.1)**
X1	**99.2** *(103.0)**	4.6	4.7 *(1.6)**
L1	**110.4** *(109.0)**	2.2	2.0 *(3.5)**
C1	**112.7** *(116.0)**	2.4	2.1 *(4.5)**
ICI 'Plytron'			
23/9	**73.8**	4.4	6.0
29/8	**90.4**	2.5	2.8
35/8	**94.7**	1.2	1.3

** Courtaulds Values*

Table 7.3-1: *Summary of ILSS results using the CRAG short beam shear test method; test speed 1.5 mm/min ; each sample included five test pieces.*

CRAG specifies a flexural failure mode as invalid. The interpretation of failure modes was found to be difficult. Interlaminar failure often was accompanied by fibre kinking as shown in Figure 7.3-2. Compressive failure is promoted by the loading roller, and results are likely to be different for different roller geometries or when the roller is padded, as described for the 4-point bend test. Since shear deformation, as depicted in Figure 7.3-2 (a) and (b), is found in all test pieces the compression kinks can be thought to be secondary effects. This is because after interlaminar failure bending deformation increases thus increasing compression surfaces stresses.

APC-2 test pieces did not fail catastrophically but by shear yielding as shown in Figure 7.3–2 (b). The test usually was stopped only because deflections became too large and the test piece was jammed between the rollers. Since compression kinks were found in these test pieces, as well as in the epoxy ones, it is suggested that compression failure was not primary and the values obtained are representative for the interlaminar shear strength. It is important to note here, that if failure is triggered by compression failure, a correlation of the compressive strength of the material and ILSS is obvious and does not prove the influence of shear properties on the compressive strength.

On almost all glass fibre-reinforced nylon specimens relatively large tensile failure zones under the roller were found indicating a flexural rather than a shear type of failure (Figure 7.3-2 (c)).

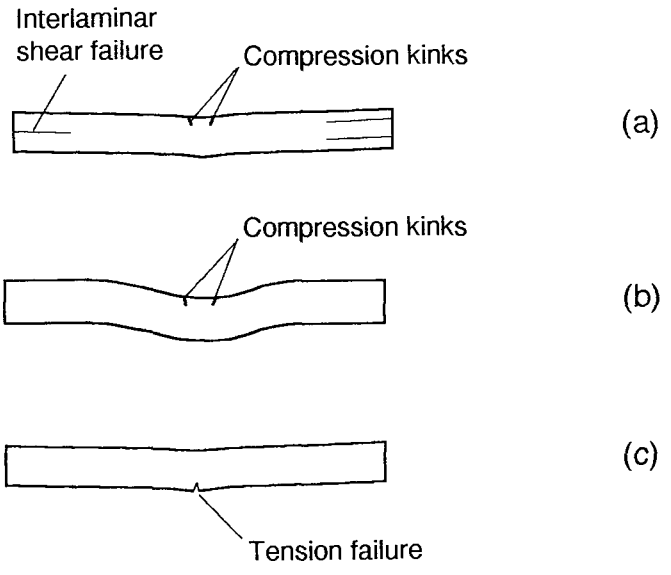


Figure 7.3-2: Illustration of failure modes of short beam shear test pieces.

Keeping in mind what was said above it appears that fibre surface treatment, as expected, has a pronounced effect on the ILSS (although not on the compressive strength for this

material as shown in Chapter 6). The results are in reasonable agreement with the Courtaulds values. The influence of exceeding the shelf live of the prepreg and undercuring cannot be assessed accurately since it is not known by exactly how long the life was exceeded (estimate: several months), or to what extent the laminate was undercured. But it can be said that there is a significant influence[+], particularly of the undercuring, which, of course, is obvious.

Nevertheless, the tests are meaningful since the objective is to compare ILSS and compressive strength (Section 9.5). The highest ILSS results were obtained for APC-2, largely a consequence of very high shear strains which can be achieved with APC-2. In Figure 7.3-3 a few typical 'maximum shear stress' versus crosshead displacement curves are presented. The shear stress for these specimens is calculated using Equation 7.3-1, replacing the ultimate load by the instantaneous load. Here it can be seen that APC-2 actually yields noticeably at lower stresses than the epoxies, but because there is no sudden failure, possibly because of a stronger interfacial bond, higher ultimate stresses are achieved.

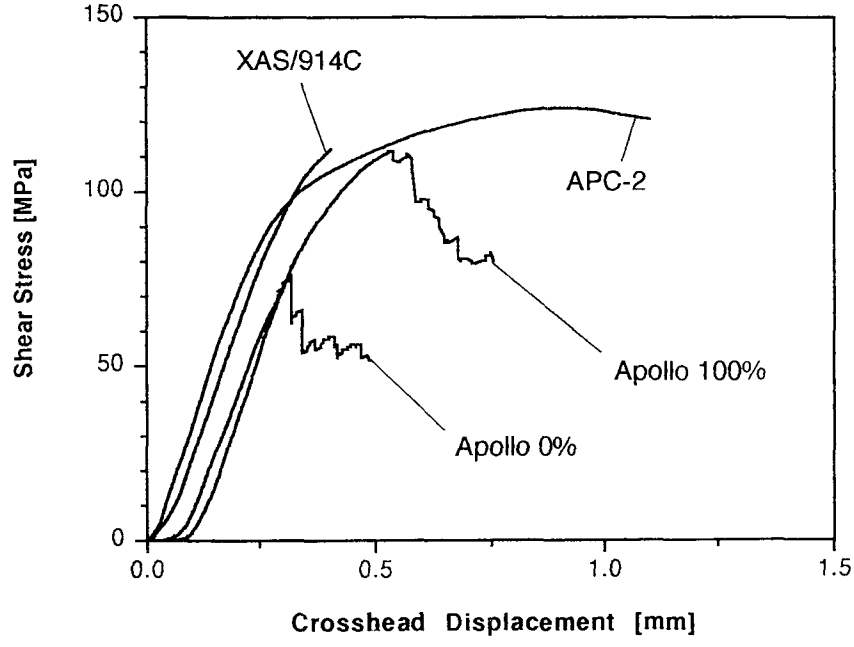


Figure 7.3-3: Some typical 'shear' stress-displacement curves from short beam shear tests.

[+] Ciba Geigy value: approximately 100MPa for both XAS/914C and XAS/913C

7.4 In-plane Shear Stress-Strain Response

In-plane shear properties are difficult to measure. The variety of methods reflects this fact and so far a unique method has not been agreed on. A simple and widely accepted method is the tension test of a ±45° lay-up. CRAG and ASTM, for example, specify this test for determination of in-plane shear properties. Tests in the present investigation are based on the CRAG recommendation. Test piece dimensions are shown in Figure 7.4-1.

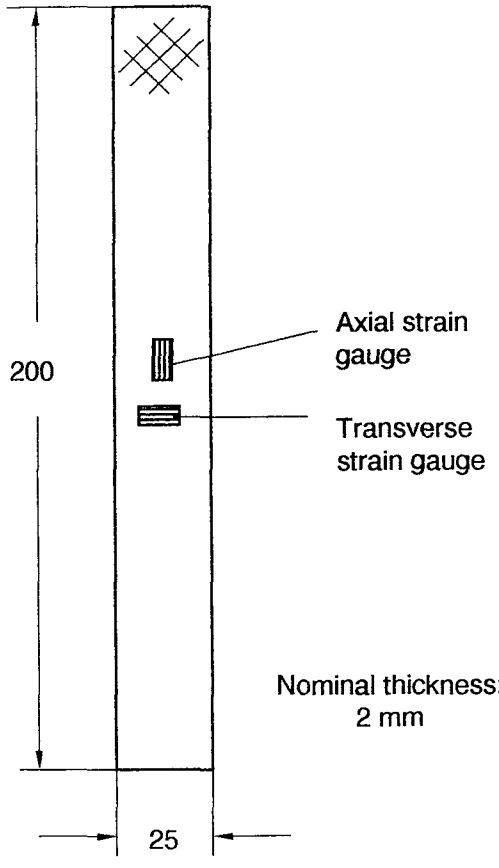


Figure 7.4-1: Test piece for determination of in-plane shear properties.

The lay-up used was $[(\pm 45°)_4]_S$, i.e. 16 plies and a nominal thickness of 2 mm. Tests were carried out for APC-2 and XAS/914C. During the test axial and transverse strains ε_{ax} and ε_{tr} are recorded and shear stress τ and shear strain γ, assuming a pure shear stress state, are calculated as:

$$\tau = 0.5P/A \qquad (7.4\text{-}1)$$

and

$$\gamma = \varepsilon_{ax} - \varepsilon_{tr} \qquad (7.4\text{-}2)$$

where P is the applied axial tensile load, and A is the cross-sectional area. The assumption of a uniform pure shear stress state in the 45° direction, of course, is an approximation, since the in-plane shear stresses at the specimen edges must be zero. Near the edges a complex three-dimensional stress state is to be expected. 'Scissoring' of the plies under tension causes the ply angle to change from 45° to lower values causing additional stress components. The absolute stress values should therefore be disregarded as a direct measure for the in-plane shear strength. Nevertheless, it is believed that the in-plane shear behaviour at moderate strains is reflected adequately by this method and therefore employed for lack of a better one.

The strain gauge circuit only allowed recording up to about 3.5 % axial strain so that consequently the shear strain recordings are limited to about 7%. This poses no real limitation as the portion of the shear stress-strain curve needed for later analysis is basically the one below 3 % shear strain.

Figure 7.4-2 shows the five shear stress-strain curves obtained for APC-2 test pieces. In contrast to the compression stress-strain curves these curves exhibit some scatter in their characteristics. Particularly for specimen #5 a flatter curve than for the other four was obtained.

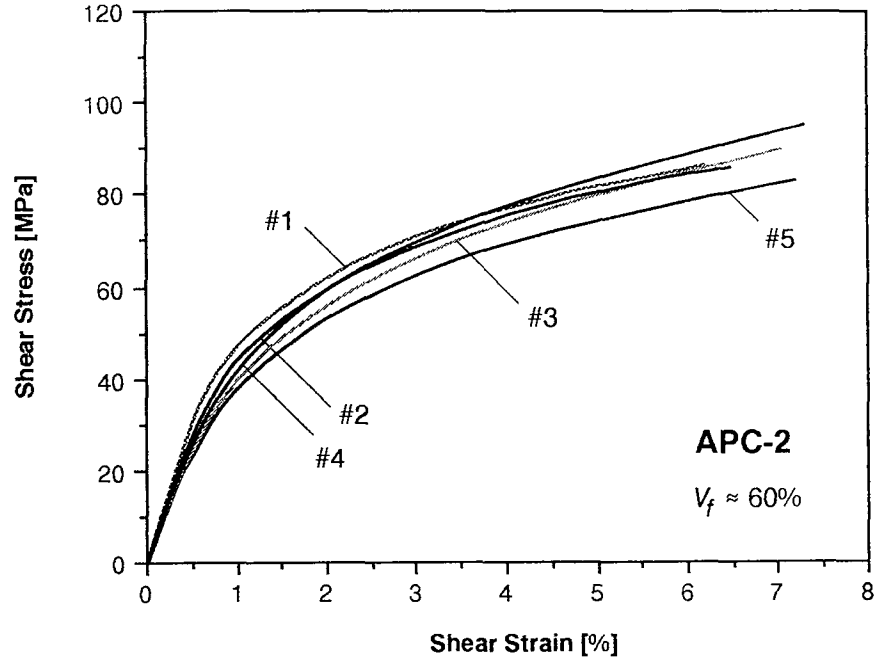


Figure 7.4-2: Typical shear stress-strain curves of APC-2 obtained by tension of a ±45° test piece.

The next figure shows the results for XAS/914C. Six specimens in total were tested, the test speed again being 5 mm/min for specimens #2 to #6 as for the APC-2 specimens. Specimen #1 was tested approximately six months after the laminate was produced and the result used in the early stages of the project. The rate of crosshead motion was 1 0 mm/min in this test. The curves of specimens #2, #3 and #4 (#4 is tested only to the yielding point) are remarkably close. Therefore, the difference to the curve of specimen #1 seems surprising. Since #2 to #4 were tested approximately 24 months after laminate production, 'ageing' effects cannot be excluded to explain the difference, although they were stored in a vacuum oven. Viscoelasticity could also play a role making results dependent on the test speed. The similarity of the slopes of the curves in the plasticity zone, however, makes an influence of the test speed of the observed magnitude unlikely.

The curves for test pieces #5 and #6 clearly show the influence of moisture take-up on the shear performance of the composite. The specimens were immersed in water for approximately 10 months and assumed to be saturated.

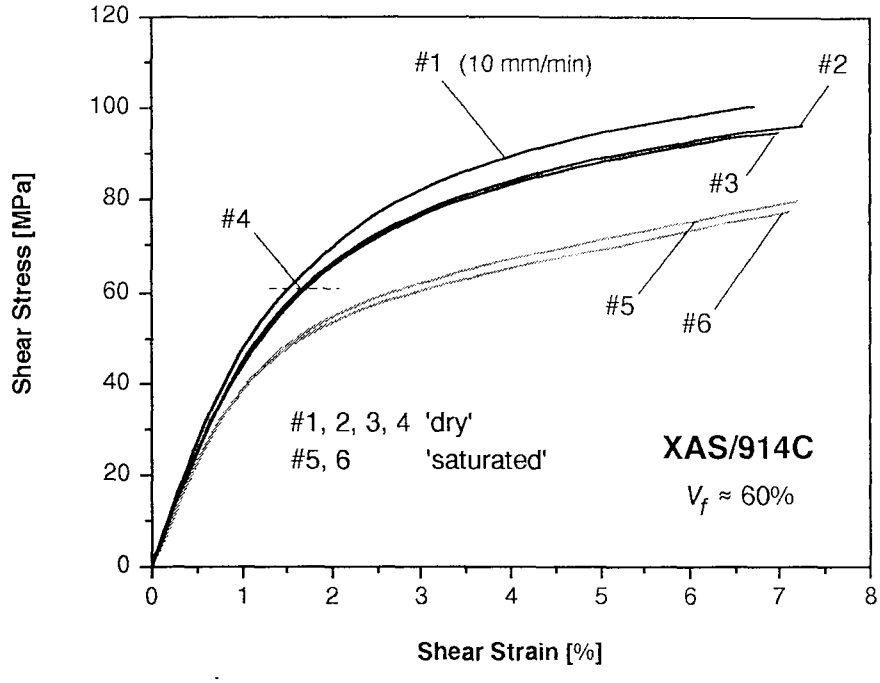


Figure 7.4-3: Typical shear stress-strain curves of XAS/914C obtained by tension of a ±45° test piece.

Material	No	Ultimate shear stress [MPa]	Shear modulus 0.5% secant [GPa]
XAS/914C 'dry'	1	-	5.30
	2	123	5.05
	3	127	5.05
XAS/914C 'saturated'	5	139	4.53
	6	140	4.53
APC-2 'dry'	1	151	6.15
	2	-	4.93
	3	164	5.35
	4	-	5.61
	5	-	4.73

Table 7.4-1: Mechanical properties from in-plane shear tests.

Ultimate stresses and 0.5% secant shear moduli are listed in Table 7.4-1. From the few results it can be deduced that moisture take-up reduces the shear modulus by approximately 10%, but ultimate (apparent) shear stresses seem to be increased. APC-2

shows the highest ultimate shear stresses, and the modulus is slightly higher than that for XAS-914C. Since the shear curves are used in the analytical section, functions were required to fit the experimental data. Fifth order polynomials were found to fit the data satisfactorily in the range of 0% to 5%. Better representation of the curve characteristics can be achieved with fewer coefficients by using exponential functions, e.g.

$$\tau = A + B\gamma + C\,e^{-\gamma} + D\,e^{-2\gamma} \qquad (7.4\text{-}3)$$

Both types of curve fit are illustrated in Figure 7.4-4.

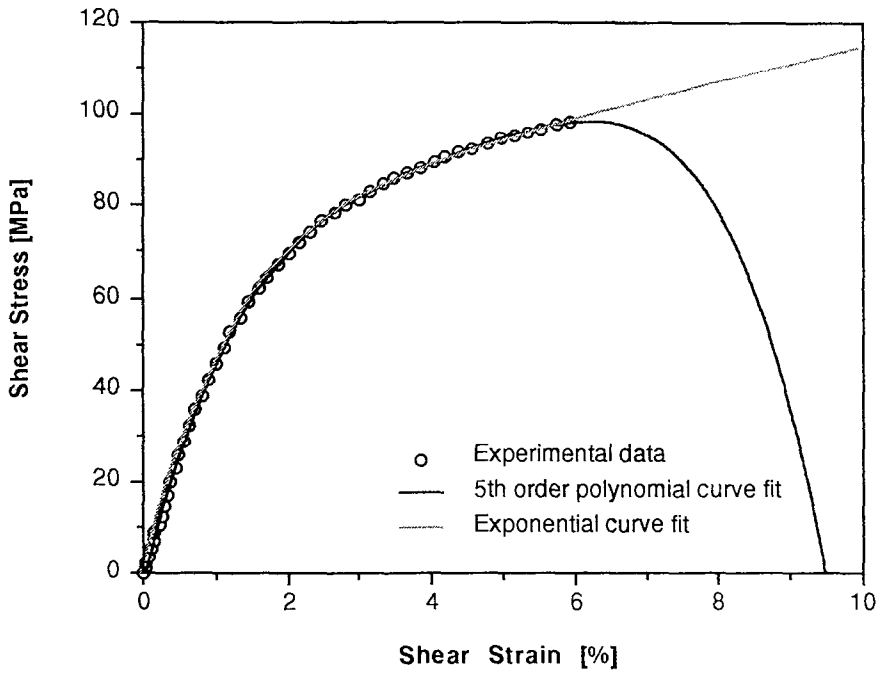


Figure 7.4-4: Polynomial and exponential curve fits to a typical shear curve.

Table 7.4-2 shows the coefficients of Equation 7.4-3 for the curves chosen as being representative. The curve of APC-2 test piece #4 has been chosen since it is almost identical with the mean curve fit of all APC-2 specimens.

Test piece	Condition	A	B	C	D
XAS/914 #1	'dry'	74.82	4.02	-97.77	22.69
XAS/914 #2	'dry'	71.27	3.66	-91.52	20.11
XAS/914 #5/6 (mean)	'saturated'	53.59	3.52	-47.50	-5.81
APC-2 #4	'dry'	57.29	4.66	-44.26	-12.75

Table 7.4-2: Coefficients of representative shear stress-strain curve fits.

Finally, the representative shear stress-strain curves are shown in Figure 7.4-5. Direct comparison of the XAS/914C and the APC-2 confirms the trend observed in the short beam shear tests. The APC-2 specimens yield at lower strains but reach higher stress levels at high strains (Table 7.4-1). The initial shear stiffness of APC-2 is slightly higher than that of XAS/914C.

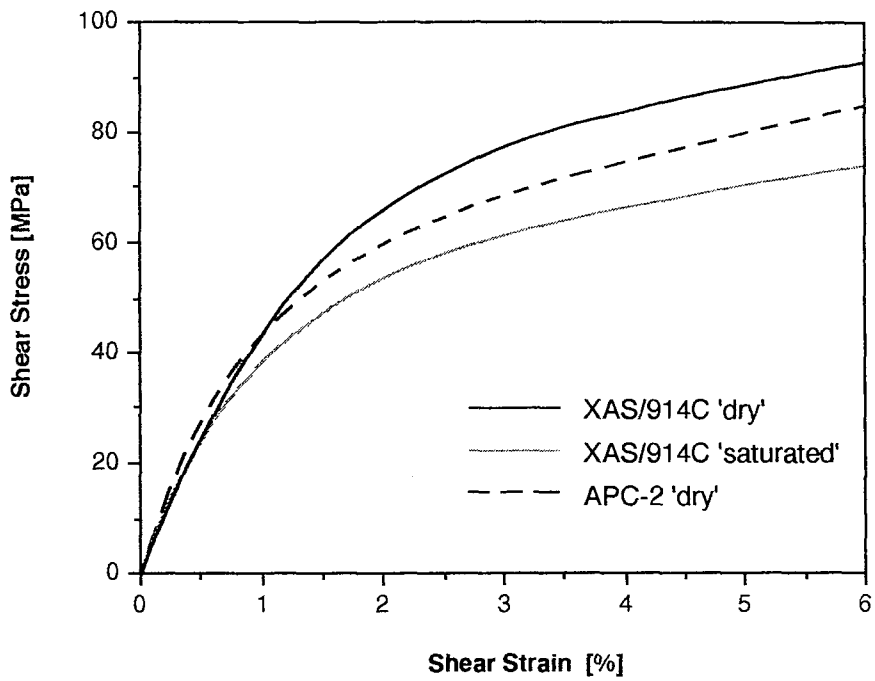


Figure 7.4-5: Representative shear stress-strain curve fits for XAS/914C and APC-2.

CHAPTER 8 QUANTIFICATION OF FIBRE MISALIGNMENT

The importance of fibre alignment for the compressive strength of continuous fibre composites has been pointed out earlier. In this chapter an approach to characterise and quantify the alignment of fibres within various composites is presented.

8.1 Description of the Technique

Basically, the technique proposed by Yugartis, 1987, is applied. It will be described briefly below and for simplicity the symbols in Yugartis' paper are used.

The technique is based on the simple observation that a plane section of a straight circular fibre is an ellipse.

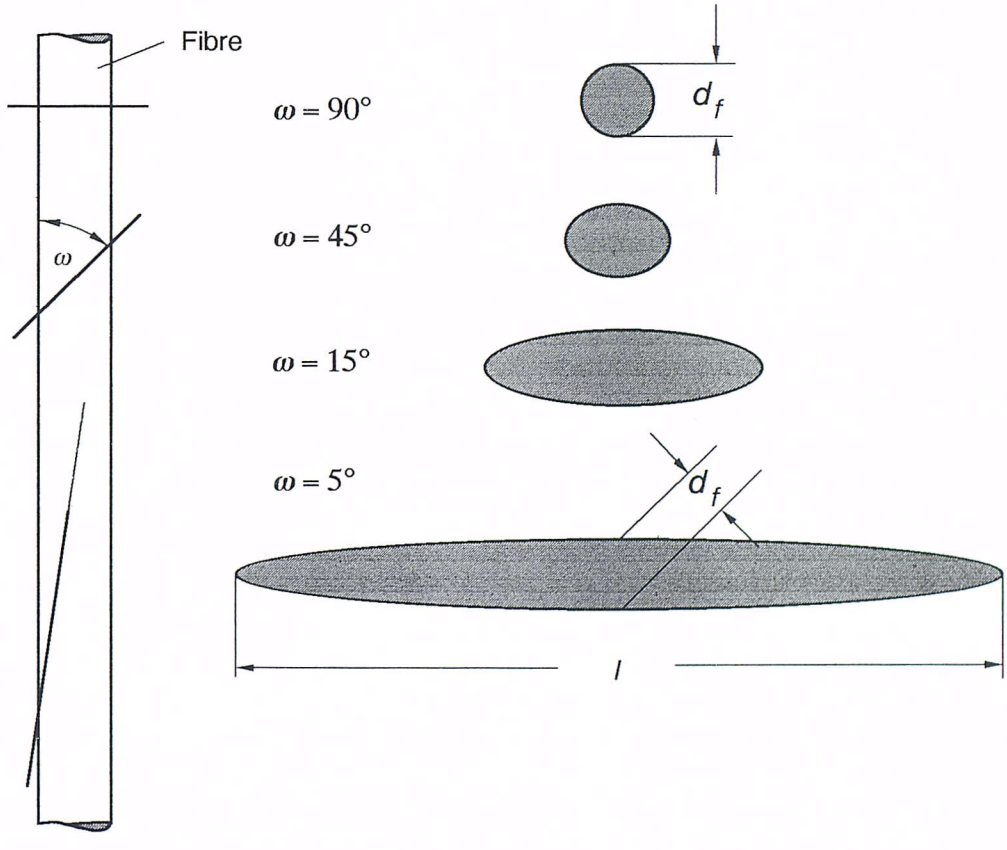


Figure 8.1-1: Cross-sections of circular fibres sectioned at different angles.

The smaller of the major axes equals the fibre diameter when the sectioning plane is perpendicular to the fibre plane. The angle of the cutting plane (see Figure 8.1-1) and the length of the longer major axis are related by:

$$\sin\omega = \frac{d_f}{l} \tag{8.1-1}$$

where d_f is the fibre diameter and l the major axis of the ellipse. The idea is then to evaluate the distribution of fibre angles within the composite by determining the axis ratios of a sectioned sample. Figure 8.1-2 defines the angles when regarding a sectioned composite.

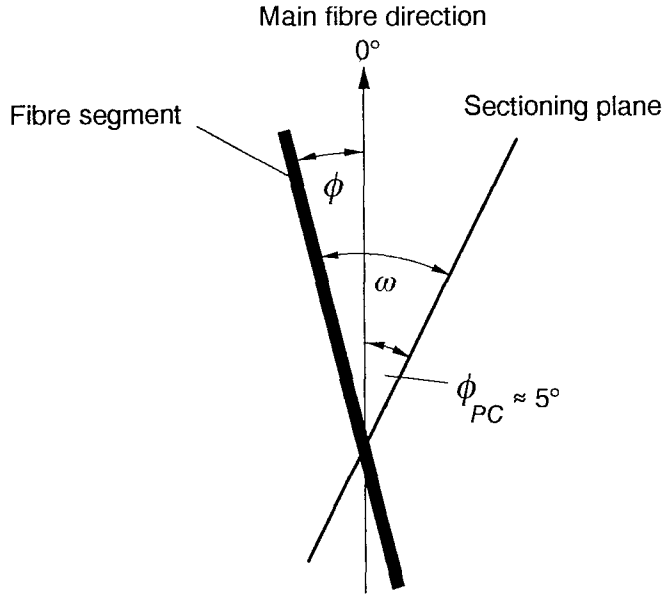


***Figure 8.1-2:** Definition of fibre angles in a sectioned composite sample.*

As implied above, two assumptions have to be made to get valid information: firstly, fibres are straight over short sections of at least twenty fibre diameters and, secondly, fibres have a circular cross-section and equal diameters. The first assumption is justified regarding Figure P-21 where a reflected light microscopy photograph of unidirectional XAS/914C is shown. The assumption of circular fibre cross-section is justified from Yugartis' measurements. The distribution of fibre diameters was judged to be narrow with a standard deviation of approximately 5% of the mean fibre diameter.

The choice of the sample intersection angle ϕ_{PC} is of great importance since it determines the resolution of the technique. Figure 8.1-3 illustrates that the angle should be as small as possible. The limit here is that the assumption of straight segments is less likely to be fulfilled for long intersections. On the other hand, it must be larger than the greatest expected misalignment angle as the technique fails for $\omega < 0$. Figure 8.1-3 shows conspicuously that the chosen angle of 5 degrees offers good resolution on both sides of the intersection angle. For greater intersection angles the resolution would be very low for greater fibre angles, say 10°.

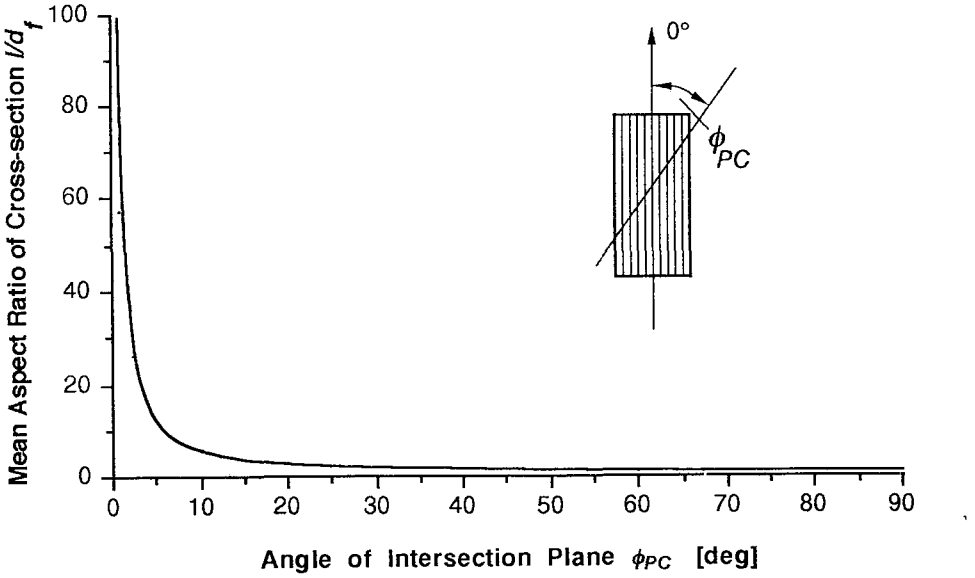


Figure 8.1-3: Illustration of the sensitivity of the technique to the sample intersection angle.

In the present investigation the practical procedure starts by sectioning a composite sample of a typical thickness of 2 mm at an angle of approximately 5°. The sample is then cast in polyester resin and polished carefully. Care has to be taken that the polished surface remains flat, i.e. that all fibres are sectioned at the same angle. Proper polishing is a prerequisite for a meaningful fibre angle analysis. Over-polishing can damage the edges of the elliptic fibre cross-sections. Insufficient polishing on the other hand results in part of the cross-section being left concealed under resin. Figure P-20 gives examples of micrographs taken from samples used in the present investigation. Note the variation of the cross-sections of intersected fibres in different layers and within a layer as well.

The next step is the determination of the aspect ratios of the elliptic fibre cross-sections. This was done in the present study in a semi-automatic way by using an image analyser. For this purpose the sample was placed under a microscope and a video camera attached to it transmitted the image to an image analyser. On the screen of this the image can then be processed using an external drawing board and various software features. Ideally the objects, which are the individual fibre cross-sections in this case, should be clearly distinguishable from the background. In practice this is very difficult to automate since all information is digitised and the computer cannot interpret the information as the human eye can. It is, therefore, necessary that the identified objects can be treated individually as illustrated in Figure 8.1-4. This increases the capability of the system significantly.

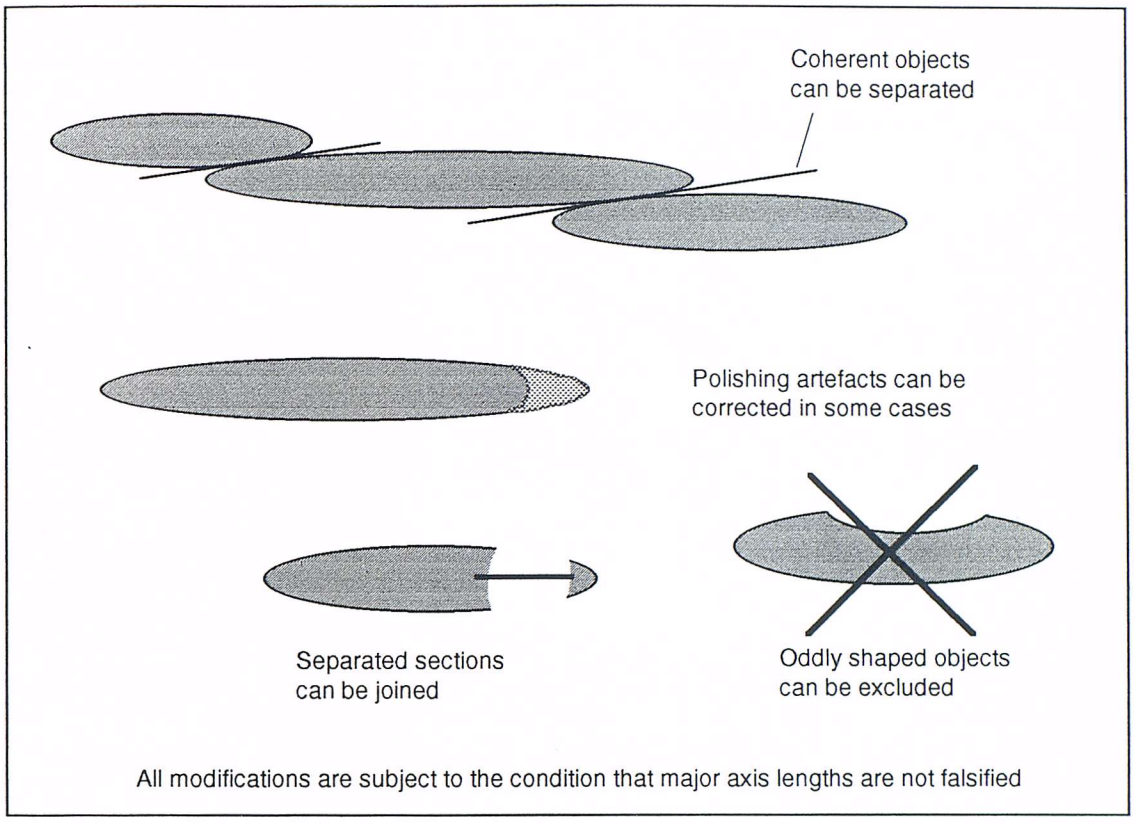


Figure 8.1-4: Possibilities of manipulating objects using an image analyser.

Most important is the initial setting of thresholds which requires some experience in order to achieve repeatable results. Although the resolution is limited, the image analyser was found to be a powerful tool. The limitation of the resolution is basically the pixel size of the screen which, with the chosen settings, was about 6% of the fibre diameter. Therefore, it was thought that the measurement of the aspect ratios was more accurate than assuming a constant fibre diameter and measuring the ellipse lengths only. Usually 1000 values per sample were measured by scanning the sample, avoiding double scanning. The data were then stored on disc and further processed by a FORTRAN program on a PC. After filtering and correcting the data for distortion of the video camera the next program steps are:

- Calculation of the angle ω from Equation 8.1-1
- Sorting of the angles ω_i into class intervals

A class interval width of half a degree was chosen in agreement with Yugartis' work. The width is not a critical parameter and can be changed easily in the program if it is felt necessary.

The distribution of relative fibre angles is now available in the form of a discrete distribution as illustrated in Figure 8.1-5 for XAS/914C.

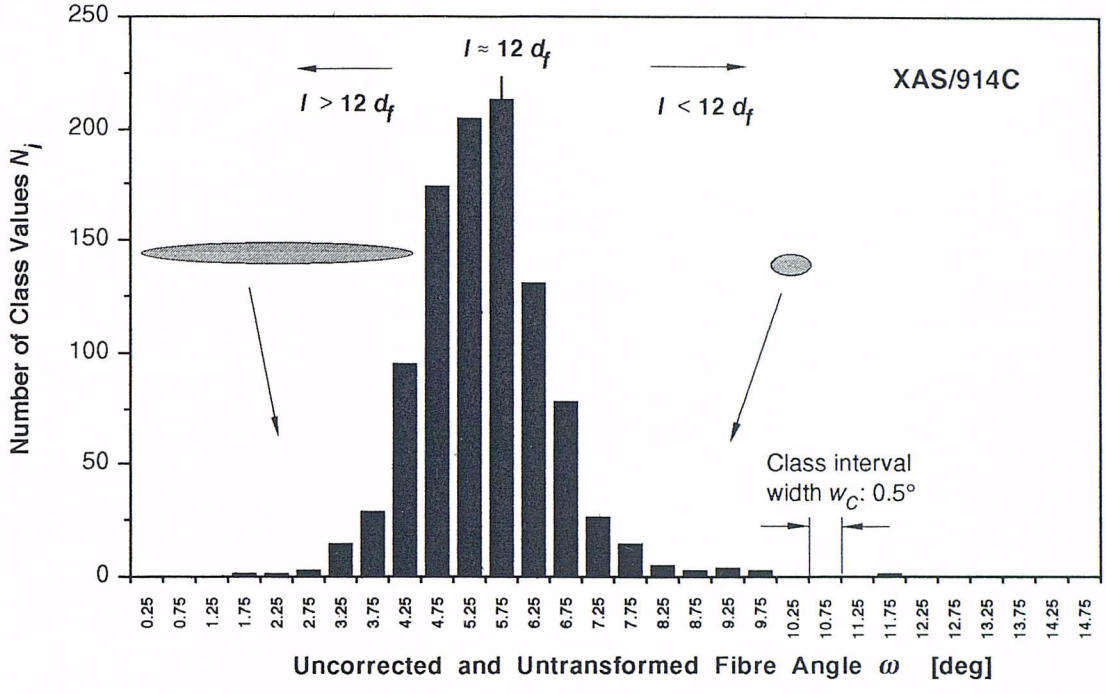


Figure 8.1-5: Classification of relative fibre angles.

Yugartis proposes a correction for counting bias since in a limited observation area smaller objects are more likely to be counted than large ones. The correction yields:

$$f_V(\omega_i) = \frac{\frac{N_i}{\tan \omega_i}}{\sum_{1}^{m} \frac{N_i}{\tan \omega_i}} \qquad (8.1\text{-}2)$$

where $f_V(\omega_i)$ is the volume fraction of fibre at an angle ω_i; ω_i and n_i are class interval mean and number of values within a class interval, respectively, and m is the total number of class intervals.

8.2 Statistical Data Analysis

After correcting for counting bias, the distribution of the fibre orientation is given in the form of a discrete function as illustrated in Figure 8.2-1.

If the distribution is symmetric the transformation from the relative angle ω to the fibre angle with respect to the main zero direction ϕ is simply (see Figure 8.1-2):

$$\phi = \omega - \phi_{PC} \tag{8.2-1}$$

where ϕ_{PC} is the mean of the distribution $f_V(\omega)$. As pointed out by Yurgartis, the assumption of a symmetric distribution is reasonable. Any distortion of the distribution is due to the fact that negative angles of ω, i.e. angles anti-clockwise greater than the angle of the cutting plane are counted as positive. Consequently, this does not cause a problem as long as most of the fibres are oriented within $\pm\phi_{PC}$, which can be assumed for high performance composite systems. However, if the distribution is wider the procedure outlined above should only be taken as an approximation. Ideally, the intersection angle ϕ_{PC} should then be increased. But one could find oneself in a trade-off situation since the resolution decreases rapidly in this range of angles as mentioned earlier.

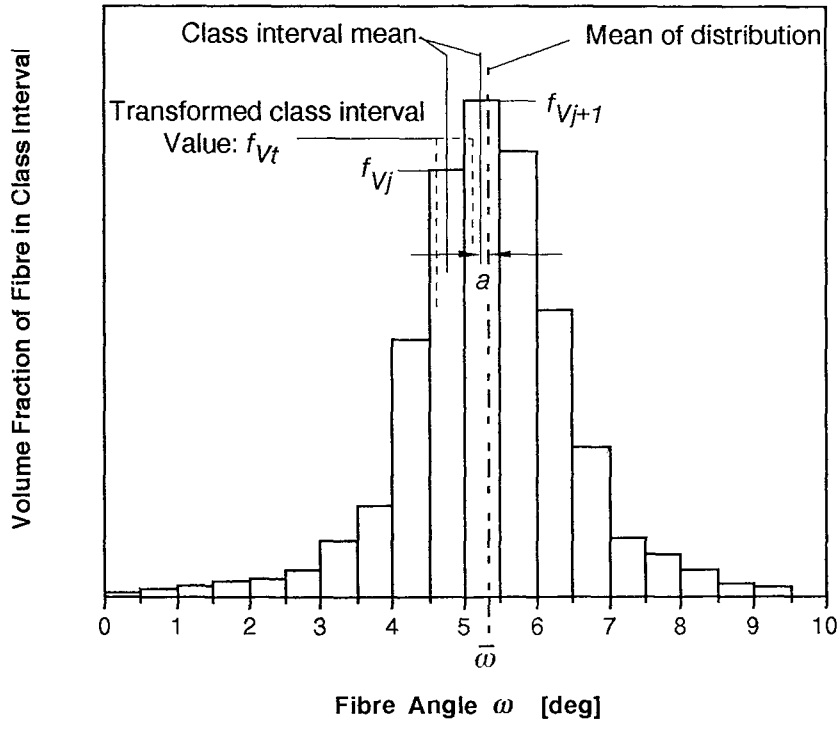


Figure 8.2-1: Untransformed corrected discrete distribution of fibre angles.

Generally, the mean of a discrete function of m class intervals with a mean of x_i and the relative class frequencies $\tilde{f}$ is given as:

$$\bar{x} = \sum_{i=1}^{m} \tilde{f}_i(x_i)x_i \tag{8.2-2}$$

with

$$\sum_{i=1}^{m} \tilde{f}_i(x_i) = 1 \tag{8.2-3}$$

Applied on the distribution of fibre angles, the mean fibre angle relative to the sectioning plane becomes:

$$\bar{\omega} = \sum_{i=1}^{m} f_V(\omega_i)\omega_i \tag{8.2-4}$$

As in Equation 8.1-2, $f_V(\omega_i)$ denotes the volume fraction of fibre at an angle ω_i; ω_i being the class interval mean.

The distribution can now be transformed with the mean of the distribution becoming the origin of the transformed distribution. Since the distribution mean generally does not coincide with a class interval mean, the class values have to be redistributed. Equally distributed values within a class interval of the discrete function are assumed for this purpose. The value of the transformed class interval is then calculated from relevant proportions of the untransformed class intervals it overlays (see Figure 8.2-1):

$$f_{Vt} = \left(1 - \frac{a}{w_c}\right) f_{Vj} + \left(\frac{a}{w_c}\right) f_{Vj+1} \tag{8.2-5}$$

where a is the difference of distribution mean and the next smaller class interval mean and w_c is the class interval width.

Finally, it is necessary to characterise the form of the distribution. The simplest approach is to do so by determining the standard deviation, a large standard deviation being an indication of poor overall alignment whereas a smaller one would characterise a more narrow angle distribution. Physically the standard deviation could be regarded as a mean value of fibre misorientation.

Using the notation from above, the variance of a discrete distribution may be expressed as:

$$\sigma_{n-1}^2 = \frac{n}{n-1} \sum_{i=1}^{m} \tilde{f}_i(x_i)(x_i - \bar{x})^2 \tag{8.2-6}$$

where n is the total number of values in all class intervals. The standard deviation is the square root of the variance. Since the number of measured values in the present investigation is around 1000, the fraction in Equation 8.2-6 can be neglected so that one obtains for the standard deviation of the fibre angle distribution:

$$\sigma = \left(\sum_{i=1}^{m} f_v(\omega_i) \left(\omega_i - \bar{\omega}\right)^2 \right)^{\frac{1}{2}} \tag{8.2-7}$$

In the present study the standard deviation was calculated using the values of ω only within the interval $\pm\phi_{PC}$. The reasoning behind this is that a few strongly misaligned fibres might have no physical significance, i.e. they might not affect average mechanical properties, but they would disproportionately influence the standard deviation. As discussed before, this is only a constraint in the case when the measured distribution is an approximation because of the condition $\omega<\phi_{PC}$. For most high quality prepregs the calculation is justifiable.

The following alternative of characterising the distribution is proposed by the present author. Positive and negative class interval values are added. This is justified since the described method does not correlate fibre angle and location, therefore positive and negative values are of equal status. The fraction of fibre volume oriented at angles $\pm\phi_i$ is obtained as:

$$f_V(|\phi_i|) = f_V(\phi_i) + f_V(-\phi_i) \tag{8.2-8}$$

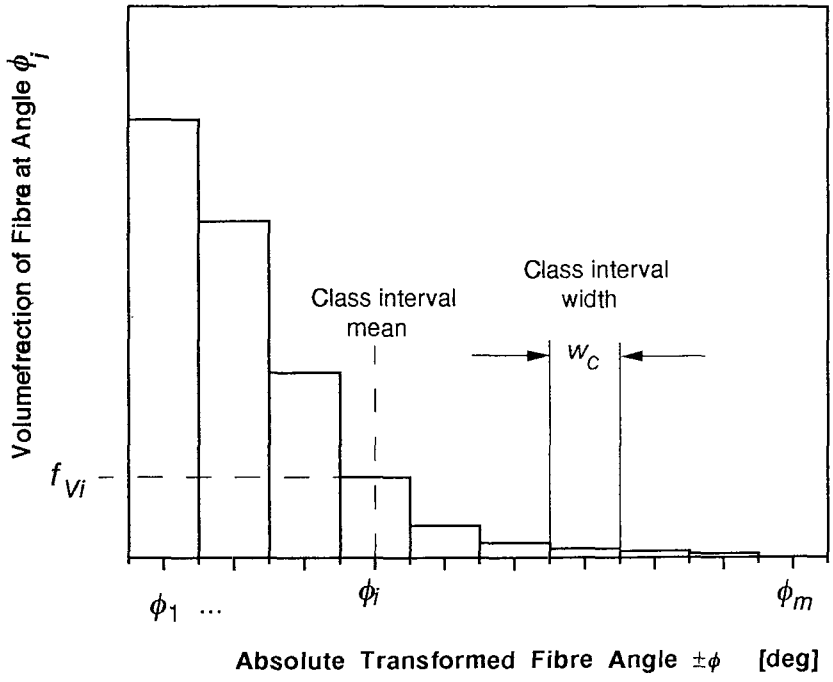


Figure 8.2-2: Absolute fibre angle distribution used for determination of a representative mean deviation from the zero direction.

The mean angle is determined from this, now non-symmetric, distribution (see Figure 8.2-2) as:

$$\bar{\phi} = \sum_{i=1}^{m} f_V(\phi_i)\,\phi_i \tag{8.2-9}$$

This is equivalent with applying Equation 8.2-4 on the transformed distribution replacing ω_i with the absolute value of ϕ_i . The only difference is that the class intervals in the distribution above are redistributed in order to include the centre class interval and to use equal class interval widths. With smaller increments this step is not necessary.

So far, only in-plane fibre misalignment has been discussed. Clearly, fibres are misaligned in space, i.e. out-of-plane misalignment has to be considered as well. As Yugartis showed, both cases of misalignment can be examined separately by choosing appropriate intersection angles. In the present investigation only in-plane misalignment was investigated since it was thought that due to lower fibre constraint in the layer plane in-plane misalignment is the more serious one. This is confirmed by Yugartis' measurements, who found that the out-of-plane fibre misalignment of cured APC-2 laminates is significantly lower than in-plane misalignment. However, for other systems this should be the subject of further investigation.

A more fundamental problem with the method for determination of fibre misalignment as described above is the fact that from the final distribution of fibre angles the shape of fibre misalignment is not known. In particular, there is no distinction between 'intrinsic' short wave length fibre misalignment and misalignment of a whole layer, e.g. caused when laying up. Scanning of an individual layer within a sample should give an estimate of the average lay-up misalignment. This, again, is a topic for further investigation. In the present investigation the lay-up error is estimated to be about ±0.25°, as mentioned in Chapter 3.

8.3 Results for Several CFRP Systems

In-plane analysis has been applied on six different systems for which compression data were available: XAS/914C, AS4/PEEK (APC-2), Apollo 43-750/9106C with 4 different levels of fibre surface treatment: 0%, 10%, 50% and 100% of the standard surface treatment. For the XAS/914C composite a comparative analysis was carried out measuring the ellipse aspect ratios manually from micrographs using a vernier caliper.

Figure 8.3-1 shows the transformed distribution of fibre misalignment for XAS/914C using the image analyser. The distribution is nearly symmetric and narrow with respect to the angle of the sectioning plane. For this case the choice of the intersection angle is certainly adequate, and one could even reduce the angle to about 3 degrees to gain a better resolution. A cumulative plot of the above distribution is given in the following Figure 8.3-2. From this it can be seen that about 90% of the fibre volume lie within ±1.5 degrees of the main fibre direction.

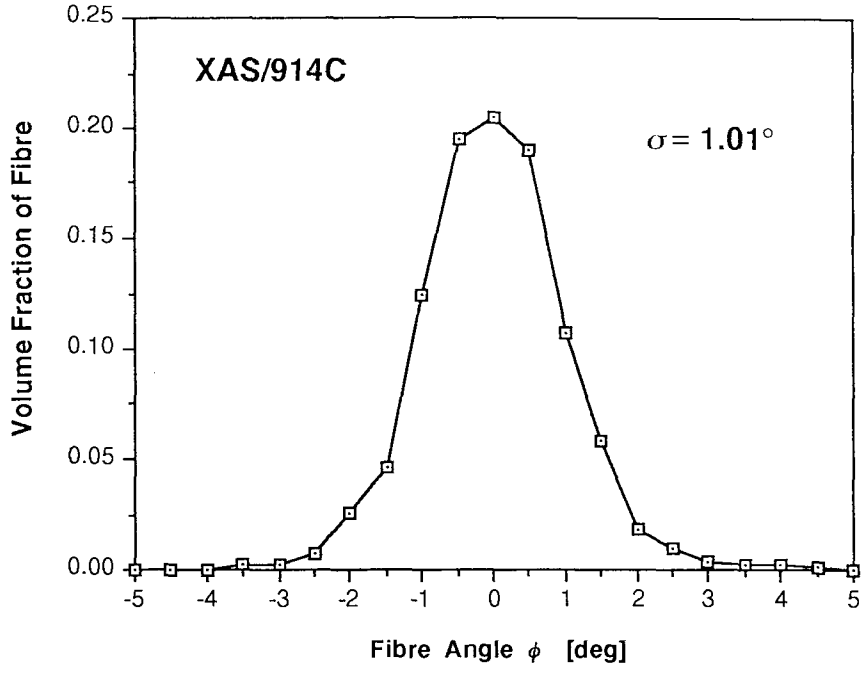


Figure 8.3-1: Fibre angle distribution for XAS/914C using an image analyser.

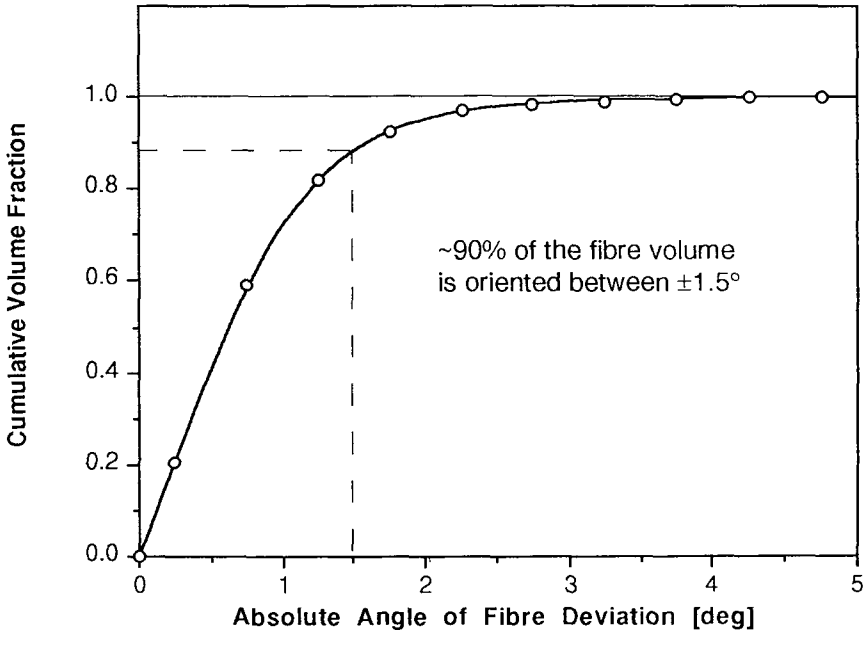


Figure 8.3-2: Cumulative fibre angle distribution for XAS/914C.

In Figure 8.3-3 the comparison between image analyser and manual measurement is presented. 270 cross-sections were evaluated manually and 1000 with the image analyser. The agreement of the two methods is surprisingly good bearing in mind that the resolution of both procedures is different.

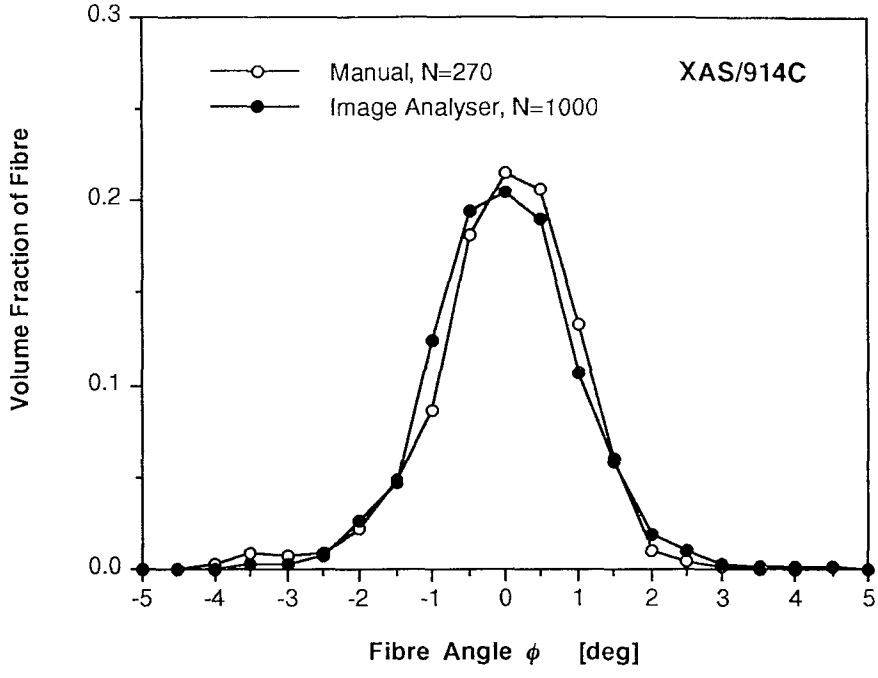


Figure 8.3-3: Comparison of image analyser and manual measurement.

The distribution for APC-2 shown in Figure 8.3-4 is clearly wider (σ = 1.53°) than the one for XAS/914C (Figure 8.3-5), though still fairly symmetric. Part of the reason for the wider distribution might be poor layer alignment in APC-2 as the laying-up of thermoplastic prepregs is somewhat more difficult than laying up tacky epoxy ones. However, comparison of the micrographs of XAS/914C and APC-2 would suggest that 'intrinsic' fibre waviness is more pronounced in the thermoplastic.

The value for the standard deviation determined in this investigation lies between the values measured by Yugartis (1987) and Mrse and Piggot (1990). Using the same method, they determined the standard deviation of the fibre angle distribution of unidirectional APC-2 as 1.94° and 1.36°, respectively.

Finally, the results for the Apollo fibre composites are shown in Figure 8.3-6. Again, the distributions seem to be reasonably symmetric, with the exception of the material containing non-treated fibres (0%). In this case approximately 10 % of the fibre volume was outside the angle window of ±5°. The distributions of the Apollo samples seem to be similar to the APC-2 results apart from the 10% one which is more narrow. This is clearly reflected in the distributions' standard deviation listed in Table 8.3-1.

In the following chapter the correlation between the fibre misalignment, as determined here, and compressive strength will be discussed.

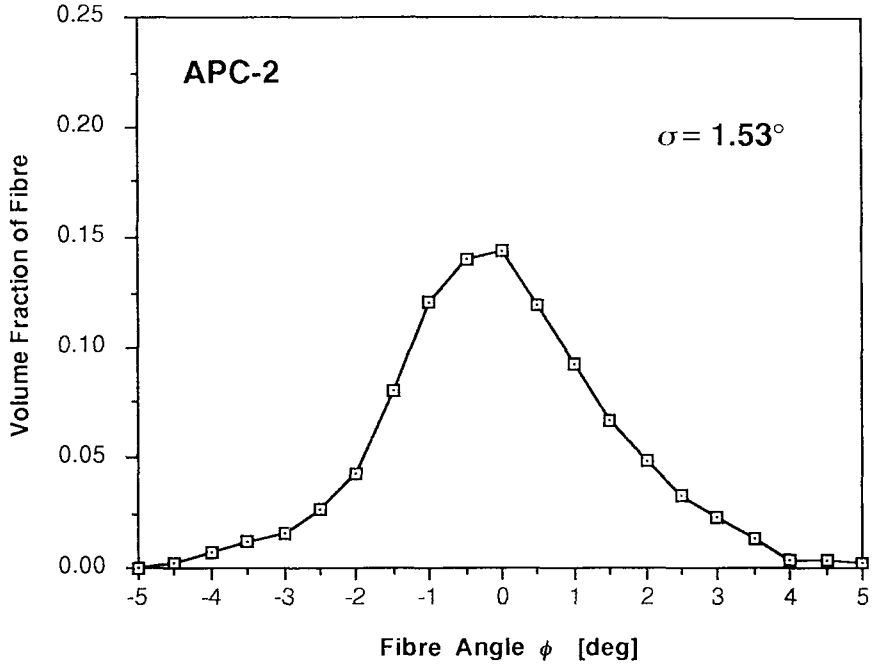


Figure 8.3-4: Fibre angle distribution for AS4/PEEK (APC-2).

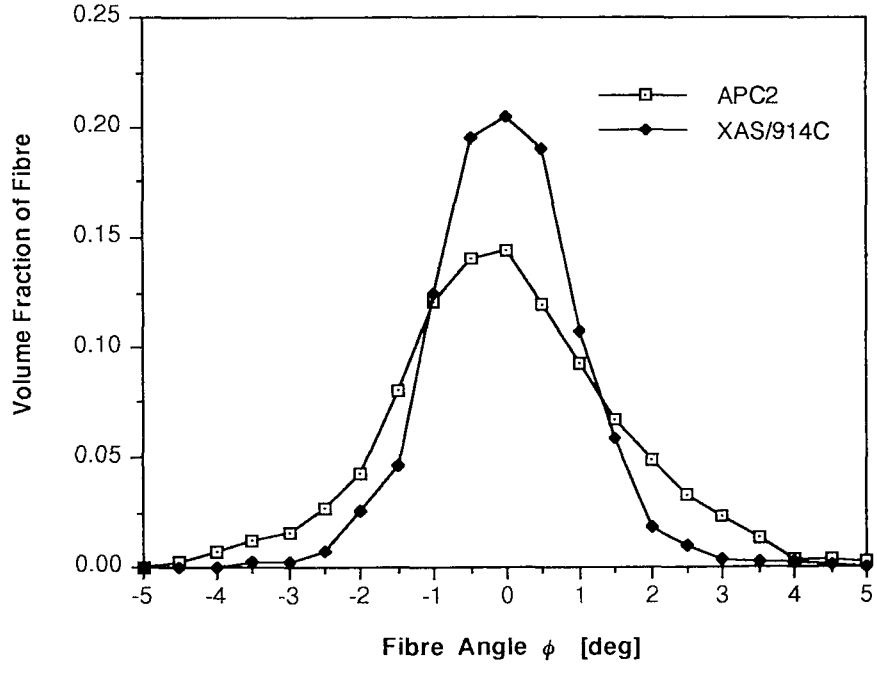


Figure 8.3-5: Comparison of fibre angle distribution for AS4/PEEK and XAS/914C.

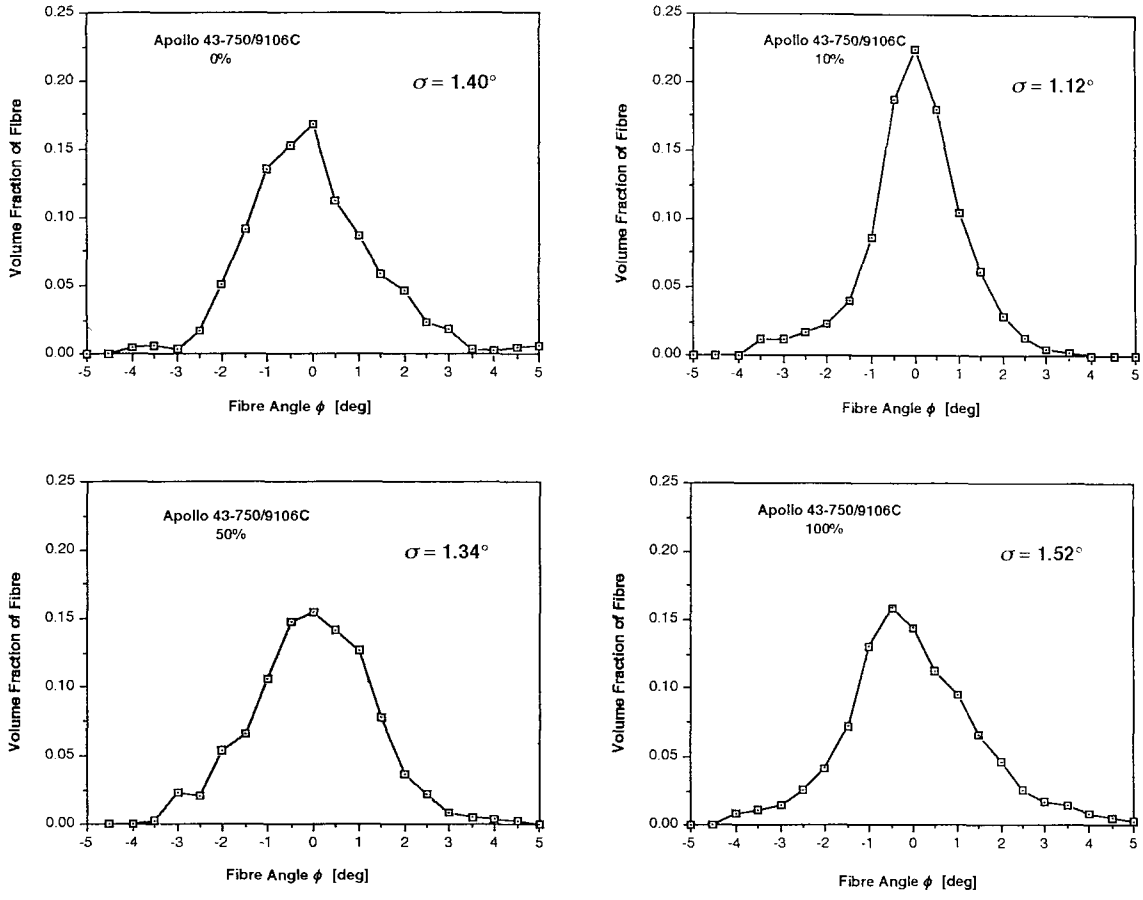


Figure 8.3-6: Transformed fibre angle distributions for Apollo 43-750/9106C containing fibres with 0%, 10%, 50% and 100% surface treatment.

Material	Fraction of fibre volume included in the analysis Σf_{Vi} [%]	Mean angle of untransformed distribution $\bar{\omega}$ [deg]	Standard deviation of transformed distribution σ [deg]	Mean of distribution of absolute angles $\bar{\phi}$ [deg]
XAS/914C	99.9	5.29	1.01	0.81
APC-2	97.6	5.49	1.53	1.21
Apollo 0%	90.2	5.28	1.40	1.08
Apollo 10%	99.9	5.25	1.12	0.87
Apollo 50%	99.7	5.24	1.34	1.07
Apollo 100%	99.6	6.12	1.52	1.17

Table 8.3-1: Results of the statistical analysis of fibre angle distributions.

Figure 8.3-7 summarises the results in the form of cumulative plots of the distributions. The better aligned composites are distinctly recognised by their steeper curve. In Figure 8.3-8 a summary of the incremental distributions of the absolute angles is shown.

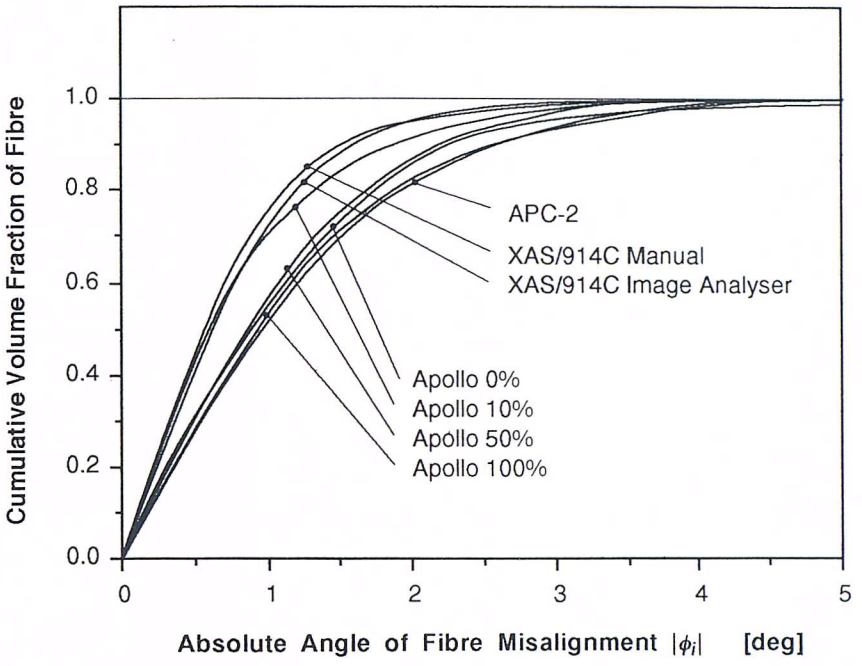


Figure 8.3-7: Results of the fibre angle analysis; cumulative plots.

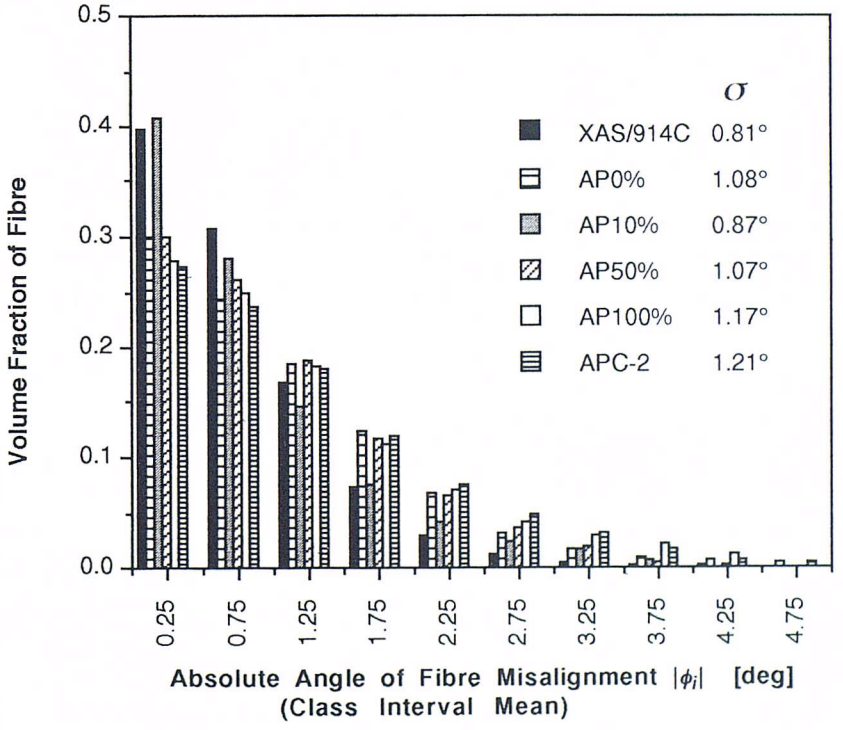


Figure 8.3-8: Results of the fibre angle analysis; distribution of absolute angles.

CHAPTER 9 DISCUSSION OF EXPERIMENTAL FINDINGS

9.1 Proof of Proposed Test Method

In this section some of the experiences gathered with the proposed test method will be described and discussed. This will lead to an assessment of the feasibility of the method.

Frictional effects

A major fixture-introduced effect which has to be considered with compression testing is friction. As mentioned previously, friction might give misleading results for strength as well as for the modulus of elasticity. Jamming of the specimen because of transverse deformation when using the modified ASTM D695 method, for instance, can add an unknown load to the overall load, thus falsifying the strength as well as the modulus .

The influence of friction in the proposed ICSTM method was estimated by determining the axial modulus of elasticity of a unidirectional test piece and arranging the end blocks in different ways, as illustrated in Figure 9.1-1.

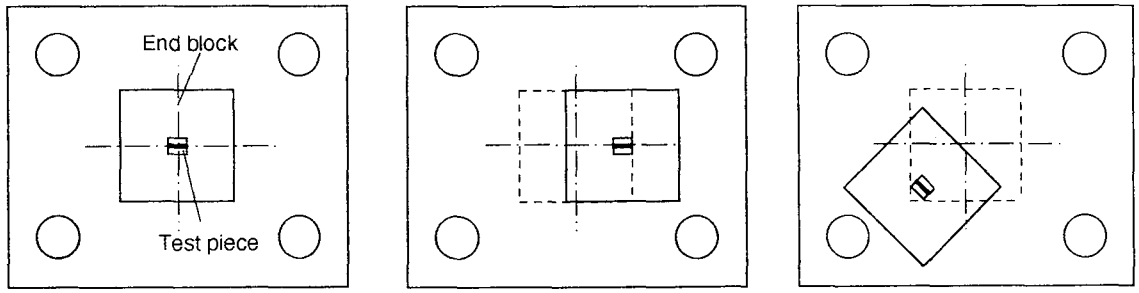


Figure 9.1-1: Illustration of test fixture arrangement for assessment of frictional effects.

The eccentric position of the test piece would increase any friction and lead to an increased apparent modulus, if significant. In the standard position the measured modulus for a particular specimen varied approximately ±1% when the test was repeated and the same procedure of determining the modulus was used. For the three positions illustrated in Figure 9.1-1 the following values were determined as the mean of three tests each:

Position	Modulus [GPa]
(a)	111.1
(b)	111.6
(c)	109.5

These results were within the usual scatter and, since friction would lead to an increased rather than reduced apparent modulus, they indicate that there is no significant frictional influence to be taken into account using this fixture. The four-pillar die set obviously is very well suited for ensuring axial loading.

At this point, a note on the measurement of the axial modulus of elasticity will be made. It was noticed that the method of modulus determination can substantially influence the result. Graphical determination from the stress-strain curve, for instance, can result in a difference of up to 5% from values calculated from curve fits, even when care is taken to be precise. The order of the curve fit plays a role as well. Figure 9.1-2 (b) illustrates how even small friction at the first instance of loading can influence the value of the modulus if the initial part of the curve is not disregarded. In some cases this was found to falsify the result, particularly when using the CRAG method. It is therefore recommended to inspect the stress-strain curve before the modulus is determined and to extrapolate the linear portion if necessary. The situation is more difficult if friction is proportional to the load, Figure 9.1-2 (c). The curve cannot then be corrected since the amount of friction is unknown, stressing the need to minimise frictional effects.

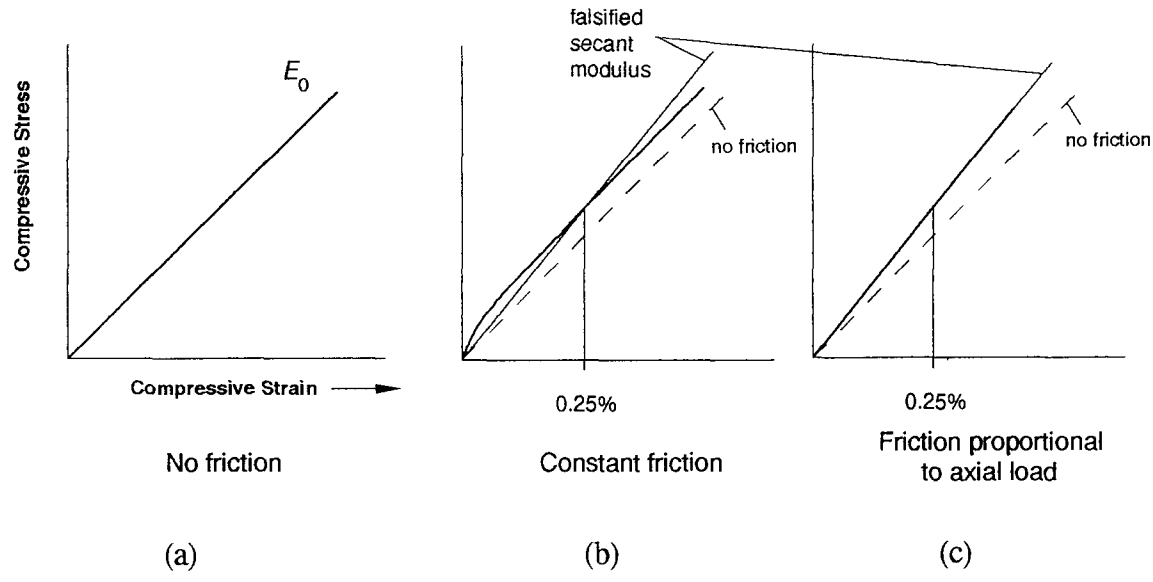


Figure 9.1-2: *Effects of friction on the apparent modulus of elasticity.*

Reproducibility

In order to gain some information on reproducibility of results using the ICSTM method a young student not experienced with testing, but familiar with the testing machine, was asked to conduct compression tests independently, using the ICSTM method with standard test pieces. The specimens were supplied and only a brief introduction to handling of the test rig was given.

The student carried out the five tests in less than one hour, the test pieces not being equipped with strain gauges, producing a mean UCS of 1653 MPa[+] with a coefficient of variation of 2.4 %.

The results of the testing short course (Section 6.1) indicate a similar tendency: the ultimate compressive stress measured using the ICSTM method is largely independent of the tester's influence. However, it has to be noted that test piece preparation might influence the results as pointed out earlier. The results of these tests are compared with the results from the parametric study gauge length (Chapter 5) in Figure 9.1-3 (see also Table T-34).

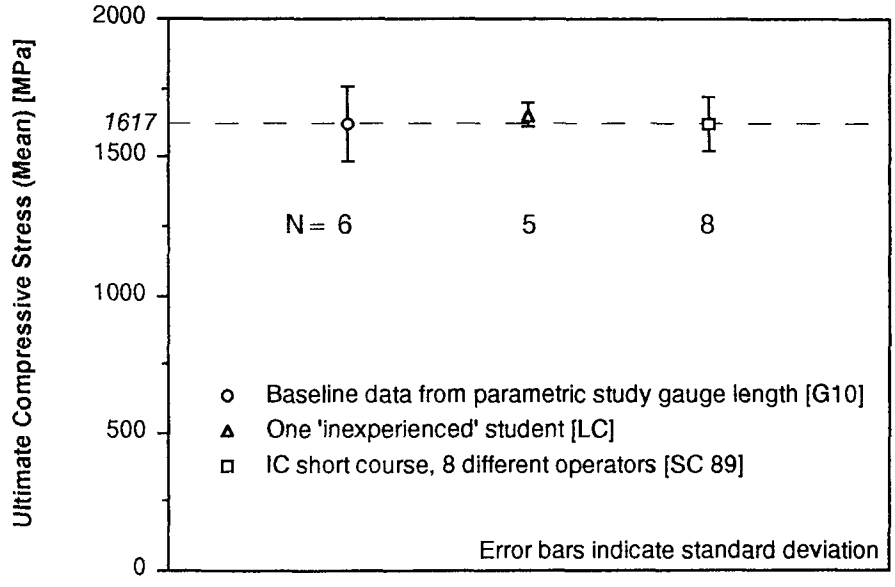


Figure 9.1-3: Influence of operator on the test results using the ICSTM method.

[+] Specimen thickness was measured as produced; therefore, the UCS values should be corrected as proposed in Chapter 3.

Note that the variation of the standard deviation of test results as depicted in Figure 9.1-3 is not typical. The samples G10 and LC exhibited scatter of results above and below average (coefficient of variation C_V = 8.6% and 2.4%, respectively) which can most probably not be attributed to operator influence since both were carried out by only one operator at a time. From the different familiarity with the test the opposite trend in the scatter of results would have been expected.

The influence of specimen production was demonstrated by testing of three specimens produced by a Birmingham University student[++]. The test pieces were tabbed individually and specimens #1 and # 2 were not machined after end tab bonding. The mean value of the three tests (see Table T-29) was 1500 MPa. Whilst it is not clear whether the condition of the laminate (moisture content, volume fraction etc.) influenced the result it is felt that specimen production as specified in Chapter 3 will certainly lead to better reproducibility.

With regard to the variation of results observed with other methods, it can be concluded that the proposed method improves repeatability and reproducibility of compression tests.

Clamping constraints

Through-thickness stresses are suspected of promoting compressive failure at the tab tip. Using the ICSTM method, these stresses can be controlled to a certain extent by the torque applied to the clamping bolts of the end blocks. In the standard tests the applied torque was 10 Nm to the bolt near the loaded specimen end and 5 Nm to the bolt near the gauge section. These values were purely empirical, but proved to yield satisfactory results. A torque of 5 Nm was regarded as being just sufficient to align the test piece sufficiently without straining the gauge section.

In a series of tests the influence of the torque on the ultimate compressive stress was determined. The bolt torque on the specimen end was held constant whereas the torque on the 'inner' bolt was varied between 5 and 30 Nm. Figure 9.1-4 shows the results of this investigation. For torques higher than 15 Nm a large drop in the compressive strength is apparent. The value for 20 Nm is about the same as that measured with IITRI and CRAG methods in most cases. This again demonstrates that the method of load introduction used by the ICSTM method reduces stress concentrations leading to higher overall failure stresses.

[++] Laminate and test pieces produced at Birmingham University.

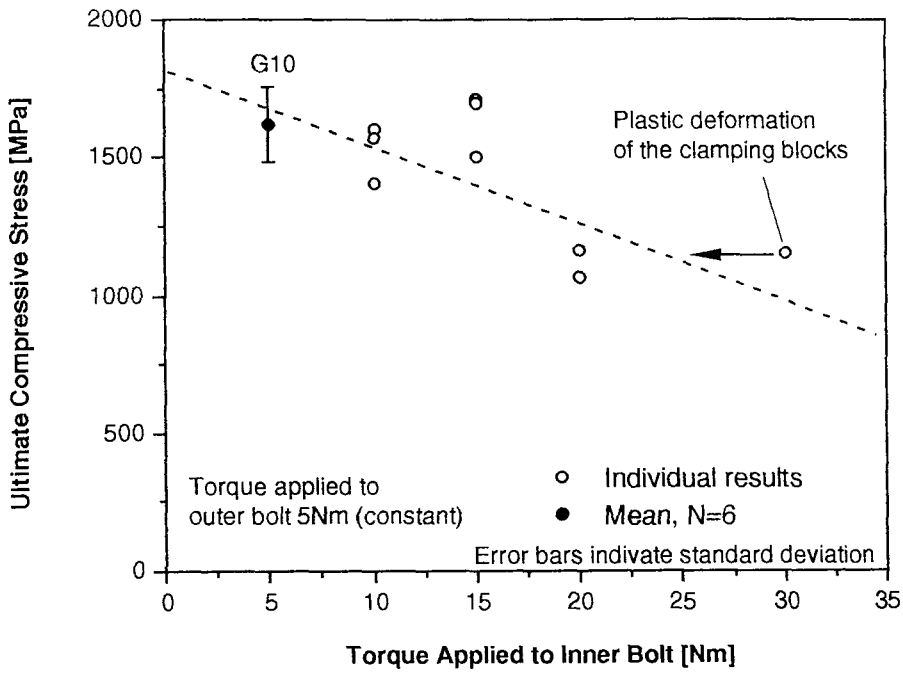


Figure 9.1-4: Influence of clamping pressure on apparent compressive strength using the ICSTM method.

It cannot be argued with certainty whether the reduction of compression strength is due to through-thickness deformation or to additional shear loading and suppressing tab tip debonding. Whatever the reason, the point is made clear, that a loading condition, as present in the indirect compression methods, reduces the measured strength.

Versatility

The compilation of test results in Chapter 6 proved the versatility of the proposed method. Various kinds of composites have been tested successfully, and the results gained are believed to be meaningful. Testing in general was fast and efficient and problems of removing the fractured test piece occurred only occasionally. The relatively unrestrained access to the specimen was found to be useful when strain gauges were used. Also, the alignment of the blocks could be checked during the test and in some cases, e.g. when testing the woven cross-ply GRP, the gap between the blocks allowed the observation of the initiation of failure.

Assessment of results

Finally, some more general observations regarding irregularities in the stress-strain curves, which give the tester valuable information on the validity of the test, are described. Figure 9.1-5 shows typical stress-strain curves, which were all frequently

observed, and combinations thereof, when using the ICSTM method. Most of the curves shown have also been observed when using other methods. It is clear from these observations that without the knowledge of the stress-strain curve up to fracture the test result loses much of its value. Therefore, it is suggested that the test piece must be instrumented with strain gauges in order to be able to assess test results, otherwise the results produced might be meaningless. And it is strongly recommended to use a 'gauge specimen', i.e. for instance a strain gauged machined steel test piece, to identify any misalignment of the compression fixture before testing.

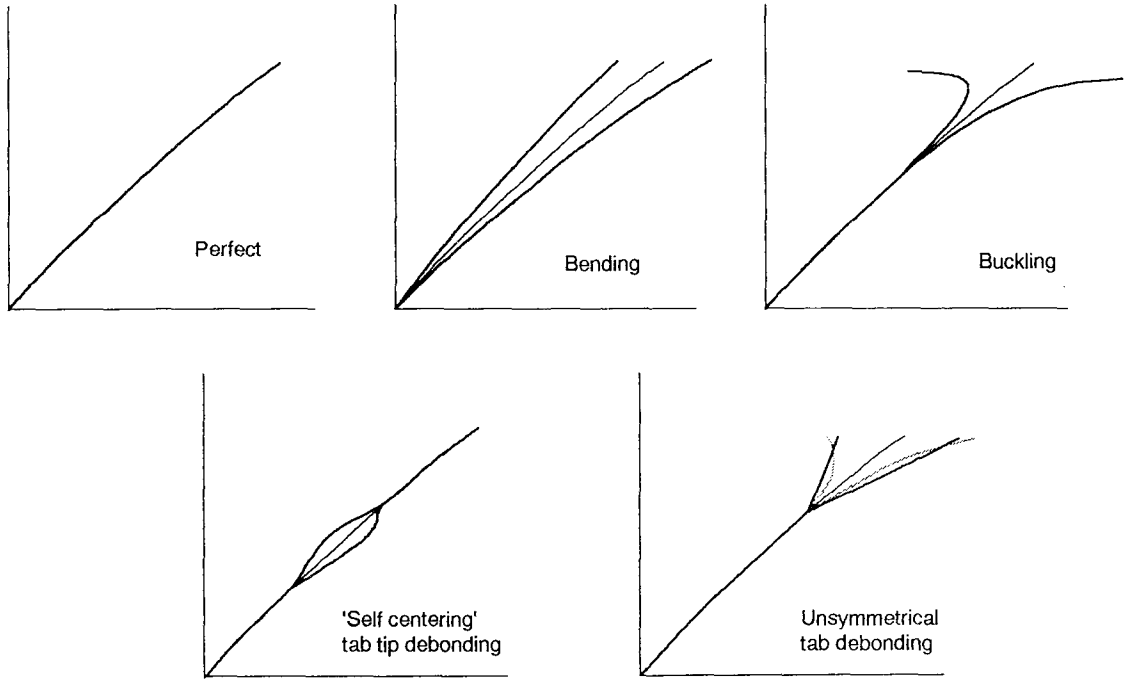


Figure 9.1-5: Some typical compressive stress-strain curves observed using the ICSTM method.

Conclusions

In conclusion, the proposed method proved to be very easy to use. The versatility for a range of different test pieces and testing conditions has been shown. Frictional effects can be neglected and in general test piece constraints are reduced. Repeatabilty of test results was good and, as far as preliminary results show, reproducibility is also good.

9.2 Influence of Test Method

Many authors have addressed the topic of influence of the test method on the measured compressive strength of a composite. This was evident in the literature review in Chapter 2. In Chapter 5 the factors thought to influence the test result were summarised and discussed. It was suggested that a combination of all the factors given can account for the variation of test results.

In this section an attempt will be made to assess test method-typical influence from the experience gathered during the project, although it was often found difficult to distinguish between general parameters, e.g. care in specimen preparation or experience of the operator, and features which can be attributed to a particular test method.

Figure 9.2-1 summarises all axial compression test results for XAS/914C obtained in the present investigation. It should be noted that all test pieces, apart from the one used in the Birmingham method, were tabbed with square, i.e. non-tapered, GRP tabs.

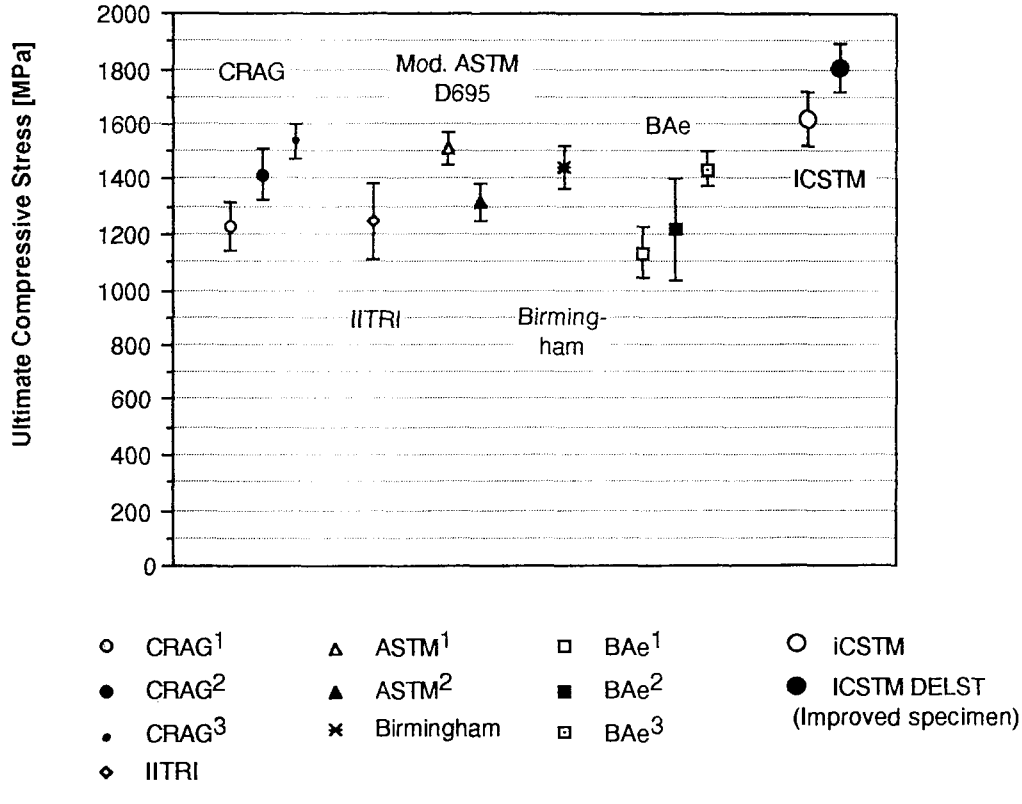
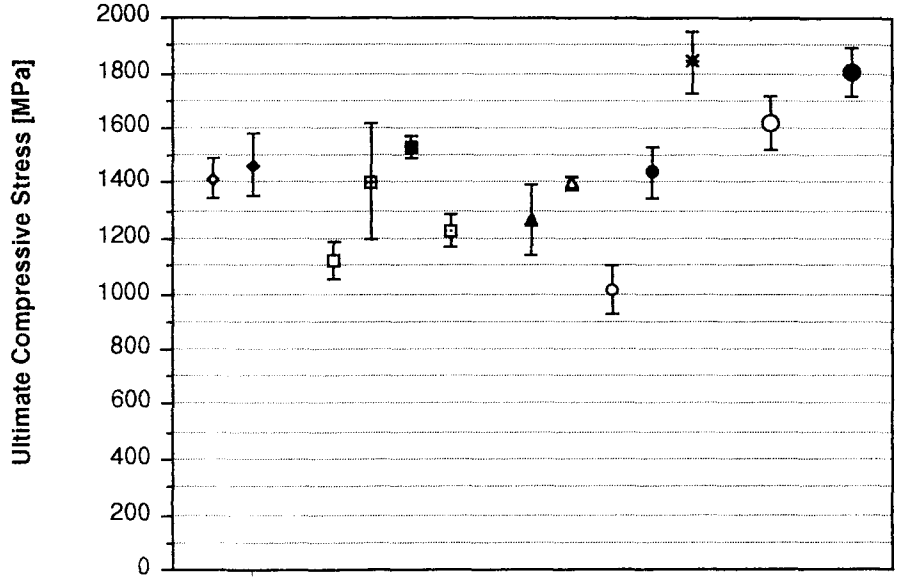


Figure 9.2-1: Results of tests carried out in the present study for the compressive strength of XAS/914C using different test methods and specimen configurations; abbreviations as in Table 6.1.1-1.

There are clear trends as indicated in Chapter 6. Indirect methods yielded low results compared to the methods where the load is partially introduced by shear and partially through the end. Slight changes in specimen clamping resulted in changes of up to 30% of the measured compressive strength. These results suggest that there is too much variation possible and since there is no consensus on a general optimum design the indirect methods of current specification are not recommended for testing practice. Odom and Adams (1990) report high results for using test pieces with steel tabs. This would indicate that factors such as tab debonding as observed with the ICSTM method play an important role as well when using other test methods.

The results presented are in general agreement with results reported in the literature. Figure 9.2-2 shows some of the published data for XAS/914C using different test methods.



◇ Barker (1987) partly plain section
◆ ibid. waisted gauge section
□ LEE (1987) Celanese 12.5 mm gl.
⊞ ibid. Celanese 6 mm gl. 1st attempt
■ ibid. Celanese 6 mm gl. 2nd attempt
⊡ ibid. end-loaded specimen
▲ Woolstencroft et al. (1981) Celanese method
△ Woolstencroft et al. (1981) RAE method
○ ibid. BAe modulus specimen
● ibid. modified ASTM D695 (t = 2 mm)
✱ ibid. modified Celanese (gl. 4 mm)
O ICSTM method standard specimen (gl. 10 mm)
● ICSTM method Improved specimen (DELST) (gl. 10 mm)

Figure 9.2-2: *Published test results for the compressive strength of XAS/914C using different test methods and specimen configurations.*

The only exception is the high result attributed to the modified Celanese. This result was, as mentioned earlier, reported by a German company using a specimen of only 4 mm gauge length. Further evidence that the variation of data gained using one particular test method can be greater than the variation between methods is the range of results reported for the IITRI method using AS4/3501 as specified in Chapter 2. In other words, although repeatability of test results may be given, reproducibility when using indirect test methods can be quite poor.

The ICSTM method yielded the highest results in the present study when using the standard specimen. Results were further increased when the improved test piece with debond inserts was employed. And, importantly, the results were consistent. They seemed only weakly dependent on test piece parameters as long as premature buckling of the test piece could be avoided. Also, experience from testing practice, summarised in Section 9.1, indicates that operator influence is minimised for this method, i.e. sensitivity to slight alterations in the set-up seems to be small. This is thought to be a consequence of reduced stress concentrations, particularly the ones caused by through-thickness loading. The generally higher test results gained with methods using end-loaded specimens would support this assumption.

Macrobuckling has been identified as a major problem in compression testing. Since most test methods specify certain specimen dimensions, this is an important aspect when assessing a method. On the other hand this is rather a problem purely of specimen lay-out, stressing the need for strain gauge instrumenting of the test piece in order to get meaningful results.

Concluding, it is felt that mixed end/shear load introduction is superior to load introduction by shear alone, as long as end failures can be avoided. Indirect methods seem to influence specimen failure by through-thickness loading. Tab tapering (or modified gripping as specified in Section 4.1) is a compromise which unfortunately conflicts with the requirements to avoid macrobuckling. This has been shown to be a major problem with unidirectional composites.

If restrictions of industry are taken into consideration, data being based on the most widespread standards, the BAe rig is recommended for use since it was simple to operate and lacks the drawbacks of Celanese-type fixtures. With appropriate specimen design it is felt that variations encountered when using different indirect methods can be reduced.

The proposed new method is the most promising of the examined methods, yielding the most meaningful values with the least effort and low variability.

However, considering limitations of coupon compression tests in general, as discussed in Section 5.6, more work is necessary to qualify other methods where the slenderness ratio of the test piece is not imposing severe restrictions, as, for example, with the IITRI mini-sandwich beam (Kim and Crasto, 1990) or multidirectionally laminated test pieces.

9.3 Influence of Test Piece Parameters

Test piece parameters have been identified to play an important role when assessing and comparing different test methods. Several test piece parameters, influencing the compressive strength result when using the ICSTM test method, were examined directly or indirectly as described in Chapter 5. The basic finding of this investigation was that, except for the slenderness ratio of the test piece, other parameters influenced the test results, mostly through debonding of tab tips. That meant that if a certain specimen type was prone to tab debonding the measured result, i.e. the apparent compressive strength, was higher. Stiff end tabs, for example, whilst causing high stress concentrations debonded for just this reason and, therefore, reduced stress concentrations and led to high strength results. Waisting of the specimen in order to minimise stress concentration, on the other hand, was found to shift the stress where interlaminar failure occurred to regions where disturbance of the balance led to catastrophic failure. The opposite of the initial intention was therefore achieved. This hardly controllable mechanism was found to override other parameters. It indicates the importance of stress concentration at the tab tips. Tapering of the tabs, as mentioned before, was thought to be no solution since the specimen slenderness ratio has a detrimental influence on the measured strength via macrobuckling of the test piece.

Figure 9.3-1 simplifies these findings. It is an illustration of a plausible effect of combinations of loading and properties of the tabbing on the test result, the 'apparent compressive strength'. The chart was found to be valid for the modified ASTM D695 and the ICSTM method and it is suggested to be applicable to other methods as well. The effect of through-thickness loading when using the ICSTM method has qualitatively been demonstrated in Section 9.1. The effect in other methods could be that of suppressing tab tip debonding plus additional deformation of surface fibres. It is believed that a significant portion of the variety of results quoted in the literature can be reduced to dependence on these factors.

The introduction of the bond inserts is supposed to reduce the influence of tabbing material properties. It was found that if the total axial tab stiffness is about one third of the specimen stiffness end failure of the test pieces could be avoided. The stiffness of the

tabs should be as small as possible. Tabs, therefore, should be as thin as possible from the view of stress concentrations but stiff enough to prevent the specimen ends from brooming. Thinner tabs are also preferred since they provide greater lateral stiffness and therefore increase the buckling load of the test piece. Because the stress concentration at the tab tips is controlled by a combination of factors it is difficult to predict a certain effect. That is thought to be the reason for the high variation, as mentioned before, particularly when the additional complication of macroscopic buckling is taken into account.

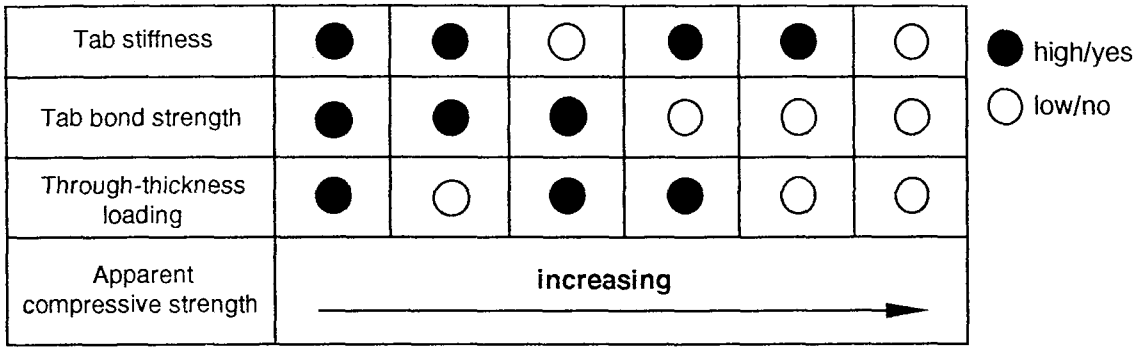


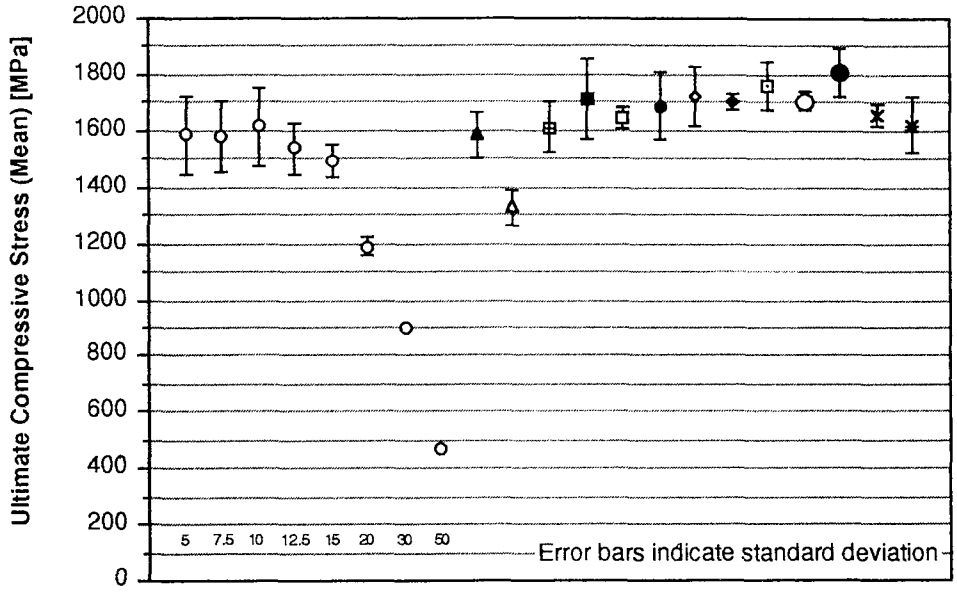
Figure 9.3-1: Effect of tabbing properties on measured compressive strength.

An important result of the study on the slenderness ratio was the finding that even relatively short test pieces could fail by macroscopic instability. 10 mm was found to be the minimum gauge length for a 16-ply laminate in order to have an unconstrained area. It is suggested that specimens with debond inserts or specimens where delaminations occur well before fracture (e.g. milled test pieces as described in Section 5.2.3) would allow one to reduce the unsupported length to, say, 7.5 mm, because the weakly bonded area experiences much lower constraints than when bonded. Unfortunately, these tests, although prepared, could not be finished within the project. This should, therefore, be a topic for further investigation.

The surprising fact that deliberately induced layer misalignment did not seem to influence the result significantly is believed to be due to constraints of the test rig on the specimen, as pointed out in Chapter 5. Flexural tests with specimens containing deliberately misaligned fibres might give a more realistic picture of the influence of fibre alignment on the compressive strength.

Generally, more investigations with the improved specimen are desirable. With the findings of this work in mind it would be interesting to again examine the parameters using an optimised test piece.

To give a concluding summary, all results of the parametric investigation discussed in Chapter 5 are shown in Figure 9.3-2 and listed in Table T-32.



Symbols denote deviation from standard test piece (Figure 5.2-1):

- ○ Gauge length 5.0 to 50 mm (G5-G50)
- ▲ Nominal thickness 1.5 mm (T12)
- △ Nominal thickness 1.0 mm, gauge length 7,5 mm (T8)
- ⊞ Width 5.0 mm (W5)
- ■ Lay-up ±1° (PM1)
- □ Fibres 2° off-axis (COA2)
- ● Smooth gauge surface (PP3)
- ◇ Machined gauge section (SGG)
- ◆ ditto + all surfaces ground flat (SGGF)
- ⊡ Initial tab debonds by bending (DEB)
- ○ Tab debonds/PTFE tape (DELPT)
- ● Tab debonds/Cellulose tape (DELPT)

Other results

- × Student X (LC)
- ✱ IC short course 1989 (SC 89)

Figure 9.3-2: Test results for the compressive strength of XAS/914C using the ICSTM method and varying test piece parameters.

9.4 Interpretation of Flexure Test Results

The question to be asked with respect to the high strains achieved in the flexure tests is whether the test measures the tensile and compression properties of the composite in a realistic way. To answer the question, an attempt will be made to predict the force-strain curve from the four-point bend tests as shown in Figure 7.2-2, using the elastic tension-compression properties of the composite (Equation 7.1-1).

The procedure is divided into two parts:

1. Considering material nonlinearity:

   Determination of surface strains in the centre of the test piece caused by a bending moment, using the nonlinear stress-strain relationship of the composite.

2. Considering geometric nonlinearity:

   Determination of the relationship of applied load to bending moment acting on the specimen centre, which is nonlinear due to large deformations.

Starting with the first problem, engineering bending theory is assumed to be valid, i.e. strains are linear through thickness and through-thickness stresses are neglected.

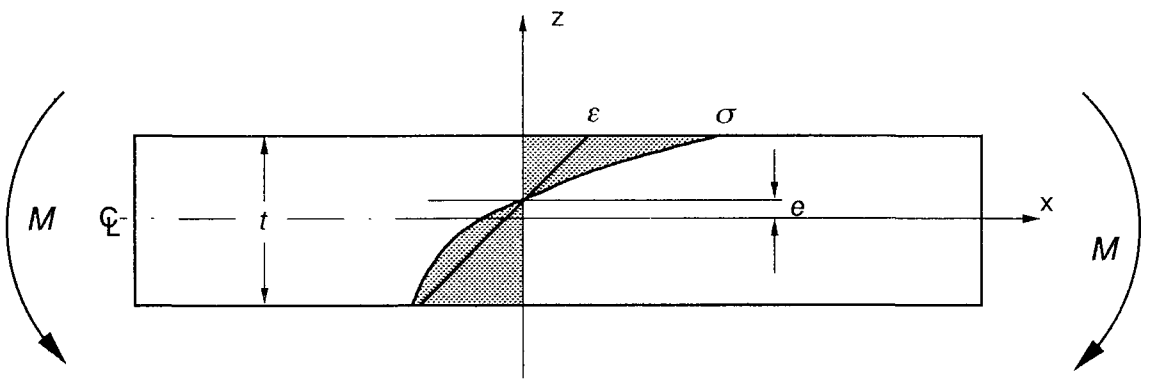


Figure 9.4-1: Sketch of strain and stress distribution in the flexure specimen

Assuming different elastic properties in tension and compression, a shift e of the neutral axis is anticipated. The distribution of strains can be written as:

$$\varepsilon(z) = \varepsilon_0(z - e) \tag{9.4-1}$$

with

$$\frac{dz}{d\varepsilon} = \frac{1}{\varepsilon_0} \tag{9.4-2}$$

The nonlinear stress-strain relation is expressed by (compare Equation 7.1-1.):

$$\sigma(\varepsilon) = A\varepsilon + B\varepsilon^2 + C\varepsilon^3 \tag{9.4-3}$$

For equilibrium over the cross-section two conditions have to be fulfilled:

1. Balance of horizontal forces

$$\int_{-z_0}^{z_0} \sigma(z)dz = 0 \tag{9.4-4}$$

2. Balance of moments on centre line:

$$\int_{-z_0}^{z_0} \sigma(z)zdz = \frac{M}{w} \tag{9.4-5}$$

where w is the width of the test piece. These conditions combined with Equations 9.4-1 to 9.4-3 yield:

$$\frac{1}{\varepsilon_0}\int_{\varepsilon_c}^{\varepsilon_t} [A\varepsilon + B\varepsilon^2 + C\varepsilon^3]d\varepsilon = 0 \tag{9.4-6}$$

and

$$\frac{1}{\varepsilon_0^2}\int_{\varepsilon_c}^{\varepsilon_t} [A\varepsilon_0 e\varepsilon + (A + B\varepsilon_0 e)\varepsilon^2 + (B + C\varepsilon_0 e)\varepsilon^3 + C\varepsilon^4]d\varepsilon = \frac{M}{w} \tag{9.4-7}$$

with the tensile and compressive surface strains being:

$$\varepsilon_t = \varepsilon_0\left(\frac{t}{2} - e\right) \tag{9.4-8}$$

$$\varepsilon_c = -\varepsilon_0\left(\frac{t}{2} + e\right) \tag{9.4-9}$$

And after straightforward integration one obtains:

$$C\left(\frac{t^3}{4}e + te^3\right)\varepsilon_0^2 - B\left(\frac{t^3}{12} + te^2\right)\varepsilon_0 + Ate = 0 \tag{9.4-10}$$

and

$$C\left(\frac{t^5}{80}+\frac{t^3e^2}{4}\right)\varepsilon_0^3-\frac{Bet^3}{6}\varepsilon_0^2+\frac{At^3}{12}\varepsilon_0=\frac{M}{w} \tag{9.4-11}$$

A computer program is used to solve the quadratic Equation 9.4-10 in ε_0 for increments of e and calculates the corresponding moment from Equation 9.4-11. With the surface strains from Equation 9.4-8 and 9.4-9 the relation $M(\varepsilon)$ is known. And with the linear relation between the applied load P and the moment M acting on the centre cross-section of the flexure specimen (for the loading geometry shown in Figure 7.2-1):

$$M=\frac{Ps}{8} \tag{9.4-12}$$

the relation $P(\varepsilon)$ can be calculated.

Figure 9.4-2 shows the predicted curve $P(\varepsilon)$ for the geometry of specimen #3 (Section 7.2). For comparison the experimental data are plotted as well. The difference of tensile and compressive strains is predicted accurately as illustrated in Figure 9.4-3, but the nonlinearity of the experimental curve is not matched. Note that although the elastic response in tension is stiffening, the overall stiffness of the test piece (mean value of the surface strain signals) is decreasing, which is predicted correctly in its tendency. This is caused by the stiffness decrease in compression overriding the stiffness increase in tension.

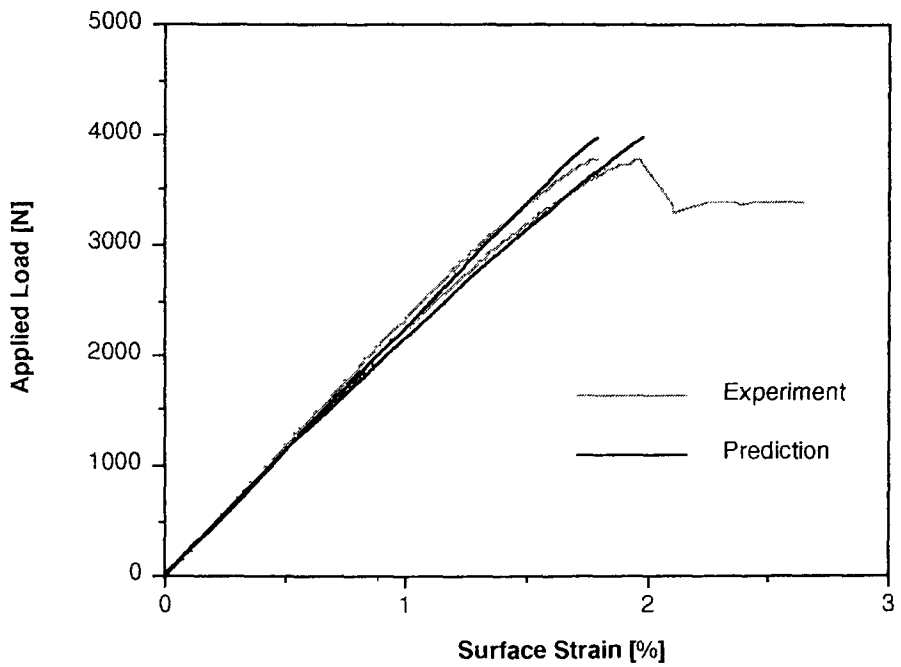


Figure 9.4-2: Geometric linear prediction assuming test conditions described in Section 7.2 and test results for four-point bend test.

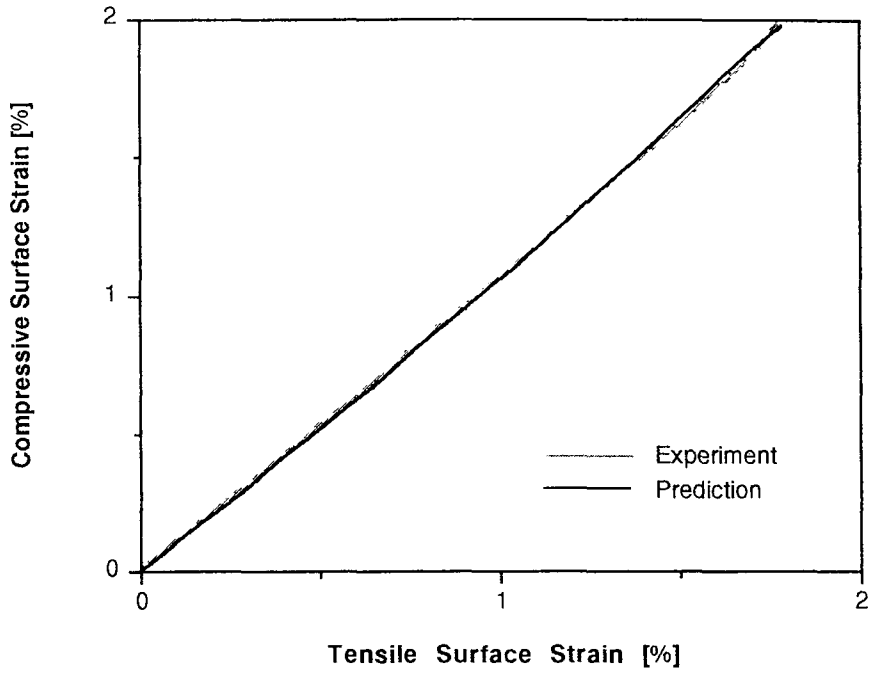


Figure 9.4-3: *Geometric linear prediction and test results for four point bend test, compressive versus tensile surface strains.*

Next, the relation of the applied load and the moment acting on the centre cross-section of the test piece is examined. For this purpose deflections of the test piece and associated changes of direction of the forces are taken into account. Ideally, deflections are measured in the test or determined by an iterative finite element analysis continuously updating the structure. However, it is felt that an assessment using first order deflections as described below might be sufficient. The geometry and abbreviations used in the following are defined in Figure 9.4-4.

The beam is split into two segments according to Figure 9.4-4. The first beam segment is subjected to a pure end moment M, the second one to a vertical end load $P/2$. First order deflections and distortions are calculated using the following:

Deflections of the single elements:

$$a = \frac{Ml_a^2}{2EI} \qquad \text{and} \qquad b' = \frac{Pl_b^3}{6EI} \tag{9.4-13}$$

Deflection of the beam end:

$$b = b' + l_b \tan\alpha \tag{9.4-14}$$

Distortions of the single elements:

$$\alpha = \frac{Ml_a}{EI} \qquad \text{and} \qquad \beta' = \frac{Pl_b^2}{4EI} \tag{9.4-15}$$

With

$$l_a = l_b = \frac{s}{4} \tag{9.4-16}$$

and Equation 9.4-12 the distortion of the beam end becomes:

$$\beta = \alpha + \beta' = \frac{3Ps^2}{64EI} \tag{9.4-17}$$

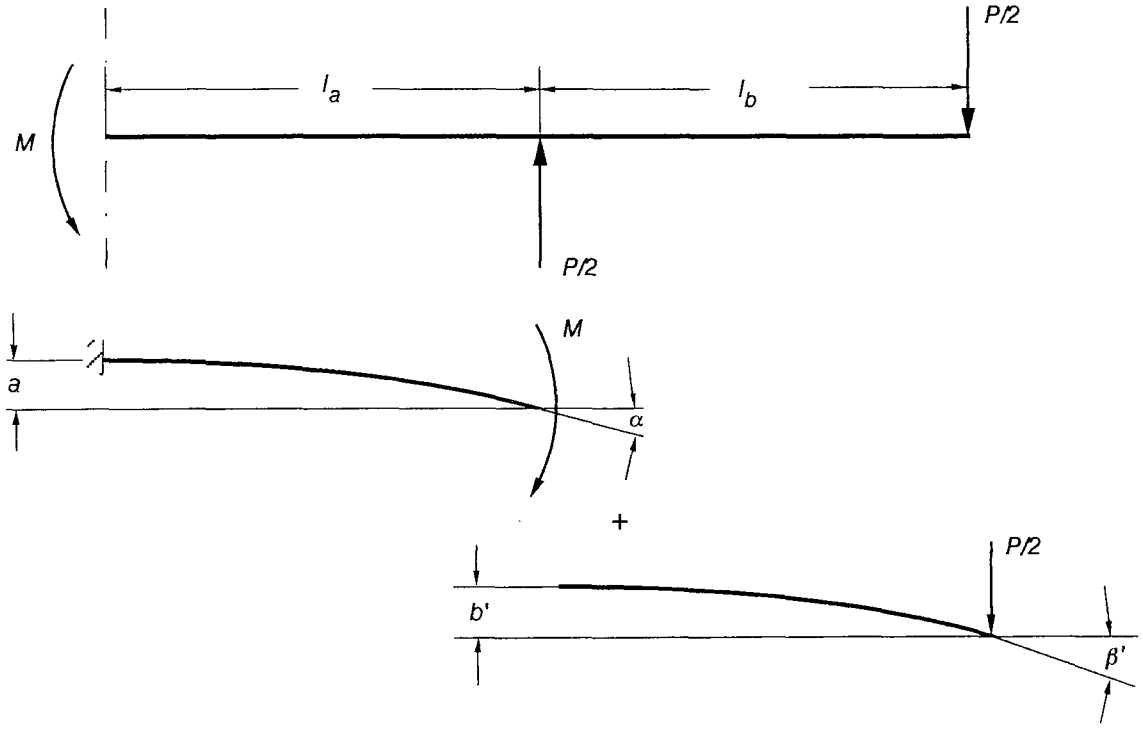


Figure 9.4-4: *Deflections of the flexure specimen.*

The deformations are calculated using the actual specimen geometry and a constant average modulus of elasticity of $E = 120$ GPa. With this information the general case illustrated in Figure 9.4-5 can be examined. Frictional forces are included, as there is a movement between the rollers and the test piece. Denoting the coefficient of friction with μ frictional forces are calculated as:

$$F_i = \mu P_i,\ i=a,\ b \tag{9.4-18}$$

Vertical balance of forces yields:

$$P_a = P_b \frac{\cos\beta + \mu\sin\beta}{\cos\alpha - \mu\sin\alpha} \tag{9.4-19}$$

Equilibrium of the forces acting on the loading roller gives:

$$P = 2P_a(\cos\alpha - \mu\sin\alpha) \tag{9.4-20}$$

where, as before, P denotes the force measured in the experiment.

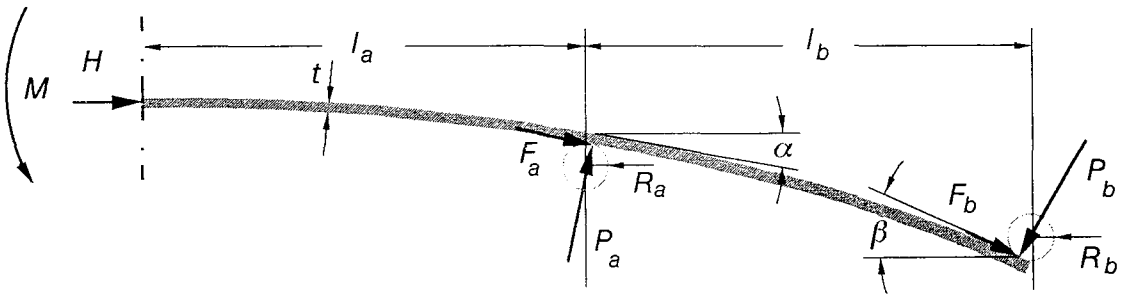


Figure 9.4-5: *Forces acting on the flexure specimen.*

A balance of moments on the specimen centre using Equations 9.4-18 to 9.4-20 yields the expression for the bending moment which acts on the centre under a load *P*:

$$M = M_{lin}\, C_{corr} \tag{9.4-21}$$

where

$$M_{lin} = \frac{P}{2} l_b \tag{9.4-22}$$

and the correction factor:

$$C_{corr} = \frac{1}{l_b}\left\{ X_1 + \frac{\sin\beta - \mu\cos\beta}{\cos\beta + \mu\sin\beta} X_2 - X_3 - \frac{\sin\alpha + \mu\cos\alpha}{\cos\alpha - \mu\sin\alpha} X_4 \right\} \tag{9.4-23}$$

where the dimensions X_i are defined as:

$$\begin{aligned} X_1 &= l_a + l_b - R_b \sin\beta \\ X_2 &= a + b - \frac{t}{2}\cos\beta - R_b\,(1 - \cos\beta) \\ X_3 &= l_a + R_a \sin\alpha \\ X_4 &= a + \frac{t}{2}\cos\alpha + R_a(1 - \cos\alpha) \end{aligned} \tag{9.4-24}$$

Equation 9.4-21 describes how the linear bending moment, i.e. specimen deformations not considered, has to be corrected in order to get the true bending moment $M(P)$. In order to include the nonlinearity in the model described above, the applied force from the linear case has to be divided by this correction factor.

Figure 9.4-6 shows the correction factor versus the tensile surface strain for the test piece #4. Obviously, the amount of friction acting on the specimen has a significant influence on the centre moment. It should be noted that, for low frictional coefficients and high strains, the factor is higher than 1, which would result in a load-strain curve with decreasing slope, as observed in the experiment.

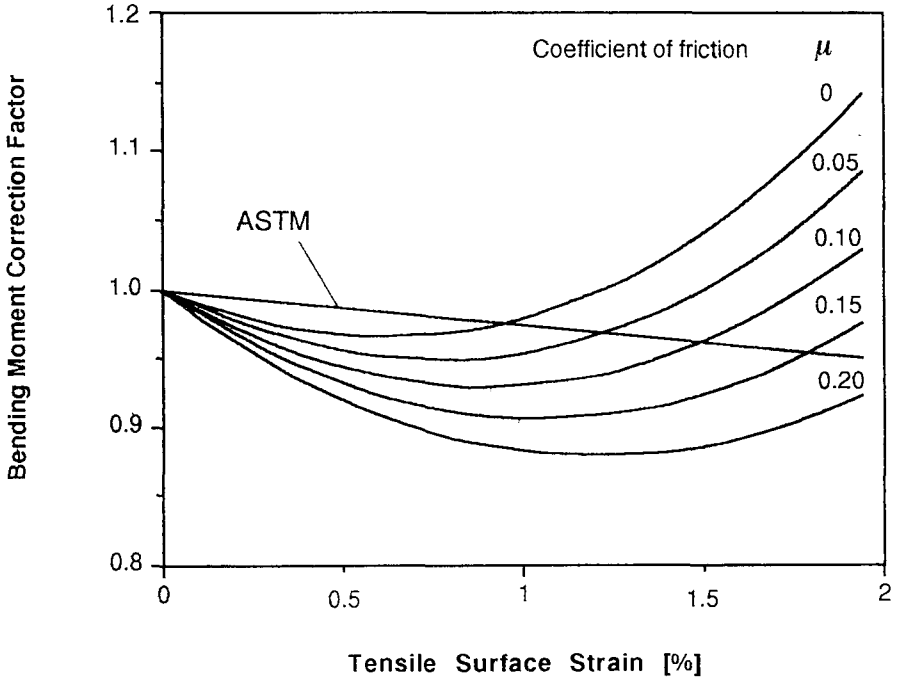


Figure 9.4-6: *Bending moment correction factor versus tensile surface strain.*

Figure 9.4-7 finally shows the prediction of surface strains assuming a friction coefficient of 0.05 and roller radii of 4 and 3 mm for loading and support rollers, respectively. The fit of the experimental data is very good, particularly if it is considered that the deformations and stiffness of the beam are only calculated from first-order deflections. The nonlinear character of the curve is more pronounced for smaller values of μ, as is to be expected from Figure 9.4-6.

The horizontal resultant H (Figure 9.4-5) can be expressed as:

$$H = \frac{P}{2}\left(\frac{\sin\beta - \mu\cos\beta}{\cos\beta + \mu\sin\beta} - \frac{\sin\alpha + \mu\cos\alpha}{\cos\alpha - \mu\sin\alpha}\right) \qquad (9.4\text{-}25)$$

Again, it greatly depends on the frictional forces and can be compressive or tensile. However, for a friction factor of 0.05 the resulting additional axial stress at fracture stress is -3 MPa and can therefore be neglected. Also, shear stresses have not been considered in this analysis since they are assumed to be small.

The correction factor recommended by the ASTM standard is seen to match the conditions of the test only if high coefficients of friction and high strains are assumed; otherwise the correlation to the predicted values is poor. Therefore, the calculation of stresses using the equations given in the ASTM standard cannot be recommended.

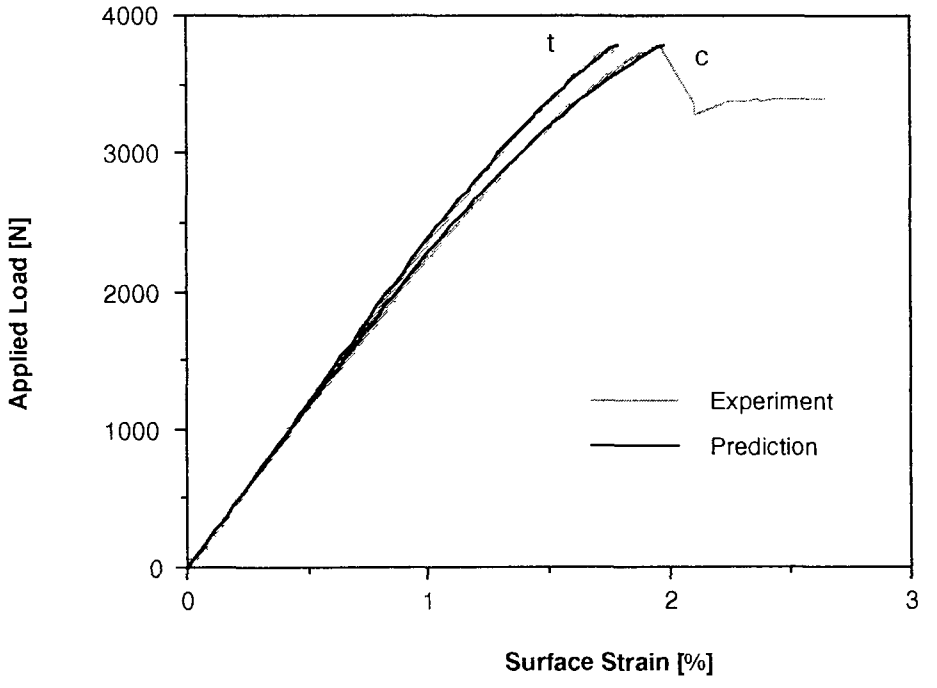


Figure 9.4-7: Nonlinear prediction of the load-strain response of the flexure test piece.

Using Equations 9.4-8 and 9.4-9, the shift of the neutral axis e due to different elastic behaviour in tension and compression can be expressed as:

$$e = \frac{\frac{\varepsilon_t}{\varepsilon_c} + 1}{1 - \frac{\varepsilon_t}{\varepsilon_c}} \frac{t}{2} \tag{9.4-26}$$

where ε_t and ε_c are tension and compression surface strains, respectively, and t is the test piece thickness. With the strains at first failure for specimens #3 and#4 from Table 7.2-1 the shift of the neutral axis amounts to 2.0 and 2.5 % of the test piece thickness, i.e. 0.04 mm and 0.05 mm, respectively.

The conclusion of the findings described above is that the elastic behaviour of the test piece in a four-point bend test can be described satisfactorily from knowledge of the elastic behaviour in individual tension and compression tests. The absence of significant stress concentrations could explain the increased level of failure strains in compression as well as in tension.

9.5 Correlation of Compressive Strength and Other Mechanical Properties

The results of short beam shear tests and determination of fibre angle distribution have been outlined in Chapter 7 and 8, respectively. In this section a correlation between these properties and the compressive strength as determined using the ICSTM method will be investigated.

Basically, the interlaminar shear strength of four groups of unidirectional composites has been determined:

1. 43-750/9106C containing fibres of different surface treatment;
2. XAS-fibre reinforced epoxies of different cure condition;
3. AS4 fibre-reinforced PEEK (APC-2); and
4. glass fibre-reinforced nylon with different fibre volume fractions.

Figure 9.5-1 presents the short beam interlaminar shear strength versus the compressive strength determined using the ICSTM method; one could say 'apparent ILSS versus apparent compressive strength'.

For the three composites containing XAS-fibres a linear correlation of ILSS and UCS can be recognised. The result for APC-2 lies below this line. Significantly, the four Apollo-fibre systems containing fibres of different surface treatment exhibit a pronounced influence of the surface treatment on ILSS, but their UCS is almost independent of the interfacial properties. In Chapter 6 it has been said that most of the glass fibre/nylon compression specimens failed in a macrobuckling mode; whereas in Chapter 7 it has been pointed out that most ILSS specimens failed in a mixed shear/(tensile)flexural mode. Ultimate stresses for both types of failure can be regarded as proportional to the fibre volume fraction so that a linear relationship as found in Figure 9.5-1 is to be expected.

Short beam interlaminar shear strength seems to be a weak indicator of the compressive strength of a composite system but not an exclusive one. In other words:

there is a trend towards higher compressive strengths for high values of ILSS, but high ILSS is not necessarily equivalent to high compressive strength of the system.

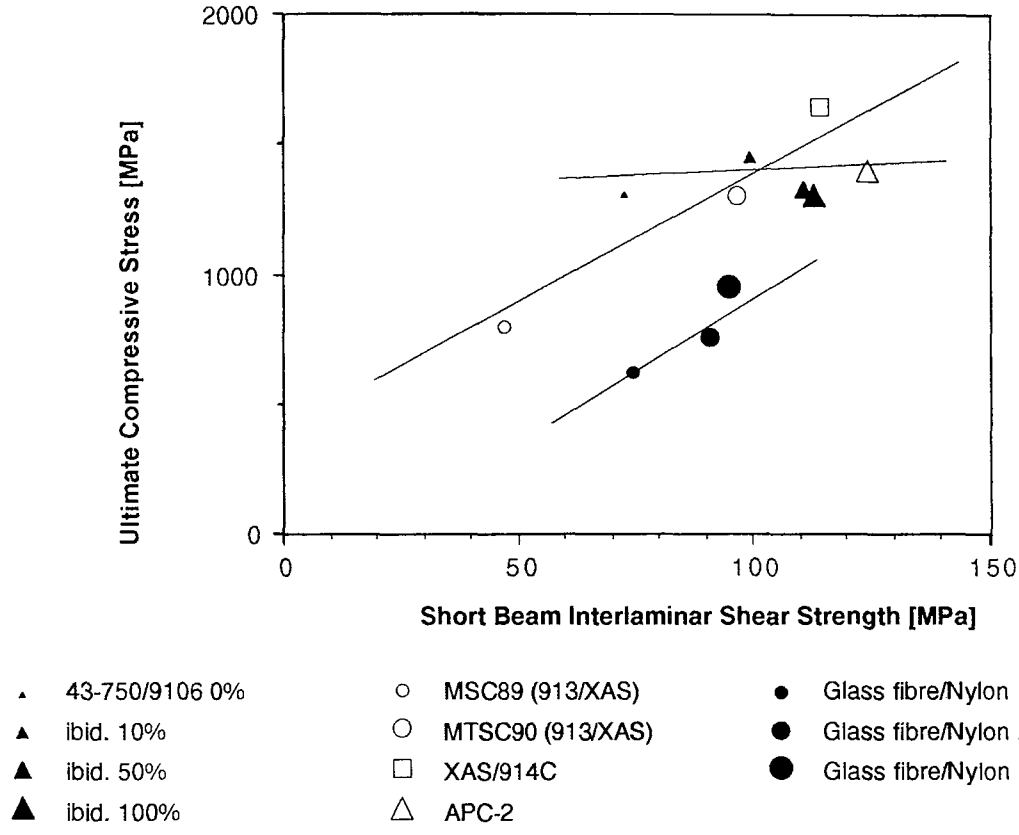


Figure 9.5-1: Compressive strength (ICSTM method with standard specimen) versus short beam ILSS for several unidirectional composites.

The second important factor in this context has been identified as the quality of fibre alignment. It has been outlined previously that it is difficult to find a typical quantitative measure, particularly a quantitative measure which distinguishes between different qualities of fibre misalignment: the overall (rotational layer) misalignment and the localised short wavelength fibre misalignment. In Chapter 8 a method of determining the total distribution of in-plane fibre misalignment has been employed on some unidirectional composites:

1. 43-750/9106C containing fibres of different surface treatment;
2. XAS/914C;
3. AS4 fibre-reinforced PEEK (APC-2).

The standard deviation of the distributions determined (as described in Chapter 8) will be used as a measure for the quality of fibre alignment in the composite. The component of

rotational misalignment due to off-axis plies is therefore neglected, which is probably not a great source of error if the laminates are laid-up carefully. Separate scanning of single layers and comparison with the results of the whole specimen would allow an assessment of the error as pointed out in Chapter 8. Since time restrictions of the project did not allow further investigations, these comparisons have not been carried out but are suggested for further work.

Figure 9.5-2 shows the results of the fibre alignment analysis versus the compressive strength determined with the ICSTM method, using different specimen types The figure allows some interesting conclusions. Regarding the compression results of all materials gained using the ICSTM method with standard specimen, a linear correlation, regardless of the ILSS results, can be stated. Particularly interesting is the Apollo 43-750/9106C material with fibres of 10% surface treatment which yielded somewhat higher compression strength results than the others: this material has the best fibre alignment of the 9106C composites.

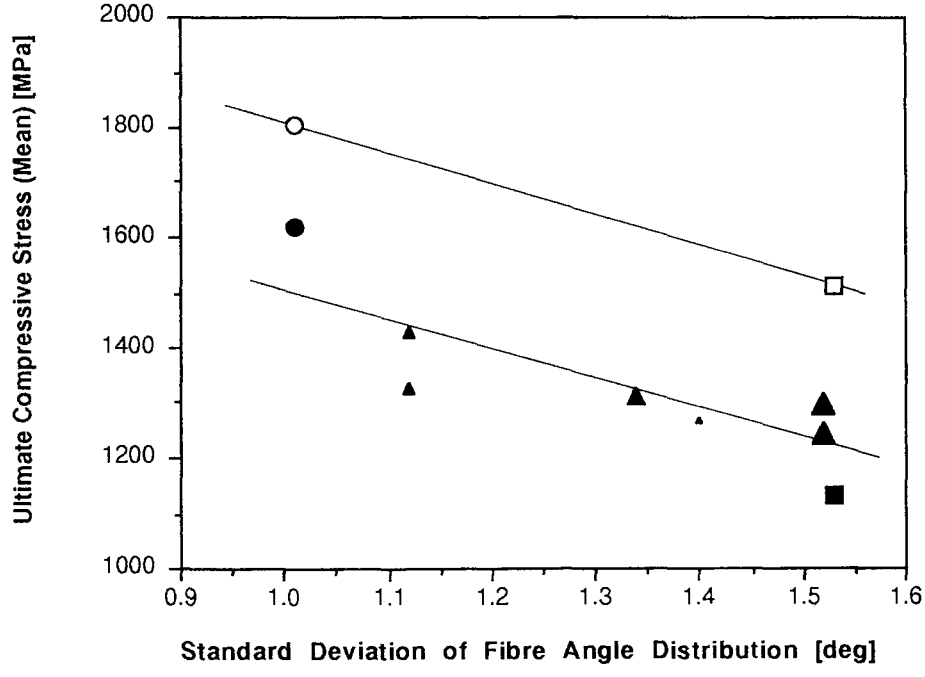


Figure 9.5-2: Compressive strength of several unidirectional CFRP versus fibre alignment.

XAS/914C was found to have the best fibre alignment of the systems examined accompanied by the highest compressive strength. And likewise, APC-2, although of comparable interlaminar strength, was found to exhibit the highest degree of misalignment and lowest compressive strength. A similar trend is found for the two materials if compression data gained with an improved specimen (with debond inserts) are compared.

Concluding, it is suggested that fibre alignment is an important factor of the compressive strength of a unidirectional composite. Elastic shear data such as the shear modulus have not been considered here. But it can be stated that since the shear modulus of the epoxy systems are about equal, the shear modulus of APC-2 is slightly higher, no direct correlation between the shear stiffness and the compressive strength could be found. The influence of the interlaminar shear strength on the compressive strength could not be fully explored since too little data for composites with comparable and small fibre alignment were available. The deformation behaviour in the short beam shear tests indicates that a composite shear yield stress is possibly a better measure of compressive performance. This will be examined in more detail in Chapter 11.

9.6 Significance of Coupon Compression Testing

It has been shown that with appropriate specimen design using the ICSTM rig, compressive failure stresses and strains of test coupons can be increased significantly compared to standard test methods. For XAS/914C average compressive failure strains of almost 2% could be realised, higher than any published data for comparable slenderness ratios. When macrobuckling of the specimen occurred compressive strains in the centre of the gauge section, the location of the strain gauges, reached strains as high as 2.5 % without signs of compressive failure in this vicinity. Similarly, the results for the other CFRP systems examined, Apollo 43-750/9106 and APC-2, were significantly higher than reported from other methods. Specimens of both systems did not show signs of macrobuckling and failure was usually initiated near the end tab edges. Only in very few cases failure occurred in the centre of the gauge section.

The fact that XAS/914C test pieces buckled is on the one hand an indication that failure was premature and the full compressive potential of the material was not reached yet. On the other hand, however, it introduces interesting questions. Why does the test piece never fail in the centre where local compressive stresses are the highest? Is it a consequence of high stress concentrations at the tab tip at lower stresses than in the gauge

centre? Or is it a consequence of a suppressed failure mode in the centre, e.g. due to a complex stress state?

Strains of 2.5% and above without apparent damage have been observed in flexure specimens where similar conditions as in the buckling test piece are present. Multidirectional test pieces including 0°-layers failed at strains over 2%. And for the sandwich column used in a IITRI rig Crasto and Kim (1990) reported failure strains significantly higher than for the coupon test piece. Common for the three test methods is that only a thin layer of material is loaded. The relatively high failure strains would support an argument of size effect. But it can also be argued that shear stresses are reduced in all three cases. The more so for the flexure specimen which seems to yield the highest failure strains. In-plane constraint of 0°-layers exists in a multidirectional specimen, particularly when 90°-layers are present, as well as in the sandwich column where thin laminates are bonded onto a core. This could hinder in-plane deformation of initially deflected fibre bundles, thus increasing the compressive load carrying capability.

However, this condition is not present in the flexure test. Here, no lateral constraint is imposed. Higher failure strains could be explained if local shear instability, as indicated in Chapter 2 and further discussed in Chapter 11, is assumed as the compressive failure mode. The amplitude of initially wavy fibres, or rather fibre bundles, is increased under compression. If the whole cross-section is not under uniform compressive strain the less strained fibres offer some restraint to the geometric deformation of the more strained ones (see Chapter 11). In the flexure specimen, where the through-thickness strain gradient is high, the fibres under tension are likely to stabilise the compressed ones, both in-plane and out-of-plane. The resistance of fibres under compression to geometric deformation which, finally, leads to an unstable state is increased. As a consequence, the failure strain of the outer layers is higher than in the uniformly strained laminate.

From the nature of compression failure one would expect a local worst misalignment or flaw to trigger failure. But since the same failure location is always observed in coupon test pieces it is very likely that stress concentrations override the effect of local imperfections in the uniformly stressed material.

Although there is no direct proof, it is felt that the true compressive strength of unidirectional composites lies between the results of the alternative methods described above and coupon tests in their optimum form, e.g. ICSTM method. All signs indicate that a combination of axial direct and shear stress concentrations cause premature failure of coupon specimens. Constraints existent in the other methods inhibit compressive failure to a certain extent.

Published test results, shown below, for the compressive strength of APC-2 would confirm this hypothesis:

Crasto and Kim (1990), IITRI mini sandwich beam:	1570 MPa
Crasto and Kim (1990), four-point flexure:	1630 MPa
Mrse and Piggot (1990), mini sandwich beam:	1610 MPa
Mrse and Piggot (1991), mini sandwich beam:	1680 MPa

The ICSTM method with improved specimen yielded a result of 1511 MPa. This result, if somewhat lower, is in the same range as the above mentioned ones. Particularly if results gained with standard coupon tests are considered (see Section 6.1.4)

One big advantage of the classical coupon test over tests involving sandwiches is relatively easy specimen preparation. For the ICSTM method a very simple procedure of specimen preparation has been described in Chapter 3.

A real limitation of coupon testing is buckling of the test piece. Specimens have to designed carefully to avoid macroinstability. Figures F-16 and F-17 contain guidelines for adequate specimen lay-out. However, it is possible that a uniform stress field may not be realised so that microfailure occurs before macrofailure regarding the decreasing modulus of elasticity of CFRP with compressive strain.

In conclusion, it is felt that it has been shown that by simple means stress concentrations can be reduced in routine testing. This should allow the determination of design allowables from coupon tests. It should be noted that this investigation is rather the beginning of a development (Figure 9.6-1), and further research will be necessary to draw firm conclusions.

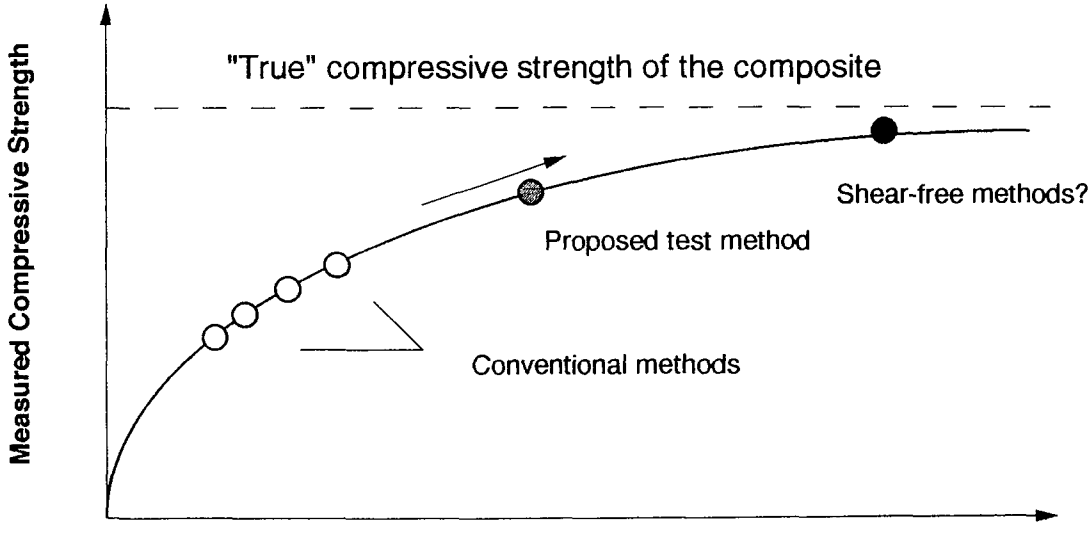


Figure 9.6-1: A view of compression testing practice.

CHAPTER 10 MACRO INSTABILITY OF THE TEST PIECE

In Chapter 5 evidence of macroinstability of unidirectional test pieces even at relatively short gauge lengths was presented. Using a conventional buckling analysis, calculated critical buckling stresses are much higher than the measured ones. In the light of the experimental findings a modified analysis will therefore be examined in this chapter. Some similarities will be found to the case of micromechanical instability which is discussed in the next chapter.

10.1 General Aspects on Buckling of Columns

As an introduction, the basic principles of buckling will be reviewed. The state of a compressively loaded, initially straight, column is stable as long as the load is below the critical load. As soon as the critical load or buckling load is reached, the straight form becomes unstable; the bifurcation point is reached. That means that two shapes are possible: the straight form or a deflected one including bending and shear deformation of the column. Since in a real structure there is always a small imperfection, the deflected form is always preferred. In other words, when the buckling load is reached the column or strut will jump into the bent form commonly referred to as buckling. This transition is of a sudden nature if the imperfection is small; one could say the more sudden the smaller the initial imperfection.

A more figurative image of the buckling process, which often is not very clearly defined, might be the following (Timoshenko and Gere, 1961): a small lateral force, applied on a column under a compressive load smaller than the buckling load, will cause a lateral deflection of the column. If the lateral force is removed the column will resume the initial shape. The critical load or the buckling load of an ideal column is then defined as the compression load at which the lateral deflection remains when the lateral load is taken away.

For an ideally straight column the bifurcation point can be estimated by an energy balance. The bifurcation point is the point where the energy stored in the deflected structure due to bending (and shear) equals the work done by the applied load. Clearly, the buckling load can also be determined by a force balance. The result in both cases depends on the estimate of the buckled shape but the error due to different shape assumptions is not large provided the end conditions are fulfilled (Timoshenko and Gere, 1961).

It can be shown that with any initial imperfection the lateral deflections grow infinitely when the buckling load of the ideal column is approached, so that it can be concluded that as long as the stresses are in the elastic region the apparent buckling load is the same regardless of the initial imperfection. From a linear analysis, i.e. the deflected shape is modelled neglecting second order terms, the critical load is the maximum load the column can sustain. A nonlinear analysis, however, shows that an increase in load is possible beyond the buckling load. These facts are illustrated in Figure 10.1-1, where α denotes the ratio of applied load to critical load.

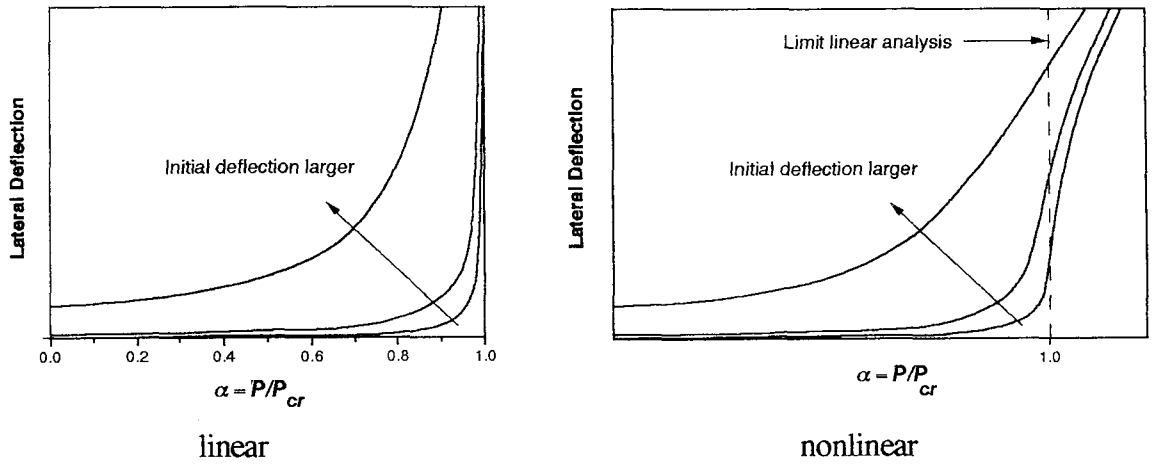


Figure 10.1-1: *Load deflection behaviour under compression of columns with imperfections.*

The classical elastic Euler buckling stress for a strut is given as:

$$\sigma_{Eu} = \frac{C\pi^2 E}{s^2} \qquad (10.1\text{-}1)$$

C is a constant taking into account the end support condition of the strut, i.e. the manner in which it is clamped. The value of C is 1 for both ends hinged and 4 for both ends clamped. Any practical realisation should lie between these two extremes. s is the slenderness ratio, which for a rectangular cross-section of thickness t is calculated as:

$$s = \frac{g}{t}\sqrt{12} \qquad (10.1\text{-}2)$$

where g denotes the unsupported (gauge) length. E is the bending modulus of elasticity which equals the longitudinal modulus for isotropic materials. Dealing with composites the situation is different. The bending modulus of a multidirectional laminate can differ substantially from the longitudinal modulus depending on the stacking sequence of the laminate.

Large initial imperfections in the case of metals pose the problem of reaching the elastic limit on the concave face before the buckling load is reached. In order to estimate the buckling load from test data within the elastic region Southwell proposed a method known as the 'Southwell plot' (Timoshenko and Gere, 1961). Assuming that the lateral deflection δ of the midpoint of the column is due to an initial imperfection a, the following relation is obtained:

$$\frac{\delta}{P} P_{cr} - \delta = \kappa \tag{10.1-3}$$

where P_{cr} is the buckling load, P the load corresponding to δ, and κ equals the initial deflection a. It can be shown that in the general case of a combination of an initial deflection a and an eccentricity in the load application e, Equation 10.1-3 is valid with $\kappa = a+e$. If the the ratio δ/P is plotted against the measured deflection δ the points fall on a straight line and the intersection with the δ-axis gives the value of the initial imperfection, or the sum of initial imperfection and eccentricity, respectively. The inverse slope of the line gives the critical load. These relations, of course, are valid for stress, i.e. load divided by the cross-sectional area.

In Figure 10.1-2 an example for an aluminium alloy is given using Equation 5.2.4-9 (Chapter 5) to calculate the central deflection from the measured surface strains. The specimen chosen buckles well before the elastic limit in pure compression is reached. The Southwell plot predicts the buckling stress from the data within the elastic region as 266 MPa. This compares well with the ultimate compressive stress of 253 MPa measured in the experiment.

Composites behave quasi-elastically until fracture; therefore, the buckling load can often be estimated from the maximum load. However, if the failure stress is reached before the tangent modulus vanishes, i.e. the stress-strain curves are horizontal, the method described above allows an estimate of the buckling load. Equation 10.1-1 is valid only within the elastic region of the material. As an extension for the plastic region, the 'reduced modulus' (Figure 10.1-3) has been introduced, given for a rectangular cross-section as (Timoshenko and Gere, 1961):

$$E_r = \frac{4EE_t}{\left(\sqrt{E} + \sqrt{E_t}\right)^2} \tag{10.1-4}$$

Generally, E_r depends on the shape of the cross-section since the shift of the neutral axis, i.e. the amount of shift on the nonlinear stress-strain curve, depends on the moment of inertia of the cross-section.

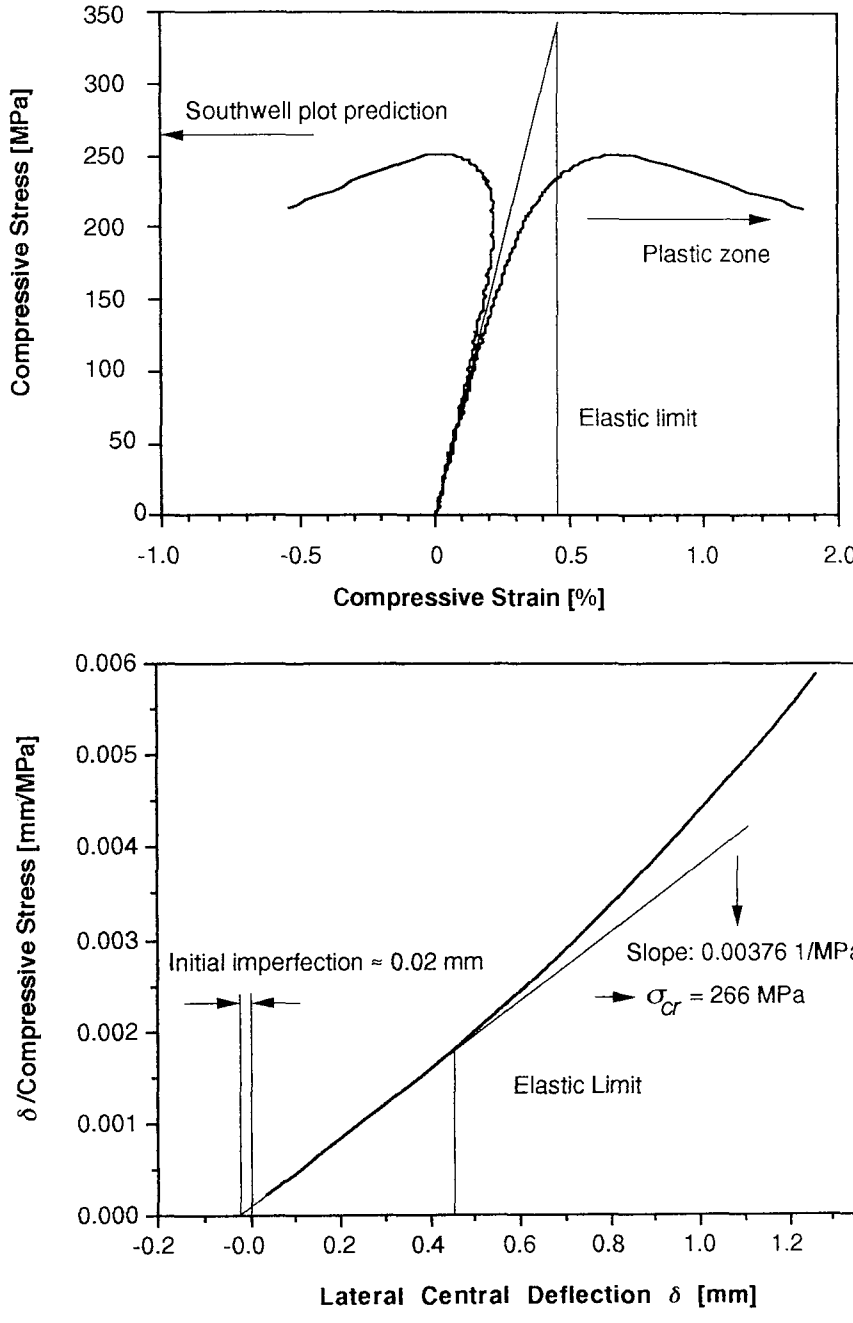


Figure 10.1-2: Application of the Southwell plot: (a) Compressive stress-strain curve of an aluminium alloy specimen (gauge length 50 mm, thickness 2 mm); (b) Southwell plot using the data from (a).

The buckling load can then be calculated by replacing the elastic modulus by the reduced modulus. In practice, however, using the tangent modulus, which is only a material property and independent of the cross-section, proved to give satisfactory results for aluminium rods (Timoshenko and Gere, 1961). This is thought to be because the elastic unloading of the concave side is compensated by an overall load increase, therefore the tangent modulus controls the deformation behaviour.

Buckling in the plastic zone might pose a realistic danger in metal constructions. Plasticity of metals is an important aspect of fail safe design which, as a matter of fact, prevented the breakthrough of composites in a variety of applications. However, with respect to stability problems plasticity has to be considered carefully.

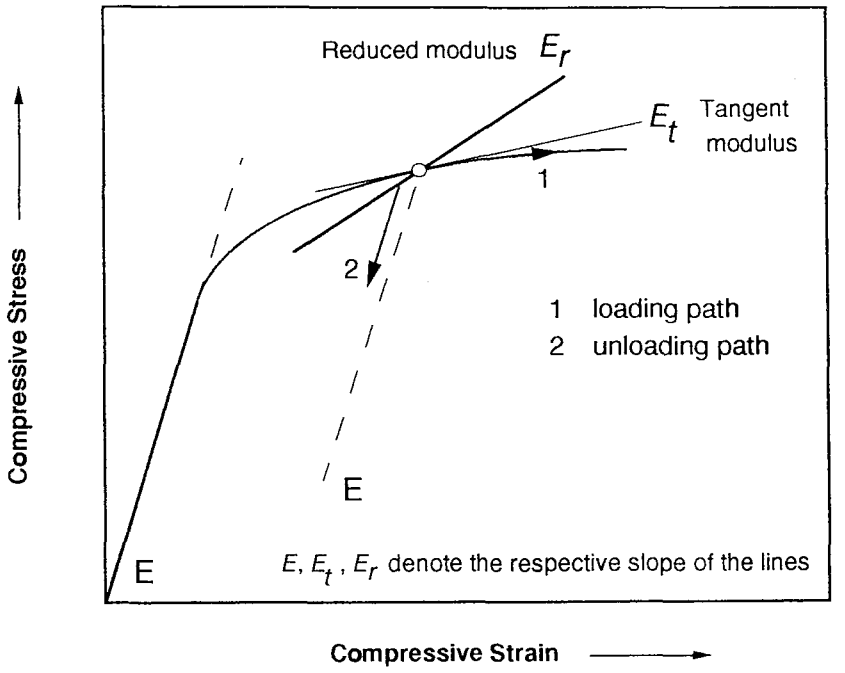


Figure 10.1-3: Illustration of reduced modulus in plasticity zone of metals.

10.2 Modifications of Euler Equations for Composites

Dealing with composites, and CFRP in particular, two aspects have to be regarded. The first is the low shear stiffness of composites and the second the nonlinear nature of the stress-strain response.

10.2.1 Shear Correction

For isotropic materials such as metals the elastic constants, shear modulus G and longitudinal modulus E, are related by:

$$\frac{E}{G} = 2(1+\nu) \qquad (10.2.1\text{-}1)$$

With typical values for ν of 0.3 for steel and 0.33 for aluminium one obtains for the ratio of the elastic moduli a value of approximately 2.6 and 2.66, respectively. The ratio for XAS/914C is about 25 which is an order of magnitude higher. In the deduction of

Equation 10.1-1 the shear deformation of the column was neglected, a reasonable assumption for metals. Inclusion of shear deformation yields for the critical stress (Timoshenko and Gere, 1961):

$$\sigma_{cr} = \sigma_{Eu} \frac{1}{1 + n\,\sigma_{Eu}/G} \qquad (10.2.1\text{-}2)$$

Here, σ_{Eu} is the Euler buckling stress from Equation 10.1-1 and n is a factor dependent upon the cross-section shape. For a rectangular cross-section the value of n is 1.2. G is the composite (out-of-plane) shear modulus. Note that it is treated here as a constant.

The correction of the Euler buckling stress according to Equation 10.2.1-2 is included in ASTM D3410.

10.2.2 Nonlinear Elastic Properties

It was mentioned before that the compressive stress-strain response of unidirectional CFRP is nonlinear, a fact which is evident from the tests carried out in this investigation and is observed for other systems as well (e.g. Hahn and Williams, 1986). The test method proposed allowed the recording of strains to higher levels than observed so far, thus strengthening the assumption of a modulus of elasticity decreasing with strain (Figure 10.2.2-1).

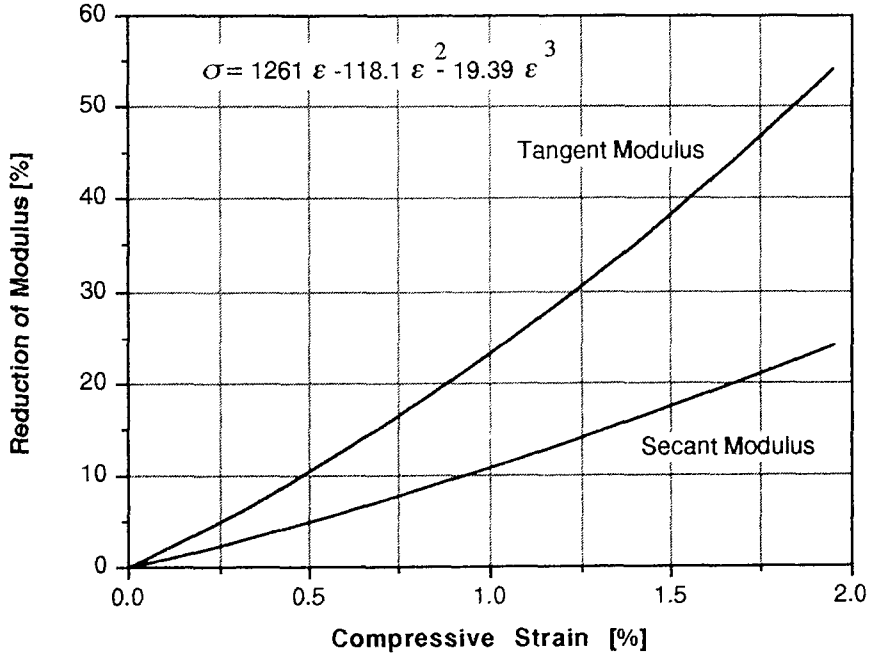


Figure 10.2.2-1: Reduction of longitudinal modulus of elasticity of XAS/914C under compression.

The cause for the observed nonlinearity is most likely to be found in the elastic behaviour of the fibre itself. Tests with repeated loading indicate that the nonlinearity is of an elastic nature, as shown in Figure 10.2.2-2, where the loading and unloading phase of a compression test is shown.

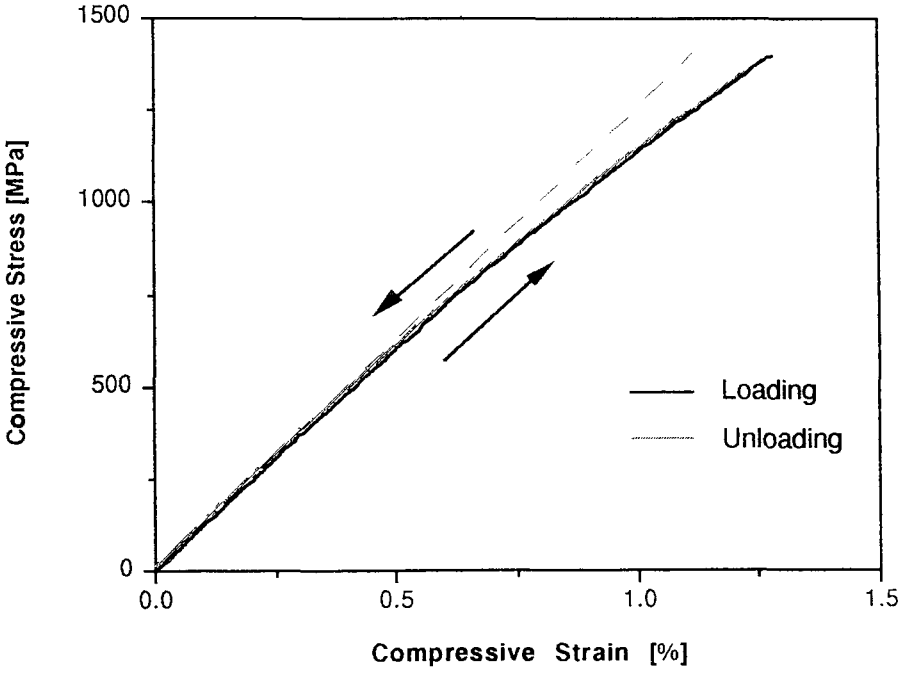


Figure 10.2.2-2: Demonstration of the nonlinear elastic nature of the stress-strain response of XAS/914C under compression.

A modification of the foregoing equations including the instantaneous modulus of elasticity is therefore proposed. The critical compressive stress is calculated using Equation 10.2.1-2, but now the Euler buckling stress is given by:

$$\sigma_{Eu} = \frac{C\pi^2 E_t(\varepsilon^*)}{s^2} \qquad (10.2.2\text{-}1)$$

where E_t is the tangent longitudinal modulus of elasticity and ε^* is the strain at the instant of buckling. Note that E_t is a function of the axial compressive strain ε. Using this equation, the critical stress has to be determined iteratively. Figure 10.2.2-3 compares the critical stress calculated using the different equations cited above. The tangent modulus of elasticity is calculated as the first derivative of the stress:

$$E_t(\varepsilon) = \sigma'(\varepsilon) \qquad (10.2.2\text{-}2)$$

where the stress-strain curve is approximated by an average third order polynomial curve fit of the sample DELST (Figure F-10, Table T-18):

$$\sigma = 1261\ \varepsilon - 118.1\ \varepsilon^2 - 19.39\ \varepsilon^3 \qquad (10.2.2\text{-}3)$$

where ε is to be taken in % (positive) and σ in MPa. Strictly, the predictions using a variable modulus are only valid up to stresses which have been measured. For the predictions the stress-strain curves above the measured values are extrapolated and it is not known if a third order polynomial curve fit is adequate (Section 6.1.2)

Figure 10.2.2-3 clearly shows the impact of the modifications of the Euler equations on the predicted buckling stress. Particularly the introduction of the tangent modulus of elasticity reduces the predicted values for small slenderness ratios. For example, the slenderness ratio of a test piece with a thickness of 2 mm and 10 mm gauge length is 17.32. Assuming ideally clamped-clamped conditions, the Euler buckling stress is 16600 MPa; including shear deformation and assuming a shear modulus of $G = 5.0$ GPa the prediction is reduced to approximately 3350 MPa. The inclusion of a reduced tangent modulus of elasticity finally yields a critical stress of about 2100 MPa, which is roughly one eighth of the Euler stress. Considering the fact that the end constraints might not be 'ideally-clamped' in reality, the buckling stress is in the region of stresses which can be realised with the ICSTM method.

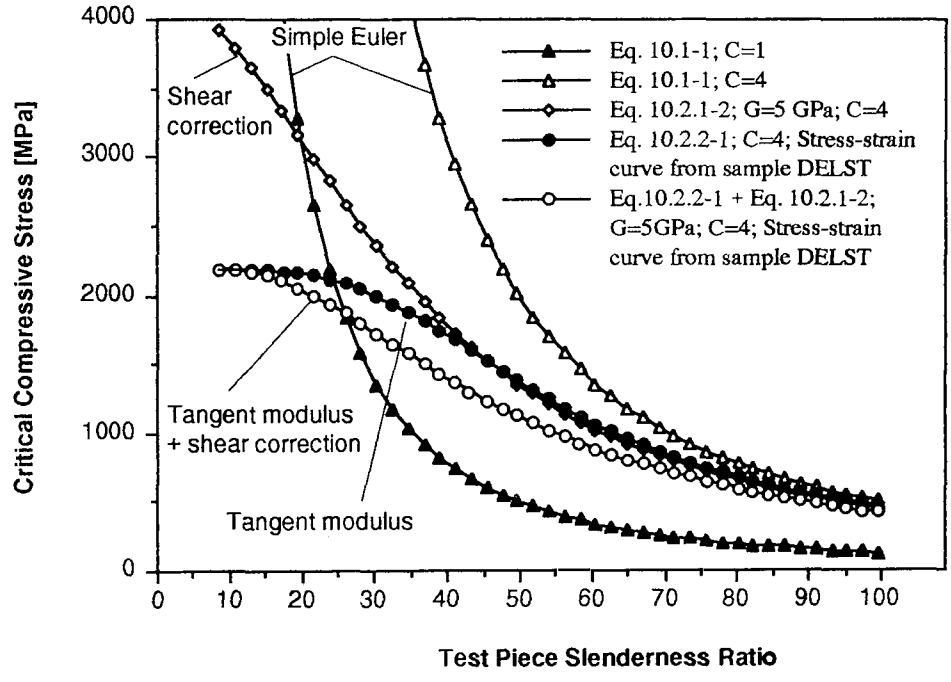


Figure 10.2.2-3: Comparison of buckling stress predictions.

10.3 Comparison with Experimental Results and Discussion

In this section the experimental results from the parameter study of test piece geometry are compared with the predictions of the critical stress described in the previous section. The test results where bifurcation of the surface strains occurred, indicating buckling of the test piece, are distinguished from the ones showing no bifurcation. In the following the in-plane shear modulus of the composite, as determined in Chapter 7, is used rather than the out-of-plane shear modulus. It is believed that this approximation is justifiable.

Figure 10.3-1 shows predicted critical stresses using the shear modified Euler equation including tangent modulus of elasticity (Equations 10.2.1-2 and 10.2.2-1) for several clamping conditions. The two extremes, clamped-clamped ($C = 4$) and hinged-hinged ($C = 1$), envelop the experimental data for which bifurcation was observed. Slender specimens lay close to the clamped-clamped condition, whereas the short ones are close to hinged-hinged. This is reasonable since the ratio of 'bedding'-stiffness to specimen bending stiffness is higher for the slender test pieces so that their clamping condition can be regarded as almost perfectly rigid. For the short specimens, failing at much higher stress levels, the lateral compliance of the tabs and the clamping bolts might allow some rotation, thus reducing the clamping factor.

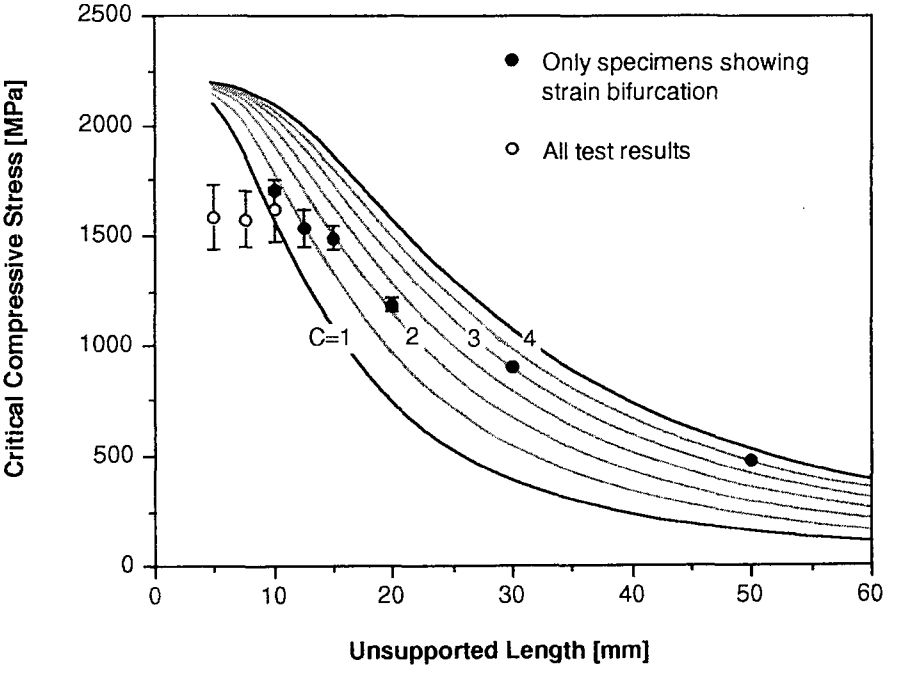


Figure 10.3-1: Comparison of experimental results and buckling predictions using Equations 10.2.1-2 and 10.2.2-1 to -3 with initial in-plane shear modulus G = 5.0 GPa.

Interesting results are obtained when the shear modulus used in the calculation is not taken as the initial in-plane shear modulus but a reduced value. Figure 10.3-2 shows the impact on the predicted critical stress introduced by such a reduction of the shear modulus, here from 5.0 GPa to 2.5 GPa. Figure F-17 shows a variety of critical stress versus slenderness ratio plots which can be used for specimen design for various composites.

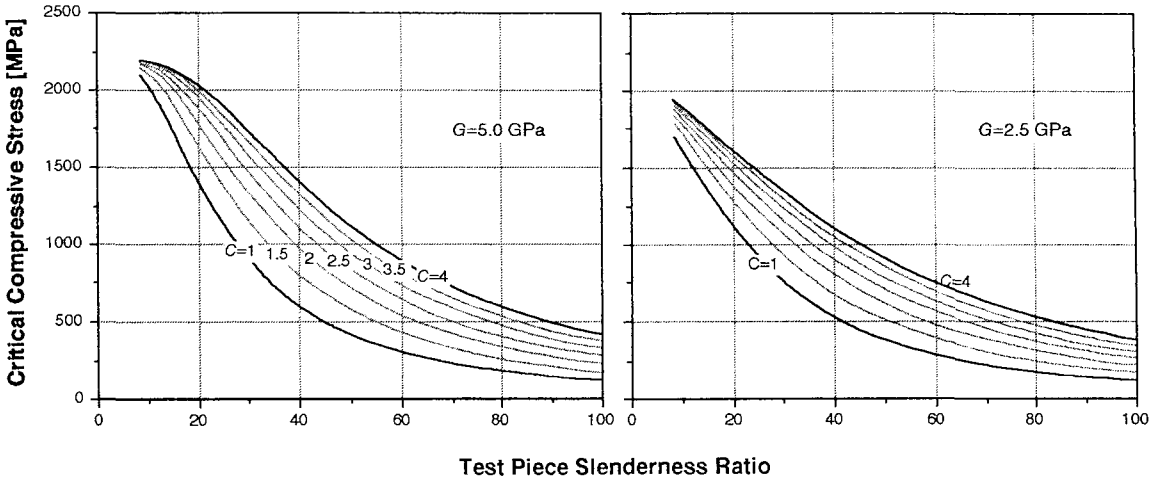


Figure 10.3-2: Critical stresses versus slenderness ratio using different values for the composite shear modulus.

Finally, Figure 10.3-3 shows predictions using shear correction and tangent modulus of elasticity for various values of the shear modulus and for clamping factors $C = 4$ and $C = 3$. Conspicuously, the experimental data fit the curve G = 2.5 GPa, half the initial in-plane shear modulus, and C = 4 very well, particularly when compared to the predictions using the simple Euler equation or the shear corrected Euler equations which are shown in Figure 10.3-4.

This approach of using a reduced shear modulus is reasonable, as is the assumption of a changing clamping condition with slenderness ratio. It is likely that both effects play a role. Because of imperfect fibre alignment the matrix experiences shear deformation under axial compression, as pointed out in Chapter 2. This, in turn, might lead to an overall shear stiffness reduction since the shear stress-strain response of most matrix materials is nonlinear. This will be examined further in the next chapter. Obviously, the use of a constant reduced shear modulus is unlikely to be correct, but good fit of the data suggest that a function $G(\sigma_c)$ exists. That has been pointed out earlier by Hayashi (1989). Experimentally this function is difficult to determine, considering that even the determination of the initial shear modulus is somewhat dubious.

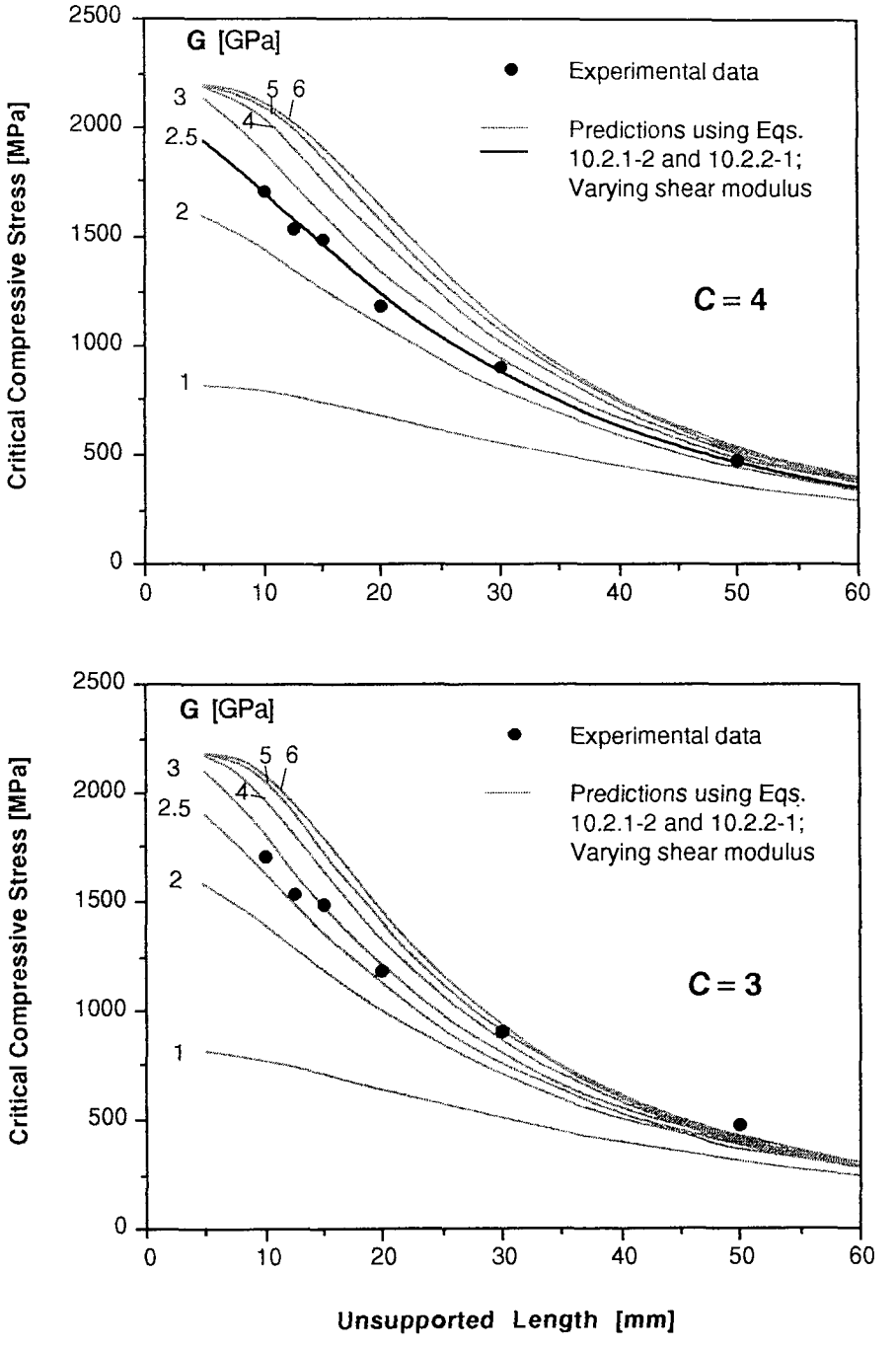


Figure 10.3-3: Comparison of test results and predictions for varying values of shear modulus and two clamping factors.

In the present study the ICSTM method and a standard compression test piece was used to investigate the function $G(\sigma_c)$. The lower block of the rig was supported by a rotational bearing and the moment necessary to twist the test piece was measured. The rotational deformation of the test piece, measured by ±45° strain gauges, was believed to be proportional to the shear stiffness. The test was then repeated under various axial loads so that the (constant) friction could be eliminated. Finally, however, the test was

abandoned because it was thought that decoupling of the shear induced by the axial load on the deformed test piece was not possible. A more detailed analysis considering geometric effects could possibly lead to a solution.

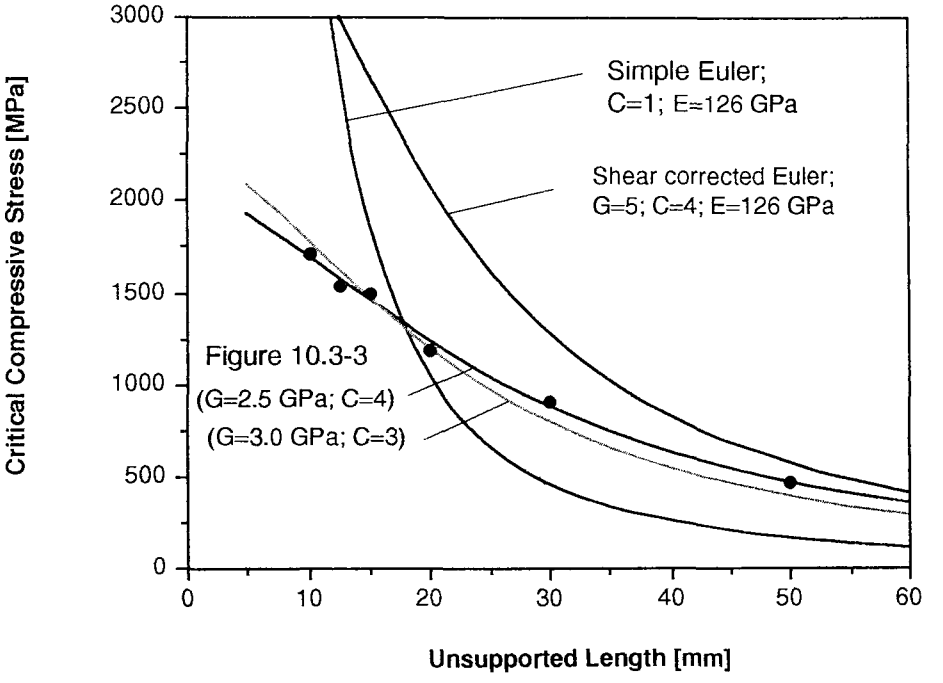


Figure 10.3-4: Comparison of experimental data and common methods of buckling prediction.

The conclusion of the comparison is that in order to predict macroscopic instability of CFRP columns it is vital to include not only shear deformation but, in particular, varying modulus of elasticity. That is, knowledge of the stress-strain curve of the composite is necessary to predict buckling stresses. Comparison with test data showed that critical stresses can then be predicted conservatively by assuming a hinged-hinged condition for small slenderness ratios. The assumption of a reduced shear modulus of half the initial in-plane shear modulus with clamped-clamped ends led to a good prediction of critical stresses for XAS/914C for the whole range of specimen slenderness ratios examined. Figure 10.3-4 gives a good impression how common buckling analysis overpredicts the buckling stresses of unidirectional CFRP.

CHAPTER 11 MICROMECHANICAL MODEL TO PREDICT COMPRESSIVE FAILURE

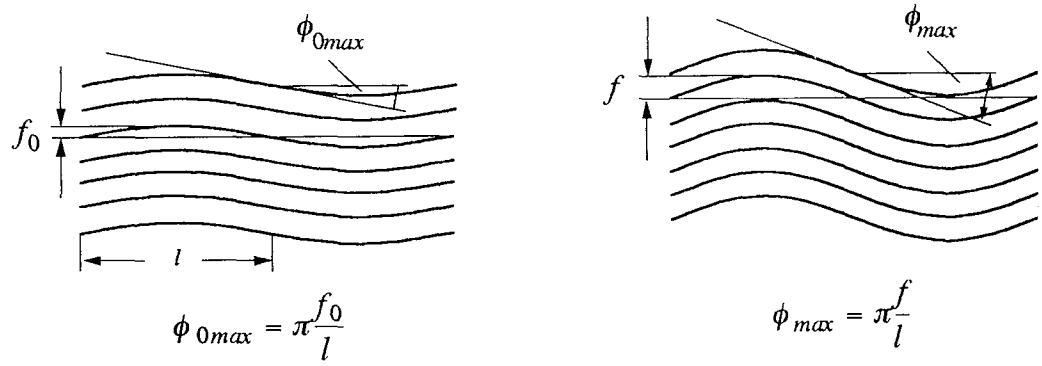
In the previous chapter global instability, where deflections of the test piece are relevant, was examined incorporating material nonlinearities. It has been shown how a combined shear and bending instability led to buckling of the test piece. A similar investigation is carried out in this chapter on a micro level, i.e. fibre deformations are relevant. A graphical solution of the microinstability model is presented, and the factors determining the compressive strength are discussed.

11.1 Derivation of the Model

The model presented in Section 11.1.1 is similar to the one developed by Wang (1978) and modified by Hahn (1986). The main feature of these models is that they assume initially non-straight fibres. Under axial compression initial deflections are increased eventually leading to failure by shear instability. As pointed out in Chapter 2, this mode of microbuckling, referred to as 'plastic microbuckling' by Fleck and Budiansky (1990) is in contrast to the classical elastic microbuckling analysis by Rosen (1964) where straight fibres are assumed and an elastic buckling analysis is carried out.

11.1.1 Micromechanical Strength Model

Sinusoidal initial fibre deflection is assumed within a composite element as shown in Figure 11.1.1, which might represent a segment of a fibre bundle.



(a) initial state (b) axially compressed

Figure 11.1.1-1: Idealised fibre deflection in the composite.

The lateral fibre deflection will be expressed as :

$$v_0(x) = f_0 \sin\frac{\pi}{l}x \qquad (11.1.1\text{-}1)$$

where l denotes the half wave length and f_0 the amplitude of the initial fibre deflection. Under axial compression the fibre deflection is assumed to be magnified to:

$$v(x) = f \sin\frac{\pi}{l}x \qquad (11.1.1\text{-}2)$$

The simplification is made that there is no displacement gradient in the y-direction, i.e. the analysis is essentially one-dimensional:

$$\frac{\partial u}{\partial y} = \frac{\partial v}{\partial y} = 0 \qquad (11.1.1\text{-}3)$$

The maximum angle between fibre and laminate 0°-direction occurs in the vicinity of minimum fibre curvature and can be expressed in terms of initial deflections:

$$\phi_{0max} = \pi\frac{f_0}{l} \qquad (11.1.1\text{-}4)$$

and in the loaded composite:

$$\phi_{max} = \pi\frac{f}{l} \qquad (11.1.1\text{-}5)$$

where f_0/l and f/l are dimensionless terms characterising the initial fibre deflection and fibre deflection under compression, respectively, as illustrated in Figure 11.1.1-1. In the following the subscript 'max' will be omitted when referring to ϕ_{0max}, i.e. $\phi_0 = \phi_{0max}$.

The stress field is derived from the displacement field by considering the constitutive equations of the composite material. The balance of moments on the typical repeating element shown in Figure 11.1.1-2 yields:

$$\frac{\partial M}{\partial x}dx + \tau\Delta y dx - \sigma_c\Delta y\frac{\partial v}{\partial x}dx = 0 \qquad (11.1.1\text{-}6)$$

and with the simplification from above:

$$\frac{dM}{dx} + \tau\Delta y - \sigma_c\Delta y\frac{dv}{dx} = 0 \qquad (11.1.1\text{-}7)$$

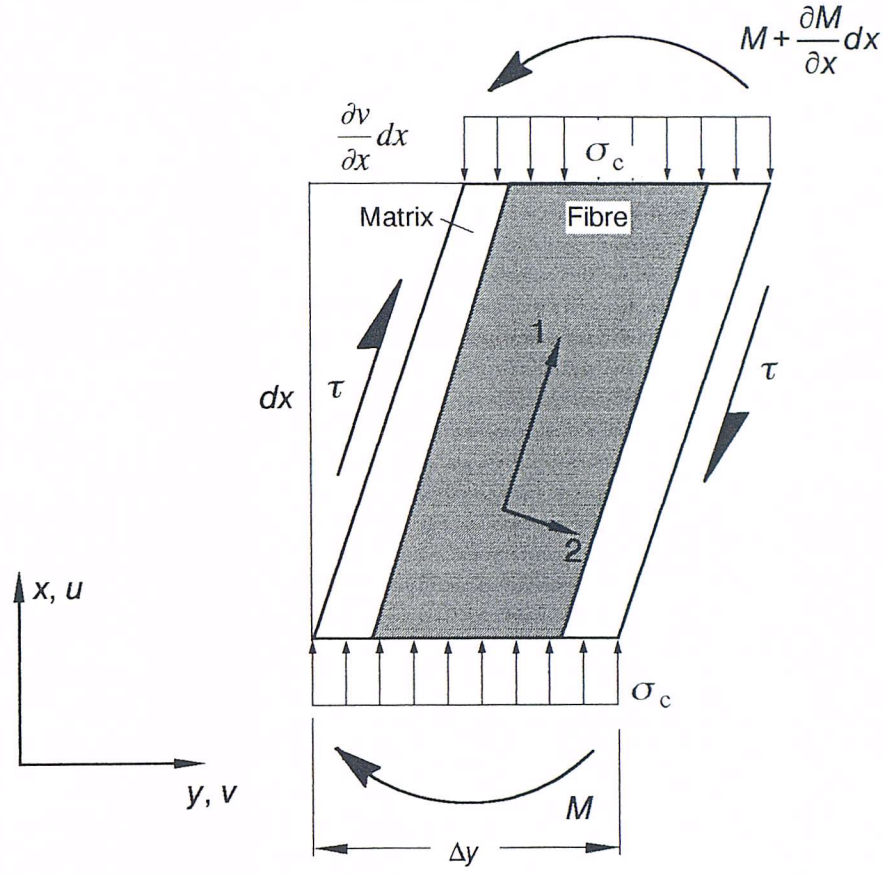


Figure 11.1.1-2: Forces acting on a repeating composite element under axial compression.

Equation 11.1.1-7 includes a bending, a shear and a compression term. As deflections are small, engineering theory is assumed and the bending contribution of the matrix is neglected. The bending moment can then be written:

$$M = -E_f I_f \frac{d^2(v - v_0)}{dx^2} \qquad (11.1.1\text{-}8)$$

with E_f and I_f denoting the modulus of elasticity and the second moment of area of the fibre, respectively. The shear response of the composite element is assumed to be nonlinear and may be expressed as:

$$\tau(\gamma) = G_s(\gamma)\gamma \qquad (11.1.1\text{-}9)$$

where $G_s(\gamma)$ is the composite secant shear modulus at a given shear strain γ. The shear strain can be calculated from the deformations, considering also Equation 11.1.1-3, as:

$$\gamma = \frac{d(v - v_0)}{dx} \tag{11.1.1-10}$$

or with Equations 11.1.1-1 and 11.1.1-2:

$$\gamma = \pi \frac{(f - f_0)}{l} \tag{11.1.1-11}$$

With Equation 11.1.1-10 the differential Equation 11.1.1-7 becomes:

$$-\frac{E_f I_f}{\Delta y} \frac{d^3(v - v_0)}{dx} + G_s(\gamma) \frac{d(v - v_0)}{dx} - \sigma_c \frac{dv}{dx} = 0 \tag{11.1.1-12}$$

And with Equations 11.1.1-1 and 11.1.1-2:

$$\sigma_c = \left[\frac{\pi^2}{l^2} \frac{E_f I_f}{\Delta y} + G_s(\gamma) \right] \left(1 - \frac{f_0}{f} \right) \tag{11.1.1-13}$$

This equation expresses the equilibrium compressive stress on a composite element for a fibre deflection magnified by the factor f/f_0. Since σ_c is independent of x, a solution for the postulated displacement field only exists if the secant shear modulus is assumed to be constant along the x-axis. Since the shear strain in the x-direction is not constant, the shear modulus is not constant. The equilibrium compressive stress is therefore taken as the minimum stress, which is obtained for the minimum secant shear modulus, i.e. the shear modulus at the maximum shear strain.

In order to consider the influence of the bending term an assessment of the absolute fibre waviness has to be made. Using absolute dimensions, the bending term of Equation 11.1.1-13 can be written as:

$$\pi^2 \frac{V_f E_f}{12} \left(\frac{d_f}{l} \right)^2 \tag{11.1.1-14}$$

assuming that

$$d_f = V_f \, \Delta y \tag{11.1.1-15}$$

and a rectangular fibre cross-section (two-dimensional model). Figure P-21, shows a section of unidirectional CFRP (XAS/914C) polished parallel to the fibres. From some individual fibres it can be estimated that the ratio of fibre diameter and half wave length of deflection d_f/l is certainly less than, say, 1/50. Taking this value and 60 GPa[+] for the

[+] Tangent modulus of elasticity is used, since the composite is under compression (see Chapter 10).

composite axial modulus at fracture, the bending term becomes 40 MPa which would be around 1% of the secant shear modulus G_S at fracture[++] . The bending term under these conditions can be neglected. If, however, the half wave length is only, to give another example, 10 times the diameter the bending term would contribute 25 %, which cannot be neglected. Therefore, the analysis for other materials, particularly those containing less stiff fibres or fibres with strong induced waviness, might require the inclusion of the bending term. A question remaining at this point is why the kink band length in CFRP is typically between 10 and 20 fibre diameters indicating a pre-failure 'waviness pattern' of these dimensions, since this cannot be found in micrographs.

Neglecting the bending term and including Equation 11.1.1-11, Equation 11.1.1-13 reduces to:

$$\sigma_c = \sigma_c(\gamma) = G\frac{\gamma}{\gamma + \pi\frac{f_0}{l}} \qquad (11.1.1\text{-}16)$$

or in terms of the maximum fibre angle initially present in the composite (see Figure 11.1.1-1):

$$\sigma_c = \frac{\tau(\gamma)}{\gamma + \phi_0} \qquad (11.1.1\text{-}17)$$

The compressive equilibrium stress on a composite element is now expressed in terms of shear stress at the location of maximum shear strain and initial maximum fibre angle. The ultimate compressive stress, i.e. the compressive strength of the material, is the maximum of this function. With a known shear stress-strain relationship for the composite this equation can be solved numerically or graphically, as shown in the next section, as a function of initial deflections. If the shear curve can be approximated analytically as a function $\tau = \tau(\gamma)$ the condition for the compressive stress in Equation 11.1.1-16 being a maximum becomes:

$$\tau(\gamma^*) - [\gamma^* + \phi_0]\frac{d\tau}{d\gamma}(\gamma^*) = 0 \qquad (11.1.1\text{-}18)$$

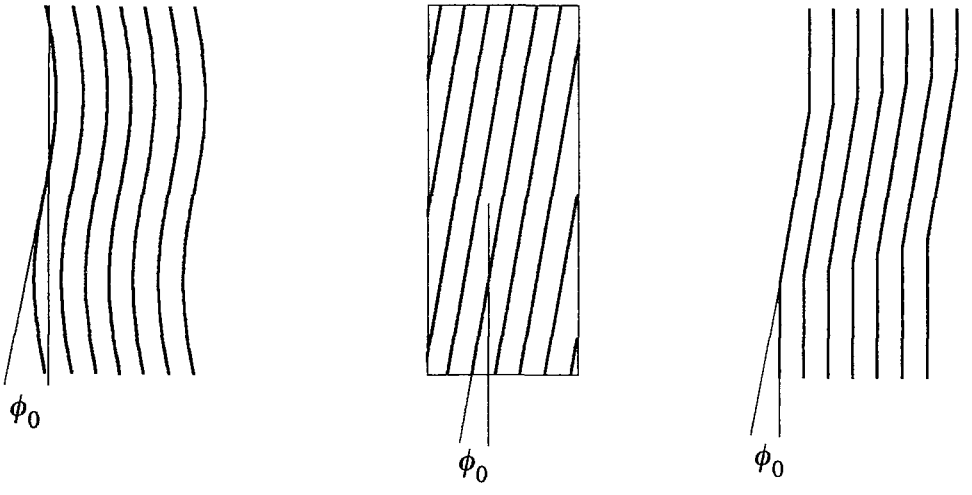
where γ^* is the shear strain at failure. With Equation 11.1.1-18 inserted into Equation 11.1.1-17, the ultimate compressive stress is obtained as:

$$\sigma_{cu} = \frac{d\tau}{d\gamma}(\gamma^*) = G_t(\gamma^*) \qquad (11.1.1\text{-}19)$$

The compressive strength equals the tangent shear modulus of the composite at the shear strain where instability due to Equation 11.1.1-16 occurs.

[++] Secant shear modulus at fracture assumed to be 4GPa (see Section 11.1.2)

Hahn and Williams (1986) derive Equation 11.1.1-17 multiplied by the fibre volume fraction V_f by regarding a fibre element rather than a fibre/matrix volume element. Wisnom (1990) deduces Equation 11.1.1-17 by regarding a unidirectional layer of straight fibres aligned at an angle of ϕ_0 to the fibre axis (Figure 11.1.1-3 (b)). Argon (1972) and Fleck and Budianski (1990) obtain a similar result by regarding a band of kinked parallel fibres (Figure 11.1.1-3 (c)) as described in Chapter 2. All derivations have in common that a shear/compression coupling exists, i.e. the composite is subjected to shear when compressed axially, and other stress components are neglected. To recall, this condition is approximately given at the vicinity of minimum fibre curvature if sinusoidal fibre waviness as shown in Figure 11.1.1-3 (a) is assumed.



(a) present model
Wang (1978)
Hahn and Williams (1986)

(b)
Wisnom (1990)

(c)
Argon (1972)
Fleck and Budiansky (1990)

Figure 11.1.1-3: *Different idealisations of the unloaded unidirectional composite.*

11.1.2 Graphical Solution

In the previous section the compressive strength has been defined as the ultimate compressive stress:

$$\sigma_{cu} = \left(\frac{\tau(\gamma)}{\varphi(\gamma)} \right)_{max} \qquad (11.1.2\text{-}1)$$

The maximum of the ratio of $\tau(\gamma)$ and $\varphi(\gamma)$ from Equation 11.1.2-1, i.e. the compressive strength of the composite, has been determined graphically by the present author as

outlined below. The method allows one to determine the ultimate compressive stress from the shear stress-strain curve and a typical angle of fibre misalignment.

The measured shear stress-strain curve of the composite may be available as shown in Figure 7.4-3, e.g. from ±45° tension test. In Figure 11.1.2-1 the linear function $\varphi(\gamma) = \gamma+\phi_0$ where γ is the shear strain and ϕ_0 is the typical maximum angle of initial fibre misalignment, as described previously, is added to the shear curve. The scale for this function can be chosen freely and the following derivation is not affected by its value.

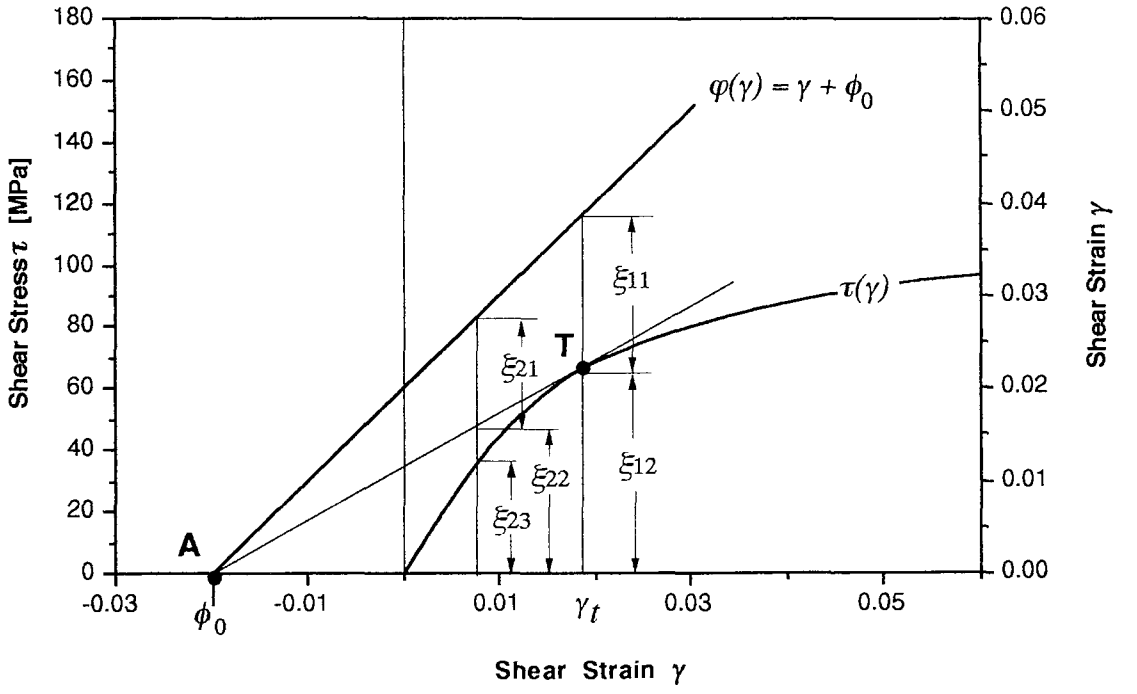


Figure 11.1.2-1: *Graphical determination of the ultimate compressive stress.*

It can be deduced from geometry:

$$\frac{\xi_{11}}{\xi_{12}} = \frac{\xi_{21}}{\xi_{22}} \tag{11.1.2-2}$$

and:

$$\frac{\xi_{11} + \xi_{12}}{\xi_{12}} = \frac{\xi_{21} + \xi_{22}}{\xi_{22}} \tag{11.1.2-3}$$

and with $\xi_{23} < \xi_{22}$ it follows:

$$\frac{\xi_{12}}{\xi_{11} + \xi_{12}} > \frac{\xi_{23}}{\xi_{21} + \xi_{22}} \tag{11.1.2-4}$$

so that it can be concluded for the 'tangent shear strain' γ_t (Figure 11.1.2-1):

$$\left(\frac{\tau}{\varphi}\right)_{\gamma=\gamma_t} > \left(\frac{\tau}{\varphi}\right)_{\gamma<\gamma_t} \qquad (11.1.2\text{-}5)$$

This can be shown equally for values $\gamma > \gamma_t$ if the sign of curvature of the shear stress-strain curve does not change. As this is valid for most real composite systems, one can assume that for a given initial misalignment the maximum ratio as defined above is given at the tangent point of curve (A-T) and the stress-strain curve. The compressive strength of the composite is the slope of that line (Equation 11.1.1-19).

This result can also be deduced from Equation 11.1.1-18 which gives the condition for the applied compressive stress being a maximum, slightly rewritten, as:

$$\tau' = \frac{\tau}{\gamma + \phi_0} \qquad (11.1.2\text{-}6)$$

The tangent on the shear-stress strain curve intersecting the abscissa at $-\phi_0$ fulfills this condition.

The compressive strength can be read directly if the secondary axis of the graph is dimensioned as shown in Figure 11.1.2-2, i.e. if the scale of the secondary coordinate axis is equal to the scale of the primary coordinate axis divided by the maximum graph window value γ_W of the abscissa (shear strain).

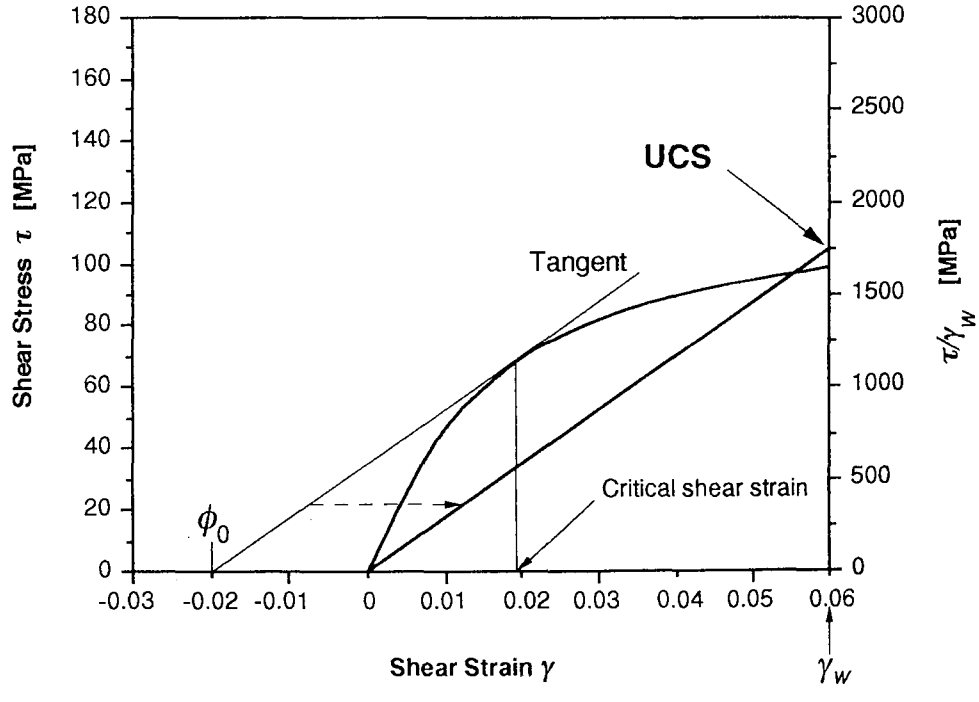


Figure 11.1.2-2: *Direct reading of the ultimate compressive stress.*

11.1.3 Discussion of the Model Parameters

The main parameters are the shear response of the composite and the fibre orientation. Factors determining the shear stress-strain response of the composite are the initial stiffness or shear modulus, the ultimate shear stress and the ductility of the material, i.e. the shape of the stress-strain curve. In order to separate these parameters the shear curve is idealised here as:

$$\tau = -\tau_u \exp\left\{-\left[\frac{G}{\tau_u}\gamma + p\gamma^2\right]\right\} + \tau_u \qquad (11.1.3\text{-}1)$$

where τ_u denotes the shear strength of the composite, G is the initial shear modulus and p is a shape parameter defining the gradient of curvature of the curve. The postulate that the curvature does not change sign, true for polymers, yields the condition:

$$p < \frac{1}{2}\left(\frac{G}{\tau_u}\right)^2 \qquad (11.1.3\text{-}2)$$

As a numerical example, an initial composite shear modulus G = 5.0 GPa and an ultimate (asymptotic) shear stress τ_u = 100 MPa are assumed. The maximum value of p is then 1250. Smaller values of p result in 'flatter' shear curves as illustrated in Figure 11.1.3.1–1. The maximum value of p represents a curve closer to the elastic-perfectly plastic shape.

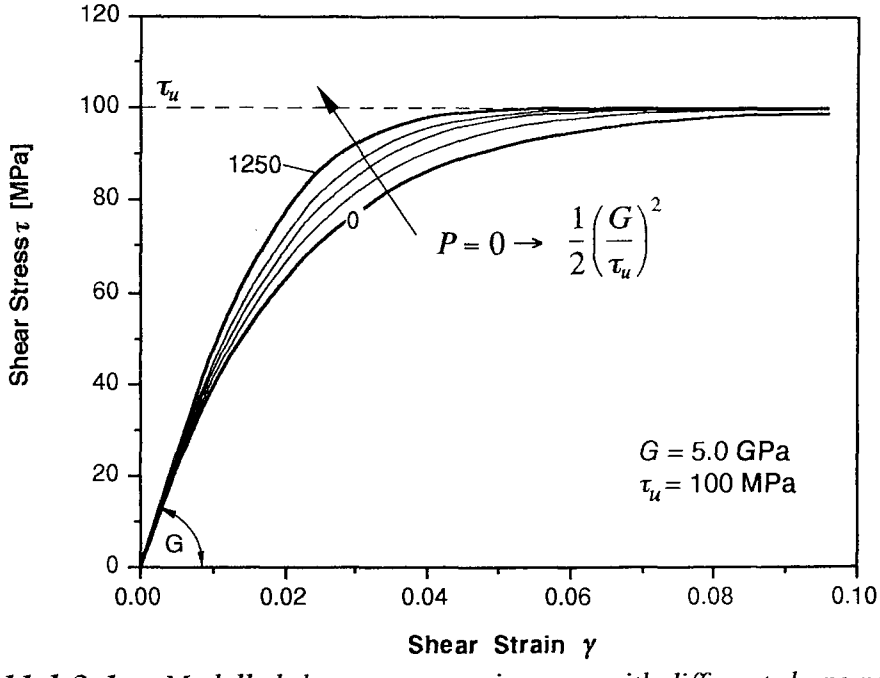


Figure 11.1.3-1: Modelled shear stress-strain curve with different shape parameters.

The question to be examined is to what extent the individual parameters influence the compressive strength of the composite. In Figure 11.1.3-2 the extremes of curve shapes, with shear modulus and ultimate shear stress being constant, are illustrated. If the shear behaviour is ideally elastic-perfectly plastic the point where shear instability occurs is clearly defined as the yield point. As soon as the shear response deviates from the ideal case, the amount of fibre misalignment determines the instability strain. In the numerical example from above the ultimate compressive stress predictions vary between 1720 MPa and 2670 MPa (see Figure 11.1.3-2) for the same values of fibre misalignment (1°), shear modulus (5 GPa) and shear strength (100 MPa). From Figure 11.1.3-2 it becomes also clear that for vanishing misalignment ($f_0/l \rightarrow 0$ or $\phi_0 \rightarrow 0$) the inelastic solution converges towards the elastic solution:

$$\frac{f_0}{l} \rightarrow 0: \quad \sigma_{cu} \rightarrow G$$

And the same is true for any misalignment with increasing shear strength:

$$\tau_u \rightarrow \infty: \quad \sigma_{cu} \rightarrow G$$

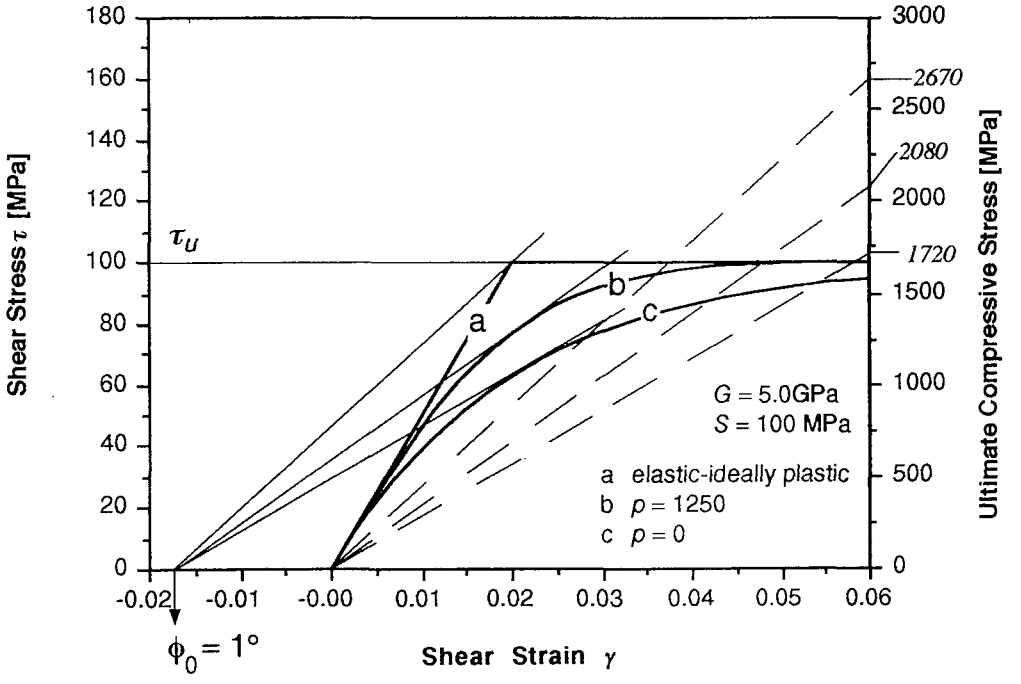


Figure 11.1.3-2: Influence of the shape of the shear stress-strain curve on the ultimate compressive stress.

In Figure 11.1.3-3 the results of the parametric study are presented. Shear modulus, shear strength and shape parameter have each been varied within certain limits whilst

keeping the others constant. The ultimate compressive stress is then plotted versus initial fibre misalignment.

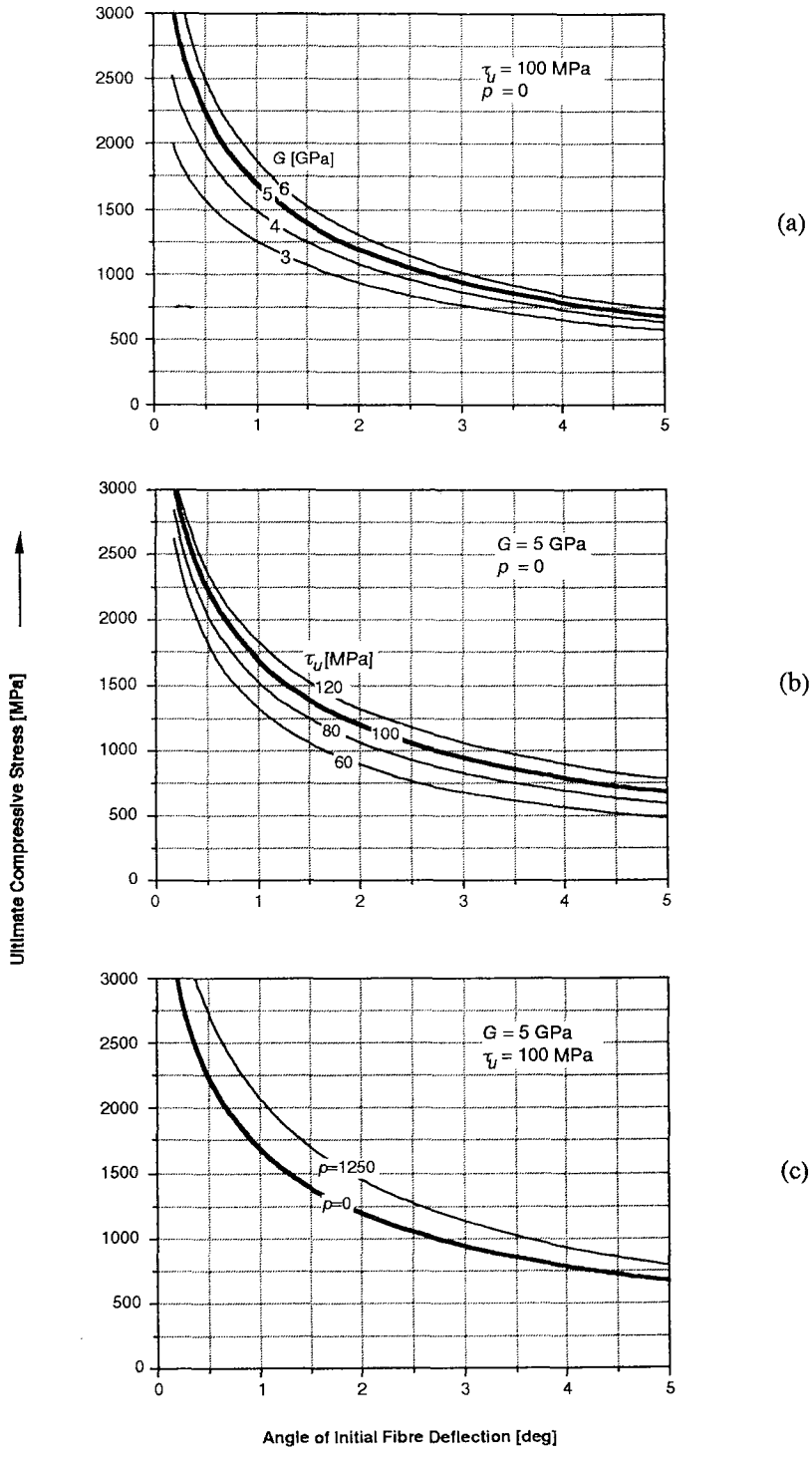


Figure 11.1.3-3: Influence of variation of shear modulus (a), shear strength (b) and shape of the shear stress-strain curve (c) on the ultimate compressive stress versus initial fibre deflection

The graphs show that an increase in shear modulus or in shear strength would be translated into an increased compressive strength as long as the other parameter is kept constant. However, if, for instance, the curve exhibits a more nonlinear characteristic at the same time the compressive strength could be lower. This was found to be the case for APC-2 compared to XAS/914C in the present investigation. Modulus and ultimate shear stress of the thermoplastic composite were slightly higher but the shape parameter smaller (see Figure 7.3-2). Predictions for the two systems will be discussed in detail in Section 11.2.2.

For very small angles of fibre misalignment the parametric study predicts that the impact of a shear modulus variation would be greater than that of a shear strength variation. As pointed out above, the ultimate compressive stress approaches the elastic solution, i.e. the shear modulus, for vanishing fibre misalignment; therefore, any increase in modulus will proportionally be translated into increase of compressive strength.

11.1.4 Modelling the Stress-Strain Response

It has often been argued that the nonlinear stress-strain response of CFRP is, at least partly, caused by fibre waviness, increasing under axial compression and decreasing under axial tension. If that were the case, a typical mean fibre waviness could be estimated by matching the experimentally determined stress-strain curve by a simplified micromechanical model. This in turn would allow a realistic input into the failure model described in Section 11.1.1.

In the following a simple (two-dimensional) model formulated in FORTRAN is described in order to predict the load-displacement response of a composite with initial fibre waviness.

The total axial strain of the composite is thought to be composed of a linear elastic portion and a geometric (nonlinear) portion due to fibre curvature, which is assumed to be sinusoidal as described in Section 11.1.1.

$$\varepsilon_{tot}(\gamma) = \varepsilon_{el}(\gamma) + \varepsilon_{geom}(\gamma) \qquad (11.1.4\text{-}1)$$

γ is the maximum average shear strain in the composite as defined in Section 11.1.1 and can be calculated from the relative fibre displacement f/l using Equation 11.1.1-11.

The elastic portion of the axial strain is simply calculated from:

$$\varepsilon_{el} = \frac{\sigma_c}{E_0} \tag{11.1.4-2}$$

where σ_c is the applied compressive stress and E_0 is the initial axial modulus of the composite. Since deflections are small, the geometric portion can be approximated as the difference of the arc length of the fibre half wave in each strain increment:

$$\varepsilon_{geom}(\gamma) = \frac{s(\gamma) - s_0}{l} \tag{11.1.4-3}$$

with $s(\gamma)$ and s_0 denoting the fibre arc length at the shear strain γ and the initial length, respectively. The arc length s is determined by:

$$s = \int_{x_1}^{x_2} \sqrt{1 + (v'(x))^2}\, dx \tag{11.1.4-4}$$

where $v(x)$ is the function of fibre deflection (Equations 11.1.1-1 and 11.1.1-2). This integration is carried out numerically using Simpson's rule:

$$\int_a^b y\, dx \approx \frac{b-a}{3n}\left[y_a + 4y_1 + 2y_2 + 4y_3 + \ldots + 2y_{n-2} + 4y_{n-1} + y_b\right] \tag{11.1.4-5}$$

The whole program works in increments of shear strain as illustrated in the flowchart shown in Figure 11.1.4-1. For a given shear strain the equivalent geometric deformation is calculated and with the equilibrium compressive stress the elastic deformation, assuming straight fibres and composite modulus of elasticity, is determined. The total deformation normalised to the half wave length of initial fibre deflection plotted versus the compressive stress gives the (calculated) stress-strain curve of the composite.

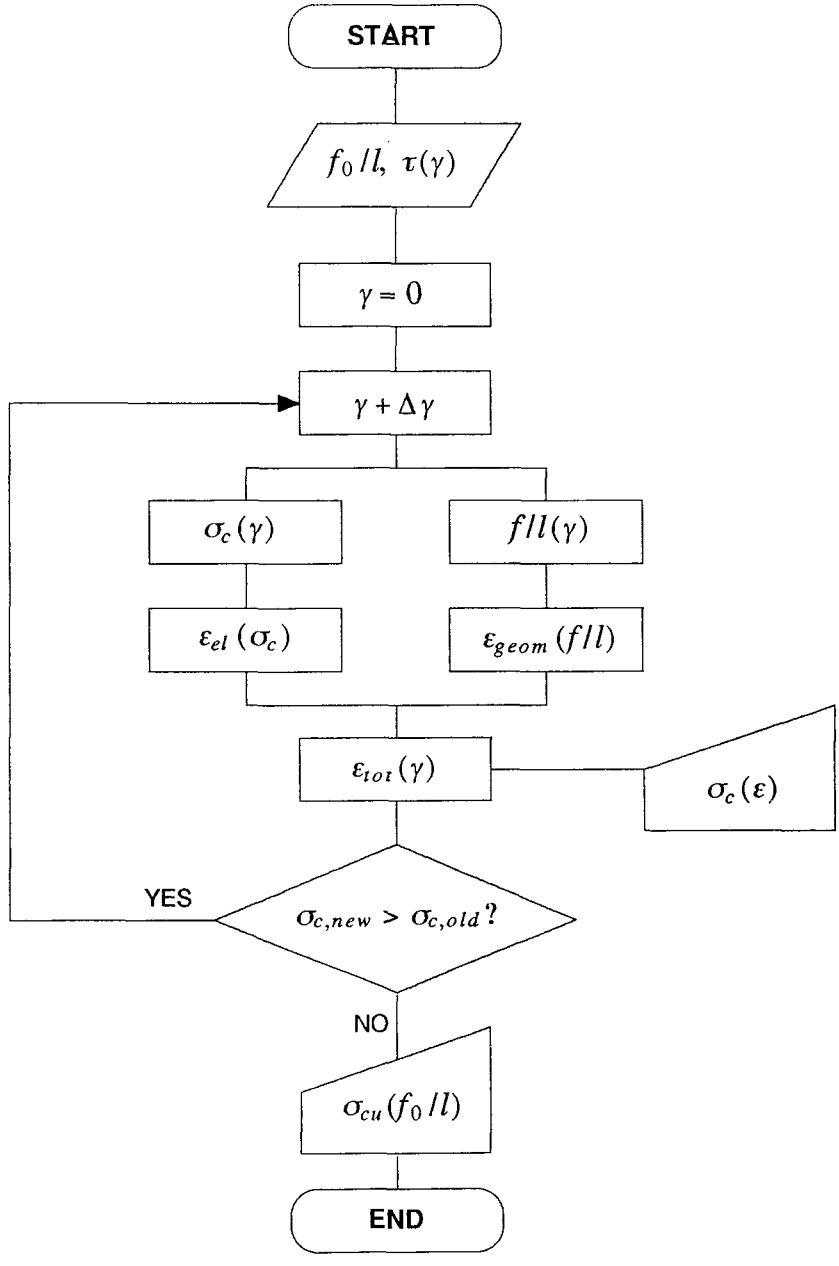


Figure 11.1.4-1: *Flowchart of the computer program to model the stress-strain response of a unidirectional CFRP composite.*

In Section 11.2.1 the stress-strain curve of XAS/914C using the experimentally determined input parameters will be presented and the result discussed.

11.2 Input of Experimental Data

In this section the results of the experimental investigations described in Chapters 7 and 8 will be used to predict the compressive strength of the composite. Of particular interest, obviously, are the shear stress-strain curves for XAS/914C and APC-2 from ±45° tension tests, and the results of the fibre angle analysis.

11.2.1 Stress-Strain Response

Figure 11.2.1-1 shows the stress-strain response calculated for various values of initial fibre waviness. In the calculations the shear stress-strain curve of a typical XAS/914C sample (5 specimens DELST) is used and the composite modulus is assumed to be a constant value (126 GPa).

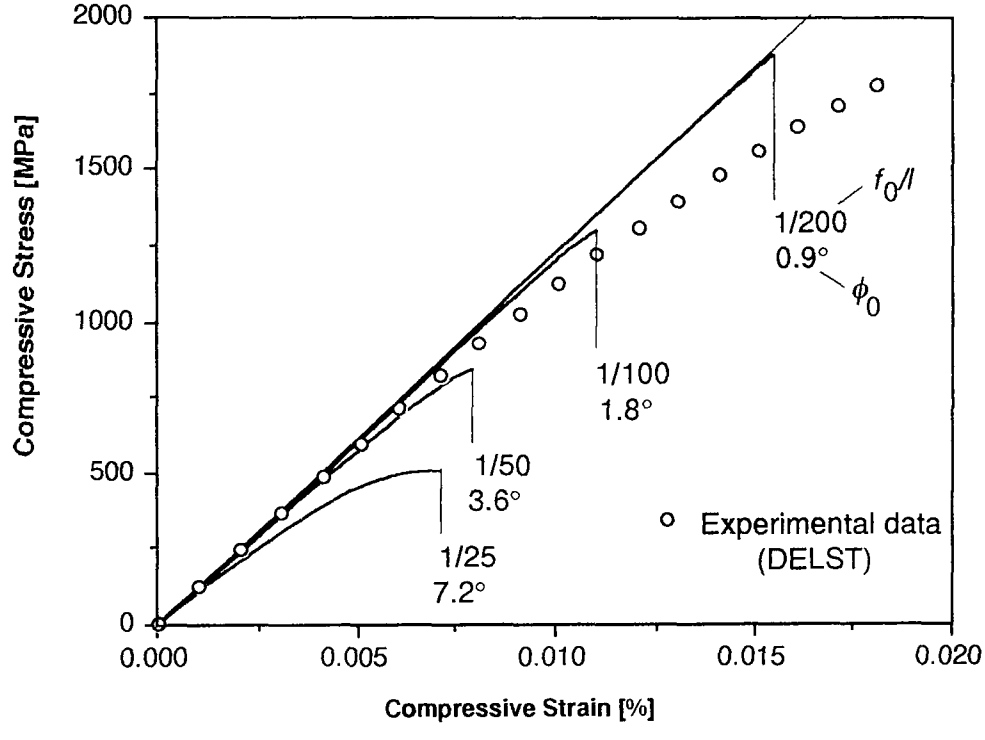


Figure 11.2.1-1: Modelled stress-strain response of a unidirectional composite for various initial fibre deflections.

The figure clearly shows that only for small values of f_0/l, i.e. for strongly misaligned fibres, does the stress-strain curve show significant nonlinearity. For realistic angles of misalignment the geometric portion of the deformation is negligible. The aim to deduce a characteristic average angle of misalignment by fitting the predicted stress-strain curve to

the experimental data can therefore not be realised. Failure of individual bundles of fibres as a cause of nonlinearity can most certainly be excluded since the macroscopic stress-strain response is elastic (Chapter 10) and completely recoverable. Also, failure of a bundle of a size significant enough to have some effect on a macroscopic level would influence the equilibrium of the neighbouring fibres causing catastrophic failure of the composite. Therefore, as pointed out in an earlier chapter, the nonlinearity must be caused by nonlinear elastic behaviour of the carbon fibre itself. To summarise, the following findings support this postulate:

1. Although an analysis of fibre angle distribution could not be carried out due to lack of time in the present project, micrographs of samples of GRP polished at 5° to the fibre axis were found, by visual inspection, to exhibit a degree of fibre misalignment comparable to APC-2, or even worse. Despite this fact the stress-strain curves of GRP are almost linear (Chapter 6). Therefore, geometric deformation of the fibres cannot play a significant role.
2. Above calculations of stress-strain curves.
3. Resent research (Melanitis and Galiotis, 1990) proved by means of Raman spectroscopy on single carbon fibres glued on acrylic beams that the stress-strain response of a fibre is nonlinear to the same extent the composite is.

11.2.2 Strength Prediction

Figure 11.2.2-1 shows the predicted compressive strength versus typical initial fibre misalignment angle for dry and saturated XAS/914C and dry APC-2. For small angles of initial misalignment the predicted compressive stress approaches the composite shear modulus, since the compressive strength is given as the slope of the shear stress-strain curve at the instability shear strain. The critical shear strain is small for small angles of initial misalignment and increases with increasing initial misalignment (compare, for instance, the graphical solution shown in Figure 11.1.2-2). Therefore, the prediction curves reflect the inverse characteristic of the shear stress-strain curves of the composite. For small angles of misalignment, the gradient of the predicted compressive strength over misalignment angle is steep, decreasing significantly between 0.5 and 1.5° of initial fibre misalignment. Translated into practical terms, that means that composites containing well aligned fibres are more prone to variation in compressive strength when varying fibre curvature than less well aligned ones. For instance fibre deflections induced by load introduction might have a different effect for different types of composites.

The individual curves exhibit clear characteristics as expected from the equivalent shear stress-strain curves. The predicted compressive strength of 'dry' XAS/914C is about 15% higher than the one for saturated XAS/914C. These results are in good agreement to test data published by Barker and Balasundaram (1987) who tested various laminates of XAS/914C under different temperatures and saturations. The APC-2 prediction lies between 5 and 10% beneath the XAS/914C curve for the same misalignment angles.

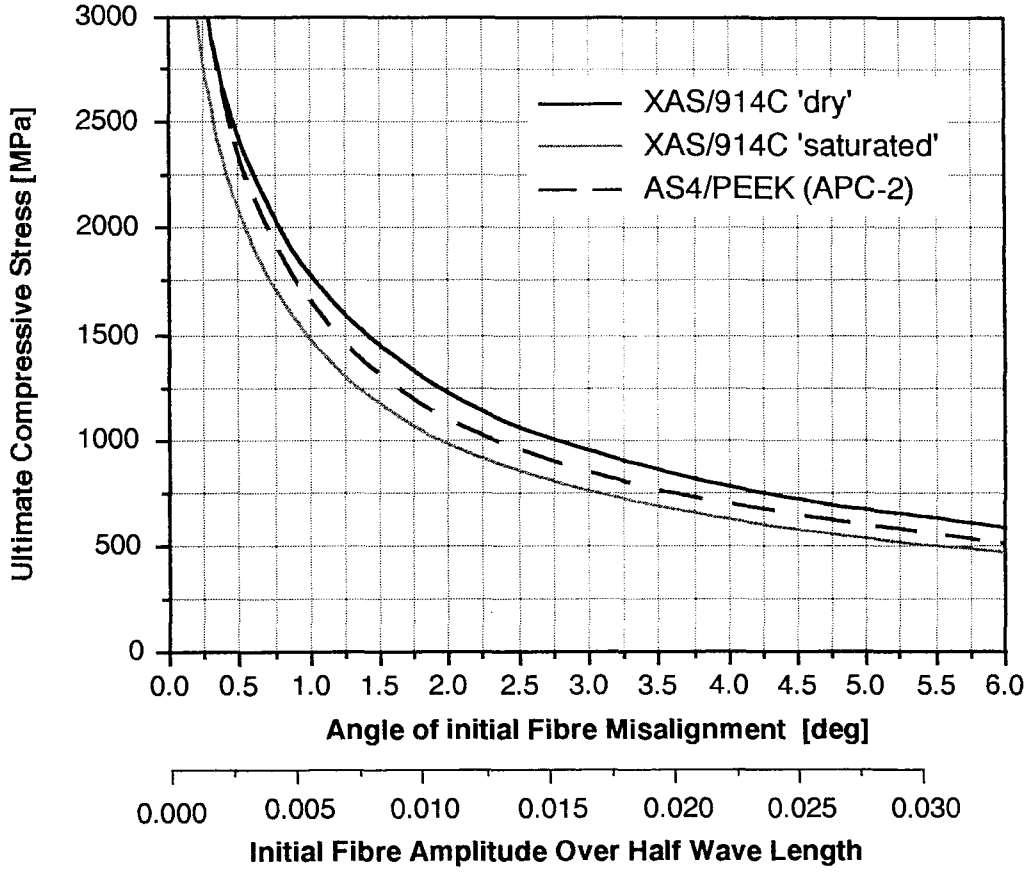


Figure 11.2.2-1: Ultimate compressive stress versus initial fibre deflection.

In order to predict not only trends but also absolute values of the compressive strength a typical angle of misalignment has to be defined. As indicated earlier, this is the main problem when using the model described in this chapter since the fibres are not uniformly misaligned but rather in a statistical manner. In Chapter 8 two methods to define a typical angle from the distribution of fibre angles have been suggested: the standard deviation of the fibre angle distribution and a 'linearised' standard deviation, i.e. the weighted mean of the absolute fibre angle distribution. Based on these angles the results for the predicted compressive strength of the above mentioned composites are summarised in Table 11.2.2-1.

Material	UCS based on the standard deviation of transformed distribution of fibre angles [MPa]	UCS based on mean of distribution of absolute fibre angles [MPa]
XAS/914C (dry)	1775	1970
XAS/914C (sat.)	1470	1650
APC-2	1295	1490
Apollo 0%	(1500*/1225**)	(1715*/1420**)
Apollo 10%	(1685*/1390**)	(1910*/1590**)
Apollo 50%	(1530*/1250**)	(1725*/1425**)
Apollo 100%	(1425*/1165**)	(1645*/1355**)

* Values based on the shear stress-strain curves of 'dry' XAS/914C

* *Values based on the shear stress-strain curves of 'saturated' XAS/914C

Table 11.2.2-1: *Prediction of the compressive strength of the composites examined.*

It is interesting to note that for the angles specified above local shear instability occurs at rather low (maximum) average shear stress levels as can be seen from Figure 11.2.2-2, where the shear strain at failure is plotted against initial fibre misalignment.

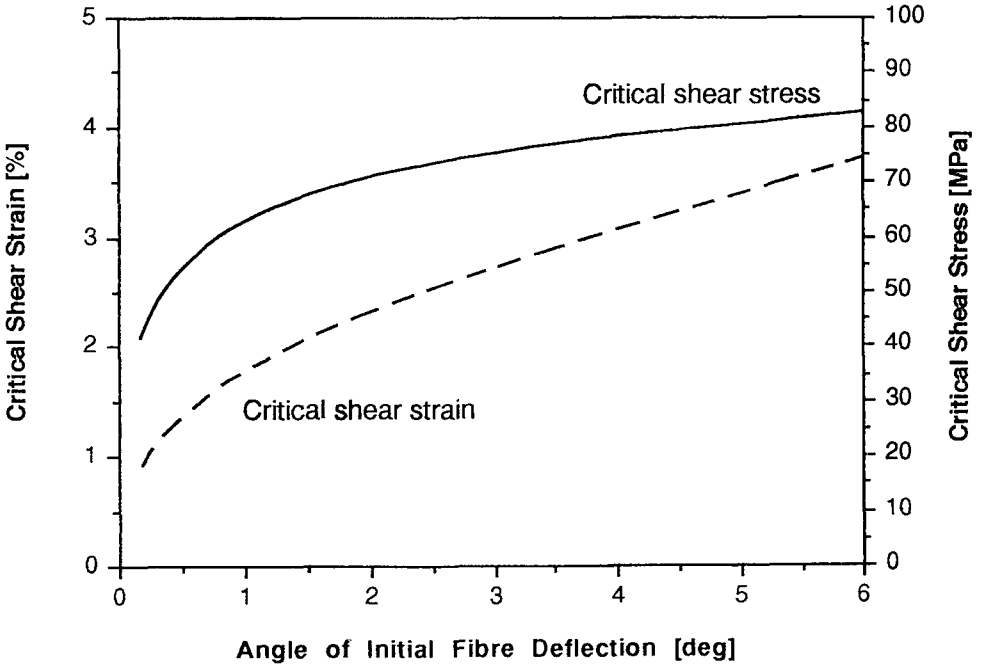


Figure 11.2.2-2: *Critical values versus initial fibre deflection for XAS/914C.*

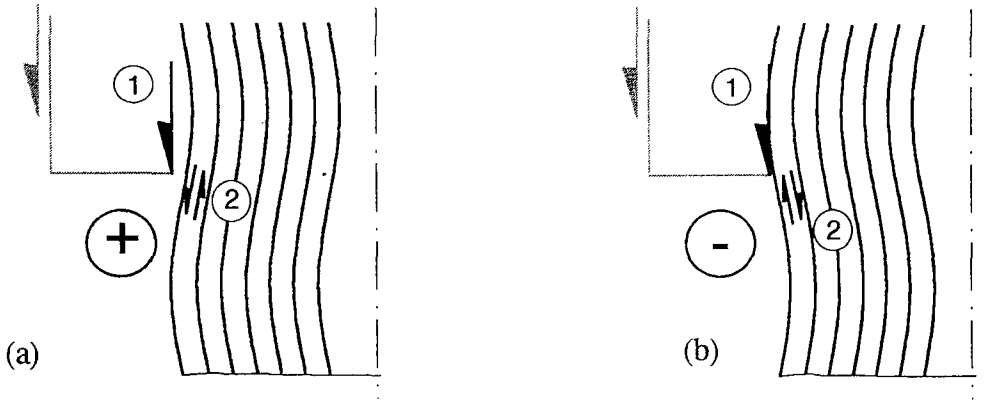
For the mentioned materials the critical average failure shear strain is only in the region of 1-2%, corresponding to a critical shear stress of between 45 and 70 MPa. This could at least qualitatively explain why the compressive strength apparently is not dependent on the fibre surface treatment, i.e. on interfacial properties, of the composite. In Section 11.3 this will be further analysed.

Before discussing the predictions in detail an important aspect of the compressive failure process will be reviewed.

11.2.3 Influence of Superposed Shear Stresses

In the failure process proposed the shear stress-strain response of the composite plays a key role. Modifications in the curve would result in a change of compressive strength as pointed out in the previous section. In this section the effects that superposed shear stresses, caused for example by load introduction, might have on the compressive strength of unidirectional systems will be examined.

First of all, a convention of signs is necessary. Obviously, the stress state induced in a unidirectional composite under compression is three-dimensional and very complex. Again, the situation will be simplified by splitting induced shear deformations into in-plane and out-of-plane components, corresponding to the direction of fibre deflection. Superposed shear stresses can either increase or decrease existing shear deformation as sketched in Figure 11.2.3-1. In the following the worst case of added stresses is assumed.



① Shear deformation caused by load introduction

② Shear deformation induced by axial compression because of non-axial fibres

Figure 11.2.3-1: Sketch of modes of shear superposition: (a) increased or (b) decreased shear deformation caused by load introduction.

Figure 11.2.3-2 illustrates how the model proposed in Section 11.1.1 is applied when shear stresses are superposed: the shear stress-strain relation is obtained by adding the superposed shear stress (or strain) value to the incremental value, i.e. the incremental procedure uses the section of the original shear stress-strain curve above the superposed shear stress (strain). The terms 'induced' shear strain and stress refer to stresses and strains induced when misaligned fibres are axially compressed.

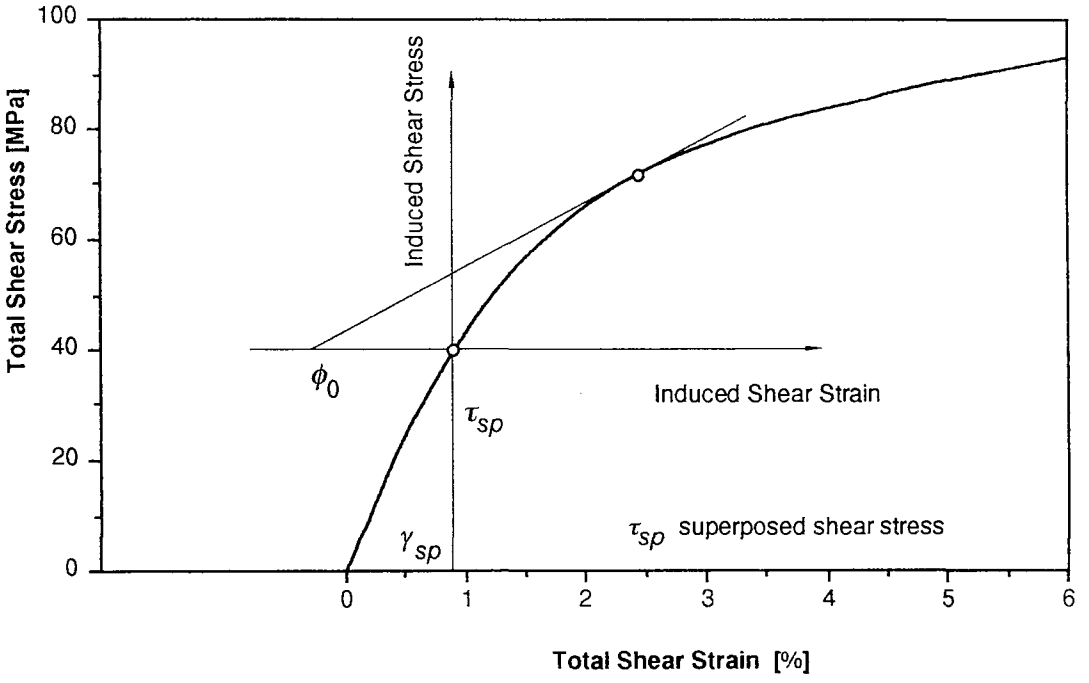


Figure 11.2.3-2: *Illustration of the method to determine the compressive strength with shear stresses superposed.*

The results of the calculations, in increments of 10 MPa superposed shear stresses, are shown in Figure 11.2.3-3 for XAS/914C and Figure 11.2.2-4 for APC-2, respectively. The impact of superposed shear stresses on the compressive strength of a composite is clearly visible from these figures. As expected from the mechanics of failure, the compressive strength approaches zero when the shear stress approaches the shear strength of the composite. The asymptotical value of about 400 MPa reflects the constant slope of the composite shear-stress strain curve at shear strains above 3% which is probably an artefact of the particular shear test. Since the validity of the model in these boundary regions is questionable because of model simplifications, the results for the high shear stresses should only be taken as a tendency.

An interesting observation at this point is that the reduction in apparent compressive strength when using the same specimen in the CRAG and the ICSTM rig can very well be explained by higher shear stresses through load introduction .

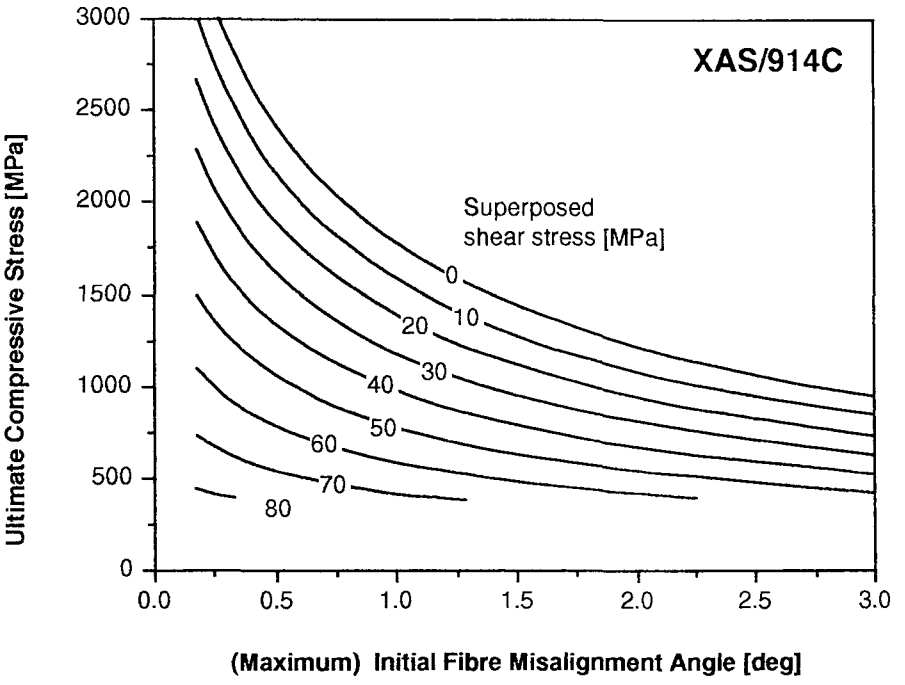


Figure 11.2.3-3: The influence of superposed shear stresses on the predicted compressive strength of XAS/914C.

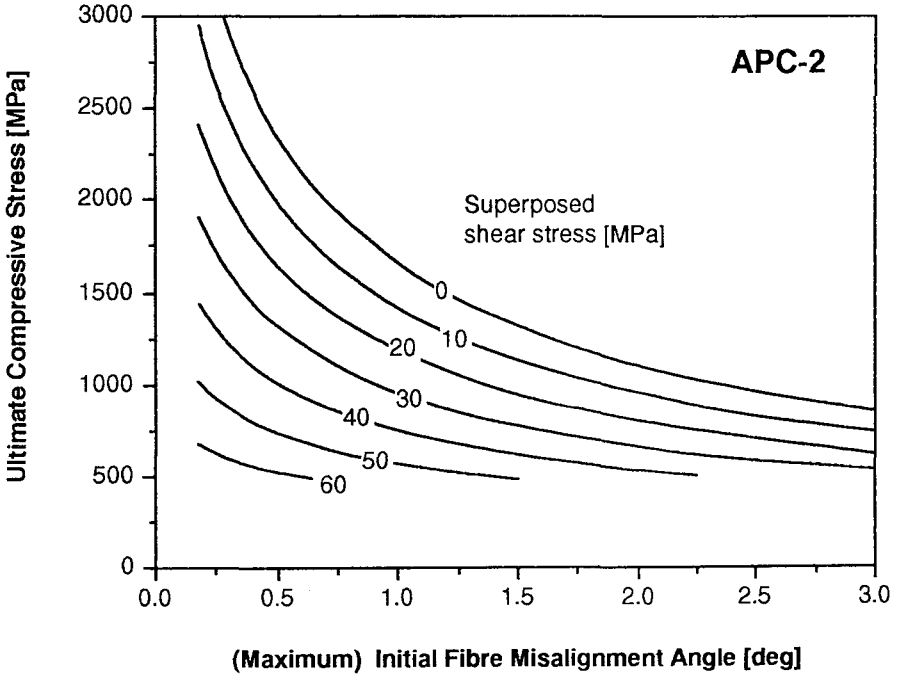


Figure 11.2.3-4: The influence of superposed shear stresses on the predicted compressive strength of AS4/PEEK (APC-2).

11.3 Concluding Discussion

11.3.1 Discussion of the Predictions

Firstly, the strength predictions will be compared to the experimental results of this investigation. Since only the shear stress-strain curves of XAS/914C and APC-2 have been measured, the results of these two composites will be considered primarily.

When comparing experimental results with analytical predictions stress concentrations have to be considered. The finite element study has shown that axial direct and shear stress concentrations exist in the vicinity of the tab tip. In the previous section it has been shown how shear stresses can affect the compressive strength of the composite. Clearly, axial direct stress concentrations lower the average failure stress as well by initiating compressive failure in the vicinity of higher axial compressive stress. It has been stressed in Chapter 5 that realistic values were not to be expected from a linear finite element model. Even if the exact stress field were known a two-dimensional micromechanical analysis would be necessary to assess failure initiation. It is a problem similar to defining a typical angle of misalignment. A complex problem is reduced to basically a one-dimensional one. However, it is believed that some reasonable conclusions can be drawn by assuming a typical (critical) average stress concentration, e.g. caused by shear stresses.

In Figure 11.3.1-1 the compression test results are plotted onto the prediction graphs of the previous section. The typical angle of fibre misalignment is taken, as pointed out earlier, as the standard deviation or as the mean of the absolute fibre angle distribution.

Regarding the results based on the standard deviation first, the compressive strength of APC-2 is over-predicted by approximately 15% when the result for the specimen with debond insert is taken. The result of the machined specimen would suggest a superposed shear stress of 10 MPa. Similarly, the results for XAS/914C specimens with debond insert are correctly predicted, and a superposed shear stress of 10 MPa is suggested for the standard specimen. Based on the mean value of the absolute fibre distribution the APC-2 value for the specimen with debond insert is correctly predicted and a superposed shear stress of approximately 20 MPa suggested for the machined specimen. A superposed shear stress of approximately 10 MPa for the specimen with debond insert and approximately 17 MPa for the standard specimen is suggested for XAS/914C. These predictions are more reasonable than the ones based on the standard deviation. It has to be recalled that some of the XAS/914C specimens failed in a macrobuckling mode. Therefore, the test results should be over-predicted by a larger margin than for APC-2

where macrobuckling is not observed. Due to higher axial failure stresses superposed shear stresses are higher for XAS/914C than for APC-2. The predicted compressive failure stress for XAS/914C without superposed shear stresses is 1970 MPa which would correspond to an extrapolated compressive strain of around 2.2 % (compare Figure 7.1-4). Such values have been recorded in various tests as discussed in Section 9.6. The results for APC-2, using the specimen with debond insert, are predicted correctly, i.e. it is implied that the coupon gives realistic results. This is a reasonable assumption since of each sample of 5 specimens one failed centrally, which has not been observed for XAS/914C. It indicates that local fibre misorientations in APC-2 are more likely to trigger failure than in XAS/914C.

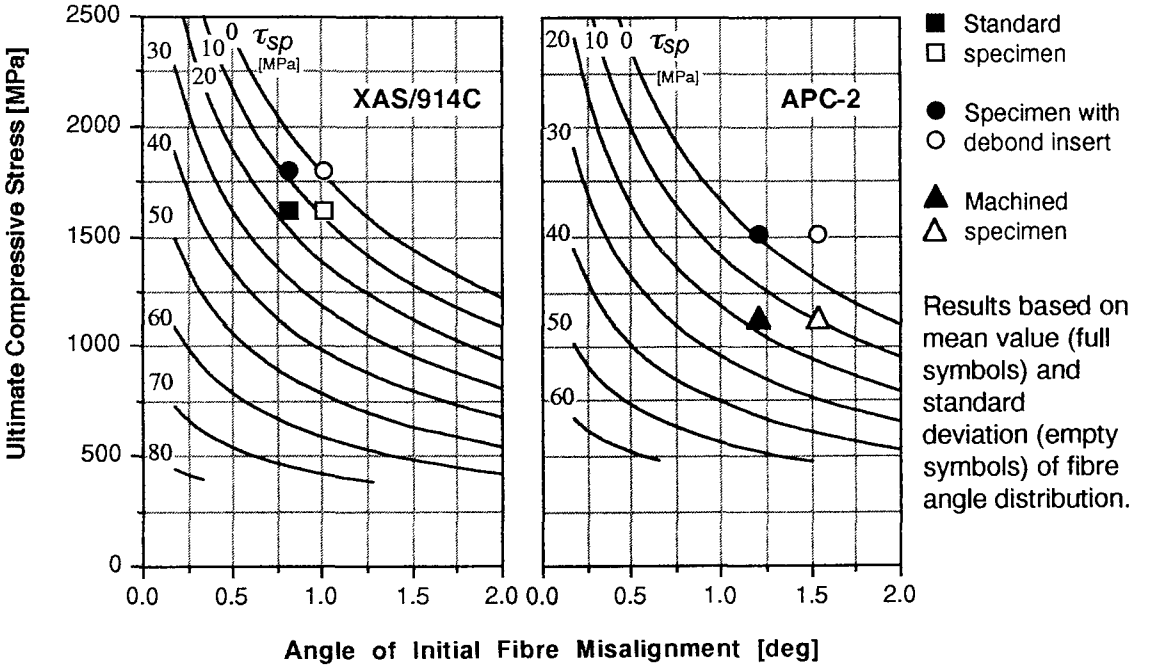


Figure 11.3.1-1: Comparison of predicted and measured values for the compressive strength of XAS/914C and APC-2.

The interpretations of the above show that using the mean of the absolute fibre angle distribution gives answers which could describe experimental findings better than using the standard deviation. As described in Chapter 8, standard deviation uses quadratic terms, whereas these terms are linear in the calculation of the mean. Therefore, the physical difference of both angles is the weight they assign to the fibres which differ from the 0°-direction. The result that the 'linear formulation' describes the test results in a better way leads to the conclusion that a 'smearing' effect is to be considered when describing compression failure of a composite. That simply means that there is an interaction between fibre bundles of different levels of misalignment. Bundles with small

misalignment support others with greater misalignment thus reducing shear deformation, which in turn leads to a greater misalignment of the straight bundles. This mechanism has also been suggested earlier (Section 9.2) to explain the higher strains achieved under conditions where strong bending, i.e. strain gradients, exist. Fibre bundles in outer layers are constrained in their in-plane deformation by inner, less highly loaded, fibre bundles. Since the gradient is very steep in thin flexure test pieces, this constraint is believed to have significant influence. The greater the thickness, i.e. the smaller the gradient, the smaller the effect. Such a size effect has been found in experiments by Wisnom (1991).

Interfacial properties do play an important role in the model. Experimentally it has been shown that there is a certain correlation between the compressive strength and the ultimate shear stress (Section 9.5) as determined, for example, by a short beam shear test. The analytical model has shown that the shear yielding characteristics are responsible for the compressive performance rather than the ultimate shear stress. If shear failure is assumed to be of interfacial nature rather than matrix yield, it will depend on factors such as fibre surface treatment. It is therefore to be expected that fibre surface treatment affects the compressive strength of the composite. It is suggested that the graphical solution in case of interfacial failure can be determined as shown in Figure 11.3.1-2.

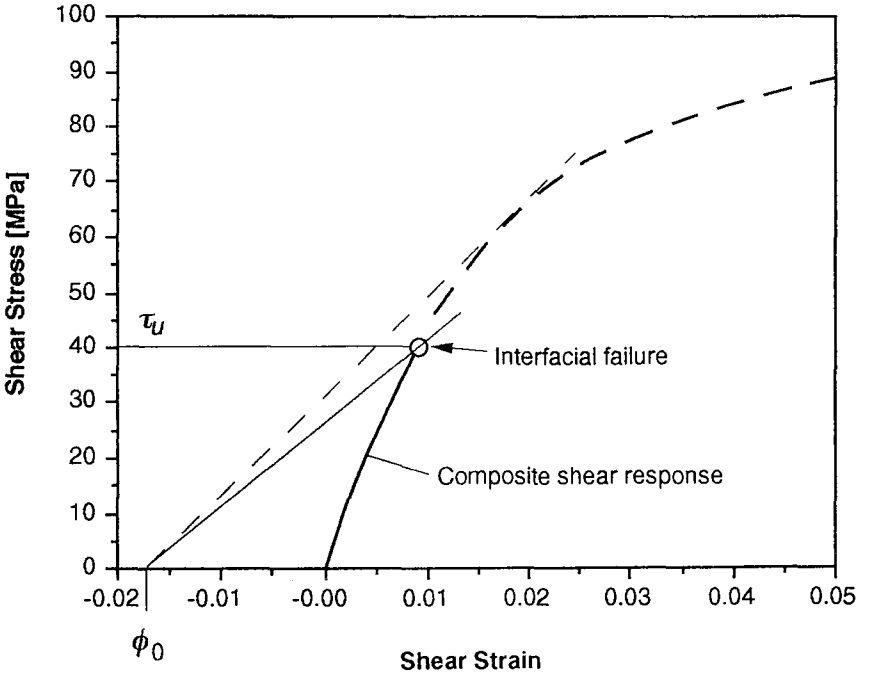


Figure 11.3.1-2: Graphical determination of the compressive strength in case of interfacial failure.

Unfortunately, it is not known how the stresses calculated from the short beam shear stresses correspond to the in-plane shear stress values of the ±45° tests. The lowest ILSS value has been measured for Apollo 43-750/9106C, containing fibres without surface treatment, as 72.7 MPa. If it is assumed that ILSS values are roughly in-plane shear strength values, it could be deduced that the mean composite shear stress when instability occurs is lower than this lowest measured value (compare Figure 11.2.2-2). Shear instability would occur before the interfacial strength is reached. However, influence of fibre surface treatment on compressive performance has been reported for other systems and lay-ups, (e.g. Curtis and Morton, 1982). It is suggested that if the interface is weak other factors, such as tensile interface stresses, might gain influence on the compressive failure mode. Tensile interface stresses might be caused by the different Poisson deformation of fibre and matrix (Woolstencroft, 1982) or, if the composite is modelled as described in this chapter, by the difference in fibre radius of neighbouring fibres in the vicinity of maximum curvature.

Figure 11.3.1-3 shows the test results for Apollo 43-750/9106C, containing fibres with different levels of surface treatment, versus the initial fibre misalignment angle. The test results are compared to predictions for the epoxy system XAS/914C in 'dry' and 'saturated' condition since the shear stress-strain curves for the Apollo-systems have not been measured. As before, the two typical average angles are used.

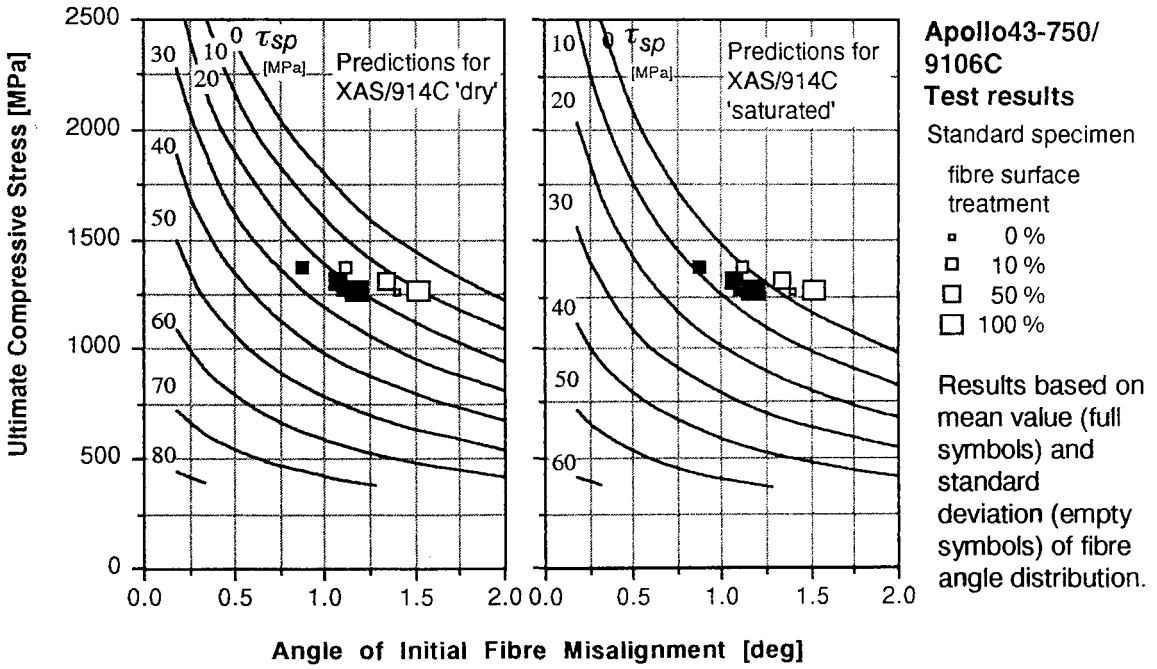


Figure 11.3.1-3: Assessment of the test results for Apollo 43-750/9106C using the ICSTM compression test method (standard specimen) on the basis of predictions for XAS/914C in dry and saturated conditions.

It is assumed that the shear performance of Apollo 43-750/9106C lies somewhere between that of 'dry' and that of 'saturated' XAS/914C+; the predictions then follow the tendency observed for the composites described above. The predictions based on the mean value of the absolute fibre angle distribution suggest a superposed shear stress of 10 to 15 MPa . Again, it seems that the values based on the standard deviation over-predict the compressive strength of the composite. A certain amount of superposed shear stress has to be postulated, because failure of the specimen was in almost all cases initiated near the tab tip.

11.3.3 General Comments on Compression Failure

In this section some aspects of modelling compression failure considering experimental evidence will be discussed.

Since plastic shear deformation takes place before shear instability occurs, it could be argued that this non-reversible deformation should be reflected in a non-elastic axial stress-strain curve. But the stress-strain curve is reversible as, for instance, illustrated in Figure 10.2.2-2. In fact, that is not a contradiction because as shown in Section 11.2.1 the geometric, partly plastic deformation, is very small for highly aligned composites. This can be assumed at least shortly before failure and, due to the nature of compressive failure, the test cannot be reversed just before failure since the point of failure is not known. Also, nonlinearity caused by plastic shear deformation is probably overridden by nonlinear axial response of the matrix.

Although there is some indication that the effect of misalignment is smeared by interaction between fibres, it is likely that a few isolated kinks or strongly misaligned fibre bundles will trigger compressive failure. If the misalignment angle is large (compare Figure 11.2.1-1) geometric fibre deformation is of the same order as axial compression deformation. At the point of shear instability axial elastic strain can be accommodated by further geometric deformation. The load is redistributed and catastrophic failure does not necessarily follow. This situation is probably seen in woven cross-ply CFRP. If, however, the kink angle is small, say below 2° as in highly aligned unidirectional CFRP, geometric deformation when loading the composite axially is

---

+ This assumption is reasonable since the performance of 9106 was qualified as not being satisfactory by the manufacturers. IISS data, however, are comparable to the the 914 epoxy. Possibly, the shear response of the composite is more nonlinear as in the case of saturated XAS/914C.

negligible compared to the axial deformation. Local shear instability, therefore, causes large geometric deformation when the axial strain is 'released'. Failure then is catastrophic. The buckled bundle disturbs the equilibrium of the neighbourhood, leading to a spread of the kinked zone. Fleck and Budiansky (1990) have shown that once a kink is initiated only small axial compressive stress is needed for the failure front to progress.

Since stress concentrations in test coupons are usually highest on the surfaces, failure is expected to be initiated there. This coincides with the experimental observations. An exception is possibly the case of 'quarter-point' failure when the coupon buckles. Through-thickness shear stresses then are highest in the centre of the specimen at approximately quarter gauge length, the location of failure as discussed in Section 5.2.

Generally, compressive failure involves kink bands, i.e. a half wave length, rather than a complete or several wave lengths, although microbuckling involving several wave lengths has been observed occasionally (e.g. Figure P-4). The fact of predominant kinking can be explained by the fact that even if fibre bundles posses a wavy form in the composite it is unlikely that the wave will be symmetric. Instability will occur at the section with the largest amplitude or, if amplitudes are similar, where the stress field promotes instability.

An illustration of frequently observed 'reflection' of kink bands on free edges (reported in Chapter 4, also referred to as forked or wedge-type failure in Chapter 5) is given in Figure 11.3.2-1.

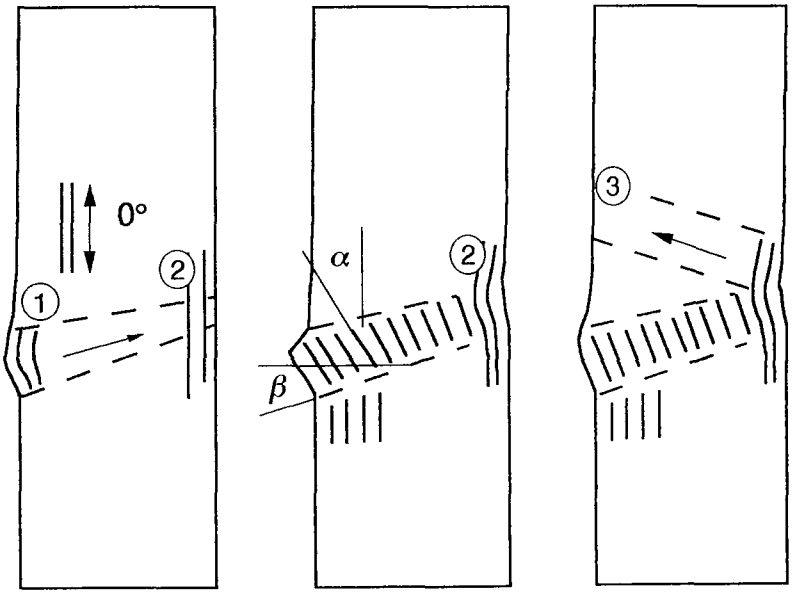


Figure 11.3.2-1: Illustration of propagation of kink bands at a free specimen edge.

Region 1 is momentarily unloaded when failure is initiated. The kink spreads to region 2, deforming fibres on the free surface whilst at region 1 fibres have fractured in the vicinity of highest curvature. Optical micrographs show that fibres adjacent to the kink band remain straight after fibre failure (compare Figures P-4 (a) to (c)). Unlike the fibres in region 1 the deformed fibres in region 2 are still under compressive stress, since the load bearing capability of the kink band is small, and a 'reflected' kink is is initiated. When the first kink is established over the width the kinked fibres lock up (Fleck and Budiansky, 1990). Due to the elastic energy stored in the test rig and specimen the load is built up again to a lower level when the test is interrupted at first failure in displacement controlled tests. The 'reflected' kink might therefore be promoted to region 3. This goes on, until the remaining compressive stress is too low to promote the kink. If a failed specimen was deliberately further loaded this mechanism could be provoked until the kink had travelled through the whole specimen.

11.3.3 Conclusions

In conclusion, it has been shown that all the current experimental findings could be verified by the simple analytical model. Compressive failure could be predicted for two quite different CFRP systems without having to fit input data to experimental results. The mean angle of fibre misalignment as defined in Chapter 8 provides reasonable predictions when used to predict shear instability from the nonlinear composite shear stress-strain curve. Fibre alignment has been shown to be such an important factor when assessing the compressive strength of a composite that models not including this parameter cannot be accepted. The influence of moisture was reflected in the shear-stress strain curve and the consequence on compressive strength was predicted correctly. Unfortunately, the effect of temperature on the compressive strength could not be examined in the present investigation. But, as Wang (1978) pointed out, test results for higher temperatures could be predicted satisfactorily by using input data for fibre misalignment which fitted the room temperature test and the shear stress-strain curve at the relevant temperature.

CHAPTER 12 CONCLUSIONS AND SUGGESTIONS FOR FUTURE WORK

12.1 Conclusions of the Experimental Work

Conclusions of compression testing generally

* The large variation of test results found in the published scientific literature has been repeated in the experiments carried out in this investigation using XAS/914C. It has been suggested that this is largely a consequence of specimen design rather than specific for a certain test method. Support for this assumption is the large variation of results gained with a particular method. However, in the present investigation it was found that methods introducing the load by mixed shear/end-loading in general give more consistent results.

* Compressive failure is catastrophic and spreads across the cross-section, separating the test piece. In all cases some longitudinal splitting was present but it is thought that this is a post-failure event. Failure in almost all cases initiated at external stress concentrators such as tab tips or points of contact with the testing jig.

* A new test method combining features of established methods but avoiding their shortcomings has been proposed. It uses an end-loaded tabbed test piece and frictional effects are eliminated by the use of a die set. For XAS/914C significantly higher test results could be realised than reported so far for test pieces with equivalently unconstrained gauge section. The method is very versatile as it can easily be adapted to a range of different test piece geometries.

* The most significant test piece parameters when using the proposed method have been identified as the slenderness ratio of the test piece and the mechanism of tab tip debonding. Tab tip debonding was found to reduce stress concentrations and fibre deflections at the tab tip. These factors are thought to be detrimental to the measured compressive strength of a coupon and particularly severe for indirect test methods.

* The combination of tab stiffness and bond strength is crucial for the strain at which tab tip debonding occurs. Test pieces machined from unidirectional laminates proved to be suitable, since the high tab stiffness caused tip delamination at low strains. If tab tips debonded at strains near the failure strains the resulting instantaneous (often sudden) load eccentricity could cause premature failure. Application of debond inserts yielded the desired effect as well.

* Tab tip debonding did not lower the buckling stress, i.e. the effective unsupported length was not changed significantly. However, the resulting strain signals in some cases resembled the ones typical for macrobuckling of the test piece.
* Further factors influencing the test result were found to be the method of specimen production and the care and experience of the operator. Often it is found that the second attempt yields higher results than the first one under apparently unchanged conditions.
* The effect of layer misalignment is suppressed when using short specimens since shear deformation is hindered by the test rig.

General findings regarding CFRP

* Carbon fibre-reinforced plastics behave nonlinear-elastically up to fracture both in tension and compression, i.e. the tensile and compressive stress-strain curves are nonlinear and reversible. A consequence of this is that the axial modulus of elasticity is increasing in tension and, to a higher degree, decreasing in compression.
* The nonlinear character of the stress-strain behaviour has been proven experimentally to be caused by the nonlinear nature of the fibres themselves. GRP, glass fibres being isotropic, behaves almost linearly up to fracture although fibre misalignment was found to be similar in GRP and CFRP. Also, the fact that the stress-strain behaviour of CFRP is elastic puts weight to the argument.
* The decreasing modulus in compression contributes to the tendency of macroscopic buckling at high strains. This could be verified analytically by assuming that the local modulus is responsible for the buckling behaviour rather than the initial or secant modulus.
* Compressive failure in the CFRP systems examined, including XAS/914C and APC-2, is by fibre microbuckling with consequent development of a kink band.
* Longitudinal splitting and brushing of specimen ends is a post-failure effect.
* It has been suggested that stress gradients, for example when bending a laminate, allow higher compressive stresses compared to the uniaxial stress state to be realised because of the support effect of the less stressed regions.

Significance of coupon compression testing

* If failure is by microbuckling and not by macroscopic instability of the test piece, then the coupon test gives lower bound of compressive strength. Unfortunately, it

is difficult to assess how low.

* Failure strains in other tests such as flexure and compression of multidirectional laminates are usually higher than the ones gained in coupon tests. Results of these tests should always be taken into account as a reference when assessing the compressive strength of a system, considering the previous topic.

* Use of the method presented in this study is recommended in order to obtain meaningful results.

* Variation of coupon test results allows conclusions on the sensitivity of the compressive strength of a laminate in complex stress. This is of great practical importance for structural applications.

Recommendations for the testing practice

* It is essential that test pieces are instrumented with strain gauges which allow separate reading of opposing surface strains. The true failure sequence is often not possible by examining the fractured test piece. Effects such as bending, asymmetrical tab debonding, interlaminar failure or wrongly loading the testing jig, which all can lead to premature failure or falsified results, can be identified through the stress-strain curve. In particular, macrobuckling of the test piece has to be recognised, which is hardly possible without separate strain readings.

* Measurement of test piece dimensions, although regarded as a trivial issue, should be considered as a source of error. When fabric peel plies are used when manufacturing the laminates the imprinted surface pattern can falsify the thickness measurement, which is of consequence particularly in flexure tests. Insufficient machining of edges, i.e. leaving scratches or wedging the edges, can, if not influence the failure, at least cause misleading measurement of the test piece width (or thickness if the gauge section is machined).

* Specimen surfaces in contact with the grips have to be flat in order to avoid test piece bending. Although accuracy of test piece machining is not confined to compression testing, this is of particular importance with short compression test pieces. Obviously, when the load is introduced at the ends additionally these end surfaces have to be flat and square. In the present investigation a simple and very effective procedure to produce suitable test pieces has been presented.

* The stress-strain curve has to be analysed carefully before determining the modulus of elasticity. Particularly in the initial part, where the modulus is read from, the

curve can be falsified by friction. Procedures calculating the modulus automatically are dismissed.

In order to achieve meaningful results using indirect compression test methods (e.g. CRAG, Celanese, IITRI) the following measures are recommended:

* It was found that when the tab ends emerged slightly from the grips, equivalent to tapering of the tabs, the measured strength results was increased. Since the constraints were reduced, this is thought to be a more realistic test.
* There is evidence that the mechanism of tab debonding is beneficial for indirect test as well as for test methods using end-loaded test pieces.
* The grips must have the right roughness in order to avoid slipping of the specimen without having to apply excessive transverse pressure. On the other hand, it has been observed that serrations in the grips, whilst ensuring safe grip, promoted premature failure.
* The CRAG fixture has to be adjusted carefully to the test piece dimensions. Since the method generally is prone to large variation of results, it is not recommended.
* British Aerospace rig was found to be the most convenient methods of the indirect ones and is therefore recommended.
* Change method for ICSTM method.

12.2 Conclusions of Theoretical Investigations

* Load-strain behaviour of four-point flexure test pieces could be described using the stress-strain curves from axial coupon tests.
* Shear deformation and decreasing modulus of elasticity were found to be important parameters when analysing macroscopic instability of CFRP coupons. Buckling stresses could be predicted satisfactorily when the tangent modulus of elasticity and shear correction were used. It was found that both clamping factor and effective shear modulus are likely to decrease with increasing compressive stress.
* Microbuckling has been predicted by using a simple analysis assuming that failure is by shear instability. The main input parameters determining the compressive strength of the laminate are initial fibre waviness and the shear response of the composite.
* Input of an experimentally determined mean value of the initial fibre angle distribution and the shear response of the composite from a ±45° tension test led to

satisfactory predictions of the compressive strength of two systems with quite different compressive properties: XAS/914C and APC-2.

* Using the kinematics of the strength model, it could be demonstrated that the nonlinear stress-strain characteristic, in particular under compression, is not caused by geometric effects due to fibres not being perfectly aligned, but by nonlinear elastic behaviour of carbon fibres.

* The strength model also allowed one to explain experimental evidence (e.g. some low test results using indirect test methods) by a combination of hardware-introduced effects such as stress concentrations (shear and axial) and surface fibre deformation.

Recommendations for Structural Applications

Basically, what was said for a test piece holds true for any structure. Unidirectional CFRP has proven to be extremely sensitive to contact stresses. Specimens failed at 60 % of their potential maximum load when the CFRP was in pressure contact with steel edges (Birmingham method). In flexure test pieces failure occurred at considerably lower failure stresses when the loading rollers were not padded. Simple measures such as padding the roller could raise the compressive capability significantly (as a matter of fact, tensile failure occurred when the rollers were padded and compressive failure could not be provoked). Also, it was suggested that additional fibre deflection caused by load introduction causes premature failure. Consequently, apart from obvious stress raisers, such as notches and holes, the following should be considered in structural applications:

* Shear stresses due to load introduction should be as low as possible in compressively loaded components.

* Dangerous short wave fibre deflections could be caused by contact with other components. Creep of the CFRP should be considered as well. For instance, support fixtures might indent a cylindrical structure under compression in long term applications.

* Unidirectional layers in general should be sandwiched, e.g. by angle plies.

* One should aim for good fibre alignment with the load axis. In particular, fibres should be as straight as possible. This could be achieved by putting fibres under slight tension during curing and cool-down.

12.3 Suggestions for Future Work

In the present investigation several questions have been answered only partially. Although trends have been predicted correctly, further work on the following topics is desirable.

Experimentally

Regarding coupon compression testing the following investigations are thought to be useful:

* A test method has been proposed and proven, basically using one particular carbon fibre reinforced plastic. It would be desirable to verify the results on different materials. Also, the parametric investigation which in this study has been carried out using a 'standard' test piece would yield interesting information on a test piece with debond inserts.
* Optimising the specimen design to avoid macrobuckling. It has been suggested to use a 16-ply test piece with a gauge length of approximately 7 mm. Preferably, the test piece should be machined from a thicker panel or have debond inserts in order not to constrain the gauge section.

The problems of load introduction pose severe limitation on the reliability of coupon compression testing for material development and quality control. It has therefore been suggested that the unidirectional coupon tests should be challenged by test methods with reduced stress concentrations:

* Further assessment of deriving unidirectional compression properties from testing multidirectional laminates.
* Further assessment of flexure testing as a method to determine compressive properties of unidirectional materials. In particular, it is suggested to use flexure tests in order to assess the influence of an overall misalignment of the laminate or single layers, since the reaction forces in coupon tests do not allow one to assess these parameters.
* The promising results achieved using sandwich columns (Kim and Crasto, 1990) encourage the use of the test configuration introduced in the present study for loading of sandwich columns as illustrated in Figure 12.3-1. It has been shown

that stress concentrations caused by load introduction can be significantly reduced using an end-loaded specimen with debond inserts. It would be interesting to find out what results the advantages of testing a sandwich column, i.e. testing of very thin laminates, combined with reduced stress concentrations from load introduction would yield.

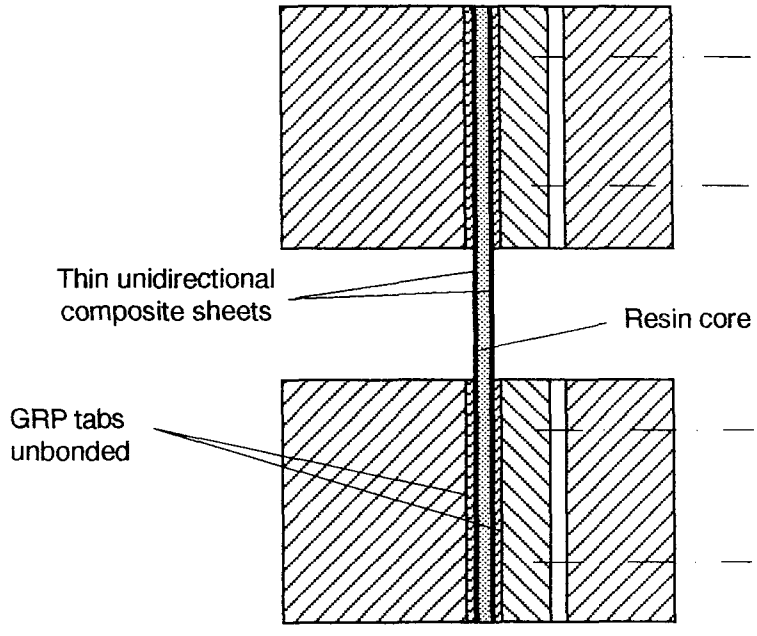


Figure 12.3-1: Proposal for the use of a sandwich column in the ICSTM test rig shown in Figure 5.1-4.

Fibre alignment measurements

* Measurement of out-of-plane misalignment and comparison to the in-plane misalignment analysed in the present study.
* Analysis of single layers in order to obtain information about the contribution of misaligned layers to the overall fibre angle distribution.
* Examination of different materials, e.g. glass fibre-reinforced plastics.
* Determination of the quality of fibre misalignment. Although there is some (visual) evidence of fibres being misaligned in bundles, there is no means to quantify wavelength and spatial distribution of single bundles.

There remains some uncertainty about the validity of ±45° tension tests for determination of the shear response. In particular, viscoelastic effects have been suggested to influence the results. This should be a topic of further investigation.

Analytical work

* Moving from a basically one-dimensional model to a true two-dimensional one would allow interaction of misaligned fibre bundles to be taken into account. As a first step, a fibre distribution as determined in Chapter 8 could be assumed.
* The transfer of data gained from coupon tests requires a better knowledge of the three-dimensional stress state in a test piece. A nonlinear finite element model including plasticity would yield useful information.

Principal Conclusions

- **Most conventional test methods, although yielding meaningful results in their optimum form, allow too much influence of the particular tester for them to be recommended as standard test methods**
- **Application of strain gauges are a prerequisite for compression testing in order to assess the validity of the test, particularly in order to identify macro-instability.**
- **Disagreement of predicted and measured compressive strength of CFRP is largely a consequence of the influence of the testing conditions. Unidirectional CFRP is extremely sensitive to stress concentrations.**
- **The ICSTM method proposed in this work combines simplicity of specimen production, ease of use and re-peatabilty of realistic results for a range of materials.**
- **Fibre alignment and shear response are the main parameters governing the compressive strength of unidirectional high strength carbon fibre-reinforced plastics.**

REFERENCES

ADAMS, D.F and LEWIS, E.Q., "Influence of Specimen Gage Length and Loading Method on the Axial Compressive Strength of a Unidirectional Composite Material". *Experimental Mechanics.* A Journal of the Society for Experimental Mechanics Inc., Vol. 31, No 1, March 1991, pp. 14-20.

ADAMS, D.F. and ODOM, E.M., "Influence of Specimen Tabs on the Compressive Strength of a Unidirectional Composite Material". *Journal of Composite Materials*, Vol. 25, June 1991, pp. 774-786.

ADAMS, D.F., "A Comparison of Composite Material Compression Test Methods in Current Use". Proceedings of the 34th International SAMPE Symposium, Anaheim, May 8-11 1989, pp. 1422-1433.

ADSIT, N.R., "Compression Testing of Graphite/Epoxy". *Compression Testing of Homogeneous Materials and Composites*, ASTM STP 808, Richard Chait and Ralph Papirno, Eds., American Society for Testing and Materials, 1983, pp. 175-186.

American Society for Testing and Materials, ASTM D695-85 , "Standard Test Method for Compressive Properties of Rigid Plastics", 1985.

American Society for Testing and Materials, ASTM D790M-84 : "Flexural Properties of Unreinforced and Reinforced Plastics and Electrical Insulating Materials (Metric)", 1984.

American Society for Testing and Materials, ASTM D3410-87: "Standard Test Method for Compressive Properties of Unidirectional or Crossply Fiber-Resin Composites", 1987.

American Society for Testing and Materials, ASTM D3518, "Standard Practise for In-plane Shear Stress-Strain Response of Unidirectional Reinforced Plastics", 1976.

ARGON, A., In: "Treatise on Materials Science and Technology". H. Herman, Ed., Vol. 1, Academic Press, New York and London, 1972, pp. 106-114.

ARGYRIS, J., EBERLE, K. and HAEBERLE, J., "Lebensdauerkennwerte aus Betriebsbelastungen von kohlefaserverstärkten Kunststofflaminaten". DFG Final Report, Institute for Computer Applications, University of Stuttgart, June 1988.

BARKER, A.J. and BALASUNDARAM,V., "Compression Testing of Carbon Fibre-Reinforced Plastics Exposed to Humid Environments". *Composites*, Vol. 18, No. 3, July 1987, pp. 217-226.

BERG, J.S. and ADAMS, D.F., "An Evaluation of Composite Material Compression Test Methods". *Journal of Composites Technology and Research*, Vol. 11, No.2, Summer 1989, pp. 41-46.

BERG, J.S. and ADAMS, D.F., "An Evaluation of Composite Material Compression Methods". Mechanical Engineering Department, University of Wyoming, Report UW-CMRG-R-88-106, 1988.

BOGETTI, T.A., GILLESPIE, J.W. Jr. and PIPES, R.B., "Evaluation of the IITRI Compression Test Method for Stiffness and Strength Determination". *Composites Science and Technology*, No. 1, January 1988, pp. 57- 76.

BOLL, D.J., JENSEN R.M., CORDNER, L. and BASCOM W.D., "Compression Behavior of Single Carbon Filaments Embedded in an Epoxy Polymer". *Journal of Composite Materials*, Vol. 24, Feb. 1990. Technomic Publishing Co. Inc., 1990, pp. 208-219.

BUDIANSKY, B., "Micromechanics". *Computers & Structures*, Vol. 16, No. 1-4, 1983, pp. 3-12.

CHAMIS, C.C. and SINCLAIR, J.H., "Longitudinal Compressive Failure Modes in Fiber Composites: End Attachment Effects on IITRI Type Test Specimens". *Journal of Composites, Technology and Research*, Vol. 7, No. 4, Winter 1985, pp. 129-135.

CHAMIS, C.C., "Simplified Composite Micromechanical Equations for Strength, Fracture Toughness and Environmental Effects". SAMPE Quarterly, July 1984, pp. 41-55.

CHANG, F.-K. and LESSARD, L.B., "Effect of Load Distribution on the Fiber Buckling Strength of Unidirectional Composites". *Journal of Composite Materials*, Vol. 25, No. 1, Jan. 1991, pp. 65-87.

CHAPLIN, C.R., "Compressive Fracture in Unidirectional Glass-Reinforced Plastics". *Journal of Materials Science*, Vol.12, 1977, pp. 347-352.

CHOU, T.-W., and KELLY, A., "The Effect of Transverse Shear on the Longitudinal Compressive Strength of Fibre Composites". *Journal of Materials Science*, Vol. 15, 1980, pp. 327-331.

CLARK, R.K and LISAGOR, W.B., "Compression Testing of Graphite/Epoxy Composite Materials". *Test Methods and Design Allowables for Fibrous Composites, ASTM STP 734*, C.C. Chamis, Ed; American Society for Testing and Materials, 1981, pp. 152-165.

CRASTO, A.S. and ANDERSON D.P., "Correlation of Structure and Compressive Strength in Pitch-Based Graphite Fibers". Proceedings of the American Society for Composites - Fifth Technical Conference: "*Composite Materials in Transition*". Technomic Publishing Company Inc., Lancaster, Pennsylvania, 1990.

CRASTO, A.S. and KIM, R.Y., "Compression Strengths of Advanced Composites from a Novel Mini-Sandwich Beam". *SAMPE Quarterly*, Vol. 22, No 3, 1990, pp. 29-39.

CURTIS, P.T. and WHITEHEAD D.L., "The Effect of Fabrication Induced Surface Roughness on the Compressive and Flexural Properties of Carbon Fibre Reinforced Plastics". Royal Aerospace Establishment, Technical Report TR 90034, July 1990.

CURTIS, P.T., and MORTON, J., "The Effect of Fibre Surface Treatment on the Compressive Strength of CFRP Laminates". Royal Aircraft Establishment, Technical Report 82047, 1982.

CURTIS, P.T., and MORTON, J., "The Effect of Fibre Surface Treatment on the Compressive Strength of CFRP Laminates". *Progress in Science and Engineering of Composites*, T. Hayashi, K. Kawata and S. Umekawa, Eds., ICCM-IV, Tokyo, 1982, pp. 219-228.

CURTIS, P.T. (Ed.), "CRAG Test Methods for the Measurement of the Engineering Properties of Fibre-Reinforced Plastics". Royal Aerospace Establishment, Technical Report 88012, 1988.

DAVIS, J.G., "Compressive Strength of Fibre-Reinforced Composite Materials". *Composite Reliability, ASTM STP 580*, American Society for Testing and Materials, 1975, pp. 364-377.

EVANS, A.G. and ADLER, W.F., "Kinking as a Mode of Structural Degradation in Carbon Fibre Composites". *Acta Metallurgica*, Vol. 26, 1978, pp. 725-738.

EWINS, P.D. and HAM, A.C., "The Nature of Compressive Failure in Unidirectional Carbon Fibre-Reinforced Plastics". Royal Aircraft Establishment, Technical Report 73057, 1973.

EWINS, P.D., "Tensile and Compressive Test Specimens for Unidirectional Carbon Fibre Reinforced Plastics". Royal Aircraft Establishment, Technical Report 71217, 1971.

FLECK, N.A. and BUDIANSKY B., "Compressive Failure of Fibre Composites due to Microbuckling". Proceedings of IUTAM Symposium, Troy, New York, May 29-June 1, 1990. Springer Verlag 1991. Included in the Report of the Cambridge University Engineering Department, CUED/C-MATS/TR.176, October 1990.

GEDNEY, C.C., PASCUAL, C.R. and KOLKAILAH, F.A., "Comparison of ASTM Standard Compression Test Methods of Graphite/Epoxy Composite Specimens". Proceedings of 32nd International SAMPE Symposium, April 1987, pp 1015-1025.

GRESZCZUK, L.B., "Compressive Strength and Failure Modes of Unidirectional Composites". *Analysis of the Test Methods for High Modulus Fibres and Composites, ASTM STP 521*, American Society for Testing and Materials, 1973, pp. 192-217.

GRESZCZUK, L.B., "Microbuckling Failure of Circular Fibre-Reinforced Composites". *AIAA Journal*, Vol. 13, No. 10, October 1975, pp. 1311-1318.

GRIMES, G.C., "Experimental Study of Compression-Compression Fatigue of Graphite/Epoxy Composites". *Test Methods and Design Allowables for Fibrous Composites, ASTM STP 734*, C.C. Chamis, Ed; American Society for Testing and Materials, 1981, pp. 281-337.

GRUBER, M.B., OVERBEEKE, J.L. and CHOU, T.-W., "A Reusable Sandwich Beam Concept for Composite Compression Test". *Journal of Composite Materials*, Vol. 16, May 1982, pp. 162-171.

HAHN, H.T. and WILLIAMS J.G., "Compression Failure Mechanisms in Unidirectional Composites". Proceedings of the 6th International Conference on Composite Materials and 2nd European Conference on Composite Materials, London 1987, F.L. Matthews, N.C.R. Buskell, J.M. Hodginson, Eds., Elsevier Applied Science, 1987, Vol. 1, pp. 115-139.

HAHN, H.T. and WILLIAMS, J.G., "Compression Failure Mechanisms in Unidirectional Composites". *Composite Materials: Testing and Design (Seventh Conference), ASTM STP 893*, J.M. Whitney, Ed., American Society for Testing and Materials, Philadelphia, 1986, pp. 115-139.

HAHN, H.T., "Analysis of Kink Band Formation Under Compression". Proceedings of the 6th International Conference on Composite Materials and 2nd European Conference on Composite Materials, London 1987, F.L. Matthews, N.C.R. Buskell, J.M. Hodgkinson, Eds., Elsevier Applied Science, 1987, Vol. 1, pp. 269-277.

HAHN, H.T., and SOHI, M.M., "Buckling of a Fibre Bundle Embedded in Epoxy". *Composites Science and Technology*, Vol. 27, 1986, pp. 25-41.

HANASAKI, S. and HASEGAWA, Y., "Compressive Strength of Unidirectional Fibrous Composites". *Journal of Composite Materials*, Vol. 8, July 1974, pp.306-309.

HANCOX, N.L., "The Compression Strength of Unidirectional Carbon Fibre Reinforced Plastic". *Journal of Materials Science*, Vol. 10, 1975, pp. 234-242.

HART-SMITH, L.J., "Generation of Higher Composite Material Allowables Using Improved Test Coupons". Proceedings of the 36th International SAMPE Symposium, San Diego, April 15-18, 1991, pp. 1029-1043.

HAWTHORNE, H.M. and TEGHTSOONIAN, E., "Axial Compression Fracture in Carbon Fibres". *Journal of Materials Science*, Vol. 10, 1975, pp. 41-51.

HAYASHI, T. and KOYAMA, K., "Theory and Experiments of Compressive Strength of Unidirectionally Fiber-Reinforced Composite Materials. Proceedings of the International Conference on Mechanical Behaviour of Materials, Kyoto, Japan, 1971, Vol. 5, pp. 104-112.

HAYASHI, T., "Compression Strength of Unidirectionally Fibre- Reinforced Composite Materials". Proceedings of the Seventh International Reinforced Plastics Conference, Brighton, UK, 1970, Paper No. 11.

HAYASHI, T., "Effective Shear Modulus of Composite Materials under Normal Stress". Proceedings of the First European Conference on Composite Materials ECCM-1, A.R. Bunsell, P. Lamicq and A. Massiah, Eds., September 1985, Bordeaux, France, pp. 434-439.

HENRAT, P., "Compression Properties of High Performance Composites Tested With Different Methods". Proceedings of the 8th European Chapter Conference SAMPE: *Looking Ahead for Materials and Processes*. J. de Bossu, G. Briens and P. Lissac, Eds., Elsevier Science Publishers B.V., Amsterdam, 1987, pp. 389-399.

HERRMANN, L.R., WILLIAM, E.M. and CHAN, S.T.K., "Response of Reinforcing Wires to Compressive States of Stress". *Journal of Composite Materials*, Vol. 1, 1967, pp. 212-226.

HOFER, K.E. and RAO, P.N., "A New Static Compression Fixture for Advanced Composite Materials". *Journal of Testing and Evaluation*, JTEVA, Vol. 5, No. 4, July 1977, pp. 278-283.

KIM, R.Y. and TSAI S.W., "A Compressive Test Method for Ring Specimens". Proceedings of the 33rd International SAMPE Symposium, March 7-10, 1988, pp. 1159-1168.

KRETSIS, G., "Mechanical Characterisation of Hybrid Glass/Carbon Fibre-Reinforced Plastics". Ph.D.-thesis, Imperial College, University of London, February 1987.

KUKULA, S.J., "A Finite Element Study of Compression Tests for Advanced Composite Materials". MSc-thesis submitted to the University of London. Centre for Composite Materials, Imperial College of Science, Technology and Medicine, September 1989.

KULKARNI, S.V., RICE, J.S. and ROSEN, B.W., "An Investigation of the Compressive Strength of Kevlar 49/Epoxy Composites". *Composites*, Vol. 6, No. 5, September 1975, pp. 217-225.

KUMAR, S. and HELMINIAK T.E., "Compressive Strength of High Performance Fibers". *SAMPE Journal*, Vol. 26, No. 2, March/April 1990, pp. 51-61.

LAGER, J.R. and June, R.R., "Compressive Strength of Boron/Epoxy Composites". *Journal of Composite Materials*, Vol. 3, Jan. 1969, pp. 48-56.

LAMOTHE, R.M. and NUNES, J., "Evaluation of Fixturing for Compression Testing of Metal Matrix and Polymer/Epoxy Composites". *Compression Testing of Homogeneous Materials and Composites, ASTM STP 808*, Richard Chait and Ralph Papirno, Eds., American Society for Testing and Materials, 1983, pp. 241-253.

LANIR, Y., and FUNG, Y.C.B., "Fiber Composite Columns Under Compression". *Journal of Composite Materials*, Vol. 6, July 1972, pp. 387-400.

LEE, R.J., "Compression Strength of Aligned Carbon Fibre Reinforced Thermoplastic Laminates". *Composites*, Vol. 18, No. 1, January 1987, pp. 35-39.

LEE, S.-Y., and SPRINGER, G.S., "Effects of Cure on the Mechanical Properties of Composites". *Journal of Composite Materials*, Vol. 22, January 1988, pp. 15-29.

LEESER, D. and LEACH, D., "Compressive Properties of Thermoplastic Matrix Composites". Proceedings of the 34th International SAMPE Symposium, Anaheim, May 8-11 1989, pp.1464-1473.

MADHUKAR, M.S. and DRZAL, L.T., "Effect of Fibre-Matrix Adhesion on Longitudinal (0°) Compressive Properties of Graphite/Epoxy Composites". Proceedings of the American Society for Composites - Fifth Technical Conference: "*Composite Materials in Transition*". Technomic Publishing Company Inc., Lancaster, Pennsylvania, 1990, pp. 849-858.

MARTINEZ, G.M., PIGOTT, M.R., BAINBRIDGE, D.M.R., and HARRIS, B., "The Compressive Strength of Composites with Kinked, Misaligned and Poorly Adhering Fibres". *Journal of Materials Science*, Vol. 16, 1981, pp. 2831-2836.

MELANITIS, N. and GALIOTIS, C., "Compressional Behaviour of Carbon Fibres. Part I: A Raman Spectroscopic Study". *Journal of Materials Science*, Vol. 25, No. 12, December 1990, pp. 5081-5090.

MRSE, A. and PIGGOT, M.R., "Relation Between Fibre Divagation and Compressive properties of Fibre Composites". Proceedings of the 35th International SAMPE Symposium, Anaheim, April 2-5 1990, pp. 2236-2244.

MRSE, A. and PIGGOT, M.R., "Mechanism of Compressive Failure in Fibre Composites". Proceedings of the First International Conference on Deformation and Fracture of Composites, March 25-27, 1991, University of Manchester, Manchester, UK, Plastics and Rubber Institute, London, pp. 8/1-8/7.

NORITA, T., KITANO, A. and NOGUCHI, K., "Compressive Strength of Fibre Reinforced Composite Materials - Effect of Fibre Properties". Proceedings of the Fourth Japan-U.S. Conference on Composite Materials, June 27-29, 1988, Washington, D.C., Technomic Publishing Company Inc., Lancaster, Pennsylvania, 1988, pp. 548-557.

Normenstelle Luftfahrt im DIN Deutsches Institut für Normung e. V., DIN 29971/5.1.2.8, "Druckfestigkeit und Elastizitätsmodul aus Druckversuch (Compression Strength and Modulus of Elasticity in Compression)". April 1987.

ODOM, E.M. and ADAMS, D.F., "Failure Modes of Unidirectional Carbon/Epoxy Composite Compression Specimens". *Composites*, Vol. 21, Number 4, July 1990, pp. 289-296.

PARRY, T.V. and WRONSKY, A.S., "Kinking and Compressive Failure in Uniaxially Aligned Carbon Fibre Composite Tested Under Superposed Hydrostatic Pressure". *Journal of Materials Science*, Vol.17, 1982, pp. 893-900.

PIGGOT, M.R. and WILDE, P., "Compressive Strength of Aligned Steel Reinforced Epoxy Resin". *Journal of Materials Science*, Vol 15, 1980, pp. 2811-2815.

PIGGOT, M.R., and HARRIS, B., "Compression Strength of Carbon, Glass and Kevlar-49 Fibre-Reinforced Polyester Resins". *Journal of Materials Science*, Vol. 15, 1980, pp. 2523-2538.

PIGOTT, M.R., "A Theoretical Framework for the Compressive Properties of Aligned Fibre Composites". *Journal of Materials Science*, Vol. 16, 1981, pp. 2837-2845.

PINNELL, M.F., KNIGHT, M. and PINNELL, W.B., "A Fractographic and Experimental Analysis of Composite Compression Test Methods". Proceedings of the American Society for Composites - Fifth Technical Conference: "*Composite Materials in Transition*". Technomic Publishing Company Inc., Lancaster, Pennsylvania, 1990, pp. 819-826.

POON, C., LEE, S., GOULD, R. and SCOTT, R.F., "Compression Testing of Advanced Composite Laminates". Proceedings of the 34th International SAMPE Symposium, Anaheim, May 8-11 1989, pp. 2498-2505.

PORT, K.F., "The Compressive Strength of Carbon Fibre-Reinforced Plastics". Royal Aircraft Establishment, Technical Report 82083, 1982.

POTTER, R.T., "Some Fractographic Investigations of Compressive Failures in Carbon Fibre-Reinforced Plastics". Royal Aircraft Establishment, Technical Report 86049, 1986.

PRANDY, J.M. and HAHN H.T., "Compressive Strength of Carbon Fibers". Proceedings of the 35th International SAMPE Symposium, Anaheim, April 2-5, 1990, pp. 1657-1670.

PURSLOW, D. and COLLINGS, T.A., "A Test Specimen for Compression Strength and Modulus of Unidirectional Carbon Fibre Reinforced Plastic Laminates". Royal Aircraft Establishment, Technical Report 72096, 1972.

PURSLOW, D., "Some Fundamental Aspects of Composites Fractography". *Composites*, Vol. 12, October 1981, pp. 241-247.

REISS, R., YAO, T.-M., and CLARK, R.K., "Effect of Load Introduction in Compression Testing of Composite Laminates". *Compression Testing of Homogeneous Materials and Composites, ASTM STP 808*, Richard Chait and Ralph Papirno, Eds., American Society for Testing and Materials, 1983, pp. 200-220.

ROSEN, B.W., "Mechanics of Composite Strengthening". *Fiber Composite Materials*, American Society of Metals, 1964, pp. 58 ff.

RYDER, J.T. and BLACK, E.D., "Compression Testing of Large Gauge Length Composite Coupons". *Composite Materials; Testing and Design (Fourth Conference), ASTM STP 617*, American Society for Testing and Materials, 1977, pp. 170-189.

SADOWSKY,M.A., PU, S.L. and HUSSAIN, M.A., "Buckling of Microfibres". *Journal of Applied Mechanics*, December 1967, pp. 1011-1016.

SCHUERCH, H., "Prediction of Compressive Strength in Uniaxial Boron Fibre-Metal Matrix Composite Materials". *Journal of the American Institute of Aeronautics and Astronautics*, Vol. 4, No. 1, January 1966, pp. 102-106.

SHUART, M.J., "An Analysis of Shear Failure Mechanisms for Compression-Loaded $[\pm 0]_S$ Laminates". *Journal of Composite Materials*, Vol. 23, March 1989, pp. 251-263.

SHUART, M.J., "An Evaluation of the Sandwich Beam Compression Test Method for Composites". *Test Methods and Design Allowables for Fibrous Composites, ASTM STP 734*, C.C. Chamis, Ed; American Society for Testing and Materials, 1981, pp. 152-165.

SINCLAIR, J.H. and CHAMIS, C.C., "Compressive Behavior of Unidirectional Fibrous Composites". *Compression Testing of Homogeneous Materials and Composites, ASTM STP 808*, Richard Chait and Ralph Papirno, Eds., American Society for Testing and Materials, 1983, pp. 155-174.

SMOOT, M.A., "Compressive Response of Hercules AS1/3501-6 Graphite/Epoxy Composites". Report No. CCM-82-16, Centre for Composite Materials, University of Delaware, Newark 1982.

SOUTIS, C. and FLECK, N.A., "Investigation of the Compressive Strength of CFRP Under Static Loading". Report of the Cambridge University Engineering Department, CUED/C-MAT/TR, January 1988.

SOUTIS, C., "Measurement of the Static Compressive Strength of Carbon Fibre-Epoxy Laminates". *Composites Science and Technology*, Vol. 42, No. 4, 1991, pp. 373-392.

STEIF, P.S., "A Simple Model for the Compressive Failure of Weakly Bonded, Fiber-Reinforced Composites". *Journal of Composite Materials*, Vol. 22, Sept. 1988, pp. 818-828.

Suppliers of Advanced Composite Materials Association, Recommended Method SRM 1-88: SACMA *Recommended Test Method for Compressive Properties of Oriented Fibre-Resin Composites*, Washington, DC, 1989.

SWANSON, S.R., COLVIN, G.E. Jr. and HASLAM, C.L., "Measurements of the Compression Behavior of AS4/3501-6 and IM7/8551-7 Carbon/Epoxy". Proceedings of the 33rd International SAMPE Symposium, March 7-10, 1988, pp. 1571-1581.

SWIFT, D.G., "Elastic Moduli of Fibrous Composites Containing Misaligned Fibres". *Journal of Physics. D: Applied Physics*, Vol. 8, 1975, pp. 223-240.

TAN, S.C., "Stress Analysis and the Evaluation of Celanese and IITRI Compression Test Specimens". Proceedings of the American Society for Composites - Fifth Technical Conference: "*Composite Materials in Transition*". Technomic Publishing Company Inc., Lancaster, Pennsylvania, 1990, pp. 827-838.

TIMOSHENKO, S.P. and GERE, J.M., *Theory of Elastic Stability*. Second Edition, McGraw-Hill, 1961.

TSAI, S.W. and HAHN, H.T., *Introduction to Composite Materials*. Technomic Publishing Company, Westport, Connecticut, 1980, pp. 416 ff.

TSUSHIMA, E., "Intrinsic Strength of Carbon Fiber by Loop Testing". *SAMPE Quarterly*, 1989, pp. 2042-2053.

WANG, A.S.D., "A Non-Linear Microbuckling Model Predicting the Compressive Strength of Unidirectional Composites". American Society of Mechanical Engineers (ASME) Paper No. 78-WA/Aero-1, presented at the Winter Annual Meeting, San Francisco, Calif., Dec 10-15, 1978, pp.3-8.

WEAVER, C.W., and WILLIAMS, J.G., "Deformation of a Carbon-Epoxy Composite Under Hydrostatic Pressure". *Journal of Materials Science*, Vol. 10, 1975, 1323-1333.

WESTBERG, R.L. and ABDALLAH, M.G., "An Experimental and Analytical Evaluation of Three Compressive Test Methods for Unidirectional Graphite/Epoxy Composites". Report No. RI-86B12100, Hercules Inc., Magna, Utah, May 1987.

WHITNEY, J.M. and GUIHARD S.K., "Failure Modes in Compression Testing of Composite Materials". Proceedings of the 36th International Sampe Symposium, San Diego, April 15-18, 1991, pp. 1069-1078.

WILKINSON, E., PARRY, T.V., and WRONSKI, A.S., "Compressive Failure in Two Types of Carbon Fibre-Epoxide Laminates". *Composites Science and Technology*, Vol. 26, 1986, pp. 17-29.

WISNOM M.R., "The Effect of Specimen Size on the Bending Strength of Unidirectional Carbon Fibre-Epoxy". *Composite Structures*, Vol. 18, 1991, pp. 47-63.

WISNOM, M.R., "The Effect of Fibre Misalignment on the Compressive Strength of Unidirectional Carbon Fibre/Epoxy. *Composites*, Vol. 21, No. 5, September 1990, pp. 403-407.

WOOLSTENCROFT, D. H., HARESCEUGH, R.I. and CURTIS, A.R., "The Compressive Behaviour of Carbon Fibre-Reinforced Plastic". *Progress in Science and Engineering of Composites*, T. Hayashi, K. Kawata and S. Umekawa, Eds., ICCM-IV, Tokyo, 1982, pp. 439-445.

WOOLSTENCROFT, D.H., CURTIS, A.R. and HARESCEUGH, R.I., "A Comparison of Test Techniques Used for the Evaluation of the Unidirectional Compressive Strength of Carbon Fibre Reinforced Plastic". *Composites*, Vol. 12, No. 4, October 1981, pp. 275-281.

WRONSKY, A.S., and PARRY, T.V., "Compressive Failure and Kinking in Uniaxially Aligned Glass-Resin Composite Under Superposed Hydrostatic Pressure". *Journal of Materials Science*, Vol.17, 1982, pp. 3656-3662.

YEH, J.R., and TEPLY, J.L., "Compressive Response of Kevlar/Epoxy Composites". *Journal of Composite Materials*, Vol. 22, March 1988, pp. 245-257.

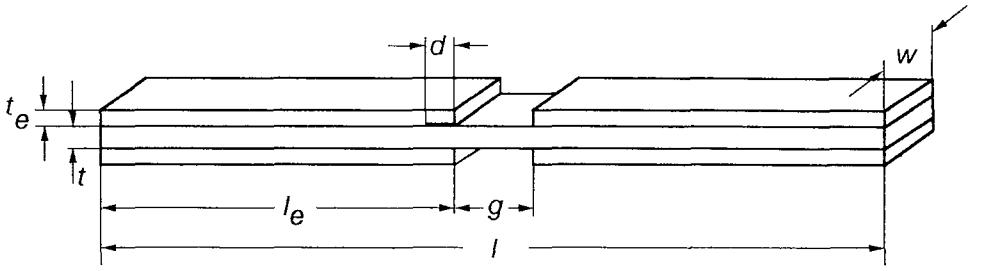
YUGARTIS, S.W., "Measurement of Small Angle Fibre Misalignments in Continous Fibre Composites". *Composites Science and Technology*, Vol. 30, 1987, pp. 279-293.

FIGURES

F-1 to F-18

Note :

C1: Signal of the strain gauge facing the operator



t	nominal laminate thickness	t_e	thickness of end tab
l	test piece length	g	gauge length
w	test piece width	d	length of debond insert (if applicable)
l_e	length of end tab		

Tabbing material: woven cross-ply glass fibre/epoxy

Test Method	t	l	w	l_e	t_e	g	d
CRAG	2	110	10	50	1.7/2.2	10	-
BAe	2	110	10	50	1.7	10	-
IITRI	2	132.5	12.5	60	1.7	12.5	-
ASTM D695[1]	2	75	10	35	2.2	5	-
ASTM D695[2]	1	75	10	35	1.7	5	-
ICSTM (standard)	2	90	10	40	1.7	10	-
ICSTM (insert)	2	90	10	40	1.7	10	5

All dimensions in mm

Figure F-1: *Compression test piece dimensions.*

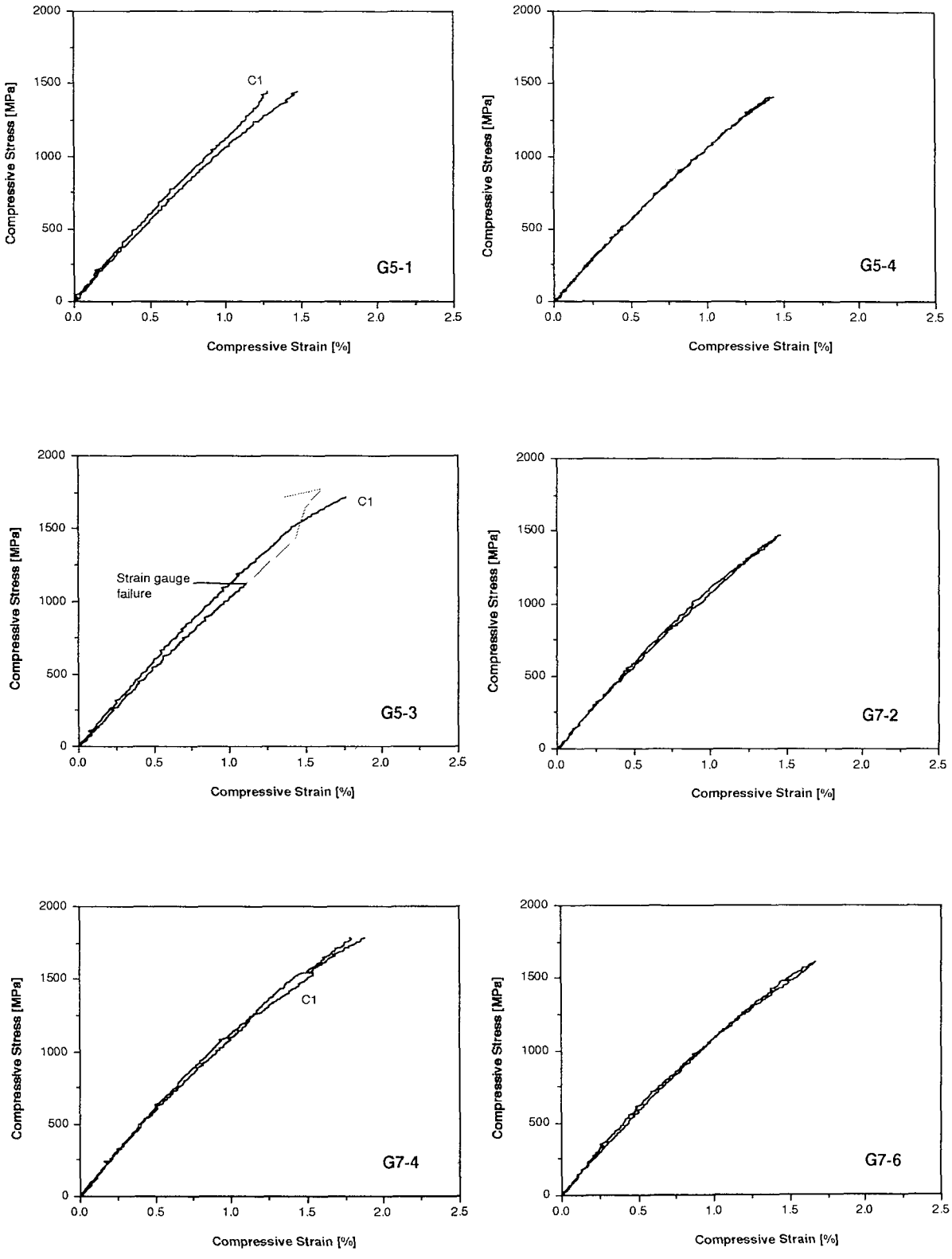


Figure F-2: Stress-strain curves of unidirectional XAS/914C using the ICSTM compression test method with standard test piece; gauge lengths 5 and 7.5 mm.

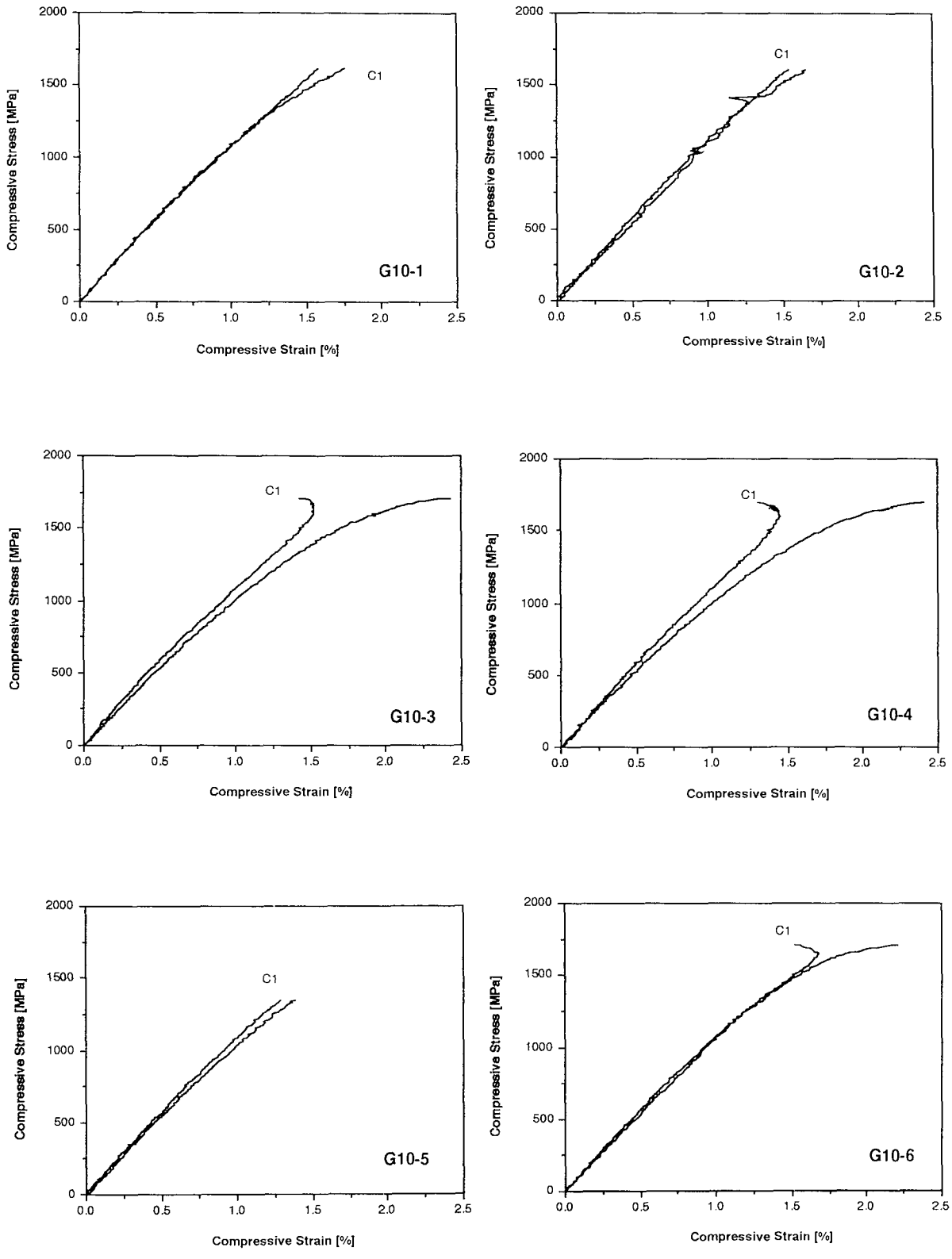


Figure F-3: Stress-strain curves of unidirectional XAS/914C using the ICSTM compression test method with standard test piece; gauge length 10 mm.

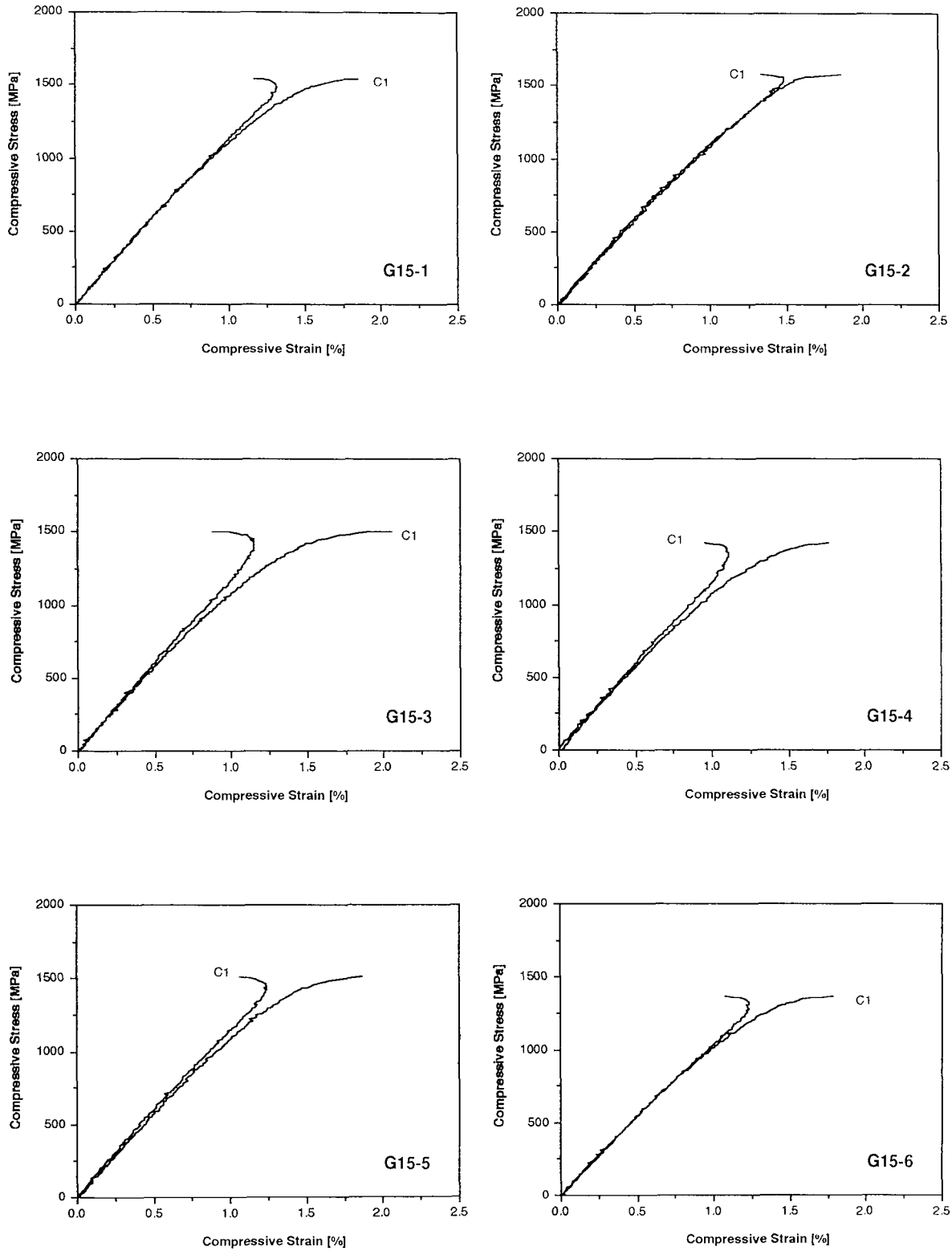


Figure F-4: Stress-strain curves of unidirectional XAS/914C using the ICSTM compression test method with standard test piece; gauge length 15 mm.

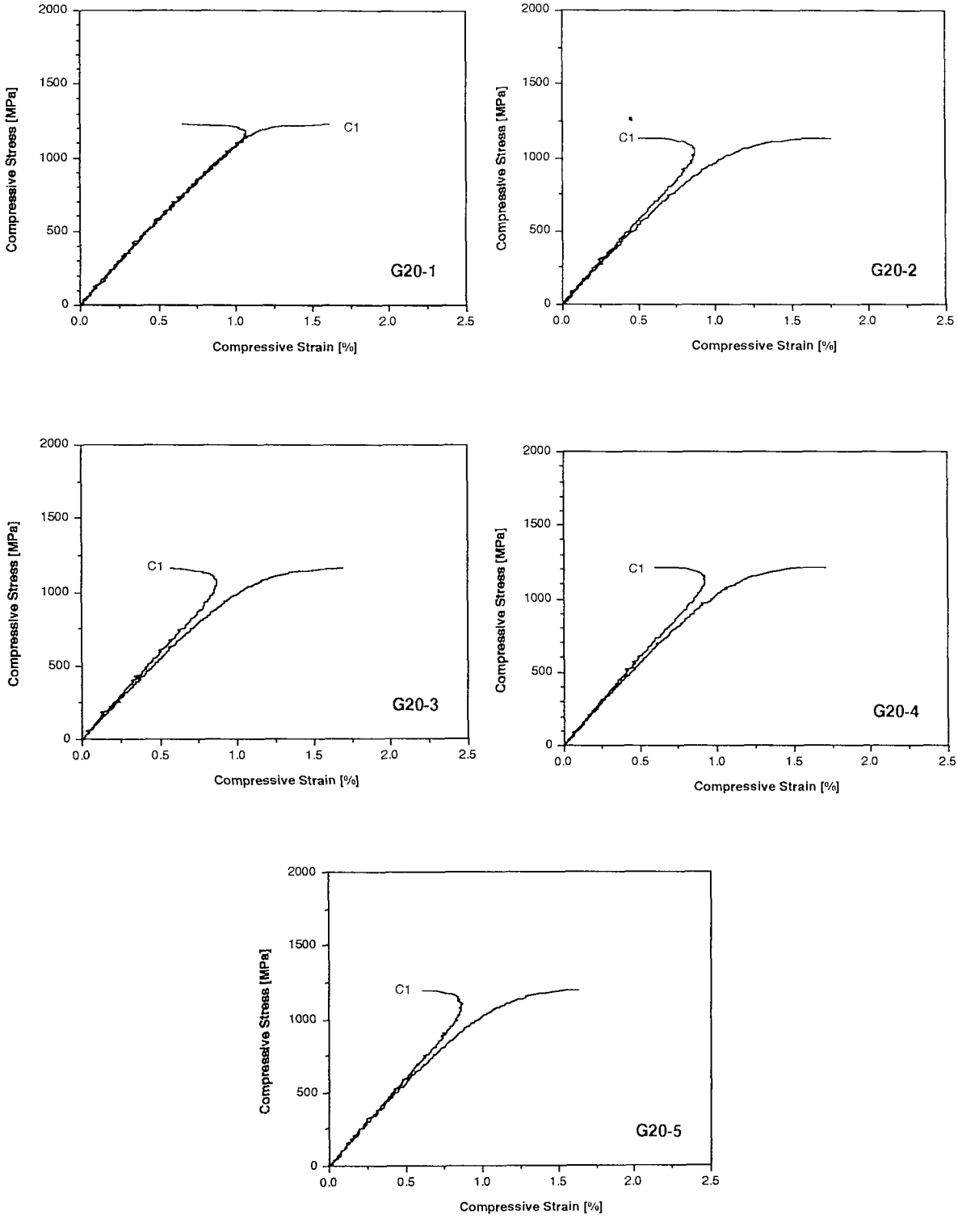


Figure F-5: *Stress-strain curves of unidirectional XAS/914C using the ICSTM compression test method with standard test piece; gauge length 20 mm.*

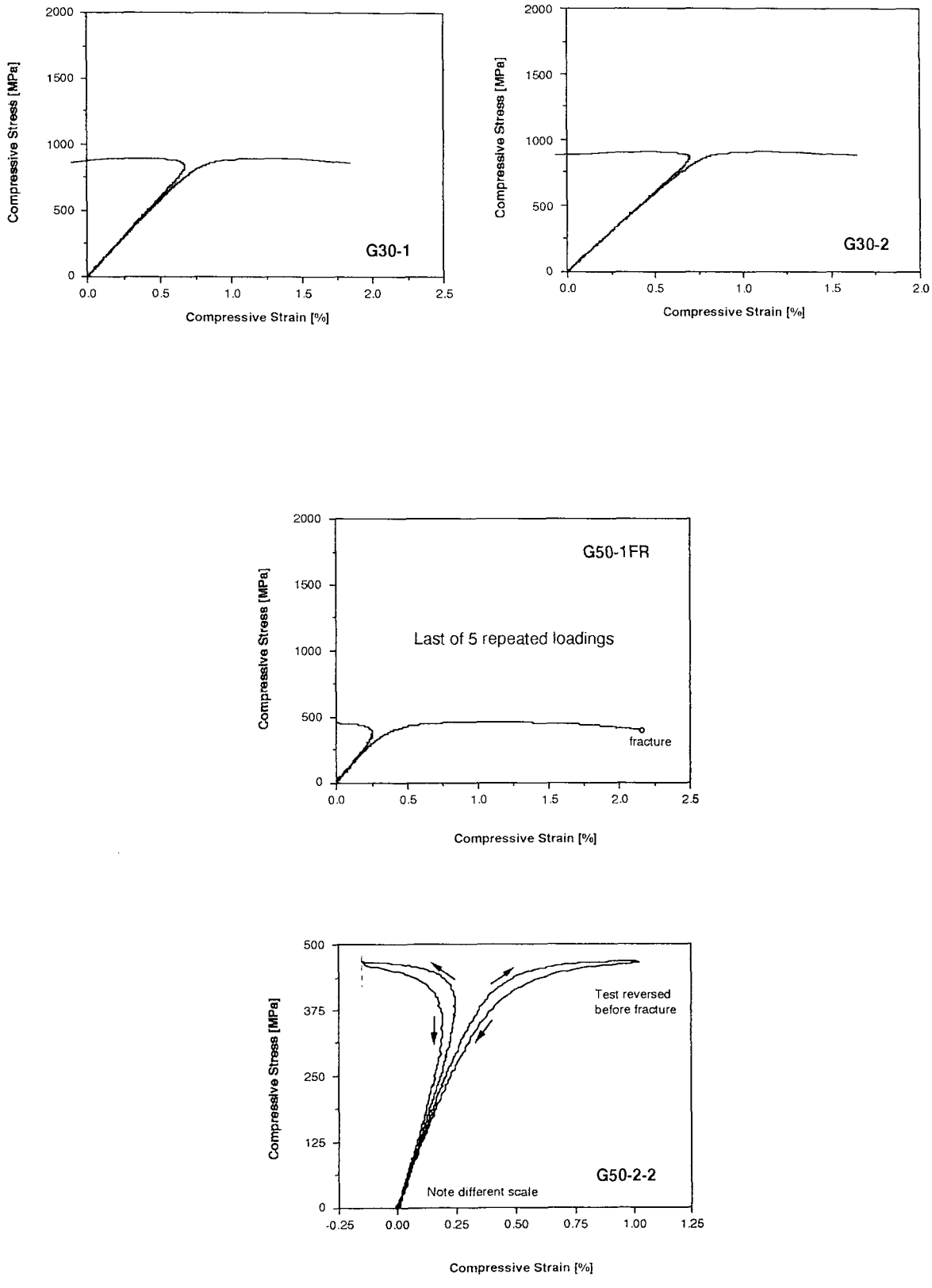


Figure F-6: Stress-strain curves of unidirectional XAS/914C using the ICSTM compression test method with standard test piece; gauge length 30 and 50 mm.

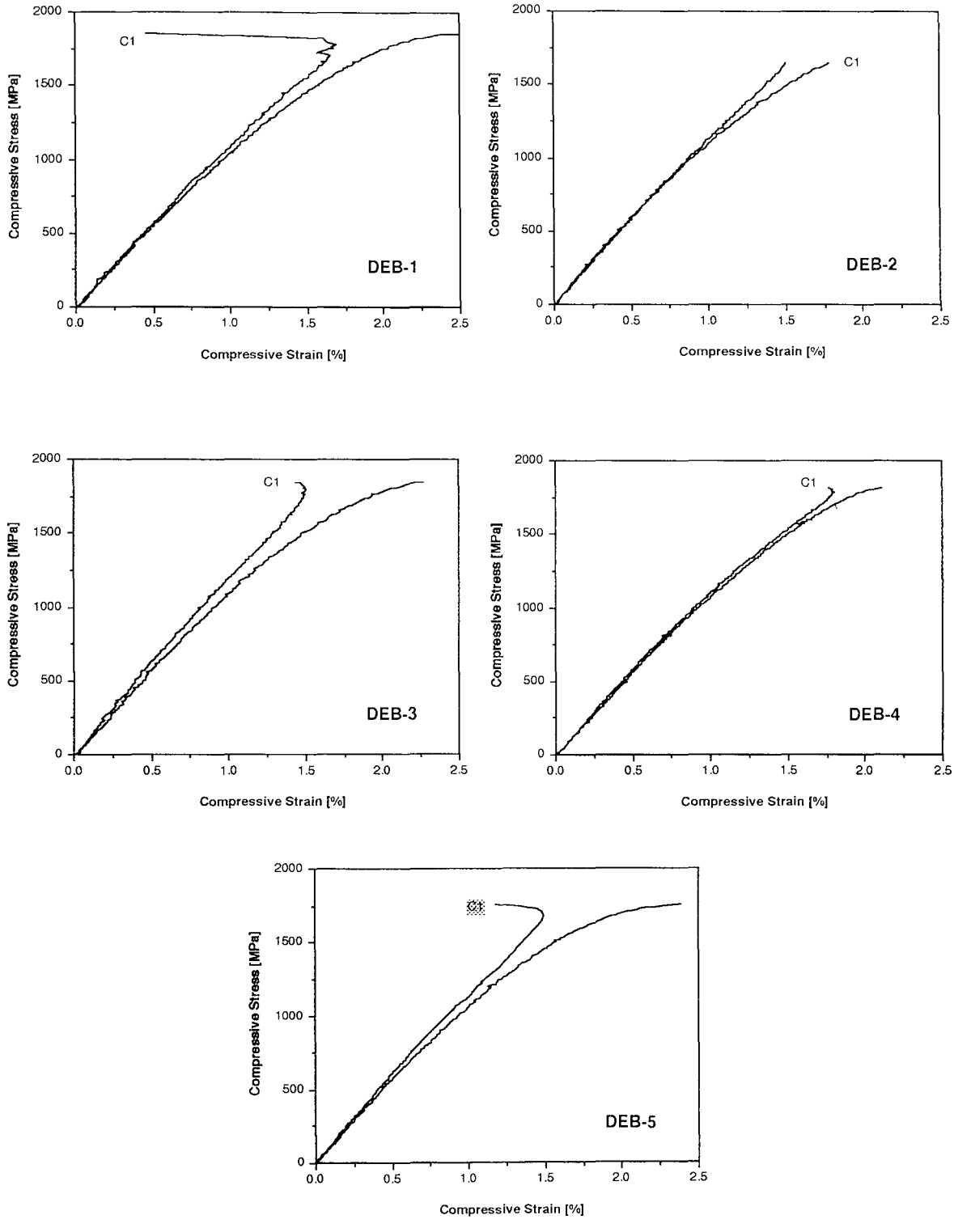


Figure F-7: *Stress-strain curves of unidirectional XAS/914C using the ICSTM compression test method; test piece gauge length 10 mm; initial debond by bending.*

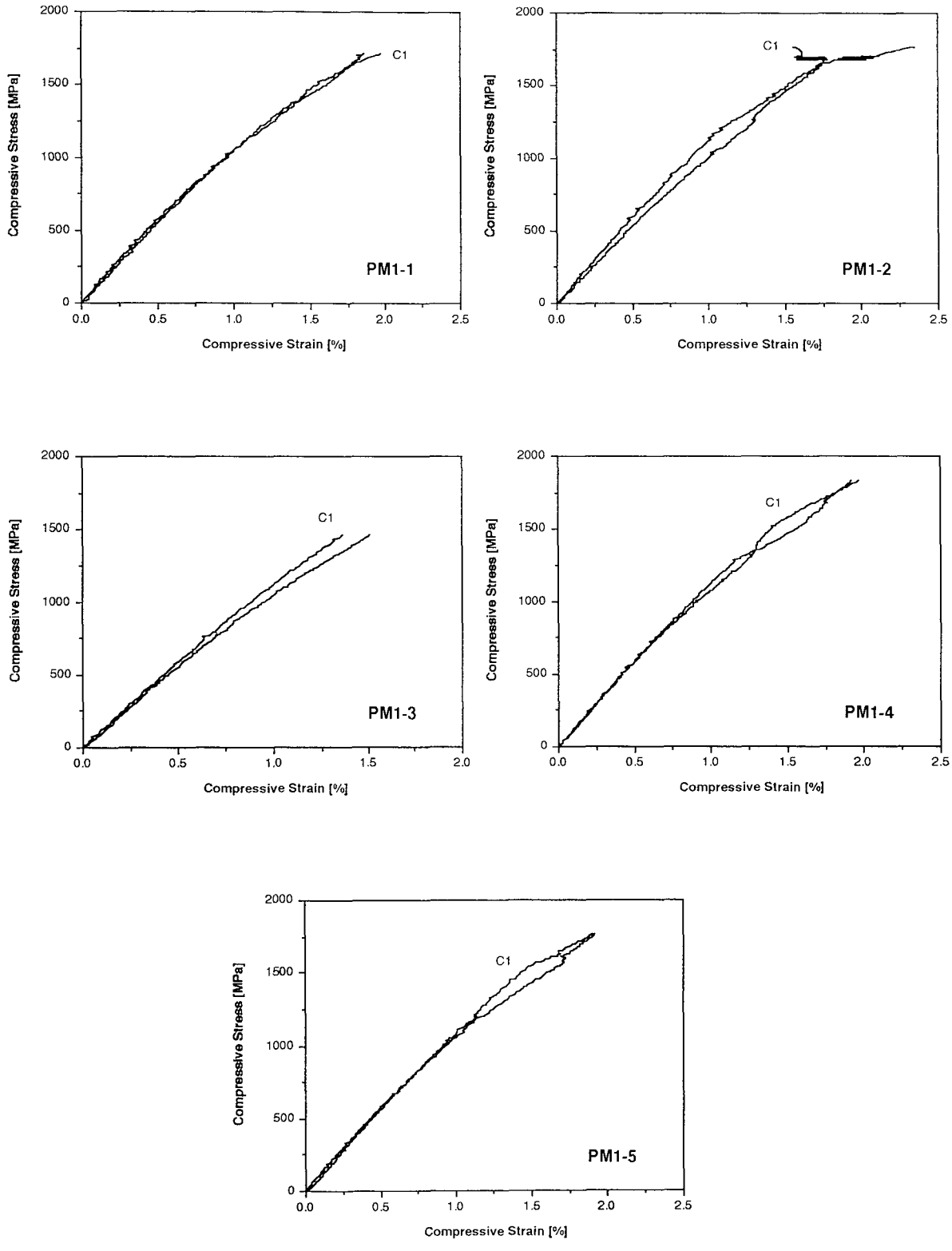


Figure F-8: Stress-strain curves of quasi-unidirectional XAS/914C using the ICSTM compression test method; quasi-unidirectional lay-up$[(\pm 1°)_4]_S$; 10 mm gauge length.

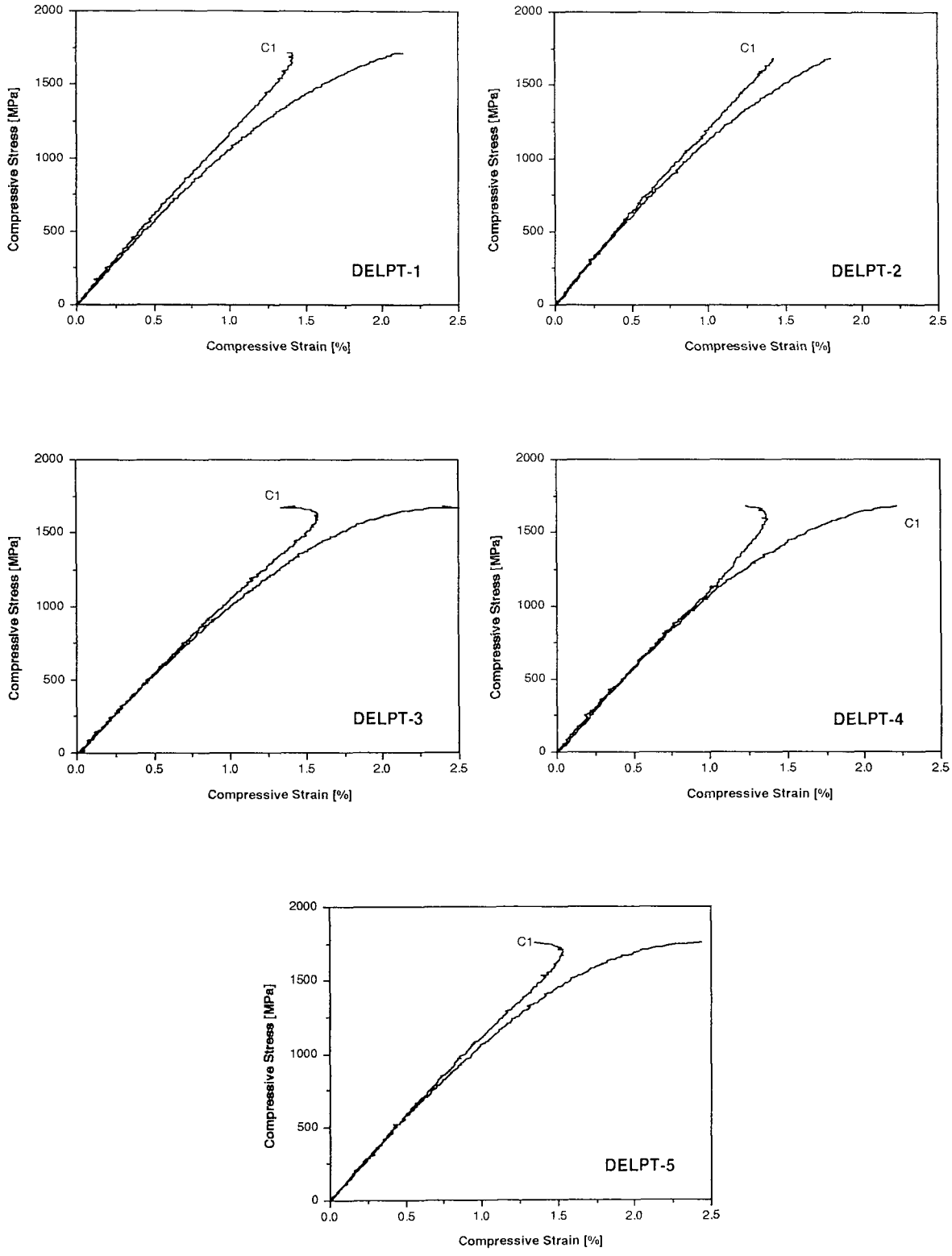


Figure F-9: Stress-strain curves of unidirectional XAS/914C using the ICSTM compression test method; test piece gauge length 10 mm; tap tip debond by inserting a 5 mm strip of PTFE tape.

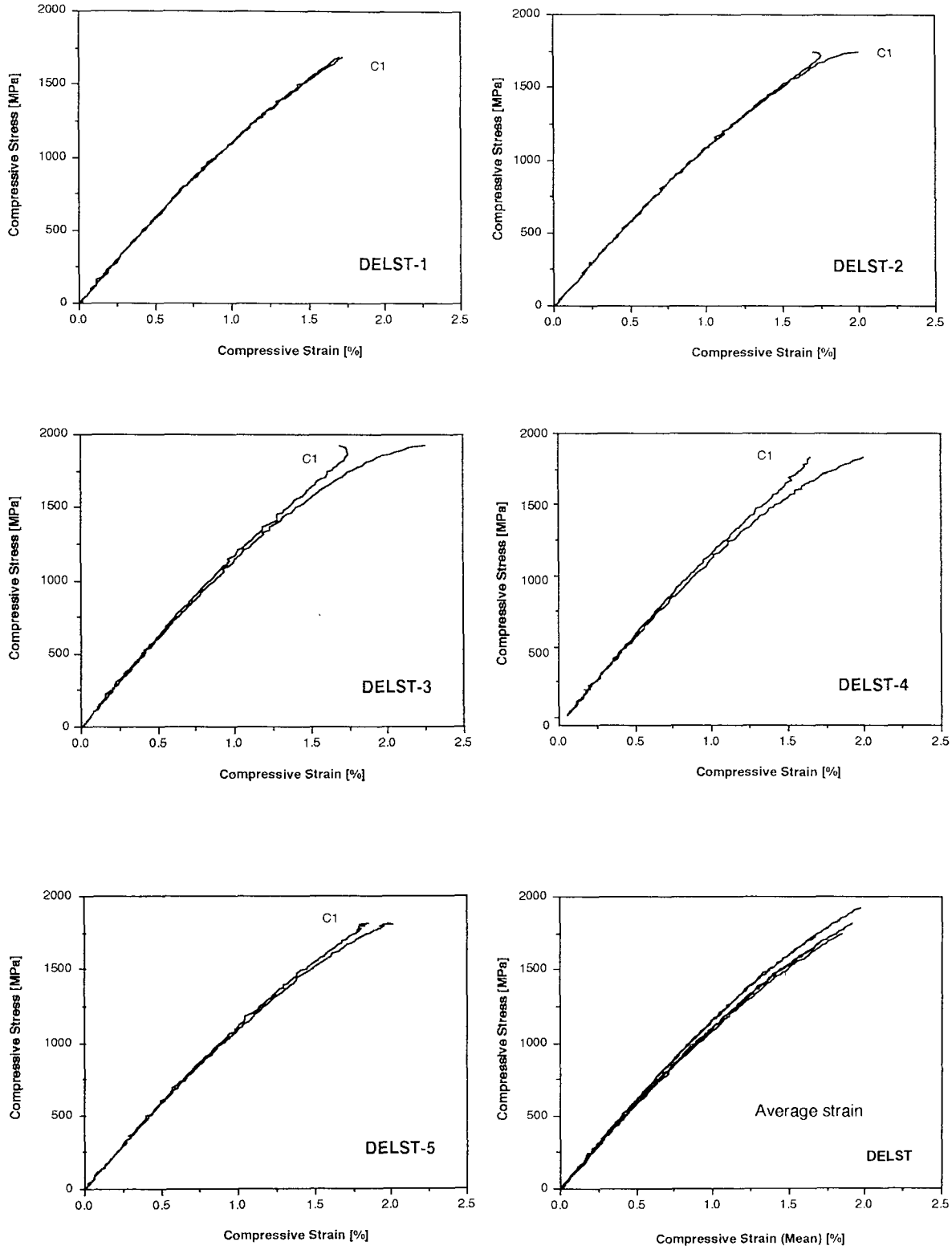


Figure F-10: *Stress-strain curves of unidirectional XAS/914C using the ICSTM compression test method; test piece gauge length 10 mm; tap tip debond by inserting a 5 mm strip of cellulose adhesive tape.*

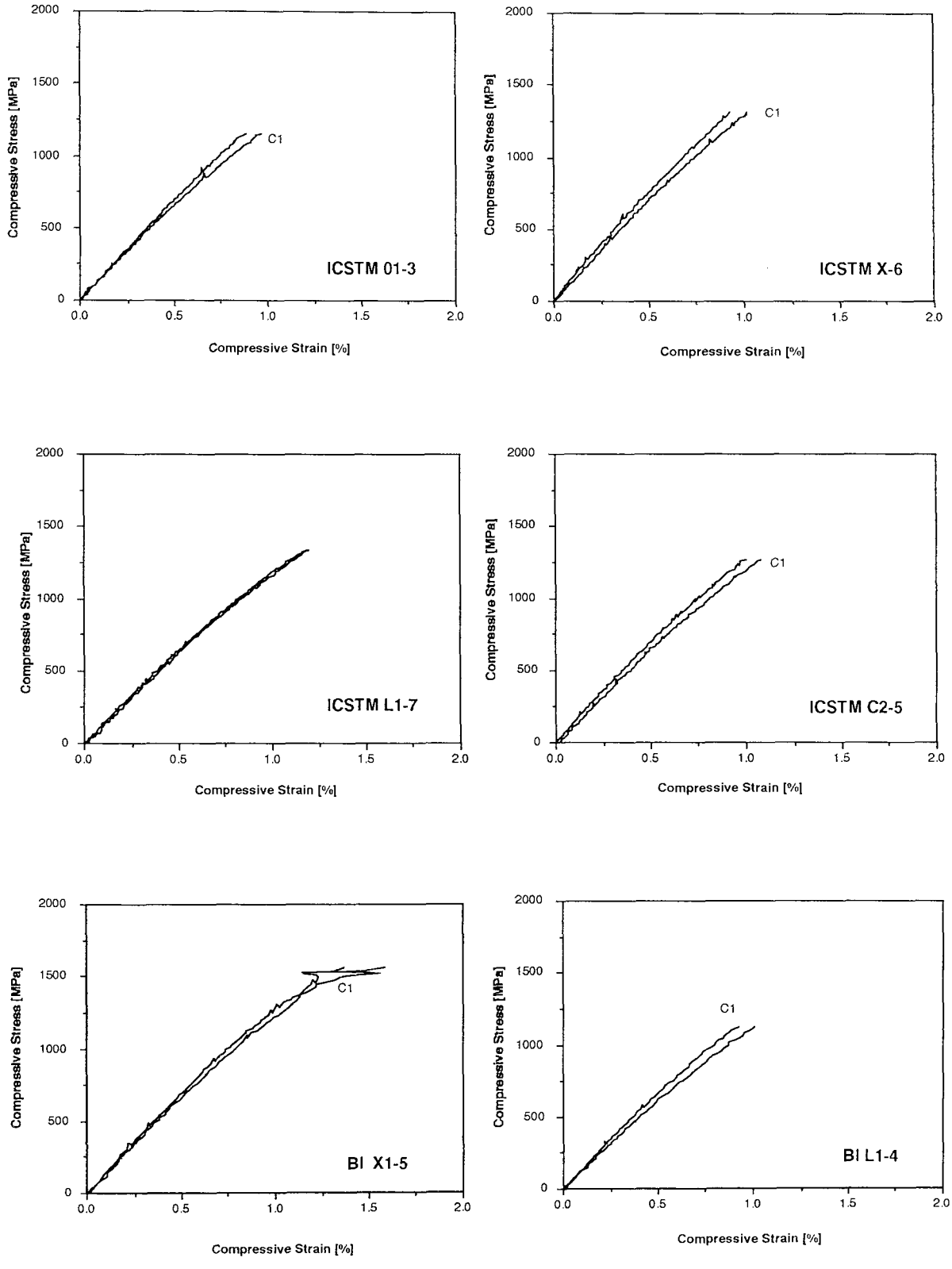


Figure F-11: Some typical stress-strain curves of unidirectional Apollo/9106C with different levels of fibre surface treatment using the ICSTM and the Birmingham (BI) method.

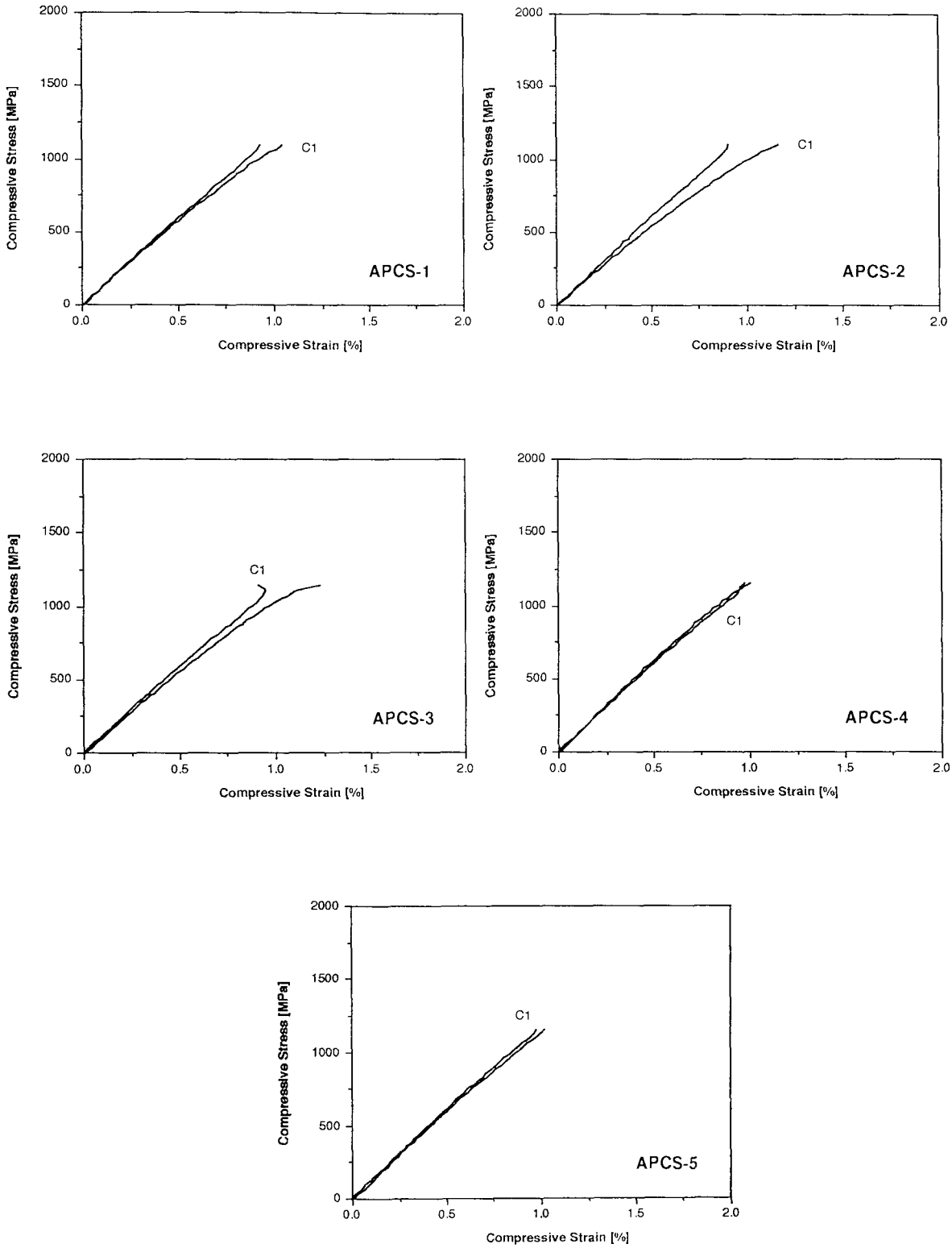


Figure F-12: *Stress-strain curves of unidirectional APC-2 using the ICSTM compression test method; test piece 10 mm machined gauge section.*

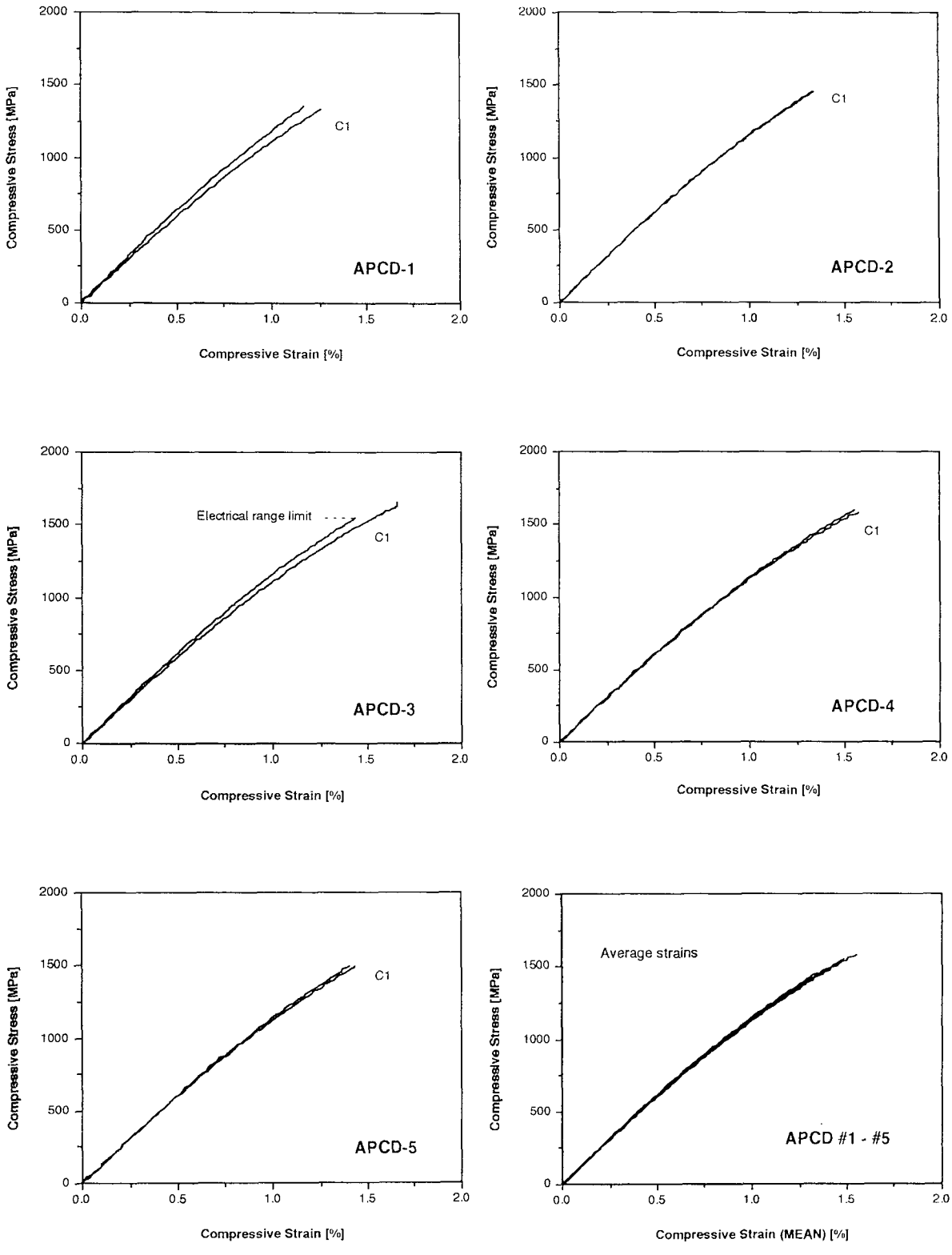


Figure F-13: *Stress-strain curves of unidirectional APC-2 using the ICSTM compression test method; test piece gauge length 10 mm with 5 mm debond (cellulose tape) insert.*

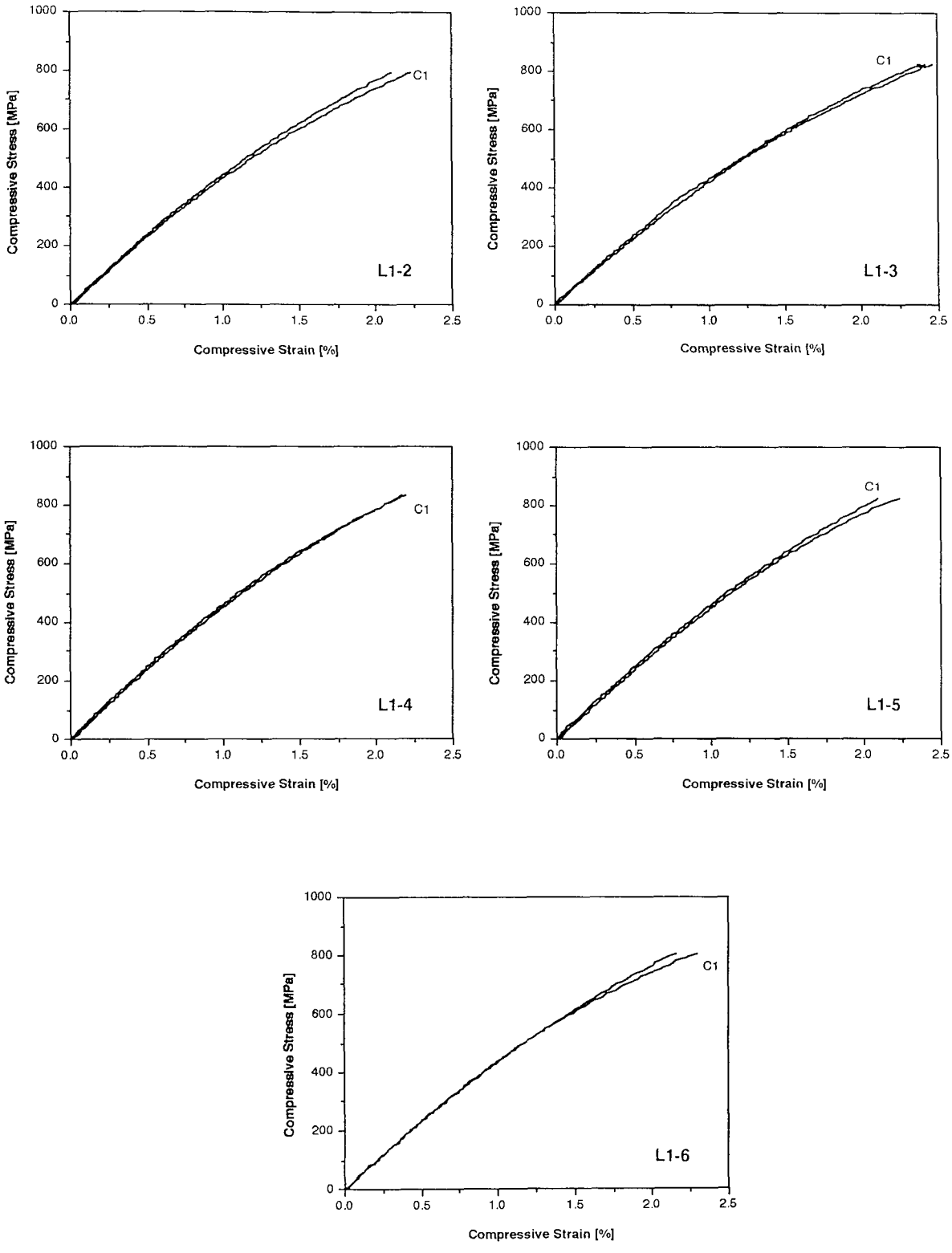


Figure F-14: *Stress-strain curves of quasi-isotropic XAS/914C (laminate L1) using the ICSTM compression test method with sandwiched test piece.*

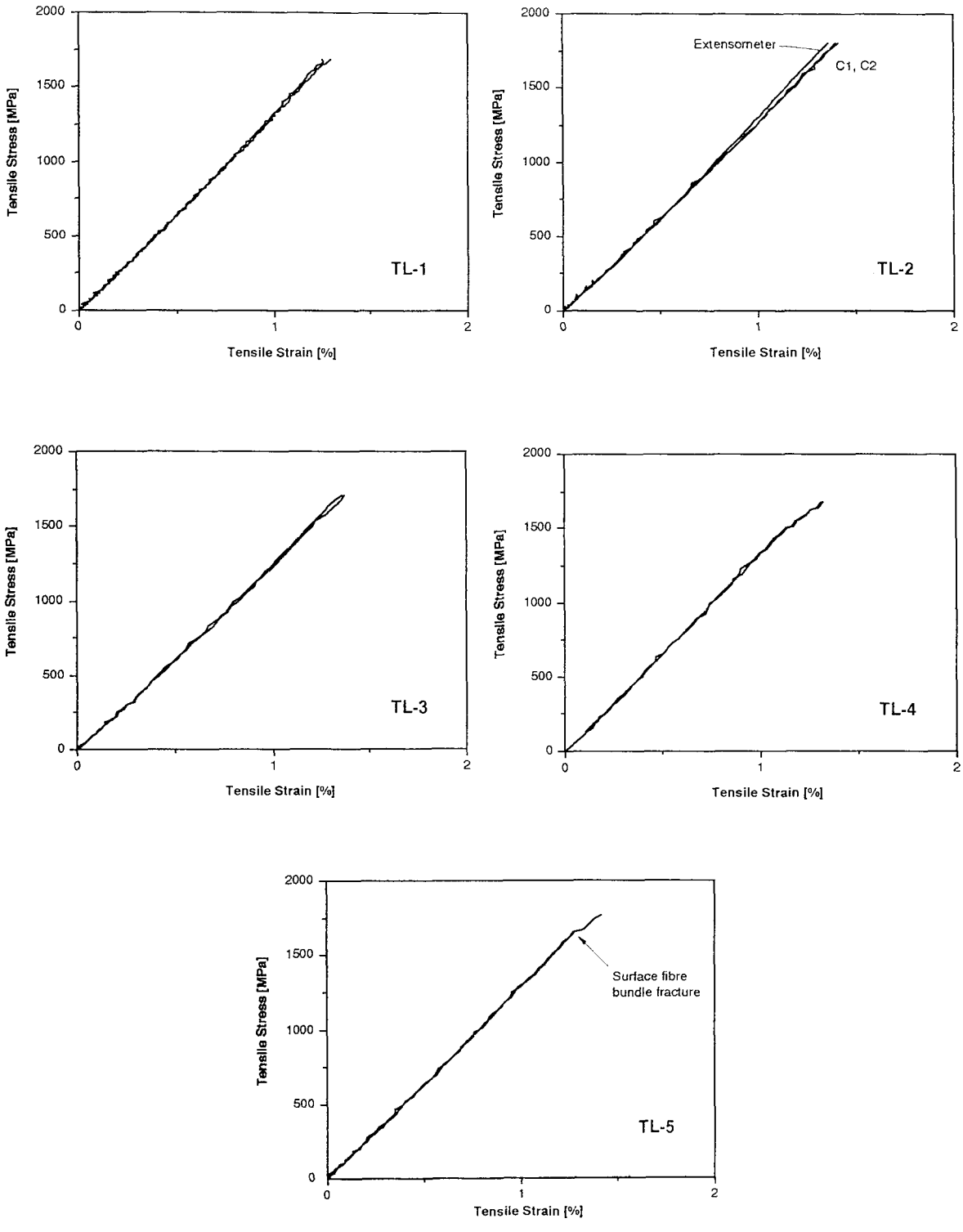


Figure F-15: *Stress-strain curves of unidirectional XAS/914C; tension tests.*

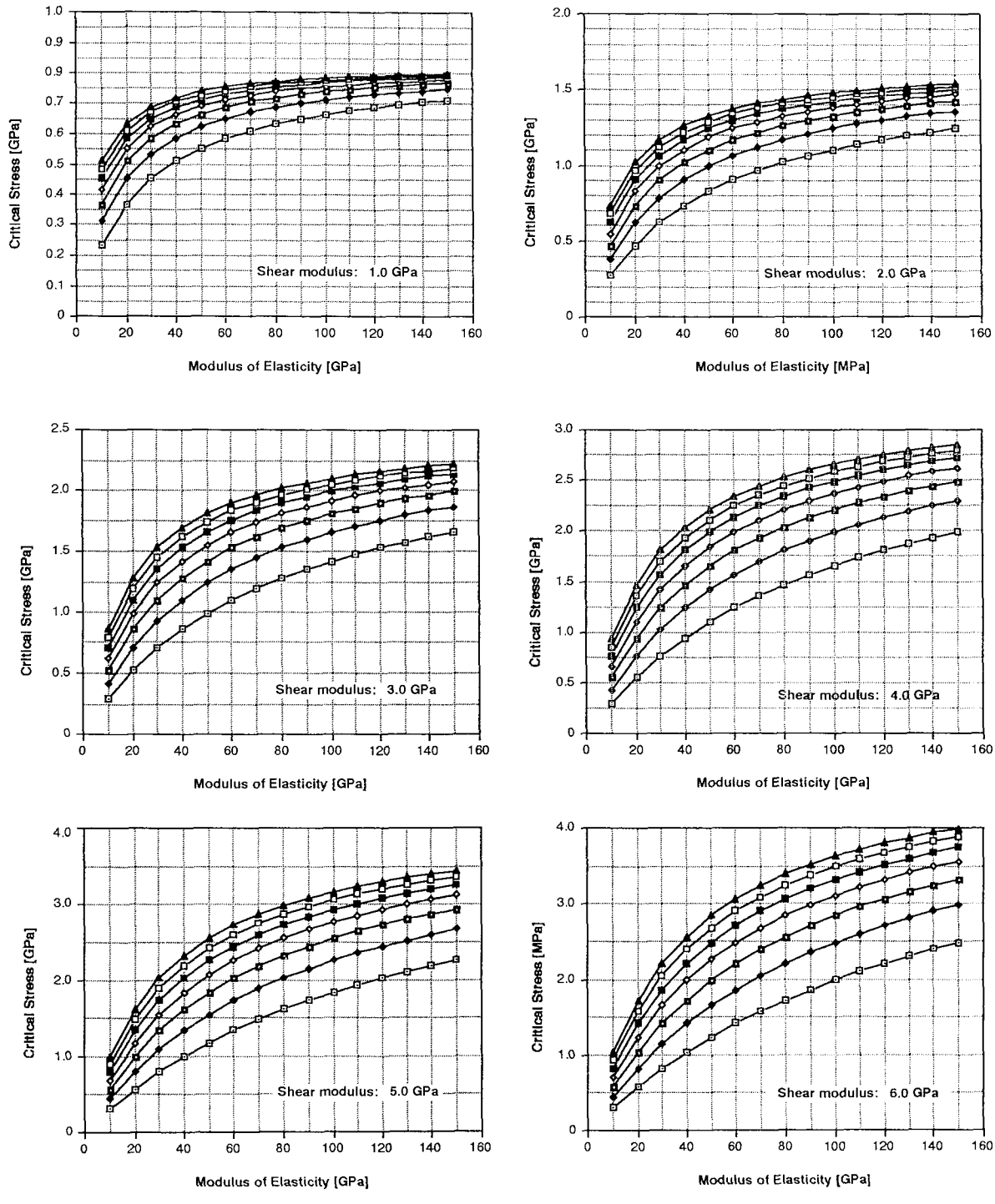


Figure F-16: Critical compressive stress versus longitudinal modulus of elasticity for different clamping conditions for an orthotropic column with rectangular cross-section of 2 mm thickness and 10 mm unsupported length.

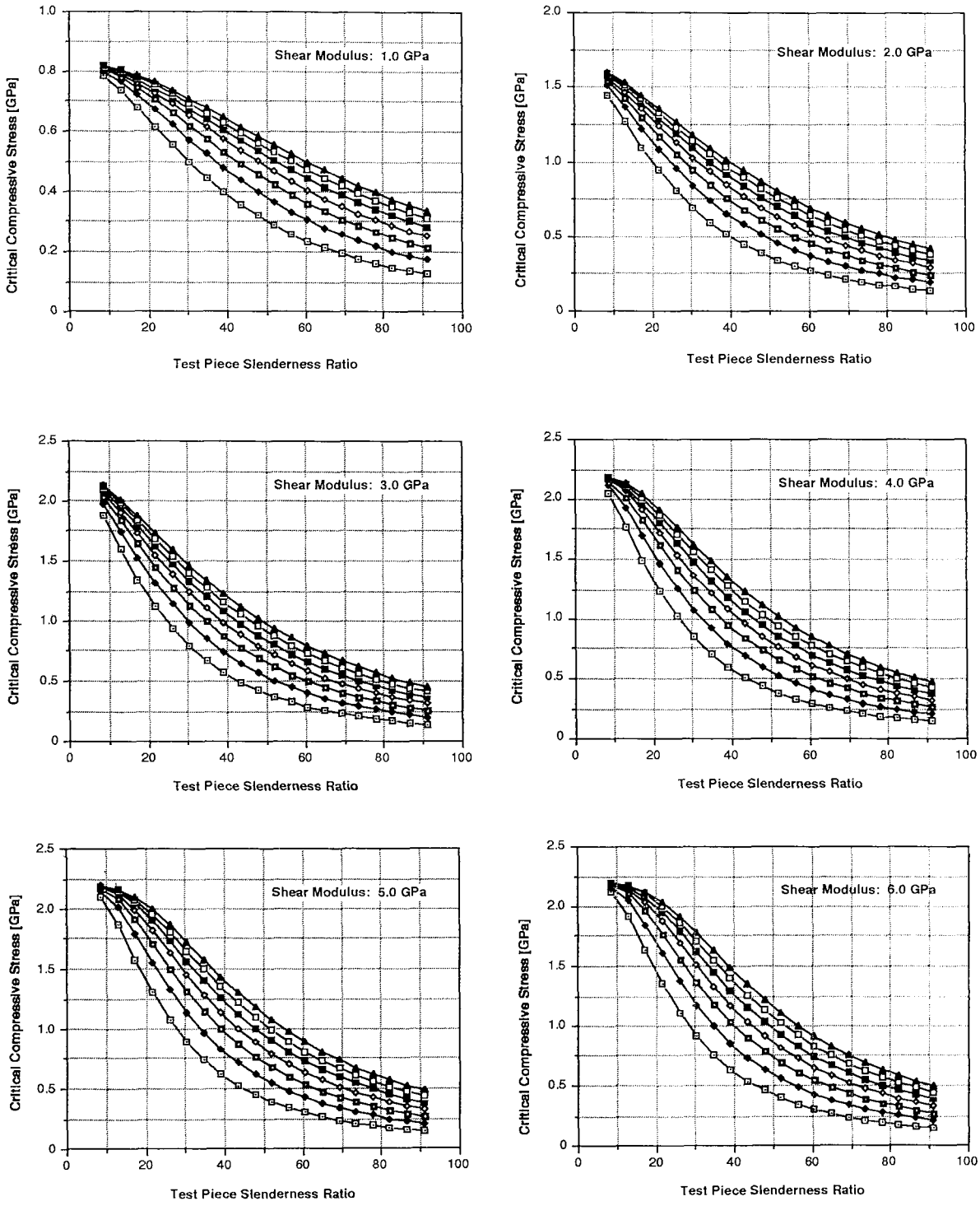


Figure F-17: Critical compressive stress versus test piece slenderness ratio for different clamping conditions for an orthotropic column with rectangular cross-section.

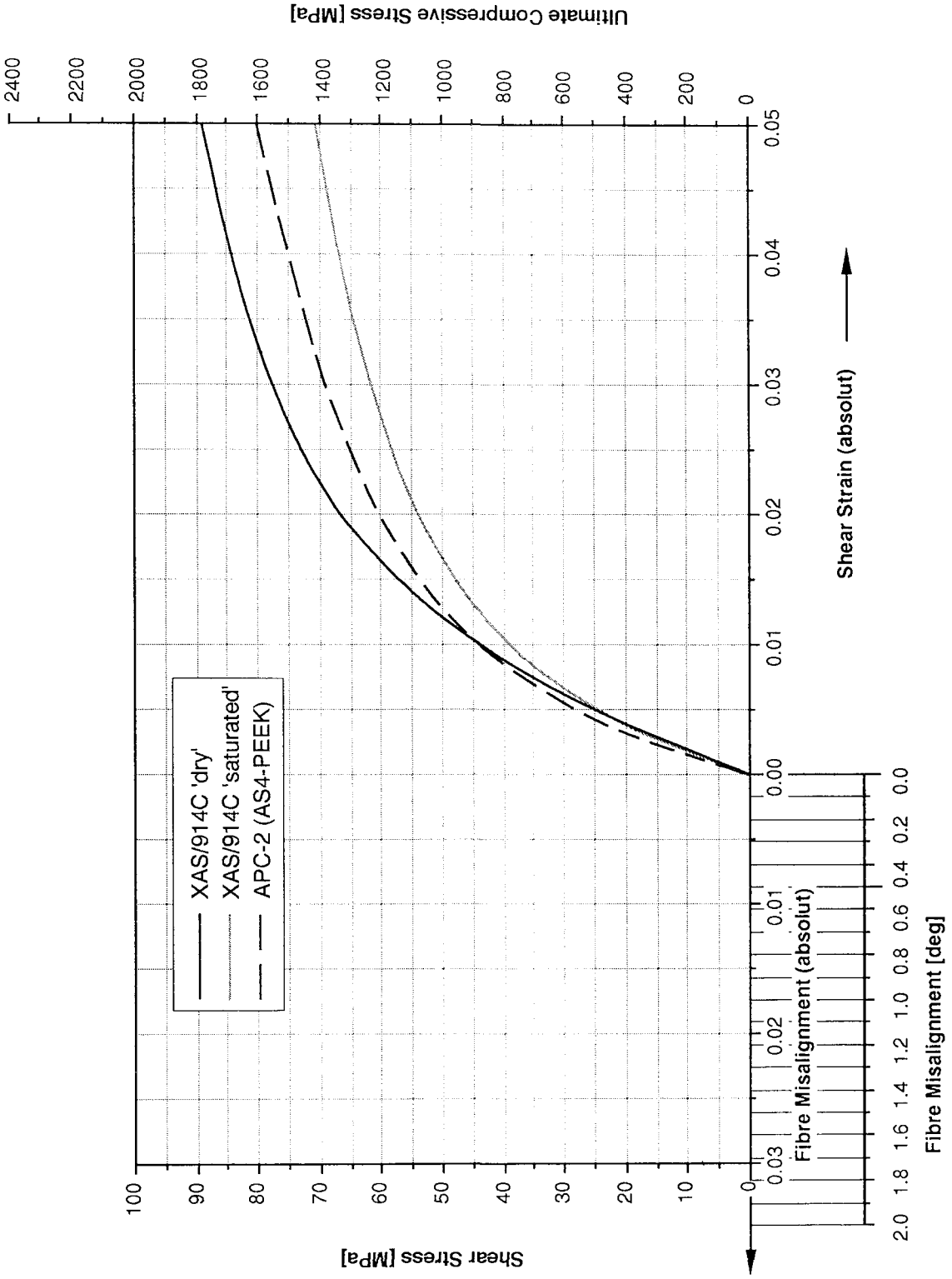
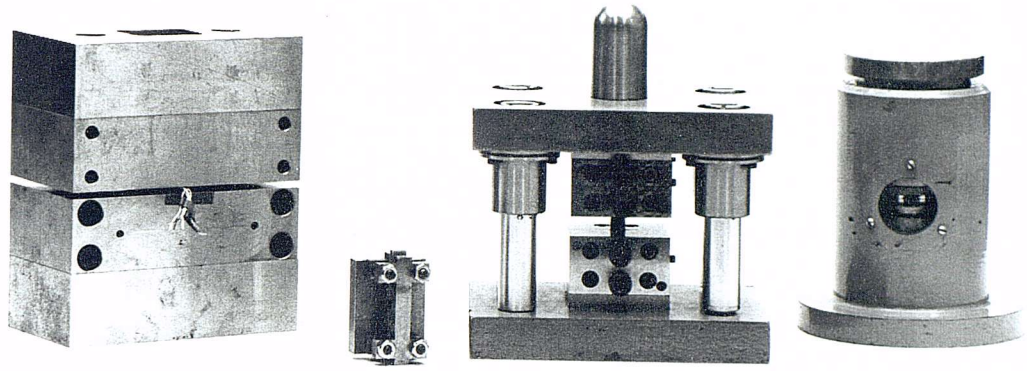


Figure F-18: *Chart for graphical solution of compressive strength for a given angle of misalignment; shear curves of XAS/914C ('dry' and 'saturated') and APC-2 are given.*

PHOTOGRAPHS

Figures P-1 to P-21



IITRI *ASTM D695 modified* *ICSTM* *CRAG*

***Figure P-1**: Various compression test jigs; same scale.*

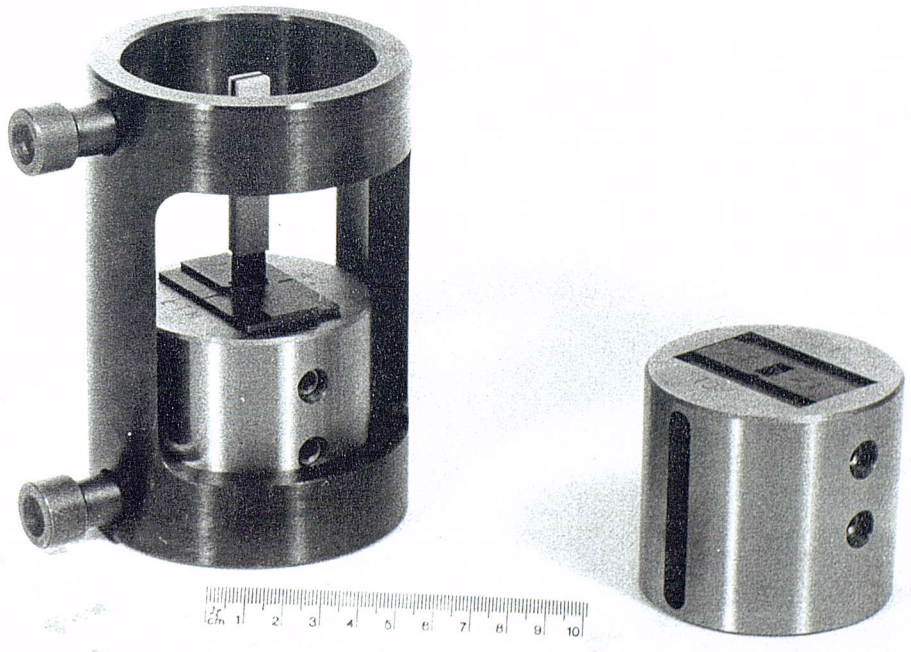


***Figure P-2**: British Aerospace compression jig.*

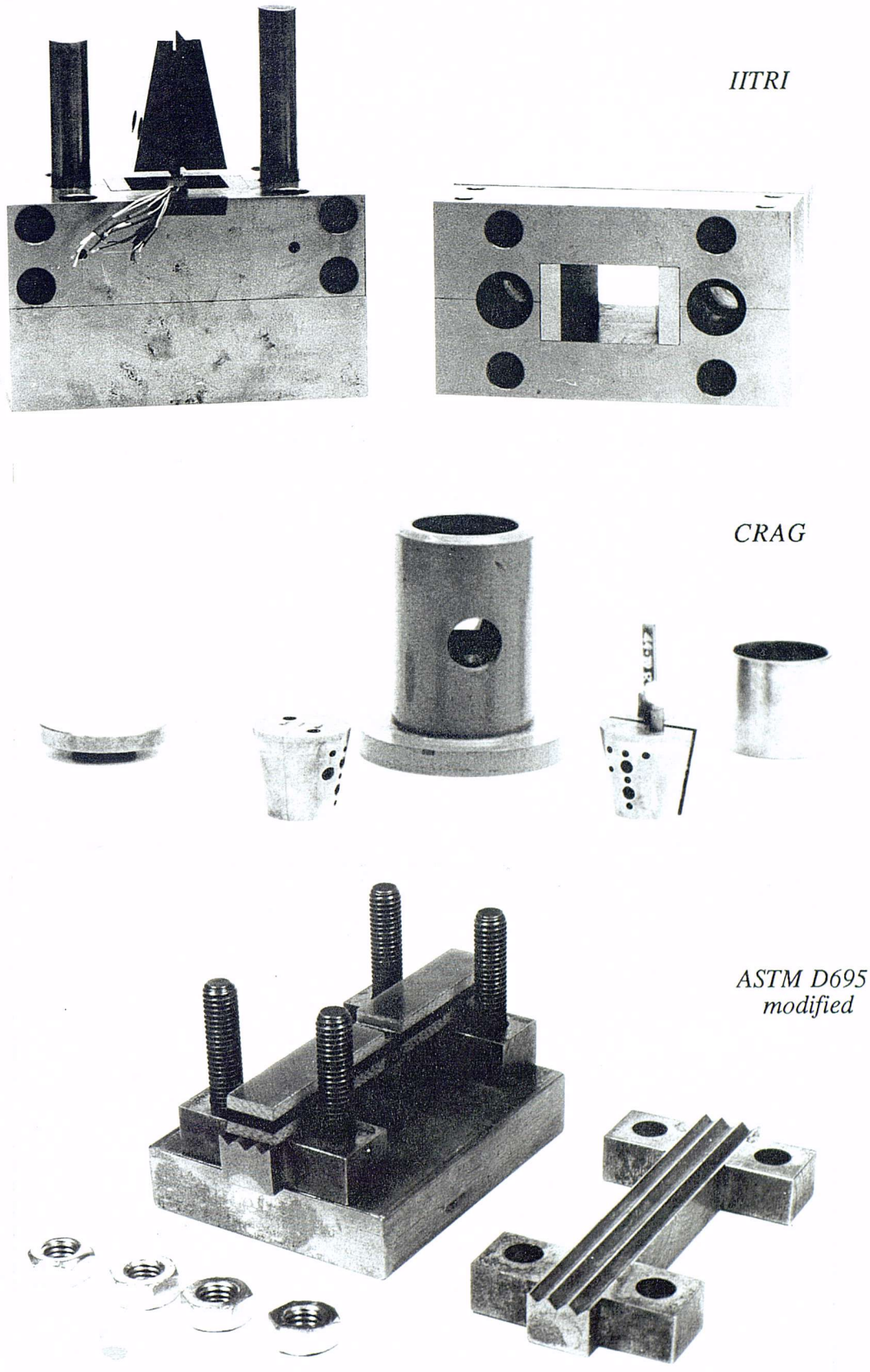
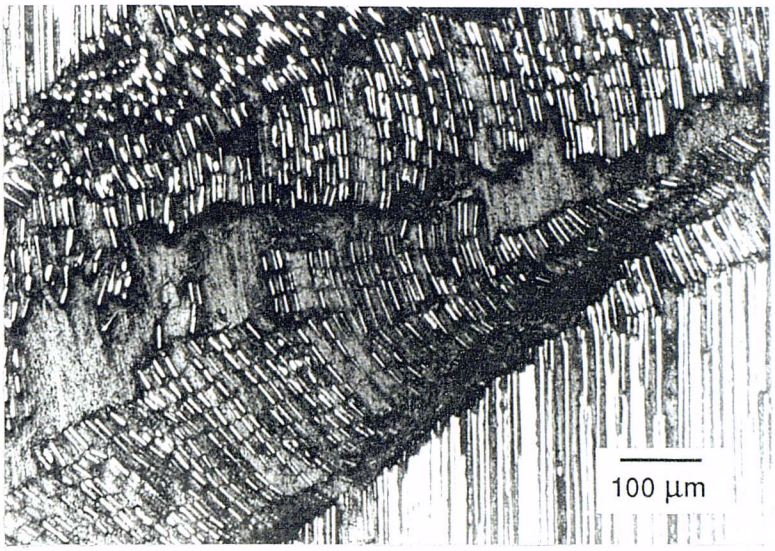
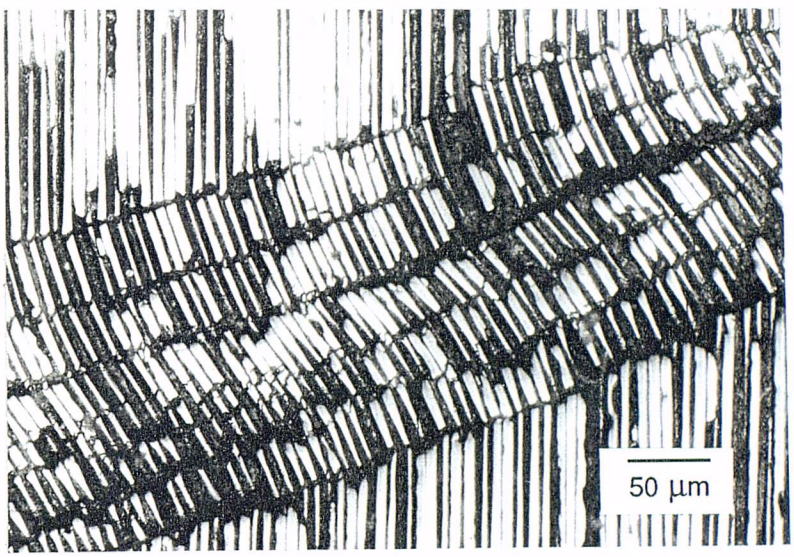


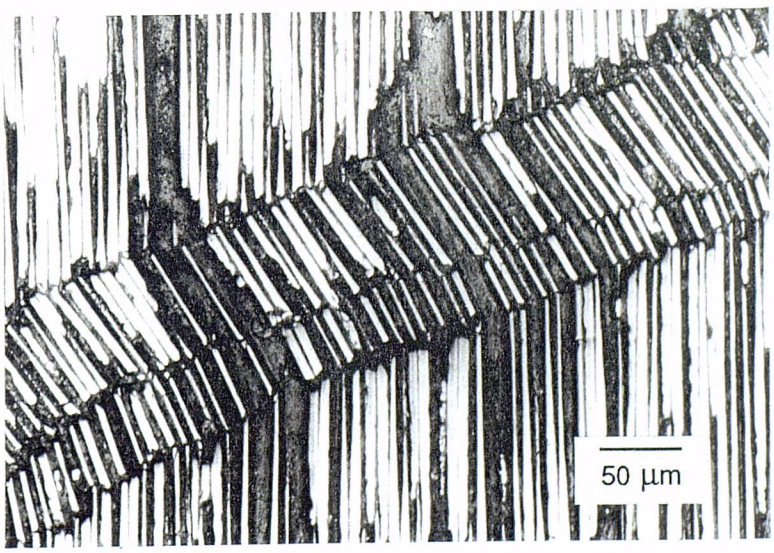
***Figure P-3**: Compression jigs with specimens mounted; disassembled; not same scale.*



(a)

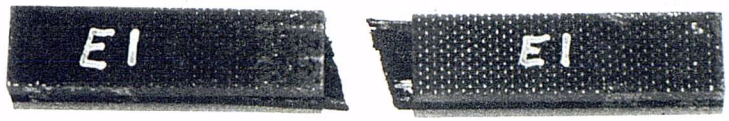
(b)



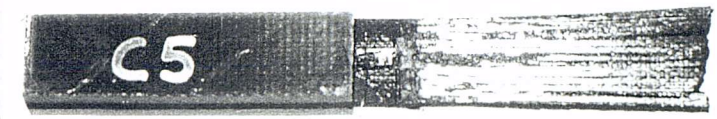


(c)

***Figure P-4**: Micrographs of compressive failure modes of CFRP; (a) in-phase buckling of fibres forming a band including several wave lengths of buckled fibres; (b) and (c) kink bands.*



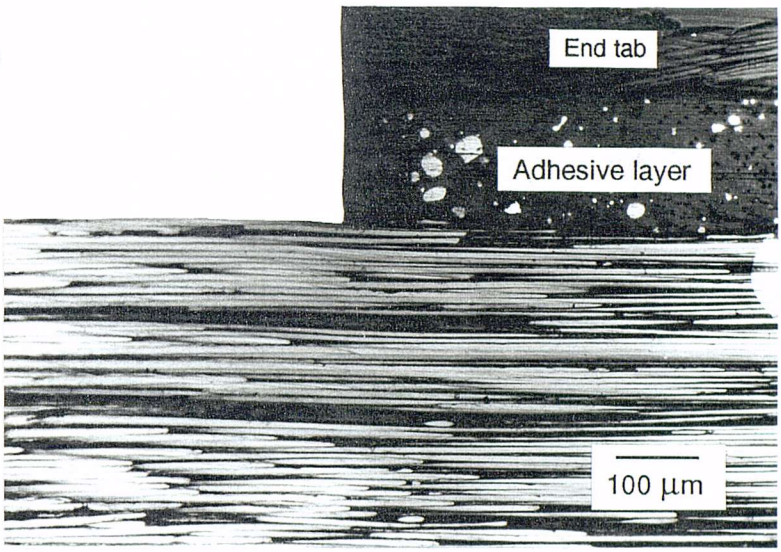
(a)



(b)

Figure P-5: *Typical compressive failure of a CFRP test piece using the modified ASTM D695 method; (a) gauge section failure (b) end failure.*

Figure P-6: *Micrograph of the tab tip region; specimen through-thickness loaded by a clamping device.*



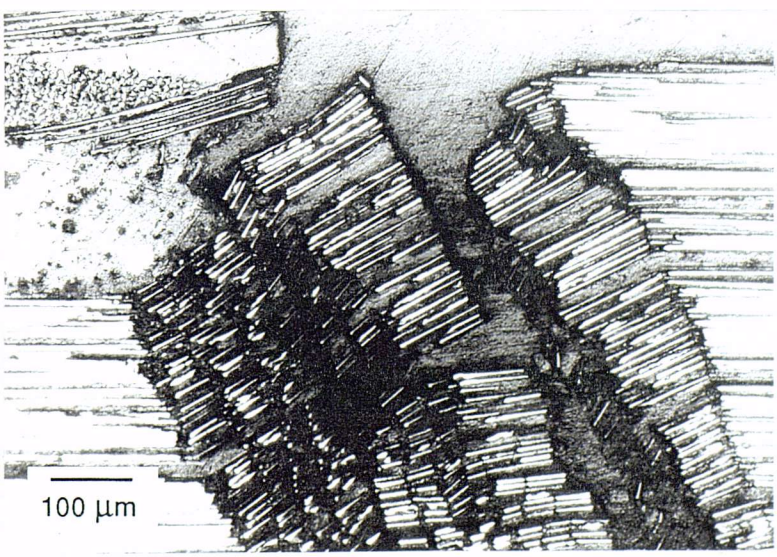


Figure P-7: *Micrograph of compressive failure initiated at tab tip.*

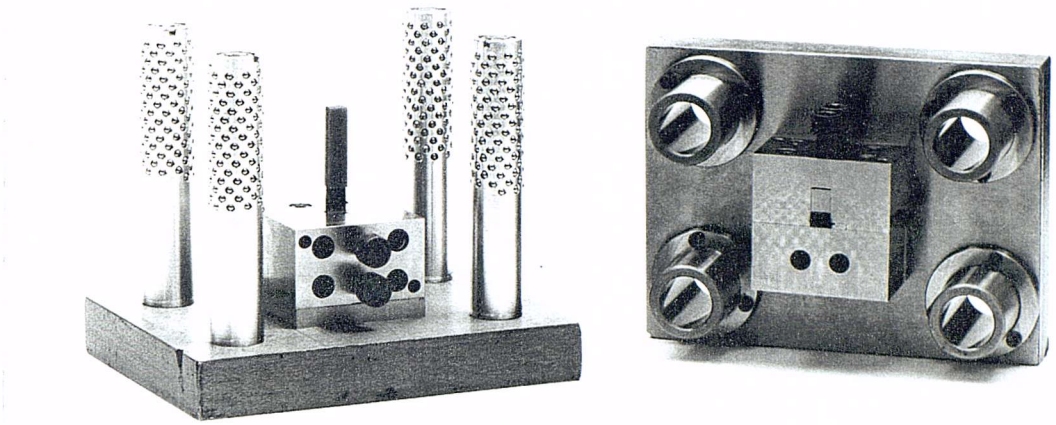


Figure P-8: *ICSTM compression rig; disassembled.*

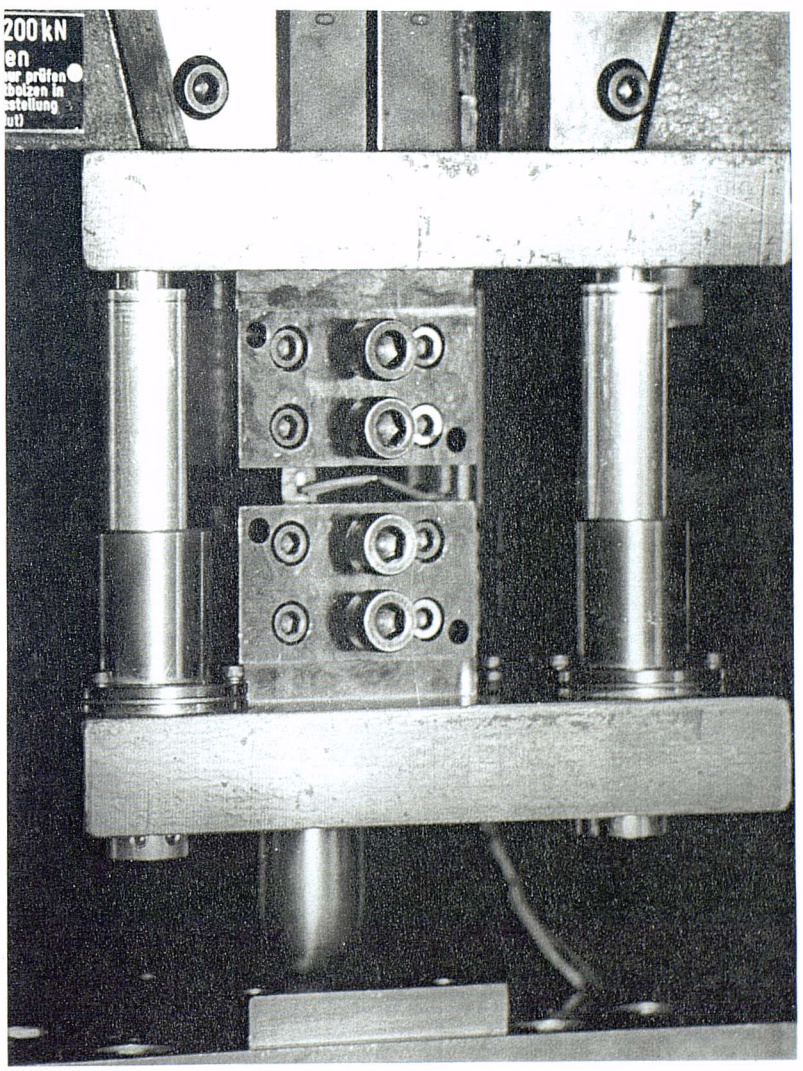


Figure P-9: *ICSTM compression rig mounted in universal testing machine.*

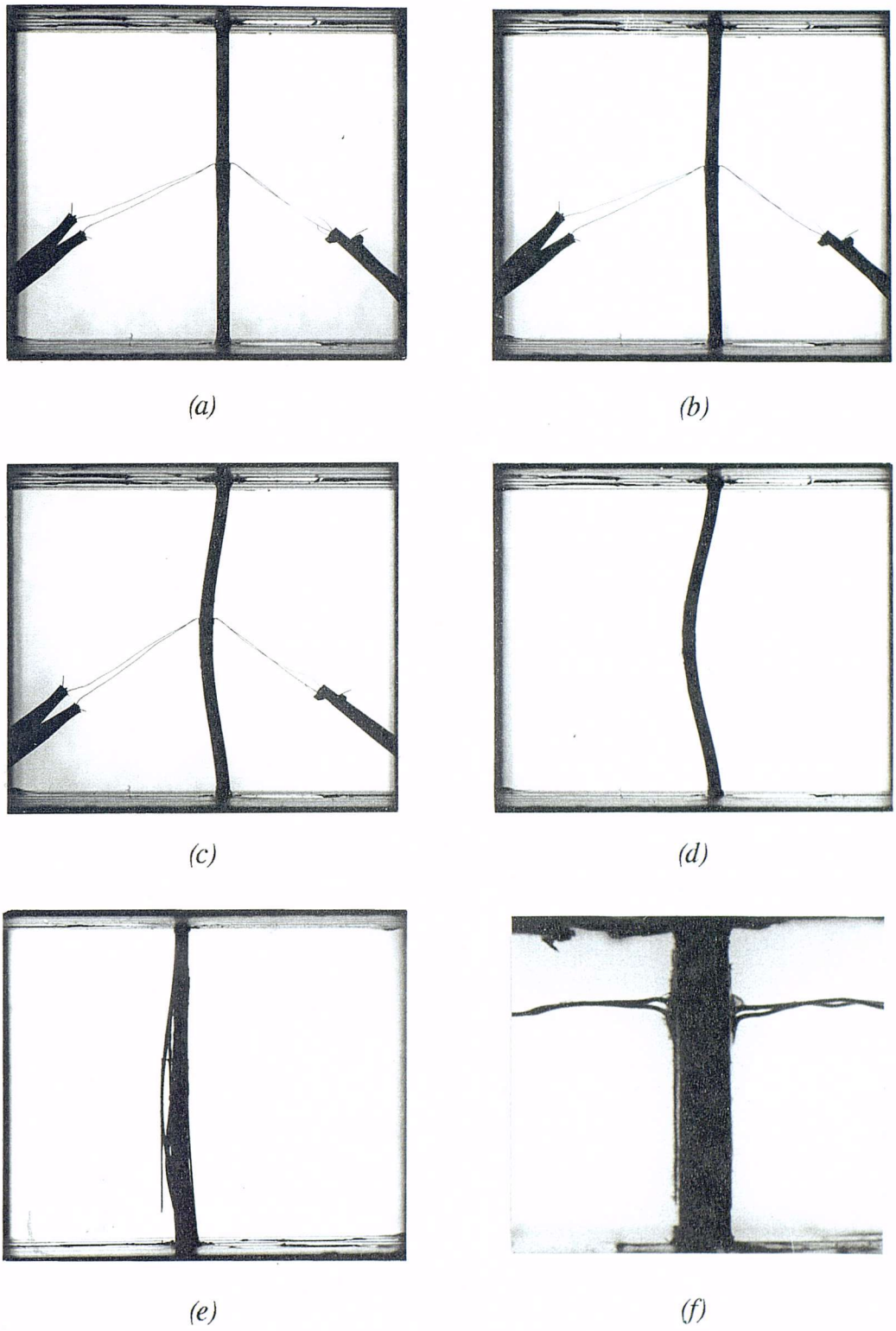


Figure P-10: *Buckling of a CFRP test piece with 50 mm (a)-(e) and 10 mm (f) gauge length using the ICSTM method; (a) initial state; (b) onset of buckling; (c) buckled shape, increased deflection; (d) shape just before failure; (e) fractured test piece; (f) 10 mm test piece just before failure.*



(a) XAS/914C; 50 mm gauge length. (G50-2; UCS 475 MPa)

(b) XAS/914C; 30 mm gauge length. (G30-2; UCS 908 MPa)





(c) XAS/914C 10 mm gauge length (G10-6; UCS 1712 MPA)



(d) XAS/914C; 7.5 mm gauge length. (G7-4, UCS 1785 MPA)



1. DELST-4; UCS 1837 MPA *2. PM1-4; UCS 1831 MPA*

(e) XAS/914C; compressive failure under end tabs.



1. APCS-2; UCS 1111 MPa *2. APCS-1; UCS 1101 MPa*

(f) APC-2(AS4/PEEK)

Figure P-11: *Macroscopic failure modes of compression test pieces using the ICSTM method; details in Chapter 5.*

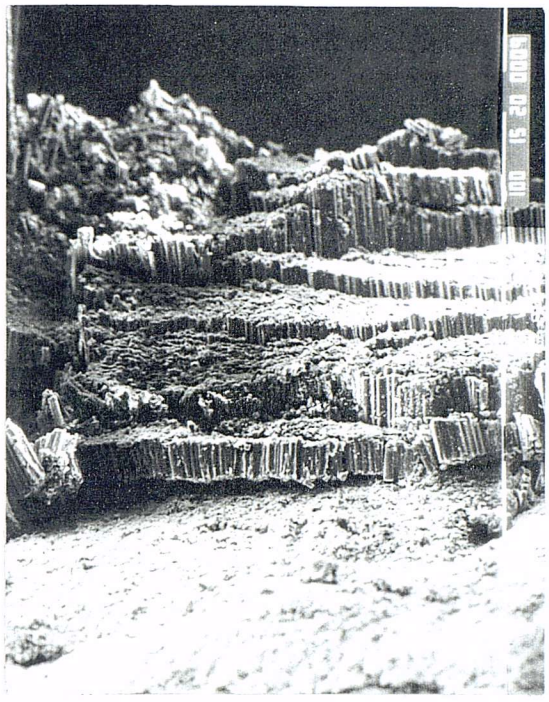


Figure P-12: Scanning electron micrograph of the compression fracture surface of a XAS/914C test piece.

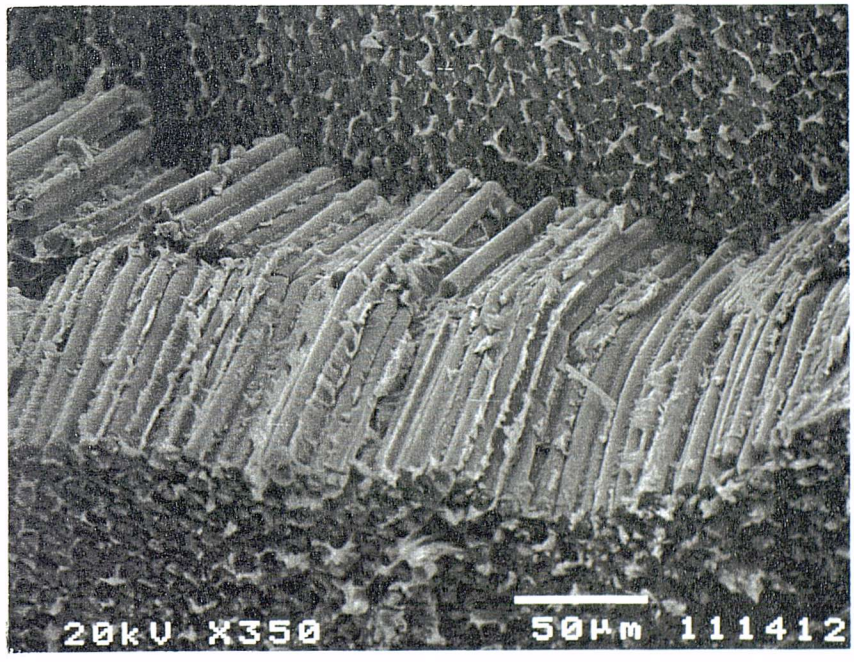


Figure P-13: *Scanning electron micrograph showing the compression fracture surface of an APC-2 test piece; note the bent but unfractured fibres (right); buckled fibres fractured at vicinity of highest curvature form a kink band (left).*



***Figure P-14**: Scanning electron micrograph of a kink band surface in APC-2 (AS4/PEEK) showing ends of fibres failed in flexure.*

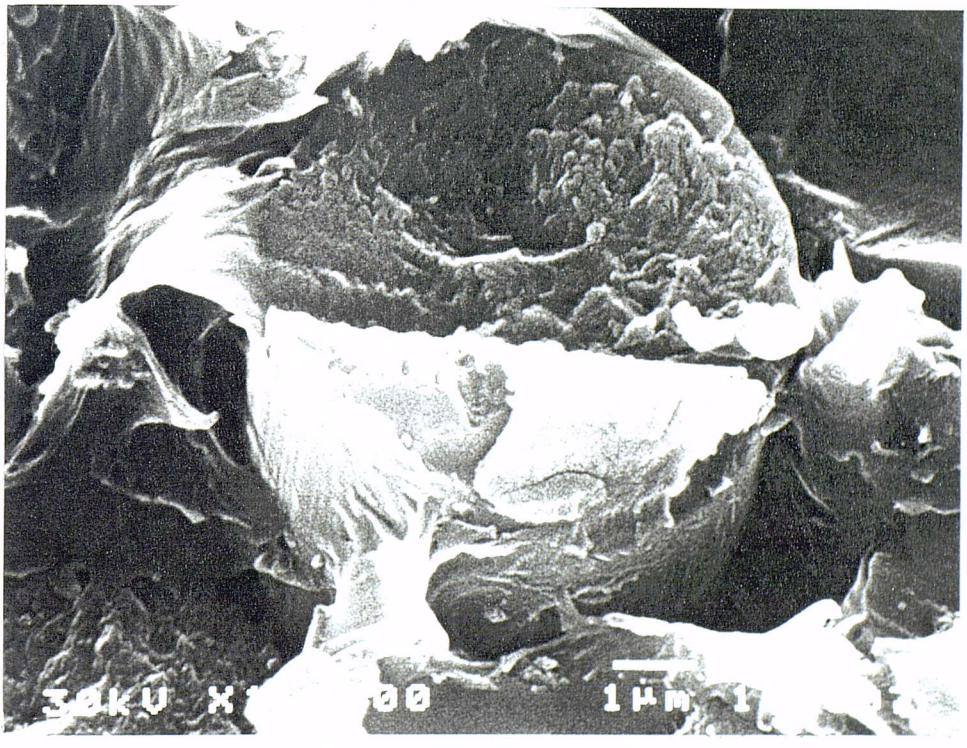


***Figure P-15**: Scanning electron micrograph at higher magnification of centre fibre end in Figure P-14 (x10000) showing details of flexural fibre failure.*

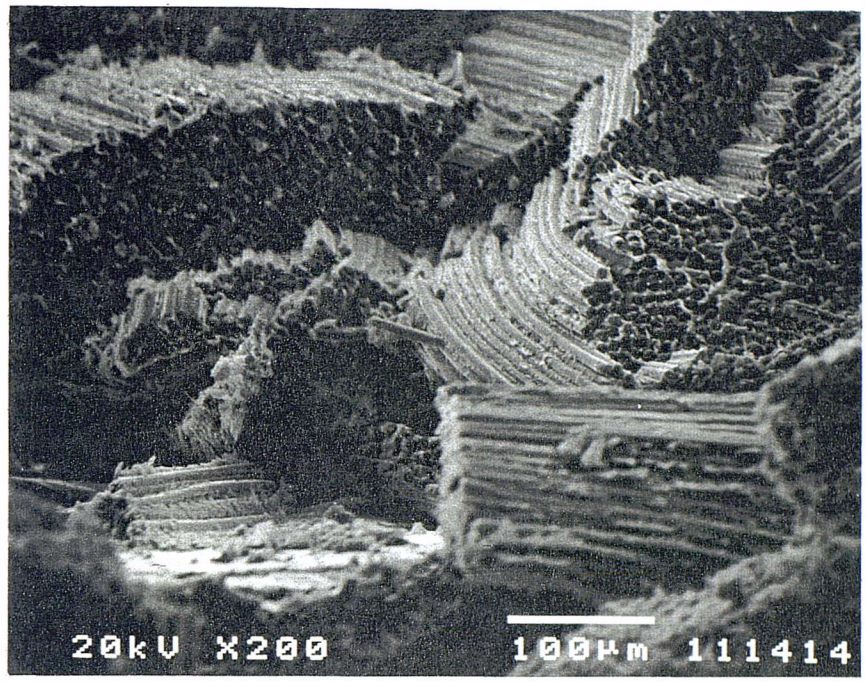
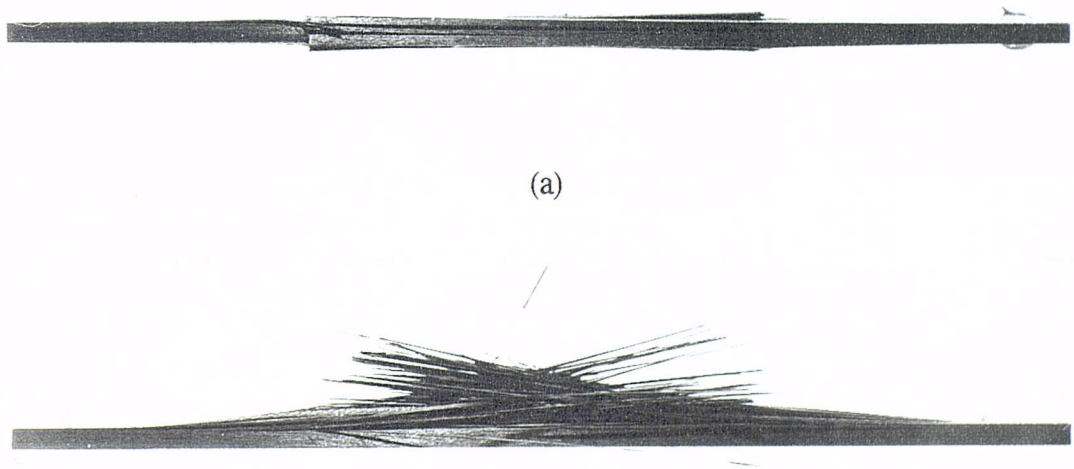


Figure P-16: *Scanning electron micrograph of a compression fracture surface in APC-2 (AS4/PEEK) showing bundles of buckled fibres.*



(a)

(b)

Figure P-17: *Fractured ASTM D790M-84 four-point bend test pieces; (a) compressive failure above rollers using a standard jig; (b) tensile failure above rollers using rollers with plastic sleeves.*

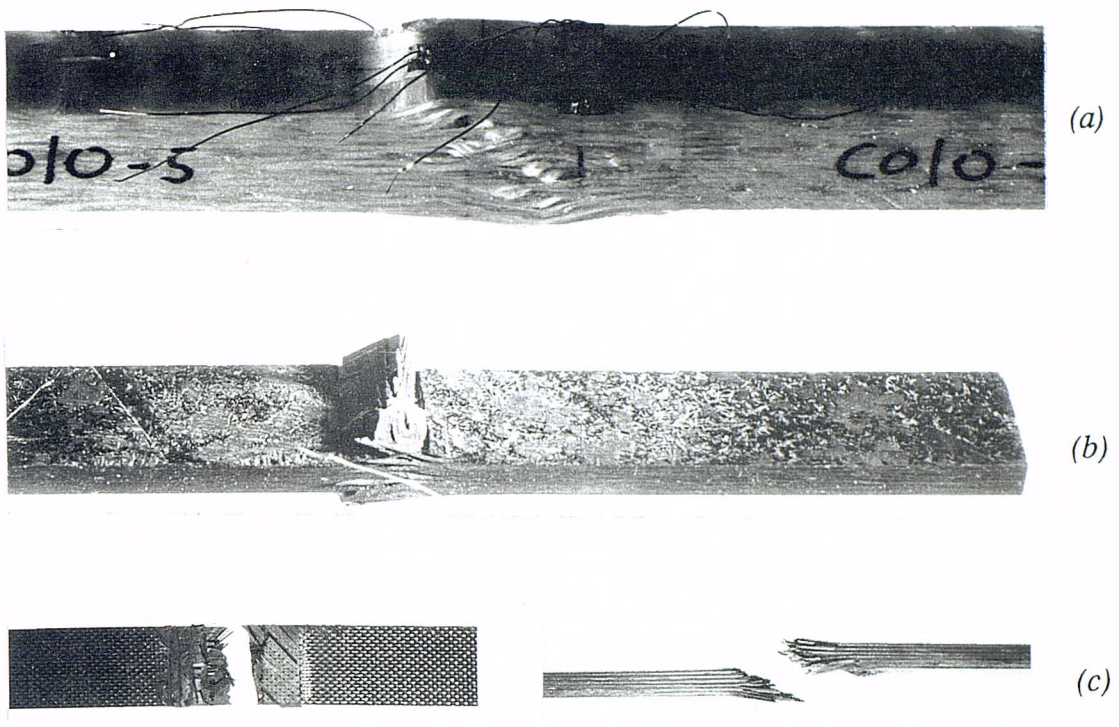


Figure P-18: *Compression failure of non-standard specimens using the ICSTM method: (a) thick woven crossply GRP; (b) woven crossply CFRP; (c) multidirectional CFRP; width of test piece 10 mm in all cases.*

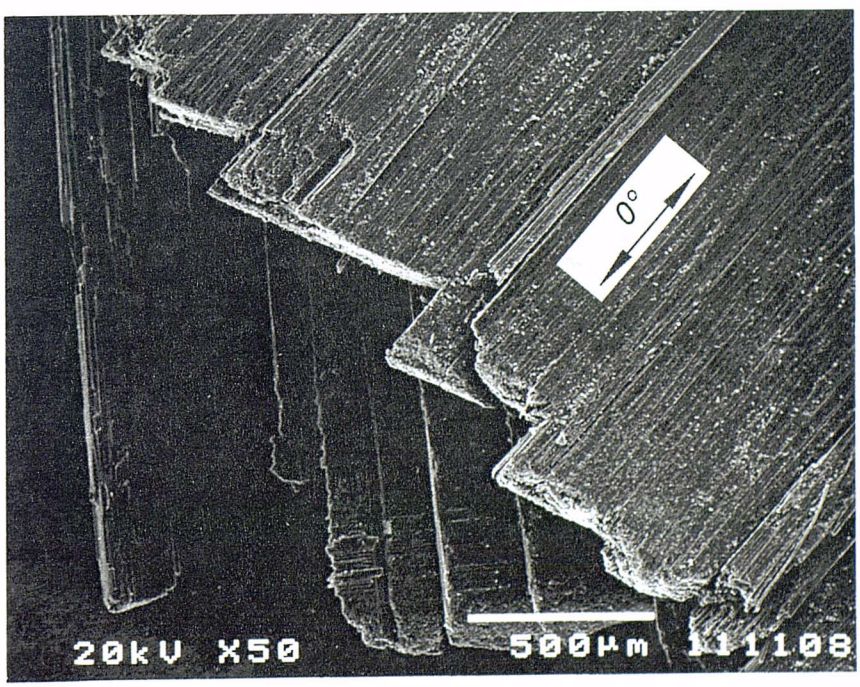
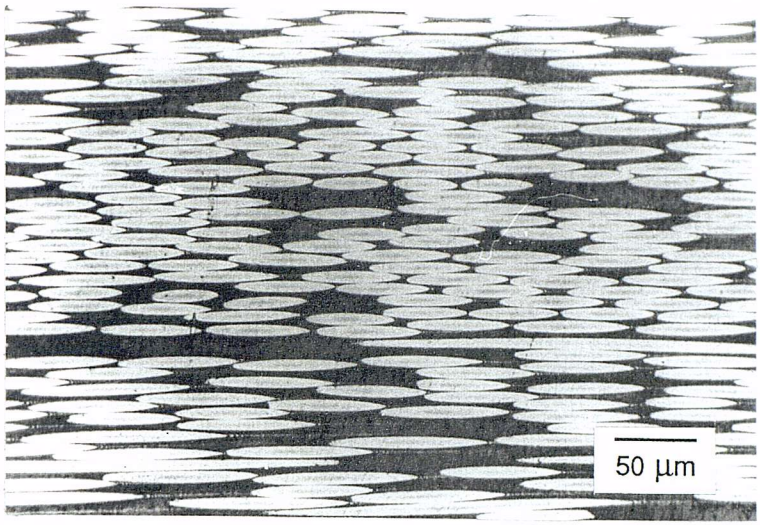


Figure P-19: *Scanning electron micrograph of the compression fracture surface in the 0°-ply of multi-directional XAS/914C; lay-up: $[(+45/-45/0/90)_3]_S$; 45°-plies removed.*



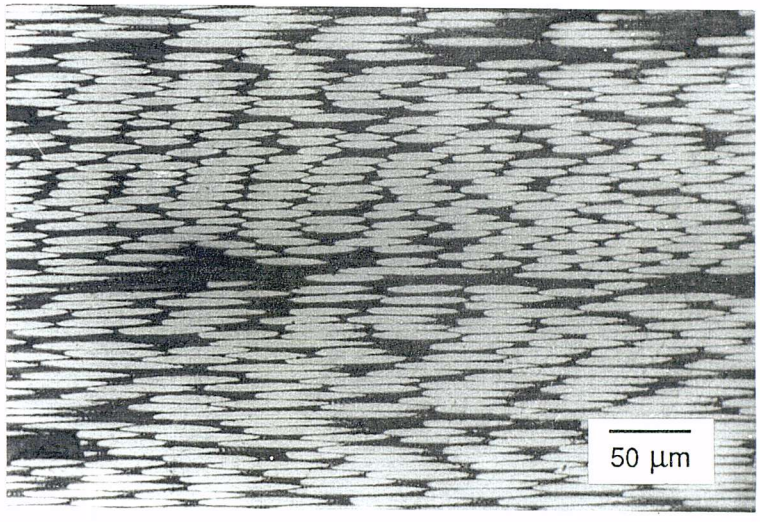


Figure P-20: *Micrographs taken from polished samples of unidirectional CFRP intersected at an angle of approximately 5°.*

(a) APC-2 (AS4/PEEK)

(b) Apollo 43-750/9106C 0% fibre surface treatment

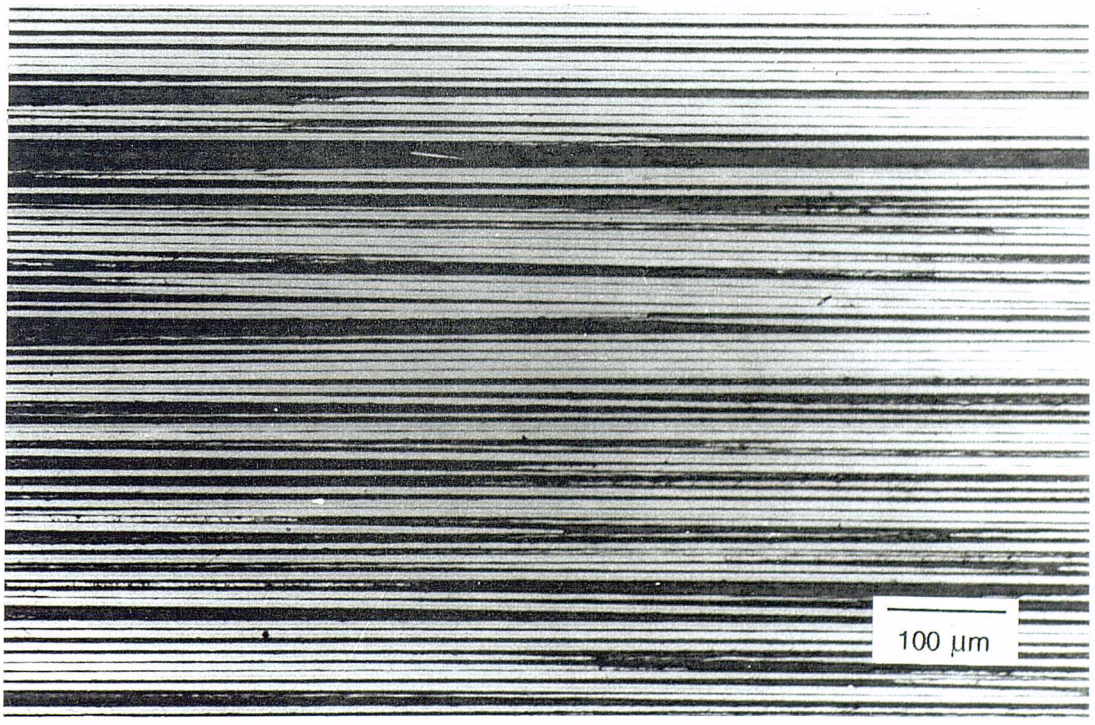


Figure P-21: *Sample of unidirectional XAS/914C polished parallel to the fibres.*

TABLES

T-1 to T-34

Abbreviations and terms used in the tables:

UCS	Ultimate compressive stress
UCSN	Ultimate compressive strain
UTS	Ultimate tensile stress
UTSN	Ultimate tensile strain
MOD	Longitudinal modulus of elasticity (0.25 % secant)
t	Measured thickness of the test piece
w	Measured width of the test piece
A	Cross-sectional area: $A = w\,t$
Test speed:	Rate of testing machine crosshead displacement
Bolt torque:	Torque applied to the clamping bolts of the ICSTM rig near the specimen end/near the gauge section

G5 XAS/914C			Test method: ICSTM/Standard specimen; 5 mm gauge length Test speed: 1.5 mm/min Bolt torque: 10/5 Nm Test pieces instrumented with 1 mm strain gauges			
No	*t* [mm]	*w* [mm]	*A* [mm^2]	**UCS** [MPa]	**MOD** [GPa]	Notes
1	2.12	10.01	21.22	**1442**	119.9	-
2	2.01	9.97	20.04	-	N/A	End failure; rig loaded
3	2.05	10.00	20.50	**1716**	118.2	-
4	2.08	10.01	20.82	**1418**	116.7	-
5	1.94	10.01	19.42	**1651**	N/A	-
6	1.98	10.01	19.82	**1695**	N/A	Reload at 225 MPa

Statistics	Mean	σ_{n-1}	C_V [%]
UCS [MPa]	**1584**	**143.1**	**9.0**
MOD [GPa]	**118.3**	-	-

***Table T-1:** Test results for the compressive strength of XAS/914C; gauge length 5 mm.*

G7 XAS/914C			Test method: ICSTM/Standard specimen; 7.5 mm gauge length Test speed: 1.5 mm/min Bolt torque: 10/5 Nm Test pieces instrumented with 1 mm strain gauges			
No	*t* [mm]	*w* [mm]	*A* [mm^2]	**UCS** [MPa]	**MOD** [GPa]	Notes
1	2.08	10.02	20.84	**1480**	-	-
2	1.96	9.98	19.56	**1477**	122.2	-
3	2.10	10.00	21.00	**1634**	121.8	Reload at 533 MPa
4	2.11	9.98	21.06	**1785**	127.0	-
5	2.00	10.01	20.02	**1471**	-	-
6	2.05	10.00	20.50	**1615**	122.8	-

Statistics	Mean	σ_{n-1}	C_V [%]
UCS [MPa]	**1577**	**125.4**	**8.0**
MOD [GPa]	**123.5**	**2.4**	**2.0**

***Table T-2:** Test results for the compressive strength of XAS/914C; gauge length 7.5 mm.*

G10 XAS/914C			Test method: ICSTM/Standard specimen; **10 mm** gauge length Test speed: 1.5 mm/min Bolt torque: 10/5 Nm Test pieces instrumented with 2 mm strain gauges			
No	*t* [mm]	*w* [mm]	*A* [mm^2]	**UCS** [MPa]	**MOD** [GPa]	Notes
1	2.09	9.99	20.88	**1620**	117.4	-
2	2.12	9.98	21.16	**1618**	117.1	-
3	2.12	9.93	21.05	**1712**	115.0	-
4	2.12	9.98	21.16	**1694**	116.2	-
5	2.12	10.01	21.22	**1348**	114.3	No obvious cause for low strength value
6	2.12	10.00	21.20	**1712**	111.5	-

Statistics	Mean	σ_{n-1}	C_V [%]
UCS [MPa]	**1617**	**138.8**	**8.6**
MOD [GPa]	**115.3**	**2.19**	**1.9**

Table T-3: *Test results for the compressive strength of XAS/914C; gauge length 10 mm.*

G12 XAS/914C			Test method: ICSTM/Standard specimen; **12.5 mm** gauge length Test speed: 1.5 mm/min Bolt torque: 10/5 Nm Test pieces instrumented with 2 mm strain gauges			
No	*t* [mm]	*w* [mm]	*A* [mm^2]	**UCS** [MPa]	**MOD** [GPa]	Notes
1	2.10	9.96	20.92	-	115.4	End failure at 1452 MPa
2	2.12	10.00	21.20	**1626**	116.3	-
3	2.12	9.99	21.18	**1441***	116.8	*End tab debond before failure
4	2.13	9.99	21.28	**1614**	117.4	-
5	2.12	9.96	21.12	**1446**	116.2	-
6	2.13	9.98	21.26	**1552**	118.9	-

Statistics	Mean	σ_{n-1}	C_V [%]
UCS [MPa]	**1536**	**88.8**	**5.8**
MOD [GPa]	**116.8**	**1.21**	**1.0**

Table T-4: *Test results for the compressive strength of XAS/914C; gauge length 12.5 mm.*

G15 XAS/914C			Test method: ICSTM/Standard specimen; **15 mm** gauge length Test speed: 1.5 mm/min Bolt torque: 10/5 Nm Test pieces instrumented with 2 mm strain gauges			
No	*t* [mm]	*w* [mm]	*A* [mm^2]	**UCS** [MPa]	**MOD** [GPa]	Notes
1	2.13	9.99	21.28	**1546**	122.6	-
2	2.1	9.93	20.85	**1581**	121.4	-
3	2.13	9.97	21.24	**1506**	121.4	-
4	1.97	9.98	19.66	**1431**	119.0	-
5	2.06	9.89	20.37	**1510**	121.8	-
6	2.01	10.02	20.14	**1369**	119.1	-

Statistics	Mean	σ_{n-1}	C_V [%]
UCS [MPa]	**1491**	**55.9**	**3.7**
MOD [GPa]	**119.7**	**4.00**	**3.3**

Table T-5: *Test results for the compressive strength of XAS/914C; gauge length 15 mm.*

G20 XAS/914C			Test method: ICSTM/Standard specimen; **20 mm** gauge length Test speed: 1.5 mm/min Bolt torque: 0/0 Nm Test pieces instrumented with 2 mm strain gauges			
No	*t* [mm]	*w* [mm]	*A* [mm^2]	**UCS** [MPa]	**MOD** [GPa]	Notes
1	2.15	10	21.50	**1227**	120.4	-
2	2.16	9.87	21.32	**1148**	116.1	-
3	2.15	9.99	21.48	**1157**	116.9	Reloaded at 593 MPa Bolt torque 10/5
4	2.16	10.02	21.64	**1213**	120.6	-
5	2.16	9.98	21.56	**1193**	120.0	-

Statistics	Mean	σ_{n-1}	C_V [%]
UCS [MPa]	**1188**	**34.4**	**2.9**
MOD [GPa]	**118.8**	**2.13**	**1.8**

Table T-6: *Test results for the compressive strength of XAS/914C; gauge length 20 mm.*

G30 XAS/914C			Test method: ICSTM/Standard specimen; **30 mm** gauge length Test speed: 1.5 mm/min Bolt torque: 10/5 Nm Test pieces instrumented with 2 mm strain gauges			
No	t [mm]	w [mm]	A [mm^2]	**UCS** [MPa]	**MOD** [GPa]	Notes
1	2.10	10.00	21.00	**893**	119.5	-
2	2.07	9.96	20.62	**908**	122.7	-
Statistics			Mean		σ_{n-1}	C_V [%]
UCS [MPa]			**900**		-	-
MOD [GPa]			**121.1**		-	-

Table T-7: *Test results compressive strength of XAS/914C; gauge length 30 mm.*

G50 XAS/914C			Test method: ICSTM/Standard specimen; **50 mm** gauge length Test speed: 1.5 mm/min Bolt torque: 10/5 Nm Test pieces instrumented with 2 mm strain gauges			
No	t [mm]	w [mm]	A [mm^2]	**UCS** [MPa]	**MOD** [GPa]	Notes
1	2.11	10.01	21.12	**469**	120.2	-
2	2.02	9.87	19.94	**475**	128.8	-
Statistics			Mean		σ_{n-1}	C_V [%]
UCS [MPa]			**472**		-	-
MOD [GPa]			**124.5**		-	-

Table T-8: *Test results compressive strength of XAS/914C; gauge length 50 mm.*

T8 XAS/914C	Test method: ICSTM/Standard specimen; 7.5 mm gauge length Laminate: 8 plies; 1 mm nominal thickness Test speed: 1.5 mm/min Bolt torque: 5/5 Nm Test pieces instrumented with 2 mm strain gauges.					
No	*t* [mm]	*w* [mm]	*A* [mm^2]	**UCS** [MPa]	**MOD** [GPa]	Notes
1	1.03	9.96	10.26	**1283**	121.6	-
2	0.99	9.98	9.88	**1387**	127.9	-
3	1.03	9.92	10.22	**1297**	122.4	-
4	1.03	9.94	10.24	**1397**	118.9	-
5	1.03	9.97	10.27	**1267**	117.9	-

Statistics	Mean	σ_{n-1}	C_V [%]
UCS [MPa]	**1326**	**61.1**	**4.6**
MOD [GPa]	**121.7**	**3.91**	**3.2**

Table T-9: *Test results for the compressive strength of XAS/914C; 8-ply laminate.*

T12 XAS/914C	Test method: ICSTM/Standard specimen; 10 mm gauge length Laminate: 12 plies; 1.5 mm nominal thickness Test speed: 1.5 mm/min Bolt torque: #1,2: 15/5 Nm, #3,4,5: 5/5 Nm Test pieces instrumented with 2 mm strain gauges.					
No	*t* [mm]	*w* [mm]	*A* [mm^2]	**UCS** [MPa]	**MOD** [GPa]	Notes
1	1.59	9.85	15.66	**1454**	115.6	-
2	1.54	9.94	15.31	**1586**	120.7	-
3	1.53	9.95	15.22	**1581**	121.3	-
4	1.55	10.00	15.50	**1633**	124.2	-
5	1.58	9.82	15.52	**1665**	119.9	-

Statistics	Mean	σ_{n-1}	C_V [%]
UCS [MPa]	**1584**	**80.4**	**5.1**
MOD [GPa]	**120.3**	**3.11**	**2.6**

Table T-10: *Test results for the compressive strength of XAS/914C; 12-ply laminate.*

SGG XAS/914C	Test method: ICSTM Gauge section machined from 4 mm laminate Test pieces instrumented with 2 mm strain gauges Test speed: 1.5 mm/min Bolt torque: 15/15 Nm					
No	t [mm]	w [mm]	A [mm^2]	**UCS** [MPa]	**MOD** [GPa]	Notes
1	2.06	9.80	20.19	**1763**	N/A	Loaded to 1000 MPa - torque 5/0 Nm; reload to failure with 15/15 Nm
2	1.88	9.78	18.39	**1551***	N/A	* significant bending
3	2.03	9.84	19.98	**1814**	N/A	-
4	1.95	9.85	19.21	**1726**	N/A	-
5	2.02	9.85	19.90	**1757**	N/A	-

Statistics	Mean	σ_{n-1}	C_V [%]
UCS [MPa]	**1722**	**100.8**	**5.9**
MOD [GPa]	N/A	N/A	N/A

Table T-11: *Compressive strength of XAS/914C; specimen machined from 32-ply laminate.*

SGGF XAS/914C	Test method: ICSTM Gauge section machined from 4 mm laminate; surfaces of tabs ground. Test pieces instrumented with 2 mm strain gauges Test speed: 1.5 mm/min Bolt torque: # 1,2: 5/5 Nm # 3-5: 15/15 Nm					
No	t [mm]	w [mm]	A [mm^2]	**UCS** [MPa]	**MOD** [GPa]	Notes
1	2.00	9.72	19.44	**1707**	119.8	-
2	2.01	9.77	19.64	**(1604)**	N/A	End failure after 'tab' delamination at 1604 MPa
3	2.01	9.67	19.44	**1693**	N/A	-
4	2.06	9.77	20.13	**1741**	N/A	-
5	2.01	9.24	18.57	**1680**	N/A	-

Statistics	Mean	σ_{n-1}	C_V [%]
UCS [MPa]	**1705**	**26.3**	**1.5**
MOD [GPa]	N/A	N/A	N/A

Table T-12: *Compressive strength of XAS/914C; specimen machined from 32-ply laminate; additional machining of the tab surfaces.*

DEB 914C/XAS	Test method: ICSTM Debonding of tab tips by bending of the test piece; debond length 6-8 mm Test speed: 1.5 mm/min Bolt torque: 10/5 Nm

No	*t* [mm]	*w* [mm]	*A* [mm^2]	**UCS** [MPa]	**MOD** [GPa]	Notes
1	2.11	10	21.10	**1864**	118.4	-
2	1.99	9.96	19.82	**1653**	122.7	-
3	2.15	9.95	21.39	**1719**	125.9	-
4	2.15	9.95	21.39	**1818**	120.4	-
5	2.07	9.97	20.64	**1752**	120.6	-

Statistics	Mean	σ_{n-1}	C_V [%]
UCS [MPa]	**1761**	**82.7**	**4.7**
MOD [GPA]	**121.6**	**2.85**	**2.3**

Table T-13: Influence of initial tab tip debonding on the compressive strength of XAS/914C.

PP3 XAS/914C	Test method: ICSTM Smooth surface finish of gauge section, peel ply Tygavac RF 260/P3 Test speed: 1.5 mm/min Bolt torque: 10/5 Nm

No	*t* [mm]	*w* [mm]	*A* [mm^2]	**UCS** [MPa]	**MOD** [GPa]	Notes
1	2.13	9.98	21.26	**1706**	-	Crackling sounds during test
2	2.15	9.97	21.44	**1921**	-	-
3	2.14	9.94	21.27	**1618**	-	-
4	2.15	9.95	21.39	**1656**	113.6	-
5	2.15	10.00	21.50	**1636**	115.5	-
6	2.15	9.99	21.48	**1592**	-	-

Statistics	Mean	σ_{n-1}	C_V [%]
UCS [MPa]	**1688**	**120.4**	**7.1**
MOD [GPA]	**114.6**	-	-

Table T-14: Influence of surface finish on the compressive strength of XAS/914C.

PM1 XAS/914C			Test method: ICSTM Ply lay-up $[(\pm 1°)_8]_s$ Test speed: 1.5 mm/min Bolt torque: 5/10 Nm			
No	*t* [mm]	*w* [mm]	*A* [mm^2]	**UCS** [MPa]	**MOD** [GPa]	Notes
1	2.11	10.00	21.10	**1717**	117.7	Tab tip debond
2	2.12	9.96	21.12	**1773**	116.9	Tab tip debond
3	2.12	9.97	21.14	**1466**	119.3	No tab tip debond
4	2.12	9.96	21.12	**1831***	122.9	*Failure under tab; tab tip debond
5	2.13	9.96	21.21	**1762**	118.8	Tab tip debond

Statistics	Mean	σ_{n-1}	C_V [%]
UCS [MPa]	**1710**	**142.2**	**8.3**
MOD [GPA]	**119.1**	**2.31**	**1.9**

Table T-15: *Influence of layer alignment on the compressive strength of XAS/914C.*

COA2 XAS/914C			Test method: ICSTM Unidirectional laminate machined at 2° to the fibre direction Test speed: 1.5 mm/min			
No	*t* [mm]	*w* [mm]	*A* [mm^2]	**UCS** [MPa]	**MOD** [GPa]	Notes
1	2.12	9.96	21.12	**1638**	N/A	-
2	2.07	9.95	20.60	**1651**	N/A	-
3	2.12	9.92	21.03	**1615**	N/A	-
4	2.13	9.97	21.24	**1626**	N/A	-
5	2.13	9.95	21.19	**1712**	N/A	-

Statistics	Mean	σ_{n-1}	C_V [%]
UCS [MPa]	**1648**	**38.0**	**2.3**

Table T-16: *Influence of laminate alignment on the compressive strength of XAS/914C.*

DELPT XAS/914C	Test method: ICSTM Debonding of tab tips by inserting of a PTFE strip Debond length: 5 mm Test speed: 1.5 mm/min Bolt torque: 10/5 Nm

No	t [mm]	w [mm]	A [mm^2]	**UCS** [MPa]	**MOD** [GPa]	Notes
1	2.12	9.94	21.07	**1720**	121.9	-
2	2.04	9.96	20.32	**1687**	127.0	Failure at end of debond insert
3	2.12	9.95	21.09	**1675**	111.6	-
4	2.09	9.92	20.73	**1684**	118.9	
5	2.13	9.98	21.26	**1756**	118.5	-

Statistics	Mean	σ_{n-1}	C_V [%]
UCS [MPa]	**1704**	**33.5**	**2.0**
MOD [GPa]	**119.6**	**5.61**	**4.7**

Table T-17: *Influence of initial tab tip debonding on the compressive strength of XAS/914C; debond by inserting 5 mm PTFE tape.*

DELST XAS/914C	Test method: ICSTM Debonding of tab tips by inserting of a strip of cellulose tape Debond length: 5 mm Test speed: 1.5 mm/min Bolt torque: 10/5 Nm

No	t [mm]	w [mm]	A [mm^2]	**UCS** [MPa]	**MOD** [GPa]	Notes
1	1.90	9.98	18.96	**1698**	121.3	Failure at end of debond insert
2	1.89	9.96	18.82	**1754**	119.8	-
3	2.05	9.98	20.46	**1928**	126.3	Failure at end of debond insert
4	1.99	9.87	19.64	**1837**	126.6	Failure under tab after debonding
5	2.1	9.95	20.89	**1815**	121.1	-

Statistics	Mean	σ_{n-1}	C_V [%]
UCS [MPa]	**1806**	**87.0**	**4.8**
MOD [GPa]	**123.0**	**3.19**	**2.6**

Table T-18: *Influence of initial tab tip debonding on the compressive strength of XAS/914C; debond by inserting 5 mm cellulose adhesive tape.*

APCS AS4/PEEK - ICI			Test method: ICSTM Gauge section machined from 4 mm thick laminate Test pieces instrumented with 2 mm strain gauges Test speed: 1.5 mm/min Bolt torque: 10/5 Nm			
No	*t* [mm]	*w* [mm]	*A* [mm^2]	**UCS** [MPa]	**MOD** [GPa]	Notes
1	1.97	9.95	19.60	**1101**	120.3	-
2	1.98	9.97	19.74	**1111**	118.2	Cracking sound before **central** failure
3	1.97	9.96	19.62	**1153**	117.7	Cracking sound before failure
4	1.99	9.96	19.82	**1149**	127.7	-
5	2.00	9.92	19.84	**1152**	125.7	-

Statistics	Mean	σ_{n-1}	C_V [%]
UCS [MPa]	**1133**	**25.1**	**2.2**
MOD [GPa]	**121.9**	**4.5**	**3.7**

Table T-19: *Compressive strength of APC-2/AS4; machined specimen.*

APCD AS4/PEEK - ICI			Test method: ICSTM 5 mm adhesive cellulose tape under tab tip Test pieces instrumented with 2 mm strain gauges Test speed: 1.5 mm/min Bolt torque: 10/5 Nm			
No	*t* [mm]	*w* [mm]	*A* [mm^2]	**UCS** [MPa]	**MOD** [GPa]	Notes
1	2.23	9.98	22.26	**1353**	127.1	-
2	2.22	9.95	22.09	**1456**	128.5	-
3	2.22	9.91	22.00	**1658**	126.0	central failure
4	2.22	9.96	22.11	**1597**	125.4	-
5	2.23	9.94	22.17	**1493**	125.4	-

Statistics	Mean	σ_{n-1}	C_V [%]
UCS [MPa]	**1511**	**119.7**	**7.9**
MOD [GPa]	**126.5**	**1.3**	**1.1**

Table T-20: *Compressive strength of APC-2; specimen with debond insert.*

Apollo 43-750/ 9106C			Test method: ICSTM Test speed: 2 mm/min Thickness measured as moulded (if no strain gauges are applied)			
Lay-up	No	*t* [mm]	*w* [mm]	*A* [mm^2]	**UCS** [N]	Notes
01	1	2.30	9.76	22.45	**1180**	strain gauged
01	2	2.39	9.66	23.09	**1356***	-
01	3	2.38	9.66	22.99	**1155**	strain gauged
01	4	2.47	9.63	23.79	**1345**	-
01	5	2.39	9.73	23.25	**1292**	strain gauged
01	6	2.48	9.62	23.86	**(1373*)**	-
01	7	2.38	9.6	22.85	**1378**	-
01	8	2.44	9.06	22.11	**1081***	-
X1	1	2.40	9.96	23.90	**1356***	-
X1	2	2.38	10.03	23.87	**1394***	-
X1	3	2.39	9.87	23.59	**1297***	-
X1	4	2.39	9.95	23.78	**1338**	-
X1	5	2.34	9.95	23.28	**1251**	-
X1	6	2.38	10.02	23.85	**1325**	strain gauged
X1	7	2.37	9.92	23.51	**1360**	strain gauged; reloaded after loading up to 700 MPa.
X1	8	2.25	9.95	22.39	**1300**	strain gauged
L1	1	2.65	9.95	26.37	**(1325*)**	-
L1	2	2.64	9.96	26.29	**1362***	-
L1	3	2.65	9.99	26.47	**(1339*)**	-
L1	4	2.62	9.97	26.12	**1381**	-
L1	5	2.56	9.95	25.47		-
L1	6	2.56	9.96	25.50	**1277**	strain gauged
L1	7	2.55	9.98	25.45	**1338**	strain gauged
L1	8	2.62	9.96	26.10	**1371**	strain gauged
L1	9	2.63	9.8	25.77	**1121**	-

Table T-21: .....Continued on next page....

Apollo 43-750/ 9106C			Test method: ICSTM Test speed: 2 mm/min Thickness measured as moulded (if no strain gauges are applied)			
Lay-up	No	t [mm]	w [mm]	A [mm^2]	**UCS** [N]	Notes
C1	1	2.25	9.74	21.92	**1245**	-
C1	2	2.27	9.65	21.91	**1045**	-
C1	3	2.29	9.81	22.46	**(1090)**	failure under end tab
C1	4	2.24	9.8	21.95	**1371**	-
C1	5	2.25	9.52	21.42	**1195**	strain gauged
C1	6	2.28	9.83	22.41	**1305**	strain gauged
C1	7	2.29	9.83	22.51	**1299**	strain gauged
C1	8	2.30	9.67	22.24	**1383***	failure in the centre of gauge section
C1	9	2.27	9.79	22.22	**1284**	-
C2	1	2.42	9.99	24.18	**1234**	strain gauged
C2	2	2.39	9.92	23.71	**1284**	-
C2	3	2.43	9.93	24.13	**1299***	-
C2	4	2.41	9.95	23.98	**(1341*)**	failure under end tab
C2	5	2.32	9.99	23.18	**1266**	strain gauged
C2	6	2.35	9.92	23.31	**1288**	-
C2	7	2.35	9.88	23.22	-	-
C2	8	2.40	9.99	23.98	**1244**	-
C2	9	2.42	9.9	23.96	**1330**	-

UCS [MPa]	Mean	σ_{n-1}	C_V [%]
01	**1270**	**115.2**	**9.1**
01-#6	1255	116.0	9.2
X1	**1328**	**44.6**	**3.4**
L1	**1314**	**84.5**	**6.4**
L1-#1,3	1308	99.0	7.6
C1	**1246**	**117.0**	**9.4**
C1-#3	1266	108.2	8.6
C2	**1286**	**37.8**	**2.9**

** kinking under the tab before gauge section failure*

Table T-21: *Test results for the compressive strength of Apollo 43-750/9106C with different levels of fibre surface treatment; ICSTM method with standard specimen.*

Apollo 43-750/ 9106C			Test method: Birmingham Test speed: 2 mm/min Failure mode: E End failure C Central failure G Failure where specimen emerges from block				
Lay-up	No	t [mm]	w [mm]	A [mm^2]	**UCS** [N]	Failure mode	Bolt torque [Nm]
01	1	1.53	9.995	15.29	**1353**	G	15/15
01	2	1.61	9.995	16.09	**1289**	G	15/15
01	3	1.64	10.00	16.40	**(1317)**	E	15/15
01	4	1.58	9.995	15.79	**1367**	G	15/10
01	5	1.54	9.995	15.39	**1386**	G	15/10
01	6	1.64	9.995	16.39	**1150**	G	15/15
X1	1	1.55	9.995	15.49	**1387**	G	15/15
X1	2	1.51	10.00	15.10	**1375**	G	15/15
X1	3	1.55	10.01	15.52	**1395**	G	15/15
X1	4	1.54	9.995	15.39	**1538**	G	15/10
X1	5	1.52	10.00	15.20	**1563**	G	15/10
L1	1	1.62	10.00	16.20	**1368**	C	15/15
L1	2	1.61	10.00	16.10	**1410**	G	15/15
L1	3	1.61	10.005	16.11	**1359**	C	15/15
L1	4	1.6	10.00	16.00	**1120**	C	15/15
L1	5	1.28	10.00	12.80	**1393**	C	15/10
C2	3	1.61	10.00	16.10	**(1236)**	E	15/15
C2	4	1.64	10.005	16.41	**(1327)**	E	15/15
C2	5	1.59	10.005	15.91	**(1376)**	E	15/15
C2	6	1.59	10.005	15.91	**(1357)**	E	15/15
C2	7	1.58	10.00	15.80	**1304**	C	20/10
C2	8	1.58	10.01	15.82	**1256**	G	20/10
C2	9	1.58	10.00	15.80	**1364**	G	20/15
C2	10	1.63	10.00	16.30	**1286**	C	20/10

UCS [MPa]	Mean	σ_{n-1}	C_V [%]
01	**1310**	**86.0**	**6.6**
01-#3	1309	96.1	7.3
X1	**1452**	**91.0**	**6.3**
L1	**1330**	**119.1**	**9.0**
C2	**1313**	**51.7**	**3.9**
C2-#7-10	1303	45.5	3.5

Table T-22: *Test results for the compressive strength of Apollo 43-750/9106C with different levels of fibre surface treatment; Birmingham method.*

ICI/'Plytron'			Test method: ICSTM/standard test piece Test speed: 3 mm/min Bolt torque: 10/5 Nm				
Nom. V_f[%]	No	t [mm]	A [mm^2]	**UCS** [MPa]	**UCSN** [%]	**MOD** [GPa]	Failure
23	1	1.95	18.93	**721**	3.38	23.2	B
23	2	1.94	19.26	**542**	3.06	20.0	-
23	3	1.94	18.86	**696**	3.39	22.4	B
23	4	1.96	19.40	**519**	2.70	20.8	-
23	5	1.96	19.46	**624**	3.35	20.0	B
29	1	1.86	18.49	**770**	3.13	25.6	B
29	2	1.89	18.79	**727**	3.16	24.0	-
29	3	1.88	18.65	**823**	3.29	26.4	B
29	4	1.90	18.87	**850**	3.14	28.0	B
29	5	1.87	18.61	**635**	2.86	23.2	-
35	1	1.99	19.76	**991**	3.29	30.4	B
35	2	1.97	19.44	**924**	3.27	31.2	B
35	3	1.95	19.38	**892**	2.95	32.0	B
35	4	1.94	19.26	**937**	2.97	32.8	B
35	5	1.93	19.16	**1006**	3.13	32.8	B

UCS [MPa]	Mean	σ_{n-1}	C_V[%]
V_f=23%	**620**	**89.8**	**14.5**
V_f=29%	**761**	**85.0**	**11.2**
V_f=35%	**950**	**47.5**	**5.0**
MOD [GPa]	Mean	σ_{n-1}	C_V[%]
V_f=23%	**21.3**	**1.45**	**6.8**
V_f=29%	**25.4**	**1.91**	**7.5**
V_f=35%	**31.8**	**1.04**	**3.3**

Table T-23: Test results compressive strength of ICI 'Plytron' with different levels of fibre volume fraction. 'B' in the column 'Failure' indicates bifurcation of the strain signals

LIVCW woven cross-ply CFRP $[(0°, 90°)_3]_s$	Test method: ICSTM/multidirectional Test piece sandwiched between GFRP tabs, unbonded Test pieces instrumented with 2 mm strain gauges Test speed: 1.5 mm/min Bolt torque: 10/0 Nm					
No	t [mm]	w [mm]	A [mm^2]	**UCS** [MPa]	**MOD** [GPa]	Notes
1	2.93	9.97	29.21	**707**	64.8	-
2	2.93	10.01	29.33	**644**	56.8	-
3	2.91	9.95	28.95	**721**	57.6	-
4	2.93	10.01	29.33	**629**	-	-
5	2.97	9.99	29.67	**694**	-	-
6	2.94	9.92	29.16	**584**	58.4	restart after loading to 143 and then 200 MPa, bending
7	2.97	9.93	29.49	**606**	56.8	-
8	2.97	9.91	29.43	**673**	58.4	-
9	2.97	9.97	29.61	**705**	51.2	-
10	2.95	9.95	29.35	**671**	60.0	-

Statistics	Mean	σ_{n-1}	C_V[%]
UCS [MPa]	**663**	46.2	**7.0**
MOD [GPa]	**58.0**	**3.78**	**6.5**

Table T-24: *Test results compressive strength of woven cross-ply CFRP.*

LIVCWAL woven cross-ply CFRP $[(0°, 90°)_3]_s$	Test method: ICSTM Test pieces tabbed with Al-tabs at Liverpool University Test speed: 1.5 mm/min Bolt torque: 10/0 Nm					
No	t [mm]	w [mm]	A [mm^2]	**UCS** [MPa]	**MOD** [GPa]	Notes
1	2.95	9.96	29.38	**(563)**	N/A	Failure under tab at serration in Al-tab
2	3.01	9.94	29.92	**(488)**	N/A	Failure under tab at serration in Al-tab
3	2.92	9.94	29.02	**(530)**	N/A	Failure under tab at serration in Al-tab
4	2.98	9.89	29.47	**(604)**	N/A	Failure under tab at serration in Al-tab
5	2.95	9.99	29.47	**667**	N/A	central failure

Statistics	Mean	σ_{n-1}	C_V[%]
UCS [MPa]	**(570)**	68.8	**12.1**
MOD [GPa]	N/A	N/A	N/A

Table T-25: *Test results compressive strength of woven cross-ply CFRP; aluminium end tabs; specimens manufactured at Liverpool University.*

L1 XAS/914C $[(+45°, -45°, 0°, 90°)_3]_S$	Test method: ICSTM/multidirectional Test piece sandwiched between GFRP tabs, unbonded Test pieces #1-6 instrumented with 2 mm strain gauges Test speed: 1.5 mm/min Bolt torque 10/0 Nm

No	*t* [mm]	*w* [mm]	*A* [mm^2]	**UCS** [MPa]	**MOD** [GPa]	Notes
1	3.10	10.01	31.03	**752**	N/A	-
2	3.10	10.01	31.03	**797**	48.6	-
3	3.07	9.92	30.45	**842**	47.7	-
4	2.98	9.97	29.71	**832**	50.5	-
5	2.98	9.97	29.71	**828**	48.7	-
6	2.97	9.98	29.64	**805**	50.4	-
7	3.02	10.00	30.20	**762**	N/A	-
8	3.10	9.90	30.69	**801**	N/A	-
9	3.06	10.00	30.60	**710**	N/A	-
10	3.04	9.96	30.28	**743**	N/A	-

Statistics	Mean	σ_{n-1}	C_V [%]
UCS [MPa]	**787**	43.6	**5.5**
MOD [GPa]	**49.2**	**1.2**	**2.5**

Table T-26: *Compressive strength of quasi-isotropic XAS/914C; lay-up L1.*

TL XAS/914C	Test method: Tension; 2 mm thickness; GRP tabs 50x10x2.6 Test pieces instrumented with 2 mm strain gauges Test speed: 5 mm/min

No	*t* [mm]	*w* [mm]	*A* [mm^2]	**UTS** [MPa]	**UTSN** [%]	**MOD** [GPa]	Notes
1	2.1	9.95	20.89	**1941**	1.45	125.8	Test speed 2 mm/min
2	2.02	9.83	19.86	**1819**	1.41	121.4	Extensometer for comparison
3	2.02	10.02	20.24	**1742**	1.39	118.2	-
4	2.05	9.94	20.38	**1841**	1.35	122.9	-
5	2.03	10.05	20.40	**1819**	1.42	121.9	-

Statistics	Mean	σ_{n-1}	C_V [%]
UTS [MPa]	**1832**	**71.4**	**3.9**
MOD [GPa]	**122.0**	**2.7**	**2.3**

Table T-27: Test results tensile strength of XAS/914C.

NT XAS/914C **Bolt Torque**				Test method: ICSTM/ standard test piece Test speed: 1.5 mm/min Thickness measured as moulded No strain gauges applied		
No	*t* [mm]	*w* [mm]	*A* [mm^2]	**UCS** [MPa]	Bolt torque [Nm]	Notes
1	2.10	9.87	20.73	**1632**	10/10	-
2	1.94	9.90	19.21	**1569**	10/10	-
3	1.94	9.87	19.15	**1400**	10/10	-
4	2.05	9.85	20.19	**1697**	15/10	-
5	2.01	9.86	19.82	**1702**	15/10	-
6	1.91	9.84	18.79	**1503**	15/10	-
7	2.09	9.89	20.67	**1059**	20/10	-
8	2.10	9.90	20.79	**1165**	20/10	-
9	2.11	9.87	20.83	**1154**	(30)/10	Clamping blocks deform plastically

Torque [Nm]	**UCS** Mean [MPa]	σ_{n-1} [MPa]	C_V [%]
10/10	**1534**	**120.0**	**7.82**
15/10	**1634**	**113.5**	**6.94**
20/10	**1112**	**(75.0)**	**(6.74)**

Table T-28: *Influence of clamping bolt torque on the measured compressive strength of XAS/914C.*

DC XAS/914C				Test method: ICSTM Test speed: 1.5 mm/min Bolt torque 10/5 Nm Specimens manufactured by Debby Carr, Birmingham University	
No	*t* [mm]	*w* [mm]	*A* [mm^2]	**UCS** [MPa]	Notes
1	2.04	9.96	20.32	**1342**	-
2	1.96	9.56	18.74	**1612**	-
3	(2.03) 1.99*	9.98	19.86	**1543**	Tab surfaces ground flat before testing; tab tips debonded by bending of the test piece * resin pimples removed in gauge section

Table T-29: *Test results compressive strength of XAS/914C; specimens produced at Birmingham University.*

Sample	N	UCS (Mean) [MPA]	σ_{n-1} [MPA]	C_V [%]
G5	5	1584	143.1	9.0
G7	6	1577	125.4	8.0
G10	6	1617	138.8	8.6
G12	5	1536	88.8	5.8
G15	6	1491	55.9	3.7
G20	5	1188	34.4	2.9
G30	2	900	-	-
G50	2	472	-	-
T8	5	1326	61.1	4.6
T12	5	1584	80.4	5.1
W5	5	1611	90.9	5.6
SGG	5	1722	100.8	5.9
SGGF	4	1705	26.3	1.5
DEB	5	1761	82.7	4.7
PM1	5	1710	142.2	8.3
COA2	5	1648	38.0	2.3
PP3	6	1688	120.4	7.1
DELST	5	1806	87.0	4.8
DELPT	5	1704	33.5	2.0
LC	5	1653	40.4	2.4
PM1D	4	1691	88.4	5.2
SC89	8	1622	96.6	6.0

Table T-30: *Summary of parameter study compressive strength of XAS/914C using the ICSTM method; abbreviations see Section 9.3.*

APPENDIX A1

Paper presented at ASM-3
Applied Solid Mechanics-3
University of Surrey
Guildford, April 6/7 1989

published by
Elsevier Applied Science

COMPRESSION TEST METHODS FOR COMPOSITES AND THEORIES PREDICTING THE COMPRESSIVE STRENGTH OF UNIDIRECTIONAL CFRP

J.G. HAEBERLE
F.L. MATTHEWS
Department of Aeronautics
Imperial College, Prince Consort Road, London SW7 2BY

ABSTRACT

Following a literature survey, compression test methods for composites have been classified and assessed. Our own experiments and microscopic examinations confirm some conclusions of the literature survey. An overview of reported compressive failure modes of unidirectional CFRP is given and mechanisms of failure initiation described. Some analytical models predicting the compressive strength of unidirectional CFRP are presented.

INTRODUCTION

Many specific static and dynamic properties of modern composite materials are superior to those of metals. Composites, however, are far from replacing metals because of some typical shortcomings due to their orthotropic nature. One major factor limiting the application of composites in primary structures is their low compressive strength after impact and at elevated temperatures. An increase of the compressive strength of current composite systems without sacrificing other properties, as for instance impact strength, is therefore desirable. This necessarily involves a better understanding of the complex compressive failure mechanisms and of their parameters. Although there has been research on the subject for more than twenty years, a unique analytical model predicting the compressive strength from the properties of the constituents is still not available.

Generally, the compressive strength of a composite system is understood to be the compressive strength of the unidirectional material, i.e. of a test piece made of unidirectional material loaded parallel to the fibres. Most real structures are laminated multidirectionally, a one-dimensional stress state is rather exceptional and constraints are quite different to those present in the specimen test. It seems nevertheless reasonable to regard this strength value as a fundamental material property.

The inherent orthotropy of composites, i.e. stiffness and strength in the fibre direction are very high and transverse to the fibres very low, makes testing of unidirectional composites very difficult. As test methods originally designed for metals cannot in most cases be applied

to composites, new methods had to be developed. This paper is thus divided into two sections: firstly, the results of a literature survey on compression test methods, concentrating on currently used techniques, will be presented; then, in the second section, compressive failure modes reported for unidirectional CFRP and parameters of the compressive strength are discussed, and some strength prediction models are described.

1. COMPRESSION TEST METHODS FOR COMPOSITES

Due to the nature of stability problems, compression testing requires a high level of precision and great care in carrying out the experiments. The individual tester's experience with the specific jig is therefore important and might influence the test results to a considerable extent. This is reflected by the great variety of published data for the compressive strength of composites [1, 2]. As a consequence, contradictory assessments of a test method by different authors can confuse the reader. Before comparing test methods some fundamental aspects of compression testing deserve attention.

Generating a uniform one-dimensional stress state is the main objective of a compression test fixture. The need to prevent overall buckling of the compressed specimen complicates the situation. Nowadays coupon specimens, cut from panels with a typical thickness of about 2 mm, are used for testing rather than rods. Therefore, the gauge length of these relatively thin specimens has to be short or they must be supported by an anti-buckling device. Short specimens with a typical gauge length from 5 to 12.5 mm are preferred for testing unidirectional material. Long gauge length, side-supported, specimens are used for testing multidirectional laminates, so that angle ply fibres are not constrained by the grips.

Stress concentrations due to load introduction increase with the degree of orthotropy of the material tested. Thus, stress concentrations present the most serious problems for unidirectional lay-ups and may cause premature failure of the specimen (figure 4). This problem will be discussed later. There are three basic methods of introducing a compressive load into the specimen: direct loading of the specimen end; loading the specimen by shear; and mixed direct and shear loading.

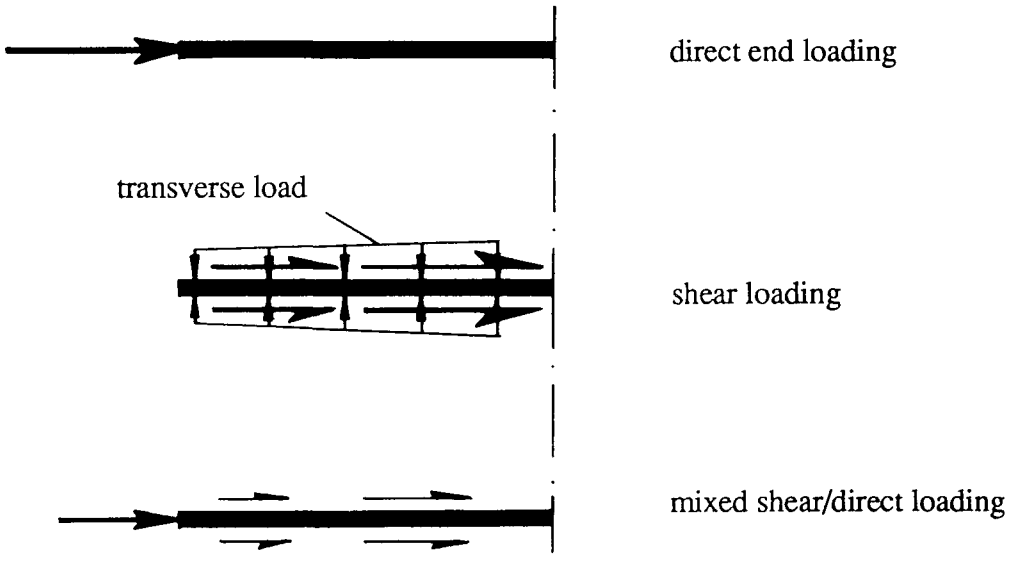


Figure 1. Different methods of load introduction into a compressive specimen

Direct loading of the specimen end as specified for instance in ASTM D695 'Test Methods for Rigid Plastics' is not suitable for high strength composites. Because of the low transverse strength and the low interlaminar strength of these materials the specimens fail by end crushing, sometimes referred to as 'brooming', and/or longitudinal splitting.

Shear loading of the specimen end, which is usually tabbed in the same manner as for a tension specimen, is the commonest method. Shape, material and precision of the end tabs are likely to influence the failure mode and strength result. One of the first fixtures using this principle is the Celanese fixture, developed at the Celanese Research Center and later adapted as ASTM D3410 standard [3]. The specimen is held in conical wedge grips which are accommodated in tapered sleeves. An outer cylinder maintains alignment of the parts. When the load is applied to the sleeves, it will be transmitted to the specimen by shear through friction between the specimen and the grips. This fixture needs careful adjustment to the specimen's thickness. Otherwise, non-uniform load distribution on the cones will lead to distortion of the sleeves and friction with the outer cylinder.

The German standard DIN 59273 and CRAG [4] specify slightly modified versions of the Celanese fixture and specimens. A more fundamental modification of the Celanese fixture was developed by the Illinois Institute of Technology Research Institute (IITRI). Here, tapered grips, which fit into matching pockets in massive steel blocks, are used rather than conical ones, so that specimens of different thicknesses can be easily accommodated. The steel blocks are aligned by pillar guides and linear ball bearings.

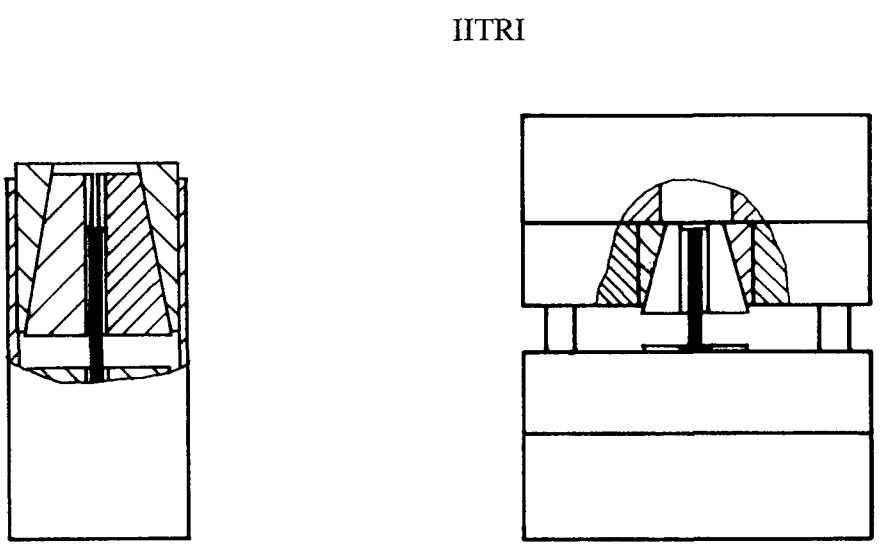


Figure 2. The Celanese and IITRI compression fixtures, shown schematically

The Wyoming University modified Celanese fixture uses trapezoidal wedge grips similar to the IITRI fixture, but with a conical surface of constant radius. Note that in the case of all the above mentioned fixtures the specimen end is loaded transversely in order to generate the shear load.

A typical representative fixture for mixed shear and end loading is the configuration proposed by Purslow and Collings and modified by Port at the Royal Aircraft Establishment (RAE) [5]. The specimen, which is waisted to force failure in the centre of the gauge length, is bonded into slots in aluminium end blocks. The amount of shear loading depends on the properties of the adhesive as well as on the thickness of the bond layer. Great care is needed in specimen preparation.

A modified ASTM D695 specimen (BOEING 1979) [2,5] is loaded in a similar way. The end-tabbed and overall-supported specimen with a gauge length of 5 mm is purely end-loaded. A certain amount of the load is introduced to the specimen by shear through the end tabs, depending on the stiffness of the tabs and bond layer. An additional alignment device is recommended. Although the specimen needs careful preparation the test jig is of remarkable simplicity. Due to the transverse constraint of Poisson's deformation the specimen may experience some transverse loading.

A variation of the RAE method is the fixture developed at Birmingham University [6]. Here, an RAE-type specimen with a waisted gauge section is clamped within steel cubes at the end rather than being bonded. Thus, the specimen end is loaded directly and a portion of the load is transmitted by shear depending on the clamping force. Mounting of the specimen is very simple, but due to clamping there is a certain amount of transverse loading.

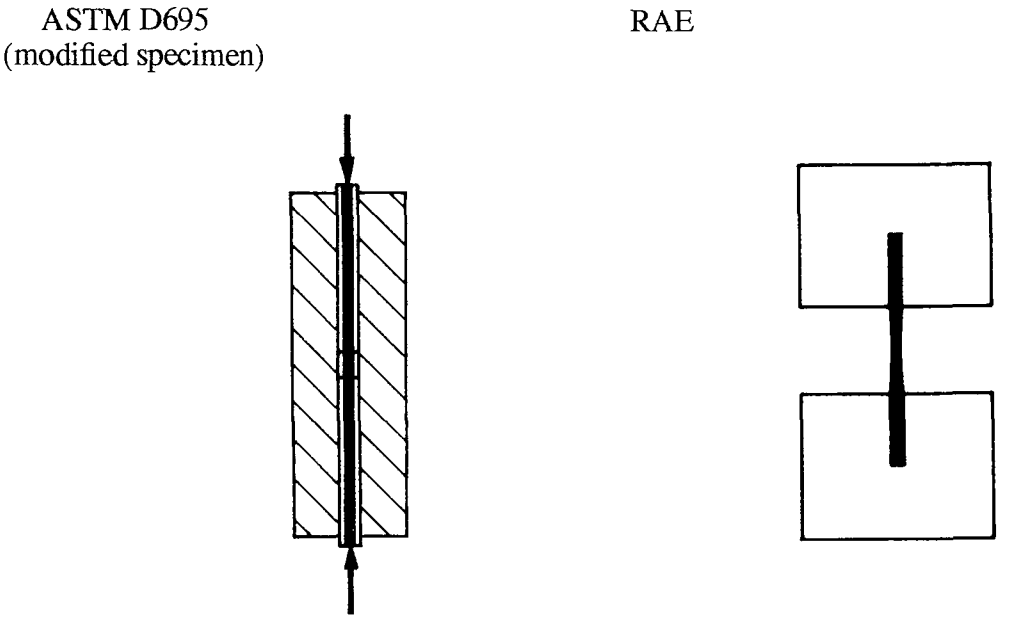


Figure 3. Modified ASTM D695 and RAE fixtures, shown schematically

Waisting the specimen, which in fact is an optimized form of tabbing, has to be carried out carefully in order to maintain a symmetric specimen, otherwise one would be likely to introduce bending and cause premature failure. Port [5] showed that interfacial splitting due to excessive shear stresses can be avoided when the specimen is waisted following the taper contour equation, which gives the minimum gauge length:

$$l_{min} = \ln(D/d)\, d\, S_c/S_{is} \qquad (1)$$

where l_{min} is the minimum gauge length, D the nominal specimen thickness, d the minimum specimen thickness, S_c is the compressive strength, S_{is} is the interlaminar shear strength.

Stress concentrations at the ends of the end tabs of unwaisted specimens initiate failure at local stress levels which can be significantly higher than the measured overall stress level. Therefore, strength results obtained with unwaisted specimens are to be regarded as a lower bound for the compressive strength. It is, on the other hand, unclear how damaging of surface fibres when the specimen's waist is machined influences compressive failure initiation.

Long gauge length specimens, i.e. multidirectional laminates, are either end-tabbed and shear-loaded or, as for instance recommended in CRAG [4], end-loaded with end fittings to prevent brooming.

Sandwich specimens are designed rather as sandwich beams than sandwich columns, and are loaded in four-point bending. The top cover composite sheet is the specimen to be tested. A metal honeycomb core and a bottom cover sheet with greater stiffness and strength ensure that the specimen fails on the compressive side. In this way very thin specimens can be tested. The high costs of this type of specimen led to the development of a reusable sandwich beam [7]. Here, the core in the test section is made of plexiglas and a CFRP sheet used as tension face. On the compression side the specimen, rather than being bonded, is clamped between two aluminium end caps.

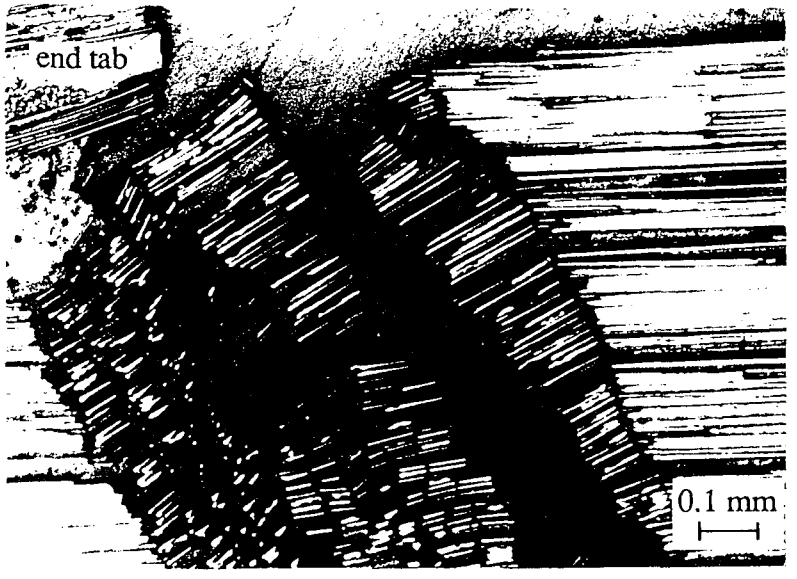


Figure 4. Compressive failure starting at the edge of end tab

Comparison of test methods

Now, some of the test methods mentioned will be assessed, starting from published comparative studies. Lamothe and Nunes [8] investigated the influence of fixture design on the compressive properties of glass-, Kevlar- and carbon/epoxy systems, as well as on FP alumina/aluminum and FP alumina/magnesium composites. Both methods employed, the IITRI and the Celanese, gave similar results for the tangent modulus. The IITRI method, however, was found to yield higher strength results and less scatter in data for the epoxy composites. The authors found both methods unsuitable for testing of metal matrix composites due to premature adhesive shear failure. Following an extensive review on compression test methods Berg and Adams [9] compared the IITRI, the Wyoming-modified Celanese method and a Wyoming end-loaded specimen configuration. The materials used were CFRP and GFRP in unidirectional and quasisotropic lay-up. The IITRI method again gave the highest strength results and lowest scatter of results for unidirectional composites, a fact attributed to the superior rigidity and consequently better specimen alignment of the IITRI fixture compared to the Wyoming rig. The end-loaded fixture using an unwaisted untabbed specimen surprisingly gave similar strength results as the Wyoming fixture. Strength and modulus data for the quasi-isotropic laminates were similar for all the three methods. Comparing data gained with strain

gauges and extensometers it was concluded that both methods are equivalent, but strain gauges are recommended. Extensometers, though easier to mount, are likely to be damaged at specimen failure. Adsit [1] stated, regarding results of a testing round robin including a sandwich beam, that Celanese and IITRI methods give comparable results. The IITRI method, however, appeared to be easier to use and more flexible to varying specimen thickness. Reducing the gauge length of the Celanese specimen down to a length of 6 mm leads to increasing compressive strength results as shown by Lee [10]. Results achieved with specimens of different gauge length should therefore be handled with care. This is confirmed by the investigations of Woolstencroft et al. [2] on a CFRP system. They compared a range of test methods including the standard Celanese method; a modified version using a waisted specimen with a gauge length of only 4 mm; the RAE method; and the modified ASTM D695 method. They found that the modified Celanese specimen yielded strength results some 50% higher than the standard version. A (linear) finite element analysis, however, revealed a poor distribution of longitudinal stress and noticeable transverse stresses in the centre of the gauge length from which they concluded that the specimen was not measuring a true compressive strength. According to the finite element analysis the ASTM specimen had a reasonable stress distribution, second only to the RAE specimen which offers the most uniform distribution with negligible transverse stresses. A design value, calculated as the mean minus three times the standard deviation of the strength results of the test, was used to assess the methods. The standard Celanese, giving a low mean value and high scatter, as well as the ASTM D695, with a reasonable mean but high scatter of results, were rejected as test methods. Because of the relatively high mean of the RAE method combined with a remarkably low scatter of results, they finally recommended that method as the most suitable to characterise compressive properties of CFRP. Port, however, demonstrated that this specimen exhibited macro instability and therefore measured a buckling strength [5]. This could explain why the scatter of test results achieved with the RAE method was so low. Port consequently proposed a new standard specimen with reduced slenderness ratio. He also reports similar strength results for the new RAE specimen and the modified Celanese specimen when the slenderness ratio of the latter is increased to the same order as that of the RAE specimen. The fixture proposed by Barker [6] employs the new RAE standard specimen with the attractive feature that the specimen is not bonded, but clamped. Barker reports similar results gained with both methods and stresses the merits of an untabbed unbonded specimen when testing under various environmental conditions. Our own experiments, although at an early stage, showed that scatter of test results achieved with the ASTM D695 modified specimen can be substantially reduced by a careful preparation of the specimen surfaces [11]. The method offers the advantage of very low fixture-introduced bending, and easy handling. We also found that CRAG and IITRI specimens, cut to length, yielded higher results when tested according to the modified ASTM D695 method than when tested in the standard fixture.

The sandwich beam was found to give results consistent with those achieved with the IITRI method [1]. The properties of the core can influence the failure mode of the beam [12]. If the core takes a certain amount of the bending load, which is the case with the plexiglas core of the reusable sandwich beam, the neutral axis of the beam must be known before the load on the specimen can be determined. This is not simple, because the elastic behaviour of the cover sheets is not linear, therefore the neutral axis is dependent on the strain state. It should also be noted that transverse stresses are built up when the curved specimen is compressivly loaded. These stresses are supposed to inhibit the compressive failure process to a certain amount. That tendency can be observed in compression/tension fatigue tests of a reusable sandwich specimen [13].

Almost all authors report that the modulus of elasticity seems only weakly dependent on the test method. Care only has to be taken to exclude interaction of specimen and side support or friction between sleeves and cones, as for instance in the Celanese rig.

2. THEORIES PREDICTING THE COMPRESSIVE STRENGTH OF UNIDIRECTIONAL CFRP

Any strength prediction for a given material is possible only when the failure mode of the material is known. Unfortunately, observations of the failure process in unidirectional composites are almost impossible because the event is sudden and catastrophic. Post-failure analysis of the fracture surfaces is very difficult and may be misleading when the sudden release of stored elastic energy of the specimen, the testing rig, and the testing machine destroys the evidence of initial failure. That is why it is often difficult to distinguish between primary and secondary failure modes.

Failure modes reported for CFRP specimens include: macrobuckling of the specimen [5]; crushing of the specimen end and longitudinal splitting [14]; interfacial failure [5, 14, 15]; microbuckling of fibres in several wavelengths [16] or in a kink band pattern [11, 16-19]; shear failure of the specimen [20] and shear fracture of fibres at several locations [19].

Shear failure of the specimen, which is to be regarded as an upper limit for the compressive strength of any material, was observed at room temperature by Ewins and Ham [20]. Moving to higher temperatures, they discovered that the failure mode changed to a microbuckling type. Port [5] states that such a transition is not encountered in currently used CFRP systems and that failure is always of a microbuckling type, regardless of temperature. This is due to the fact that modern matrices are less brittle and stiff than the early systems so that the fibres fail by buckling before their compressive strength is reached. Shear failure of single fibres at several locations, causing gradual failure of the composite, was observed only for high-modulus fibre bundles embedded in epoxy resin [19].

Microbuckling of fibres or fibre bundles, i.e.local micro-instability, is accepted by most authors as the principal failure mode of currently-used high strength carbon fibre-reinforced plastics, although the mechanisms triggering failure are still unclear. In soft matrices fibres were found to buckle over several wavelengths [16], but failure of a kinking type is usually observed in CFRP. In stiffer matrices the brittle carbon fibres are likely to break immediately after buckling at two locations due to additional bending stresses. Since the buckled fibre disturbs the equilibrium of neighbouring fibres the kink band defined by rotated fibre segments which may experience further breakage during the failure process will spread across the specimen as shown in figure 5.

The boundary planes of the kink bands are usually inclined at an angle of approximately 65 to 75 degrees to the fibre direction either in the thickness or width direction . The specimen, therefore, exhibits fracture surfaces in these planes. Crossing kink bands and kink bands 'reflected' at the edge of the specimen have been observed frequently. Longitudinal splitting is likely to occur as a secondary effect when transverse tensile stresses are developed due to kinematic incompatibility in the matrix, or when a kink band meets a void. Whether the angle of kink band inclination and the kink band width are of significance is still unclear.

Early investigators assumed buckling of initially straight fibres in a shear mode (antisymmetric buckling). Models based on the classical buckling theory for bars on an elastic foundation yielded results which overpredicted the compressive strength of composites by a large margin. One of the first models was that of Rosen [21] where the compressive strength is only dependent on the (initial) matrix shear modulus G_m and the fibre volume fraction V_f:

$$S_c = G_m/(1-V_f) \qquad (2)$$

More detailed investigations, for instance incorporating a three-dimensional continuum rather than treating matrix and fibre as two-dimensional plates, brought similar results. Only the introduction of nonlinear models including initial fibre deflection yielded somewhat more realistic predictions, as shown later.

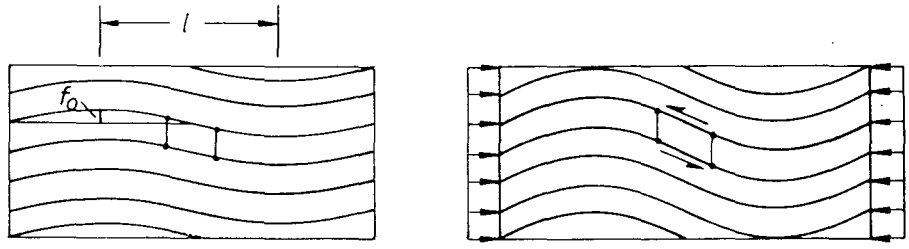


Figure 5. Kink bands in a specimen failed under compression

Weaver and Williams tested CFRP with a fibre volume fraction of 36% under hydrostatic pressure [14] and found increasing compressive strength with increasing pressure. They observed specimen failure by end crushing and longitudinal splitting from the end as well as debond failures in the specimen body at low pressures. At higher pressures the failure mode changed to a kinking type. The bond failures can be attributed to transverse tension stresses which are diminished by high pressure. High transverse tension stresses are generated when fibres buckle in an extensional, i.e. symmetric, mode, which is assumed to be the lowest energy buckling mode in composites with low fibre volume fraction. For composites with high volume fraction these results cannot be regarded as relevant. Transverse tension stresses in the matrix, on the other hand, are also caused by the mismatch of Poisson's ratio of matrix and fibre, matrix cooling shrinkage and moisture absorption. They may reach significant values as pointed out by Woolstencroft [22] and cause matrix/fibre bond failure thus initiating fibre microbuckling.

Parry and Wronsky carried out compression tests with CFRP containing type 3 carbon fibres under hydrostatic pressure [15]. They used specimens in dogbone shape with circular cross section. Failure was by fibre kinking preceded by some longitudinal splits and interfacial failure starting from the centre of the waist at low pressure. At higher pressures longitudinal splitting was suppressed. Interfacial failure seems to be a specimen design problem (equation 1) as was longitudinal splitting from the specimen end in the case mentioned above. The ultimate compressive stress was strongly dependent on pressure. They rejected therefore any model based on shear stress controlled failure such as reported by Ewins and Ham, which would be much less pressure dependent. Also, theories where the compressive strength is based on the matrix shear modulus as proposed by Rosen were ruled out, because the initial matrix shear modulus is only weakly dependent on pressure. The shear strength of the composite, however, increases in a similar range as the compressive strength. They considered therefore models based on the shear strength rather than the modulus as more suitable to predict the ultimate compressive stress.

A nonlinear model which assumes local shear instability triggering failure is described analytically by several authors [16, 23, 24] as follows. The fibres may be deflected in the stress-free state of the composite as depicted in Figure 6a and described by a sine function.



(a) (b)

Figure 6. Initial fibre deflection in the composite

Under a compressive load the fibre deflection will increase, causing mainly shear deformation in the intermediate matrix (figure 6b). Regarding a fibre element one obtains for the condition of equilibrium of outer and inner stresses [16]:

$$\sigma_c = V_f \tau(\gamma) / (\gamma + \pi f_0/l) \qquad (3),$$

where σ_c is the applied compressive stress, $\tau(\gamma)$ is the interlaminar shear stress due to the shear strain γ and f_0/l is the ratio of initial fibre deflection to wavelength (figure 6).

Note that other authors [23, 24] get the same result without the factor V_f, because they regard the forces as acting on a fibre/matrix element rather than on a fibre element. The maximum of the right hand side of Eq.(3) gives the ultimate compressive stress, i.e. the compressive strength. If the shear stress-strain curve $\tau(\gamma)$ for the composite is known explicitly, the shear strain at which instability occurs can be calculated from the condition:

$$\tau(\gamma^*) - (\gamma^* + \pi f_0/l)\, \tau'(\gamma^*) = 0 \qquad (4),$$

where $\tau' = d\tau/d\gamma$ and with Eq. (3) we get for the ultimate compressive stress:

$$\sigma_{cu} = V_f \tau'(\gamma^*) = V_f G_{lt}(\gamma^*) \qquad (5).$$

The compressive strength is equal to the local tangent shear modulus of the composite at the strain defined by Eq.(4) multiplied by the fibre volume fraction. If the explicit equation for the stress strain curve is not known an incremental procedure as proposed by Wang [23[has to be applied.

Unfortunately, f_0/l is at best a statistical quantity and difficult to measure for a given composite. Wang, therefore, proposed the following procedure to prove the validity of the strength prediction model. Firstly, the shear-stress strain behaviour of the composite is determined from stress-strain curves of a $\pm 45^\circ$ laminate under tension. With these data a value for f_0/l is selected so that the predicted result matches the experimental value in a particular test condition. f_0/l is then regarded as a material property independent of test conditions. Applying the theory with shear stress-strain curves from different test conditions, i.e. temperatures, Wang found that predicted results agreed reasonably well with the experimental results.

If a linear elastic-perfectly plastic shear stress-strain behaviour of the composite with shear yield stress S_{is} and shear yield strain γ_y is assumed, the compressive strength is given by:

$$S_c = V_f S_{is} /(\gamma_y+\pi f_0/l) = V_f G_{lt} /(1+\beta) \quad (6),$$

where $\beta = (f_0/l) /\gamma_y$,

or

$$S_c = S_{is} /(\gamma_y+\pi f_0/l) = G_{lt} /(1+\beta) \quad (7),$$

when a fibre/matrix element is regarded as a free body (see above) [24].

Hahn and Williams [16] calculated the factor β from representative results and took G_{lt} as the initial modulus of the composite. Using equation 6 they then found in general a reasonable agreement of predicted compressive strength and experimental data for different composite systems. Only for a resin tensile modulus less than 3 GPa was the compressive strength over-predicted.

Empirical equations predicting the compressive strength of CFRP from other mechanical properties of the composite are presented by Sinclair and Chamis [25]. They propose that as an upper bound the compressive strength of the composite can be calculated from the compressive strength of the fibre, which is taken as 90% of the fibre tensile strength. The compressive strength for the composite is then :

$$S_c = 0.9\ S_t \quad (8),$$

where S_t is the tensile strength of the composite. As an estimate for the lower bound for the compressive strength they suggest equations including the flexural strength S_{fl} or the interlaminar short beam strength S_{is} of the composite and the matrix tensile strength S_{tm}:

$$S_c = S_{fl} /(3 - S_{fl}/S_{tm}) \quad (9)$$

and

$$S_c = 10S_{is} + 2.5\ S_{tm} \quad (10).$$

Equations 9 and 10 were found to provide a reasonable estimate for a variety of composite systems according to unpublished Lewis Research Center data [25].

Finally, the more general failure mode of macrobuckling will be discussed briefly. Macrobuckling is understood as an overall instability of the specimen, describing a structural rather than a material property. Therefore macrobuckling of the specimen should be avoided during testing. The Euler buckling equations allow a rough estimate of the maximum specimen length or specimen slenderness ratio, defined as the ratio of specimen length to radius of gyration of the cross section. A correction of these equations for highly anisotropic materials, which includes shear deformation in the differential equation of the deflected beam, seems to be reasonable for unidirectional composites. Shear deflections should be taken into consideration, especially when the specimen is relatively short [26, 27].
The critical Euler stress is given by:

$$\sigma_{cr} = C\pi^2 E/s^2 \quad (11),$$

where E is the bending modulus of elasticity, which can be approximated by the longitudinal modulus for unidirectional materials. The bending modulus of multidirectional laminates can be very different for various stacking sequences, causing different buckling behaviour, where-

as the longitudinal modulus is almost independent of the stacking sequence. The slenderness ratio s can be written as 3.46 l/d for rectangular crossections, where l is the free buckling length and d is the thickness. C is a constant dependent on the constraint conditions of the specimen ends. Its value is 1.0 for a hinged/hinged condition; the greatest value is 4.0 for a clamped/clamped condition.

The critical stress when shear deformation is included is given by [27]:

$$\sigma_{cr} = \sigma_E/(1+n\sigma_E/G) \qquad (12),$$

where σ_E is the critical Euler buckling stress, G is the shear modulus of the composite and n is a dimensionless factor depending on the cross section. For a rectangular cross section n is 1.2.

Since the constraint conditions of the specimen usually are not known exactly, the application of these equations is limited. Tests with material of well-known linear elastic behaviour such as metals may allow somewhat realistic assumptions of these conditions. But even when the constraint constants are known some questions remain. The modulus of elasticity is not a constant, but decreases with increasing strain. Therefore buckling might occur earlier than expected from linear buckling theory [5]. And, due to debonding of the end tabs at increasing load, the free specimen length may change during the test [28].

Macrobuckling failure of a specimen designed close to the critical length is difficult to detect. That is because macrobuckling may be introduced by local microbuckling of fibres, consequently disturbing the overall stability of the specimen. Although the specimen may fail in a compressive manner it will appear as if it failed in macrobuckling. On the other hand, macro instability causes additional stresses due to bending. These can initiate microbuckling failure and the specimen will show evidence of a 'real' compressive failure although it failed due to instability. Interfacial splitting again may occur as a post-buckling effect to add further complications.

CONCLUSIONS

Test methods

The literature survey on compression methods for composites showed that short gauge length specimens are used for testing unidirectional material, and specimens with a long, supported, gauge length are used for multidirectional laminates. Load introduction is either by shear or by mixed shear/end loading. The published test data suggest that the influence of the individual researcher and the individual rig might be bigger than the influence of the test method itself. In other words, if the specification of each test method could be carefully fulfilled, the difference in test results gained with different test methods would be less significant. However, test results from specimens with different slenderness ratios are to be compared with caution.

Ease of use of the rig and the cost of rig and specimen manufacturing are important criteria when choosing a test method. The IITRI fixture was found by most authors to be easy to use and the specimen is relatively simple. Care has to be taken to ensure good alignment when loading the specimen. Another advantage of this method is that it is widely used, as well as Celanese-type fixtures which yield consistent results. Partially end-loaded specimens require great care in machining, but they are likely to experience less stress concentrations due to load introduction. The Birmingham method is interesting, because it uses an untabbed specimen and because mounting of the specimen is very simple. Simplicity of the rig is the big advantage of the ASTM D695 method with a modified specimen.

The modulus of elasticity was found to be independent of the test method. Strain gauges are recommended for strain recording rather than extensometers.

Strength prediction

Most authors accept micobuckling failure of a kinking type as the principal failure mode of modern high-strength CFRP. But the mechanisms of failure initiation are still unclear. Therefore a model predicting the compressive strength of unidirectional CFRP from fundamental properties of the constituents of the composite is not yet available. Models assuming local shear instability to be the mechanism triggering failure considering initially deflected fibres and nonlinear matrix shear behaviour look promising. The shortcoming of these models is that the fibre misalignment is very difficult to quantify *a priori*, thus making a verification of the model difficult. In addition, the shear stress-strain behaviour of the composite is difficult to measure and requires considerable experimental effort. However, even simplified models showed reasonable agreement with the experimental data.

ACKNOWLEDGEMENTS

The authors wish to acknowledge the support of the Ministry of Defence (Procurement Executive)

REFERENCES

1. Adsit, N.R., Compression Testing of Graphite/Epoxy. Compression Testing of Homogeneous Materials and Composites, ASTM STP 808, Richard Chait and Ralph Papirno, Eds., American Society for Testing and Materials, 1983, pp. 175-186.

2. Woolstencroft, D.H., Curtis, A.R. and Haresceugh, R.I., A Comparison of Test Techniques Used for the Evaluation of the Unidirectional Compressive Strength of Carbon Fibre Reinforced Plastic. Composites, Vol. 12, No. 4, October 1981.

3. American Society for Testing and Materials, ASTM D3410-75 (reapproved 1982): Standard Test Method for Compressive Properties of Unidirectional or Crossply Fiber-Resin Composites, 1975.

4. Curtis, P.T., CRAG Test Methods for the Measurement of the Engineering Properties of Fibre-Reinforced Plastics. Royal Aircraft Establishment, Technical Report 85099, 1985.

5. Port, K.F., The Compressive Strength of CFRP. Royal Aircraft Establishment, Technical Report 82083, 1982.

6. Barker, A.J., Balasundaram,V., Compression Testing of Carbon Fibre-Reinforced Plastics Exposed to Humid Environments. Composites, Vol. 18, No. 3, July 1987.

7. Gruber, M.B., Overbeeke, J.L. and Chou, T.-W., A Reusable Sandwich Beam Concept for Composite Compression Test. J. Comp. Mat., Vol. 16 (May 1982), pp. 162-171.

8. Lamothe, R.M. and Nunes, J., Evaluation of Fixturing for Compression Testing of Metal Matrix and Polymer/Epoxy Composites. In Compression Testing of Homogeneous Materials and Composites, ASTM STP 808, R. Chait and R. Papirno, Eds., American Society for Testing and Materials, 1983, pp. 241-253.

9. Berg, J.S. and Adams, D.F., An Evaluation of Composite Material Compression Methods, Mechanical Engineering Department, University of Wyoming, Report UW-CMRG-R-88-106, 1988.

10. Lee, R.J., Compression Strength of Aligned Carbon Fibre-Reinforced Thermoplastic Laminates. Composites, Vol. 18, No. 1, January 1987.

11. Haeberle, J. and Matthews, F.L., The Compressive Mechanical Properties of Fibre-Reinforced Materials. Second Interim Report, Department of Aeronautics, Imperial College, London, January 1989.

12. Shuart, M.J., An Evaluation of the Sandwich Beam Compression Test Method for Composites. In Test Methods and Design Allowables for Fibrous Composites, ASTM STP 734, C.C. Chamis, Ed; American Society for Testing and Materials, 1981, pp. 152-165.

13. Argyris, J., Eberle, K. and Haeberle, J., Lebensdauerkennwerte aus Betriebsbelastungen von kohlefaserverstaerkten Kunststofflaminaten, DFG Abschlussbericht, Institut fuer Computeranwendungen, Universitaet Stuttgart, June 1988.

14. Weaver, C.W., and Williams, J.G., "Deformation of a Carbon-Epoxy Composite Under Hydrostatic Pressure". J. Mater. Sci., Vol. 10, 1975, pp. 1323-1333.

15. Parry, T.V. and Wronsky, A.S., Kinking and Compressive Failure in Uniaxially Aligned Carbon Fibre Composite Tested Under Superposed Hydrostatic Pressure. J. Mat. Sci., Vol.17, 1982, pp. 893-900.

16. Hahn, H.T. and Williams, J.G., Compression Failure Mechanisms in Unidirectional Composites. In Composite Materials: Testing and Design (7. Conference), ASTM STP 893, J.M. Whitney, Ed., American Society for Testing and Materials, Philadelphia, 1986, pp. 115-139.

17. Evans, A.G., Adler, W.F., "Kinking as a Mode of Structural Degradation in Carbon Fibre Composites". Acta Metallurgica, Vol. 26, 1978, pp. 725-738.

18. Potter, R.T., Some Fractographic Investigations of Compressive Failures in Carbon Fibre-Reinforced Plastics. Royal Aircraft Establishment, Technical Report 86049, 1986.

19. Hahn, H.T., and Sohi, M.M., Buckling of a Fibre Bundle Embedded in Epoxy. Composites Science and Technology, Vol. 27, 1986, pp. 25-41.

20. Ewins, P.D. and Ham, A.C., The Nature of Compressive Failure in Unidirectional Carbon Fibre-Reinforced Plastics. Royal Aircraft Establishment, Technical Report 73057, 1973.

21. Rosen, B.W., In Mechanics of Composite Strengthening, American Society of Metals Seminar, Philadelphia, Pa, October 1964.

22. Woolstencroft, D. H., Haresceugh, R.I., Curtis, A.R., The Compressive Behavior of Carbon Fibre-Reinforced Plastic. In Progress in Science and Engineering of Composites, T. Hayashi, K. Kawata and S. Umekawa, Eds., ICCM-IV, Tokyo, 1982.

23. Wang, A.S.D., A Nonlinear Microbuckling Model Predicting the Compressive Strength of Unidirectional Composites. ASME Paper No. 78-WA/Aero-1, American Society of Metals, 1978.

24. Tsai, S.W. and Hahn, H.T., Introduction to Composite Materials. Technomic Publishing Company, Westport, Connecticut, 1980.

25. Sinclair, J.H. and Chamis, C.C., Compressive Behavior of Unidirectional Fibrous Composites. In Compression Testing of Homogenous Materials and Composites, ASTM STP 808, R. Chait and R. Papirno, Eds., 1983, pp.155-174.

26. Timoshenko, S.P. and Gere, J.M., Theory of Elastic Stability. Second Edition, McGraw-Hill, 1961.

27. Chou, T.-W., and Kelly, A., The Effect of Transverse Shear on the Longitudinal Compressive Strength of Fibre Composites. J. Mater. Sci., Vol. 15, 1980, pp. 327-331.

28. Chamis, C.C. and Sinclair, J.H., Longitudinal Compressive Failure Modes in Fiber Composites: End Attachement Effects on IITRI Type Test Specimens. J. of Composites, Technology and Research, Vol 7, No 4, Winter 1985, pp. 129-135.

APPENDIX A2

Paper presented at ECCM-4
Fourth European Conference on Composite Materials
Developments in the Science and Technology of Composite Materials
Stuttgart, September 25-28, 1990

published by
Elsevier Applied Science

STUDIES ON COMPRESSIVE FAILURE IN UNIDIRECTIONAL CFRP USING AN IMPROVED TEST METHOD

J.G. HAEBERLE, F.L.MATTHEWS

Imperial College of Science, Technology and Medicine
Department of Aeronautics
Prince Consort Road - London SW7 2BY - England

ABSTRACT

A new test method for compression testing of unidirectional composites is proposed. It includes elements of established methods and, it is suggested, combines their advantages and avoids their shortcomings. A major postulate was to keep the rig and the specimen as simple as possible whilst at the same time reducing specimen constraints. Test results comparing different test methods are presented. The effect of some factors of specimen preparation on the measured strength is summarised. A specimen design which offers a more uniform stress distribution emerges from the observations made during testing. The failure mode of macrobuckling is then examined considering the nonlinear elastic behaviour of unidirectional CFRP.

INTRODUCTION

Following a literature review /1/ it was felt that an intensive study was necessary in order to establish the most meaningful test method for compression testing of composites. In short, the conclusions of the survey were that the compressive strength of a unidirectional CFRP system is difficult to determine, and to a large extent the experimental result is dependent on many factors such as method of load introduction, specimen design and preparation, and fixture alignment, to name a few. A series of experiments led to the development of the test method described below.

I - EXPERIMENTAL PROCEDURE

1.1 Test Method

The design of the rig is based on the fixture developed at Birmingham University /2/, but an end loaded tabbed specimen with a gauge length of 10 mm is used, rather than

a waisted untabbed RAE-type specimen as proposed by Barker and coworkers /2/. The specimen is only slightly clamped in end blocks and loaded on its ends. This resembles the loading configuration of the Boeing modified ASTM D695 method with the advantage that end failures of the test piece are avoided. By means of a high precision die set frictional effects are minimised and axial loading of the test piece is guaranteed. Figure 1 shows the main features of the rig and the specimen. The other methods used for the comparison are the CRAG (modified Celanese); IITRI; and the modified ASTM D695 method. A short description of these methods is found in /1/.

1.2 Materials and test piece preparation

The material used throughout the tests was Fibredux 914C/Courtaulds XA-S. The cured panels were postcured in the recommended cycle and stored in vacuum. After grit-blasting, end tab plates were bonded onto the CFRP panels using room temperature curing adhesive. From these plates the individual test pieces were cut on a diamond-tipped saw. The tab surfaces were then ground flat (see Figure 1) and the test pieces instrumented with strain gauges on either side of the gauge section. All tests were carried out at room temperature.

1.3 Parameters examined

The parameters examined were: surface of the the gauge section by using different peel plies in the autoclave; fibre misalignment: material cut 2° off axis from a unidirectional panel and material layed up ±1°; thickness and length of the gauge section: 8, 12 and 16 plies and 5 to 20 mm respectively; and specimen width: 10 and 5 mm. Different end tab materials were included as well, the standard being 0/90° glass fibre/epoxy.

II - TEST RESULTS AND DISCUSSION

2.1 Comparison of different test methods

Results from a testing short course where different methods were compared are summarised in Figure 2. The mean strength result achieved with the proposed method is considerably higher than those obtained with CRAG and IITRI, a fact that can be attributed partly to lower stress concentrations introduced by the testing hardware, since the specimens have similar dimensions. It can be shown that, for instance, transverse forces as experienced by the test piece in the Celanese rig could cause additional curvature of surface fibres near the tab edge, resulting in premature failure of the specimen; see Figure 3. In practice the new (ICSTM) rig proved to be reliable and the easiest to use.

2.2 Influence of parameters of test piece production

None of the parameters listed above influenced the measured apparent strength significantly when identical slenderness ratios were compared. The only factor which seemed to influence the result was the end tab/CFRP interface as described below.
FE calculations predict high longitudinal stress peaks near the edge of the end tab. The stiffer the tab the higher are these predicted stress peaks. Surprisingly, specimens where the gauge section was machined out from thicker material showed comparatively high

test results, although these tabs resembled the stiffest in the present investigation. What seemed to be a contradiction of the FE analysis could be explained after a close examination of the specimens during the test. Figure 4 (a) shows a typical stress strain curve for these specimens. The local divergence of the strain gauge signals on opposite sides of the gauge section could be identified as the start of interlaminar shear failure starting at the corner of end tab and gauge section, i.e. the start of delamination of the end tab. Therefore stress concentrations were relieved in this critical area, allowing higher average failure stresses. This mechanism is thought to be a further reason for the higher results achieved with the ICSTM jig as the through-thickness pressure with the indirect (i.e. when the load is introduced by shear) compression test methods reduces the tendency of the tab tips to debond. Somewhat erratic delaminations account for a part of the scatter found in compression testing of composites.

2.3 Improved Specimen

It was found that, indeed, failure stresses up to 13% higher than these obtained with the standard specimen could be achieved when the delamination of the tab edges was controlled. This was realised by including a small strip of PTFE tape into the adhesive layer or by just leaving out a strip of some 5 mm beside the gauge section when grit-blasting the panels. Five specimens produced in that way gave a mean value of 1806 MPa with a coefficient of variation of 4.8 %; see Figure 2 (DELST).

2.4 Failure modes

The fracture surfaces of all the broken specimens looked similar macroscopically regardless of the test method or the parameter of manufacture. In almost all cases failure started near the end of the gauge section, adjacent to the tab edge. The fracture surfaces usually were inclined at an angle of about 75° to the fibre axis either in thickess or in width direction of the specimen. This indicated a fibre-kinking type of failure with a sharply defined band of kinked fibres, as sometimes observed in arrested failures /3/. The massive post-failure damage to the surfaces usually made it impossible to verify the kink bands microscopically.

The higher stresses achieved with the improved specimen presented a new problem. As can be seen from Figure 4 (d) even specimens of 10 mm gauge length now failed in a macro buckling mode, i.e. overall specimen instability, as indicated by the diverging signals of the opposing strain gauges. The Euler equations are known to overpredict the buckling stress for short composite bars by a large margin. If, however, the local tangent modulus of elasticity $E_t(\varepsilon)$, which decreases considerably with strain as pointed out in Figure 5, rather than the initial modulus is considered to be relevant, and the shear deformation is included in the differential equation of the buckled shape, the prediction of the critical stress becomes much more realistic. The critical stress for macro instability of the test piece can then be calculated using the following equation /4/:

$$\sigma_{cr} = \sigma_{Eu}\, 1/(1+n\, \sigma_{Eu}/G),$$

where the Euler buckling stress is taken here as:

$$\sigma_{Eu} = C\, \pi^2\, E_t(\varepsilon^*) / s^2.$$

n is a geometric factor subject to the cross section (n=1.2 for a rectangular cross section), G is the initial shear modulus of the material, C is a factor to characterise the

end conditions of the compressed bar (C=1 for hinged and C=4 for built-in ends), s is the slenderness ratio of the bar and ε^* is the mean failure strain. The equation is solved iteratively and plotted for several clamping conditions in Figure 6. It can be seen how the shear deformation gains influence on the buckling stress for small slenderness ratios. The test results for specimens of different gauge lengths are included in Figure 6. The standard specimens with gauge lengths of 12.5 mm and more, which failed mainly in a macro buckling mode, and the improved specimen with 10 mm gauge length seem to fit the curve with a clamping constraint constant C of about 1.8 reasonably well. There is a tendency towards smaller values of C with decreasing slenderness ratio of the test piece. This might be explained by the higher stiffness of the shorter specimens compared to the test rig. It should be mentioned that macrobuckling of the specimen, which is elastic initially, initiates compressive failure on a microlevel, but at unknown local stress levels. Local compressive strains of elastically buckled specimens often exceeded 2%. The fracture surface and its location, however, gives no evidence of the initial type of failure.

CONCLUSIONS

High strength results achieved with the method presented indicate that stress concentrations which cause premature failure of coupon specimens are reduced compared to conventional test methods. The more so when the test piece is prepared so that the end tab edge can debond easily and symmetrically without sacrificing lateral support, as it would if the edges were tapered. It is, however, evident from the results that test coupons with standard dimensions might not be suitable to determine the compressive strength of high strength CFRP systems. The decreasing modulus of elasticity might lead to a buckling failure of the test piece even for smaller slenderness ratios than those presented.

ACKNOWLEDGEMENTS

The authors wish to acknowledge the support of the Ministry of Defence (Procurement Executive).

REFERENCES

1. Haeberle, J.G. and Matthews, F.L., "Compression Test Methods for Composites and Theories Predicting the Compressive Strength of Unidirectional CFRP." Proceedings of the conference "Applied Solid Mechanics-3", April 6/7 1989 at the University of Surrey, Guildford, Elsevier Applied Science, 1989.

2. Barker, A.J. and Balasundaram, V., "Compression Testing of Carbon Fibre-Reinforcd Plastics Exposed to Humid Environments". Composites, Vol. 18, No. 3, July 1987.

3. Haeberle, J.G. and Matthews, F.L., "The Compressive Mechanical Properties of Fibre- Reinforced Plastics". Third Interim Report, Department of Aeronautics, Imperial College, London, May 1989, (unpublished).

4. Timoshenko, S.P. and Gere, J.M., "Theory of Elastic Stability", McGraw-Hill Kogakusha Ltd, Tokyo, 1961

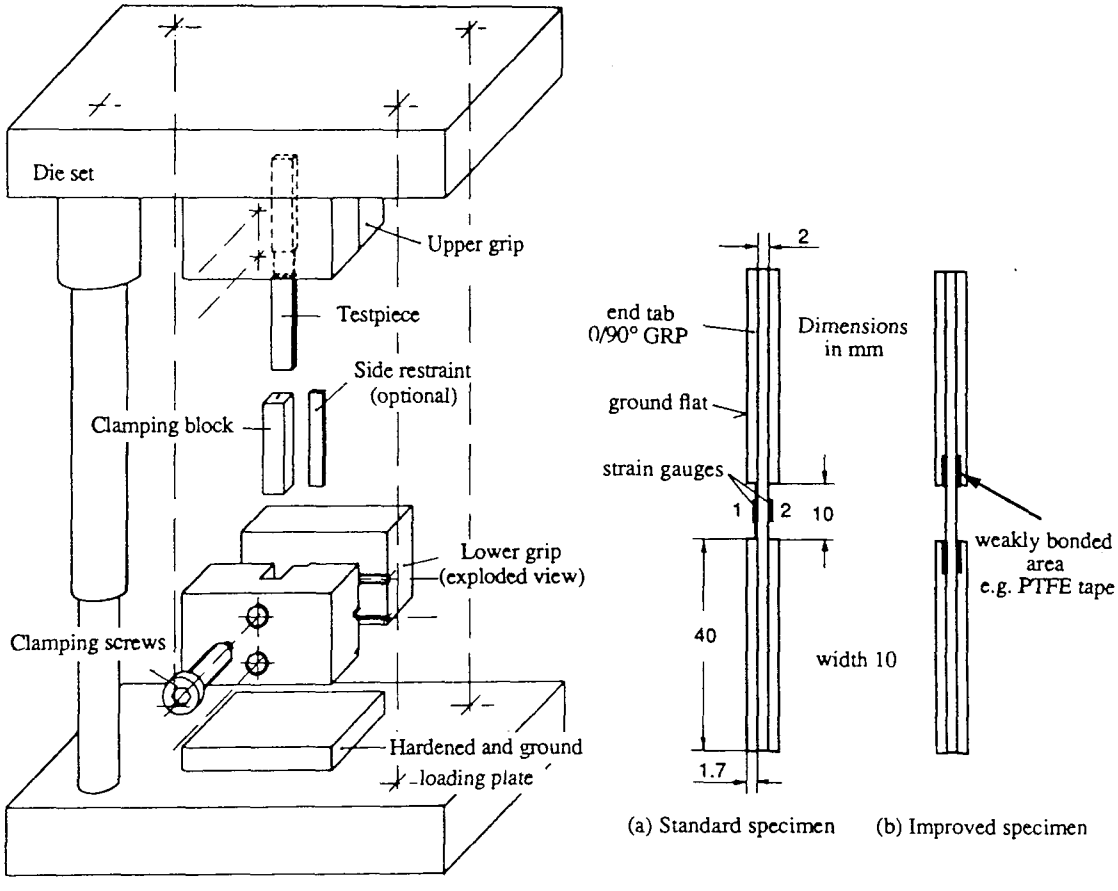


Fig. 1: Imperial College (ICSTM) compression test rig and specimen

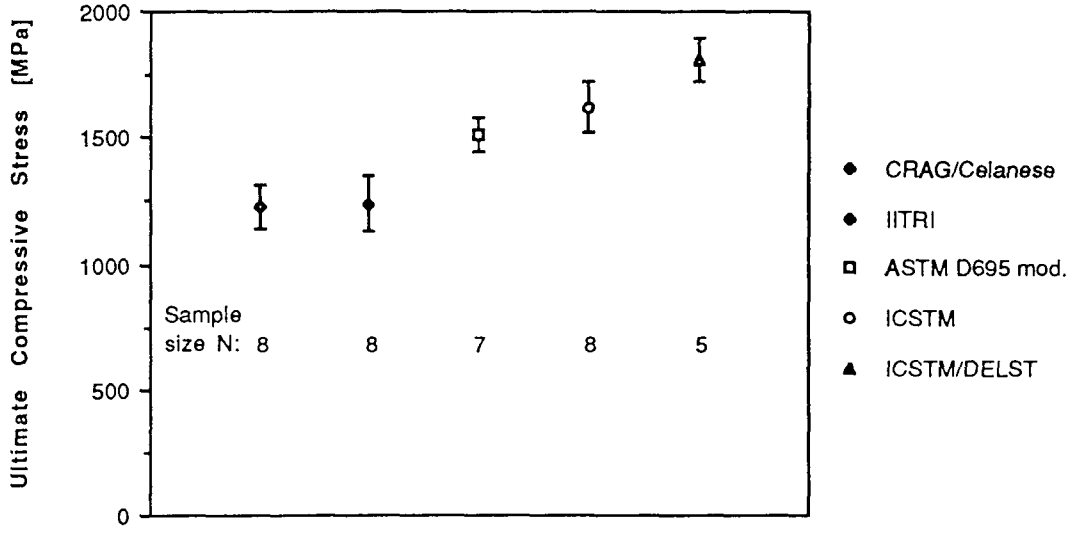


Fig. 2: Results for the compressive strength of 914C/XA-S using different test methods

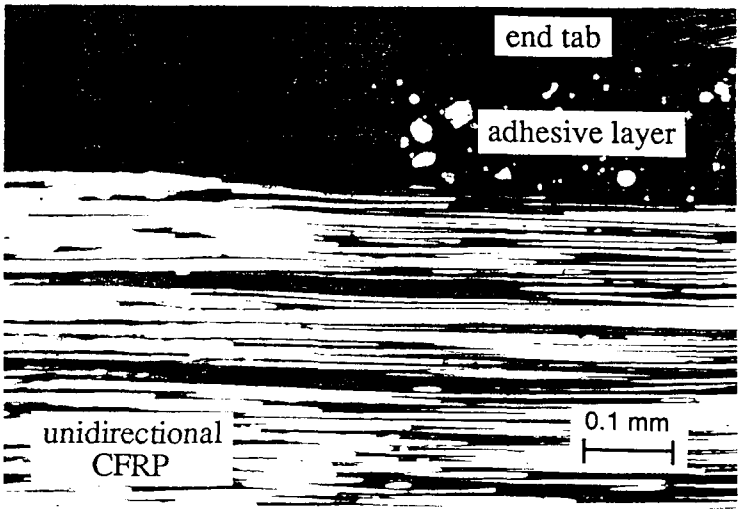


Fig. 3:

Illustration of the effect of through-thickness loading on the curvature of fibre bundles.

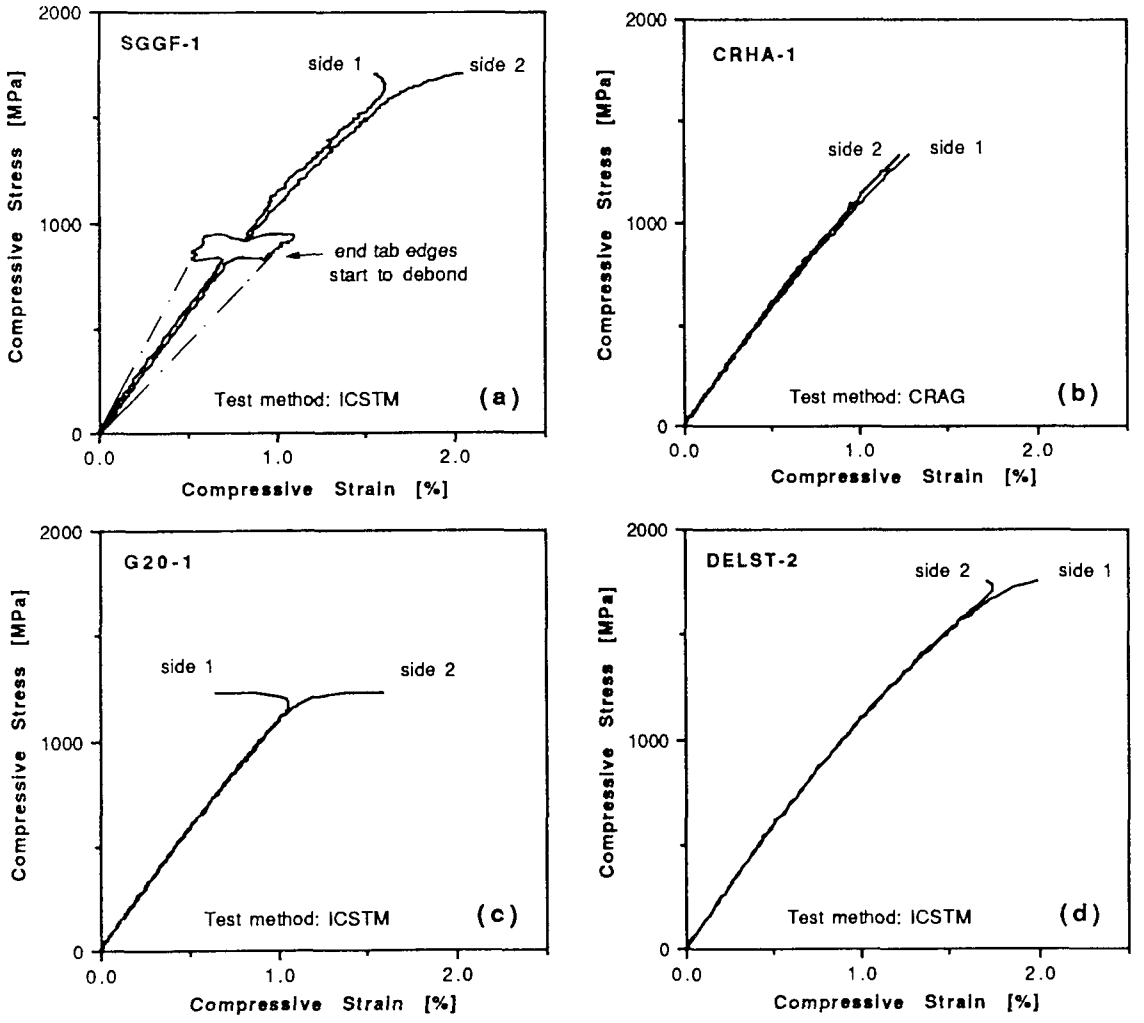


Fig. 4: Typical compressive stress strain curves, indicating debonding of end tab edges (a); failure without macro buckling (b); macro buckling: of a specimen with 20 mm gauge length (c) and of an improved specimen with 10 mm gauge length (d)

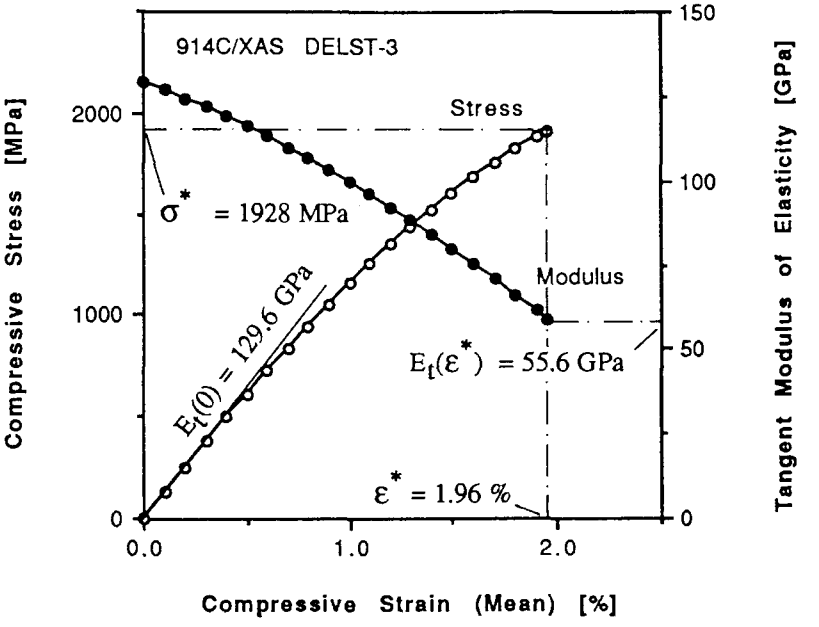


Fig. 5: Tangent longitudinal modulus of elasticity for a typical stress strain curve

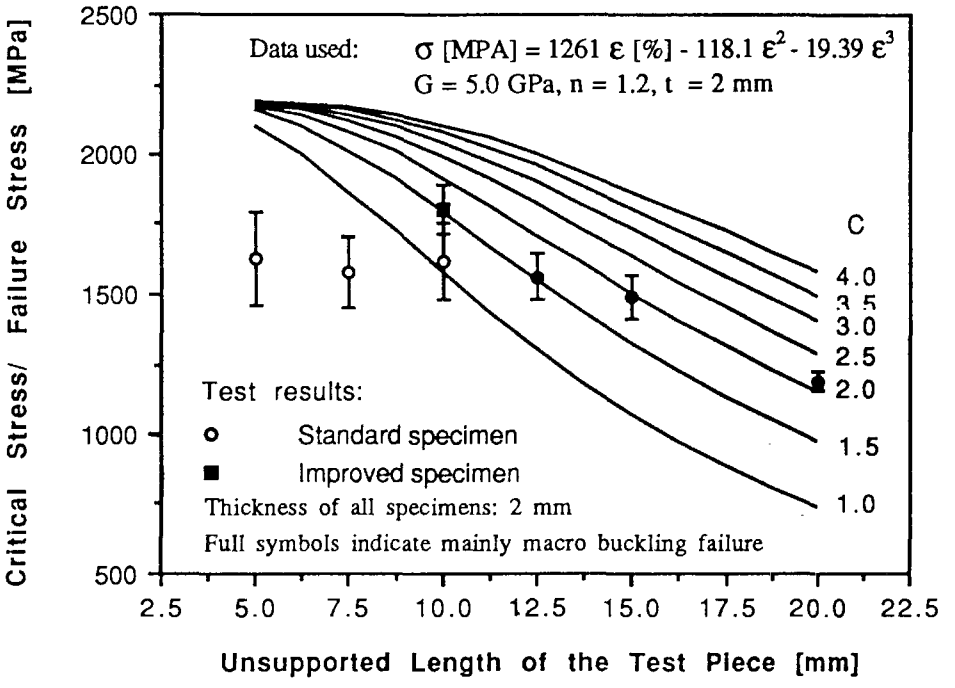


Fig. 6: Variation of the critical compressive stress for macro buckling with gauge length of the testpiece including test results of specimens with different gauge lengths